INTER

International Network on Timber Engineering Research

Proceedings

Meeting 47

01 - 04 September 2014

Bath, United Kingdom

Edited by Rainer Görlacher

Timber Scientific Publishing
KIT Holzbau und Baukonstruktionen
Karlsruhe, Germany
2014

Publisher:
Timber Scientific Publishing
KIT Holzbau und Baukonstruktionen
Reinhard-Baumeister-Platz 1
76131 Karlsruhe
Germany
2014

ISSN 2199-9740

Table of Contents

1	List of Participants		1
2	Minutes of the Meeting		3
3	Peer Review of Papers for the CIB-W18 Proceedings		17
4	Current List of CIB-W18 Papers		19
5	INTER Papers Bath, United Kingdom 2014		65
	47 - 5 - 1	Strength Grading of Split Glulam Beams - J Viguier, J-F Boquet, J Dopeux, L Bléron, F Dubois, S Aubert	67
	47 - 6 - 1	Compression Strength and Stiffness Perpendicular to the Grain – Influences of the Material Properties, the Loading Situation and the Gauge Length- C Le Levé, R Maderebner, M Flach	81
	47 - 7 - 1	Discussion of testing and Evaluation Methods for the Embedment Behaviour of Connections - S Franke, N Magnière	93
	47 - 7 - 2	Dowel-type Connections in LVL Made of Beech Wood - P Kobel, A Frangi, R Steiger	103
	47 - 7 - 3	Resistance of Connections in Cross-Laminated Timber under Brittle Block Tear-Out Failure Mode - P Zarnani, P Quenneville	117
	47 - 7 - 4	Study on Nail Connections in Deformed State - S Svensson, J Munch-Andersen	131
	47 - 7 - 5	Design Model for Inclined Screws under Varying Load to Grain Angles - R Jockwer, R Steiger, A Frangi	141
	47 - 12 - 1	Calculation of Cylindrical Shells from Wood or Wood Based Products and Consideration of the Stress Relaxation - P Aondio, S Winter, H Kreuzinger	155
	47 - 12 - 2	Hybrid Glulam Beams Made of Beech LVL and Spruce Laminations - M Frese	167
	47 - 12 - 3	Design for the Spreading under a Compressive Stress in Glued Laminated Timber - D Lathuilliere, L Bléron, J-F Bocquet, F Varacca, F Dubois	179
	47 - 12 - 4	Design of CLT Beams with Rectangular Holes or Notches - M Flaig	193
	47 - 12 - 5	Properties of Cross Laminated Timber (CLT) in Compression Perpendicular to Grain - R Brandner, G Schickhofer	209

47 - 15 - 1	Advanced Modelling of Timber-framed Wall Elements for Application in Engineering Practice - T Vogt, W Seim	225
47 - 15 - 2	A Buckling Design Approach for ‘Blockhaus’ Timber Walls Under In-plane Vertical Loads - C Bedon, M Fragiacomo, C Amadio, A Battisti	241
47 - 15 - 3	Capacity Design Approach for Multi-storey Timber-frame Buildings - D Casagrande, T Sartori, R Tomasi	255
47 - 15 - 4	Design Models for CLT Shearwalls and Assemblies Based on Connection Properties - I Gavric, M Popovski	269
47 - 15 - 5	Effects of Design Criteria on an Experimentally-based Evaluation of the Behaviour Factor of Novel Massive Wooden Shear Walls - L Pozza, R Scotta, D Trutalli, A Polastri, A Ceccotti	281
47 - 15 - 6	An Elastoplastic Solution for Earthquake Resistant Rigid Timber Shear Walls - Wei Yuen Loo, P Quenneville, Nawawi Chouw	295
47 - 15 - 7	In-Plane Racking Tests of Continuous Sheathed Wood Structural Panel Wall Bracing - T Skaggs, E Keith, Borjen Yeh, P Line, N Waltz	309
47 - 15 - 8	Design of Floor Diaphragms in Multi-Storey Timber Buildings - D Moroder, T Smith, S Pampanin, A Palermo, A H Buchanan	323
47 - 16 - 1	Fire Design of Glued-laminated Timber Beams with Regard to the Adhesive Performance Using the Reduced Cross-Section Method - M Klippel, J Schmid, A Frangi, G Fink	337

6 INTER Notes Bath, United Kingdom 2014 349

	Critical Discussion on Properties of Beech LVL - C Sandhaas, M Frese	351
	Withdrawal Strength Dependency on Timber Conditioning - J Munch-Andersen	355
	Execution of Timber Structures - K Nore, T Toratti, J Munch-Andersen, J Schmid, A Just	359
	Cross laminated Timber Made of Regional Wood from Shizuoka Area - Part 1: Project Outlines and Mechanical Properties of CLT - K Kobayashi, M Yasumura	363
	Cross Laminated Timber Made of Regional Wood from Shizuoka Area - Part 2: Seismic Performance of CLT Structures - M Yasumura, K Kobayashi, M Okabe	367
	Modelling the Bending Strength of Glued Laminated Timber using Machine-Grading Indicators - G Fink, A Frangi, J Köhler	371

1 List of Participants

AUSTRIA

R Brandner	Technical University of Graz
C Le Levé	University of Innsbruck

BELGIUM

K De Proft	Belgian Technical Centre of Wood Transformation and Furniture

CANADA

G Doudak	University of Ottawa
F Lam	University of British Columbia, Vancouver
M Popovski	FPInnovations, Vancouver
I Smith	University of New Brunswick

CROATIA

V Rajcic	University of Zagreb

DENMARK

A Hansen	Via University College
J Munch-Andersen	Danish Timber Information, Lyngby
S Svensson	Technical University of Denmark

FRANCE

D Lathuilliere	University of Lorraine
J Viguier	University of Lorraine

GERMANY

P Aondio	Technical University of Munich
H J Blaß	Karlsruhe Institute of Technology (KIT)
P Dietsch	Technical University of Munich
M Flaig	Karlsruhe Institute of Technology (KIT)
M Frese	Karlsruhe Institute of Technology (KIT)
R Görlacher	Karlsruhe Institute of Technology (KIT)
W Moorkamp	FH Aachen, University of Applied Sciences
C Sandhaas	Karlsruhe Institute of Technology (KIT)
W Seim	University Kassel
J-W van de Kuilen	Technical University of Munich
T Uibel	FH Aachen, University of Applied Sciences
T Vogt	University Kassel

IRELAND

A Harte	National University of Ireland, Galway

ITALY

M Fragiacomo	University of Sassari, Alghero
L Pozza	University of Padova
R Scotta	University of Padova
R Tomasi	University of Trento
D Trutalli	University of Padova

JAPAN

K Kobayashi	Shizuoka University
M Yasumura	Shizuoka University

NEW ZEALAND

A H Buchanan	University of Canterbury, Christchurch
Wei Yuen Loo	University of Auckland
P Quenneville	University of Auckland
F Scheibmair	University of Auckland

NORWAY

G Glaso	Norwegian Institute of Wood Technology (NTI)
K Nore	Norwegian Institute of Wood Technology (NTI)

SWEDEN

J Schmid	SP Wood Technology
E Serrano	Lund University

SWITZERLAND

L Boccadoro	ETH Zurich
G Fink	ETH Zurich
S Franke	Bern University of Applied Sciences
R Jockwer	Swiss Federal Laboratories for Material Science (EMPA) Dübendorf
P Kobel	ETH Zürich
R Steiger	Swiss Federal Laboratories for Material Science (EMPA) Dübendorf

UNITED KINGDOM

A Bradley	University of Bath
D Brandon	University of Bath
J Bregulla	BRE
P Fleming	University of Cambridge
R Harris	University of Bath
C Malaga	Imperial College
J Marcroft	Marcroft Timber Consultancy
C O’Neill	Queens University Belfast
K Ranasinghe	TRADA, High Wycombe
T Reynolds	University of Bath
Wen-Shao Chang	University of Bath
J Walker	Ecos Maclean

USA

T Skaggs	American Plywood Association, Tacoma
B Yeh	American Plywood Association, Tacoma

2 Minutes of the Meeting (by F Lam)

CHAIRMAN'S INTRODUCTION

Prof. Hans Blass welcomed the delegates to the International Network of Timber Engineering Research (INTER). This is the first INTER meeting after the successful series of 46 CIB W18 Meetings has ended and CIB W18 does not exist anymore. INTER will allow the continuation of our tradition of yearly meetings to discuss research results with the aim of transferring the information into practical application.

Past Chair of CIB W18, Chris Stieda from Forintek Canada Corp., now FPInnovations, passed away at the beginning of this year. A minute of silence was observed by the group in commemoration of Dr. Chris Stieda.

The Chair thanked Richard Harris (University of Bath) for hosting the INTER meeting. The first CIB W18 meeting took place in 1973 in Princes Risborough in England. Further CIB W18 meetings in UK include 1978 in Perth,, Scotland, 1991 in Oxford, England and 2004 in Edinburg, Scotland.

There are 22 papers accepted for this meeting. Papers brought directly to the meeting would not be accepted for presentation, discussions, or publication. Same rule applies to papers where none of the authors is present or papers which are not defended by one of the authors. The papers were selected based on the review process for abstract. The four acceptance criteria are: state of the art; originality; (assumed) content; and relation to codes or standards. Each criterion was judged with a scale of 0 (bad) to 5 (very good) leading to an overall grade. Reviewing was performed by 13 reviewers and a total of 13 submitted abstracts were not accepted.

The presentations are limited to 20 minutes each, allowing time for meaningful discussions after each presentation. The Chair asked the presenters to conclude the presentation with a general proposal or statements concerning impact of the research results on existing or future potential applications and development in codes and standards.

There are 6 topics covered in this meeting: Fire (2), Structural stability (8), Laminated members (5), Timber joints and fasteners (5), Stresses for solid timber (1), and Strength grading (1). Numbers in parentheses are the number of papers presented in each topic.

The participants have the possibility of presenting notes towards the end of the technical session. R Görlacher has brought a list of intended note presentations. Participants intending to present notes that are not on the list should notify R Görlacher accordingly.

Questions regarding the proceedings should be directed towards R. Görlacher. An address list of the participants will be circulated for verification of accuracy.

GENERAL TOPICS

Discussions took place about the conduct of INTER to ensure that we can continue to be a self-supporting group. The issue of joining other organization such as IABSE as working group was discussed. It was concluded that INTER should be continued as it is now as joining other organization would need membership also. A Buchanan supports the motion and recognizes the contribution of Karlsruhe Institute of Technology towards CIB W18 and now INTER. The group discussed the issue of the danger of becoming too small and at the same time the group does not want to become too big such that the intensive discussions were diluted. The current balance is ideal and should be maintained via word of mouth.

J Schmid asked about the issue of referenced papers and publication from the INTER meetings. H Blass responded that the group has received recognition of the CIB W18 meeting proceedings with Thomson Reuters Web of Knowledge as ISI conference proceeding series. The group will seek the same status for INTER proceedings. Hard copies of the proceedings will continue to be available. Special publication of a journal is possible; however more work is needed requiring a guest editor. Per CIB W18, INTER reviews the submitted abstracts for acceptance. Papers are then reviewed by the group via the intensive discussion and question period. Papers presented can also be reviewed to ensure scientific rigor. Proceedings from past CIB W18 meetings and INTER meetings will be available on-line.

BJ Yeh commented that official liaison with code committees is not available. H Blass suggested that individual participants of INTER serve on code committees and can bring forth INTER or CIB W18 topics and papers to the code committees. Official liaison is not needed as funding support is not available. H Blass commented that in past meetings reports from code committees were made but it lacked general interest. BJ Yeh suggested that INTER participants that are also members of various code committees members make their committees aware that INTER has replaced CIB W18.

3 FIRE

47 - 16 - 1 *Fire Design of Glued-laminated Timber Beams with Regard to the Adhesive Performance Using the Reduced Cross-Section Method* - **M Klippel, J Schmid, A Frangi G Fink**

Presented by J Schmid

BJ Yeh asked how to define adhesive quality system. J Schmid answered that there is no adhesive classification system that focuses on fire performance. This paper showed non-structural adhesives go below 0.3. Adhesive industry would like to see a certification process but this is not available. BJ Yeh commented that a heat durability standard has been available in N. America for 7 years requiring adhesives to be qualified for heat durability to eliminate low performance adhesives. This is also in the ISO standard.

W Seim asked how to define the strength at 100 C. J Schmid responded that KΘ can't be established from fire tests. This can be established only from backward calculations of fire test data of joints – lap shear tests.

K Ranasinghe asked about the glue line. J Schmid responded that since the glue line deals with shear strength, it is a different issue.

A Buchanan discussed the reduced cross section method and commented that in this paper the zero strength layer varied from 3 mm to 22 mm is a concern. He received confirmation from J Schmid that the zero strength layer depended on sectional size and the number sides exposed. A Buchanan stated that there was overlapping response between good and bad adhesives; therefore, the lack of influence of adhesive is not expected. J Schmid responded that the work was compared to fire test results using mean values and agreed that more details are needed.

S Svensson asked about the conductivity of wood and adhesive. J Schmid stated that the same conductivity was considered for wood and adhesive. S Svensson stated that glue can lead to heat transfer which can affect the results.

F Lam asked whether vertical or horizontal finger joints were used and whether there would be an influence in terms of heat transfer of the glue. J Schmid stated horizontal finger joints were used and that he is not sure whether there is a finger joint orientation effect.

STRUCTURAL STABILITY

47 - 15 - 1 *Advanced Modelling of Timber-framed Wall Elements for Application in Engineering Practice* - **T Vogt, W Seim**

Presented by T Vogt

P Quenneville asked whether the analysis was liner elastic. T Vogt responded no because the nails are yielding. P Quenneville asked whether different wall configurations will lead to different overstrength factors. T Vogt responded that the paper presented in the last CIB W18 meeting in Vancouver showed different overstrength factors for different connectors. Next step could be to develop overstrength factors for all connection types.

F Lam commented that when a wall undergoes reverse cyclic lateral loading the nails could move at an angle to the long axis of the stud. This movement depends on the wall aspect ratio. He questioned whether the presented approach can fully consider this aspect. T Vogt responded that the overstrength factor was defined as the ratio between the mean values of the response and confirmed that for walls with different aspect ratios the overstrength factors established from this approach is valid.

R Brandner received clarification about the position of the holddown devices and their elastic behaviour.

WY Loo questioned about the force displacements in the timber and commented that the use of Cartesian spring pair may work better.

E Serrano further commented that nonlinear coupled springs rather than single springs are needed to consider the behaviour of the nails.

I Smith stated that overstrength factors should be considered for the entire structure rather than for a wall.

A Buchanan commented that cyclic behaviour is important for seismic and asked whether the procedures can handle reverse cyclic. T. Vogt responded that it is not possible yet.

H Blass commented that the differences from values in EC5 are not that big. T. Vogt agreed. W Seim commented that force based design and time history approach are not appropriate for this model. Performance analysis needs push over analysis as an upper bound. The presented approach can provide this information easily.

M Fragiacomo discussed that this type of approach is still missing in Eurocode and suggested that the approach should aim for upper 95th percentile not the mean strength.

47 - 15 - 2 *A Buckling Design Approach for 'Blockhaus' Timber Walls Under In-plane Vertical Loads* - **C Bedon, M Fragiacomo, C Amadio, A Battisti**

Presented by M Fragiacomo

H Blass asked which shear modulus was considered for G and whether the rolling shear modulus should be considered and would it make a difference. M Fragiacomo agreed that the rolling shear modulus could be used and would make a difference. He also stated that a static friction coefficient μ of 0.2 was used initially but the results were different. There were discussions that the existence of gaps between the layers could decrease the bending stiffness assumed in the model. M Fragiacomo responded that the model is isotropic with smeared results. S Svensson commented that the longitudinal stiffness does not influence the lateral capacity. A Fragiacomo further discussed some of the assumptions in the FE analysis in terms of the interaction between logs and their contacts.

P. Quenneville suggested that half walls to be considered.

G Doudak and M Fragiacomo discussed the issues of modeling elastoplastic buckling, geometric nonlinearity and material nonlinearity. M Fragiacomo stated that the static friction coefficient μ was taken to reflect the mean response. R Tomasi commented that the model for buckling with contribution of torsional and movement out of plane was available in previous paper. M. Fragiacomo added that calibration factors were used in the model.

P Dietsch commented that the geometric eccentricity of L/400 in EC5 applies to one member not a wall with multiple members. Loads will shift in lumber and L/400 may be low for the wall system.

47 - 15 - 3 *Capacity Design Approach for Multi-storey Timber-frame Buildings* - **D Casagrande, T Sartori, R Tomasi**

Presented by R Tomasi

A Buchanan commented that the paper is good. In high ductility system where the weak link is to be identified for yielding to take place, other components are to be oversized. In multistory building using this approach of minimum values, is there possibility of soft storey collapse? If so which storey should be chosen? R Tomasi responded that yielding in each storey should be closely sequenced. This is similar to a braced system. The current model can't calculate so accurately. The designers can decide on the accuracy and which storey is allowed to become a soft storey in small buildings. In medium ductility class same issues exit. Here all the fasteners can yield.

P Quenneville commented that slide 16 shows the rigid and fuse items are not isolated from each other. Incompatibility of deformation between the two systems can occur. He suggested additional provisions be provided. R Tomasi agreed.

I Smith asked how to identify systems prone to disproportional damage. R Tomasi responded that simple cantilever model was considered in this paper. In practice there are secondary elements that can improve the robustness of the building. This should not be a practical problem. He further stated that using q factor of 5 may not be consistent with the behaviour of some of the buildings.

M Fragiacomo questioned plasticization along the entire wall or just assumed the ground floor plasticizing. He stated that distributed plasticization is another method to dissipate energy and wondered which method is better. R Tomasi responded that distributed plasticization was not found in time series analysis and further discussion on the topic is needed. M Popovski stated that in experiments of platform frame, plasticization occurred in one storey not the entire wall.

47 - 15 - 4 *Design Models for CLT Shearwalls and Assemblies Based on Connection Properties* - **I Gavric, M Popovski**

Presented by M Popovski

A Buchanan stated that the out of plane wall contributions offers big potential for CLT structures but depends on connection between the orthogonal walls. The use of nails or screws devices means that there is no attempt to come up with uncoupled devices between tension and shear. M Popovski agreed and further commented that we do not know the real resistance of the building even though buildings have been built.

W Seim stated that comparing different models is important to establish upper and lower bounds. He stated that model D3A is pure rocking and questioned equilibrium in this model. M Popovski answered that it is assumed that some device such as shear key will take the sliding mode.

I Smith stated that design code should not tell engineers how to do structural analysis. M Popovski agreed.

R Tomasi asked about the rules for the position of the holddown devices. M Popovski stated that it is up to the designers but the position of the holddown devices will make a difference and should be considered. There were discussions whether the presence of lintel beams in the 3-D model affect the structural performance.

M Fragiacomo stated that the 3-D system is conservative because out-of plane wall contributions were not considered in design. M Popovski responded that this is not always the case as it depends on the placement of the connection devices.

47 - 15 - 5 *Effects of Design Criteria on an Experimentally-based Evaluation of the Behaviour Factor of Novel Massive Wooden Shear Walls* - **L Pozza, R Scotta, D Trutalli, A Polastri, A Ceccotti**

Presented by D Trutalli

BJ Yeh asked that the hysteresis loops of the staple wall did not seem to reach the ultimate capacity. D Trutalli stated that they did not have breakage of the staples.

G Doudak asked how to justify q=4 between rigid and deformable panels. D Trutalli answered that test results are needed to help justify q=4.

F Lam received clarification that the staple system is the Hundegger system.

A Buchanan questioned the use of q as a wall ranking method. He questioned how to account for the poor performance of low stiffness walls with high q.

H Blass stated that the gaps between members and the performance of the base connections will also influence the wall response. D Trutalli responded that the base connectors were chosen with respect to the deformability of the panels.

M Fragiacomo asked what kind of failures was observed. D Trutalli answered that normal failures were observed with glued walls. With the unglued walls staples did not break.

I smith asked about the peak acceleration in the building. D Trutalli said that they do not have the information.

M Yasumura asked whether vertical load was applied. D Trutalli answered that 18.5 kN/m vertical load was applied. He also confirmed that 15 earthquakes were used in simulations to establish the q factor.

47 - 15 - 6 *An Elastoplastic Solution for Earthquake Resistant Rigid Timber Shear Walls* - **Wei Yuen Loo, P Quenneville, Nawawi Chouw**

Presented by WY Loo

I Smith commented about pounding against the ground and asked about the pounding within the structure itself. WY Loo responded that strong bracketed connections can be used and architecture details can be designed to prevent pounding against other parts of the structure.

W Seim received clarification of the friction device and explanations of the re-centering concept. He questioned how this system would work with wind loads where the loading is in mostly one direction only. WY Loo answered that wind load is not a problem because the system is very rigid.

M Fragiacomo commented that re-centering without restoring force is surprising. WY Loo responded that with this connection which emulates a plastic hinge that has special attributes numerical simulations results show that re-centering is available. With CLT walls which work as load bearing structures self centering is expected.

A Buchanan commented about the relatively large wall with small shear key therefore the sliding plates must provide some resistance to lateral sliding. WY Loo responded that the perpendicular to grain sliding plates can sway and are not expected to provide shear resistance.

M Fragiacomo pointed out that the static test show residual set. WY Loo responded that the numerical result of dynamic analysis shows re-centering was observed.

47 - 15 - 7 *In-Plane Racking Tests of Continuous Sheathed Wood Structural Panel Wall Bracing* - **T Skaggs, E Keith, Borjen Yeh, P Line, N Waltz**

Presented by T Skaggs

P Quenneville received confirmation that the deflections being sensitive to boundary conditions are sensitive at 40% as well as at the predicted load.

J Marcroft asked whether there was vertical load on the return wall. T Skaggs responded no and the return wall only had anchor bolts.

47 - 15 - 8 *Design of Floor Diaphragms in Multi-Storey Timber Buildings* - **D Moroder, T Smith, S Pampanin, A Palermo, A H Buchanan**

Presented by A Buchanan

WY Loo and A Buchanan discussed about wall flexibility in that it is the relative stiffness of the floor and wall and that the torsional response is important.

R Tomasi commented on the definition of flexibility of diaphragm and suggested that perhaps we need rules based on the type of construction (concrete topping floors for example). A Buchanan stated that we should be consistent rather than specifying such rules.

M Popovski provided information that in Canada diaphragm flexibility is now defined by 50% of the diaphragm deflection is greater than the deflection of the lateral load resistance system. This affects the R factor. I smith stated that in tall buildings you will not do this type of design. All agreed as wind rather than seismic will govern.

LAMINATED MEMBERS

47 - 12 - 1 *Calculation of Cylindrical Shells from Wood or Wood Based Products and Consideration of the Stress Relaxation* - **P Aondio, S Winter, H Kreuzinger**

Presented by P Aondio

H Blass asked about extrapolation from the 90 days tests and would one be able to use the LVL. P Aondio responded that there was no extrapolation and the LVL cannot be used because something is needed to distribute the stresses in the ring direction.

R Harris asked about plotting the relaxation versus time in terms of log of time. P Aondio stated that this has not been considered. R Harris stated that bonding wood is commonly done with for example glue laminated beams. P Aondio explained utilization factor and that the curve glue-laminated beams calculations from Eurocode are different. Also lower capacity of curved glulam beams would come from Eurocode.

S Svensson asked if there is an effect on how many plies. P Aondio responded that the study only dealt with 3 plies because thicker laminates would be too stiff. S Svensson commented that in slide 7 the curved glulam was painted and there should be no moisture gradient in the wood and that in actual service climate the condition can be more variable than stated in service class one.

M Fragiacomo received confirmation that 3% strain on top and bottom of the member and that the stress relaxation model was linear. M Fragiacomo recommended checking the stress level with respect to validity of linearity of the model.

47 - 12 - 2 Hybrid Glulam Beams Made of Beech LVL and Spruce Laminations - **M Frese**

Presented by M Frese

S Franke commented about the finger joint tests where 4 out of 49 had gluing deficiency. He asked whether they were ignored during the calculations. M Frese responded yes because the deficiencies were due to prototype manufacturing problems.

P Dietsch commented that in the spruce laminate the stresses exceeded the strength on the model and that tests should be done to confirm the simulations. M Frese responded that in reality spruce laminate can fail first and the material can carry additional load resulting from stress redistribution.

E Serrano commented about the failure mode of the Karlsruhe model and wondered how many elements would have failed prior to complete collapse. M Frese said that the information is available from the analysis.

S Svensson discussed shear failure between the LVL and solid wood laminate. M Frese responded that the shear stresses between the interface of the LVL and solid wood was checked. Since only two beech LVL laminate were present, the shear stresses at the interface were not as big as the shear stresses in the center line.

R Brandner asked about the assumption of normality for MOE and whether one could get negative MOE values from the simulations. M Frese responded that the simulation procedure did not seem to show negative MOE values. R Brander also commented on the distance between finger joint in the LVL that there is no need to joint with such high frequencies which would yield even higher results. M Frese responded that this is a manufacturing issue. It might be difficult to bring long length LVL broads into existing glulam plants.

BJ Yeh asked about shear failure model and commented that LVL hybrid glulam is a commercial product in N. America for many years. M Frese agreed that shear failure might occur when large number of LVL laminates is used because the LVL has relatively low shear strength.

J Munch-Andersen commented that one should use distribution of the upper tail MOE rather than the lower tail.

F Lam received confirmation that there is no restriction of finger joint position between adjacent LVL or solid sawn laminations in Europe.

J W van de Kuilen commented that the manufacturers may have different machine settings for MOE which can change its distribution.

S Franke received confirmation that the calculation method is based on glulam values not laminate values.

47 - 12 - 3 Design for the Spreading under a Compressive Stress in Glued Laminated Timber - **D Lathuilliere, L Bléron, J-F Bocquet, F Varacca, F Dubois**

Presented by D Lathuilliere

S Svensson asked was the friction between the loading head and wood considered. D

Lathuillier responded no.

F Lam asked about the size effect adjustment Ksb and received confirmation that the coefficient was established from regression.

I Smith stated that more simplification is better and asked about the consideration of B Madsen test results. He received discussions that B Madsen's results were considered via the Eurocode confirmation.

S Franke commented about the use of 1% offset for proportional limit. He stated that one should try different method as the results depend on the specimen depth such that if different specimen depths were considered the 1% offset method would result in difficulties for comparing the results.

47 - 12 - 4 Design of CLT Beams with Rectangular Holes or Notches - **M Flaig**

Presented by M Flaig

I Smith asked how different would the results be compared to stress analysis based on isotropic material. M Flaig responded that the stress concentration factor depends on the ratio of the stiffness so isotropic solution would have errors.

A Buchanan stated that the work of M Fragiacomo on LVL with cross band should be referenced. He asked suppose the beams were made with plywood, would results apply to CLT made with thinner layers. M Flaig responded that no because the shear stress distribution would be different.

BJ Yeh received clarification of the definition of the cross area, size of the hole and side of the CLT. BJ Yeh and M Flaig discussed that the glue space between the board size depends on the width of the laminate.

R Jockwer stated that in slide 17 initial cracking of the notched beam cannot be avoided. M Flaig responded that there is an unglued gap so the vertical bending failure was secondary failure.

E Serrano asked about the local effect in terms of relationship between the corner and the gap in relation to the use of the model and design. M Flaig responded that the model can only take into consideration of the full laminate. There were some tested beams and model of beams with different corners and gaps.

P Quenneville asked how reliable is the model if the torsional contribution is ignored since one cannot control the gap locations. M Flaig responded that this difference is less important with deeper beam relative to notch size. P Quenneville asked what the contribution of the torsional component is. M Flaig responded 100% because the beam would not work without torsional resistance. P Quenneville asked where the size of the crossing area is used. M Flaig responded only 150 mm assuming smaller width.

S. Svensson asked if rolling shear stress was available. M Flaig responded yes near the surface of the beam. There was discussion that the k factor does not depend on the shape of the corner. I Smith added that dry shrinkage will lead to cracks therefore rounded corner should be ignored.

M Fragiacomo asked about edge glue situation. H Blass responded that edge gluing should be ignored and one may assume 150 mm laminar width.

47 - 12 - 5 Properties of Cross Laminated Timber (CLT) in Compression Perpendicular to Grain - **R Brandner, G Schickhofer**

Presented by R Brandner

Erik Serrano asked for clarification of the uplift. R Brandner responded that under eccentric loading there could be uplift if the unloaded side was not restrained. Erik Serrano asked how to handle the unbonded edge joint. R Brandner responded that the spreading of load from first layer was neglected.

S Svensson stated that there are mechanic based solutions from Green's book for orthotropic material.

W Seim asked should moisture dependency not be covered by k_{mod}. R Brandner responded that this is a topic for discussion but the compression perpendicular to grain case is particularly sensitive to moisture influence.

J Schmidt received confirmation that the 20% increase compared to glulam can be attributed to locking effect. J Schmidt asked if this effect can be expected if the product was made at high moisture content compared to in service conditions. R Brandner responded that the capability to glue at green condition is questionable. In any case locking effect will still be present.

R Tomasi and R Brandner discussed horizontal stresses in the compression component in the 1st layer and horizontal stresses in tension in the 2nd layer in that tension transfer should be restricted.

TIMBER JOINTS AND FASTENERS

47 - 7 - 1 *Discussion of testing and Evaluation Methods for the Embedment Behaviour of Connections* - **S Franke, N Magnière**

Presented by S Franke

H Blass asked about the foundation modulus for the stiffness. He asked what do you do with the stiffness. S Franke responded that it would not be used for strength design. H Blass stated that we almost never used the stiffness values. P Quenneville stated that the information can be used in studying connection behaviour but its use in estimating connection stiffness is challenging. H Blass stated this is only for research purposes so far. He commented that there are similar data on fasteners for timber concrete joints, inclined screws etc. Stiffness data is hidden and never used in practice.

P Quenneville stated that why use the full hole test where we never have uniform stress distribution. S Franke responded that in some cases half hole test can easily split therefore full hole test is used. H Blass stated that in performing test with brittle material where splitting could occur reinforcement could be used to prevent splitting. H Blass added that this reinforcement is intended to allow embedment strength to be measured not connection strength.

I Smith stated that back in history a lot of work was done. The biggest variable was who did the test. Devices were developed to prevent splitting of the wood but not practical.

S Svensson added less human error with the simplest way possible is desired.

JW van de Kuilen stated that the quality of steel etc. can add to the variability and he agreed that the simplest way possible should be adopted.

P Quenneville questioned whether 0.05d offset or 5 mm offset is more appropriate.

J Munch Anderson stated that correction or calibration factors should be considered with the easy method. H Blass questioned how to do embedment strength tests for staples in OSB where OSB core and face have different embedment strengths. F Lam stated that in such cases one should do connection test.

I Smith stated that ASTM standard is intended for product comparisons.

P Quenneville said that the 5 mm offset and yield strength values are needed for mixed brittle failure mode for connection design.

J W van de Kuilen stated that the line from Eurocode is correct. If you sought refinements, the connection does not become safer as you cannot get good correlations between dowel embedment and connection behaviour.

47 - 7 - 2 *Dowel-type Connections in LVL Made of Beech Wood* - **P Kobel, A Frangi, R Steiger**

Presented by P Kobel

JW Van de Kuilen received clarification that the steel grades were S355 for the dowels and 8.8 for the bolts. P Kobel said that the quality of the steel was not checked but will do so later. Also he assumed over-strength of 25%.

P Quenneville asked whether net tension failures were observed. P Kobel said that for bolted connection with 2 rows of bolts it was observed. P Quenneville stated that one cannot use the net tension data in the connection test. P Kobel agreed. He said that the net tension failure happened only once and since then the test configuration was changed to avoid this mode.

R Brandner and P Quenneville discussed that for cross banded LVL, net cross section failure needed to be checked by designers.

C Sandhaas commented about different strength properties of beech LVL.

H Blass asked how many cross band is needed. P Kobel responded that they are still working on it. He further confirmed that bolts were needed to prevent the opening failure mode shown in the code provision.

W Seim commented that with a better material whether EC5 spacing rules would still work.

J Munch Andersen commented that more investigation is needed for increasing the load capacity per fastener. One should consider load per fastener rather than spacing rules.

P Quenneville asked about the cross banded LVL pricing. P Kobel said no information is available. P Quenneville stated that if LVL has high price, one might lose economical advantage for any gain in capacity.

47 - 7 - 3 *Resistance of Connections in Cross-Laminated Timber under Brittle Block Tear-Out Failure Mode* - **P Zarnani, P Quenneville**

Presented by P Quenneville

S Franke stated that in the model side plane was neglected. In the tests there was some shear transfer as there was no cut made in the specimen. If you made the cut it would fit the model. P Quenneville agreed.

S Franke referred to slide 16 where t_{ef} was the only check. He asked if the nail was smaller than the 1st laminar, is it possible that the failure would extend into the cross layer with rolling shear and tension. P Quenneville said it is possible.

I Smith asked what kind of end distances would be needed to avoid the alarming failures shown in some of the slides. P Quenneville responded that in a practical case 500 kN of load transfer in a shear wall was needed. Use up to 1 m wide connection and use LVL on the outside to provide the tensile resistance in the outside laminate. Depending on the load, the bottom end distance is not that significant; the length and width of the connection are more important.

A Buchanan stated for high strength and stiffness applications rivets are best and control of deflection in building needs stiffer fasteners. He commented that ductility can be put into some devices. For example for post tension rocking walls, yielding steel devices are used.

One needs stiffness of the connections otherwise one will lose the post tension effect. He has a question in the problem with high stresses in CLT where LVL are used in CLT as mix material. Is it easy to handle mix material with various thicknesses and grades. P Quenneville responded that one still needs more work and discussion about the practical example in New Zealand. He said mobilizing the entire thickness may be more desirable.

47 - 7 - 4 *Study on the Rope-effect on the Load-carrying Capacity of Nailed Connections* - **S Svensson, J Munch-Andersen**

Presented by S Svensson

H Blass commented that the present rope effect in EC5 is based on a theory that does not take into consideration actual fasteners. The angle φ needed in the study depends on splitting tendency. In this present EC5 this is not considered because the value of the angle is unsure. He asked how do you provide assurance of the value of the angle φ. S Svensson responded that in the elastic part the angle φ is approximately 1, 1.5, 2 degrees. In full plasticity for mild steel the angle φ is approximately 4 to 5 degrees. H Blass asked how to guarantee this angle before localized splitting of the timber. S Svensson agreed that this is a topic of future research. J Munch Andersen added that this paper aims to gain more understanding and insight with physically correct approach. H Blass asked can you quantify the contribution of the rope effect which has two parts one of which is already in the EC5. There was discussion that if the contribution is not that much, is it worthwhile to consider this because the angle φ may be different.

JW van de Kuilen referred to an old paper from TU Delft from J Kuipers and T van der Put on the same topic. He asked as annular ringed nails were used what type of yield moment was calculated for this type of fasteners. S Svensson responded that the values came from the manufacturer. JW van de Kuilen stated nails with cutoff round head will also behave differently.

I Smith commented about Johansson's work in 1941.

47 - 7 - 5 *Design Model for Inclined Screws under Varying Load to Grain Angles* - **R Jockwer, R Steiger, A Frangi**

Presented by R Jockwer

H Blass asked why this type of connections was considered when you would have openings. R Jockwer responded that for the reinforcement case such as notched beams this has relevance. H Blass asked would you not incline the screws to avoid opening effect even in the reinforcement cases. In the notch case there is an opening component. Also for example CLT wall connected at the corner there would be an opening case. H Blass received confirmation that in such cases where the opening reduced the embedment, the withdrawal length was also reduced.

H Blass stated that back calculation of the embedment strength can be affected by the existence of friction forces even though Teflon was used. Friction can still be transferred where the calculated embedment in the paper is significantly higher than the values in literature. R Jockwer agreed.

J Munch Andersen commented about the contribution of the head of the screw potentially increasing the fastener capacity due to rope effect.

M Frese commented that pulling test of the inclined screws at 45 degree, relative movement of both pieces was observed. In the case of the notched beam, the beam is bonded which will restrict horizontal movement. He asked if the tests reflect reality. R Jockwer responded that in the test only at larger deformation such lateral movement was observed so the test should be valid.

S Svensson asked did you monitor the bending angles of all of the screws. R Jockwer stated only a few cases were observed and they did not keep the failed screws. S Svensson asked why the compression mode was not tried. R Jockwer responded that similar tests were done in the literature; their results offered comparisons for this study.

STRESSES FOR SOLID TIMBER

47 - 6 - 1 *Compression Strength and Stiffness Perpendicular to the Grain – Influences of the Material Properties, the Loading Situation and the Gauge Length*- **C Le Levé, R Maderebner, M Flach**

Presented by C Le Levé

D Brandon commented that the side movement of the specimens were observed; the fixity of the top and bottom plates could affect the results. WS Loo also commented on the load head actuator fixity. C Le Levé agreed that it is possible that the fixity could influence results.

R Görlacher stated that MOE values should not depend on loading situation. As the stresses in the specimens are not uniform; therefore, differences in stiffness were observed. As such one should consider referencing the stiffness rather than MOE.

S. Franke said that influence of annual ring was reported. He asked how you would propose to handle this in codes. C Le Levé responded that in the test standard one should specify annual ring orientation. S Franke further commented that if the test set up was modified, one would get the EN results. P Dietsch added that it is important to talk about issues related to test standard.

F Lam commented that there are too many conclusions from this paper. The author should focus on only a few most relevant points.

S Svensson commented about clear wood testing. He asked can reaction wood be ignored and why not look into representative sample rather than clear wood.

JW van de Kuilen commented that Eurocode is considering removal of density and lowering compression strength perpendicular to grain values. He commented that slide 6 showed local failure only and asked why care about the area underneath the failure zone.

H Blass added that the consequence of failure is excessive deformation; code design rules included consideration of low consequence of failure.

STRESS GRADING

47 - 5 - 1 *Strength Grading of Split Glulam Beams* - **J Viguier, J-F Boquet, J Dopeux, L Bléron, F Dubois, S Aubert**

Presented by J Viguier

J Munch Andersen commented that old data showed reduced strength of 4 MPa with one cut and 8 MPA with two cuts. He commented that it is very difficult to show things are different in terms of using statistics.

P Quenneville commented that statistical comparisons were made at the mean and 5th percentile comparisons are more appropriate.

R Brandner asked why the bending test done on edge for the boards. J Viguier responded that grading is done by calibrated machines in edge bending in France. R Brandner commented that recently more machines in Europe are calibrated based on tensile strength.

JW van de Kuilen asked whether the boards were checked for the grade quality. J Viguier responded that it will be done later. JW van de Kuilen stated that different manufacturing procedures may influence grade distribution.

E Serrano and J Viguier discussed about two cuts to split a beam into three in terms of the quality of the thin member.

R Steiger commented that tools can be used to qualify uncertainties. In Slide 18 and 19 using effective cross section for stiffness properties maybe possible but for strength is inappropriate. J Viguier explained the procedure using the ratio between the values of moment of inertia of the full board and the reduced cross section to get the weakest section and to get the reduced Moe. Then the relationship between MOR and MOE was used to get the strength.

S Franke asked whether this can be done with tension grading. J Viguier answered yes. It is better with tension grading. S Franke also commented that the increase of density of the resawn beam could explain the increase in strength. J Viguier responded the density increase is little.

NOTES

Six notes were presented

ANY OTHER BUSINESS

P Dietsch presented information on CEN TC 250 /SC5 current status.

The group is in general agreement that this type of code and standards activities information exchange is useful and should be included in future meetings.

P Quenneville reported on activities in Canada and Australia/NZ

P Dietsch presented background information on COST Action FP1402 Basis of structural timber design – from research to standards

M Fragiacomo presented background information on COST Action FP1404 Fire safe use of bio-based building products.

VENUE AND PROGRAMME FOR NEXT MEETING

Next venue will be in Croatia – Solaris Beach Resort the week of Aug 24 to 28, 2015.

V Rajcic will host the next meeting and presented an invitation to the participants.

The 2016 venue will be in Graz Austria to be hosted by G Schickhofer.

The 2017 venue will be in Japan to be hosted by M Yasumura.

CLOSE

Chairman thanked R Harris and the supporting group for hosting and organizing the excellent meeting. Meeting closed.

3 Peer review of papers for the INTER Proceedings

Experts involved:

Members of the INTER group are a community of experts in the field of timber engineering.

Procedure of peer review

- Submission of manuscripts: all members of the INTER group attending the meeting receive the manuscripts of the papers at least four weeks before the meeting. Everyone is invited to read and review the manuscripts especially in their respective fields of competence and interest.

- Presentation of the paper during the meeting by the author

- Comments and recommendations of the experts, discussion of the paper

- Comments, discussion and recommendations of the experts are documented in the minutes of the meeting and are printed on the front page of each paper.

- Final acceptance of the paper for the proceedings with
  - no changes
  - minor changes
  - major changes
  - or reject

- Revised papers are to be sent to the editor of the proceedings and the chairman of the INTER group

- Editor and chairman check, whether the requested changes have been carried out.

4 Current List of CIB W18 and INTER Papers

Technical papers presented to CIB-W18(A) are identified by a code CIB-W18(A)/a-b-c, and

Technical papers presented to INTER are identified by a code INTER/a-b-c, where:

a denotes the meeting at which the paper was presented.

1 Princes Risborough, England; March 1973
2 Copenhagen, Denmark; October 1973
3 Delft, Netherlands; June 1974
4 Paris, France; February 1975
5 Karlsruhe, Federal Republic of Germany; October 1975
6 Aalborg, Denmark; June 1976
7 Stockholm, Sweden; February/March 1977
8 Brussels, Belgium; October 1977
9 Perth, Scotland; June 1978
10 Vancouver, Canada; August 1978
11 Vienna, Austria; March 1979
12 Bordeaux, France; October 1979
13 Otaniemi, Finland; June 1980
14 Warsaw, Poland; May 1981
15 Karlsruhe, Federal Republic of Germany; June 1982
16 Lillehammer, Norway; May/June 1983
17 Rapperswil, Switzerland; May 1984
18 Beit Oren, Israel; June 1985
19 Florence, Italy; September 1986
20 Dublin, Ireland; September 1987
21 Parksville, Canada; September 1988
22 Berlin, German Democratic Republic; September 1989
23 Lisbon, Portugal; September 1990
24 Oxford, United Kingdom; September 1991
25 Åhus, Sweden; August 1992
26 Athens, USA; August 1993
27 Sydney, Australia; July 1994
28 Copenhagen, Denmark; April 1995
29 Bordeaux, France; August 1996
30 Vancouver, Canada; August 1997
31 Savonlinna, Finland; August 1998
32 Graz, Austria, August 1999
33 Delft, The Netherlands; August 2000
34 Venice, Italy; August 2001
35 Kyoto, Japan; September 2002
36 Colorado, USA; August 2003
37 Edinburgh, Scotland, August 2004
38 Karlsruhe, Germany, August 2005

39 Florence, Italy, August 2006
40 Bled, Slovenia, August 2007
41 St. Andrews, Canada 2008
42 Dübendorf, Switzerland 2009
43 Nelson, New Zealand 2010
44 Alghero, Italy 2011
45 Växjö,Sweden 2012
46 Vancouver, Canada 2013
47 Bath, United Kingdom 2014

b denotes the subject:

1 Limit State Design
2 Timber Columns
3 Symbols
4 Plywood
5 Stress Grading
6 Stresses for Solid Timber
7 Timber Joints and Fasteners
8 Load Sharing
9 Duration of Load
10 Timber Beams
11 Environmental Conditions
12 Laminated Members
13 Particle and Fibre Building Boards
14 Trussed Rafters
15 Structural Stability
16 Fire
17 Statistics and Data Analysis
18 Glued Joints
19 Fracture Mechanics
20 Serviceability
21 Test Methods
100 CIB Timber Code
101 Loading Codes
102 Structural Design Codes
103 International Standards Organisation
104 Joint Committee on Structural Safety
105 CIB Programme, Policy and Meetings
106 International Union of Forestry Research Organisations

c is simply a number given to the papers in the order in which they appear:

Example: CIB-W18/4-102-5 refers to paper 5 on subject 102 presented at the fourth meeting of W18.

Listed below, by subjects, are all papers that have to date been presented to W18 and INTER. When appropriate some papers are listed under more than one subject heading.

LIMIT STATE DESIGN

1-1-1 Limit State Design - H J Larsen

1-1-2 The Use of Partial Safety Factors in the New Norwegian Design Code for Timber Structures - O Brynildsen

1-1-3 Swedish Code Revision Concerning Timber Structures - B Noren

1-1-4 Working Stresses Report to British Standards Institution Committee BLCP/17/2

6-1-1 On the Application of the Uncertainty Theoretical Methods for the Definition of the Fundamental Concepts of Structural Safety - K Skov and O Ditlevsen

11-1-1 Safety Design of Timber Structures - H J Larsen

18-1-1 Notes on the Development of a UK Limit States Design Code for Timber - A R Fewell and C B Pierce

18-1-2 Eurocode 5, Timber Structures - H J Larsen

19-1-1 Duration of Load Effects and Reliability Based Design (Single Member) - R O Foschi and Z C Yao

21-102-1 Research Activities Towards a New GDR Timber Design Code Based on Limit States Design - W Rug and M Badstube

22-1-1 Reliability-Theoretical Investigation into Timber Components Proposal for a Supplement of the Design Concept - M Badstube, W Rug and R Plessow

23-1-1 Some Remarks about the Safety of Timber Structures - J Kuipers

23-1-2 Reliability of Wood Structural Elements: A Probabilistic Method to Eurocode 5 Calibration - F Rouger, N Lheritier, P Racher and M Fogli

31-1-1 A Limit States Design Approach to Timber Framed Walls - C J Mettem, R Bainbridge and J A Gordon

32 -1-1 Determination of Partial Coefficients and Modification Factors- H J Larsen, S Svensson and S Thelandersson

32 -1-2 Design by Testing of Structural Timber Components - V Enjily and L Whale

33-1-1 Aspects on Reliability Calibration of Safety Factors for Timber Structures – S Svensson and S Thelandersson

33-1-2 Sensitivity studies on the reliability of timber structures – A Ranta-Maunus, M Fonselius, J Kurkela and T Toratti

41-1–1 On the Role of Stiffness Properties for Ultimate Limit State Design of Slender Columns– J Köhler, A Frangi, R Steiger

TIMBER COLUMNS

2-2-1 The Design of Solid Timber Columns - H J Larsen

3-2-1 The Design of Built-Up Timber Columns - H J Larsen

4-2-1 Tests with Centrally Loaded Timber Columns - H J Larsen and S S Pedersen

4-2-2 Lateral-Torsional Buckling of Eccentrically Loaded Timber Columns- B Johansson

5-9-1 Strength of a Wood Column in Combined Compression and Bending with Respect to Creep - B Källsner and B Norén

5-100-1 Design of Solid Timber Columns (First Draft) - H J Larsen

6-100-1 Comments on Document 5-100-1, Design of Solid Timber Columns - H J Larsen and E Theilgaard

6-2-1 Lattice Columns - H J Larsen

6-2-2 A Mathematical Basis for Design Aids for Timber Columns - H J Burgess

6-2-3 Comparison of Larsen and Perry Formulas for Solid Timber Columns- H J Burgess

7-2-1 Lateral Bracing of Timber Struts - J A Simon

8-15-1 Laterally Loaded Timber Columns: Tests and Theory - H J Larsen

17-2-1 Model for Timber Strength under Axial Load and Moment - T Poutanen

18-2-1 Column Design Methods for Timber Engineering - A H Buchanan, K C Johns, B Madsen

19-2-1 Creep Buckling Strength of Timber Beams and Columns - R H Leicester

19-12-2 Strength Model for Glulam Columns - H J Blaß

20-2-1 Lateral Buckling Theory for Rectangular Section Deep Beam-Columns- H J Burgess

20-2-2 Design of Timber Columns - H J Blaß

21-2-1 Format for Buckling Strength - R H Leicester

21-2-2 Beam-Column Formulae for Design Codes - R H Leicester

21-15-1 Rectangular Section Deep Beam - Columns with Continuous Lateral Restraint - H J Burgess

21-15-2 Buckling Modes and Permissible Axial Loads for Continuously Braced Columns - H J Burgess

21-15-3 Simple Approaches for Column Bracing Calculations - H J Burgess

21-15-4 Calculations for Discrete Column Restraints - H J Burgess

22-2-1 Buckling and Reliability Checking of Timber Columns - S Huang, P M Yu and J Y Hong

22-2-2 Proposal for the Design of Compressed Timber Members by Adopting the Second-Order Stress Theory - P Kaiser

30-2-1 Beam-Column Formula for Specific Truss Applications - W Lau, F Lam and J D Barrett

31-2-1 Deformation and Stability of Columns of Viscoelastic Material Wood - P Becker and K Rautenstrauch

34-2-1 Long-Term Experiments with Columns: Results and Possible Consequences on Column

34-2-2 Proposal for Compressive Member Design Based on Long-Term Simulation Studies – P Becker, K Rautenstrauch

35-2-1 Computer Simulations on the Reliability of Timber Columns Regarding Hygrothermal Effects- R Hartnack, K-U Schober, K Rautenstrauch

36-2-1 The Reliability of Timber Columns Based on Stochastical Principles - K Rautenstrauch, R Hartnack

38-2-1 Long-term Load Bearing of Wooden Columns Influenced by Climate – View on Code - R Hartnack, K Rautenstrauch

SYMBOLS

3-3-1 Symbols for Structural Timber Design - J Kuipers and B Norén

4-3-1 Symbols for Timber Structure Design - J Kuipers and B Norén

28-3-1 Symbols for Timber and Wood-Based Materials - J Kuipers and B Noren

PLYWOOD

2-4-1 The Presentation of Structural Design Data for Plywood - L G Booth

3-4-1 Standard Methods of Testing for the Determination of Mechanical Properties of Plywood - J Kuipers

3-4-2 Bending Strength and Stiffness of Multiple Species Plywood - C K A Stieda

4-4-4 Standard Methods of Testing for the Determination of Mechanical Properties of Plywood - Council of Forest Industries, B.C.

5-4-1 The Determination of Design Stresses for Plywood in the Revision of CP 112 - L G Booth

5-4-2 Veneer Plywood for Construction - Quality Specifications - ISO/TC 139. Plywood, Working Group 6

6-4-1 The Determination of the Mechanical Properties of Plywood Containing Defects - L G Booth

6-4-2 Comparsion of the Size and Type of Specimen and Type of Test on Plywood Bending Strength and Stiffness - C R Wilson and P Eng

6-4-3 Buckling Strength of Plywood: Results of Tests and Recommendations for Calculations - J Kuipers and H Ploos van Amstel

7-4-1 Methods of Test for the Determination of Mechanical Properties of Plywood - L G Booth, J Kuipers, B Norén, C R Wilson

7-4-2 Comments Received on Paper 7-4-1

7-4-3 The Effect of Rate of Testing Speed on the Ultimate Tensile Stress of Plywood - C R Wilson and A V Parasin

7-4-4 Comparison of the Effect of Specimen Size on the Flexural Properties of Plywood Using the Pure Moment Test - C R Wilson and A V Parasin

8-4-1 Sampling Plywood and the Evaluation of Test Results - B Norén

9-4-1 Shear and Torsional Rigidity of Plywood - H J Larsen

9-4-2 The Evaluation of Test Data on the Strength Properties of Plywood - L G Booth

9-4-3 The Sampling of Plywood and the Derivation of Strength Values (Second Draft) - B Norén

9-4-4 On the Use of the CIB/RILEM Plywood Plate Twisting Test: a progress report - L G Booth

10-4-1 Buckling Strength of Plywood - J Dekker, J Kuipers and H Ploos van Amstel

11-4-1 Analysis of Plywood Stressed Skin Panels with Rigid or Semi-Rigid Connections- I Smith

11-4-2 A Comparison of Plywood Modulus of Rigidity Determined by the ASTM and RILEM CIB/3-TT Test Methods - C R Wilson and A V Parasin

11-4-3 Sampling of Plywood for Testing Strength - B Norén

12-4-1 Procedures for Analysis of Plywood Test Data and Determination of Characteristic Values Suitable for Code Presentation - C R Wilson

14-4-1 An Introduction to Performance Standards for Wood-base Panel Products - D H Brown

14-4-2 Proposal for Presenting Data on the Properties of Structural Panels - T Schmidt

16-4-1 Planar Shear Capacity of Plywood in Bending - C K A Stieda

17-4-1 Determination of Panel Shear Strength and Panel Shear Modulus of Beech-Plywood in Structural Sizes - J Ehlbeck and F Colling

17-4-2 Ultimate Strength of Plywood Webs - R H Leicester and L Pham

20-4-1 Considerations of Reliability - Based Design for Structural Composite Products - M R O'Halloran, J A Johnson, E G Elias and T P Cunningham

21-4-1 Modelling for Prediction of Strength of Veneer Having Knots - Y Hirashima

22-4-1 Scientific Research into Plywood and Plywood Building Constructions the Results and Findings of which are Incorporated into Construction Standard Specifications of the USSR - I M Guskov

22-4-2 Evaluation of Characteristic values for Wood-Based Sheet Materials - E G Elias

24-4-1 APA Structural-Use Design Values: An Update to Panel Design Capacities - A L Kuchar, E G Elias, B Yeh and M R O'Halloran

STRESS GRADING

1-5-1 Quality Specifications for Sawn Timber and Precision Timber - Norwegian Standard NS 3080

1-5-2 Specification for Timber Grades for Structural Use - British Standard BS 4978

4-5-1 Draft Proposal for an International Standard for Stress Grading Coniferous Sawn Softwood - ECE Timber Committee

16-5-1 Grading Errors in Practice - B Thunell

16-5-2 On the Effect of Measurement Errors when Grading Structural Timber- L Nordberg and B Thunell

19-5-1 Stress-Grading by ECE Standards of Italian-Grown Douglas-Fir Dimension Lumber from Young Thinnings - L Uzielli

19-5-2 Structural Softwood from Afforestation Regions in Western Norway - R Lackner

21-5-1 Non-Destructive Test by Frequency of Full Size Timber for Grading - T Nakai

22-5-1 Fundamental Vibration Frequency as a Parameter for Grading Sawn Timber - T Nakai, T Tanaka and H Nagao

24-5-1 Influence of Stress Grading System on Length Effect Factors for Lumber Loaded in Compression - A Campos and I Smith

26-5-1 Structural Properties of French Grown Timber According to Various Grading Methods - F Rouger, C De Lafond and A El Quadrani

28-5-1 Grading Methods for Structural Timber - Principles for Approval - S Ohlsson

28-5-2 Relationship of Moduli of Elasticity in Tension and in Bending of Solid Timber - N Burger and P Glos

29-5-1 The Effect of Edge Knots on the Strength of SPF MSR Lumber - T Courchene, F Lam and J D Barrett

29-5-2 Determination of Moment Configuration Factors using Grading Machine Readings - T D G Canisius and T Isaksson

31-5-1 Influence of Varying Growth Characteristics on Stiffness Grading of Structural Timber - S Ormarsson, H Petersson, O Dahlblom and K Persson

31-5-2 A Comparison of In-Grade Test Procedures - R H Leicester, H Breitinger and H Fordham

32-5-1 Actual Possibilities of the Machine Grading of Timber - K Frühwald and A Bernasconi

32-5-2 Detection of Severe Timber Defects by Machine Grading - A Bernasconi, L Boström and B Schacht

34-5-1 Influence of Proof Loading on the Reliability of Members – F Lam, S Abayakoon, S Svensson, C Gyamfi

36-5-1 Settings for Strength Grading Machines – Evaluation of the Procedure according to prEN 14081, part 2 - C Bengtsson, M Fonselius

36-5-2 A Probabilistic Approach to Cost Optimal Timber Grading - J Köhler, M H Faber

36-7-11 Reliability of Timber Structures, Theory and Dowel-Type Connection Failures - A Ranta-Maunus, A Kevarinmäki

38-5-1 Are Wind-Induced Compression Failures Grading Relevant - M Arnold, R Steiger

39-5-1 A Discussion on the Control of Grading Machine Settings – Current Approach, Potential and Outlook - J Köhler, R Steiger

39-5-2 Tensile Proof Loading to Assure Quality of Finger-Jointed Structural timber - R Katzengruber, G Jeitler, G Schickhofer

40-5-1 Development of Grading Rules for Re-Cycled Timber Used in Structural Applications - K Crews

40-5-2 The Efficient Control of Grading Machine Settings - M Sandomeer, J Köhler, P Linsenmann

41-5-1 Probabilistic Output Control for Structural Timber - Fundamental Model Approach – M K Sandomeer, J Köhler, M H Faber

42-5-1 Machine Strength Grading – a New Method for Derivation of Settings - R Ziethén, C Bengtsson

43-5-1 Quality Control Methods - Application to Acceptance Criteria for a Batch of Timber - F Rouger

43-5-2 Influence of Origin and Grading Principles on the Engineering Properties of European Timber - P Stapel, J W v. d. Kuilen, A Rais

44-5-1 Assessment of Different Knot-Indicators to Predict Strength and Stiffness Properties of Timber Boards - G Fink, M Deublein, J Köhler

44-5-2 Adaptive Production Settings Method for Strength Grading - G Turk, A Ranta-Maunus

44-5-3 Initial Settings for Machine Strength Graded Structural Timber - R Ziethén, C Bengtsson

47-5-1 Strength Grading of Split Glulam Beams - J Viguier, J-F Boquet, J Dopeux, L Bléron, F Dubois, S Aubert

47-6-1 Compression Strength and Stiffness Perpendicular to the Grain – Influences of the Material Properties, the Loading Situation and the Gauge Length- C Le Levé, R Maderebner, M Flach

STRESSES FOR SOLID TIMBER

4-6-1 Derivation of Grade Stresses for Timber in the UK - W T Curry

5-6-1 Standard Methods of Test for Determining some Physical and Mechanical Properties of Timber in Structural Sizes - W T Curry

5-6-2 The Description of Timber Strength Data - J R Tory

5-6-3 Stresses for EC1 and EC2 Stress Grades - J R Tory

6-6-1 Standard Methods of Test for the Determination of some Physical and Mechanical Properties of Timber in Structural Sizes (third draft) - W T Curry

7-6-1 Strength and Long-term Behaviour of Lumber and Glued Laminated Timber under Torsion Loads - K Möhler

9-6-1	Classification of Structural Timber - H J Larsen
9-6-2	Code Rules for Tension Perpendicular to Grain - H J Larsen
9-6-3	Tension at an Angle to the Grain - K Möhler
9-6-4	Consideration of Combined Stresses for Lumber and Glued Laminated Timber - K Möhler
11-6-1	Evaluation of Lumber Properties in the United States - W L Galligan and J H Haskell
11-6-2	Stresses Perpendicular to Grain - K Möhler
11-6-3	Consideration of Combined Stresses for Lumber and Glued Laminated Timber (addition to Paper CIB-W18/9-6-4) - K Möhler
12-6-1	Strength Classifications for Timber Engineering Codes - R H Leicester and W G Keating
12-6-2	Strength Classes for British Standard BS 5268 - J R Tory
13-6-1	Strength Classes for the CIB Code - J R Tory
13-6-2	Consideration of Size Effects and Longitudinal Shear Strength for Uncracked Beams - R O Foschi and J D Barrett
13-6-3	Consideration of Shear Strength on End-Cracked Beams - J D Barrett and R O Foschi
15-6-1	Characteristic Strength Values for the ECE Standard for Timber - J G Sunley
16-6-1	Size Factors for Timber Bending and Tension Stresses - A R Fewell
16-6-2	Strength Classes for International Codes - A R Fewell and J G Sunley
17-6-1	The Determination of Grade Stresses from Characteristic Stresses for BS 5268: Part 2 - A R Fewell
17-6-2	The Determination of Softwood Strength Properties for Grades, Strength Classes and Laminated Timber for BS 5268: Part 2 - A R Fewell
18-6-1	Comment on Papers: 18-6-2 and 18-6-3 - R H Leicester
18-6-2	Configuration Factors for the Bending Strength of Timber - R H Leicester
18-6-3	Notes on Sampling Factors for Characteristic Values - R H Leicester
18-6-4	Size Effects in Timber Explained by a Modified Weakest Link Theory- B Madsen and A H Buchanan
18-6-5	Placement and Selection of Growth Defects in Test Specimens - H Riberholt
18-6-6	Partial Safety-Coefficients for the Load-Carrying Capacity of Timber Structures - B Norén and J-0 Nylander
19-6-1	Effect of Age and/or Load on Timber Strength - J Kuipers
19-6-2	Confidence in Estimates of Characteristic Values - R H Leicester
19-6-3	Fracture Toughness of Wood - Mode I - K Wright and M Fonselius
19-6-4	Fracture Toughness of Pine - Mode II - K Wright
19-6-5	Drying Stresses in Round Timber - A Ranta-Maunus
19-6-6	A Dynamic Method for Determining Elastic Properties of Wood - R Görlacher
20-6-1	A Comparative Investigation of the Engineering Properties of "Whitewoods" Imported to Israel from Various Origins - U Korin
20-6-2	Effects of Yield Class, Tree Section, Forest and Size on Strength of Home Grown Sitka Spruce - V Picardo
20-6-3	Determination of Shear Strength and Strength Perpendicular to Grain - H J Larsen

21-6-1 Draft Australian Standard: Methods for Evaluation of Strength and Stiffness of Graded Timber - R H Leicester

21-6-2 The Determination of Characteristic Strength Values for Stress Grades of Structural Timber. Part 1 - A R Fewell and P Glos

21-6-3 Shear Strength in Bending of Timber - U Korin

22-6-1 Size Effects and Property Relationships for Canadian 2-inch Dimension Lumber - J D Barrett and H Griffin

22-6-2 Moisture Content Adjustements for In-Grade Data - J D Barrett and W Lau

22-6-3 A Discussion of Lumber Property Relationships in Eurocode 5 - D W Green and D E Kretschmann

22-6-4 Effect of Wood Preservatives on the Strength Properties of Wood - F Ronai

23-6-1 Timber in Compression Perpendicular to Grain - U Korin

24-6-1 Discussion of the Failure Criterion for Combined Bending and Compression - T A C M van der Put

24-6-3 Effect of Within Member Variability on Bending Strength of Structural Timber - I Czmoch, S Thelandersson and H J Larsen

24-6-4 Protection of Structural Timber Against Fungal Attack Requirements and Testing- K Jaworska, M Rylko and W Nozynski

24-6-5 Derivation of the Characteristic Bending Strength of Solid Timber According to CEN-Document prEN 384 - A J M Leijten

25-6-1 Moment Configuration Factors for Simple Beams- T D G Canisius

25-6-3 Bearing Capacity of Timber - U Korin

25-6-4 On Design Criteria for Tension Perpendicular to Grain - H Petersson

25-6-5 Size Effects in Visually Graded Softwood Structural Lumber - J D Barrett, F Lam and W Lau

26-6-1 Discussion and Proposal of a General Failure Criterion for Wood - T A C M van der Put

27-6-1 Development of the "Critical Bearing": Design Clause in CSA-086.1 - C Lum and E Karacabeyli

27-6-2 Size Effects in Timber: Novelty Never Ends - F Rouger and T Fewell

27-6-3 Comparison of Full-Size Sugi (Cryptomeria japonica D.Don) Structural Performance in Bending of Round Timber, Two Surfaces Sawn Timber and Square Sawn Timber - T Nakai, H Nagao and T Tanaka

28-6-1 Shear Strength of Canadian Softwood Structural Lumber - F Lam, H Yee and J D Barrett

28-6-2 Shear Strength of Douglas Fir Timbers - B Madsen

28-6-3 On the Influence of the Loading Head Profiles on Determined Bending Strength - L Muszyñsky and R Szukala

28-6-4 Effect of Test Standard, Length and Load Configuration on Bending Strength of Structural Timber- T Isaksson and S Thelandersson

28-6-5 Grading Machine Readings and their Use in the Calculation of Moment Configuration Factors - T Canisius, T Isaksson and S Thelandersson

28-6-6 End Conditions for Tension Testing of Solid Timber Perpendicular to Grain - T Canisius

29-6-1 Effect of Size on Tensile Strength of Timber - N Burger and P Glos

29-6-2 Equivalence of In-Grade Testing Standards - R H Leicester, H O Breitinger and H F Fordham

30-6-1 Strength Relationships in Structural Timber Subjected to Bending and Tension - N Burger and P Glos

30-6-2 Characteristic Design Stresses in Tension for Radiata Pine Grown in Canterbury - A Tsehaye, J C F Walker and A H Buchanan

30-6-3 Timber as a Natural Composite: Explanation of Some Peculiarities in the Mechanical Behaviour - E Gehri

31-6-1 Length and Moment Configuration Factors - T Isaksson

31-6-2 Tensile Strength Perpendicular to Grain According to EN 1193 - H J Blaß and M Schmid

31-6-3 Strength of Small Diameter Round Timber - A Ranta-Maunus, U Saarelainen and H Boren

31-6-4 Compression Strength Perpendicular to Grain of Structural Timber and Glulam - L Damkilde, P Hoffmeyer and T N Pedersen

31-6-5 Bearing Strength of Timber Beams - R H Leicester, H Fordham and H Breitinger

32-6-1 Development of High-Resistance Glued Robinia Products and an Attempt to Assign Such Products to the European System of Strength Classes - G Schickhofer and B Obermayr

32-6-2 Length and Load Configuration Effects in the Code Format - T Isaksson

32-6-3 Length Effect on the Tensile Strength of Truss Chord Members - F Lam

32-6-4 Tensile Strength Perpendicular to Grain of Glued Laminated Timber - H J Blaß and M Schmid

32-6-5 On the Reliability-based Strength Adjustment Factors for Timber Design - T D G Canisius

34-6-1 Material Strength Properties for Canadian Species Used in Japanese Post and Beam Construction - J D Barrett, F Lam, S Nakajima

35-6-1 Evaluation of Different Size Effect Models for Tension Perpendicular to Grain Design - S Aicher, G Dill-Langer

35-6-2 Tensile Strength of Glulam Perpendicular to Grain - Effects of Moisture Gradients - J Jönsson, S Thelandersson

36-6-1 Characteristic Shear Strength Values Based on Tests According to EN 1193 - P Glos, J Denzler

37-6-1 Tensile Strength of Nordic Birch - K H Solli

37-6-2 Effect of Test Piece Orientation on Characteristic Bending Strength of Structural Timber - P Glos, J K Denzler

37-6-3 Strength and Stiffness Behaviour of Beech Laminations for High Strength Glulam - P Glos, J K Denzler, P W Linsenmann

37-6-4 A Review of Existing Standards Related to Calculation of Characteristic Values of Timber - F Rouger

37-6-5 Influence of the Rolling-Shear Modulus on the Strength and Stiffness of Structural Bonded Timber Elements - P Fellmoser, H J Blass

38-6-1 Design Specifications for Notched Beams in AS:1720 - R H Leicester

38-6-2 Characteristic Bending Strength of Beech Glulam - H J Blaß, M Frese

38-6-3 Shear Strength of Glued Laminated Timber - H Klapp, H Brüninghoff

39-6-1 Allocation of Central European hardwoods into EN 1912 - P Glos, J K Denzler

39-6-2	Revisiting EN 338 and EN 384 Basics and Procedures - R Steiger, M Arnold, M Fontana
40-6-1	Bearing Strength Perpendicular to the Grain of Locally Loaded Timber Blocks - A J M Leijten, J C M Schoenmakers
40-6-2	Experimental Study of Compression and Shear Strength of Spruce Timber - M Poussa, P Tukiainen, A Ranta-Maunus
40-6-3	Analysis of Tension and Bending strength of Graded Spruce Timber - A Hanhijärvi, A Ranta-Maunus, H Sarkama, M Kohsaku, M Poussa, J Puttonen
41-6-1	Design of Inclined Glulam Members with an End Notch on the Tension Face - A Asiz, I Smith
41-6-2	A New Design Approach for End-notched Beams - View on Code - K Rautenstrauch, B Franke, S Franke, K U Schober
41-6-3	The Design Rules in Eurocode 5 for Compression Perpendicular to the Grain - Continuous Supported Beams - H J Larsen, T A C M van der Put, A J M Leijten
41-6-4	Size Effects in Bending – J K Denzler, P Glos
42-6-1	Variability of Strength of European Spruce - A Ranta-Maunus, J K Denzler
42-6-2	Impact Loaded Structural Timber Elements Made from Swiss Grown Norway Spruce - R Widmann, R Steiger
42-6-3	Modelling the Bending Strength of Timber Components –Implications to Test Standards - J Köhler, M Sandomeer, T Isaksson, B Källsner
43-6-1	The Bearing Strength of Timber Beams on Discrete Supports - A Jorissen, B de Leijer, A Leijten
44-6-1	Impact of Material Properties on the Fracture Mechanics Design Approach for Notched Beams in Eurocode 5 - R Jockwer, R Steiger, A Frangi, J Köhler
44-6-2	Interaction of Shear Stresses and Stresses Perpendicular to the Grain - R Steiger, E Gehri
46-6-1	Enhanced Design Approach for Reinforced Notched Beams - R Jockwer, A Frangi, E Serrano, R Steiger
47-6-1	Compression Strength and Stiffness Perpendicular to the Grain – Influences of the Material Properties, the Loading Situation and the Gauge Length- C Le Levé, R Maderebner, M Flach

TIMBER JOINTS AND FASTENERS

1-7-1	Mechanical Fasteners and Fastenings in Timber Structures - E G Stern
4-7-1	Proposal for a Basic Test Method for the Evaluation of Structural Timber Joints with Mechanical Fasteners and Connectors - RILEM 3TT Committee
4-7-2	Test Methods for Wood Fasteners - K Möhler
5-7-1	Influence of Loading Procedure on Strength and Slip-Behaviour in Testing Timber Joints - K Möhler
5-7-2	Recommendations for Testing Methods for Joints with Mechanical Fasteners and Connectors in Load-Bearing Timber Structures - RILEM 3 TT Committee
5-7-3	CIB-Recommendations for the Evaluation of Results of Tests on Joints with Mechanical Fasteners and Connectors used in Load-Bearing Timber Structures - J Kuipers
6-7-1	Recommendations for Testing Methods for Joints with Mechanical Fasteners and Connectors in Load-Bearing Timber Structures (seventh draft) - RILEM 3 TT Committee

6-7-2	Proposal for Testing Integral Nail Plates as Timber Joints - K Möhler
6-7-3	Rules for Evaluation of Values of Strength and Deformation from Test Results - Mechanical Timber Joints - M Johansen, J Kuipers, B Norén
6-7-4	Comments to Rules for Testing Timber Joints and Derivation of Characteristic Values for Rigidity and Strength - B Norén
7-7-1	Testing of Integral Nail Plates as Timber Joints - K Möhler
7-7-2	Long Duration Tests on Timber Joints - J Kuipers
7-7-3	Tests with Mechanically Jointed Beams with a Varying Spacing of Fasteners - K Möhler
7-100-1	CIB-Timber Code Chapter 5.3 Mechanical Fasteners;CIB-Timber Standard 06 and 07 - H J Larsen
9-7-1	Design of Truss Plate Joints - F J Keenan
9-7-2	Staples - K Möhler
11-7-1	A Draft Proposal for International Standard: ISO Document ISO/TC 165N 38E
12-7-1	Load-Carrying Capacity and Deformation Characteristics of Nailed Joints - J Ehlbeck
12-7-2	Design of Bolted Joints - H J Larsen
12-7-3	Design of Joints with Nail Plates - B Norén
13-7-1	Polish Standard BN-80/7159-04: Parts 00-01-02-03-04-05. "Structures from Wood and Wood-based Materials. Methods of Test and Strength Criteria for Joints with Mechanical Fasteners"
13-7-2	Investigation of the Effect of Number of Nails in a Joint on its Load Carrying Ability - W Nozynski
13-7-3	International Acceptance of Manufacture, Marking and Control of Finger-jointed Structural Timber - B Norén
13-7-4	Design of Joints with Nail Plates - Calculation of Slip - B Norén
13-7-5	Design of Joints with Nail Plates - The Heel Joint - B Källsner
13-7-6	Nail Deflection Data for Design - H J Burgess
13-7-7	Test on Bolted Joints - P Vermeyden
13-7-8	Comments to paper CIB-W18/12-7-3 "Design of Joints with Nail Plates"- B Norén
13-7-9	Strength of Finger Joints - H J Larsen
13-100-4	CIB Structural Timber Design Code. Proposal for Section 6.1.5 Nail Plates - N I Bovim
14-7-1	Design of Joints with Nail Plates (second edition) - B Norén
14-7-2	Method of Testing Nails in Wood (second draft, August 1980) - B Norén
14-7-3	Load-Slip Relationship of Nailed Joints - J Ehlbeck and H J Larsen
14-7-4	Wood Failure in Joints with Nail Plates - B Norén
14-7-5	The Effect of Support Eccentricity on the Design of W- and WW-Trussed with Nail Plate Connectors - B Källsner
14-7-6	Derivation of the Allowable Load in Case of Nail Plate Joints Perpendicular to Grain - K Möhler
14-7-7	Comments on CIB-W18/14-7-1 - T A C M van der Put

15-7-1 Final Recommendation TT-1A: Testing Methods for Joints with Mechanical Fasteners in Load-Bearing Timber Structures. Annex A Punched Metal Plate Fasteners - Joint Committee RILEM/CIB-3TT

16-7-1 Load Carrying Capacity of Dowels - E Gehri

16-7-2 Bolted Timber Joints: A Literature Survey - N Harding

16-7-3 Bolted Timber Joints: Practical Aspects of Construction and Design; a Survey - N Harding

16-7-4 Bolted Timber Joints: Draft Experimental Work Plan - Building Research Association of New Zealand

17-7-1 Mechanical Properties of Nails and their Influence on Mechanical Properties of Nailed Timber Joints Subjected to Lateral Loads - I Smith, L R J Whale, C Anderson and L Held

17-7-2 Notes on the Effective Number of Dowels and Nails in Timber Joints - G Steck

18-7-1 Model Specification for Driven Fasteners for Assembly of Pallets and Related Structures - E G Stern and W B Wallin

18-7-2 The Influence of the Orientation of Mechanical Joints on their Mechanical Properties - I Smith and L R J Whale

18-7-3 Influence of Number of Rows of Fasteners or Connectors upon the Ultimate Capacity of Axially Loaded Timber Joints - I Smith and G Steck

18-7-4 A Detailed Testing Method for Nailplate Joints - J Kangas

18-7-5 Principles for Design Values of Nailplates in Finland - J Kangas

18-7-6 The Strength of Nailplates - N I Bovim and E Aasheim

19-7-1 Behaviour of Nailed and Bolted Joints under Short-Term Lateral Load - Conclusions from Some Recent Research - L R J Whale, I Smith and B O Hilson

19-7-2 Glued Bolts in Glulam - H Riberholt

19-7-3 Effectiveness of Multiple Fastener Joints According to National Codes and Eurocode 5 (Draft) - G Steck

19-7-4 The Prediction of the Long-Term Load Carrying Capacity of Joints in Wood Structures - Y M Ivanov and Y Y Slavic

19-7-5 Slip in Joints under Long-Term Loading - T Feldborg and M Johansen

19-7-6 The Derivation of Design Clauses for Nailed and Bolted Joints in Eurocode 5 - L R J Whale and I Smith

19-7-7 Design of Joints with Nail Plates - Principles - B Norén

19-7-8 Shear Tests for Nail Plates - B Norén

19-7-9 Advances in Technology of Joints for Laminated Timber - Analyses of the Structural Behaviour - M Piazza and G Turrini

19-15-1 Connections Deformability in Timber Structures: A Theoretical Evaluation of its Influence on Seismic Effects - A Ceccotti and A Vignoli

20-7-1 Design of Nailed and Bolted Joints-Proposals for the Revision of Existing Formulae in Draft Eurocode 5 and the CIB Code - L R J Whale, I Smith and H J Larsen

20-7-2 Slip in Joints under Long Term Loading - T Feldborg and M Johansen

20-7-3 Ultimate Properties of Bolted Joints in Glued-Laminated Timber - M Yasumura, T Murota and H Sakai

20-7-4 Modelling the Load-Deformation Behaviour of Connections with Pin-Type Fasteners under Combined Moment, Thrust and Shear Forces - I Smith

21-7-1 Nails under Long-Term Withdrawal Loading - T Feldborg and M Johansen

21-7-2 Glued Bolts in Glulam-Proposals for CIB Code - H Riberholt

21-7-3 Nail Plate Joint Behaviour under Shear Loading - T Poutanen

21-7-4 Design of Joints with Laterally Loaded Dowels. Proposals for Improving the Design Rules in the CIB Code and the Draft Eurocode 5 - J Ehlbeck and H Werner

21-7-5 Axially Loaded Nails: Proposals for a Supplement to the CIB Code - J Ehlbeck and W Siebert

22-7-1 End Grain Connections with Laterally Loaded Steel Bolts A draft proposal for design rules in the CIB Code - J Ehlbeck and M Gerold

22-7-2 Determination of Perpendicular-to-Grain Tensile Stresses in Joints with Dowel-Type Fasteners - A draft proposal for design rules - J Ehlbeck, R Görlacher and H Werner

22-7-3 Design of Double-Shear Joints with Non-Metallic Dowels A proposal for a supplement of the design concept - J Ehlbeck and O Eberhart

22-7-4 The Effect of Load on Strength of Timber Joints at high Working Load Level - A J M Leijten

22-7-5 Plasticity Requirements for Portal Frame Corners - R Gunnewijk and A J M Leijten

22-7-6 Background Information on Design of Glulam Rivet Connections in CSA/CAN3-086.1-M89 - A proposal for a supplement of the design concept - E Karacabeyli and D P Janssens

22-7-7 Mechanical Properties of Joints in Glued-Laminated Beams under Reversed Cyclic Loading - M Yasumura

22-7-8 Strength of Glued Lap Timber Joints - P Glos and H Horstmann

22-7-9 Toothed Rings Type Bistyp 075 at the Joints of Fir Wood - J Kerste

22-7-10 Calculation of Joints and Fastenings as Compared with the International State - K Zimmer and K Lissner

22-7-11 Joints on Glued-in Steel Bars Present Relatively New and Progressive Solution in Terms of Timber Structure Design - G N Zubarev, F A Boitemirov and V M Golovina

22-7-12 The Development of Design Codes for Timber Structures made of Compositive Bars with Plate Joints based on Cyclindrical Nails - Y V Piskunov

22-7-13 Designing of Glued Wood Structures Joints on Glued-in Bars - S B Turkovsky

23-7-1 Proposal for a Design Code for Nail Plates - E Aasheim and K H Solli

23-7-2 Load Distribution in Nailed Joints - H J Blass

24-7-1 Theoretical and Experimental Tension and Shear Capacity of Nail Plate Connections - B Källsner and J Kangas

24-7-2 Testing Method and Determination of Basic Working Loads for Timber Joints with Mechanical Fasteners - Y Hirashima and F Kamiya

24-7-3 Anchorage Capacity of Nail Plate - J Kangas

25-7-2 Softwood and Hardwood Embedding Strength for Dowel type Fasteners - J Ehlbeck and H Werner

25-7-4 A Guide for Application of Quality Indexes for Driven Fasteners Used in Connections in Wood Structures - E G Stern

25-7-5 35 Years of Experience with Certain Types of Connectors and Connector Plates Used for the Assembly of Wood Structures and their Components- E G Stern

25-7-6 Characteristic Strength of Split-ring and Shear-plate Connections - H J Blass, J Ehlbeck and M Schlager

25-7-7 Characteristic Strength of Tooth-plate Connector Joints - H J Blass, J Ehlbeck and M Schlager

25-7-8 Extending Yield Theory to Screw Connections - T E McLain

25-7-9 Determination of k_{def} for Nailed Joints - J W G van de Kuilen

25-7-10 Characteristic Strength of UK Timber Connectors - A V Page and C J Mettem

25-7-11 Multiple-fastener Dowel-type Joints, a Selected Review of Research and Codes - C J Mettem and A V Page

25-7-12 Load Distributions in Multiple-fastener Bolted Joints in European Whitewood Glulam, with Steel Side Plates - C J Mettem and A V Page

26-7-1 Proposed Test Method for Dynamic Properties of Connections Assembled with Mechanical Fasteners - J D Dolan

26-7-2 Validatory Tests and Proposed Design Formulae for the Load-Carrying Capacity of Toothed-Plate Connectored Joints - C J Mettem, A V Page and G Davis

26-7-3 Definitions of Terms and Multi-Language Terminology Pertaining to Metal Connector Plates - E G Stern

26-7-4 Design of Joints Based on in V-Shape Glued-in Rods - J Kangas

26-7-5 Tests on Timber Concrete Composite Structural Elements (TCCs) - A U Meierhofer

27-7-1 Glulam Arch Bridge and Design of it's Moment-Resisting Joints - K Komatsu and S Usuku

27-7-2 Characteristic Load - Carrying Capacity of Joints with Dowel - type Fasteners in Regard to the System Properties - H Werner

27-7-3 Steel Failure Design in Truss Plate Joints - T Poutanen

28-7-1 Expanded Tube Joint in Locally DP Reinforced Timber - A J M Leijten, P Ragupathy and K S Virdi

28-7-2 A Strength and Stiffness Model for the Expanded Tube Joint - A J M Leijten

28-7-3 Load-carrying Capacity of Steel-to Timber Joints with Annular Ring Shanked Nails. A Comparison with the EC5 Design Method - R Görlacher

28-7-4 Dynamic Effects on Metal-Plate Connected Wood Truss Joints - S Kent, R Gupta and T Miller

28-7-5 Failure of the Timber Bolted Joints Subjected to Lateral Load Perpendicular to Grain - M Yasumura and L Daudeville

28-7-6 Design Procedure for Locally Reinforced Joints with Dowel-type Fasteners - H Werner

28-7-7 Variability and Effects of Moisture Content on the Withdrawal Characteristics for Lumber as Opposed to Clear Wood - J D Dolan and J W Stelmokas

28-7-8 Nail Plate Capacity in Joint Line - A Kevarinmäki and J Kangas

28-7-9 Axial Strength of Glued-In Bolts - Calculation Model Based on Non-Linear Fracture Mechanics - A Preliminary Study - C J Johansson, E Serrano, P J Gustafsson and B Enquist

28-7-10 Cyclic Lateral Dowel Connection Tests for seismic and Wind Evaluation - J D Dolan

29-7-1 A Simple Method for Lateral Load-Carrying Capacity of Dowel-Type Fasteners - J Kangas and J Kurkela

29-7-2 Nail Plate Joint Behaviour at Low Versus High Load Level - T Poutanen

29-7-3 The Moment Resistance of Tee and Butt - Joint Nail Plate Test Specimens - A Comparison with Current Design Methods - A Reffold, L R J Whale and B S Choo

29-7-4 A Critical Review of the Moment Rotation Test Method Proposed in prEN 1075 - M Bettison, B S Choo and L R J Whale

29-7-5 Explanation of the Translation and Rotation Behaviour of Prestressed Moment Timber Joints - A J M Leijten

29-7-6 Design of Joints and Frame Corners using Dowel-Type Fasteners - E Gehri

29-7-7 Quasi-Static Reversed-Cyclic Testing of Nailed Joints - E Karacabeyli and A Ceccotti

29-7-8 Failure of Bolted Joints Loaded Parallel to the Grain: Experiment and Simulation - L Davenne, L Daudeville and M Yasumura

30-7-1 Flexural Behaviour of GLT Beams End-Jointed by Glued-in Hardwood Dowels - K Komatsu, A Koizumi, J Jensen, T Sasaki and Y Iijima

30-7-2 Modelling of the Block Tearing Failure in Nailed Steel-to-Timber Joints - J Kangas, K Aalto and A Kevarinmäki

30-7-3 Cyclic Testing of Joints with Dowels and Slotted-in Steel Plates - E Aasheim

30-7-4 A Steel-to-Timber Dowelled Joint of High Performance in Combination with a High Strength Wood Composite (Parallam) - E Gehri

30-7-5 Multiple Fastener Timber Connections with Dowel Type Fasteners - A Jorissen

30-7-6 Influence of Ductility on Load-Carrying Capacity of Joints with Dowel-Type Fasteners - A Mischler

31-7-1 Mechanical Properties of Dowel Type Joints under Reversed Cyclic Lateral Loading - M Yasumura

31-7-2 Design of Joints with Laterally Loaded Dowels - A Mischler

31-7-3 Flexural Behaviour of Glulam Beams Edge-Jointed by Lagscrews with Steel Splice Plates - K Komatsu

31-7-4 Design on Timber Capacity in Nailed Steel-to-Timber Joints - J Kangas and J Vesa

31-7-5 Timber Contact in Chord Splices of Nail Plate Structures - A Kevarinmäki

31-7-6 The Fastener Yield Strength in Bending - A Jorissen and H J Blaß

31-7-7 A Proposal for Simplification of Johansen`s Formulae, Dealing With the Design of Dowelled-Type Fasteners - F Rouger

31-7-8 Simplified Design of Connections with Dowel-type fasteners - H J Blaß and J Ehlbeck

32-7-1 Behaviour of Wood-Steel-Wood Bolted Glulam Connections - M Mohammad and J H P Quenneville

32-7-2 A new set of experimental tests on beams loaded perpendicular-to-grain by dowel-type joints- M Ballerini

32-7-3 Design and Analysis of Bolted Timber Joints under Lateral Force Perpendicular to Grain - M Yasumura and L Daudeville

32-7-4 Predicting Capacities of Joints with Laterally Loaded Nails - I Smith and P Quenneville

32-7-5 Strength Reduction Rules for Multiple Fastener Joints - A Mischler and E Gehri

32-7-6 The Stiffness of Multiple Bolted Connections - A Jorissen

32-7-7	Concentric Loading Tests on Girder Truss Components - T N Reynolds, A Reffold, V Enjily and L Whale
32-7-8	Dowel Type Connections with Slotted-In Steel Plates - M U Pedersen, C O Clorius, L Damkilde, P Hoffmeyer and L Esklidsen
32-7-9	Creep of Nail Plate Reinforced Bolt Joints - J Vesa and A Kevarinmäki
32-7-10	The Behaviour of Timber Joints with Ring Connectors - E Gehri and A Mischler
32-7-11	Non-Metallic, Adhesiveless Joints for Timber Structures - R D Drake, M P Ansell, C J Mettem and R Bainbridge
32-7-12	Effect of Spacing and Edge Distance on the Axial Strength of Glued-in Rods - H J Blaß and B Laskewitz
32-7-13	Evaluation of Material Combinations for Bonded in Rods to Achieve Improved Timber Connections - C J Mettem, R J Bainbridge, K Harvey, M P Ansell, J G Broughton and A R Hutchinson
33-7-1	Determination of Yield Strength and Ultimate Strength of Dowel-Type Timber Joints – M Yasumura and K Sawata
33-7-2	Lateral Shear Capacity of Nailed Joints – U Korin
33-7-3	Height-Adjustable Connector for Composite Beams – Y V Piskunov and E G Stern
33-7-4	Engineering Ductility Assessment for a Nailed Slotted-In Steel Connection in Glulam– L Stehn and H Johansson
33-7-5	Effective Bending Capacity of Dowel-Type Fasteners - H J Blaß, A Bienhaus and V Krämer
33-7-6	Load-Carrying Capacity of Joints with Dowel-Type Fasteners and Interlayers - H J Blaß and B Laskewitz
33-7-7	Evaluation of Perpendicular to Grain Failure of Beams caused by Concentrated Loads of Joints – T A C M van der Put and A J M Leijten
33-7-8	Test Methods for Glued-In Rods for Timber Structures – C Bengtsson and C J Johansson
33-7-9	Stiffness Analysis of Nail Plates – P Ellegaard
33-7-10	Capacity, Fire Resistance and Gluing Pattern of the Rods in V-Connections – J Kangas
33-7-11	Bonded-In Pultrusions for Moment-Resisting Timber Connections – K Harvey, M P Ansell, C J Mettem, R J Bainbridge and N Alexandre
33-7-12	Fatigue Performance of Bonded-In Rods in Glulam, Using Three Adhesive Types - R J Bainbridge, K Harvey, C J Mettem and M P Ansell
34-7-1	Splitting Strength of Beams Loaded by Connections Perpendicular to Grain, Model Validation – A J M Leijten, A Jorissen
34-7-2	Numerical LEFM analyses for the evaluation of failure loads of beams loaded perpendicular-to-grain by single-dowel connections – M Ballerini, R Bezzi
34-7-3	Dowel joints loaded perpendicular to grain - H J Larsen, P J Gustafsson
34-7-4	Quality Control of Connections based on in V-shape glued-in Steel Rods – J Kangas, A Kevarinmäki
34-7-5	Testing Connector Types for Laminated-Timber-Concrete Composite Elements – M Grosse, S Lehmann, K Rautenstrauch
34-7-6	Behaviour of Axially Loaded Glued-in Rods - Requirements and Resistance, Especially for Spruce Timber Perpendicular to the Grain Direction – A Bernasconi
34-7-7	Embedding characteristics on fibre reinforcement and densified timber joints - P Haller, J Wehsener, T Birk

34-7-8	GIROD – Glued-in Rods for Timber Structures – C Bengtsson, C-J Johansson
34-7-9	Criteria for Damage and Failure of Dowel-Type Joints Subjected to Force Perpendicular to the Grain – M Yasumura
34-7-10	Interaction Between Splitting and Block Shear Failure of Joints – A J M Leijten, A Jorissen, J Kuipers
34-7-11	Limit states design of dowel-fastener joints – Placement of modification factors and partial factors, and calculation of variability in resistance – I Smith, G Foliente
34-7-12	Design and Modelling of Knee Joints - J Nielsen, P Ellegaard
34-7-13	Timber-Steel Shot Fired Nail Connections at Ultimate Limit States - R J Bainbridge, P Larsen, C J Mettem, P Alam, M P Ansell
35-7-1	New Estimating Method of Bolted Cross-lapped Joints with Timber Side Members - M Noguchi, K Komatsu
35-7-2	Analysis on Multiple Lag Screwed Timber Joints with Timber Side Members - K Komatsu, S Takino, M Nakatani, H Tateishi
35-7-3	Joints with Inclined Screws - A Kevarinmäki
35-7-4	Joints with Inclined Screws - I Bejtka, H J Blaß
35-7-5	Effect of distances, Spacing and Number of Dowels in a Row an the Load Carrying Capacity of Connections with Dowels failing by Splitting - M Schmid, R Frasson, H J Blaß
35-7 6	Effect of Row Spacing on the Capacity of Bolted Timber Connections Loaded Perpendicular-to-grain - P Quenneville, M Kasim
35-7-7	Splitting Strength of Beams Loaded by Connections, Model Comparison - A J M Leijten
35-7-8	Load-Carrying Capacity of Perpendicular to the Grain Loaded Timber Joints with Multiple Fasteners - O Borth, K U Schober, K Rautenstrauch
35-7-9	Determination of fracture parameter for dowel-type joints loaded perpendicular to wooden grain and its application - M Yasumura
35-7-10	Analysis and Design of Modified Attic Trusses with Punched Metal Plate Fasteners - P Ellegaard
35-7-11	Joint Properties of Plybamboo Sheets in Prefabricated Housing - G E Gonzalez
35-7-12	Fiber-Reinforced Beam-to-Column Connections for Seismic Applications - B Kasal, A Heiduschke, P Haller
36-7-1	Shear Tests in Timber-LWAC with Screw-Type Connections - L Jorge, H Cruz, S Lopes
36-7-2	Plug Shear Failure in Nailed Timber Connections: Experimental Studies - H Johnsson
36-7-3	Nail-Laminated Timber Elements in Natural Surface-Composite with Mineral Bound Layer - S Lehmann, K Rautenstrauch
36-7-4	Mechanical Properties of Timber-Concrete Joints Made With Steel Dowels - A Dias, J W G van de Kuilen, H Cruz
36-7-5	Comparison of Hysteresis Responses of Different Sheating to Framing Joints - B Dujič, R Zarnić
36-7- 6	Evaluation and Estimation of the Performance of the Nail Joints and Shear Walls under Dry/Humid Cyclic Climate - S Nakajima
36-7-7	Beams Transversally Loaded by Dowel-Type Joints: Influence on Splitting Strength of Beam Thickness and Dowel Size - M Ballerini, A Giovanella
36-7-8	Splitting Strength of Beams Loaded by Connections - J L Jensen

36-7-9 A Tensile Fracture Model for Joints with Rods or Dowels loaded Perpendicular-to-Grain - J L Jensen, P J Gustafsson, H J Larsen

36-7-10 A Numerical Model to Simulate the Load-Displacement Time-History of Mutiple-Bolt Connections Subjected to Various Loadings - C P Heine, J D Dolan

36-7-11 Reliability of Timber Structures, Theory and Dowel-Type Connection Failures - A Ranta-Maunus, A Kevarinmäki

37-7-1 Development of the "Displaced Volume Model" to Predict Failure for Multiple-Bolt Timber Joints - D M Carradine, J D Dolan, C P Heine

37-7-2 Mechanical Models of the Knee Joints with Cross-Lapped Glued Joints and Glued in Steel Rods - M Noguchi, K Komatsu

37-7-3 Simplification of the Neural Network Model for Predicting the Load-Carrying Capacity of Dowel-Type Connections - A Cointe, F Rouger

37-7-4 Bolted Wood Connections Loaded Perpendicular-to-Grain- A Proposed Design Approach - M C G Lehoux, J H P Quenneville

37-7-5 A New Prediction Formula for the Splitting Strength of Beams Loaded by Dowel Type Connections - M Ballerini

37-7-6 Plug Shear Failure: The Tensile Failure Mode and the Effect of Spacing - H Johnsson

37-7-7 Block Shear Failure Test with Dowel-Type Connection in Diagonal LVL Structure - M Kairi

37-7-8 Glued-in Steel Rods: A Design Approach for Axially Loaded Single Rods Set Parallel to the Grain - R Steiger, E Gehri, R Widmann

37-7-9 Glued in Rods in Load Bearing Timber Structures - Status regarding European Standards for Test Procedures - B Källander

37-7-10 French Data Concerning Glued-in Rods - C Faye, L Le Magorou, P Morlier, J Surleau

37-7-11 Enhancement of Dowel-Type Fasteners by Glued Connectors - C O Clorius, A Højman

37-7-12 Review of Probability Data for Timber Connections with Dowel-Type Fasteners - A J M Leijten, J Köhler, A Jorissen

37-7-13 Behaviour of Fasteners and Glued-in Rods Produced From Stainless Steel - A Kevarinmäki

37-7-14 Dowel joints in Engineered Wood Products: Assessment of Simple Fracture Mechanics Models - M Snow, I Smith, A Asiz

37-7-15 Numerical Modelling of Timber and Connection Elements Used in Timber-Concrete-Composite Constructions - M Grosse, K Rautenstrauch

38-7-1 A Numerical Investigation on the Splitting Strength of Beams Loaded Perpendicular-to-grain by Multiple-dowel Connections – M Ballerini, M Rizzi

38-7-2 A Probabilistic Framework for the Reliability Assessment of Connections with Dowel Type Fasteners - J Köhler

38-7-3 Load Carrying Capacity of Curved Glulam Beams Reinforced with self-tapping Screws - J Jönsson, S Thelandersson

38-7-4 Self-tapping Screws as Reinforcements in Connections with Dowel-Type Fasteners- I Bejtka, H J Blaß

38-7-5 The Yield Capacity of Dowel Type Fasteners - A Jorissen, A Leijten

38-7-6 Nails in Spruce - Splitting Sensitivity, End Grain Joints and Withdrawal Strength - A Kevarinmäki

38-7-7 Design of Timber Connections with Slotted-in Steel Plates and Small Diameter Steel Tube Fasteners - B Murty, I Smith, A Asiz

39-7-1 Effective in-row Capacity of Multiple-Fastener Connections - P Quenneville, M Bickerdike

39-7-2 Self-tapping Screws as Reinforcements in Beam Supports - I Bejtka, H J Blaß

39-7-3 Connectors for Timber-concrete Composite-Bridges - A Döhrer, K Rautenstrauch

39-7-4 Block Shear Failure at Dowelled Double Shear Steel-to-timber Connections - A Hanhijärvi, A Kevarinmäki, R Yli-Koski

39-7-5 Load Carrying Capacity of Joints with Dowel Type Fasteners in Solid Wood Panels - T Uibel, H J Blaß

39-7-6 Generalised Canadian Approach for Design of Connections with Dowel Fasteners - P Quenneville, I Smith, A Asiz, M Snow, Y H Chui

40-7-1 Predicting the Strength of Bolted Timber Connections Subjected to Fire - M Fragiacomo, A Buchanan, D Carshalton, P Moss, C Austruy

40-7-2 Edge Joints with Dowel Type Fasteners in Cross Laminated Timber - H J Blaß, T Uibel

40-7-3 Design Method against Timber Failure Mechanisms of Dowelled Steel-to-Timber Connections - A Hanhijärvi, A Kevarinmäki

40-7-4 A EYM Based Simplified Design Formula for the Load-carrying Capacity of Dowel-type Connections - M Ballerini

40-7-5 Evaluation of the Slip Modulus for Ultimate Limit State Verifications of Timber-Concrete Composite Structures - E Lukaszewska, M Fragiacomo, A Frangi

40-7-6 Models for the Predictions of the Ductile and Brittle Failure Modes (Parallel-to-Grain) of Timber Rivet Connections - M Marjerrison, P Quenneville

40-7-7 Creep of Timber and Timber-Concrete Joints. - J W G van de Kuilen, A M P G Dias

40-7-8 Lag Screwed Timber Joints with Timber Side Members- K Komatsu, S Takino, H Tateishi

41-7-1 Applicability of Existing Design Approaches to Mechanical Joints in Structural Composite Lumber - M Snow, I Smith, A Asiz, M Ballerini

41-7-2 Validation of the Canadian Bolted Connection Design Proposal - P Quenneville, J Jensen

41-7-3 Ductility of Moment Resisting Dowelled Joints in Heavy Timber Structures - A Polastri, R Tomasi, M Piazza, I Smith

41-7-4 Mechanical Behaviour of Traditional Timber Connections: Proposals for Design, Based on Experimental and Numerical Investigations. Part I: Birdsmouth - C Faye, P Garcia, L Le Magorou, F Rouger

41-7-5 Embedding Strength of European Hardwoods - U Hübner, T Bogensperger, G Schickhofer

42-7-1 Base Parameters of Self-tapping Screws - G Pirnbacher, R Brandner, G Schickhofer

42-7-2 Joints with Inclined Screws and Steel Plates as Outer Members - H Krenn, G Schickhofer

42-7-3 Models for the Calculation of the Withdrawal Capacity of Self-tapping Screws - M Frese, H J Blaß

42-7-4 Embedding Strength of New Zealand Timber and Recommendation for the NZ Standard - S Franke, P Quenneville

42-7-5 Load Carrying Capacity of Timber-Wood Fiber Insulation Board – Joints with Dowel Type Fasteners - G Gebhardt, H J Blaß

42-7-6 Prediction of the Fatigue Resistance of Timber-Concrete-Composite Connections - U Kuhlmann, P Aldi

42-7-7 Using Screws for Structural Applications in Laminated Veneer Lumber - D M Carradine, M P Newcombe, A H Buchanan

42-7-8 Influence of Fastener Spacings on Joint Performance - Experimental Results and Codification - E Gehri

42-7-9 Connections with Glued-in Hardwood Rods Subjected to Combined Bending and Shear Actions - J L Jensen, P Quenneville

43-7-1 Probabilistic Capacity Prediction of Timber Joints under Brittle Failure Modes - T Tannert, T Vallée, and F Lam

43-7-2 Ductility in Timber Structures - A Jorissen, M Fragiacomo

43-7-3 Design of Mechanically Jointed Concrete-Timber Beams Taking into Account the Plastic Behaviour of the Fasteners - H J Larsen, H Riberholt, A Ceccotti

43-7-4 Design of Timber-Concrete Composite Beams with Notched Connections - M Fragiacomo, D Yeoh

43-7-5 Development of Design Procedures for Timber Concrete Composite Floors in Australia and New Zealand - K Crews, C Gerber

43-7-6 Failure Behaviour and Resistance of Dowel-Type Connections Loaded Perpendicular to Grain - B Franke, P Quenneville

43-7-7 Predicting Time Dependent Effects in Unbonded Post-Tensioned Timber Beams and Frames - S Giorgini, A Neale, A Palermo, D Carradine, S Pampanin, A H Buchanan

43-7-8 Simplified Design of Post-tensioned Timber Frames - M Newcombe, M Cusiel, S Pampanin, A Palermo, A H Buchanan

44-7-1 Pull-through Capacity in Plywood and OSB - J Munch-Andersen, J D Sørensen

44-7-2 Design Concept for CLT - Reinforced with Self-Tapping Screws - P Mestek, H Kreuzinger, S Winter

44-7-3 Fatigue Behaviour of the Stud Connector Used for Timber-Concrete Composite Bridges – K Rautenstrauch, J Mueller

44-7-4 The Stiffness of Beam to Column Connections in Post-Tensioned Timber Frames – T Smith, W van Beerschoten, A Palermo, S Pampanin, F C Ponzo

44-7-5 Design Approach for the Splitting Failure of Dowel-Type Connections Loaded Perpendicular to Grain - Bettina Franke, Pierre Quenneville

46-7-1 Comparison of Design Rules for Glued-in rods and Design Rule Proposal for Implementation in European Standards - M Stepinac, F Hunger, R Tomasi, E Serrano, V Rajcic, J-W van de Kuilen

46-7-2 In-service Dynamic Stiffness of Dowel-type Connections - T Reynolds, R Harris Wen-Shao Chang

46-7-3 Design Procedure to Determine the Capacity of Timber Connections under Potential Brittle, Mixed and Ductile Failure Modes - P Zarnani, P Quenneville

46-7-4 Withdrawal Strength of Self-tapping Screws in Hardwoods - Ulrich Hübner

46-7-5 Wood Splitting Capacity in Timber Connections Loaded Transversely: Riveted Joint Strength for Full and Partial Width Failure Modes - P Zarnani, P Quenneville

46-7-6 Design Approach for the Splitting Failure of Dowel-type Connections Loaded Perpendicular to Grain- B Franke, P Quenneville

46-7-7 Beams Loaded Perpendicular to Grain by Connections - J C M Schoenmakers, A J M Leijten, A J M Jorissen

46-7-8 Influence of Fasteners in the Compression Area of Timber Members - M Enders-Comberg, H J Blaß

46-7-9 Design of Shear Reinforcement for Timber Beams - P Dietsch, H Kreuzinger, S Winter

47-7-1 Discussion of testing and Evaluation Methods for the Embedment Behaviour of Connections - S Franke, N Magnière

47-7-2 Dowel-type Connections in LVL Made of Beech Wood - P Kobel, A Frangi, R Steiger

47-7-3 Resistance of Connections in Cross-Laminated Timber under Brittle Block Tear-Out Failure Mode - P Zarnani, P Quenneville

47-7-4 Study on Nail Connections in Deformed State - S Svensson, J Munch-Andersen

47-7-5 Design Model for Inclined Screws under Varying Load to Grain Angles - R Jockwer, R Steiger, A Frangi

LOAD SHARING

3-8-1 Load Sharing - An Investigation on the State of Research and Development of Design Criteria - E Levin

4-8-1 A Review of Load-Sharing in Theory and Practice - E Levin

4-8-2 Load Sharing - B Norén

19-8-1 Predicting the Natural Frequencies of Light-Weight Wooden Floors - I Smith and Y H Chui

20-8-1 Proposed Code Requirements for Vibrational Serviceability of Timber Floors - Y H Chui and I Smith

21-8-1 An Addendum to Paper 20-8-1 - Proposed Code Requirements for Vibrational Serviceability of Timber Floors - Y H Chui and I Smith

21-8-2 Floor Vibrational Serviceability and the CIB Model Code - S Ohlsson

22-8-1 Reliability Analysis of Viscoelastic Floors - F Rouger, J D Barrett and R O Foschi

24-8-1 On the Possibility of Applying Neutral Vibrational Serviceability Criteria to Joisted Wood Floors - I Smith and Y H Chui

25-8-1 Analysis of Glulam Semi-rigid Portal Frames under Long-term Load - K Komatsu and N Kawamoto

34-8-1 System Effect in Sheathed Parallel Timber Beam Structures – M Hansson, T Isaksson

35-8-1 System Effects in Sheathed Parallel Timber Beam Structures part II. - M Hansson, T Isaksson

39-8-1 Overview of a new Canadian Approach to Handling System Effects in Timber Structures - I Smith, Y H Chui, P Quenneville

DURATION OF LOAD

3-9-1 Definitions of Long Term Loading for the Code of Practice - B Norén

4-9-1 Long Term Loading of Trussed Rafters with Different Connection Systems - T Feldborg and M Johansen

5-9-1 Strength of a Wood Column in Combined Compression and Bending with Respect to Creep - B Källsner and B Norén

6-9-1 Long Term Loading for the Code of Practice (Part 2) - B Norén

6-9-2 Long Term Loading - K Möhler

6-9-3 Deflection of Trussed Rafters under Alternating Loading during a Year - T Feldborg and M Johansen

7-6-1 Strength and Long Term Behaviour of Lumber and Glued-Laminated Timber under Torsion Loads - K Möhler

7-9-1 Code Rules Concerning Strength and Loading Time - H J Larsen and E Theilgaard

17-9-1 On the Long-Term Carrying Capacity of Wood Structures - Y M Ivanov and Y Y Slavic

18-9-1 Prediction of Creep Deformations of Joints - J Kuipers

19-9-1 Another Look at Three Duration of Load Models - R O Foschi and Z C Yao

19-9-2 Duration of Load Effects for Spruce Timber with Special Reference to Moisture Influence - A Status Report - P Hoffmeyer

19-9-3 A Model of Deformation and Damage Processes Based on the Reaction Kinetics of Bond Exchange - T A C M van der Put

19-9-4 Non-Linear Creep Superposition - U Korin

19-9-5 Determination of Creep Data for the Component Parts of Stressed-Skin Panels - R Kliger

19-9-6 Creep an Lifetime of Timber Loaded in Tension and Compression - P Glos

19-1-1 Duration of Load Effects and Reliability Based Design (Single Member) - R O Foschi and Z C Yao

19-6-1 Effect of Age and/or Load on Timber Strength - J Kuipers

19-7-4 The Prediction of the Long-Term Load Carrying Capacity of Joints in Wood Structures - Y M Ivanov and Y Y Slavic

19-7-5 Slip in Joints under Long-Term Loading - T Feldborg and M Johansen

20-7-2 Slip in Joints under Long-Term Loading - T Feldborg and M Johansen

22-9-1 Long-Term Tests with Glued Laminated Timber Girders - M Badstube, W Rug and W Schöne

22-9-2 Strength of One-Layer solid and Lengthways Glued Elements of Wood Structures and its Alteration from Sustained Load - L M Kovaltchuk, I N Boitemirova and G B Uspenskaya

24-9-1 Long Term Bending Creep of Wood - T Toratti

24-9-2 Collection of Creep Data of Timber - A Ranta-Maunus

24-9-3 Deformation Modification Factors for Calculating Built-up Wood-Based Structures - I R Kliger

25-9-2 DVM Analysis of Wood. Lifetime, Residual Strength and Quality - L F Nielsen

26-9-1 Long Term Deformations in Wood Based Panels under Natural Climate Conditions. A Comparative Study - S Thelandersson, J Nordh, T Nordh and S Sandahl

28-9-1 Evaluation of Creep Behavior of Structural Lumber in Natural Environment - R Gupta and R Shen

30-9-1 DOL Effect in Tension Perpendicular to the Grain of Glulam Depending on Service Classes and Volume - S Aicher and G Dill-Langer

30-9-2 Damage Modelling of Glulam in Tension Perpendicular to Grain in Variable Climate - G Dill-Langer and S Aicher

31-9-1 Duration of Load Effect in Tension Perpendicular to Grain in Curved Glulam - A Ranta-Maunus

32-9-1 Bending-Stress-Redistribution Caused by Different Creep in Tension and Compression and Resulting DOL-Effect - P Becker and K Rautenstrauch

32-9-2 The Long Term Performance of Ply-Web Beams - R Grantham and V Enjily

36-9-1 Load Duration Factors for Instantaneous Loads - A J M Leijten, B Jansson

39-9-1 Simplified Approach for the Long-Term Behaviour of Timber-Concrete Composite Beams According to the Eurocode 5 Provisions - M Fragiacomo, A Ceccotti

TIMBER BEAMS

4-10-1 The Design of Simple Beams - H J Burgess

4-10-2 Calculation of Timber Beams Subjected to Bending and Normal Force - H J Larsen

5-10-1 The Design of Timber Beams - H J Larsen

9-10-1 The Distribution of Shear Stresses in Timber Beams - F J Keenan

9-10-2 Beams Notched at the Ends - K Möhler

11-10-1 Tapered Timber Beams - H Riberholt

13-6-2 Consideration of Size Effects in Longitudinal Shear Strength for Uncracked Beams - R O Foschi and J D Barrett

13-6-3 Consideration of Shear Strength on End-Cracked Beams - J D Barrett and R O Foschi

18-10-1 Submission to the CIB-W18 Committee on the Design of Ply Web Beams by Consideration of the Type of Stress in the Flanges - J A Baird

18-10-2 Longitudinal Shear Design of Glued Laminated Beams - R O Foschi

19-10-1 Possible Code Approaches to Lateral Buckling in Beams - H J Burgess

19-2-1 Creep Buckling Strength of Timber Beams and Columns - R H Leicester

20-2-1 Lateral Buckling Theory for Rectangular Section Deep Beam-Columns - H J Burgess

20-10-1 Draft Clause for CIB Code for Beams with Initial Imperfections - H J Burgess

20-10-2 Space Joists in Irish Timber - W J Robinson

20-10-3 Composite Structure of Timber Joists and Concrete Slab - T Poutanen

21-10-1 A Study of Strength of Notched Beams - P J Gustafsson

22-10-1 Design of Endnotched Beams - H J Larsen and P J Gustafsson

22-10-2 Dimensions of Wooden Flexural Members under Constant Loads - A Pozgai

22-10-3 Thin-Walled Wood-Based Flanges in Composite Beams - J König

22-10-4 The Calculation of Wooden Bars with flexible Joints in Accordance with the Polish Standart Code and Strict Theoretical Methods - Z Mielczarek

23-10-1 Tension Perpendicular to the Grain at Notches and Joints - T A C M van der Put

23-10-2 Dimensioning of Beams with Cracks, Notches and Holes. An Application of Fracture Mechanics - K Riipola

23-10-3 Size Factors for the Bending and Tension Strength of Structural Timber - J D Barret and A R Fewell

23-12-1 Bending Strength of Glulam Beams, a Design Proposal - J Ehlbeck and F Colling

23-12-3 Glulam Beams, Bending Strength in Relation to the Bending Strength of the Finger Joints - H Riberholt

24-10-1 Shear Strength of Continuous Beams - R H Leicester and F G Young

25-10-1 The Strength of Norwegian Glued Laminated Beams - K Solli, E Aasheim and R H Falk

25-10-2 The Influence of the Elastic Modulus on the Simulated Bending Strength of Hyperstatic Timber Beams - T D G Canisius

27-10-1 Determination of Shear Modulus - R Görlacher and J Kürth

29-10-1 Time Dependent Lateral Buckling of Timber Beams - F Rouger

29-10-2 Determination of Modulus of Elasticity in Bending According to EN 408 - K H Solli

29-10-3 On Determination of Modulus of Elasticity in Bending - L Boström, S Ormarsson and O Dahlblom

29-10-4 Relation of Moduli of Elasticity in Flatwise and Edgewise Bending of Solid Timber - C J Johansson, A Steffen and E W Wormuth

30-10-1 Nondestructive Evaluation of Wood-based Members and Structures with the Help of Modal Analysis - P Kuklik

30-10-2 Measurement of Modulus of Elasticity in Bending - L Boström

30-10-3 A Weak Zone Model for Timber in Bending - B Källsner, K Salmela and O Ditlevsen

30-10-4 Load Carrying Capacity of Timber Beams with Narrow Moment Peaks - T Isaksson and J Freysoldt

37-10-1 Design of Rim Boards for Use with I-Joists Framing Systems - B Yeh, T G Williamson

40-10- 1 Extension of EC5 Annex B Formulas for the Design of Timber-concrete Composite Structures - J Schänzlin, M Fragiacomo

40-10-2 Simplified Design Method for Mechanically Jointed Beams - U A Girhammar

41-10-1 Composite Action of I-Joist Floor Systems - T G Williamson, B Yeh

41-10-2 Evaluation of the Prestressing Losses in Timber Members Prestressed with Unbonded Tendons - M Fragiacomo, M Davies

41-10-3 Relationship Between Global and Local MOE – J K Denzler, P Stapel, P Glos

42-10-1 Relationships Between Local, Global and Dynamic Modulus of Elasticity for Soft- and Hardwoods – G J P Ravenshorst, J W G van de Kuilen

ENVIRONMENTAL CONDITIONS

5-11-1 Climate Grading for the Code of Practice - B Norén

6-11-1 Climate Grading (2) - B Norén

9-11-1 Climate Classes for Timber Design - F J Keenan

19-11-1 Experimental Analysis on Ancient Downgraded Timber Structures - B Leggeri and L Paolini

19-6-5 Drying Stresses in Round Timber - A Ranta-Maunus

22-11-1 Corrosion and Adaptation Factors for Chemically Aggressive Media with Timber Structures - K Erler

29-11-1 Load Duration Effect on Structural Beams under Varying Climate Influence of Size and Shape - P Galimard and P Morlier

30-11-1 Probabilistic Design Models for the Durability of Timber Constructions - R H Leicester

36-11-1 Structural Durability of Timber in Ground Contact – R H Leicester, C H Wang, M N Nguyen, G C Foliente, C McKenzie

38-11-1 Design Specifications for the Durability of Timber – R H Leicester, C-H Wang, M Nguyen, G C Foliente

38-11-2 Consideration of Moisture Exposure of Timber Structures as an Action - M Häglund, S Thelandersson

LAMINATED MEMBERS

6-12-1 Directives for the Fabrication of Load-Bearing Structures of Glued Timber - A van der Velden and J Kuipers

8-12-1 Testing of Big Glulam Timber Beams - H Kolb and P Frech

8-12-2 Instruction for the Reinforcement of Apertures in Glulam Beams - H Kolb and P Frech

8-12-3 Glulam Standard Part 1: Glued Timber Structures; Requirements for Timber (Second Draft)

9-12-1 Experiments to Provide for Elevated Forces at the Supports of Wooden Beams with Particular Regard to Shearing Stresses and Long-Term Loadings - F Wassipaul and R Lackner

9-12-2 Two Laminated Timber Arch Railway Bridges Built in Perth in 1849 - L G Booth

9-6-4 Consideration of Combined Stresses for Lumber and Glued Laminated Timber - K Möhler

11-6-3 Consideration of Combined Stresses for Lumber and Glued Laminated Timber (addition to Paper CIB-W18/9-6-4) - K Möhler

12-12-1 Glulam Standard Part 2: Glued Timber Structures; Rating (3rd draft)

12-12-2 Glulam Standard Part 3: Glued Timber Structures; Performance (3 rd draft)

13-12-1 Glulam Standard Part 3: Glued Timber Structures; Performance (4th draft)

14-12-1 Proposals for CEI-Bois/CIB-W18 Glulam Standards - H J Larsen

14-12-2 Guidelines for the Manufacturing of Glued Load-Bearing Timber Structures - Stevin Laboratory

14-12-3 Double Tapered Curved Glulam Beams - H Riberholt

14-12-4 Comment on CIB-W18/14-12-3 - E Gehri

18-12-1 Report on European Glulam Control and Production Standard - H Riberholt

18-10-2 Longitudinal Shear Design of Glued Laminated Beams - R O Foschi

19-12-1 Strength of Glued Laminated Timber - J Ehlbeck and F Colling

19-12-2 Strength Model for Glulam Columns - H J Blaß

19-12-3 Influence of Volume and Stress Distribution on the Shear Strength and Tensile Strength Perpendicular to Grain - F Colling

19-12-4 Time-Dependent Behaviour of Glued-Laminated Beams - F Zaupa

21-12-1 Modulus of Rupture of Glulam Beam Composed of Arbitrary Laminae - K Komatsu and N Kawamoto

21-12-2 An Appraisal of the Young's Modulus Values Specified for Glulam in Eurocode 5- L R J Whale, B O Hilson and P D Rodd

21-12-3 The Strength of Glued Laminated Timber (Glulam): Influence of Lamination Qualities and Strength of Finger Joints - J Ehlbeck and F Colling

21-12-4 Comparison of a Shear Strength Design Method in Eurocode 5 and a More Traditional One - H Riberholt

22-12-1 The Dependence of the Bending Strength on the Glued Laminated Timber Girder Depth - M Badstube, W Rug and W Schöne

22-12-2 Acid Deterioration of Glulam Beams in Buildings from the Early Half of the 1960s - Prelimination summary of the research project; Overhead pictures - B A Hedlund

22-12-3 Experimental Investigation of normal Stress Distribution in Glue Laminated Wooden Arches - Z Mielczarek and W Chanaj

22-12-4 Ultimate Strength of Wooden Beams with Tension Reinforcement as a Function of Random Material Properties - R Candowicz and T Dziuba

23-12-1 Bending Strength of Glulam Beams, a Design Proposal - J Ehlbeck and F Colling

23-12-2 Probability Based Design Method for Glued Laminated Timber - M F Stone

23-12-3 Glulam Beams, Bending Strength in Relation to the Bending Strength of the Finger Joints - H Riberholt

23-12-4 Glued Laminated Timber - Strength Classes and Determination of Characteristic Properties - H Riberholt, J Ehlbeck and A Fewell

24-12-1 Contribution to the Determination of the Bending Strength of Glulam Beams - F Colling, J Ehlbeck and R Görlacher

24-12-2 Influence of Perpendicular-to-Grain Stressed Volume on the Load-Carrying Capacity of Curved and Tapered Glulam Beams - J Ehlbeck and J Kürth

25-12-1 Determination of Characteristic Bending Values of Glued Laminated Timber. EN-Approach and Reality - E Gehri

26-12-1 Norwegian Bending Tests with Glued Laminated Beams-Comparative Calculations with the "Karlsruhe Calculation Model" - E Aasheim, K Solli, F Colling, R H Falk, J Ehlbeck and R Görlacher

26-12-2 Simulation Analysis of Norwegian Spruce Glued-Laminated Timber - R Hernandez and R H Falk

26-12-3 Investigation of Laminating Effects in Glued-Laminated Timber - F Colling and R H Falk

26-12-4 Comparing Design Results for Glulam Beams According to Eurocode 5 and to the French Working Stress Design Code (CB71) - F Rouger

27-12-1 State of the Art Report: Glulam Timber Bridge Design in the U.S. - M A Ritter and T G Williamson

27-12-2 Common Design Practice for Timber Bridges in the United Kingdom - C J Mettem, J P Marcroft and G Davis

27-12-3 Influence of Weak Zones on Stress Distribution in Glulam Beams - E Serrano and H J Larsen

28-12-1 Determination of Characteristic Bending Strength of Glued Laminated Timber - E Gehri

28-12-2 Size Factor of Norwegian Glued Laminated Beams - E Aasheim and K H Solli

28-12-3 Design of Glulam Beams with Holes - K Riipola

28-12-4 Compression Resistance of Glued Laminated Timber Short Columns- U Korin

29-12-1 Development of Efficient Glued Laminated Timber - G Schickhofer

30-12-1 Experimental Investigation and Analysis of Reinforced Glulam Beams - K Oiger

31-12-1 Depth Factor for Glued Laminated Timber-Discussion of the Eurocode 5 Approach - B Källsner, O Carling and C J Johansson

32-12-1 The bending stiffness of nail-laminated timber elements in transverse direction- T Wolf and O Schäfer

33-12-1 Internal Stresses in the Cross-Grain Direction of Wood Induced by Climate Variation – J Jönsson and S Svensson

34-12-1 High-Strength I-Joist Compatible Glulam Manufactured with LVL Tension Laminations – B Yeh, T G Williamson

34-12-2 Evaluation of Glulam Shear Strength Using A Full-Size Four-Point Test Method – B Yeh, T G Williamson

34-12-3 Design Model for FRP Reinforced Glulam Beams – M Romani, H J Blaß

34-12-4 Moisture induced stresses in glulam cross sections – J Jönsson

34-12-5 Load Carrying Capacity of Nail-Laminated Timber under Concentrated Loads – V Krämer, H J Blaß

34-12-6 Determination of Shear Strength Values for GLT Using Visual and Machine Graded Spruce Laminations – G Schickhofer

34-12-7 Mechanically Jointed Beams: Possibilities of Analysis and some special Problems – H Kreuzinger

35-12-1 Glulam Beams with Round Holes – a Comparison of Different Design Approaches vs. Test Data - S Aicher L Höfflin

36-12-1 Problems with Shear and Bearing Strength of LVL in Highly Loaded Structures - H Bier

36-12-2 Weibull Based Design of Round Holes in Glulam - L Höfflin, S Aicher

37-12-1 Development of Structural LVL from Tropical Wood and Evaluation of Their Performance for the Structural Components of Wooden Houses. Part-1. Application of Tropical LVL to a Roof Truss - K Komatsu, Y Idris, S Yuwasdiki, B Subiyakto, A Firmanti

37-12-2 Reinforcement of LVL Beams With Bonded-in Plates and Rods - Effect of Placement of Steel and FRP Reinforcements on Beam Strength and Stiffness - P Alam, M P Ansell, D Smedley

39-12-1 Recommended Procedures for Determination of Distribution Widths in the Design of Stress Laminated Timber Plate Decks - K Crews

39-12-2 In-situ Strengthening of Timber Structures with CFRP - K U Schober, S Franke, K Rautenstrauch

39-12-3 Effect of Checking and Non-Glued Edge Joints on the Shear Strength of Structural Glued Laminated Timber Beams - B Yeh, T G Williamson, Z A Martin

39-12-4 A Contribution to the Design and System Effect of Cross Laminated Timber (CLT) - R Jöbstl, T Moosbrugger, T Bogensperger, G Schickhofer

39-12-5 Behaviour of Glulam in Compression Perpendicular to Grain in Different Strength Grades and Load Configurations - M Augustin, A Ruli, R Brandner, G Schickhofer

40-12-1 Development of New Constructions of Glulam Beams in Canada - F Lam, N Mohadevan

40-12-2 Determination of Modulus of Shear and Elasticity of Glued Laminated Timber and Related Examination - R Brandner, E Gehri, T Bogensperger, G Schickhofer

40-12-3 Comparative Examination of Creep of GTL and CLT-Slabs in Bending - R A Jöbstl, G Schickhofer,

40-12-4 Standard Practice for the Derivation of Design Properties of Structural Glued Laminated Timber in the United States - T G Williamson, B Yeh

40-12-5 Creep and Creep-Rupture Behaviour of Structural Composite Lumber Evaluated in Accordance with ASTM D 6815 - B Yeh, T G Williamson.

40-12-6 Bending Strength of Combined Beech-Spruce Glulam - M Frese, H J Blaß

40-12-7 Quality Control of Glulam: Shear Tests of Glue Lines - R Steiger, E Gehri

41-12-1 Paper withdrawn by the author

41-12-2 Bending Strength of Spruce Glulam: New Models for the Characteristic Bending Strength - M Frese, H J Blass,

41-12-3 In-Plane Shear Strength of Cross Laminated Timber - R A Joebstl, T Bogensperger, G Schickhofer

41-12-4 Strength of Glulam Beams with Holes - Tests of Quadratic Holes and Literature Test Results Compilation - H Danielsson, P J Gustafsson

42-12-1 Glulam Beams with Holes Reinforced by Steel Bars – S Aicher, L Höfflin

42-12-2 Analysis of X-lam Panel-to-Panel Connections under Monotonic and Cyclic Loading - C Sandhaas, L Boukes, J W G van de Kuilen, A Ceccotti

42-12-3 Laminating Lumber and End Joint Properties for FRP-Reinforced Glulam Beams - T G Williamson, B Yeh

43-12-4 Validity of Bending Tests on Strip-Shaped Specimens to Derive Bending Strength and Stiffness Properties of Cross-Laminated Solid Timber (CLT) - R Steiger, A Gülzow

42-12-5 Mechanical Properties of Stress Laminated Timber Decks - Experimental Study - K Karlsson, R Crocetti, R Kliger

43-12-1 Fatigue Behaviour of Finger Jointed Lumber - S Aicher, G Stapf

43-12-2 Experimental and Numercial Investigation on the Shear Strength of Glulam - R Crocetti, P J Gustafsson, H Danielsson, A Emilsson, S Ormarsson

43-12-3 System Effects in Glued Laminated Timber in Tension and Bending - M Frese, H J Blaß

43-12-4 Experimental Investigations on Mechanical Behaviour of Glued Solid timber - C Faye, F Rouger, P Garcia

44-12-1 Properties of CLT-Panels Exposed to Compression Perpendicular to their Plane- T Bogensperger, M Augustin, G Schickhofer

44-12-2 Strength of Spruce Glulam Subjected to Longitudinal Compression – M Frese, M Enders-Comberg, H J Blaß, P Glos

44-12-3 Glued Laminated Timber: A proposal for New Beam Layups - F Rouger, P Garcia

44-12-4 Glulam Beams with Internally and Externally Reinforced Holes – Test, Detailing and Design – S Aicher

44-12-5 Size Effect of Bending Strength in Glulam Beam - F Lam

46-12-1 Modelling the Bending Strength of Glued Laminated Timber - Considering the Natural Growth Characteristics of Timber - G Fink, A Frangi, J Kohler

46-12-2 In-Plane Shear Strength of Cross Laminated Timber (CLT): Test Configuration, Quantification and Influencing Parameters - R Brandner, T Bogensperger, G Schickhofer

46-12-3 Shear Strength and Shear Stiffness of CLT-beams Loaded in Plane - M Flaig, H J Blaß

46-12-4 Stiffness of Screw-Reinforced LVL in Compression Perpendicular to the Grain - C Watson, W van Beerschoten, T Smith, S Pampanin, A H Buchanan

47-12-1 Calculation of Cylindrical Shells from Wood or Wood Based Products and Consideration of the Stress Relaxation - P Aondio, S Winter, H Kreuzinger

47-12-2 Hybrid Glulam Beams Made of Beech LVL and Spruce Laminations - M Frese

47-12-3 Design for the Spreading under a Compressive Stress in Glued Laminated Timber - D Lathuilliere, L Bléron, J-F Bocquet, F Varacca, F Dubois

47-12-4 Design of CLT Beams with Rectangular Holes or Notches - M Flaig

47-12-5	Properties of Cross Laminated Timber (CLT) in Compression Perpendicular to Grain - R Brandner, G Schickhofer

PARTICLE AND FIBRE BUILDING BOARDS

7-13-1	Fibre Building Boards for CIB Timber Code (First Draft)- O Brynildsen
9-13-1	Determination of the Bearing Strength and the Load-Deformation Characteristics of Particleboard - K Möhler, T Budianto and J Ehlbeck
9-13-2	The Structural Use of Tempered Hardboard - W W L Chan
11-13-1	Tests on Laminated Beams from Hardboard under Short- and Longterm Load - W Nozynski
11-13-2	Determination of Deformation of Special Densified Hardboard under Long-term Load and Varying Temperature and Humidity Conditions - W Halfar
11-13-3	Determination of Deformation of Hardboard under Long-term Load in Changing Climate - W Halfar
14-4-1	An Introduction to Performance Standards for Wood-Base Panel Products - D H Brown
14-4-2	Proposal for Presenting Data on the Properties of Structural Panels - T Schmidt
16-13-1	Effect of Test Piece Size on Panel Bending Properties - P W Post
20-4-1	Considerations of Reliability - Based Design for Structural Composite Products - M R O'Halloran, J A Johnson, E G Elias and T P Cunningham
20-13-1	Classification Systems for Structural Wood-Based Sheet Materials - V C Kearley and A R Abbott
21-13-1	Design Values for Nailed Chipboard - Timber Joints - A R Abbott
25-13-1	Bending Strength and Stiffness of Izopanel Plates - Z Mielczarek
28-13-1	Background Information for "Design Rated Oriented Strand Board (OSB)" in CSA Standards - Summary of Short-term Test Results - E Karacabeyli, P Lau, C R Henderson, F V Meakes and W Deacon
28-13-2	Torsional Stiffness of Wood-Hardboard Composed I-Beam - P Olejniczak

TRUSSED RAFTERS

4-9-1	Long-term Loading of Trussed Rafters with Different Connection Systems - T Feldborg and M Johansen
6-9-3	Deflection of Trussed Rafters under Alternating Loading During a Year - T Feldborg and M Johansen
7-2-1	Lateral Bracing of Timber Struts - J A Simon
9-14-1	Timber Trusses - Code Related Problems - T F Williams
9-7-1	Design of Truss Plate Joints - F J Keenan
10-14-1	Design of Roof Bracing - The State of the Art in South Africa - P A V Bryant and J A Simon
11-14-1	Design of Metal Plate Connected Wood Trusses - A R Egerup
12-14-1	A Simple Design Method for Standard Trusses - A R Egerup
13-14-1	Truss Design Method for CIB Timber Code - A R Egerup
13-14-2	Trussed Rafters, Static Models - H Riberholt

13-14-3 Comparison of 3 Truss Models Designed by Different Assumptions for Slip and E-Modulus - K Möhler

14-14-1 Wood Trussed Rafter Design - T Feldborg and M Johansen

14-14-2 Truss-Plate Modelling in the Analysis of Trusses - R O Foschi

14-14-3 Cantilevered Timber Trusses - A R Egerup

14-7-5 The Effect of Support Eccentricity on the Design of W- and WW-Trusses with Nail Plate Connectors - B Källsner

15-14-1 Guidelines for Static Models of Trussed Rafters - H Riberholt

15-14-2 The Influence of Various Factors on the Accuracy of the Structural Analysis of Timber Roof Trusses - F R P Pienaar

15-14-3 Bracing Calculations for Trussed Rafter Roofs - H J Burgess

15-14-4 The Design of Continuous Members in Timber Trussed Rafters with Punched Metal Connector Plates - P O Reece

15-14-5 A Rafter Design Method Matching U.K. Test Results for Trussed Rafters - H J Burgess

16-14-1 Full-Scale Tests on Timber Fink Trusses Made from Irish Grown Sitka Spruce - V Picardo

17-14-1 Data from Full Scale Tests on Prefabricated Trussed Rafters - V Picardo

17-14-2 Simplified Static Analysis and Dimensioning of Trussed Rafters - H Riberholt

17-14-3 Simplified Calculation Method for W-Trusses - B Källsner

18-14-1 Simplified Calculation Method for W-Trusses (Part 2) - B Källsner

18-14-2 Model for Trussed Rafter Design - T Poutanen

19-14-1 Annex on Simplified Design of W-Trusses - H J Larsen

19-14-2 Simplified Static Analysis and Dimensioning of Trussed Rafters - Part 2 - H Riberholt

19-14-3 Joint Eccentricity in Trussed Rafters - T Poutanen

20-14-1 Some Notes about Testing Nail Plates Subjected to Moment Load - T Poutanen

20-14-2 Moment Distribution in Trussed Rafters - T Poutanen

20-14-3 Practical Design Methods for Trussed Rafters - A R Egerup

22-14-1 Guidelines for Design of Timber Trussed Rafters - H Riberholt

23-14-1 Analyses of Timber Trussed Rafters of the W-Type - H Riberholt

23-14-2 Proposal for Eurocode 5 Text on Timber Trussed Rafters - H Riberholt

24-14-1 Capacity of Support Areas Reinforced with Nail Plates in Trussed Rafters - A Kevarinmäki

25-14-1 Moment Anchorage Capacity of Nail Plates in Shear Tests - A Kevarinmaki and J. Kangas

25-14-2 Design Values of Anchorage Strength of Nail Plate Joints by 2-curve Method and Interpolation - J Kangas and A Kevarinmaki

26-14-1 Test of Nail Plates Subjected to Moment - E Aasheim

26-14-2 Moment Anchorage Capacity of Nail Plates - A Kevarinmäki and J Kangas

26-14-3 Rotational Stiffness of Nail Plates in Moment Anchorage - A Kevarinmäki and J Kangas

26-14-4 Solution of Plastic Moment Anchorage Stress in Nail Plates - A Kevarinmäki

26-14-5	Testing of Metal-Plate-Connected Wood-Truss Joints - R Gupta
26-14-6	Simulated Accidental Events on a Trussed Rafter Roofed Building - C J Mettem and J P Marcroft
30-14-1	The Stability Behaviour of Timber Trussed Rafter Roofs - Studies Based on Eurocode 5 and Full Scale Testing - R J Bainbridge, C J Mettern, A Reffold and T Studer
32-14-1	Analysis of Timber Reinforced with Punched Metal Plate Fasteners- J Nielsen
33-14-1	Moment Capacity of Timber Beams Loaded in Four-Point Bending and Reinforced with Punched Metal Plate Fasteners – J Nielsen
36-14-1	Effect of Chord Splice Joints on Force Distribution in Trusses with Punched Metal Plate Fasteners - P Ellegaard
36-14-2	Monte Carlo Simulation and Reliability Analysis of Roof Trusses with Punched Metal Plate Fasteners - M Hansson, P Ellegaard
36-14-3	Truss Trouble – R H Leicester, J Goldfinch, P Paevere, G C Foliente
40-14-1	Timber Trusses with Punched Metal Plate Fasteners - Design for Transport and Erection - H J Blaß

STRUCTURAL STABILITY

8-15-1	Laterally Loaded Timber Columns: Tests and Theory - H J Larsen
13-15-1	Timber and Wood-Based Products Structures. Panels for Roof Coverings. Methods of Testing and Strength Assessment Criteria. Polish Standard BN-78/7159-03
16-15-1	Determination of Bracing Structures for Compression Members and Beams - H Brüninghoff
17-15-1	Proposal for Chapter 7.4 Bracing - H Brüninghoff
17-15-2	Seismic Design of Small Wood Framed Houses - K F Hansen
18-15-1	Full-Scale Structures in Glued Laminated Timber, Dynamic Tests: Theoretical and Experimental Studies - A Ceccotti and A Vignoli
18-15-2	Stabilizing Bracings - H Brüninghoff
19-15-1	Connections Deformability in Timber Structures: a Theoretical Evaluation of its Influence on Seismic Effects - A Ceccotti and A Vignoli
19-15-2	The Bracing of Trussed Beams - M H Kessel and J Natterer
19-15-3	Racking Resistance of Wooden Frame Walls with Various Openings - M Yasumura
19-15-4	Some Experiences of Restoration of Timber Structures for Country Buildings - G Cardinale and P Spinelli
19-15-5	Non-Destructive Vibration Tests on Existing Wooden Dwellings - Y Hirashima
20-15-1	Behaviour Factor of Timber Structures in Seismic Zones. - A Ceccotti and A Vignoli
21-15-1	Rectangular Section Deep Beam - Columns with Continuous Lateral Restraint - H J Burgess
21-15-2	Buckling Modes and Permissible Axial Loads for Continuously Braced Columns- H J Burgess
21-15-3	Simple Approaches for Column Bracing Calculations - H J Burgess
21-15-4	Calculations for Discrete Column Restraints - H J Burgess

21-15-5 Behaviour Factor of Timber Structures in Seismic Zones (Part Two) - A Ceccotti and A Vignoli

22-15-1 Suggested Changes in Code Bracing Recommendations for Beams and Columns - H J Burgess

22-15-2 Research and Development of Timber Frame Structures for Agriculture in Poland- S Kus and J Kerste

22-15-3 Ensuring of Three-Dimensional Stiffness of Buildings with Wood Structures - A K Shenghelia

22-15-5 Seismic Behavior of Arched Frames in Timber Construction - M Yasumura

22-15-6 The Robustness of Timber Structures - C J Mettem and J P Marcroft

22-15-7 Influence of Geometrical and Structural Imperfections on the Limit Load of Wood Columns - P Dutko

23-15-1 Calculation of a Wind Girder Loaded also by Discretely Spaced Braces for Roof Members - H J Burgess

23-15-2 Stability Design and Code Rules for Straight Timber Beams - T A C M van der Put

23-15-3 A Brief Description of Formula of Beam-Columns in China Code - S Y Huang

23-15-4 Seismic Behavior of Braced Frames in Timber Construction - M Yasumara

23-15-5 On a Better Evaluation of the Seismic Behavior Factor of Low-Dissipative Timber Structures - A Ceccotti and A Vignoli

23-15-6 Disproportionate Collapse of Timber Structures - C J Mettem and J P Marcroft

23-15-7 Performance of Timber Frame Structures During the Loma Prieta California Earthquake - M R O'Halloran and E G Elias

24-15-2 Discussion About the Description of Timber Beam-Column Formula - S Y Huang

24-15-3 Seismic Behavior of Wood-Framed Shear Walls - M Yasumura

25-15-1 Structural Assessment of Timber Framed Building Systems - U Korin

25-15-3 Mechanical Properties of Wood-framed Shear Walls Subjected to Reversed Cyclic Lateral Loading - M Yasumura

26-15-1 Bracing Requirements to Prevent Lateral Buckling in Trussed Rafters - C J Mettem and P J Moss

26-15-2 Eurocode 8 - Part 1.3 - Chapter 5 - Specific Rules for Timber Buildings in Seismic Regions - K Becker, A Ceccotti, H Charlier, E Katsaragakis, H J Larsen and H Zeitter

26-15-3 Hurricane Andrew - Structural Performance of Buildings in South Florida - M R O'Halloran, E L Keith, J D Rose and T P Cunningham

29-15-1 Lateral Resistance of Wood Based Shear Walls with Oversized Sheathing Panels - F Lam, H G L Prion and M He

29-15-2 Damage of Wooden Buildings Caused by the 1995 Hyogo-Ken Nanbu Earthquake - M Yasumura, N Kawai, N Yamaguchi and S Nakajima

29-15-3 The Racking Resistance of Timber Frame Walls: Design by Test and Calculation - D R Griffiths, C J Mettem, V Enjily, P J Steer

29-15-4 Current Developments in Medium-Rise Timber Frame Buildings in the UK - C J Mettem, G C Pitts, P J Steer, V Enjily

29-15-5 Natural Frequency Prediction for Timber Floors - R J Bainbridge, and C J Mettem

30-15-1 Cyclic Performance of Perforated Wood Shear Walls with Oversize Oriented Strand Board Panels - Ming He, H Magnusson, F Lam, and H G L Prion

30-15-2 A Numerical Analysis of Shear Walls Structural Performances - L Davenne, L Daudeville, N Kawai and M Yasumura

30-15-3 Seismic Force Modification Factors for the Design of Multi-Storey Wood-Frame Platform Construction - E Karacabeyli and A Ceccotti

30-15-4 Evaluation of Wood Framed Shear Walls Subjected to Lateral Load - M Yasumura and N Kawai

31-15-1 Seismic Performance Testing On Wood-Framed Shear Wall - N Kawai

31-15-2 Robustness Principles in the Design of Medium-Rise Timber-Framed Buildings - C J Mettem, M W Milner, R J Bainbridge and V. Enjily

31-15-3 Numerical Simulation of Pseudo-Dynamic Tests Performed to Shear Walls - L Daudeville, L Davenne, N Richard, N Kawai and M Yasumura

31-15-4 Force Modification Factors for Braced Timber Frames - H G L Prion, M Popovski and E Karacabeyli

32-15-1 Three-Dimensional Interaction in Stabilisation of Multi-Storey Timber Frame Buildings **-** S Andreasson

32-15-2 Application of Capacity Spectrum Method to Timber Houses **-** N Kawai

32-15-3 Design Methods for Shear Walls with Openings **-** C Ni, E Karacabeyli and A Ceccotti

32-15-4 Static Cyclic Lateral Loading Tests on Nailed Plywood Shear Walls **-** K Komatsu, K H Hwang and Y Itou

33-15-1 Lateral Load Capacities of Horizontally Sheathed Unblocked Shear Walls – C Ni, E Karacabeyli and A Ceccotti

33-15-2 Prediction of Earthquake Response of Timber Houses Considering Shear Deformation of Horizontal Frames – N Kawai

33-15-3 Eurocode 5 Rules for Bracing – H J Larsen

34-15-1 A simplified plastic model for design of partially anchored wood-framed shear walls – B Källsner, U A Girhammar, Liping Wu

34-15-2 The Effect of the Moisture Content on the Performance of the Shear Walls – S Nakajima

34-15-3 Evaluation of Damping Capacity of Timber Structures for Seismic Design – M Yasumura

35-15-1 On test methods for determining racking strength and stiffness of wood-framed shear walls - B Källsner, U A Girhammar, L Wu

35-15-2 A Plastic Design Model for Partially Anchored Wood-framed Shear Walls with Openings - U A Girhammar, L Wu, B Källsner

35-15-3 Evaluation and Estimation of the Performance of the Shear Walls in Humid Climate - S Nakajima

35-15-4 Influence of Vertical Load on Lateral Resistance of Timber Frame Walls - B Dujič, R Žarnić

35-15-5 Cyclic and Seismic Performances of a Timber-Concrete System - Local and Full Scale Experimental Results - E Fournely, P Racher

35-15-6 Design of timber-concrete composite structures according to EC5 - 2002 version - A Ceccotti, M Fragiacomo, R M Gutkowski

35-15-7 Design of timber structures in seismic zones according to EC8- 2002 version - A Ceccotti, T Toratti, B Dujič

35-15-8 Design Methods to Prevent Premature Failure of Joints at Shear Wall Corners - N Kawai, H Okiura

36-15-1 Monitoring Light-Frame Timber Buildings: Environmental Loads and Load Paths – I Smith et al.

36-15-2 Applicability of Design Methods to Prevent Premature Failure of Joints at Shear Wall Corners in Case of Post and Beam Construction - N Kawai, H Isoda

36-15-3 Effects of Screw Spacing and Edge Boards on the Cyclic Performance of Timber Frame and Structural Insulated Panel Roof Systems - D M Carradine, J D Dolan, F E Woeste

36-15-4 Pseudo-Dynamic Tests on Conventional Timber Structures with Shear Walls - M Yasumura

36-15-5 Experimental Investigation of Laminated Timber Frames with Fiber-reinforced Connections under Earthquake Loads - B Kasal, P Haller, S Pospisil, I Jirovsky, A Heiduschke, M Drdacky

36-15-6 Effect of Test Configurations and Protocols on the Performance of Shear Walls - F Lam, D Jossen, J Gu, N Yamaguchi, H G L Prion

36-15-7 Comparison of Monotonic and Cyclic Performance of Light-Frame Shear Walls - J D Dolan, A J Toothman

37-15-1 Estimating 3D Behavior of Conventional Timber Structures with Shear Walls by Pseudodynamic Tests - M Yasumura, M Uesugi, L Davenne

37-15-2 Testing of Racking Behavior of Massive Wooden Wall Panels - B Dujič, J Pucelj, R Žarnić

37-15-3 Influence of Framing Joints on Plastic Capacity of Partially Anchored Wood-Framed Shear Walls - B Källsner, U A Girhammar

37-15-4 Bracing of Timber Members in Compression - J Munch-Andersen

37-15-5 Acceptance Criteria for the Use of Structural Insulated Panels in High Risk Seismic Areas - B Yeh, T D Skaggs, T G Williamson Z A Martin

37-15-6 Predicting Load Paths in Shearwalls - Hongyong Mi, Ying-Hei Chui, I Smith, M Mohammad

38-15-1 Background Information on ISO STANDARD 16670 for Cyclic Testing of Connections - E Karacabeyli, M Yasumura, G C Foliente, A Ceccotti

38-15-2 Testing & Product Standards – a Comparison of EN to ASTM, AS/NZ and ISO Standards – A Ranta-Maunus, V Enjily

38-15-3 Framework for Lateral Load Design Provisions for Engineered Wood Structures in Canada - M Popovski, E Karacabeyli

38-15-4 Design of Shear Walls without Hold-Downs - Chun Ni, E Karacabeyli

38-15-5 Plastic design of partially anchored wood-framed wall diaphragms with and without openings - B Källsner, U A Girhammar

38-15-6 Racking of Wooden Walls Exposed to Different Boundary Conditions - B Dujič, S Aicher, R Žarnić

38-15-7 A Portal Frame Design for Raised Wood Floor Applications - T G Williamson, Z A Martin, B Yeh

38-15-8 Linear Elastic Design Method for Timber Framed Ceiling, Floor and Wall Diaphragms - Jarmo Leskelä

38-15-9 A Unified Design Method for the Racking Resistance of Timber Framed Walls for Inclusion in EUROCODE 5 - R Griffiths, B Källsner, H J Blass, V Enjily

39-15-1 Effect of Transverse Walls on Capacity of Wood-Framed Wall Diaphragms - U A Girhammar, B Källsner

39-15-2 Which Seismic Behaviour Factor for Multi-Storey Buildings made of Cross-Laminated Wooden Panels? - M Follesa, M P Lauriola, C Minowa, N Kawai, C Sandhaas, M Yasumura, A Ceccotti

39-15-3 Laminated Timber Frames under dynamic Loadings - A Heiduschke, B Kasal, P Haller

39-15-4 Code Provisions for Seismic Design of Multi-storey Post-tensioned Timber Buildings - S Pampanin, A Palermo, A Buchanan, M Fragiacomo, B Deam

40-15-1 Design of Safe Timber Structures – How Can we Learn from Structural Failures? - S Thelandersson, E Frühwald

40-15-2 Effect of Transverse Walls on Capacity of Wood-Framed Wall Diaphragms—Part 2 - U A Girhammar, B Källsner

40-15-3 Midply Wood Shear Wall System: Concept, Performance and Code Implementation - Chun Ni, M Popovski, E Karacabeyli, E Varoglu, S Stiemer

40-15-4 Seismic Behaviour of Tall Wood-Frame Walls - M Popovski, A Peterson, E Karacabeyli

40-15-5 International Standard Development of Lateral Load Test Method for Shear Walls - M Yasumura, E Karacabeyli

40-15-6 Influence of Openings on Shear Capacity of Wooden Walls - B Dujič, S Klobcar, R Žarnić

41-15-1 Need for a Harmonized Approach for Calculations of Ductility of Timber Assemblies - W Muñoz, M Mohammad, A Salenikovich, P Quenneville

41-15-2 Plastic Design of Wood Frame Wall Diaphragms in Low and Medium Rise Buildings - B Källsner, U A Girhammar

41 15-3 Failure Analysis of Light Wood Frame Structures under Wind Load - A Asiz, Y H Chui, I Smith

41-15-4 Combined Shear and Wind Uplift Resistance of Wood Structural Panel Shearwalls B Yeh, T G Williamson

41-15-5 Behaviour of Prefabricated Timber Wall Elements under Static and Cyclic Loading – P Schädle, H J Blass

42-15-1 Design Aspects on Anchoring the Bottom Rail in Partially Anchored Wood-Framed Shear Walls - U A Girhammar, B Källsner

42-15-2 New Seismic Design Provisions for Shearwalls and Diaphragms in the Canadian Standard for Engineering Design in Wood - M Popovski, E Karacabeyli, Chun Ni, P Lepper, G Doudak

42-15-3 Stability Capacity and Lateral Bracing Force of Metal Plate Connected Wood Truss Assemblies - Xiaobin Song, F Lam, Hao Huang, Minjuan He

42-15-4 Improved Method for Determining Braced Wall Requirements for Conventional Wood-Frame Buildings - Chun Ni, H Rainer, E Karacabeyli

43-15-1 Influence of the Boundary Conditions on the Racking Strength of Shear Walls with an Opening - M Yasumura

43-15-2 Influence of Different Standards on the Determination of Earthquake Properties of Timber Shear Wall Systems - P Schädle, H J Blaß

43-15-3 Full-Scale Shear Wall Tests for Force Transfer Around Openings - T Skaggs, B Yeh, F Lam

43-15-4 Optimized Anchor-Bolt Spacing for Structural Panel Shearwalls Subjected to Combined Shear and Wind Uplift Forces - B Yeh, E Keith, T Skaggs

44-15-1 A Proposal for Revision of the Current Timber Part (Section 8) of Eurocode 8 Part 1 - M Follesa, M Fragiacomo, M P Lauriola

44-15-2 Influence of Vertical Loads on Lateral Resistance and Deflections of Light-Frame Shear Walls - M Payeur, A Salenikovich, W Muñoz

44-15-3 Modelling Force Transfer Around Openings of Full-Scale Shear Walls - T Skaggs, B Yeh, F Lam, Minghao Li, D Rammer, J Wacker

44-15-4 Design of Bottom Rails in Partially Anchored Shear Walls Using Fracture Mechanics - E Serrano, J Vessby, A Olsson, U A Girhammar, B Källsner

44-15-5 Notes on Deformation and Ductility Requirements in Timber Structures. - K A Malo, P Ellingsbø, C Stamatopoulos

44-15-6 Enhanced Model of the Nonlinear Load-bearing Behaviour of Wood Shear Walls and Diaphragms - M H Kessel, C Hall

44-15-7 Seismic Performance of Cross-Laminated Wood Panels - M Popovski, E Karacabeyli

44-15-8 Evaluation of Plywood Sheathed Shear Walls with Screwed Joints Tested According to ISO 21581 - K Kobayashi, M Yasumura

44-15-9 Influence of Connection Properties on the Ductility and Seismic Resistance of Multi-Storey Cross-Lam Buildings - I Sustersic, M Fragiacomo, B Dujic

46-15-1 Experimental Investigations on Seismic Behaviour of Conventional Timber Frame Wall with OSB Sheathing - Proposal of Behaviour Factor - C Faye, L Le Magorou, P Garcia, J-C Duccini

46-15-2 Capacity Seismic Design of X-Lam Wall Systems Based on Connection Mechanical Properties - I Gavric, M Fragiacomo, A Ceccotti

46-15-3 An Approach to Derive System Seismic Force Modification Factor for Buildings Containing Different LLRS's - Z Chen, C Ni, Y-H Chui, G Doudak, M Mohammad

46-15-4 Connections and Anchoring for Wall and Slab Elements in Seismic Design - M Schick, T Vogt, W Seim

46-15-5 Analytical Formulation Based on Extensive Numerical Simulations of Behavior Factor q for CLT buildings - L Pozza, R Scotta, D Trutalli, A Ceccotti, A Polastri

46-15-6 Proposal for the q-factor of Moment Resisting Timber Frames with High Ductility Dowel Connectors - D Wrzesniak, G Rinaldin, M Fragiacomo, C Amadio

46-15-7 Wind Tunnel Tests for Wood Structural Panels Used as Nailable Sheathing - B Yeh, A Cope, E Keith

47-15-1 Advanced Modelling of Timber-framed Wall Elements for Application in Engineering Practice - T Vogt, W Seim

47-15-2 A Buckling Design Approach for 'Blockhaus' Timber Walls Under In-plane Vertical Loads - C Bedon, M Fragiacomo, C Amadio, A Battisti

47-15-3 Capacity Design Approach for Multi-storey Timber-frame Buildings - D Casagrande, T Sartori, R Tomasi

47-15-4 Design Models for CLT Shearwalls and Assemblies Based on Connection Properties - I Gavric, M Popovski

47-15-5 Effects of Design Criteria on an Experimentally-based Evaluation of the Behaviour Factor of Novel Massive Wooden Shear Walls - L Pozza, R Scotta, D Trutalli, A Polastri, A Ceccotti

47-15-6 An Elastoplastic Solution for Earthquake Resistant Rigid Timber Shear Walls - Wei Yuen Loo, P Quenneville, Nawawi Chouw

47-15-7 In-Plane Racking Tests of Continuous Sheathed Wood Structural Panel Wall Bracing - T Skaggs, E Keith, Borjen Yeh, P Line, N Waltz

47-15-8 Design of Floor Diaphragms in Multi-Storey Timber Buildings - D Moroder, T Smith, S Pampanin, A Palermo, A H Buchanan

FIRE

12-16-1 British Standard BS 5268 the Structural Use of Timber: Part 4 Fire Resistance of Timber Structures

13-100-2 CIB Structural Timber Design Code. Chapter 9. Performance in Fire

19-16-1 Simulation of Fire in Tests of Axially Loaded Wood Wall Studs - J König

24-16-1 Modelling the Effective Cross Section of Timber Frame Members Exposed to Fire - J König

25-16-1 The Effect of Density on Charring and Loss of Bending Strength in Fire - J König

25-16-2 Tests on Glued-Laminated Beams in Bending Exposed to Natural Fires - F Bolonius Olesen and J König

26-16-1 Structural Fire Design According to Eurocode 5, Part 1.2 - J König

31-16-1 Revision of ENV 1995-1-2: Charring and Degradation of Strength and Stiffness - J König

33-16-1 A Design Model for Load-carrying Timber Frame Members in Walls and Floors Exposed to Fire - J König

33-16-2 A Review of Component Additive Methods Used for the Determination of Fire Resistance of Separating Light Timber Frame Construction - J König, T Oksanen and K Towler

33-16-3 Thermal and Mechanical Properties of Timber and Some Other Materials Used in Light Timber Frame Construction - B Källsner and J König

34-16-1 Influence of the Strength Determining Factors on the Fire Resistance Capability of Timber Structural Members – I Totev, D Dakov

34-16-2 Cross section properties of fire exposed rectangular timber members - J König, B Källsner

34-16-3 Pull-Out Tests on Glued-in Rods at High Temperatures – A Mischler, A Frangi

35-16-1 Basic and Notional Charring Rates - J König

37 - 16 - 1 Effective Values of Thermal Properties of Timber and Thermal Actions During the Decay Phase of Natural Fires - J König

37 - 16 - 2 Fire Tests on Timber Connections with Dowel-type Fasteners - A Frangi, A Mischler

38-16-1 Fire Behaviour of Multiple Shear Steel-to-Timber Connections with Dowels - C Erchinger, A Frangi, A Mischler

38-16-2 Fire Tests on Light Timber Frame Wall Assemblies - V Schleifer, A Frangi

39-16-1 Fire Performance of FRP Reinforced Glulam - T G Williamson, B Yeh

39-16-2 An Easy-to-use Model for the Design of Wooden I-joists in Fire - J König, B Källsner

39-16-3 A Design Model for Timber Slabs Made of Hollow Core Elements in Fire - A Frangi, M Fontana

40-16-1 Bonded Timber Deck Plates in Fire - J König, J Schmid

40-16-2 Design of Timber Frame Floor Assemblies in Fire - A Frangi, C Erchinger

41-16-1 Effect of Adhesives on Finger Joint Performance in Fire - J König, J Norén, M Sterley

42-16-1 Advanced Calculation Method for the Fire Resistance of Timber Framed Walls -S Winter, W Meyn

42-16-2 Fire Design Model for Multiple Shear Steel-to-Timber Dowelled Connections - C Erchinger, A Frangi, M Fontana

42-16-3 Comparison between the Conductive Model of Eurocode 5 and the Temperature Distribution Within a Timber Cross-section Exposed to Fire - M Fragiacomo, A Menis, P Moss, A Buchanan, I Clemente

43-16-1 Light Timber Frame Construction with Solid Timber Members – Application of the Reduced Cross-section Method - J König, J Schmid

43-16-2 Fire Exposed Cross-Laminated Timber - Modelling and Tests - J Schmid, J König, J Köhler

43-16-3 Timber-Concrete Composite Floors in Fire - J O'Neill, D Carradine, R Dhakal, P J Moss, A H Buchanan, M Fragiacomo

44-16-1 Gypsum Plasterboards and Gypsum Fibreboards – Protective Times for Fire Safety Design of Timber Structures –A Just, J Schmid, J König

46-16-1 Comparison of the Fire Resistance of Timber Members in Tests and Calculation Models - J Schmid, M Klippel, A Just, A Frangi

47-16-1 Fire Design of Glued-laminated Timber Beams with Regard to the Adhesive Performance Using the Reduced Cross-Section Method - M Klippel, J Schmid, A Frangi, G Fink

STATISTICS AND DATA ANALYSIS

13-17-1 On Testing Whether a Prescribed Exclusion Limit is Attained - W G Warren

16-17-1 Notes on Sampling and Strength Prediction of Stress Graded Structural Timber - P Glos

16-17-2 Sampling to Predict by Testing the Capacity of Joints, Components and Structures - B Norén

16-17-3 Discussion of Sampling and Analysis Procedures - P W Post

17-17-1 Sampling of Wood for Joint Tests on the Basis of Density - I Smith, L R J Whale

17-17-2 Sampling Strategy for Physical and Mechanical Properties of Irish Grown Sitka Spruce - V Picardo

18-17-1 Sampling of Timber in Structural Sizes - P Glos

18-6-3 Notes on Sampling Factors for Characteristic Values - R H Leicester

19-17-1 Load Factors for Proof and Prototype Testing - R H Leicester

19-6-2 Confidence in Estimates of Characteristic Values - R H Leicester

21-6-1 Draft Australian Standard: Methods for Evaluation of Strength and Stiffness of Graded Timber - R H Leicester

21-6-2 The Determination of Characteristic Strength Values for Stress Grades of Structural Timber. Part 1 - A R Fewell and P Glos

22-17-1 Comment on the Strength Classes in Eurocode 5 by an Analysis of a Stochastic Model of Grading - A proposal for a supplement of the design concept - M Kiesel

24-17-1 Use of Small Samples for In-Service Strength Measurement - R H Leicester and F G Young

24-17-2 Equivalence of Characteristic Values - R H Leicester and F G Young

24-17-3 Effect of Sampling Size on Accuracy of Characteristic Values of Machine Grades - Y H Chui, R Turner and I Smith

24-17-4 Harmonisation of LSD Codes - R H Leicester

25-17-2 A Body for Confirming the Declaration of Characteristic Values - J Sunley

25-17-3 Moisture Content Adjustment Procedures for Engineering Standards - D W Green and J W Evans

27-17-1 Statistical Control of Timber Strength - R H Leicester and H O Breitinger

30-17-1 A New Statistical Method for the Establishment of Machine Settings - F Rouger

35-17-1 Probabilistic Modelling of Duration of Load Effects in Timber Structures - J Köhler, S Svenson

38-17-1 Analysis of Censored Data - Examples in Timber Engineering Research - R Steiger, J Köhler

39-17-1 Possible Canadian / ISO Approach to Deriving Design Values from Test Data - I Smith, A Asiz, M Snow, Y H Chui

44-17-1 Influence of Sample Size on Assigned Characteristic Strength Values – P Stapel, G J P Ravenshorst, J W G van de Kuilen

GLUED JOINTS

20-18-1 Wood Materials under Combined Mechanical and Hygral Loading - A Martensson and S Thelandersson

20-18-2 Analysis of Generalized Volkersen - Joints in Terms of Linear Fracture Mechanics - P J Gustafsson

20-18-3 The Complete Stress-Slip Curve of Wood-Adhesives in Pure Shear - H Wernersson and P J Gustafsson

22-18-1 Perspective Adhesives and Protective Coatings for Wood Structures - A S Freidin

34-18-1 Performance Based Classification of Adhesives for Structural Timber Applications - R J Bainbridge, C J Mettem, J G Broughton, A R Hutchinson

35-18-1 Creep Testing Wood Adhesives for Structural Use - C Bengtsson, B Källander

38-18-1 Adhesive Performance at Elevated Temperatures for Engineered Wood Products - B Yeh, B Herzog, T G Williamson

39-18-1 Comparison of the Pull–out Strength of Steel Bars Glued in Glulam Elements Obtained Experimentally and Numerically - V Rajčić, A Bjelanović, M Rak

39-18-2 The Influence of the Grading Method on the Finger Joint Bending Strength of Beech - M Frese, H J Blaß

43-18-1 Comparison of API, RF and MUF Adhesives Using a Draft Australian/New Zealand Standard - B Walford

FRACTURE MECHANICS

21-10-1 A Study of Strength of Notched Beams - P J Gustafsson

22-10-1 Design of Endnotched Beams - H J Larsen and P J Gustafsson

23-10-1 Tension Perpendicular to the Grain at Notches and Joints - T A C M van der Put

23-10-2 Dimensioning of Beams with Cracks, Notches and Holes. An Application of Fracture Mechanics - K Riipola

23-19-1 Determination of the Fracture Energie of Wood for Tension Perpendicular to the Grain - W Rug, M Badstube and W Schöne

23-19-2 The Fracture Energy of Wood in Tension Perpendicular to the Grain. Results from a Joint Testing Project - H J Larsen and P J Gustafsson

23-19-3 Application of Fracture Mechanics to Timber Structures - A Ranta-Maunus

24-19-1 The Fracture Energy of Wood in Tension Perpendicular to the Grain - H J Larsen and P J Gustafsson

28-19-1 Fracture of Wood in Tension Perpendicular to the Grain: Experiment and Numerical Simulation by Damage Mechanics - L Daudeville, M Yasumura and J D Lanvin

28-19-2 A New Method of Determining Fracture Energy in Forward Shear along the Grain - H D Mansfield-Williams

28-19-3 Fracture Design Analysis of Wooden Beams with Holes and Notches. Finite Element Analysis based on Energy Release Rate Approach - H Petersson

28-19-4 Design of Timber Beams with Holes by Means of Fracture Mechanics - S Aicher, J Schmidt and S Brunold

30-19-1 Failure Analysis of Single-Bolt Joints - L Daudeville, L Davenne and M Yasumura

37 - 19 - 1 Determination of Fracture Mechanics Parameters for Wood with the Help of Close Range Photogrammetry - S Franke, B Franke, K Rautenstrauch

39-19-1 First Evaluation Steps of Design Rules in the European and German codes of Transverse Tension Areas - S Franke, B Franke, K Rautenstrauch

SERVICEABILITY

27-20-1 Codification of Serviceability Criteria - R H Leicester

27-20-2 On the Experimental Determination of Factor k_{def} and Slip Modulus k_{ser} from Short- and Long-Term Tests on a Timber-Concrete Composite (TCC) Beam - S Capretti and A Ceccotti

27-20-3 Serviceability Limit States: A Proposal for Updating Eurocode 5 with Respect to Eurocode 1 - P Racher and F Rouger

27-20-4 Creep Behavior of Timber under External Conditions - C Le Govic, F Rouger, T Toratti and P Morlier

30-20-1 Design Principles for Timber in Compression Perpendicular to Grain - S Thelandersson and A Mårtensson

30-20-2 Serviceability Performance of Timber Floors - Eurocode 5 and Full Scale Testing - R J Bainbridge and C J Mettem

32-20-1 Floor Vibrations - B Mohr

37-20-1 A New Design Method to Control Vibrations Induced by Foot Steps in Timber Floors - Lin J Hu, Y H Chui

37-20-2 Serviceability Limit States of Wooden Footbridges. Vibrations Caused by Pedestrians - P Hamm

43-20-1 The Long Term Instrumentation of a Timber Building in Nelson NZ - the Need for Standardisation - H W Morris, S R Uma, K Gledhill, P Omenzetter, M Worth

46-20-1 CLT and Floor Vibrations: a Comparison of Design Methods - A Thiel, S Zimmer, M Augustin, G Schickhofer

TEST METHODS

31-21-1 Development of an Optimised Test Configuration to Determine Shear Strength of Glued Laminated Timber - G Schickhofer and B Obermayr

31-21-2 An Impact Strength Test Method for Structural Timber. The Theory and a Preliminary Study - T D G Canisius

35-21-1 Full-Scale Edgewise Shear Tests for Laminated Veneer Lumber- B Yeh, T G Williamson

39-21-1 Timber Density Restrictions for Timber Connection Tests According to EN28970/ISO8970 - A Leijten, J Köhler, A Jorissen

39-21-2 The Mechanical Inconsistence in the Evaluation of the Modulus of Elasticity According to EN384 - T Bogensperger, H Unterwieser, G Schickhofer

40-21-1 ASTM D198 - Interlaboratory Study for Modulus of Elasticity of Lumber in Bending - A Salenikovich

40-21-2 New Test Configuration for CLT-Wall-Elements under Shear Load - T Bogensperger, T Moosbrugger, G Schickhofer

41-21-1 Determination of Shear Modulus by Means of Standardized Four-Point Bending Tests - R Brandner, B Freytag, G Schickhofer

43-21-1 Estimation of Load-Bearing Capacity of Timber Connections - J Munch-Andersen, J D Sørensen, F Sørensen

43-21-2 A New Method to Determine Suitable Spacings and Distances for Self-tapping Screws - T Uibel, H J Blaß

CIB TIMBER CODE

2-100-1 A Framework for the Production of an International Code of Practice for the Structural Use of Timber - W T Curry

5-100-1 Design of Solid Timber Columns (First Draft) - H J Larsen

5-100-2 A Draft Outline of a Code for Timber Structures - L G Booth

6-100-1 Comments on Document 5-100-1; Design of Solid Timber Columns - H J Larsen and E Theilgaard

6-100-2 CIB Timber Code: CIB Timber Standards - H J Larsen and E Theilgaard

7-100-1 CIB Timber Code Chapter 5.3 Mechanical Fasteners; CIB Timber Standard 06 and 07 - H J Larsen

8-100-1 CIB Timber Code - List of Contents (Second Draft) - H J Larsen

9-100-1 The CIB Timber Code (Second Draft)

11-100-1 CIB Structural Timber Design Code (Third Draft)

11-100-2 Comments Received on the CIB Code - U Saarelainen; Y M Ivanov, R H Leicester, W Nozynski, W R A Meyer, P Beckmann; R Marsh

11-100-3 CIB Structural Timber Design Code; Chapter 3 - H J Larsen

12-100-1 Comment on the CIB Code - Sous-Commission Glulam

12-100-2 Comment on the CIB Code - R H Leicester

12-100-3 CIB Structural Timber Design Code (Fourth Draft)

13-100-1 Agreed Changes to CIB Structural Timber Design Code

13-100-2 CIB Structural Timber Design Code. Chapter 9: Performance in Fire

13-100-3a Comments on CIB Structural Timber Design Code

13-100-3b Comments on CIB Structural Timber Design Code - W R A Meyer

13-100-3c Comments on CIB Structural Timber Design Code - British Standards Institution

13-100-4 CIB Structural Timber Design Code. Proposal for Section 6.1.5 Nail Plates - N I Bovim

14-103-2 Comments on the CIB Structural Timber Design Code - R H Leicester

15-103-1 Resolutions of TC 165-meeting in Athens 1981-10-12/13

21-100-1 CIB Structural Timber Design Code. Proposed Changes of Sections on Lateral Instability, Columns and Nails - H J Larsen

22-100-1 Proposal for Including an Updated Design Method for Bearing Stresses in CIB W18 - Structural Timber Design Code - B Madsen

22-100-2 Proposal for Including Size Effects in CIB W18A Timber Design Code - B Madsen

22-100-3 CIB Structural Timber Design Code - Proposed Changes of Section on Thin-Flanged Beams - J König

22-100-4 Modification Factor for "Aggressive Media" - a Proposal for a Supplement to the CIB Model Code - K Erler and W Rug

22-100-5 Timber Design Code in Czechoslovakia and Comparison with CIB Model Code - P Dutko and B Kozelouh

LOADING CODES

4-101-1 Loading Regulations - Nordic Committee for Building Regulations

4-101-2 Comments on the Loading Regulations - Nordic Committee for Building Regulations

37-101-1 Action Combination Processing for the Eurocodes Basis of Software to Assist the Engineer - Y Robert, A V Page, R Thépaut, C J Mettem

43-101-1 Dependant Versus Independent Loads in Structural Design - T Poutanen

STRUCTURAL DESIGN CODES

1-102-1 Survey of Status of Building Codes, Specifications etc., in USA - E G Stern

1-102-2 Australian Codes for Use of Timber in Structures - R H Leicester

1-102-3 Contemporary Concepts for Structural Timber Codes - R H Leicester

1-102-4 Revision of CP 112 - First Draft, July 1972 - British Standards Institution

4-102-1 Comparsion of Codes and Safety Requirements for Timber Structures in EEC Countries - Timber Research and Development Association

4-102-2 Nordic Proposals for Safety Code for Structures and Loading Code for Design of Structures - O A Brynildsen

4-102-3 Proposal for Safety Codes for Load-Carrying Structures - Nordic Committee for Building Regulations

4-102-4 Comments to Proposal for Safety Codes for Load-Carrying Structures - Nordic Committee for Building Regulations

4-102-5 Extract from Norwegian Standard NS 3470 "Timber Structures"

4-102-6 Draft for Revision of CP 112 "The Structural Use of Timber" - W T Curry

8-102-1 Polish Standard PN-73/B-03150: Timber Structures; Statistical Calculations and Designing

8-102-2 The Russian Timber Code: Summary of Contents

9-102-1 Svensk Byggnorm 1975 (2nd Edition); Chapter 27: Timber Construction

11-102-1 Eurocodes - H J Larsen

13-102-1 Program of Standardisation Work Involving Timber Structures and Wood-Based Products in Poland

17-102-1 Safety Principles - H J Larsen and H Riberholt

17-102-2	Partial Coefficients Limit States Design Codes for Structural Timberwork - I Smith
18-102-1	Antiseismic Rules for Timber Structures: an Italian Proposal - G Augusti and A Ceccotti
18-1-2	Eurocode 5, Timber Structures - H J Larsen
19-102-1	Eurocode 5 - Requirements to Timber - Drafting Panel Eurocode 5
19-102-2	Eurocode 5 and CIB Structural Timber Design Code - H J Larsen
19-102-3	Comments on the Format of Eurocode 5 - A R Fewell
19-102-4	New Developments of Limit States Design for the New GDR Timber Design Code - W Rug and M Badstube
19-7-3	Effectiveness of Multiple Fastener Joints According to National Codes and Eurocode 5 (Draft) - G Steck
19-7-6	The Derivation of Design Clauses for Nailed and Bolted Joints in Eurocode5 - L R J Whale and I Smith
19-14-1	Annex on Simplified Design of W-Trusses - H J Larsen
20-102-1	Development of a GDR Limit States Design Code for Timber Structures - W Rug and M Badstube
21-102-1	Research Activities Towards a New GDR Timber Design Code Based on Limit States Design - W Rug and M Badstube
22-102-1	New GDR Timber Design Code, State and Development - W Rug, M Badstube and W Kofent
22-102-2	Timber Strength Parameters for the New USSR Design Code and its Comparison with International Code - Y Y Slavik, N D Denesh and E B Ryumina
22-102-3	Norwegian Timber Design Code - Extract from a New Version - E Aasheim and K H Solli
23-7-1	Proposal for a Design Code for Nail Plates - E Aasheim and K H Solli
24-102-2	Timber Footbridges: A Comparison Between Static and Dynamic Design Criteria - A Ceccotti and N de Robertis
25-102-1	Latest Development of Eurocode 5 - H J Larsen
25-102-1A	Annex to Paper CIB-W18/25-102-1. Eurocode 5 - Design of Notched Beams - H J Larsen, H Riberholt and P J Gustafsson
25-102-2	Control of Deflections in Timber Structures with Reference to Eurocode 5 - A Martensson and S Thelandersson
28-102-1	Eurocode 5 - Design of Timber Structures - Part 2: Bridges - D Bajolet, E Gehri, J König, H Kreuzinger, H J Larsen, R Mäkipuro and C Mettem
28-102-2	Racking Strength of Wall Diaphragms - Discussion of the Eurocode 5 Approach - B Källsner
29-102-1	Model Code for the Probabilistic Design of Timber Structures - H J Larsen, T Isaksson and S Thelandersson
30-102-1	Concepts for Drafting International Codes and Standards for Timber Constructions - R H Leicester
33-102-1	International Standards for Bamboo – J J A Janssen
35-102-1	Design Characteristics and Results According to EUROCODE 5 and SNiP Procedures - L Ozola, T Keskküla
35-102-2	Model Code for the Reliability-Based Design of Timber Structures - H J Larsen

36-102-1 Predicted Reliability of Elements and Classification of Timber Structures - L Ozola, T Keskküla

36-102-2 Calibration of Reliability-Based Timber Design Codes: Choosing a Fatigue Model - I Smith

38-102-1 A New Generation of Timber Design Practices and Code Provisions Linking System and Connection Design - A Asiz, I Smith

38-102-2 Uncertainties Involved in Structural Timber Design by Different Code Formats - L Ozola, T Keskküla

38-102-3 Comparison of the Eurocode 5 and Actual Croatian Codes for Wood Classification and Design With the Proposal for More Objective Way of Classification - V Rajcic A Bjelanovic

39-102-1 Calibration of Partial Factors in the Danish Timber Code - H Riberholt

41 - 102 - 1 Consequences of EC 5 for Danish Best Practise - J Munch-Andersen

41 - 102 - 2 Development of New Swiss standards for the Assessment of Existing Load Bearing Structures – R Steiger, J Köhler

41 – 102 - 3 Measuring the CO2 Footprint of Timber Buildings – A Buchanan, S John

INTERNATIONAL STANDARDS ORGANISATION

3-103-1 Method for the Preparation of Standards Concerning the Safety of Structures (ISO/DIS 3250) - International Standards Organisation ISO/TC98

4-103-1 A Proposal for Undertaking the Preparation of an International Standard on Timber Structures - International Standards Organisation

5-103-1 Comments on the Report of the Consultion with Member Bodies Concerning ISO/TC/P129 - Timber Structures - Dansk Ingeniorforening

7-103-1 ISO Technical Committees and Membership of ISO/TC 165

8-103-1 Draft Resolutions of ISO/TC 165

12-103-1 ISO/TC 165 Ottawa, September 1979

13-103-1 Report from ISO/TC 165 - A Sorensen

14-103-1 Comments on ISO/TC 165 N52 "Timber Structures; Solid Timber in Structural Sizes; Determination of Some Physical and Mechanical Properties"

14-103-2 Comments on the CIB Structural Timber Design Code - R H Leicester

21-103-1 Concept of a Complete Set of Standards - R H Leicester

JOINT COMMITTEE ON STRUCTURAL SAFETY

3-104-1 International System on Unified Standard Codes of Practice for Structures - Comité Européen du Béton (CEB)

7-104-1 Volume 1: Common Unified Rules for Different Types of Construction and Material - CEB

37-104-1 Proposal for a Probabilistic Model Code for Design of Timber Structures - J Köhler, H Faber

CIB PROGRAMME, POLICY AND MEETINGS

1-105-1 A Note on International Organisations Active in the Field of Utilisation of Timber - P Sonnemans

5-105-1 The Work and Objectives of CIB-W18-Timber Structures - J G Sunley

10-105-1 The Work of CIB-W18 Timber Structures - J G Sunley

15-105-1 Terms of Reference for Timber - Framed Housing Sub-Group of CIB-W18

19-105-1 Tropical and Hardwood Timbers Structures - R H Leicester

21-105-1 First Conference of CIB-W18B, Tropical and Hardwood Timber Structures Singapore, 26 - 28 October 1987 - R H Leicester

INTERNATIONAL UNION OF FORESTRY RESEARCH ORGANISATIONS

7-106-1 Time and Moisture Effects - CIB W18/IUFRO 55.02-03 Working Party

5 INTER Papers, Bath, United Kingdom 2014

47 - 5 - 1 Strength Grading of Split Glulam Beams - **J Viguier, J-F Boquet, J Dopeux, L Bléron, F Dubois, S Aubert**

47 - 6 - 1 Compression Strength and Stiffness Perpendicular to the Grain – Influences of the Material Properties, the Loading Situation and the Gauge Length- **C Le Levé, R Maderebner, M Flach**

47 - 7 - 1 Discussion of testing and Evaluation Methods for the Embedment Behaviour of Connections - **S Franke, N Magnière**

47 - 7 - 2 Dowel-type Connections in LVL Made of Beech Wood - P Kobel, A Frangi, R Steiger

47 - 7 - 3 Resistance of Connections in Cross-Laminated Timber under Brittle Block Tear-Out Failure Mode - **P Zarnani, P Quenneville**

47 - 7 - 4 Study on Nail Connections in Deformed State - **S Svensson, J Munch-Andersen**

47 - 7 - 5 Design Model for Inclined Screws under Varying Load to Grain Angles - **R Jockwer, R Steiger, A Frangi**

47 - 12 - 1 Calculation of Cylindrical Shells from Wood or Wood Based Products and Consideration of the Stress Relaxation - **P Aondio, S Winter, H Kreuzinger**

47 - 12 - 2 Hybrid Glulam Beams Made of Beech LVL and Spruce Laminations - **M Frese**

47 - 12 - 3 Design for the Spreading under a Compressive Stress in Glued Laminated Timber **- D Lathuilliere, L Bléron, J-F Bocquet, F Varacca, F Dubois**

47 - 12 - 4 Design of CLT Beams with Rectangular Holes or Notches - **M Flaig**

47 - 12 - 5 Properties of Cross Laminated Timber (CLT) in Compression Perpendicular to Grain - **R Brandner, G Schickhofer**

47 - 15 - 1 Advanced Modelling of Timber-framed Wall Elements for Application in Engineering Practice - **T Vogt, W Seim**

47 - 15 - 2 A Buckling Design Approach for ‘Blockhaus’ Timber Walls Under In-plane Vertical Loads - **C Bedon, M Fragiacomo, C Amadio, A Battisti**

47 - 15 - 3 Capacity Design Approach for Multi-storey Timber-frame Buildings **- D Casagrande, T Sartori, R Tomasi**

47 - 15 - 4 Design Models for CLT Shearwalls and Assemblies Based on Connection Properties - **I Gavric, M Popovski**

47 - 15 - 5 Effects of Design Criteria on an Experimentally-based Evaluation of the Behaviour Factor of Novel Massive Wooden Shear Walls - **L Pozza, R Scotta, D Trutalli, A Polastri, A Ceccotti**

47 - 15 - 6 An Elastoplastic Solution for Earthquake Resistant Rigid Timber Shear Walls - **Wei Yuen Loo, P Quenneville, Nawawi Chouw**

47 - 15 - 7 In-Plane Racking Tests of Continuous Sheathed Wood Structural Panel Wall Bracing - **T Skaggs, E Keith, Borjen Yeh, P Line, N Waltz**

47 - 15 - 8 Design of Floor Diaphragms in Multi-Storey Timber Buildings - **D Moroder, T Smith, S Pampanin, A Palermo, A H Buchanan**

47 - 16 - 1 Fire Design of Glued-laminated Timber Beams with Regard to the Adhesive Performance Using the Reduced Cross-Section Method - **M Klippel, J Schmid, A Frangi, G Fink**

INTER

International Network on Timber Engineering Research

STRENGTH GRADING OF SPLIT GLULAM BEAMS

J Viguier

J-F Boquet

ENSTIB / LERMAB 88000 Epinal

J Dopeux

PFT Bois-Construction du Limousin 19300 Egletons

L Bléron

ENSTIB / LERMAB 88000 Epinal

F Dubois

GEMH, GC&D, Université de Limoges 19300 Egletons

S Aubert

ENSTIB / LERMAB 88000 Epinal

FRANCE

Presented by J Viguier

J Munch Andersen commented that old data showed reduced strength of 4 MPa with one cut and 8 MPA with two cuts. He commented that it is very difficult to show things are different in terms of using statistics.

P Quenneville commented that statistical comparisons were made at the mean and 5th percentile comparisons are more appropriate.

R Brandner asked why the bending test done on edge for the boards. J Viguier responded that grading is done by calibrated machines in edge bending in France. R Brandner commented that recently more machines in Europe are calibrated based on tensile strength.

JW van de Kuilen asked whether the boards were checked for the grade quality. J Viguier responded that it will be done later. JW van de Kuilen stated that different manufacturing procedures may influence grade distribution.

E Serrano and J Viguier discussed about two cuts to split a beam into three in terms of the quality of the thin member.

R Steiger commented that tools can be used to qualify uncertainties. In Slide 18 and 19 using effective cross section for stiffness properties maybe possible but for strength is inappropriate. J Viguier explained the procedure using the ratio between the values of moment of inertia of the full board and the reduced cross section to get the weakest section and to get the reduced Moe. Then the relationship between MOR and MOE was used to get the strength.

S Franke asked whether this can be done with tension grading. J Viguier answered yes. It is better with tension grading. S Franke also commented that the increase of density of the resawn beam could explain the increase in strength. J Viguier responded the density increase is little.

STRENGTH GRADING OF SPLIT GLULAM BEAMS

Viguier J[1], Bocquet J-F[1], Dopeux J[2], Bléron L[1], Dubois F[3], Aubert S[1]

[1] ENSTIB / LERMAB 88000 Epinal [2]PFT Bois-Construction du Limousin 19300 Egletons

[3]GEMH, GC&D, Université de Limoges 19300 Egletons

Keywords: Strength grading, Glulam, Resawn

1. Introduction

To produce thin glulam (<100mm), manufacturers used to split glulam member to improve productivity. Two (single resawn) or three beams (double resawn) are obtained by length sawing a full-size glulam beam. The two (or three) sub-products obtained may have different mechanical properties than the initial beam. One study (Riberholt, 2009) was conducted to evaluate the loss of the mechanical properties. This study is based on two experimental campaigns:

-the first composed of 40 beams: 20 of them were full-size beams of GL28 (225×90mm²) and the 20 others came from splitting 10 of the previous full-size beam (their cross-section is then 225×40mm²). The initial beams were made of lamellae with a tensile strength of 18N/mm². The characteristic bending strength $f_{m,k}$ of the resawn glulam was 2.9 N/mm² less and their mean elastic modulus 300 N/mm² less;

-the second composed of 16 full-size beam GL30 (180×90mm²) made of lamellae with a tensile strength equals to 22N/mm² and 16 resawn beams from 8 full-size beams of the same quality. In this case, the characteristic bending strength $f_{m,k}$ of the resawn glulam was 0.8N/mm² less and their mean elastic modulus 1000N/mm² less.

The authors showed that the mechanical properties loss of the resawn glulam can be related to the tensile strength of the outer laminations. Those results have conduct to the introduction in EN 14080 of different formulas (equation (1) and (2)) to compute the bending strength of resawn glulam.

$$f_{m,s,k} = f_{m,g,k} - \frac{96}{f_{t,0,l,k}-6} + 4 \left(in \frac{N}{mm^2}\right) for\ 1\ cut \quad (1)$$

$$f_{m,s,k} = f_{m,g,k} - \frac{96}{f_{t,0,l,k}-6} \left(in \frac{N}{mm^2}\right) for\ 2\ cuts \quad (2)$$

Where:

- $f_{(m,s,k)}$ is the characteristic bending strength of the resawn glulam;
- $f_{(m,g,k)}$ is the characteristic bending strength of the full-size glulam beam;
- $f_{(t,0,l,k)}$ is the characteristic tensile strength of the outer laminations.

The mean modulus of elasticity parallel to the grain $E_{0,s,mean}$ of the resawn glulam will be determined from the mean modulus of elasticity $E_{0,g,mean}$ of the full-size glulam from equation (3).

$$E_{0,s,mean} = E_{0,g,mean} - 500\ (in\ MPa) \quad (3)$$

To use those equations two requirements need to be fullfilled:

-the characteristic tensile strength of the laminations must be at least 18N/mm² and at most 30N/mm² and;

-the characteristic tensile strength of the inner laminations is not more than 8N/mm² lower than the characteristic tensile strength of the outer laminations.

These formulas come from tests on fullsize beams of 90mm width; the first objective of this study is to investigate the influence of the resawn on other widths. In addition, both conditions previously presented does not allow the application of these formulas for quality under GL28h, the second objective will be to quantify the influence on lower grades and more specifically the GL24h, which is commonly used in France. In a first time, destructive tests similar to the study presented above were conducted on beams of bigger sections. Then, considering that the grade attributed to a glulam beam is directly given by the mechanical grade of the lamellae, another approach based on the influence of resawn of lamellae has also been studied by destructive testing as well as using an analytical model of strength grading.

2. Destructive test on glulam

2.1. Material and methods

2.1.1. Sampling

The sample is composed of 64 specimens of spruce distributed equally between the different sections (170×400 for full-size and 80×400 for resawn) and quality (GL24h and GL28h). 24 full-size beams were made for each quality and within these beams 8 have been resawn. The different cross-sections and grades chosen should allow us to assess the influence of splitting on larger cross-sections and lower quality than those covered by EN 14080 formulas elaborated from the study presented in introduction.

2.1.2. Glulam destructive tests

All of those beams have been tested during a normalised four point bending test according to NF EN 408+A1. The global and local (E_l) moduli of elasticity in bending have been measured. Global modulus is calculated using two assumptions, the first by considering the shear modulus as infinite (E_g) and the second taking a shear modulus equal to 650 MPa (E_{gc}). The elastic modulus values were corrected to take into account the humidity of the beams and obtain the equivalent modulus at 12% moisture content, according to EN 384. Bending strength has also been measured and corrected by a scaling factor to obtain a value equivalent to 150×600 mm² cross-section beams according to EN 1194.

2.2. Results

The average values for the different elastic modulus measured and the bending strength are shown inTable 1.The loss observed on the average value of local modulus (E_l) is equal to 398 MPa for GL24h beams while it is about 532 MPa for GL28 one. The loss for E_g and E_{gc} are nearly the same, and the average values of those losses are respectively 666 and 243 MPa for GL24h and GL28h. Concerning the mean bending strength, a difference of 4 MPa is observed between the initial beam and the split one for GL24h beams. In the case of the GL28h beams, the trend is reversed and the average bending strength for split beams (39.9 MPa) is higher than for full-size beams (37.5 MPa). However, for the bending strength it is usually better to consider characteristic values.

Table 1 : Average values and coefficients of variation for different elastic modulus and bending strength

Designation	E_l (MPa)	COV (%)	E_g (MPa)	COV (%)	E_{gc} (MPa)	COV (%)	$f_{m,mean}$(MPa)	COV (%)
Beam 24	12663	9.9	11327	8.6	11935	9.0	37.1	17.1
Beam 24-R	12265	6.3	10690	4.9	11241	5.1	33.1	14.4
Beam 28	14038	7.3	12391	6.7	13114	7.1	37.5	15.1
Beam 28-R	13506	8.0	12152	6.4	12868	6.8	39.9	15.4

Table 2 shows the characteristics values of bending strength and density, calculated according to EN 14358.The differences between characteristic bending strength of the full-size beam and the resawn are different depending on the initial grade: a loss of 0.8 MPa for the GL24h and a gain of 1.2 MPa for the GL28h are observed. Concerning the density, there is no significant differences between initial and split beams.

Table 2 : Characteristic bending strength and density (5 % quantile)

Designation	$f_{m,k}$ (MPa)	ρ_k(kg.m^{-3})
Beam 24	25.3	439
Beam 24-R	24.5	441
Beam 28	27.0	460
Beam 28-R	28.2	466

2.3.Discussion

The fact that those results are not consistent with the recommendations of EN 14080 may highlight a lack concerning the influence of the initial beam cross-section.The proposed formulas were developed on beams whose cross-sections were about twice lower than those of the present study. Depending on the quality a loss or a gain is observed, and in both cases the difference between full-size beams and split beams property is low. A loss of 4 MPa is recommended by EN 14080 recommendations for GL28h beams nevertheless in this study there is no evidence of a loss, so that the influence of the resawning recommandations seems to be limited on beams with high cross-section. The influence of the resawning process should be higher on beams of lower quality following the logic proposed by EN 14080 formulas. This cannot be stated with our results, the loss on GL24h beams is only 0.8 MPa and even if in this case to the cross-section can be the cause of this result, it seems that the loss should be higher according to EN 14080. Concerning the local elastic modulus, a loss of 532 MPa and 398 MPa is observed experimentally respectively on GL28h and GL24h beams which is consistent with the loss of 500 MPa prescribed by the EN 14080 formula. Moreover, an Analysis Of Variance (ANOVA) has been made; the properties differences are not statistically significant between a full-size beam and a resawn beam (for density, modulus of elasticity and bending strength). Since these results do not allow us to conclude on the influence of the resawning process, the following method is proposed: investigate this influence on lamellae.

3. Destructive tests on lamellae

3.1. Material and methods

3.1.1. Sampling

Two initial cross-sections (45×214 and 45×174) and two qualities (C30 and C24) of spruce lamellae have been chosen. A total of 200 boards: 50 for each combination (25 full-size and 25 resawn) have been tested.

3.1.2. Destructive tests

Four points bending tests were performed according to NF EN 408+A1. Bending strength and global modulus of elasticity has been measured. Corrections have also been applied (k_h and k_l coefficient) according to EN 384.

3.2. Results

Mean and characteristics (according to EN 14358) values of density, global elastic modulus and bending strength are shown in Table 3. The actual grades based on destructive tests are lower than expected grades. The values of elastic modulus are responsible for this downgrading. Moreover, bending strength coefficients of variation are variable within each sublot. Some of them are higher than 30%.

Table 3 : Means, characteristic values (EN 14358), and coefficients of variation of density, modulus of elasticity and bending strength.

Expected grades	Designation	ρ_{mean} (kg.m^{-3})	ρ_k (kg.m^{-3})	COV (%)	$E_{0,mean}$ (MPa)	$E_{0,k}$ (MPa)	COV (%)	f_{mean} (MPa)	$f_{m,k}$ (MPa)	COV (%)	Observed grades
C24	45×214	457	385	8.4	8390	8138	21.5	37.4	16.8	29.2	C16
	45×214 R	439	380	7.1	8203	8012	17.1	36.2	25.7	15.4	C16
	45×174	435	375	7.4	7391	7148	24.1	43.5	16.2	33.3	C14
	45×174 R	462	393	7.9	10259	10058	14.7	49.7	30.2	20.9	C22
C30	45×214	500	444	5.9	10050	9857	14.1	46.7	38.2	9.7	C22
	45×214 R	489	440	5.3	9301	9092	16.8	47.8	19.6	31.4	C18
	45×174	502	443	6.1	10166	10017	10.8	54.1	39.8	14.0	C22
	45×174 R	509	440	7.2	9992	9786	15.4	54.3	38.3	15.7	C20

Table 4 shows the mechanical properties differences between full-size lamellae and resawn boards. Concerning the density the differences are very low. Regarding to the average elastic modulus, a decrease is found in 3 cases, however, a significant increase is observed in the case of C24 for a section of 45×174 mm². Finally, differences between bending strength of the four cases considered are highly variable with a maximum loss of 18.5 MPa for C30 lamellae with a cross-section of 45×214 and a maximum increase of 14 MPa for C24 lamellae with a cross-section of 45×174.

Table 4 : Differences of mechanical properties between full-size lamellae and resawn boards

		Mechanical properties differences					
Quality	Initial cross-section (mm²)	ρ_{mean} (kg.m^{-3})	ρ_k (kg.m^{-3})	$E_{0,mean}$ (MPa)	$E_{0,k}$ (MPa)	f_{mean} (MPa)	$f_{m,k}$ (MPa)
C24	45×214	-18.6	-4.5	-186.3	-125.7	-1.2	8.9
	45×174	26.7	18.8	2868.3	2909.4	6.3	14
C30	45×214	-10.8	-3.6	-749.4	-765.0	1.2	-18.5
	45×174	7.3	-3.3	-174.4	-230.8	0.2	-1.5

3.3.Discussion

These results show that it is experimentally difficult to characterize the influence of splitting on mechanical properties of lamellae. Indeed, strength grading timber and its statistical nature can lead to high variability on small numbers of boards; particularly the 5% percentile can be very influenced by the presence of one or two pieces of lower quality. This is the case for the sublot of C24 lamellae with a cross-section equals to 45×174, two boards bending strength are lower than 18 MPa, and those two values greatly affect the 5% percentile of bending strength. In the case of non-split batch of lamellae, it would be tempting to remove these boards in order to be in a situation where the actual grade obtained by destructive tests matches the expected quality, but this approach is not appropriate for batch composed of resawn lamellae since the lowest quality timber may be due to the splitting process.For obvious reasons it is not possible to destructively test the actual resawn board and due to the variability of the mechanical properties of wood it can be problematic. Furthermore, the variability of the studied batch is representative given that all boards come from the same sawmill supplied in a local way. The case on timber quality C24 for an initial cross-section of 75×214 mm² is symptomatic of this problem; the mechanical properties of full-size lamella are much lower than the split lamella and it becomes difficult to compare these two populations and it is also difficult to state a definitive rule. Furthermore, as previously an Analysis Of Variance (ANOVA) has been made; the properties differences are also not statistically significant between full-size lamellae and resawn lamellae (for density, modulus of elasticity and bending strength).That is why the next section proposes to address this problem numerically using an analytical model.

4. Numerical resawning of lamellae

4.1.Material and methods

4.1.1. Sampling and destructive tests

In this part, the sample is composed of 437 pieces of Spruce from French forest. Three different sections have been chosen: 40×100 mm², 50×150mm² and 65×200mm², the total is equally split between the three sections. The length of all boards is about 4m. Four points bending tests were performed with the same method as previously on full-size lamellae.

4.1.2. Non-destructive tests on lamellae

All boards were passed through a scanner dedicated to mechanical grading (CombiScan+) to obtain different local informations:

- Local density: the scanner is equipped with an X-Rays imaging system. Assuming that the grey levels of thereby provided images are proportional to the acquired corresponding light intensities, they can easily and accurately be converted into local densities maps. Under this condition, the Beer-Lambert’s law can be applied to determine the density for each pixel of the densities maps.

- Local nodosity: Knot Depth Ratio (KDR) is determined with the use of X-Ray Scanning (Oh *et al.,* 2009). This value represents the local knot thickness divided by the board one. This method is based on the fact that in softwood the density of knots and clear wood are highly different (around 450 kg.m^{-3} for clear wood and 1000 kg.m-^{3} for knot).This index is equal 0 in clear wood and 100% when at a given position the thickness of the board is composed entirely of knot. It varies linearly between 0 and 100%.

- Slope of Grain (SoG): The slope of grain is measured using the tracheid’s effect, by projecting a laser’s line on the surface of the boards (Simonaho*et al.,* 2004).The pattern formed by the laser dot on the surface is elliptic. The ellipse's main axis is oriented in the same direction as the slope of grain. It's possible to have the evolution of slope of grain in the entire board surface by projecting the laser's line along the board.

An example of these measures on a board is shown in Figure 1.

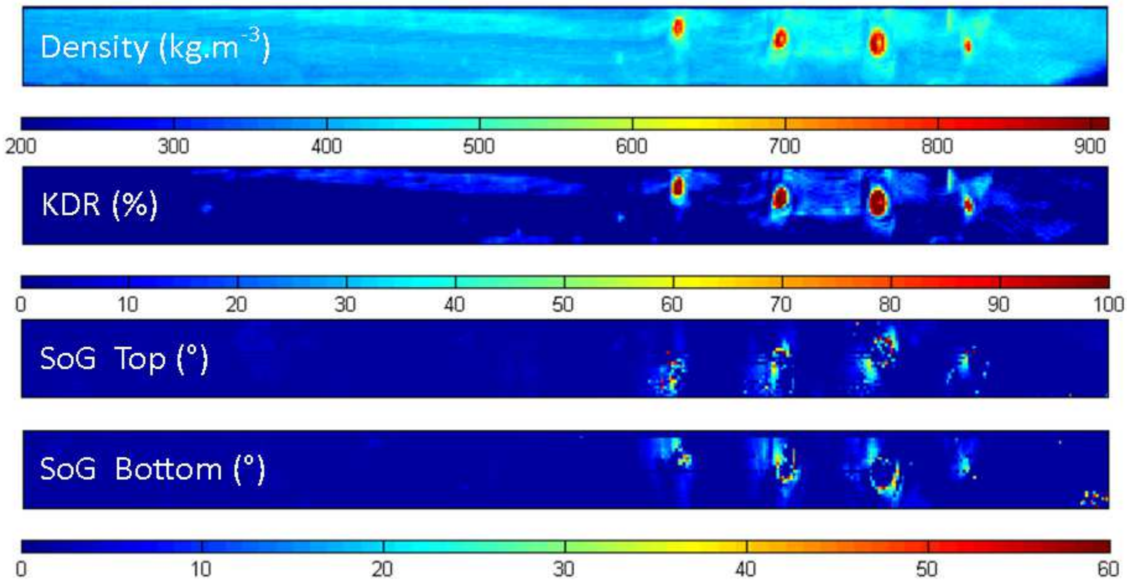

Figure 1: Local data from the scanner. From top to bottom: density map, Knot Depth Ratio and maps of slope of grain for top and bottom face of the board.

4.1.3. Analytical model

The model used to estimate elastic modulus and bending strength uses the different informations presented above. It is based on the definition of a board mechanically equivalent to the actual board where local mechanical properties variations due to singularities is taken into account by virtually reducing the thickness, the equivalent board thus obtained has therefore a variable inertia along its length. Local thickness is given by equation (4).

$$T(x,y) = [1 - KDR(x,y)] \, . \, \frac{H[\theta_{top}(x,y)] + H[\theta_{bot}(x,y)]}{2} \quad (4)$$

Where:

- T(x,y) is the local thickness of the equivalent board
- θ_{top} and θ_{bot} are the values of slope of grain measured respectively on top and bottom faces
- H(θ) is a function giving the reduction factor of a mechanical property based on slope of grain value

The H(θ) function is based on the Hankinson formula (equation (5)).

$$H(\theta) = \frac{X(\theta)}{X(\theta)} = \frac{k}{sin^n(\theta) + k.cos^n(\theta)} (5)$$

With :

- k is a constant depending of the material ($0.04<k<0.1$)
- n is a constant depending of the mechanical property ($1.5<n<2$)
- θ is the slope of grain

The local elastic modulus of the board is then determined using equation (6)

$$E_p(x) = max\begin{cases}[1 - KDR(x)]^p . E_{cw} \\ E_{min}\end{cases} \quad (6)$$

Where :

- p is a constant defined to take into account the non-linear influence of the knots
- E_{min} is the threshold of modulus of elasticity
- E_{cw} is the clearwood's modulus of elasticity based on an affix function (Guitard, 1987)

From the geometry and mechanical properties throughout the equivalent board it is then possible to calculate the deformation for a given load and therefore determine the elastic modulus of the actual board. The failure occurs when the weaker section is subject to the maximum bending moment ($M_b(x)$). Based on the assumption of the equivalence, bending strength of the actual board ($\sigma_b(x)$) can be determined by the equation (7), where I_b and $I_p(x)$ are respectively the moment of inertia of the equivalent and actual board. $Y_{NF}(x)$ is the local position of the neutral fiber and h the height of the board.

$$M_b(x) = \frac{\sigma_p . I_p(x)}{max\{y - y_{NF}(x), y_{NF}(x)\}} = \frac{\sigma_b(x) . I_b}{h/2} \quad (7)$$

4.1.4. Numerical splitting

At first, the different model parameters are optimized to obtain the best correlation (in practice the greatest coefficient of determination) between the values predicted by the model and results from destructive tests. This optimization is done on full-size boards (since destructive results are only available for full-size boards). Since the inputs of the model are images, it is possible to create boards really issued from the full-size beam and using those halves (or third) images as the new inputs of the model and then compare the predicted mechanical properties. The fact that it is possible to numerically split the boards presents a great advantage compared to the experimental methods described previously. An example of a double cut is shown in Figure 2.

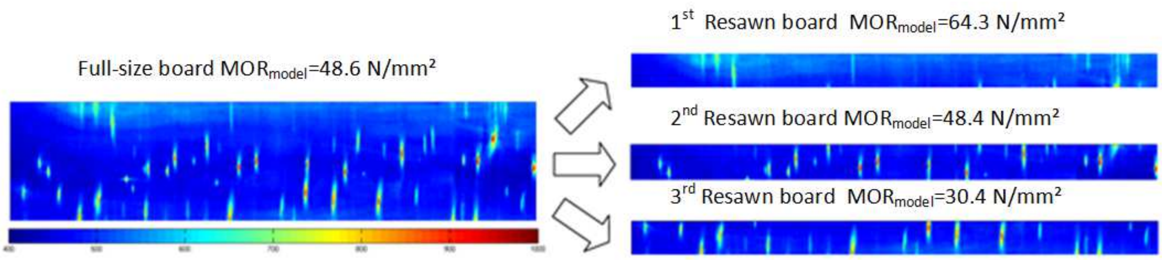

Figure 2: Numerical resawning; predicted bending strength for the full-size board and the three resawn boards.

Finally, the following data are available: density, modulus of elasticity and bending strength of the full-size board, for both boards from single cut and for the three boards from double cut.

Different groups of boards have been made depending on their characteristic bending strength corresponding to C40, C35, C30 and C24. Moreover, boards with a 40×100 mm² cross-section have been removed for the double cut in order to stay in the EN 14080 recommendations. In addition, to assess the influence of the initial height, sublots were made by grade within the different initial cross-section available. Those sublots are described in Table 5.

Table 5: Details for grades sublot for each initial cross-section; number of boards and characteristic bending strength

Grade	Single cut								Double cut					
	40×100		50×150		65×200		All cross-sections		50×150		65×200		All cross-sections	
	N	$f_{m,k}$ (MPa)	N	$f_{m,k}$ (MPa)	N	$f_{m,k}$ (MPa)	N	$f_{m,k}$ (MPa)	N	$f_{m,k}$ (MPa)	N	$f_{m,k}$ (MPa)	N	$f_{m,k}$ (MPa)
C40	44	40.14	42	40.08	5	42.25	91	40.23	42	40.21	5	42.36	47	40.30
C35	76	35.03	63	35.03	20	35.04	159	35.00	63	35.18	20	35.19	86	35.18
C30	59	30.18	47	30.10	47	30.11	155	30.02	47	30.00	47	30.12	100	30.05
C24	52	24.56	68	24.05	75	24.21	196	24.11	68	24.27	75	24.04	144	24.20

The influence of 1 or 2 cut on the characteristic bending strength of the virtual resawned boards is then evaluated. From these results, a mechanical grade is assigned to the resawn lamellae and the quality of glulam which can be manufactured from those lamellae is determined.Table 6 gives the equivalencies between GL beams grade and lamellae grade used to manufacture GL beams and the characteristic bending strength of a resawn GL beam calculated from the formulas of EN 14080.

Table 6: Equivalencies between GL beams grade and lamellae grade and characteristics bending strength of the resawn GL beam calculated from the formulas of EN 14080.

Grade GL	Grade lamella (EN338/EN14080)	$f_{m,g,k}$ (MPa)	$f_{m,s,k}$(MPa)for 1cut	$f_{m,s,k}$(MPa) for 2cut
GL20h	C18/T11	20	Determined from declared properties of the lamination	
GL22h	C22/T13	22		
GL24h	C24/T14	24		
GL26h	C27/T16	26		
GL28h	C30/T18	28	24	20
GL30h	C35/T21	30	27.6	23.6
GL32h	C40/T24	32	30.7	26.7

4.2.Results

4.2.1. Analytical model

Figure 3 shows the modulus of elasticity and bending strength obtained experimentally depending on modulus of elasticity and bending strength estimated from the model of the full-size lamellae. The model estimates the bending strength with a coefficient of determination R^2 equal to 0.67 and the modulus of elasticity with a coefficient of determination R^2 equal to 0.75.

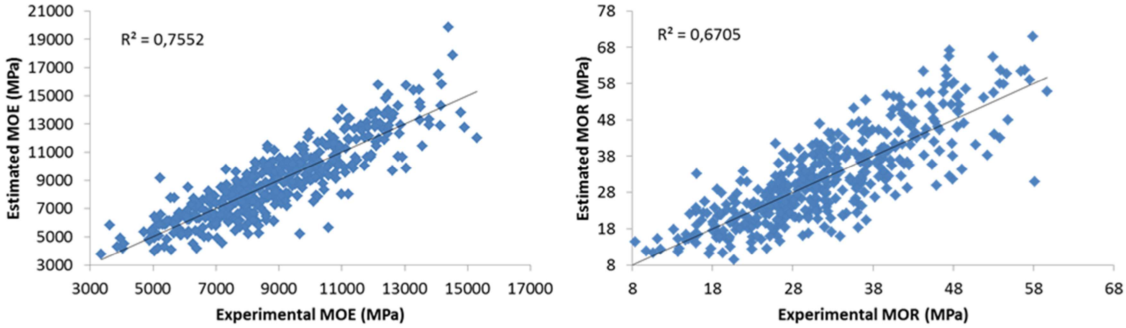

Figure 3: Estimated properties depending on measured properties for full-size lamellae.

4.2.2. Influence of the resawn process without consideration of initial height

The characteristic bending strength for the sublot obtained by resawning numerically the full-size lamellae is described Table 7. In the case of single cut two virtual boards are created, the characteristic bending strength for resawn lamellae is taken as the mean of the 5% percentile of each sublot. The same method is applied for double cut.Resawn process always leads to a decrease of the characteristic bending strength; this decrease is higher for a double cut than for single cut.

Table 7: Influence of single and double cut for four different grades

	Single cut				Double cut				
	Full-size	1st cut	2nd cut	Mean	Full-size	1st cut	2nd cut	3rd cut	Mean
C40	40.23	32.83	33.44	33.14	40.30	29.89	30.76	29.93	30.19
C35	35.00	28.31	27.93	28.12	35.18	24.75	23.25	21.76	23.25
C30	30.02	24.63	23.96	24.30	30.05	18.58	20.81	17.56	18.99
C24	24.11	18.86	18.57	18.71	24.20	13.30	16.62	11.14	13.69

From these previous results it is now possible to determine the GL beams grade manufacturable from resawn lamellae according to EN 14080. Table 8 compares this grade to the EN 14080 recommendations.

Table 8: GL beams grades manufacturable from resawn (1 or 2 cuts) lamellae compared to EN 14080 recommendations

	Single cut				Double cut			
Initial grades	1 cut 5% percentile	Grade 1 cut	Grade GLs	EN 14080	2 cuts 5% percentile	Grade 2 cuts	Grade GLs	EN 14080
GL32h/C40	33.14	C30	GL28s	GL30s	30.19	C30	GL28s	GL26s
GL30h/C35	28.12	C27	GL26s	GL26s	23.25	C22	GL22s	GL22s
GL28h/C30	24.30	C24	GL24s	GL24s	18.99	C18	GL20s	GL20s
GL24h/C24	18.71	C18	GL20s	None	13.69	Waste	Waste	None

4.2.3. Influence of initial height on the resawn process

Basis on the results of the first part of this study, it has been decided to assess the influence of the initial cross-section on the resawning process. Different sublots have been made by grade and initial cross-section. The mean characteristic bending strength of the resawn lamellae for these sublots is given Table 9. The number of boards in each sublot is indicated in bracket, sublot with less than 20 boards have been removed from the analysis since the 5% percentile is not really representative on those cases.

Table 9: Characteristic bending strength for single and double cut depending of the initial cross-section. Number of boards in each sublot is indicated in brackets, red values have been removed from the analysis.

	Single cut			Double cut	
	40×100	50×150	65×200	50×150	65×200
C40	32.89 (44)	33.91 (42)	37.44 (5)	29.21 (42)	32.03 (5)
C35	27.45 (76)	28.87 (63)	27.92 (20)	23.33 (63)	23.61 (20)
C30	22.89 (59)	24.52 (47)	26.16 (47)	17.54 (47)	21.05 (47)
C24	16.85 (52)	18.86 (68)	20.98 (75)	12.52 (68)	15.52 (75)

Figure 4 shows the difference between the characteristic bending strength of full-size lamellae and the ones issued from a single or double cut based on the initial cross-section.

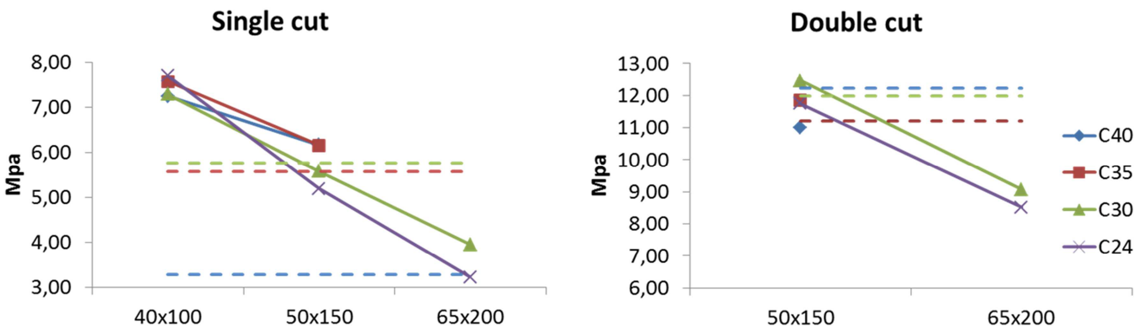

Figure 4: Difference between the characteristic bending strength of full-size lamellas and the ones from single or double cut. (Dashed lines: standards recommendations)

4.3. Discussion

The results of the first part are consistent with the recommendations of EN 14080, as only two cases did not lead to the same class of glulam. One of these cases is worse compared to the standard: the single resawn of C40 lamella (corresponding to GL32h) gives C30 lamella and allows manufacturing only GL28s although the standard formulas recommend to downgrade the beam to GL30s. However, in this example, the characteristic bending strength is equal to 33.14 MPa, which is close to C35 grade that would remain consistent with the standard. The other case seems to show that the standard is too unfavourable in the case of a double cut of a GL32h beam. The double cut on high grade glulam beams seems to have a smaller influence which can be explained by a smaller knots proportion on higher grade beams. Finally, in the second part the influence of the initial cross-section has been investigated. It clearly seems that the resawning process has a fewer influence on beam with a high initial cross-section. For a 40×100 mm² cross-section the bending strength loss due to a single cut is arround 7 MPa while it's only about 3 MPa for beams with 65×200 mm² cross-sections. The same observation can be made in the case of double cut; the loss is around 12 MPa for 50×150 mm² beams while it's only about 9 MPa for 65×200 mm² cross-sections. The Analys Of Variance shows that the bending strength differences are very significant and that the modulus of elasticity differences are not significant. This last statement on the modulus of elasticity is consistent with the conclusion of the second experimental campaign (Crocetti, 2009) since there are no reasons to believe that splitting can cause a significant reduction of MOE. On the basis of the results obtained in this study, the following recommendations are suggested:

- The characteristic bending strength of a split lamella ($f_{m,k,s}$) can be calculated by:

$f_{m,k,s} = f_{m,k} - 11 + \frac{h}{27}$ for 1cut

$f_{m,k,s} = f_{m,k} - 11 + \frac{h}{27} - 6$ for 2 cuts

The comparison between results obtained by the analytical model and by these formulas is given in Figure 5.

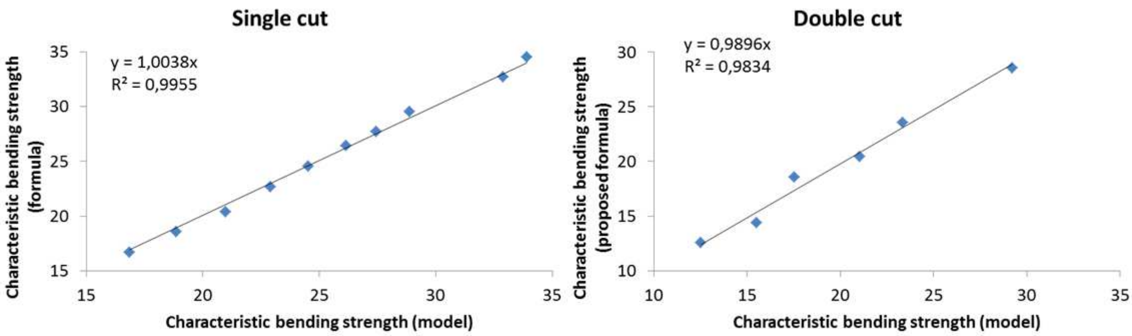

Figure 5: Comparison between results obtained by the analytical model and the formulas proposed

The grade of a glulam beam may then be deduced from these values.

5. Conclusion

The first part of the study shows that formulas of EN 14080 do not seem to apply for the cross-sections studied (higher cross-sections). Indeed, in the case of GL28, no loss was observed on the bending strength and for the GL24 the loss was very low compared to the expected values from the formulas. The second part has shown the difficulty to characterize experimentally the influence of resawning on lamellas due to the natural variability of wood and grading problem. The third part has shown a numerical approach to characterize this influence and the results seem to be consistent with the formulas of EN 14080, for both single and double resawn. Furthermore, the method proposed investigates the influence of the resawning process of lower grade glulam beams. The influence of the full-size product initial cross-section has been highlighted and a formula to calculate the bending strength of a resawn lamella has been proposed and can be used to determine the grade of a resawn glulam beam. Finally, it has been stated that the modulus of elasticity of a resawn product should not be different from the initial full-size product. A finite element model will be used in the future to characterize the mechanical behaviour of a glulam beam with lamination with mechanical properties of virtually resawn boards.

Acknowledgement

This study is supported by an ANR project (CLAMEB) for the numerical resawn part. Our gratefulness also goes to the attention of CODIFAB for funding tests and this meeting.

References

EN 14080.*: Timber Structures - Glued Laminated Timber and Glued Solid Timber - Requirements*, 2013.

EN 14358.*Timber Structures - Calculation of Characteristic 5-Percentile and Mean Values for the Purpose of Initial Type Testing and Factory Production Control*, 2007.

EN 338.*Structural Timber - Strength Classes*, 2009.

EN 384.*Structural Timber - Determination of Characteristic Values of Mechanical Properties and Density*, 2010.

EN 408.*: Structural Timber and Glued Laminated Timber - Determination of Some Physical and Mechanical Properties*, 2012.

Guitard, D. *Mécanique Du Matériau Bois et Composites*. CEPADUES.NABLA, 1987.

Jehl, Arnaud, Laurent Bléron, FabriceMeriaudeau, and Robert Collet."Contribution of Slope of Grain Information in Lumber Strength Grading," 2011.

Oh, Jung-Kwon, Kugbo Shim, Kwang-Mo Kim, and Jun-Jae Lee. "Quantification of Knots in Dimension Lumber Using a Single-Pass X-Ray Radiation."*Journal of Wood Science* 55, no. 4 (August 2009): 264–272. doi:10.1007/s10086-009-1031-7.

Riberholt, Hilmer, and Roberto Crocetti.*Bending Strength and Stiffness of Split Glulam Beams*.SP Technical Research Institute of Sweden, 2009.

Roberto Crocetti. *Stength of split glulam beams.* SP Technical Research Institude of Sweden, 2009

Simonaho, SP, J Palviainen, Y Tolonen, and R Silvennoinen."Determination of Wood Grain Direction from Laser Light Scattering Pattern."*Optics and Lasers in Engineering* 41, no. 1 (January 2004): 95–103. doi:10.1016/S0143-8166(02)00144-6.

INTER

International Network on Timber Engineering Research

COMPRESSION STRENGTH AND STIFFNESS PERPENDICULAR TO THE GRAIN – INFLUENCES OF THE MATERIAL PROPERTIES, THE LOADING SITUATION AND THE GAUGE LENGTH

C Le Levé

R Maderebner

M Flach

University of Innsbruck, Department of Engineering Science, Institute for Structural Engineering and Material Science, Unit for Timber Engineering

AUSTRIA

Presented by C Le Levé

D Brandon commented that the side movement of the specimens were observed; the fixity of the top and bottom plates could affect the results. WS Loo also commented on the load head actuator fixity. C Le Levé agreed that it is possible that the fixity could influence results.

R Görlacher stated that MOE values should not depend on loading situation. As the stresses in the specimens are not uniform; therefore, differences in stiffness were observed. As such one should consider referencing the stiffness rather than MOE.

S. Franke said that influence of annual ring was reported. He asked how you would propose to handle this in codes. C Le Levé responded that in the test standard one should specify annual ring orientation. S Franke further commented that if the test set up was modified, one would get the EN results. P Dietsch added that it is important to talk about issues related to test standard.

F Lam commented that there are too many conclusions from this paper. The author should focus on only a few most relevant points.

S Svensson commented about clear wood testing. He asked can reaction wood be ignored and why not look into representative sample rather than clear wood.

JW van de Kuilen commented that Eurocode is considering removal of density and lowering compression strength perpendicular to grain values. He commented that slide 6 showed local failure only and asked why care about the area underneath the failure zone.

H Blass added that the consequence of failure is excessive deformation; code design rules included consideration of low consequence of failure.

Compression strength and stiffness perpendicular to the grain – Influences of the material properties, the loading situation and the gauge length

Clemens Le Levé, Roland Maderebner, Michael Flach

University of Innsbruck, Department of Engineering Science, Institute for Structural Engineering and Material Science, Unit for Timber Engineering, Austria

Keywords: compression strength, stiffness, modulus of elasticity, perpendicular to the grain, supporting effect, gauge length, Videoextensometer, type of loading situation, annual ring direction, spruce wood.

Abstract

In recent years, many inconsistencies concerning the compression perpendicular to the grain have shown up. Due to the change in the concept of security the characteristic strength values were introduced to replace the permissible stresses. The design rules and their factors were reformed several times as well. These developments have led to large differences in design results of compression strength perpendicular to the grain. For this reason, investigations of the compression perpendicular to the grain are carried out in the laboratory of the University of Innsbruck. Different influences of the material properties of spruce wood as density, annual ring direction, mean width of annual rings and the supporting effect of wood grain are analysed and also other parameters as the gauge length. The results of those investigations are compared with design rules of different standards and other research projects. And it is shown that the current standards do not correctly reflect the material behaviour under compression perpendicular to the grain. Especially the large influence of the annual ring direction in the testing configuration acc. to EN 408:2012 [1] has to be taken into account.

1 Introduction

The focus of this work is on the compression perpendicular to the grain of spruce wood. This type of loading situation occurs in many joints. Especially in multi-storey buildings the high stresses perpendicular to the grain lead to relatively large deformations. To get realistic design rules it is necessary to have accurate strength and stiffness values and also a design method which covers different loading situations. In this work appropriate investigations are carried out and the results are compared with design rules of different standards and existing literature [2-5, 11-19]. Additionally the evolution and the differences of the specific design rules and their compression strength values and factors as the $k_{c,90}$-factor or the enlarged loaded area will be discussed.

The influences of density, the average width and the angle of annual rings as well as the gauge length h_0 and the supporting effect of wood grain beside the loaded area are carefully examined and their influences on the mechanical properties of spruce wood for compression perpendicular to the grain are analysed.

2 Laboratory Tests

The investigations are carried out in the laboratory of the University of Innsbruck with the universal testing machine Autograph AG-G 100 kN.

2.1 Material

The used spruce wood (Picea abies) comes from Austria. The specimens are cut and planed after being conditioned by a constant temperature of (20 ± 2) °C and relative humidity of (65 ± 5) % according to ÖNORM EN 408:2012 [1]. For the investigations specimens of clear wood are used. Their annual ring direction varies, so their influence can be researched. For each specimen the average width of the annual rings acc. to ÖNORM DIN 4074 1:2012, the annual ring direction, the wood moisture content, the gross density and the oven dry density are determined according to ÖNORM EN 13183-1:2004 and ÖNORM EN 13183-2:2002 [6-8].

2.2 Types of loading situations

The large influence of the supporting effect of wood grain beside the loaded area on the material properties perpendicular to the grain are considered in different ways in the selected standards. Therefore four types of loading situations, as shown in figure 1, are carried out. To obtain statistically reliable results at least 40 specimens of each loading situation are tested. For comparability reasons the cross section dimensions are the same for every type with 45 mm × 90 mm acc. to ÖNORM EN 408:2012 [1]. The specimen length varies depending on the type of loading situation but the unloaded end on one side remains constant with 230 mm (except for type 1). The loading area for each type is identical with 45 mm × 70 mm.

The type of loading situation 1 corresponds to the experimental setup as given in ÖNORM EN 408:2012 [1] and serves as reference. Types 2, 3 and 4 represent border cases which are determined by the different design rules of selected standards. In type 2 the loading area is at the beam end so the supporting effect of wood grain is given only on one side. In type 3 the length of the unloaded beam end is about 30 mm and corresponds to the border case of the actual code ÖNORM EN 1995-1-1:2009 [2], defining that the loaded area can be enlarged up to 30 mm on each side parallel to the grain direction. The length of the unloaded beam end of type 4 is 100 mm and reflects the design models of previous codes and the Swiss code SIA 265:2012 [11].

To get the right feed rate as defined in ÖNORM EN 408:2012 [1] of each type of loading situation preliminary investigations are conducted. The feed rate must be chosen that the maximum load $F_{c,90,max}$ is reached in (300 ± 120) seconds. So the preliminary investigations lead to feed rates between 0,5 and 1,0 mm/min (type 1 and 4). The feed rates of type 2 and 3 are 0,6 respectively 0,7 mm/min. Already here the large influence of the supporting effect of wood grain beside the loaded area is affirmed.

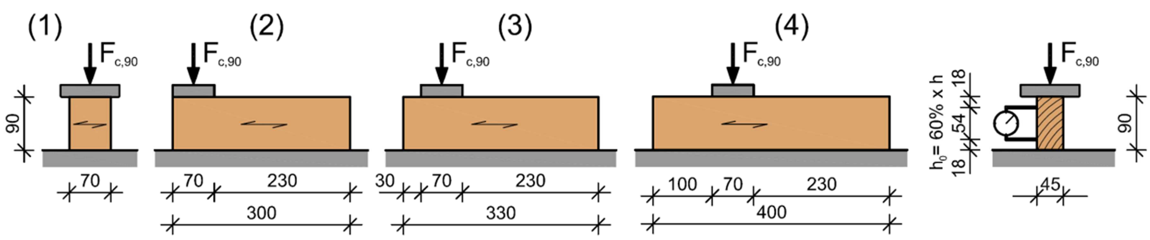

Figure 1: *Different types of loading situations*

2.3 Measurement of deformation

According to ÖNORM EN 408:2012 [1] the gauge length h_0 shall be 60 % of the specimen depth. Often tests in literature only consider the deformations over the complete specimen depth [14, 15]. Therefore, the deformations are recorded and analysed for both, the gauge length h_0 and the entire specimen depth h and their influence is determined. The feed rate of the machine indicates the deformations about the whole specimen depth and the gauge length h_0 are measured with the Videoextensometer (fig. 2). As shown in figure 3 the supporting effect of wood grain will lead to large differences between the results of both measurments methods because the main deformations will appear next to the contact area. Only the deformations of fully loaded cuboids (type 1) are more or less spread over the whole specimen depth depending on the annual ring direction and the gauge length has less influence on the results.

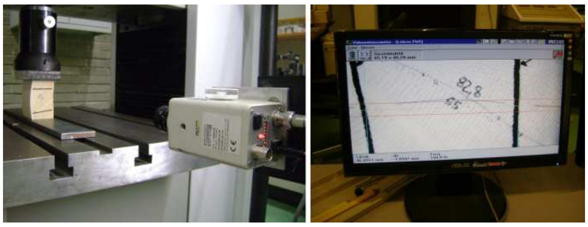

Figure 2: *Measurement of deformations with the Videoextensometer*

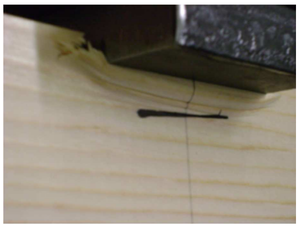

Figure 3: *Detail of deformations close to the loaded area (type 4)*

3 Test results

3.1 Compression strength and stiffness perpendicular to the grain

The determination of the strength and stiffness values perpendicular to the grain are executed as defined in ÖNORM EN 408:2012 [1]. Figure 4 shows exemplary for each type of laoding situation a stress-strain-diagram with the calculated gradient. The big discrepancies between the individual types of loading situations and the influence of the gauge length are obvious. So the strength and stiffness values increase with the length of unloaded beam end. The red lines corresponds to the results with the gauge length h_0 = 90 mm and the blue line to the results with the gauge length h_0 = 54 mm. As explained in chapter 2.3 and figure 7 the gauge length has no big influence on the test results of type 1 but with an increasing length of unloaded beam end (type 2 – 4) and a gauge length of h_0 = 54 mm the test results are clearly higher.

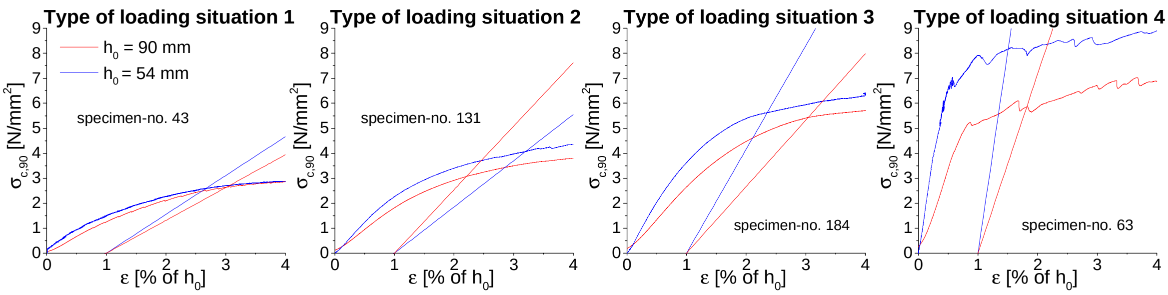

Figure 4: *Determination of strength and stiffness values acc. to EN 408:2012 [1]*

3.2 Statistical evaluation

The statistical evaluation is illustrated in table 1 and figure 5 and shows the results and the distribution of all tests. The characteristic values are calculated acc. to ÖNORM EN 384:2010 [9].

Table 1: *Test results*

		mean values	CoV	Min	Max	charact. values
type 1 (48 specimens)	density [kg/m³]	425,5	0,10	331,9	494,2	**360,2**
	mean width of annual rings [mm]	1,9	0,38	1,0	4,8	
	annual ring direction [°]	43,6	0,38	21,0	72,0	
	$f_{c,90\text{-Weg}}$ [N/mm²]	2,51	0,11	1,49	3,22	**2,17**
	$E_{c,90\text{-Weg}}$ [N/mm²]	**151,9**	0,29	75,8	265,2	108,4
	$f_{c,90\text{-Video}}$ [N/mm²]	2,41	0,11	1,40	3,07	**2,05**
	$E_{c,90\text{-Video}}$ [N/mm²]	**158,3**	0,37	70,0	349,2	102,4
type 2 (42 specimens)	density [kg/m³]	430,7	0,10	329,5	525,9	**371,1**
	mean width of annual rings [mm]	2,7	0,52	1,2	8,9	
	annual ring direction [°]	33,2	0,41	8,5	70,0	
	$f_{c,90\text{-Weg}}$ [N/mm²]	3,76	0,16	2,29	5,82	**3,07**
	$E_{c,90\text{-Weg}}$ [N/mm²]	**208,6**	0,24	116,2	367,4	154,4
	$f_{c,90\text{-Video}}$ [N/mm²]	4,03	0,17	2,31	6,42	**3,10**
	$E_{c,90\text{-Video}}$ [N/mm²]	**292,1**	0,37	151,3	741,5	172,4
type 3 (43 specimens)	density [kg/m³]	428,6	0,08	351,4	497,0	**382,1**
	mean width of annual rings [mm]	2,5	0,50	1,0	2,9	
	annual ring direction [°]	36,3	0,44	15,5	77,0	
	$f_{c,90\text{-Weg}}$ [N/mm²]	4,90	0,14	3,28	6,57	**3,82**
	$E_{c,90\text{-Weg}}$ [N/mm²]	**269,1**	0,18	165,3	393,9	205,7
	$f_{c,90\text{-Video}}$ [N/mm²]	5,29	0,14	3,25	7,20	**4,20**
	$E_{c,90\text{-Video}}$ [N/mm²]	**432,8**	0,52	261,3	1301,9	280,7
type 4 (42 specimens)	density [kg/m³]	433,5	0,10	350,8	501,8	**365,2**
	mean width of annual rings [mm]	2,3	0,51	1,0	7,2	
	annual ring direction [°]	33,3	0,49	0,0	80,0	
	$f_{c,90\text{-Weg}}$ [N/mm²]	5,32	0,24	3,37	10,27	**3,72**
	$E_{c,90\text{-Weg}}$ [N/mm²]	**329,5**	0,27	199,9	716,2	258,2
	$f_{c,90\text{-Video}}$ [N/mm²]	6,36	0,21	3,98	10,07	**4,62**
	$E_{c,90\text{-Video}}$ [N/mm²]	**501,0**	0,43	274,1	1614,4	344,4

The Box-Plots in figure 5 displays the test results of the compression strength and the modulus of elasticity perpendicular to the grain. The red symbols are the results with the gauge length over the whole specimen depth and the blue over 60 %. It is obvious that with a longer length of unloaded beam end the Coefficient of Variation (CoV) and the number of outlier increases. The outliers are all considered in the statistical evaluation because the annual ring direction is one reason for it, as described later on.

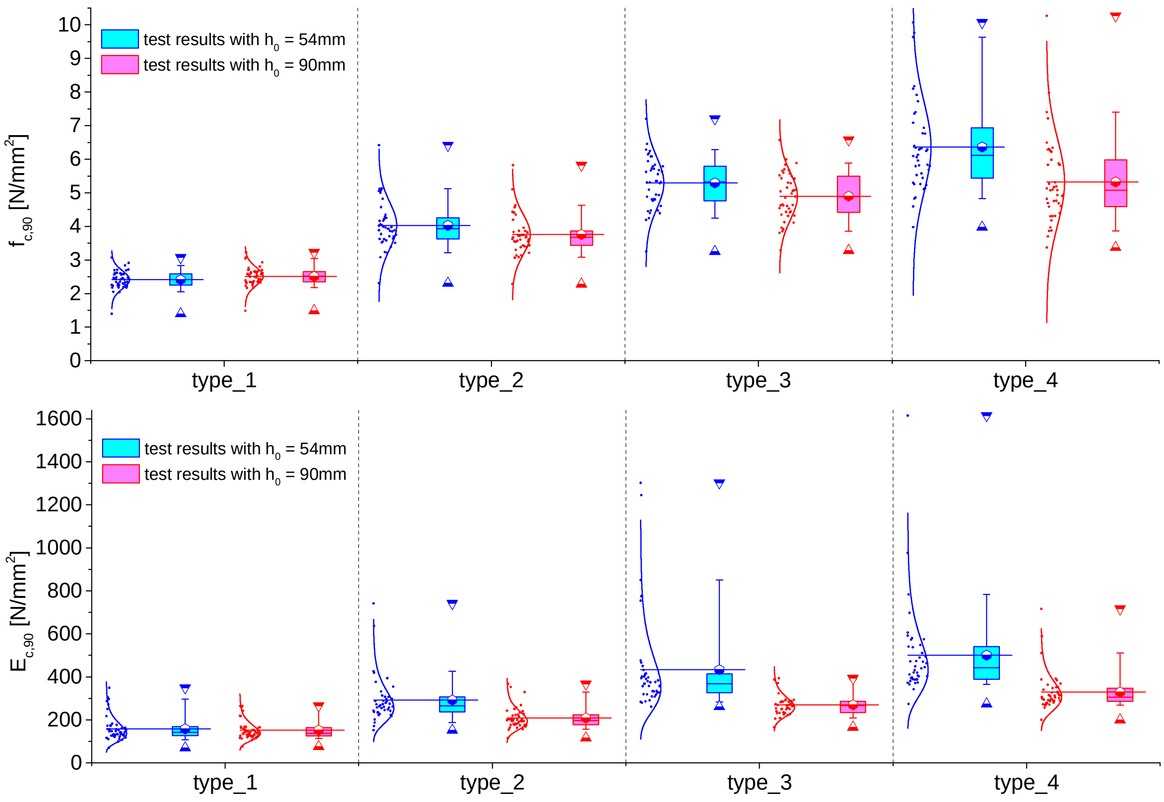

Figure 5: *Box-Plots with the results of the strength and stiffness values perpendicular to the grain*

The Box-Plot shows also the big influence of the supporting effect of wood grain on the results of the modulus of elasticity which is not considered in actual codes. The mean value of type 4 is 2,2 times respectively 3,2 times higher than the values of type 1 (depending on the gauge length). The influence of the gauge length is 4 % in type 1, 40 % in type 2, 61 % in type 3 and 34 % in type 4 in contrast to the results with h_0 = 90 mm . The influence of the gauge length is also important for the characteristic strength values with 10 % in type 3 and 24 % in type 4.

The mean value of the density ρ_{mean} of all specimens is between 425,5 und 433,5 kg/m³ and is higher than the given density ρ_{mean} = 420 kg/m³ acc. to EN 338:2009 [3] of the strength grade C24. Also the characteristic density value ρ_k which is between 360,2 and 382,7 kg/m³ is higher than in [3] with ρ_k = 350 kg/m³ for C24. In addition the sort criterion acc. to ÖNORM DIN 4074-1:2012 [6] are respected. Because of that the test results can be compared with the values of C24 respectively S10 in [3].

Figure 6 describes the relations between the density and the compression strength respectively the modulus of elasticity perpendicular to the grain. In ÖNORM EN 338:2009 [3] the compression strength perpendicular to the grain only depends on the density acc. to the equation 1 and can be enlarged in certain cases with a $k_{c,90}$ factor given in ÖNORM EN 1995 1-1:2009 [2] and an enlarged contact area. So the green line in figure 6 and type 1 can be calculated with equation 1:

$$f_{c,90}(\rho) = 0{,}007 \cdot \rho \qquad (1)$$

The green line of type 2 also considers the factor $k_{c,90}$ = 1,25 (for solid softwood timber) and the enlarged contact area acc. to equation 2:

$$f_{c,90}(\rho) = 0{,}007 \cdot \rho \cdot k_{c,90} \cdot A_{ef} / A_{real} = 0{,}0125 \cdot \rho \qquad (2)$$

The green line in type 3 and 4 is calculated as given in equation 3:

$$f_{c,90}(\rho) = 0{,}007 \cdot \rho \cdot k_{c,90} \cdot A_{ef} / A_{real} = 0{,}0143 \cdot \rho \qquad (3)$$

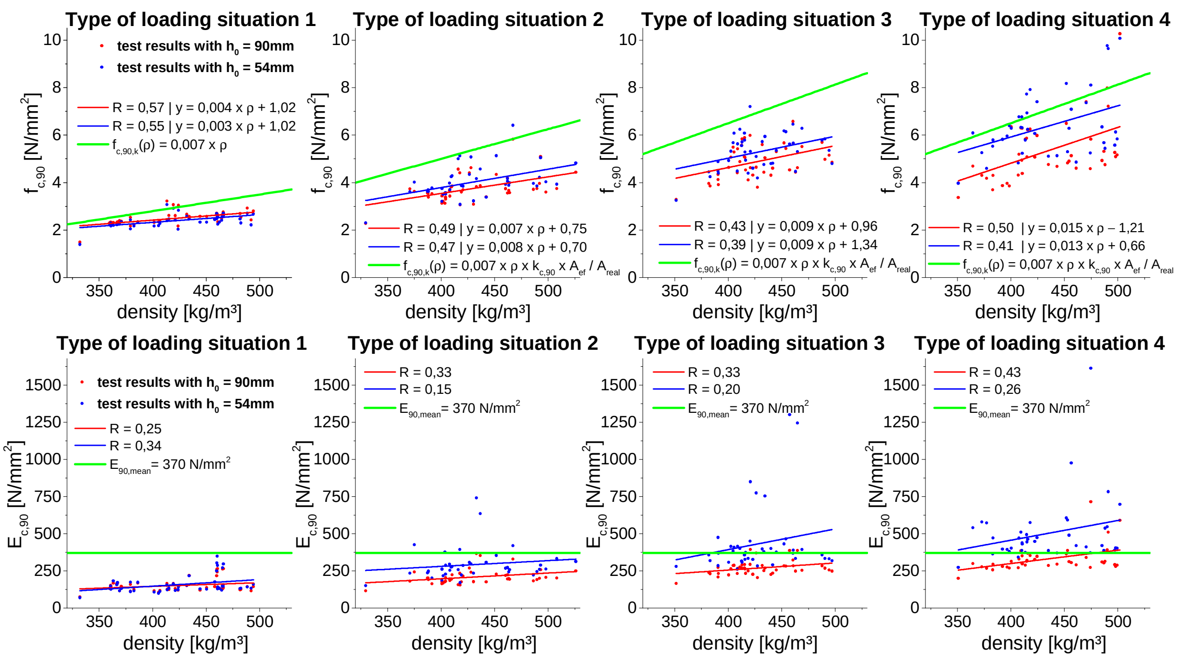

Figure 6: *Correlation between the density and the strength resp. stiffness values perp. to the grain*

The relation between the compression strength and the density of the test results is given with correlation factors up to R = 0,6. However, the gradient is smaller than given in ÖNORM EN 338:2009 and ÖNORM EN 1995-1-1:2009 [2, 3]. The regression lines in type 1 has gradients of 0,003 (resp. 0,004) and an intercept of 1,02 instead of a gradient of 0,007. The fact that almost all test results of all types of loading situations are under these green lines should be seriously considered and discussed because it is on the unsecure side.

The horizontal lines in figure 6 symbolize the constant $E_{90,mean}$ value with 370 N/mm² acc. to ÖNORM EN 338:2009 [3] of the strength grade C24. It is obvious that the test results of types 1 and 2 are clearly below. Only the test results of type 3 and 4 are in the area of the green line. This leads to the supposition that the modulus of elasticity, which did not change essentially compared to earlier codes, is not determined acc. to the actual ÖNORM EN 408:2012 [1] but with a test configuration with an unloaded beam end. Thus it should be discussed to change the values of the modulus of elasticity perpendicular to the grain in the codes and to introduce a $k_{c,90,E}$ factor. The correlation factors under R = 0,4 show that the relation between the density and the modulus of elasticity is lower than the correlation to the compression strength.

One important reason for the large discrepancies is the annual ring direction, which has a big influence on strength and stiffness properties. But it is not taken into account in ÖNORM EN 408:2012 [1]. It is even not explained how the annual ring direction has to be considered in the test configuration. For these investigations I chose by purpose to use specimens with annual ring directions between 0° and 90°. Figure 7 describes the relations between the annual ring direction and the compression strength respectively the modulus of elasticity with a quadratic regression. The angle of 0° corresponds to a tangential loading direction and 90° to a radial loading direction. A correlation coefficient up to R = 0,9 confirms this strong relation as also described in [12, 13]. The lowest results are as indicated with an annual ring direction of 45°, especially in type 1. The results of the modulus of elasticity of specimens with an unloaded beam end have a stronger relation to the annual ring direction than the compression strength.

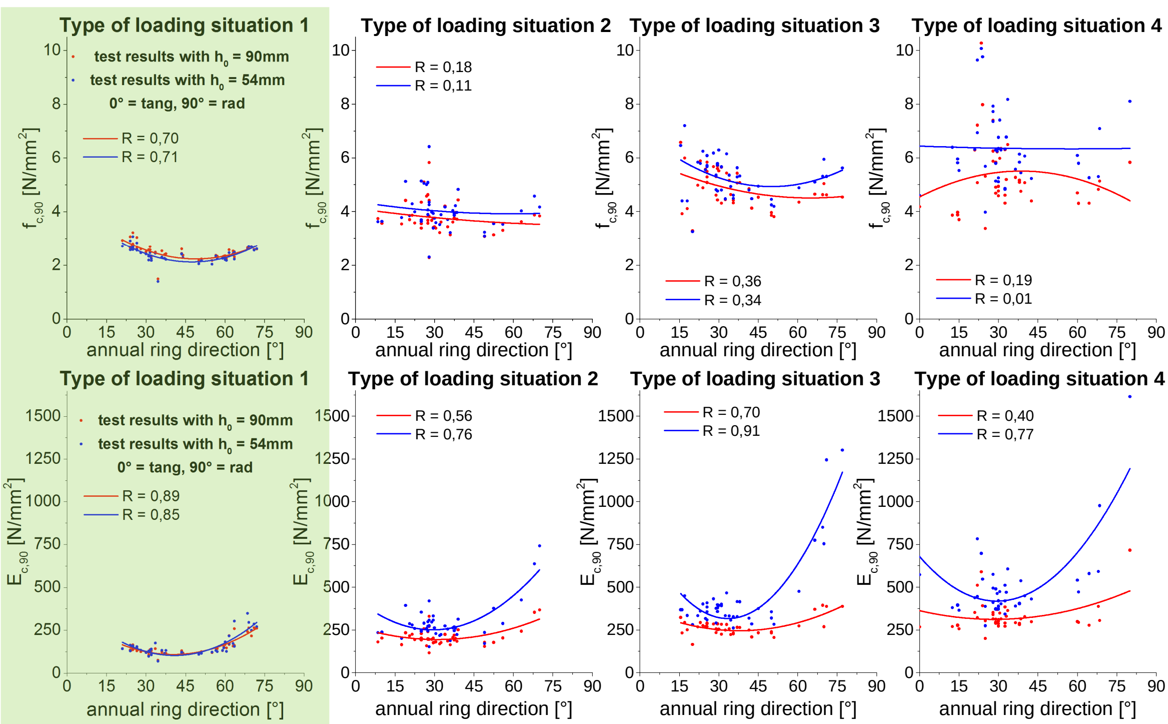

Figure 7: *Correlation between the annual ring direction and the strength resp. stiffness values*

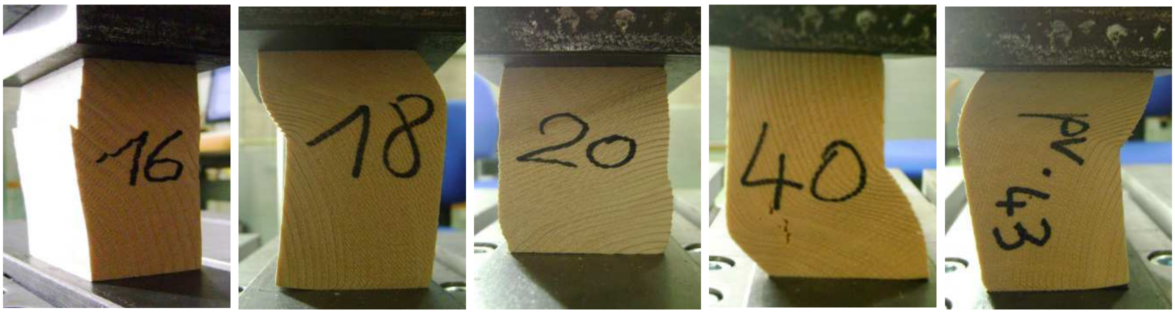

Figure 8: *Influence of the annual ring direction on the compression perpendicular to the grain*

Because the strength and stiffness values have to be determined with a test configuration acc. to ÖNORM EN 408:2012 (type 1) the strong influence of the annual ring direction with a correlation factor up to R = 0,9 (highlighted area in fig. 7) has to be taken into account. In design rules it is not useful to consider the annual ring direction but in the test configuration it has to be. As we know that the strength and the stiffness values are the smallest with an annual ring direction of 45° it could be useful to determine test configurations with defined directions. Even the old standard DIN 52192:1979 [10] has an explanation how to handle the annual ring direction but only in radial and tangential direction but not between it. In figure 8 the different deformations due to variable annual ring directions can be seen. With a radial loading direction the specimen gets uniform compressed. If the loading direction is tangential a buckling of annual rings can be observed. And by a loading direction of 45° to the annual rings a shearing between the weakest annual rings occurs (specimen no. 16).

4 Comparison of the test results with design models of selected codes and standards

Changes of the concept of security and the design rules and the introduction of the characteristic strength values have led to inconsistencies concerning the design rules of compression strength perpendicular to the grain. Furthermore, the experimental setup for determining the strength and stiffness values perpendicular to the grain has changed. Also the general design rules in the individual standards with their factors and conditions are very different from each other.

To figure out these changes the test results are compared with design rules of different versions of codes in Austria, Germany and Switzerland [2-5, 11], which are often very different from each other (figure 9 and 10). In addition to the standards also the theoretical approach of Van der Put [17, 18] is compared to the test results.

In figure 9 the design values of different codes and the results of the investigations are compared to each other. The characteristic values of the investigations are blue and the mean values red. The specific calculations are carried out in [19]. It is again recognizable that the calculated values acc. to ÖNORM EN 1995-1-1:2009 [2] (green line) are higher than the characteristic values and even the mean values of the investigations. Only the values calculated acc. to SIA 265:2012 [11] lead to a conservative designing (except for type 1). In annex C of SIA 265:2012 [11] a alternative design method for compression strenght perpendicular to the grain is proposed, which is equivalent to the design rule according to EN 1995-1-1:2009 [2].

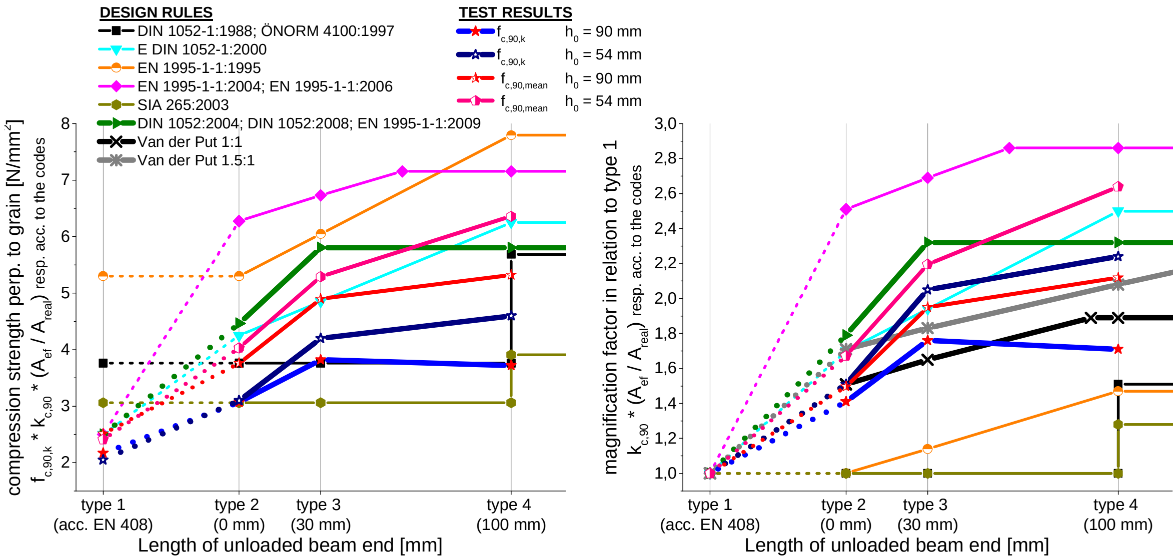

Figure 9: *Comparison of the compression strength values (left) resp. their magnification factors (right) of the test results and different codes and the approach of Van der Put*

Because the values of the different codes already strongly vary and are mostly higher than the test results, in figure 9 (right), the magnification factors depending on the length of unloaded beam end are compared. The approach of Van der Put [17, 18] (black and grey line) is also displayed and predicts better the test results. The magnification factors acc. to ÖNORM EN 1995-1-1:2009 [2] are higher than in the investigations.

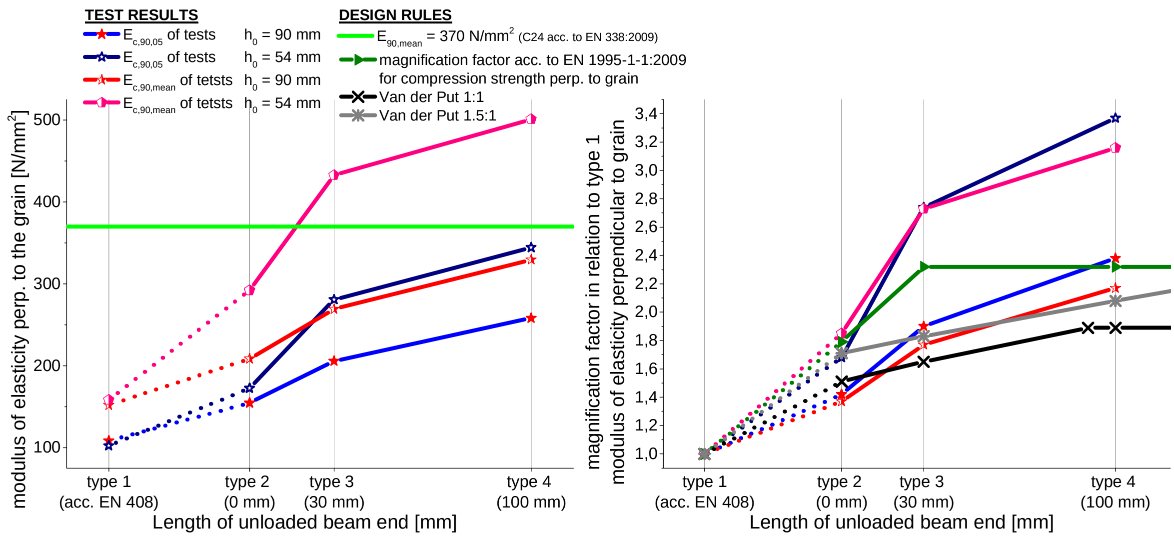

Figure 10: *Comparison of the modulus of elasticity values (left) resp. their magnification factors (right) of the test results and different codes and the approach of Van der Put*

Also the modulus of elasticity increases with the length of unloaded beam end. So the constant modulus of elasticity perpenidular to the grain $E_{90,mean}$ = 370 N/mm² acc. to ÖNORM EN 338:2009 [3] does not reflect the real material behaviour. The supporting effect of wood grain leads to a similar magnification effect as by the compression strength perpendicular to grain. In figure 10 (right) the test results are compared to the magnification factors for compression strength of ÖNORM EN 1995-1-1:2009 [2] and the approach of Van der Put. For the test results with the gauge length of 90 mm the prediction of magnification factor acc. Van der Put works very well. The magnification factor acc. to

ÖNORM EN 1995-1-1:2009 [2] leads again to higher results. But the test results with a gauge length of h_0 = 54 mm lead to a very high magnification factor up to 3,4 (type 4) which attributes to the deformations which are not in the measured area (figure 4). Therefore it should be discussed to change the actual modulus of elasticity values and to introduce a factor $k_{c,90,E}$ in the codes, which considers the supporting effect of wood grain.

5 Conclusions

The investigations show some large discrepancies between the design rules and the laboratory tests. So the bearing capacity acc. to Eurocode 5 and most other standards are much higher than acc. to the experimental results. Even the mean values of the test results regarding the strength and the stiffness values are in most cases lower than the characteristic values of the actual codes. The theoretical approach of Van der Put reflects very well the increasing strength and stiffness values due to the supporting effect of wood grain.

The strength and stiffness values are much smaller when deformations are measured over the complete specimen depth (except of type 1). The tests also show that the supporting effect of wood grain has a big effect on the modulus of elasticity, which increases similar to the compression strength. So the constant $E_{90,mean}$ value in [2, 3] does not reflect the real material behaviour. Therefore, it should be discussed to introduce a factor $k_{c,90,E}$ in the codes.

The mean value of the modulus of elasticity perpendicular to the grain of the test results of type 1 (acc. to ÖNORM EN 408:2012) is $E_{c,90,mean}$ = 152 and 158 N/mm² (table 1) and thus less than the half of the value $E_{90,mean}$ = 370 N/mm² in ÖNORM EN 338:2009 [3].

Also the characteristic values of compression strength perpendicular to the grain of the test results of type 1 are $f_{c,90,k}$ = 2,05 and 2,17 N/mm² and much lower than given in [3] for C24 with $f_{c,90,k}$ = 2,5 N/mm². Even the mean values of the test results with $f_{c,90,mean}$ = 2,41 and 2,51 N/mm² are lower.

Investigations of L. Damkilde et al., M. Poussa, M. Augustin et.al (even for glulam) and M. Poussa [13, 15 and 16] also come to similar results. With characteristic strength values of $f_{c,90,k}$ = 2,1 resp. 2,3 N/mm² for tests acc. to type 1 are also lower than the given value in ÖNORM EN 338:2009 [3].

Furthermore the dependence of the characteristic strength value perpendicular to the grain to the density according to the test results is less than defined in [3] ($f_{c,90,k} = 0.007 \cdot \rho_k$). The correlations between the density and the compression strength and stiffness values of type 1 are smaller than the correlations between the annual ring direction and the compression strength and stiffness values. So the large influence of the annual ring direction on the material properties perpendicular to grain should be taken into account in the future especially for the test method as given in [1] for determining the physical and mechanical properties.

It should also be considered whether the more complex measurements over 60% of the specimen depth are appropriate. One, because the gauge length about the complete specimen depth reflects the real deformations and second because the modulus of elasticity and the compression strength perpendicular to the grain are conservative when measured over the whole specimen depth. Also the influence of the gauge length on the results of test type 1 is not as high as on the other types of loading situations.

References

Different versions of codes are used in this paper, so the year of issue is written in the text.

[1] ÖNORM EN 408:2012. Timber structures - Structural timber and glued laminated timber - Determination of some physical and mechanical properties, Austrian Standards Institute, Wien

[2] ÖNORM EN 1995-1-1:1995 - 2009. Eurocode 5: Design of timber structures - Part 1-1: General - Common rules and rules for buildings, Wien

[3] ÖNORM EN 338:1995 - 2009. Structural Timber – Strength Classes, Austrian Standards Institute, Wien

[4] DIN 1052:1988 - 2008. Design of timber structures - General rules and rules for buildings, Beuth Verlag, Berlin

[5] ÖNORM 4100-2:1997 - 2004. Timber structures - Part 2: Design and construction, Austrian Standards Institute, Wien

[6] ÖNORM DIN 4074-1:2012. Strength grading of wood - Part 1: Coniferous sawn timber, Austrian Standards Institute, Wien

[7] ÖNORM EN 13183-1:2004 Moisture content of a piece of sawn timber - Part 1: Determination by oven dry method, Austrian Standards Institute, Wien

[8] ÖNORM EN 13183-2:2002 Moisture content of a piece of sawn timber - Part 2: Estimation by electrical resistance method, Austrian Standards Institute, Wien

[9] ÖNORM EN 384:2010 Structural timber - Determination of characteristic values of mechanical properties and density, Austrian Standards Institute, Wien

[10] DIN 52192:1979. Testing of wood; compression test perpendicular to grain, Beuth Verlag, Berlin

[11] SIA 265:2003 - 2012. Civil Engineering – Timber Structures, Schweizerischer Ingenieur- und Architektenverein, Zürich

[12] E. Gaber. Druckversuche quer zur Faser an Nadel- und Laubhölzern. In: *Holz als Roh- und Werkstoff 7/8*, Springer-Verlag, Berlin 1940

[13] L. Damkilde, P. Hoffmeyer, T.N. Pedersen. Compression Strength Perpendicular to Grain of Structural Timber and Glulam, In: *CIB-W-18/ 31-6-4*, Savonlinna, 1998

[14] H.-J. Blass, R. Görlacher. Compression perpendicular to the grain. In: *Proceedings of the 8th World Timber Engineering*, Vol. II, Lahti, 2004

[15] M. Augustin, A. Ruli, R. Brandner, G. Schickhofer. Behavior of glulam to grain in different strength grades and load configurations. In: *CIB-W18/ 39-12-6*, Florenz, 2006

[16] M. Poussa, P. Tukiainen, A. Ranta-Maunus. Experimental Study of Compression and Shear Strength of Spruce Timber. In: *CIB- W18/ 40-6-2*, Bled, 2007

[17] T. A. C. M. Van der Put. Derivation of the bearing strength perpendicular to the grain of locally loaded timber blocks. In: *Holz als Roh- und Werkstoff 66*, pages 409-417, Springer-Verlag, Berlin, 2008.

[18] A. Jorrisen, A. Leijten, B. de Leijer. The bearing strength perpendicular to grain on discrete supports. In: *CIB- W18/ 43-6-1*, Nelson, 2010

[19] C. Le Levé, R. Maderebner, M. Flach. Untersuchungen zur Querdruckfestigkeit von Fichtenholz in Abhängigkeit der Lasteinwirkung. Diploma Thesis. University of Innsbruck, Faculty of Civil Engineering, Innsbruck, 2012

INTER

International Network on Timber Engineering Research

DISCUSSION OF TESTING AND EVALUATION METHODS FOR THE EMBEDMENT BEHAVIOUR OF CONNECTIONS

S Franke
N Magnière

Bern University of Applied Sciences

SWITZERLAND

Presented by S Franke

H Blass asked about the foundation modulus for the stiffness. He asked what do you do with the stiffness. S Franke responded that it would not be used for strength design. H Blass stated that we almost never used the stiffness values. P Quenneville stated that the information can be used in studying connection behaviour but its use in estimating connection stiffness is challenging. H Blass stated this is only for research purposes so far. He commented that there are similar data on fasteners for timber concrete joints, inclined screws etc. Stiffness data is hidden and never used in practice.

P Quenneville stated that why use the full hole test where we never have uniform stress distribution. S Franke responded that in some cases half hole test can easily split therefore full hole test is used. H Blass stated that in performing test with brittle material where splitting could occur reinforcement could be used to prevent splitting. H Blass added that this reinforcement is intended to allow embedment strength to be measured not connection strength.

I Smith stated that back in history a lot of work was done. The biggest variable was who did the test. Devices were developed to prevent splitting of the wood but not practical.

S Svensson added less human error with the simplest way possible is desired.

JW van de Kuilen stated that the quality of steel etc. can add to the variability and he agreed that the simplest way possible should be adopted.

P Quenneville questioned whether 0.05d offset or 5 mm offset is more appropriate.

J Munch Anderson stated that correction or calibration factors should be considered with the easy method. H Blass questioned how to do embedment strength tests for staples in OSB where OSB core and face have different embedment strengths. F Lam stated that in such cases one should do connection test.

I Smith stated that ASTM standard is intended for product comparisons.

P Quenneville said that the 5 mm offset and yield strength values are needed for mixed brittle failure mode for connection design.

J W van de Kuilen stated that the line from Eurocode is correct. If you sought refinements, the connection does not become safer as you cannot get good correlations between dowel embedment and connection behaviour.

Discussion of testing and evaluation methods for the embedment behaviour of connections

Steffen Franke[1], Noëlie Magnière[1]

[1]Bern University of Applied Sciences, Institute for Timber Construction, Structures and Architecture, Switzerland

Keywords: Timber, embedment, standards, testing methods, full-hole test, half-hole test, evaluation methods, discussion

1 Introduction

Connections with mechanical fasteners play an important role in timber structures. Therefore their performances have to be estimated with a high reliability. The behaviour of these connections are exhaustively be characterized by its stiffness K and its capacity, for which calculation the European Yield Model (EYM) is nowadays largely accepted. In this model, the capacity of the connection is governed by the embedment f_h in the wood and by the yield moment of the fastener M_y.

The current European (EN 1995-1-1:2008) and most national design standards provide empirical formulas for the calculation of these parameters. These formulas were established based on experimental results from extensive embedment testing. These tests can nowadays be performed according to different standards where different test setups/methods and evaluation methods are given and which have been used by different researchers e.g. Whale et al. (1986), Ehlbeck and Werner (1992), Rammer and Winistorfer (2001), Sawata and Jasumura (2002), Hübner et al. (2008), Franke and Quenneville (2010, 2012), Sandhaas et al. (2013). These variances in testing and evaluation result in significant differences for both f_h and K depending on the load to grain direction and make it impossible for comparisons and to use all available test data for the evaluation of reliable calculation methods.

Therefore, a review of the different embedment test and evaluation methods has been carried out. The results highlight the major differences between American, European and international standards and their subsequent consequences on the embedment strength values obtained. Advantages, disadvantages and differences regarding these results of the methods will be addressed and discussed in the paper as a basis for a discussion with experts with the aim to define a standardised testing and evaluation method. In a close discussion with the experts at the conference, the best suitable test and evaluation methods could be agreed.

2 Methods and standards

The testing standards investigated, namely the American ASTM D5764-97a (2013), the European EN 383:2007 and the international ISO/DIS 10984-2:2008, specify different test methods, sample sizes, loading procedures and evaluation methods. A summary and comparison of the specific procedures in the different test standards are given below and discussed afterwards.

2.1 ASTM D 5764-97a (2013)

The ASTM D 5764-97a standard "Standard Test Method for Evaluating Dowel-Bearing Strength of Wood and Wood-Base Products" provides a full-hole (FH) and a half-hole (HH) testing setup, as shown in Figure 1 and Figure 2. The minimum specimen dimensions are 38 mm or 2d in thickness and the maximum of 50 mm or 4d in width and length, independent of the load-to-grain angle α, where d is the dowel diameter.

The test is conducted as to reach the maximum load in 1 to 10 min, using a constant rate of testing of usually 1.0 mm/min. There is no further information about the loading procedure. The results are given as the yield load F_{yield}, determined using the 5 %-offset method, the proportional limit load F_{prop} and the ultimate load $F_{ultimate}$. The embedment strength f_h, calculated from the yield load, is given by:

$$f_h = \frac{F_{yield}}{d \cdot t} \tag{1}$$

with d the dowel diameter and t the thickness of the test specimen. No information about the determination of foundation modulus (stiffness) K is provided.

2.2 ISO/DIS 10984-2:2008

The tests according to the international standard ISO/DIS 10984-2:2008 "Timber structures - Dowel-type fasteners - Part 2: Determination of embedding strength and foundation values" shall be carried out using a full-hole test shown in Figure 3, but it is a requirement of the test to avoid bending of the fastener under test. Thus it also allows the use of the half-hole test shown in Figure 3. The minimum specimen dimensions for tests parallel and perpendicular to grain can be found in Figure 4.

The loading procedure to be used consists of one preload cycle from $0.4 \cdot F_{max,est}$ to $0.1 \cdot F_{max,est}$ with $F_{max,est}$ as estimated maximum load ,and the force is to be increased or decreased at a constant rate, as shown in Figure 5. The maximum load is to be reached

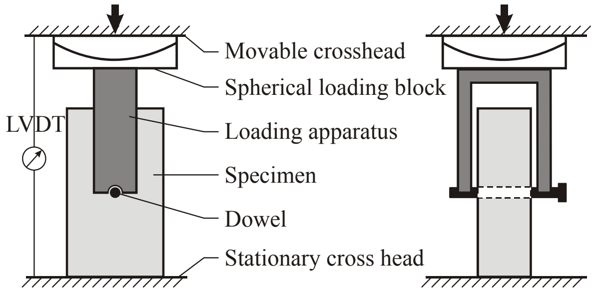

Figure 1: Test configuration full-hole test, ASTM D 5764-97a

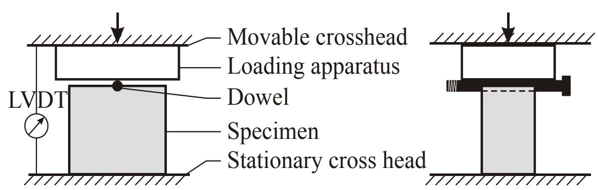

Figure 2: Test configuration half-hole test, ASTM D 5764-97a

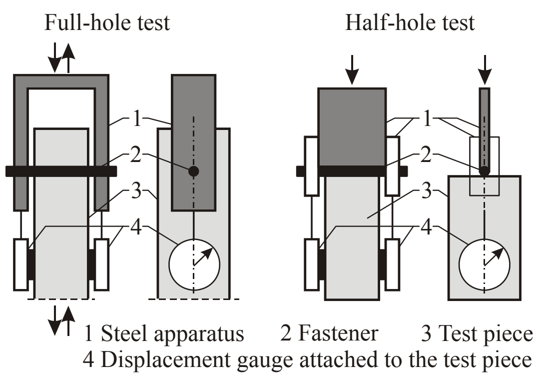

Figure 3: Test configuration, ISO/DIS 10984-2

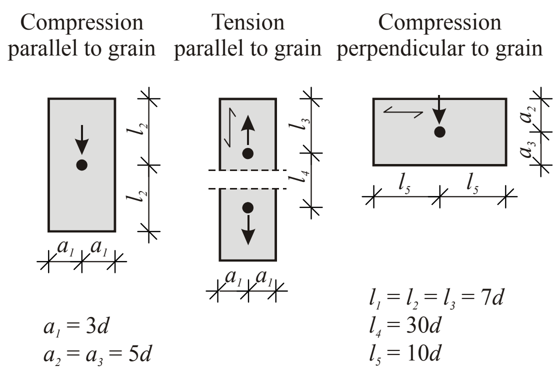

Figure 4: Sizes of test specimen, ISO/DIS 10984-2

within 300 ± 120 s. The standard includes formulas to calculate the embedment strength f_h, Eq. 2, where F_{max} is either the ultimate load or the load at 5 mm displacement, and the foundation modulus K_s, Eq. 3, where w is the displacement at 0.4 F_{max} and 0.1 F_{max}:

2.3 EN 383:2007 or DIN EN 383:2007

The European EN 383:2007 testing standards "Timber structures – Test methods, Determination of embedding strength and foundation values for dowel type fasteners" are equal to the ISO/DIS 10984-2:2008, except that it does not allows the half-hole test alternative.

2.4 Comparison and discussion

The full-hole (ASTM, ISO and EN) and half-hole (ASTM and ISO) test methods are used in the standards. The main difference between these methods is the deformation of the dowels and therefore the stiffness. Furthermore, fixing the loading plate to the dowels as for the ASTM full-hole test will influence the deformation as well. Table 1 provides a summary of the different methods and there details.

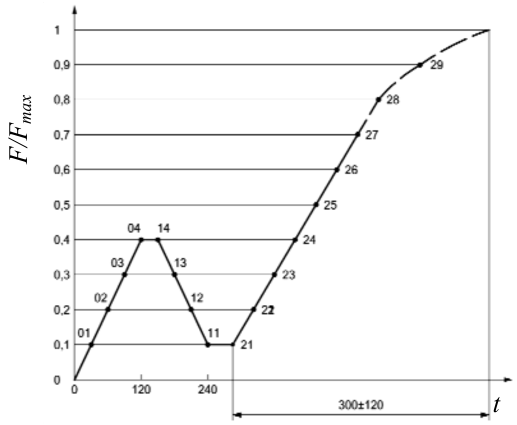

Figure 5: Loading procedure

$$f_h = \frac{F_{\max}}{b \cdot t} \tag{2}$$

$$K_s = \frac{0.4 f_{h,est}}{w_{i,\mathrm{mod}}} = \frac{0.4 f_{h,est}}{4/3 \cdot \left(w_{0.4 \cdot F} - w_{0.1 \cdot F}\right)} \tag{3}$$

Table 1: Summary of test method details

Method / detail	ASTM D 5764-97a	ISO/DIS 10984-2	EN 383
Full-hole test (FH)	(yes) only if splitting	yes	yes
Half-hole test (HH)	yes	yes	no
Loading plate fixed to dowels (full-hole test)	no	yes	yes
Specimen: Thickness t, cp. Figure 7	≥ min (38 mm or 2d)	not specified	not specified
Width w, cp. Figure 7	≥ max (50 mm or 4d)	6d for $\alpha = 0°$ 20d for $\alpha = 90°$	6d for $\alpha = 0°$ 40d for $\alpha = 90°$
Length resp. height h (loaded end), cp. Figure 7	≥ max (50 mm or 4d)	7d for $\alpha = 0°$ 5d for $\alpha = 90°$	7d for $\alpha = 0°$ 5d for $\alpha = 90°$
Loading procedure, cp. Figure 5	Monotonic, displ. controlled within 1 to 10 min	Preloading cycle, displ. controlled within 300 ± 120 s	Preloading cycle, displ. controlled within 300 ± 120 s
End of loading	0.5d displacement or after max load	u_0 + 5 mm displ. or after max load	u_0 + 5 mm displ. or after max load
Evaluation of load resp. embedment strength, cp. Eq. 1 and 2	yield load (5%-off set) or max. load	max. load or load at u_0 + 5 mm	max. load or load at u_0 + 5 mm
Evaluation of stiffness K, cp. Eq. 3	no	yes: K_i, K_s, K_e	yes: K_i, K_s, K_e

These details highlight the major differences between the three standards and their subsequent consequences on the embedment strength values obtained. E.g. the half-hole test applies the load on the full length of the fastener. This enables to obtain a result free from any influence of the fastener's bending. This gives a realistic result for the embedding strength but does not reflect the realistic stiffness of a connection due to the bending deformation of the fasteners in reality. Whereas the full-hole test rather includes the bending of the fasteners, but does not lead to a uniform stress under the dowel, which was used developing the EYM. Sandhaas et al. (2013) stated, that there are no differences between compression and tension tests, therefore no further investigations have been done.

Likewise, the embedment strength can be evaluated from the experimental stress-strain curves using two main principles: either by taking the load value corresponding to an absolute displacement of 5 mm as recommended by the EN 383:2007 and the ISO/DIS 10984-2 ($f_{h,5mm}$) or by offsetting the elastic-linear part of 5 % the fastener's diameter as suggested in the ASTM D5764-97a ($f_{h,5\%}$). Furthermore, evaluating the results at 2.1 mm ($f_{h,2.1mm}$) has been used as well. Table 2 summarizes the evaluation methods found in the literature and highlights the not consistent use and therefore non comparable results. These variations in the evaluation methods can also have a significant influence on the embedment strength of 50 % or even more within one of the test methods as shown in Franke & Magnière (2013) and Franke & Quenneville (2010, 2011, 2012). This is also shown in Figure 6 where the evaluation methods are marked on a sample load-displacement curve.

Table 2: Embedment test designs and evaluation methods found in literature

Author	Test set up	Evaluation method 5 % offset	 5 mm	 2.1 mm
Whale et al. (1986)	Equivalent to EN 383:2007 – FH		Until failure	
Ehlbeck & Werner (1992)				x
Sawata & Yasumura (2002)	EN 383:2007 – FH	x	x	
Hübner et al. (2008)	EN 383:2007 – FH		x	
Franke & Quenneville (2010, 2011, 2012)	ASTM D5764-97a – HH	x	x	

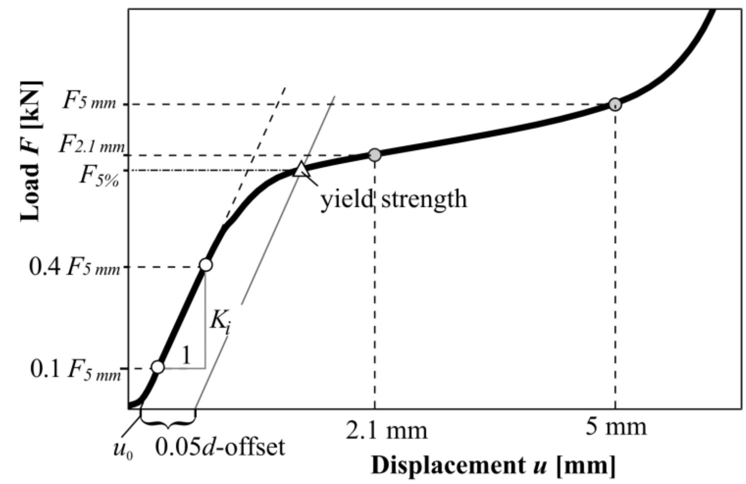

Figure 6: Evaluation methods

3 Test series

For the investigation of the differences of the test methods and evaluation methods, six test series have been carried out in order to investigate differences in relation to the load-to-grain angle *α;* three series with loading situations parallel to the grain and three for perpendicular to the grain. Within one load to grain angle *α*, two FH tests with different sizes, since the different standards use different sizes, and one HH test, where the size is comparable to the big ones of the FH test, were carried out. Focus was given to the same loaded volume resp. loaded end distance. A summary with specific information is provided in Table 3.

The same materials for the wood and for the fasteners were used for every series. The wood specimen were cut from Spruce boards, alternating in relation to the test series and conditioned at 20 °C and 65 % relative humidity until moisture equilibrium was reached. As fasteners, mild steel dowels with 12 mm in diameter of the same quality were used. The loading plates were not fixed to the dowels for all series. A sketch of the specimen according to the FH test and a specimen of each method under testing are shown in Figure 7.

Loading was applied according to the procedure used in the EN 383:2007 standard and shown in Figure 6 for all series. For the increase and decrease of the load, a constant rate of movement of 0.3 mm/min was applied.

4 Results and Discussion

The tests were analysed according to Figure 6 except of the load at 2.1 mm. The stiffness K was evaluated on the second slope (after the cycle). F_{max} is given as $F_{5\text{mm}}$ or $F_{ultimate}$ depending which occurs first. $F_{5\%}$ was used as yield load. The embedding strengths were calculated according to Eq. (1) and (2) respectively. All results as mean values are shown in Table 4. All individual curves as well as the corresponding mean curve of the FH0-

Table 3: Experimental test program

			No of		Angle	Sizes [mm], compare Fig. 4 and 6				
Series	**Name**	**Test setup**	**tests**	**Standard**	α	a_1	l_2	l_5	a_3	$w/h/t$
1	FH0-EN383	Full-Hole	5	EN 383:2007	0°	36	72	-	-	144 / 72 / 40
2	FH0-ASTM	Full-Hole	5	ASTM D5764-97a	0°	60	120	-	-	120 / 170 / 40
3	HH0-ASTM	Half-Hole	5	ASTM D5764-97a	0°	60	120	-	-	120 / 120 / 40
4	FH90-EN383	Full-Hole	5	EN 383:2007	90°	-	-	240	60	480 / 120 / 40
5	FH90-ASTM	Full-Hole	5	ASTM D5764-97a	90°	-	-	60	120	120 / 170 / 40
6	HH90-ASTM	Half-Hole	5	ASTM D5764-97a	90°	-	-	60	120	120 / 120 / 40

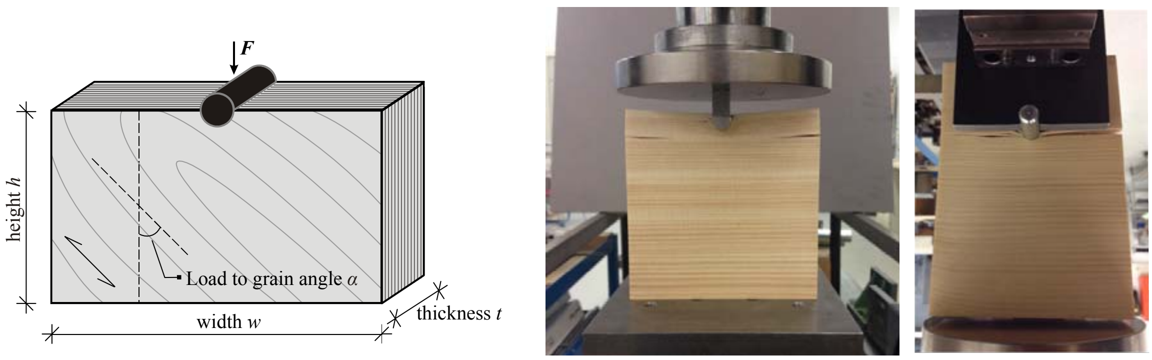

Figure 7: Specimen sizes variables and one sample HH90-ASTM and FH90-EN383 under testing

ASTM tests and FH90-ASTM tests are shown in Figure 8 with small variations. All mean curves are compared in Figure 9 for the parallel to grain tests (left) and perpendicular to grain tests (right).

4.1 Parallel to grain tests, $\alpha = 0°$

A clear difference can be seen for the parallel to grain tests in the figures and table. The HH0-ASTM test shows the highest load (30 % above the lowest) and stiffness and the FH0-EN383 test the lowest load. The difference in yield load between both FH0 tests (different specimen sizes, same method) comes to 7.5 % and between the FH0-ASTM and HH0-ASTM (same size, different method) to 20 %. Due to the relative constant plateau after yielding, there is no difference between the yield and max loads, $f_{h,max}/f_{h,5\%}$, for all series.

There is only 5 % difference in stiffness for both FH tests, compared to 73 % higher stiffness for the HH0-ASTM test.

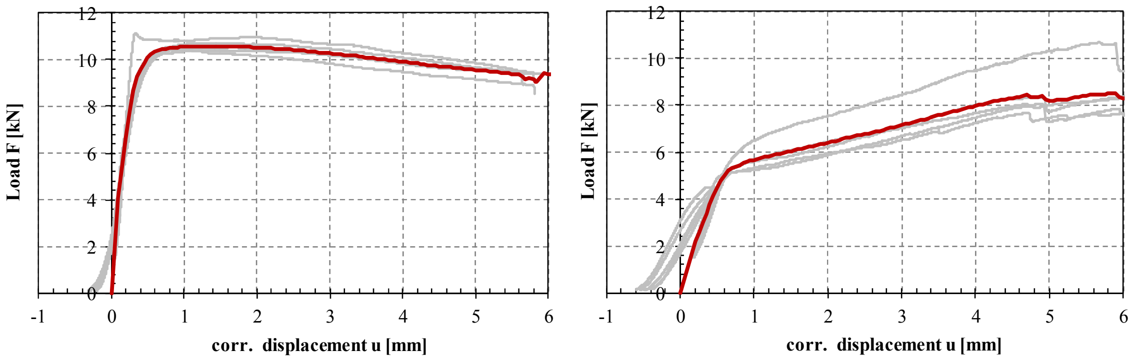

Figure 8: Individual and mean load deformation curve for FH0-ASTM (left) and FH90-ASTM (right)

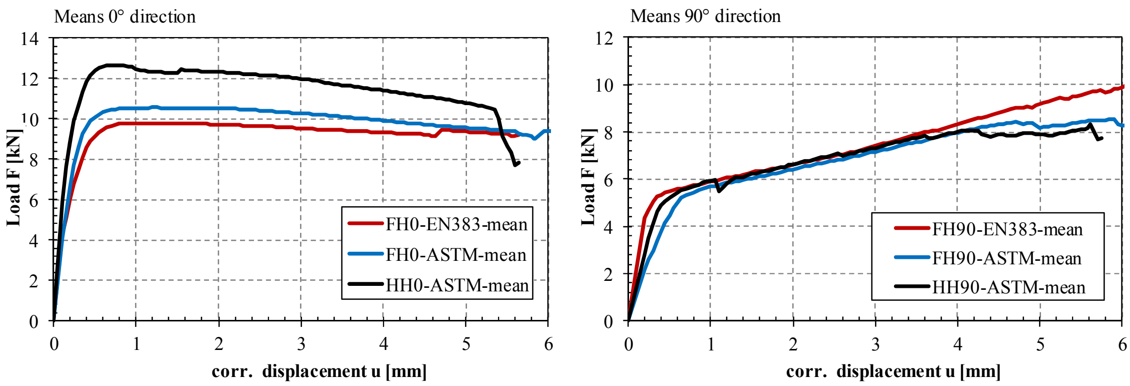

Figure 9: Comparison of the mean load deformation curves of all series

Table 4: Results of the test programs

	Slope K		$f_{h,5\%}$		$f_{h,max}$		$f_{h,max}/f_{h,5\%}$
Series	**[kN/mm]**	**COV**	**[kN]**	**COV**	**[kN]**	**COV**	**-**
FH0-EN383	34.56	13 %	(9.78)	12 %	9.83	12 %	1.00
FH0-ASTM	36.45	13 %	(10.52)	2 %	10.63	3 %	1.01
HH0-ASTM	(60.58)	20 %	12.67	1 %	12.77	1 %	1.01
FH90-EN383	18.96	14 %	(5.82)	2 %	10.22	10 %	1.76
FH90-ASTM	9.03	9 %	(5.88)	11 %	8.66	13 %	1.47
HH90-ASTM	(13.96)	30 %	5.94	18 %	8.31	13 %	1.40

4.2 Perpendicular to grain tests, $\alpha = 90°$

The results for the perpendicular to grain tests are somehow opposite. The yield loads are relatively equal to each other for all series with only 2 % difference between the lowest and highest. Due to different failure behaviours, the maximum loads differ by 23 %. Furthermore there is a significant difference between the yield and max loads, $f_{h,max}/f_{h,5\%}$, with 76, 47 and 40 %.

There are quite differences for the stiffness of 200 % between smallest and highest which are the two FH tests with different specimen sizes and 55 % between the FH90-ASTM and HH90-ASTM with same specimen sizes.

4.3 Discussion

As shown before, the variations in the test and evaluation methods have a significant influence on the embedment strength of up to 23 % even for the same evaluation method and up to 76 % between the evaluation methods. For the stiffness the influence is even up to 200 %. This shows the need for standardising respectively equalising the test and evaluation methods for both the determination of the embedment strength and stiffness for a reliable use within the design standards and to create comparability between the results of different researchers and/or species.

Following points, as marked red in Figure 10, would be necessary to discuss and to agreed on (recommendations are marked in bold):

- Determination of embedment strength:
  - Which test method: Full-hole, **Half-hole**
  - What evaluation method: $\boldsymbol{f_{5\%}}$, $f_{h,2.1mm}$, $f_{h,5mm}$
- Determination of foundation modulus (stiffness):
  - Which test method: **Full-hole,** Half-hole
  - Which modulus: Initial foundation modulus K_i,
Foundation modulus $\boldsymbol{K_S}$,
Elastic foundation modulus K_e
- Determination of u_0: **first slope**, second slope
- Specimen size: according **EN383:2007 with t ≥ min(40, 4*d*)** or
ASTM D5764-97a (2013)

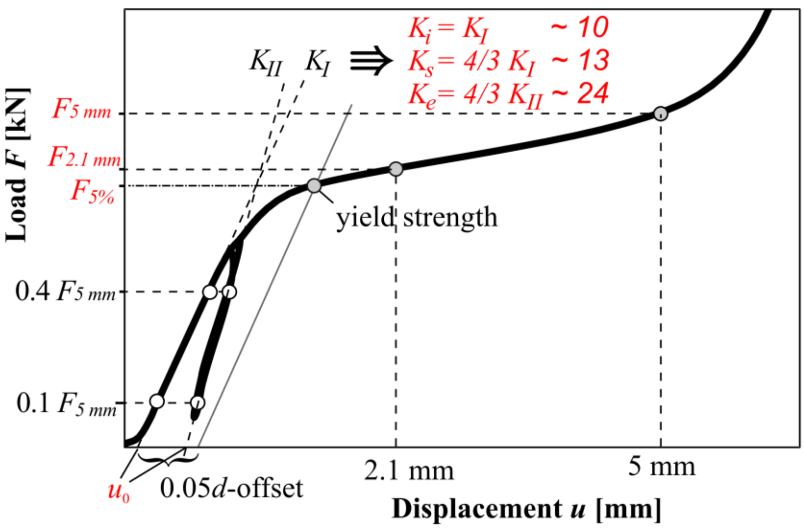

Figure 10: Evaluation methods for discussion

5 Conclusion and view

It was clearly shown, that the different testing and evaluation methods used in the standards result in different embedment strength values and foundation modules. To overcome this, specific test and evaluation methods for each value have been proposed. These needs to be discussed and agreed and could therefore proposed for code changes to provide reliable design values for safe timber structures. Comments and an excited discussion is needed and welcome.

References

ASTM International 2013: ASTM D5764-97a (2013) „Standard Test Method for Evaluating Dowel-Bearing Strength of Wood and Wood-Based Products“, West Conshohocken, United States

Ehlbeck, J., Werner, H. 1992 “Tragfähigkeit von Laubholzverbindungen mit stabförmigen Verbindungsmitteln“, Tech. Report, Versuchsanstalt für Stahl, Holz und Steine der Universität Karlsruhe, Abt. Ingenieurholzbau, Karlsruhe, Germany.

European Committee for Standardization (CEN) 2008: EN 1995-1-1:2008 “Eurocode 5 – Design of timber structures”. Brussels, Belgium

European Committee for Standardization (CEN) 2007: EN 383:2007 “Timber structures – Test methods. Determination of embedding strength and foundation values for dowel type fasteners”. Brussels, Belgium

Franke, S., Magnière, N. 2013, “The embedment failure of European beech compared to spruce wood and standards”, Materials and Joints in Timber Structures, Springer, RILEM Bookseries 9, pp. 221-229

Franke, S., Quenneville, P. 2010 “Investigation of the embedding strength of Radiata Pine and LVL”, In: WCTE 2010 – World Conference on Timber Engineering, Trentino, Italy

Franke, S., Quenneville, P. 2011 “Bolted and dowelled connections in Radiata pine and laminated veneer lumber using the European yield model”, Australian Journal of Structural Engineering, Vol 12, No 1, pp. 13-27

Franke, S., Quenneville, P. 2012 “Embedding behavior of Douglas Fir”, In: WCTE 2012 – World Conference on Timber Engineering, Auckland, New Zealand

Hübner, U., Bogensperger, T., Schickhofer, G. 2008 “Embedding Strength of European hardwoods” In: CIB-W18, Paper 41-7-5, St. Andrews, Canada

International Organization for Standardization: ISO/DIS 10984-2:2008 Timber structures – Doweltype fasteners - Part 2: Determination of embedding strength and foundation values. Geneva

Rammer, D., Winistorfer, S. 2001 “Effect of Moisture Content on Dowel-Bearing Strength” In: Wood and Fiber Science 33, Nr. 1, pp. 126-139

Sandhaas, C., Ravenshorst G. J. P., Blass H. J., and Kuilen J. W. G. 2013. “Embedment Tests Parallel-to-Grain and Ductility Aspects Using Various Wood Species” European Journal of Wood and Wood Products 71 (5), pp. 599–608

Sawata, K., Yasumura, M. 2002 “Determination of embedding strength of wood for dowel-type fasteners” In: Journal of Wood and Sciences 48, pp. 138-146

Whale, L., Smith, I., Hilson, B. 1986 “Behaviour of Nailed and Bolted Joints under Short-Term Lateral Load - Conclusions from Some Recent Research” In: Proceedings of CIB W18, Paper 19-7-1. Florence, Italy

INTER

International Network on Timber Engineering Research

DOWEL-TYPE CONNECTIONS IN LVL MADE OF BEECH WOOD

P Kobel

A Frangi

ETH Zurich, Institute of Structural Engineering

R Steiger

EMPA, Swiss Federal Laboratories for Materials Science and Technology,

Structural Engineering Research Laboratory, Dubendorf

SWITZERLAND

Presented by P Kobel

JW Van de Kuilen received clarification that the steel grades were S355 for the dowels and 8.8 for the bolts. P Kobel said that the quality of the steel was not checked but will do so later. Also he assumed over-strength of 25%.

P Quenneville asked whether net tension failures were observed. P Kobel said that for bolted connection with 2 rows of bolts it was observed. P Quenneville stated that one cannot use the net tension data in the connection test. P Kobel agreed. He said that the net tension failure happened only once and since then the test configuration was changed to avoid this mode.

R Brandner and P Quenneville discussed that for cross banded LVL, net cross section failure needed to be checked by designers.

C Sandhaas commented about different strength properties of beech LVL.

H Blass asked how many cross band is needed. P Kobel responded that they are still working on it. He further confirmed that bolts were needed to prevent the opening failure mode shown in the code provision.

W Seim commented that with a better material whether EC5 spacing rules would still work.

J Munch Andersen commented that more investigation is needed for increasing the load capacity per fastener. One should consider load per fastener rather than spacing rules.

P Quenneville asked about the cross banded LVL pricing. P Kobel said no information is available. P Quenneville stated that if LVL has high price, one might lose economical advantage for any gain in capacity.

Dowel-type connections in LVL made of beech wood

Peter Kobel[1] , Andrea Frangi[1], René Steiger[2]

[1]ETH Zurich, Institute of Structural Engineering, Switzerland

[2]EMPA, Swiss Federal Laboratories for Materials Science and Technology, Structural Engineering Research Laboratory, Dubendorf, Switzerland

Keywords: Beech, laminated veneer lumber, dowel-type connections

Abstract. Despite its favourable mechanical properties the current use of beech wood for structural purposes is still very limited. A research project at ETH Zurich and Empa aims at developing timber structures using Laminated Veneer Lumber (LVL) made of beech wood (*Fagus silvatica L.*). One part of the project focuses on dowel-type connections for large span timber truss structures, where the connections are key elements. Extensive experimental testing has been carried out, in order to assess the embedment strength (f_h) and the load-displacement behaviour of dowelled as well as bolted steel-to-timber connections in beech LVL. The investigated parameters were the cross-layer percentage, the number of fasteners in a row and the spacings of the fasteners.

The embedment strength of beech LVL with cross-layers proved to be significantly higher than respective values given by the available design formulas in Eurocode 5. The conducted connection tests showed that the use of beech LVL (with a certain amount of cross-layers) allows more efficient dowelled and bolted connections, with higher load-carrying capacities and a significant increase in ductility. Predictions using the design approach in Eurocode 5 turned out to be conservative, overestimating the negative group effect and significantly underestimating the rope effect in bolted connections.

1 Introduction

The higher strength and stiffness properties of beech wood (*Fagus silvatica L.*) as compared to most softwood species are well known. In Switzerland and other European countries beech is available in large quantities. However, beech wood is today almost entirely used for energetic purposes or non-structural applications (e.g. in the wood furniture industry). A current research project at ETH Zurich and Empa aims at developing sustainable innovative and reliable timber structures using LVL made of beech wood. Due to its industrialised production, reliable and high strength and stiffness properties, improved dimensional and form stability, LVL made of beech has a great potential for applications in high performance structural elements, for instance in large span truss structures.

In timber truss structures the connections are often governing the design of the whole structure, which can lead to overdesigned timber members and thus impose technical and economical limits on solutions in timber. In order to improve the performance of timber truss structures, the research project focuses on developing more efficient connections by applying beech LVL as truss members. Dowelled as well as bolted steel-to-timber connections are investigated.

1.1 Beech LVL

The suitability of beech wood for structural applications has been confirmed by several research projects [1]-[5]. Recent studies have also promoted the use of beech LVL for structural purposes [6],[7].

As a result of its layered structure (Fig. 1), LVL is a very homogeneous material with a very low scatter in its properties. The use of beech veneers significantly improves the strength values, as compared to softwood. The LVL material used in the project was produced by the company Hess & Co AG in Döttingen, Switzerland. It was manufactured from 2.5mm thick rotary-peeled beech veneers. In the manufacturing process the veneers were compressed to a thickness of about 2.3mm. The measured average density was 765 kg/m^3 (CoV=2.2%), obtained from 80 specimens. The cross-sectional layout consisted of veneers predominantly oriented with the grain in longitudinal direction of the LVL member, and a varying number of orthogonal cross-layers (0-23%). The cross-layer percentage of 23% was chosen in analogy to the cross-sectional layout of the existing softwood LVL product Kerto-Q. Specimens with 21%, 17% and 14% cross-layers represent a modification of the same concept. On the one hand, the cross-layers ensure dimensional and form stability of the LVL member when subjected to moisture changes. On the other hand, the anisotropic distribution of the strength values can be altered. With regard to dowel-type connections, applying cross-layers to increase the tensile strength perpendicular to the grain is particularly favourable, as commonly premature splitting failure is a prevailing factor limiting the performance of such connections. Based on manufacturer's data Table 1 exemplarily shows selected material properties of beech LVL.

Fig. 1 Example of cross-sectional layout of beech LVL with 23% of cross-layers.

Table 1 Material properties of beech LVL based on manufacturer's data [8].

Selected material properties	Beech LVL (ρ_{mean} = 730 kg/m^3)		Spruce or pine (ρ_{mean} = 480 kg/m^3)	
	No cross-layers	Cross-layers (~23%)	No cross-layers	Cross-layers (~23%)
$f_{m,0,k}$ [N/mm^2]	73.8	66.8	50	36
$f_{t,0,k}$ [N/mm^2]	72	43.3	38	27
$f_{t,90,k}$ [N/mm^2]	1.6	24.5	0.8	6.0
$E_{0,mean}$ [N/mm^2]	16'800	13'800	13'800	10'500

1.2 Design of dowel-type connections according to Eurocode 5

Connections with dowel-type fasteners are usually designed based on Johansen's yield theory [9]. Johansen's approach simplifies the behaviour of both timber and steel as ideally rigid-plastic, and estimates the load-carrying capacities for different failure modes by applying equilibrium conditions. This concept has been adopted in many current design codes (e.g. Eurocode 5 (EC 5) [10]), using additional design criteria (requirements regarding spacings and edge and end distances as well as an effective number fasteners (n_{ef})) to prevent premature failures due to splitting of the timber along the grain and plug shear failure. Moreover, depending on the type of fastener, a rope effect can be taken into account. In EC 5, for bolts the contribution of the rope effect is limited to 25% of the load-carrying capacity calculated with Johansen's model. For dowels no rope effect can be taken into account.

The relevant failure modes for dowelled connections with slotted-in steel plates and bolted connections with thin outer steel plates are summarised in Fig. 2.

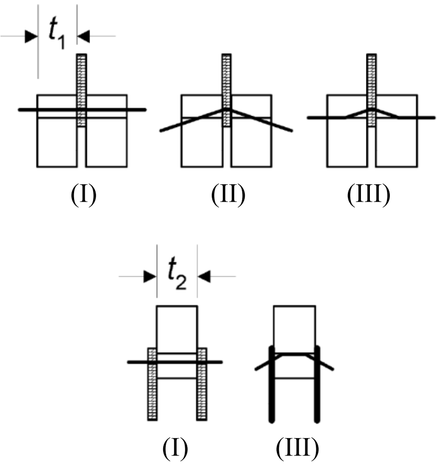

$$\begin{cases} \text{(I)} & F_{v,Rk} = f_{h,1,k} \cdot t_1 \cdot d \\ \text{(II)} & F_{v,Rk} = f_{h,1,k} \cdot t_1 \cdot d \cdot \left[\sqrt{2 + \frac{4 \cdot M_{y,Rk}}{f_{h,1,k} \cdot t_1^2 \cdot d}} - 1 \right] + \frac{F_{ax,Rk}}{4} \\ \text{(III)} & F_{v,Rk} = 2.3 \cdot \sqrt{M_{y,Rk} \cdot f_{h,1,k} \cdot d} + \frac{F_{ax,Rk}}{4} \end{cases}$$

$$\begin{cases} \text{(I)} & F_{v,Rk} = 0.5 f_{h,2,k} \cdot t \cdot d \\ \text{(III)} & F_{v,Rk} = 1.15 \cdot \sqrt{2 \cdot M_{y,Rk} \cdot f_{h,2,k} \cdot d} + \frac{F_{ax,Rk}}{4} \end{cases}$$

Fig. 2 Basic failure modes based on Johansen's yield theory for dowel-type connections with slotted-in steel plates and outer steel plates according to EC 5 design equations. (I) Embedment failure, (II) combined failure, (III) bending failure of the dowel. $F_{v,Rk}$: char. load-carrying capacity per fastener per shear plane; $f_{h,k}$: char. embedment strength; t: member thickness; d: fastener diameter; $M_{y,Rk}$: char. fastener yield moment (for dowels and bolts: $M_{y,Rk} = 0.3 f_{u,k} d^{2.6}$); $F_{ax,Rk}$: char. axial withdrawal capacity of the fastener.

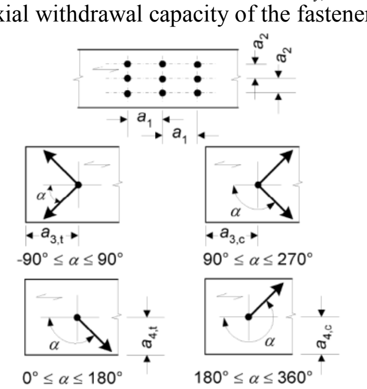

Fig. 3 Spacings and edge and end distances for dowels acc. to EC 5.

Table 2 Minimum spacings and edge and end distances for dowels and bolts according to EC 5.

Spacing and edge/end distances	Angle to grain	Minimum spacings and edge/end distances Dowels	Bolts
a_1 (parallel to grain)	0°≤α≤360°	(3+2|cosα|)d	(4+|cosα|)d
a_2 (perpendicular to grain)	0°≤α≤360°	3d	4d
$a_{3,t}$ (loaded end)	-90°≤α≤90°	max(7d;80)	max(7d;80)
$a_{3,c}$ (unloaded end)	90°≤α≤150°	$a_{3,t}$|sinα|	(1+6sinα)d
	150°≤α≤210°	max(3.5d;40mm)	4d
	210°≤α≤270°	$a_{3,t}$|sinα|	(1+6sinα)d
$a_{4,t}$ (loaded edge)	0°≤α≤180°	max((2+2sinα)d;3d)	max((2+2sinα)d;3d)
$a_{4,c}$ (unloaded edge)	180°≤α≤360°	3d	3d

Requirements regarding minimum spacings according to EC 5 are given in Table 2 and Fig. 3. The impact of the number of fasteners in a row can be accounted for by using the following reduction:

(1) $$F_{v,ef,Rk} = n_{ef} \cdot F_{v,Rk} \text{ with } n_{ef} = \min \begin{cases} n \\ n^{0.9} \cdot \sqrt[4]{\frac{a_1}{13d}} \end{cases}$$

A prerequisite for a calculation according to Johansen is the determination of the embedment strength f_h. EC 5 defines f_h as a function of the wood density ρ_k and the dowel diameter d:

(2) $$f_{h,0,k} = 0.082 \cdot (1 - 0.01 \cdot d) \cdot \rho_k \text{ for timber and LVL (loaded in grain direction)}$$

(3) $$f_{h,0,k} = 0.11 \cdot (1 - 0.01 \cdot d) \cdot \rho_k \text{ for plywoood (for any load direction)}$$

However, as these design rules have been developed mainly for softwood solid timber and glulam, their applicability for beech LVL has to be verified.

2 Experimental investigations

2.1 Embedment tests

2.1.1 Specimens and test setup

To determine the embedment strength for LVL made of beech a series of tensile embedment tests on a total of 70 specimens was carried out. In these tests the influence of different dowel diameters, cross-layer percentages in LVL and end distances of the dowels (Table 3) were studied. 40 specimens were tested strictly according to the test standard EN 383:2007 [11] (Fig. 4), with an end distance $l_3 = 7d$. For 30 specimens the end distance was reduced, thereby deviating from EN 383. During the tests the load-displacement behaviour of the dowel relatively to the timber was measured.

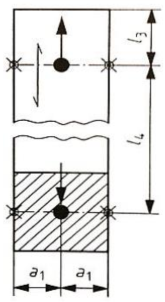

Fig. 4 Tensile embedment test acc. to EN 383: $a_1 = 3d$; $l_3 = 7d$; $l_4 = 40d$.

2.1.2 Results and comparison with the EC 5 design approach

From the tests, the embedment strength f_h is derived by deviding the load F by the projected contact area between dowel and timber. According to EN 383 F is determined either as the maximum load F_{max} or the load at a displacement of 5 mm ($F_{\Delta=5mm}$), if F_{max} is not reached before:

$$f_{h,EN383} = \frac{\{F_{\Delta=5mm}; F_{\max}\}}{d \cdot t} \tag{4}$$

EN 383 was developed mainly for solid timber and glulam specimens, where the behaviour is rather brittle and F_{max} is usually reached before the threshold displacement of 5 mm. Beech LVL with cross-layers, however, showed a much more ductile behaviour and peak values way beyond the 5 mm threshold (Fig. 6 and Fig. 8). Thus, the adequacy of the 5 mm threshold for LVL with cross-layers should be revisited. To take this into account, additionally to the approach according to EN 383, values for f_h were also calculated using strictly F_{max}.

$$f_{h,\max} = \frac{F_{\max}}{d \cdot t} \tag{5}$$

Table 3 Results of embedment tests according to EN 383.

	Configuration			f_h acc. to EN 383 (w ≤ 5 mm)				f_h from maximum load F_{max}			
	Cross-layers [%]	Dowel diameter [mm]	End dist. [mm]	$f_{h,EN383,mean}$ [N/mm²]	$w_{mean}(F_{EN})$ [mm]	n [-]	CoV [%]	$f_{h,max,mean}$ [N/mm²]	$w_{mean}(F_{max})$ [mm]	n [-]	CoV [%]
Acc. to EN 383:2007	23	- 8 -	7*d*	87	5.0	10	6.7	101	16.0	5	6.7
	0	- 12 -	7*d*	72	2.1	5	3.5	72	2.1	5	3.5
	17	- 12 -	7*d*	84	4.8	10	1.9	93	25.7	5	2.6
	23	- 12 -	7*d*	84	5.0	10	3.4	101	29.0	4	3.4
	0	- 16 -	7*d*	62	2.1	5	7.8	62	2.1	5	7.8
	14	- 16 -	7*d*	75	5.0	10	8.6	89	22.0	5	5.2
	23	- 16 -	7*d*	77	5.0	8	3.6	100*	21.0*	4	3.6*
	23	- 20 -	7*d*	75	5.0	10	5.1	104	39.0	4	5.1
l_3 reduced	0	- 12 -	5*d*	49	0.4	5	5.8	49	0.4	5	5.8
	17	- 12 -	5*d*	86	4.1	9	2.0	86	4.9	5	2.1
	0	- 16 -	5*d*	55	0.6	5	2.7	55	0.6	5	2.7
	14	- 16 -	5*d*	71	4.9	6	2.6	74	8.4	5	2.9
	23	- 8 -	3.5*d*	81	1.4	5	2.6	81	1.4	5	2.6
	23	- 16 -	3.5*d*	72	4.6	7	3.9	71	5.0	5	4.7

The results from all embedment tests are summarised in Table 3. Fig. 5 compares the test results with the expected values according to the design rules in EC 5 for solid timber and glulam made of Norway spruce and beech as well as for plywood, using the mean value of the measured density of 765 kg/m^3 in the EC 5 predictions for beech and plywood.

The mean embedment strength values obtained in beech LVL with cross-layers are higher than the corresponding values obtained from the available formulas in EC 5. Fig. 5 shows the results obtained by abiding by the 5 mm threshold given in EN 383, as well as the results using maximum values. It can be seen that also beech LVL without cross-layers yielded values above the expected values calculated with the EC 5 rules, indicating the beneficial homogenisation effect in LVL, as compared to solid timber. Cross-layers in the LVL lead to a further significant improvement, as premature splitting failures (Fig. 7, top left) is prevented, and thus a very ductile behaviour is reached, leading to higher strength values and larger deformation capacities. This positive effect of cross-layers is shown exemplarily in Fig. 6. The impact of a reduced end distance in LVL with cross-layers is illustrated in Fig. 8. While the initial behaviour is not affected, reducing the end distance promotes the occurrence of shear plug failures at an ealier stage, and thus leading to lower strength and reduced ductility.

Overall, the scatter in the results was very low, with an avarage coefficient of variation of about 4%.

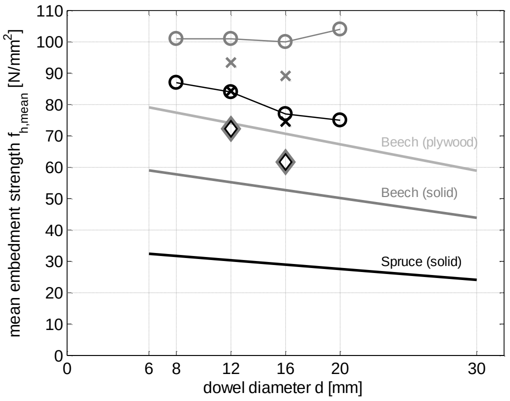

Fig. 5 Embedment strength f_h (mean values) acc. to EN 383 (l_3=7d). ○: 23% cross-layers; ×: 14% c.-l.; ◊: 0% c.-l.; ○×◊: $f_{h,EN383}$; ○×◊: $f_{h,max}$.
Acc. to EC 5: solid timber: Eq. (2), plywood: Eq. (3) with $\rho_{mean,beech}$=765kg/m^3 $\rho_{mean,spruce}$=420kg/m^3.

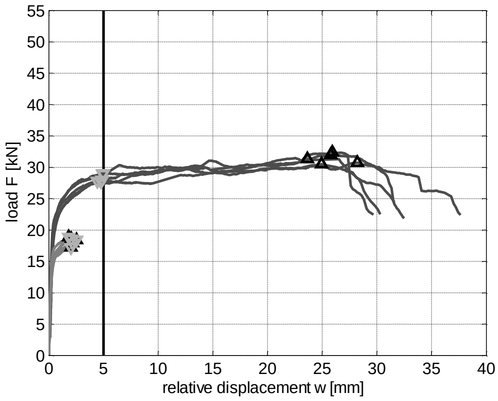

Fig. 6 Impact of cross-layers on embedment behaviour, shown for d=12mm and l_3=7d.
— 17% cross-layers (17-12-7d); — 0% c.-l. (0-12-7d).
Δ F_{max}; ▽ {$F_{\Delta=5mm}$; F_{max}} acc. to EN 383.

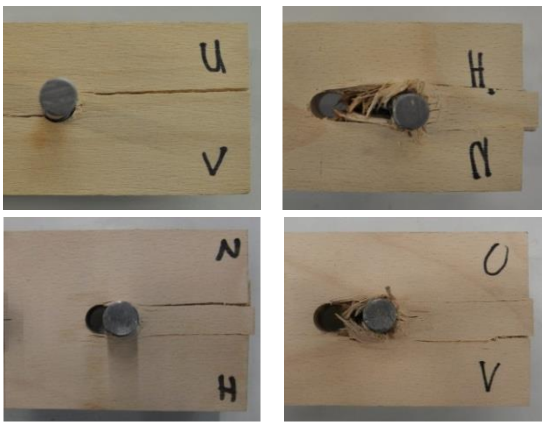

Fig. 7 Failures from embedment tests. Top left: 0-12-7d; top right: 17-12-7d; bottom left: 14-16-5d; bottom right: 14-16-7d (labels as in Table 3).

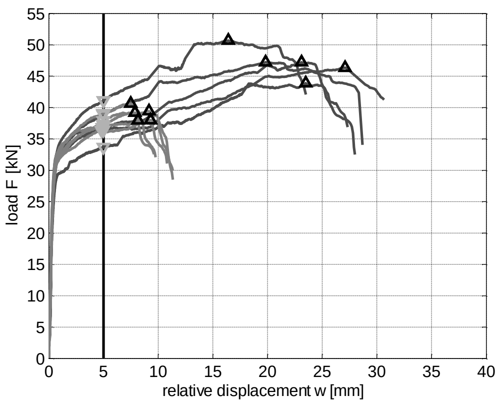

Fig. 8 Impact of end distance on embedment behaviour, shown for d=16mm and 14% cross-layers.
— 7d end distance (14-16-7d); — 5d end dist. (14-16-5d).
Δ F_{max}; ▽ {$F_{\Delta=5mm}$; F_{max}} acc. to EN 383.

2.2 Connection tests

2.2.1 Specimens and test setup

A series of 71 tensile tests on dowel-type connections was carried out according to EN 1380:2009 [12] and EN 26 891:1991 [13]. The series included dowelled connections with one and two slotted-in steel plates as well as bolted connections with outer steel plates (Fig. 9). The dowels in configurations (A) and (B) were of the steel quality S355 ($f_{u,k}$ = 510 N/mm^2), the bolts in configuration (C) were of quality 8.8 for screws ($f_{u,k}$ = 800 N/mm^2). The investigated parameters were the cross-layer percentage, the number of fasteners in a row and the spacings of the fasteners. Two different spacing patterns were used (Fig. 9, (D)). The pattern labelled "EC 5" follows the requirements for minimum spacings and end and edge distances given in EC 5, whereas in the "reduced" pattern the spacings between the fasteners and the end distance were reduced to 4*d*, which is slightly below the theoretically derived minimum spacing to prevent plug shear failures. This minumim spacing was derived from results of the embedment tests, assuming an elastic shear stress distribution in the shear planes. The reduced pattern was used to allow for the possibility of designing more compact connections and to assess corresponding consequences for the design approach.

Table 4 Test configurations of dowel-type connections.

Config-uration	Cross-layers	Fastener diameter	Spacing pattern	Rows of fasteners	No. of specimens
(A)	0 %	12 mm	EC 5	1	3
	0 %	12 mm	EC 5	2	3
	0 %	12 mm	EC 5	6	3
	0 %	12 mm	reduced	1	3
	0 %	12 mm	reduced	2	3
	0 %	12 mm	reduced	6	3
	14 %	12 mm	EC 5	1	3
	14 %	12 mm	EC 5	2	3
	14 %	12 mm	EC 5	6	3
	14 %	12 mm	reduced	1	3
	14 %	12 mm	reduced	2	3
	14 %	12 mm	reduced	6	3
	23 %	12 mm	EC 5	1	3
	23 %	12 mm	EC 5	2	3
	23 %	12 mm	EC 5	6	3
	23 %	12 mm	reduced	1	3
	23 %	12 mm	reduced	2	3
	23 %	12 mm	reduced	6	3
(B)	23 %	8 mm	EC 5	2	2
	23 %	20 mm	EC 5	2	2
	23 %	8 mm	½ EC 5	2	2
	23 %	20 mm	½ EC 5	2	2
(C)	21 %	16 mm	EC 5	1	3
	21 %	16 mm	EC 5	2	3
	21 %	16 mm	EC 5	3	3

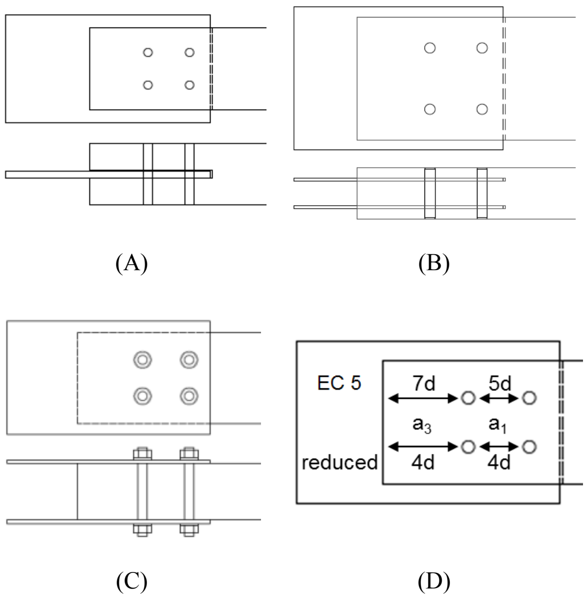

Fig. 9 Schematics of tested connections (shown for two fasteners in a row): (A),(B) – dowelled; (C) – bolted.
(D) – spacing patterns "EC 5" and "reduced".

2.2.2 Results and comparison with the EC 5 design approach

In the following selected test results are highlighted and compared to predictions using current design methods. Furthermore, the influence of the studied parameters on the behaviour of the connections is analysed.

2.2.2.1 Comparison with Johansen's yield theory

For comparison of the test results with predictions according to Johansen's yield theory as adopted in EC 5, connections with only on row of fasteners were considered, as in this case possible group effects are excluded. Results of dowelled connections (A) are shown in Fig. 10-Fig. 12. The connections were designed to fail in mode (II), i.e. combined embedment and dowel failure. The test results are compared to the corresponding theoretical values according to Johansen's yield theory. As no data about the actual mean tensile strength of the used steel dowels was available, the predictions were made based on data from [14] assuming mean values 25% above the characteristic values $f_{u,k}$. Using the values for f_h obtained from the embedment tests, a good agreement between the predictions and the test results was observed. Fig. 13 confirms that the assumed failure mode (II) could fully develop in LVL members with cross-layers.

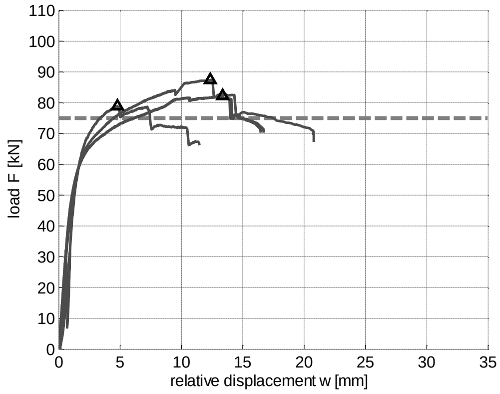

Fig. 10 Load-displacement curves of one row dowelled connections (A) in beech LVL with 0% cross-layers.
-- EC 5 prediction for mode (II) with $f_{h,EN383}$ from tests.

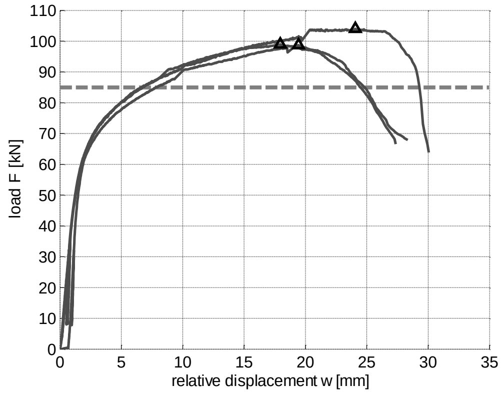

Fig. 11 Load-displacement curves of one row dowelled connections (A) in beech LVL with 14% cross-layers.
-- EC 5 prediction for mode (II) using $f_{h,EN383}$ from tests.

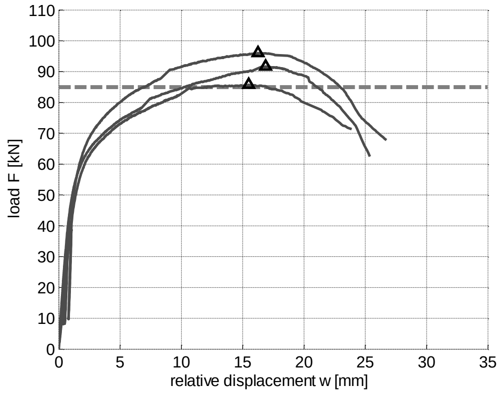

Fig. 12 Load-displacement curves of one row dowelled connections (A) in beech LVL with 23% cross-layers.
-- EC 5 prediction for mode (II) with $f_{h,EN383}$ from tests.

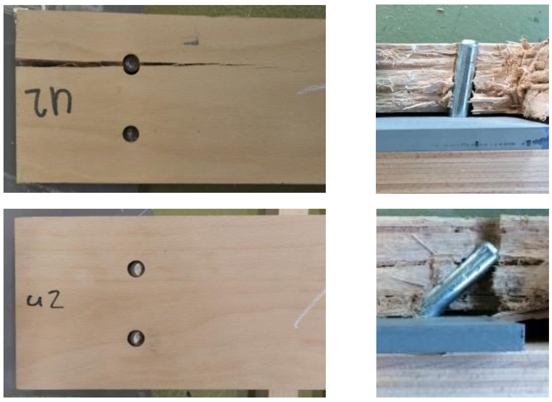

Fig. 13 Failed one row dowelled connections (A) designed to fail in mode (II). Top: 0% cross-layers; bottom: 14% cross-layers.

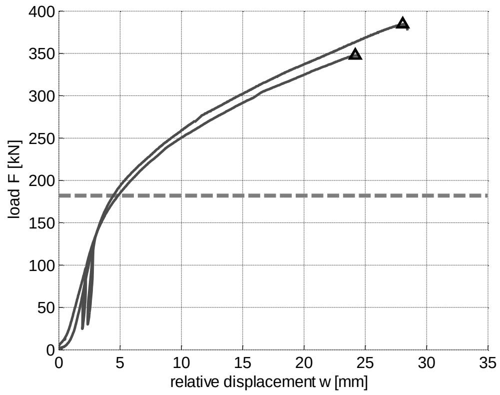

Fig. 14 Load-displacement curves of one row bolted connections (C) in beech LVL with 21% cross-layers.
-- EC 5 prediction for mode (III) with $f_{h,EN383}$ from tests.

Fig. 15 Failed one row bolted connections (C) designed to fail in mode (III), with failed bolt and visible rope effect.

In Fig. 14 the test results of the bolted connections (C) in LVL with cross-layers are compared to the predicitons obtained by applying EC 5 in. The measured load-carrying capacities were significantly higher than predicted by Johansen's approach. This discrepancy comes from a pronounced rope effect observed in the tests, which is not included to such an extent in the prediction according to EC 5 ($F_{ax}/4 \leq F_v/4$). This rope effect can develop to this extent due to the very ductile behaviour of the LVL when subjected to embedment stresses. Fig. 15 shows how embedment has taken place over the whole width of the LVL member. Theoretically, the load could be further increased until the embedment strength is reached over the whole width, which then corresponds to a ductile mode (I) failure. In the tests, however, the observed failure mode was a combined shear and tensile failure of the bolts (Fig. 15).

2.2.2.2 Impact of amount of cross-layers

The main advantage of cross-layers in LVL for dowel-type connections is the significantly increased tensile strength perpendicular to the grain, which prevents premature splitting failures and results in a very ductile behaviour of the LVL when subjected to embedment. This leads to higher load-carrying capacities, greater ductility along with better predictability, as the designated failure modes can fully develop. These effects can already be observed for one row of dowels (Fig. 10-Fig. 12), but they are even more pronounced for several rows, where group effects start impacting the behaviour of the connection (Fig. 16). With dowelled connections, tests have been carried out with 0%, 14% and 23% of cross-layers. As stated above, adding cross-layers led to a significantly improved performance of the connections. The difference between LVL with 23% compared to 14% cross-layers, however, was only marginal.

Regarding design considerations for truss structures, with members being mainly subjected to normal forces, generally a low cross-layer percentage is desirable, as a high cross-layer percentage decreases the longitudinal strength and stiffness of single truss members loaded in axial compression or tension. Therefore, the optimum amount of cross-layers has to be determined considering both the connection performance and the strength and stiffness of the members, as well as requirements for dimensional and form stability.

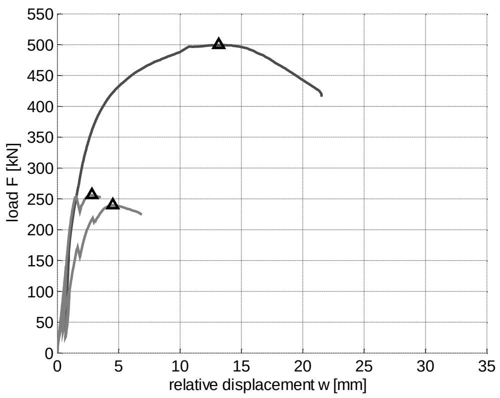

Fig. 16 Impact of amount of cross-layers for dowelled connections (A) as in Fig. 17. ▬ 14% c.-l.; ▬ 0% c.-l.

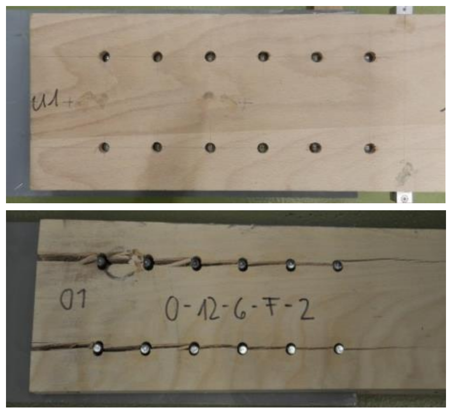

Fig. 17 Failed dowelled connections with EC 5 spacing patterns and 6 fastener rows. Top: 14% c.-l.; bottom: 0% c.l.

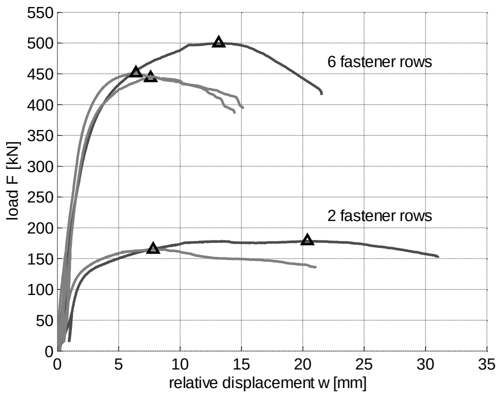

Fig. 18 Impact of spacing patterns for dowelled connections (A) as in Fig. 19. ▬ "EC 5" ▬ "reduced".

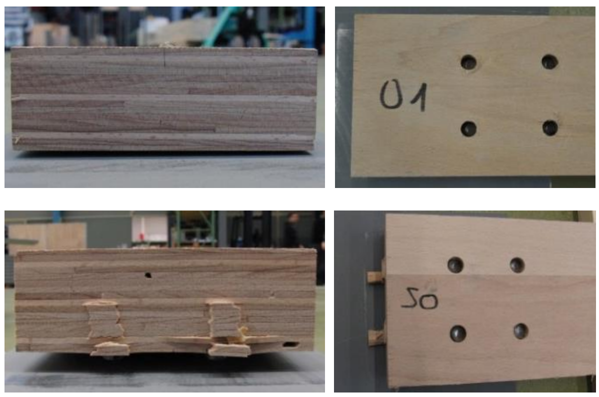

Fig. 19 Failed dowelled connections with 14% cross-layers. Top: EC 5 spacing pattern; bottom: reduced spacing pattern.

2.2.2.3 Impact of fastener spacings and end distances

The tested configurations of dowelled connections included two different spacing patterns in the loaded direction: Spacings according to EC 5 and reduced spacings (Fig. 9). Generally, compact connections with reduced spacings are desirable, in order to limit the additional material needs and the overall dimensions of the connections in the joints of the truss.

Following the spacing pattern according to EC 5 allowed the dowel failures to fully develop as designed based on the Johansen theory. Apart from embedment of the dowels, the LVL showed no visible damage (Fig. 19, top). The reduction of spacings and end distances, however, resulted in a combined dowel and plug shear failure, yielding slightly lower load-carrying capacities and a loss in ductility (Fig. 18). Shear failures are generally considered very brittle failures. However, Fig. 19 shows how the propagation of the shear plugs was impeded by the cross-layers. As a result of this, the load could be further increased even after the shear plugs had started to develop, and a certain degree of ductility could be retained.

The test results indicate the possibility to design dowel-type connections in LVL with cross-layers using reduced spacings and end distances. However, to fully exploit the load-carrying capacity of the fasteners and to maintain high ductility ratios, the requirements for spacings and end distances given by EC 5 appear to be suitable also for beech LVL. For the design it should be further considered that the chosen spacings and the resulting failure modes may also influence the level of partial safety factors to be applied when designing the connection.

2.2.2.4 Impact of number of fasteners in a row

The number of rows of fasteners was varied in the test specimens in order to assess the reduction factor experimentally and to compare it with the formula suggested in EC 5 (Eq. (1)). During testing it was observed that in dowelled connections with several rows of fasteners the side members started to bend outwards, ultimately leading to an “opening” failure (Fig. 20). This occurred only in LVL with cross-layers and can be explained with the chosen failure mode (II), for which at large deformations deviating forces arise due to the increasing inclination of the dowels. Therefore, in some of the tests the connections were clamped, preventing opening of the side members. In practice, this could be achieved by altering the failure mode (to either mode (I) or (III)) along with reducing the slenderness of side members and/or equipping some of the dowels with washers and nuts. In LVL without cross-layers no opening occurred, as the connections failed at much lower displacements due to splitting. For finally assessing the effective number of fasteners n_{ef}, only tests without opening failures were considered.

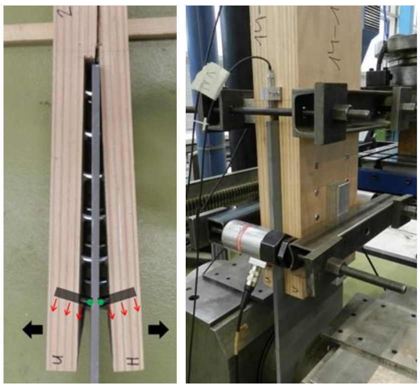

Fig. 20 Left: Opening failure in dowelled connections (A) with multiple fastener rows; right: clamping of a connection.

Fig. 21 and Fig. 22 show a comparison of the reduction factor $k_{red} = n_{ef}/n$ (reduction per fastener) derived from the test results and by applying the formula given in EC 5. This was done both for minimum spacings according to EC 5 and reduced spacings. For dowelled connections, the results show that without cross-layers n_{ef} was around or even below the given design values, whereas for LVL with cross-layers the design formula consistently proved to be conservative. However, the test results of dowelled connections indicate that a reduction factor still has to be taken into account, despite premature splitting failures being excluded. For bolted connections with outer steel plates, however, no negative group effects were observed. This might stem from the pronounced rope effect, which leads to more evenly distributed embedment stresses over the whole cross-section.

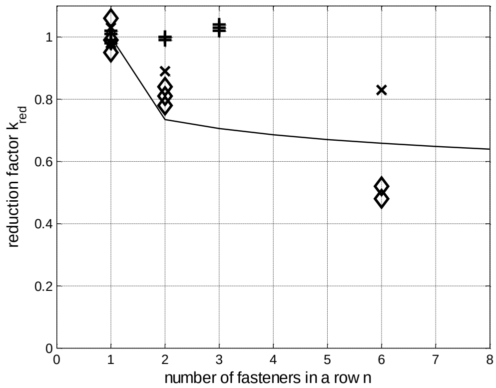

Fig. 21 Reduction factor $k_{red} = n_{ef}/n$ for EC 5 spacing patterns (a_1=5*d*). Comparison of test results with EC 5 approach from Eq. (1) (solid line). Dowelled connections (A): ◊: 0% c.l.; ×: 14%. Bolted connections: +: 21% c.-l.

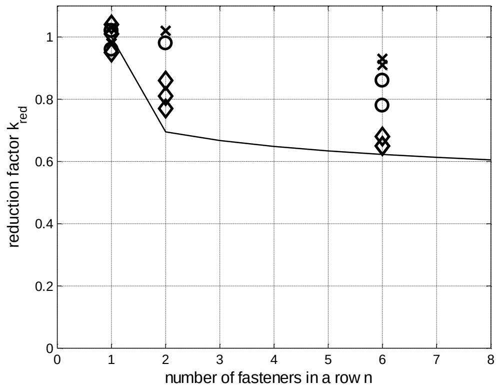

Fig. 22 Reduction factor $k_{red} = n_{ef}/n$ for reduced spacing patterns (a_1=4*d*). Comparison of test results with EC 5 approach from Eq. (1) (solid line). Dowelled connections (A): ◊: 0% c.-l.; ×: 14% c.-l.; ○: 23% c.-l.

3 Conclusions

The presented experimental investigations on dowel-type connections with dowels and bolts in beech LVL have confirmed that the favourable material properties of beech LVL are reflected in the performance of the connections:

Embedment strength

The embedment strength of beech LVL with cross-layers proved to be significantly higher than respective values given by the available design formulas in EC 5 for solid timber and glulam as well as cross-laminated timber (Norway spruce and beech). Also, the scatter in the results was low (CoV ≈ 4%) and the material showed a very ductile behaviour when subjected to embedment.

Dowel-type connections

The basic prerequisites to substantially improve the performance of dowel-type connections in joints of beech LVL structural members are:

- A sufficient amount of cross-layers in the LVL to prevent premature splitting failures and impede crack propagation is needed. In the conducted tests, a cross-layer percentage of 14% gave satisfactory results.
- “Opening” failures due to deviating forces of inclined fasteners have to be prevented. This can be achieved by an adapted geometry (slenderness of side members, failure modes) and/or by using bolts or equipping some of the dowels with washers and nuts.

Given these requirements are met, very ductile connections with high load-carrying capacities can be designed. Spacings can be adjusted depending on the requirements of the specific application. However, to fully develop the failure modes according to Johansen, the requirements for minimum spacings and end distances given in EC 5 should be met. Negative group effects have to be considered even though they are much less marked compared to connections in solid timber or glulam. Due to the potentially high load-carrying capacities per fastener, net cross-section failures can become relevant and therefore need to be verified in the design.

4 References

[1] Egner K., Kolb H. 1966: Geleimte Träger und Binder aus Buchenholz. Bauen mit Holz 68(4): 147-154.

[2] Gehri E. 1980: Möglichkeiten des Einsatzes von Buchenholz für Tragkonstruktionen. Schweizer Bauwirtschaft 79(56): 14-18.

[3] Glos P., Lederer B. 2000: Sortierung von Buchen- und Eichenschnittholz nach der Tragfähigkeit und Bestimmung der zugehörigen Festigkeits- und Steifigkeitskennwerte. Holzforschung München, TU München.

[4] Blass H.-J., Denzler J. K., Frese M., Glos P., Linsenmann P. 2005: Biegefestigkeit von Brettschichtholz aus Buche. Band 6 der Reihe Karlsruher Berichte zum Ingenieurholzbau. Lehrstuhl für Ingenieurholzbau und Baukonstruktionen. TU Karlsruhe.

[5] Schmidt M., Glos P., Wegener G. 2010: Verklebung von Buchenholz für tragende Holzbauteile. European Journal of Wood and Wood Products 68:43–57.

[6] Knorz M., van de Kuilen J.-W. 2012: Development of a high-capacity engineered wood product - LVL made of European Beech (fagus sylvatica L.). In: Proceedings of the 12th World Conference on Timber Engineering, pp. 487-497, Auckland, NZ.

[7] Dill-Langer G., Aicher S. 2014. Glulam composed of glued laminated veneer lumber made of beech wood: Superior performance in compression loading. In: Aicher S., Reinhardt H. W., Garrecht H. (eds.) Materials and Joints in Timber Structures. Springer Netherlands. pp. 603-613.

[8] Van de Kuilen, J.-W., Knorz, M., Prüfbericht Nr. 10511: Ergebnisse der Zulassungsversuche für eine ‚allgemeine bauaufsichtliche Zulassung' (abZ) von Furnierschichtholz aus Buche, 2012, Technische Universität München (TUM), Germany.

[9] Johansen, K. W. 1949: Theory of Timber Connections, IABSE, Publication No. 9, Bern, Switzerland, pp. 56-69.

[10] DIN EN 1995-1-1:2010-12. Eurocode 5: Design of timber structures - Part 1-1: General - Common rules and rules for buildings, DIN German Institute for Standardization.

[11] DIN EN 383:2007. Timber Structures - Test methods - Determination of embedment strength and foundation values for dowel type fasteners, DIN German Institute for Standardization.

[12] DIN EN 1380:2009. Timber structures - Test methods - Load bearing nails, screws, dowels and bolts, DIN German Institute for Standardization.

[13] EN 26 891:1991. Timber structures; joints made with mechanical fasten-ers; general principles for the determination of strength and deformation characteristics (ISO 6891:1983), CEN European Committee for Standardization.

[14] Erchinger, C. et al. 2006: Versuche an mehrschnittigen Stahl-Holz-Stabdübelverbindungen und Rillennagelverbindungen bei Raumtemperatur und Normbrandbedingungen. IBK Bericht, 293.

INTER

International Network on Timber Engineering Research

RESISTANCE OF CONNECTIONS IN CROSS-LAMINATED TIMBER (CLT) UNDER BLOCK TEAR-OUT FAILURE MODE

P Zarnani

P Quenneville

University of Auckland

NEW ZEALAND

Presented by P Quenneville

S Franke stated that in the model side plane was neglected. In the tests there was some shear transfer as there was no cut made in the specimen. If you made the cut it would fit the model. P Quenneville agreed.

S Franke referred to slide 16 where tef was the only check. He asked if the nail was smaller than the 1st laminar, is it possible that the failure would extend into the cross layer with rolling shear and tension. P Quenneville said it is possible.

I Smith asked what kind of end distances would be needed to avoid the alarming failures shown in some of the slides. P Quenneville responded that in a practical case 500 kN of load transfer in a shear wall was needed. Use up to 1 m wide connection and use LVL on the outside to provide the tensile resistance in the outside laminate. Depending on the load, the bottom end distance is not that significant; the length and width of the connection are more important.

A Buchanan stated for high strength and stiffness applications rivets are best and control of deflection in building needs stiffer fasteners. He commented that ductility can be put into some devices. For example for post tension rocking walls, yielding steel devices are used. One needs stiffness of the connections otherwise one will lose the post tension effect. He has a question in the problem with high stresses in CLT where LVL are used in CLT as mix material. Is it easy to handle mix material with various thicknesses and grades. P Quenneville responded that one still needs more work and discussion about the practical example in New Zealand. He said mobilizing the entire thickness may be more desirable.

Resistance of Connections in Cross-Laminated Timber (CLT) Under Block Tear-Out Failure Mode

Pouyan Zarnani, Pierre Quenneville
University of Auckland, New Zealand

Keywords: Timber, connections, CLT, Brittle failure, Plug shear, Stiffness-based model, Rivets.

1 Motivations

Timber construction has experienced considerable progress in recent years. The implementation of new engineered timber products such as Cross-laminated Timber (CLT) has played a significant role in such progress. CLT is made up of dimensional lumber glued together with structural adhesive and stacked in sheets with perpendicular orientation. It is most commonly utilised as floor and wall components across a wide range of residential and commercial building types. Due to its prefabricated elements and ease of installation, its application in mass timber multi-storey construction is growing rapidly (FPInnovations 2011). Through the emergence of such advanced engineered timber products, international building standards are revising their codes to accept high-rise timber buildings. In these types of structures, the joints need to transfer large loads and are more critical for designers. Extensive research has been conducted in Europe and more recently in Canada to evaluate the fastening capacity of different types of fasteners in CLT (Uibel, and Blass 2006, 2007; Mohammad et al. 2014). While ductile capacities calculated using yield limit equations based on the European Yield Model (EYM) are quite reliable for fastener resistance in connections, however, they do not take into account the possible brittle failure mode of the connection which could be the governing failure mode in multi-fastener joints (Zarnani and Quenneville 2014). This is the reason why the wood engineering community has dedicated a significant amount of effort over the last decades to establish a reliable predictive model to determine the capacity of timber connections under wood failure mechanisms. In recognition of this fact, a stiffness-based design approach which has already been developed by the authors and verified in LVL, glulam and lumber is adjusted to determine the connection brittle block-tear out resistance in CLT by considering the contribution of perpendicular layers.

2 Proposed design approach

The different orientation of the layers in a CLT member in comparison to glulam and Laminated Veneer Lumber (LVL) in which all the layers are laid in similar direction makes it a specific timber product. This is more important from the design perspectives as the CLT member is loaded through a joint and the stresses are distributed among the outer and inner layers. Initially, a numerical study has been conducted in order to have a better understanding of the stress distribution and the load path in CLT connections. Observations were then used to develop a closed-form analytical model.

2.1 Stress distribution in CLT

Through a simple numerical model, the parallel and perpendicular layers in a CLT member were simulated to investigate the effect of their orientation on transferring the joint load (Fig. 1). Based on potential CLT member configurations, it was assumed that the planks in a given plane are not connected on edges and that there is full load transfer between planks of different plane. To model the elastic behaviour of wood, the orthotropic stiffness properties in longitudinal, radial, and tangential axes were considered. The moduli of elasticity and rigidity and the relation among them were assumed as $E_R = E_T = E_L/20$; $G_{LR} = G_{LT} = 10G_{RT}$; and $G_{LR} = E_L/15$. Also, the Poisson's ratios were set to $\mu_{LR} = \mu_{LT} = \mu_{RT} = \mu_{TR} = 0.35$; and $\mu_{RL} = \mu_{TL} = 0.03$.

In the example shown in Fig. 1, the single shear connection consists of fasteners penetrating only the outer middle plank. In this example, the results of the FE analysis (Fig. 2a) demonstrate that about 55% of the applied load is taken by the loaded plank and the rest is distributed to the outer parallel planks adjacent to the loaded one and also to the inner parallel planks as a result of the reinforcing effect of the cross layer. In fact, the cross layer ties all adjacent parallel planks to the next layer of parallel planks (Fig. 2b). Therefore, for the joint resistance, the contribution of the other parallel planks should not be ignored even though the fasteners are not penetrating these layers.

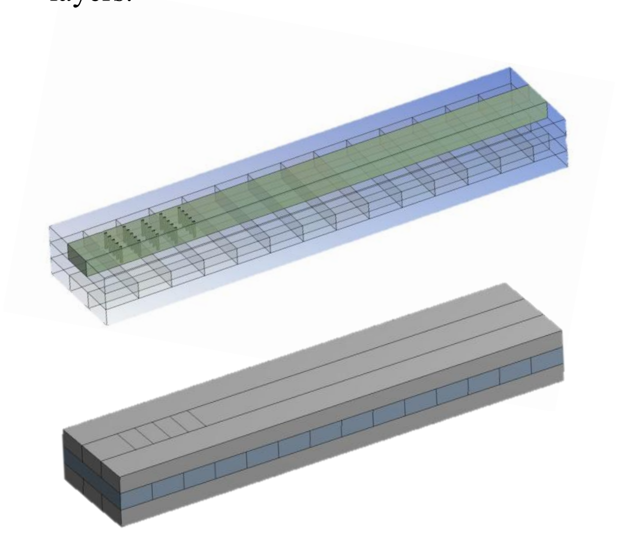

Fig. 1: Model of a CLT connection in which just the outer middle plank is loaded

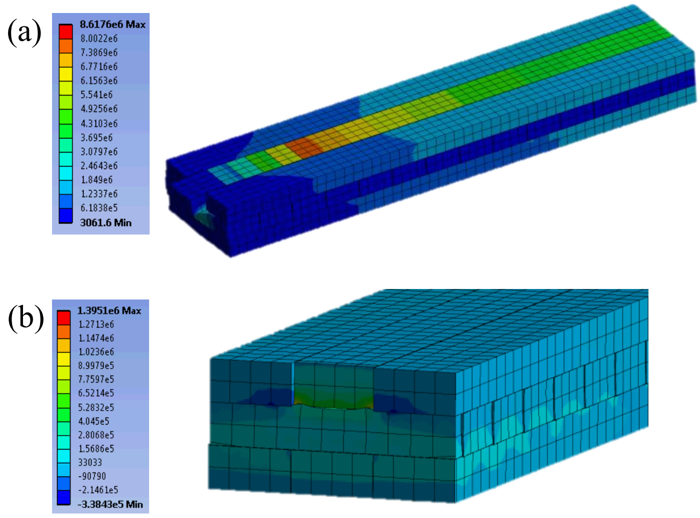

Fig. 2: Stress distribution in CLT layers: (a) tensile stress, (b) shear stress

2.2 Joint wood strength in CLT

The authors have already introduced a stiffness-based model (Fig. 3) for the prediction of wood block tear-out failure of connections in uniformly layered timber products such as LVL and glulam (Zarnani and Quenneville 2013, 2014). However, in CLT, the load transfer and stress distribution at the joint location are quite different due to the particular arrangement of the layers. Therefore, adjustments in the previously developed model are required in order to include the reinforcing effect of cross layers and determine the connection load-carrying capacity in wood brittle failure mechanisms.

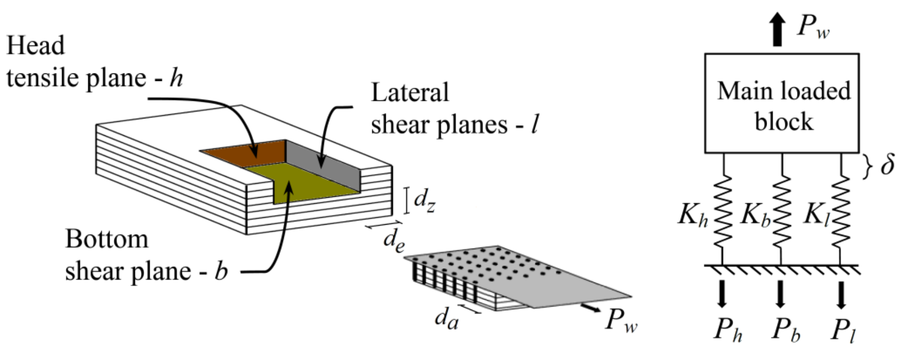

Fig. 3: Stiffness-based model developed for wood block tear-out resistance in LVL, glulam, and lumber

In the previous model developed for LVL or glulam, the applied load transfers from the wood member to the failure planes in conformity with the relative stiffness ratio of each resisting volume adjacent to the individual failure plane. As shown in Fig. 3, three resisting planes are involved including the head tensile, bottom shear and lateral shear planes. However, in the case of CLT (Fig. 4), the following considerations are necessary for the determination of the load path:

I. Disregard any contribution from the lateral shear planes ($K_l = 0$) since there is no load transfer between adjacent parallel planks. Moreover, there is no control on the positioning of the lateral planes of the joint cluster relative to the unbounded interface of the parallel planks. The worst scenario could be the matching of the lateral shear planes with the parallel planks interface.

II. Incorporate the reinforcing effect of the cross layers which contribute in transferring the load from the loaded planks at connection zone to the adjacent outer and inner parallel planks. It can be assumed as dealing with a wider and deeper joint.

In the connection shown in Figure 4, a block tear-out of depth t_{ef}, width w_c and length L_c+d_a is assumed. The wood volume of thickness d_z adjacent to the bottom shear plane is bonded to the cross layer at the glued interface. Therefore, its deformation under the acting shear force at the bottom plane decreases due to the additional stiffness resulting from the cross layer. As shown in Fig. 5a, the cross planks are restrained entirely at their bottom interface by the inner parallel planks. Also, the outer parallel planks adjacent to the loaded planks are constraining the top ends of the cross planks (Fig. 5b). Hence, the stiffness of the cross layer can be determined from the combination of its rolling and longitudinal shear deformations. Consequently, the overall stiffness corresponding to the depth under the bottom shear plane can be determined as

$$K_d = K_b + K_r + K_a \tag{1}$$

where K_b is the bottom shear plane stiffness corresponding to d_z. The K_r and K_a are the rolling and longitudinal shear stiffnesses of the cross layer, respectively. In fact, in the spring system shown in Fig. 4, a portion of the applied load will be absorbed by the head tensile plane (K_h) and the rest by the depth under the bottom shear plane (K_d). The load taken by K_d will be distributed to the residual section of the loaded planks (d_z) through K_b, to the inner parallel planks through K_r, and to the outer parallel planks adjacent to the loaded planks through K_a.

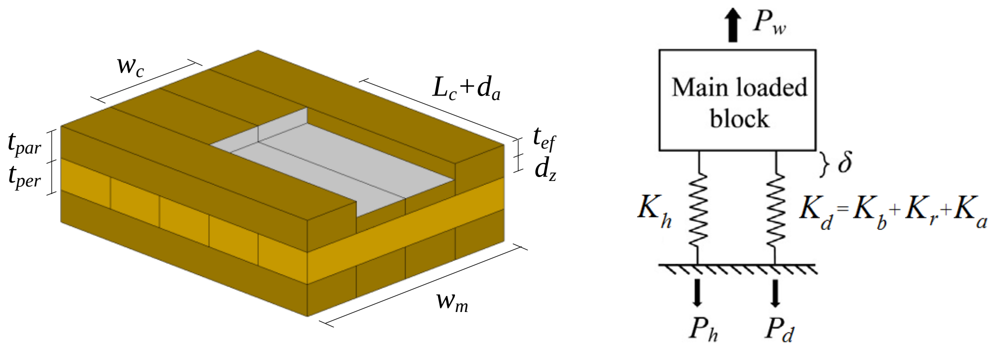

Fig. 4: Proposed stiffness-based model for wood block tear-out resistance in CLT

The K_h and K_b can be determined using the same equations provided for LVL or glulam, reported in Zarnani and Quenneville (2013). By considering the maximum rolling shear distortion of the cross layer at the connection width (w_c) to be equal to δ_r, the K_r can be expressed by Eq. (2) which takes into account the average rolling shear deformation of δ_r $(w_c+w_m)/(2w_m)$ at the entire cross layer (Fig. 5a). The K_a (Eq. 3) is derived based on the longitudinal shear deformation of the cross layer modelled as a block fixed at both ends under uniformly distributed loading (Fig. 5b). Setting the shear deformation at the top of the cross layer equal to δ_a, it is assumed that this deformation decreases linearly as it reaches the bottom part of the plank. Therefore, the average shear deformation of the cross layer at its thickness of t_{per} can be estimated as $0.5\delta_a$. In addition, the shear stiffness of this block under uniformly distributed loading is 2 times the case in which the load is applied as a concentrated load at the block centre. In Eqs. (2) and (3), G_r and G are the rolling and longitudinal shear moduli of the cross layer, respectively.

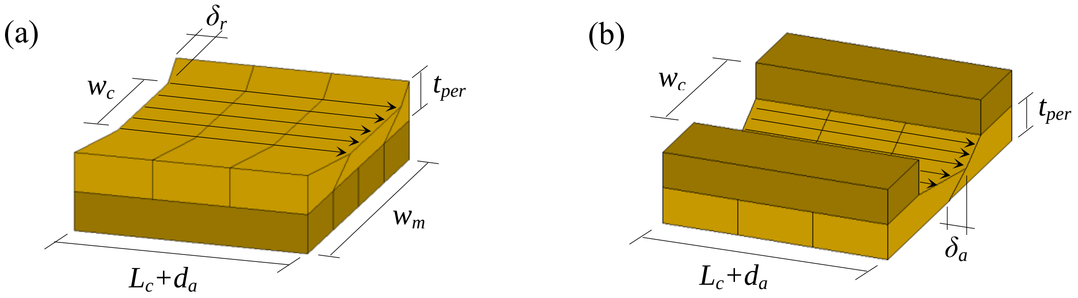

Fig. 5: Deformation of the cross layer:
(a) rolling shear deformation, (b) longitudinal shear deformation

$$K_r = \frac{G_r w_m (L_c + d_a)}{t_{per}} \times \frac{w_c + w_m}{2w_m} = \frac{G_r (L_c + d_a)(w_c + w_m)}{2t_{per}} \tag{2}$$

$$K_a = \frac{2Gt_{per}(L_c + d_a)}{w_c / 2} \times \frac{1}{2} \times 2 = \frac{4Gt_{per}(L_c + d_a)}{w_c} \tag{3}$$

By predicting the stiffness of the components contributing to the overall connection resistance, one can predict the proportion of the connection load taken by each component, $R_i = K_i / \sum K$. By further establishing the resistance of the failure planes corresponding to each of the resisting components, one can verify which of the failure planes governs the resistance of the entire connection. In fact, the connection resistance is a summation of the critical plane failure load plus the load carried by the other resisting components. The wood load-carrying capacity in a CLT connection is given by Eq. (4) which takes into account the possible situations of block tear-out failures (Fig. 6). These failure modes are specified based on the effective penetration depth of the fastener (t_{ef}) relative to the thickness and arrangement of the layers. The t_{ef} can be predicted by applying the embedment strength of CLT (Uibel and Blass 2006) and fastener characteristics in the methods reported in Zarnani and Quenneville (2012).

$$P_w = n_p \cdot \begin{cases} P_{w,I} = \min\,(p_{wh,I}, p_{wd,I}) & ,\ \text{if } t_{ef} < t_{par} \quad \text{(Mode I)} \\ P_{w,II} = \min\,(p_{wh,II}, p_{wd,II}, p_{wa,II}) & ,\ \text{if } t_{ef} = t_{par} \quad \text{(Mode II)} \\ P_{w,III} = \min\,(p_{wh,III}, p_{wd,III}, p_{wa,III}) & ,\ \text{if } t_{par} < t_{ef} < t_{par}+t_{per} \quad \text{(Mode III)} \\ P_{w,IV} = \min\,(p_{wh,IV}, p_{wd,IV}, p_{wa,IV}) & ,\ \text{if } t_{ef} = t_{par}+t_{per} \quad \text{(Mode IV)} \end{cases} \tag{4}$$

in which

$p_{wh,i}$ = wood resistance for tensile failure of head plane.

$$= f_t A_{th,i} \left(\frac{\sum K_i}{K_{h,i}}\right) \tag{5}$$

$p_{wd,i}$ = wood resistance for shear failure of bottom plane.

$$= f_{s,i} C_d A_{sd,i} \left(\frac{\sum K_i}{K_{d,i}}\right) \tag{6}$$

$p_{wa,i}$ = wood resistance for shear failure of the interface between the cross layer and the parallel planks adjacent to the loaded planks.

$$= f_{s,r} A_{sa,i} \left(\frac{\sum K_i}{K_{a,i}}\right) \tag{7}$$

n_p is the number of plates equal to 1 and 2 for one-sided joint and double-sided one, respectively. $A_{th,i}$ is the area subjected to the tensile stress and equal to $w_c t_{ef}$ for failure Mode I, and equal to $w_c t_{par}$ for the other failure modes. $A_{sd,i}$ is the area subjected to shear stress at the bottom of the block and equal to $w_c\,(L_c+d_a)$ for failure Modes I, II, and IV, and equal to $w_m\,(L_c+d_a)$ for Mode III. $A_{sa,i}$ is the area subjected to the shear stress at the interface between the cross layer and the parallel planks adjacent to the loaded planks, equal to $(w_m-w_c)(L_c+d_a)$ for failure Modes II and III, and equal to $2(w_m-w_c)(L_c+d_a)$ for failure Mode IV. f_t is the tensile strength parallel to the grain. $f_{s,i}$ is the longitudinal shear strength ($f_{s,l}$) for Mode I, and the rolling shear strength ($f_{s,r}$) for the other modes. C_d is the ratio of the average to maximum stresses on the bottom shear plane, equal to $(w_c+w_m)/(2w_m)$ for failure Mode III, and 1 for other failure modes. It should be noted that in failure Modes II and III, $d_z = 0$, therefore $K_b = 0$. In failure Modes I and IV, d_z is equal to t_{par} - t_{ef} and t_{par}, respectively. Also, in failure Modes III, and IV, the longitudinal shear deformation of the cross layer is uniform across its thickness. Therefore, $K_{a,III} = 2K_{a,I}\,(t_{ef} - t_{par})/t_{per}$ and $K_{a,IV} = 2K_{a,I}$. Moreover, in failure Mode III, the rolling shear stiffness of the residual cross layer thickness is estimated as $K_{r,III} = K_{r,I}\, t_{ef}\,/(t_{par}+t_{per} - t_{ef})$.

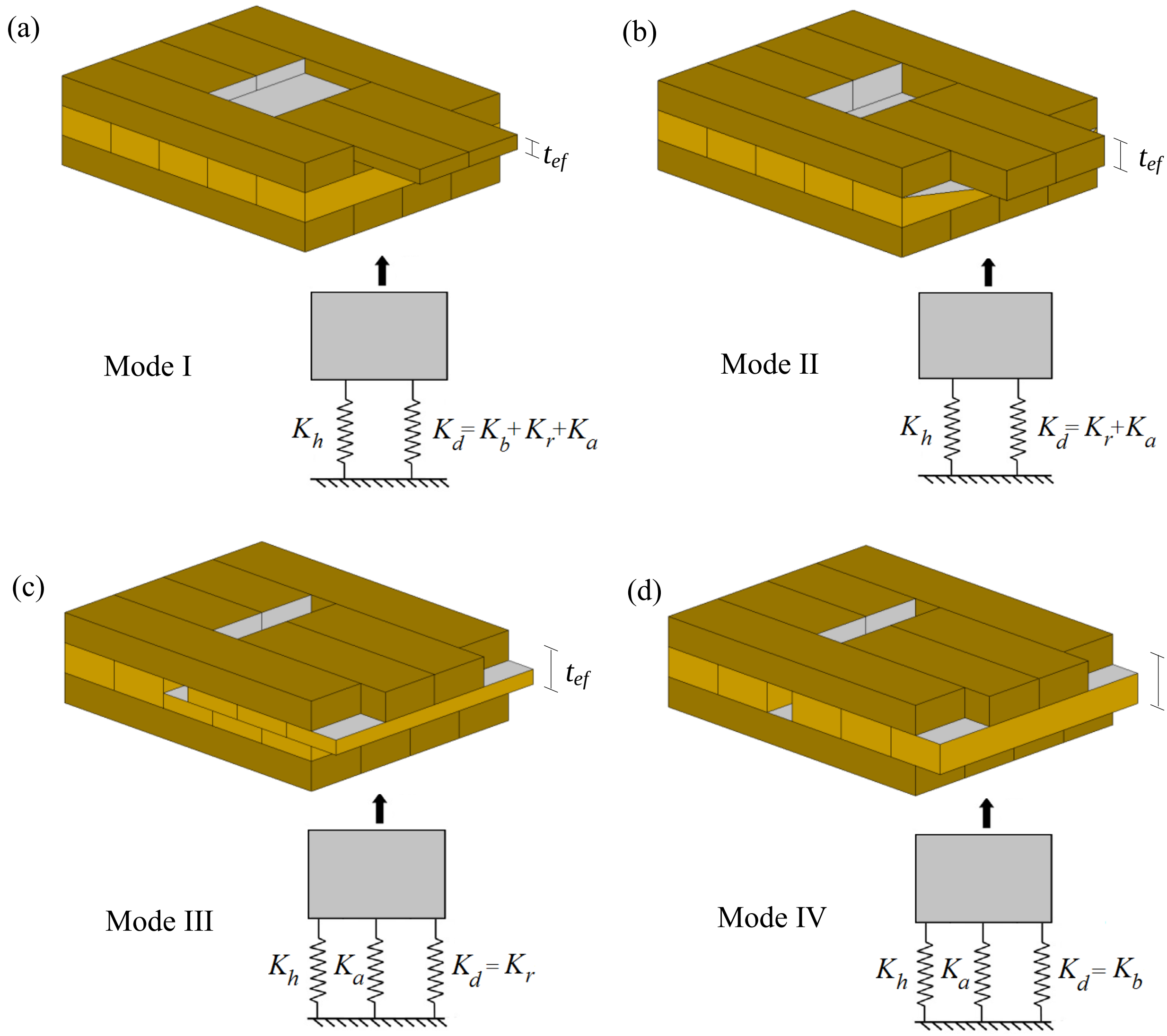

Fig. 7: Possible wood failure modes in CLT connections:
(a) $t_{ef} < t_{par}$, (b) $t_{ef} = t_{par}$, (c) $t_{par} < t_{ef} < t_{par}+t_{per}$, (d) $t_{ef} = t_{par} + t_{per}$

It is also important to note that the connection resistance corresponding to each failure mode is a summation of the critical plane failure load, plus the load carried by the other planes. Thus, when one plane fails, then the entire connection load transfers to the remaining planes in accordance with their relative stiffness ratios. It could be possible that the occurrence of the first failure of one plane does not correspond with the maximum load of the connection. Therefore, it is recommended that after the failure of one plane, one recalculates the wood resistance for the remaining planes to verify whether the residual planes can resist a higher load. In this paper, the presented equations cover the possible failure modes when the effective penetration depth of the fasteners is less than the total thickness of the first 2 layers ($t_{ef} < t_{par} + t_{per}$). For the cases in which more layers are involved, the described methodology can be applied to extend the model.

3 Testing program

Riveted connections were used to verify the model. The test configurations were selected to investigate the wood brittle failure modes and to evaluate the effect of geometry on connection strength. The rivet length and its penetration into the cross layer, the rivet group length and width, layer thicknesses and member width along with the end distance were considered. The testing program included nine groups with four replicates for each configuration. The arrangement of the plies and their relevant thicknesses can be found in Table 1. CLT specimens were manufactured from New Zealand Radiata Pine lumber stress graded 8 (SG8) with an average density of 430 kg/m^3 at12% moisture content. The thickness of the specimens varied from 145 mm to 200 mm including 5 or 7 layers in the cross-section. All specimens were conditioned to 20°C and 65% relative humidity to attain a target 12% equilibrium moisture condition (EMC) at the time of testing.

The specimens had riveted plates on the two opposite faces, resulting in a symmetric connection. The plates were 8 mm thick of 300 grade steel (f_y=300 MPa) with predrilled 6.9-mm holes to ensure the head of the rivets were rotationally fixed. Two lengths of rivets were used; 40mm long resulting in a penetration depth of L_p=28.5 mm and 65 mm long resulting in a penetration depth of L_p=53.5 mm. The geometric parameters of the connections consisted of 6 or 8 rivet rows (n_r) and 9 or 10 for the number of columns (n_c) as shown in Table 1. For all the test series, the spacing along and across the grain were set to S_c = 25 mm and S_r = 15 mm, respectively, conforming to the minimum requirements of CSA O86 (2009). The testing protocol outlined in ISO 6891(1983) was followed. The deformation of the connection was measured continuously with a pair of symmetrically placed LVDTs. A typical specimen in the testing frame is shown in Fig. 7.

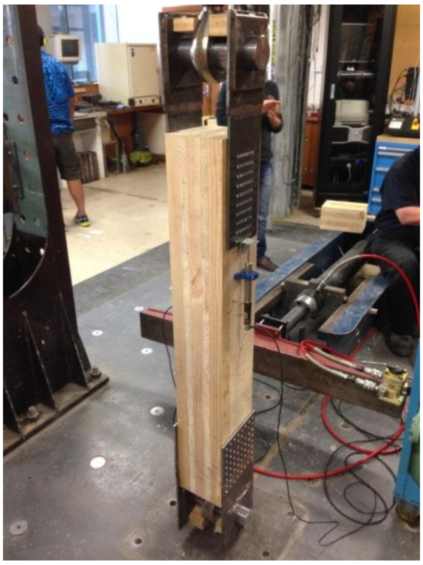

Fig. 7: Typical specimen in test set-up

Table 1: Test matrix for CLT riveted connections

<table>
<tr><th>Test group</th><th>Rivet penetration depth (mm)</th><th>No. of rows by columns</th><th>Cross-section thickness and layer arrangement (mm)</th></tr>
<tr><td>G1</td><td rowspan="6">28.5</td><td rowspan="2">6×10</td><td>175 (35/35/35/35/35)</td></tr>
<tr><td>G2</td><td>145 (35/20/35/20/35)</td></tr>
<tr><td>G3</td><td>6×9</td><td>145 (35/20/35/20/35)</td></tr>
<tr><td>G4</td><td>8×9</td><td>145 (35/20/35/20/35)</td></tr>
<tr><td>G5*</td><td rowspan="2">6×10</td><td>145 (35/20/35/20/35)</td></tr>
<tr><td>G6†</td><td>175 (35/35/35/35/35)</td></tr>
<tr><td>G7</td><td rowspan="2">53.5</td><td rowspan="2">6×10</td><td>200 (35/20/35/20/35/20/35)</td></tr>
<tr><td>G8</td><td>175 (35/35/35/35/35)</td></tr>
</table>

* With end distance of 75mm. For the other test groups: 50mm
† With member width of 350mm. For the other test groups: 200mm

4 Results and discussions

4.1 Test observations

The load-slip curve for each specimen was plotted, and the ultimate loads and the types of failure were recorded (Table 2). The peak loads ranged from 271 kN to 341 kN, indicating an overall low variability and small effect of the variables being investigated. The effect of the failure modes on the load-displacement plots is shown in Fig. 8. When brittle or mixed failure (brittle following the onset of yielding) occurred, the connection did not develop the full ductile capacity of the fasteners, and the ultimate capacity of the connection was dictated by the wood failure initiation. Specimens that failed in a brittle fashion experienced maximum displacements of 2 mm before failure. Specimens exhibiting a mixed failure suffered slightly more slip, experiencing minor plastic deformation of the fasteners before block tear-out failure occurred at a slip of 3-4.5 mm.

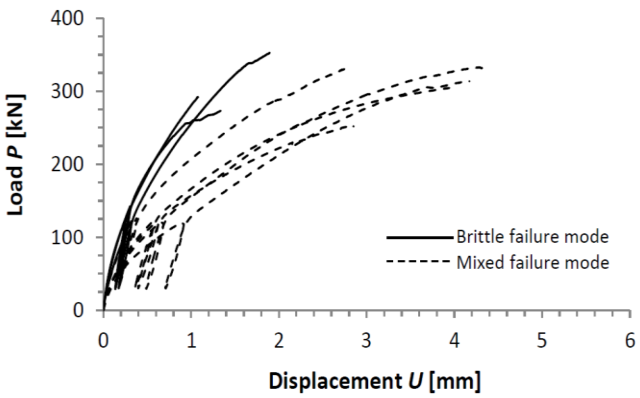

Fig. 8: Typical load-slip plots for riveted connections in CLT

Table 2: CLT connection strength and failure mode

Test group	Mean ultimate load (kN)*	Coefficient of variation (COV)	Failure mode
G1	285.7	12.3%	Mixed mode
G2	302.3	9.1%	Mixed mode
G3	5. 072	3071%	Mixed mode
G4	1. 371	3. 75%	Mixed mode
G5	1197.	371%	Mixed mode
G6	10670	3971%	Brittle mode
G7	295.8	6.3%	Brittle mode
G8	10. 73	3. 75%	Brittle mode

*4 replicates for each group.

In connections, where the rivets only penetrated the first parallel layer, a block of wood contained within the rivet group was pulled away from either one side or both sides of the specimens. A sample of failure Mode I is shown in Fig. 9a. In Fig. 9b, the specimen exhibits failure Mode II where the thickness of the failed block equals t_{par}. Also, the test observations shown in Fig. 10, demonstrate the possibility of the rolling shear failure at the interface of the outer parallel planks adjacent to the loaded one. For cases in which the penetration depth of the rivets could reach the cross layer, the block tear-out of the first layer was accompanied with the rolling shear failure at the interface of the cross layer and the adjacent outer and inner parallel planks (Fig. 11).

(a) (b)

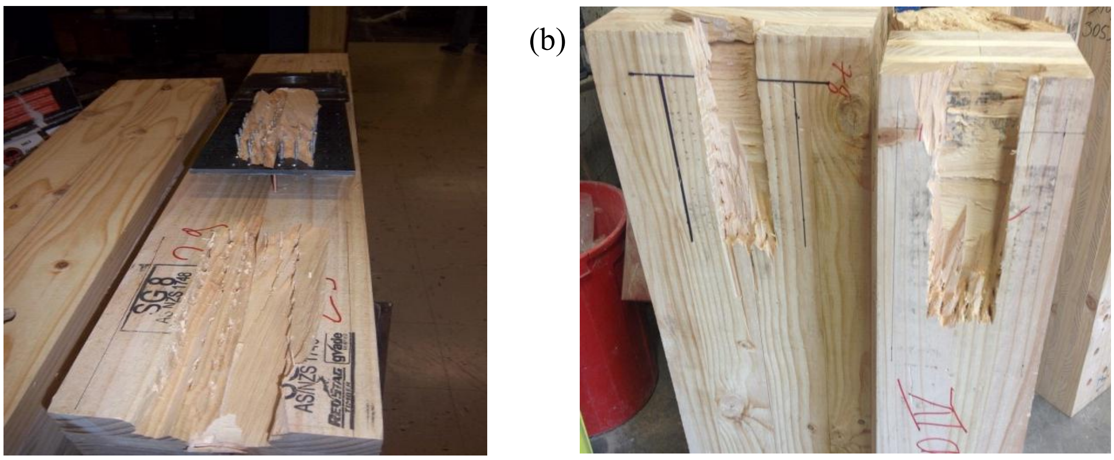

Fig. 9: Failed riveted connection showing block tear-out in the outer layer: (a) Mode I, (b) Mode II

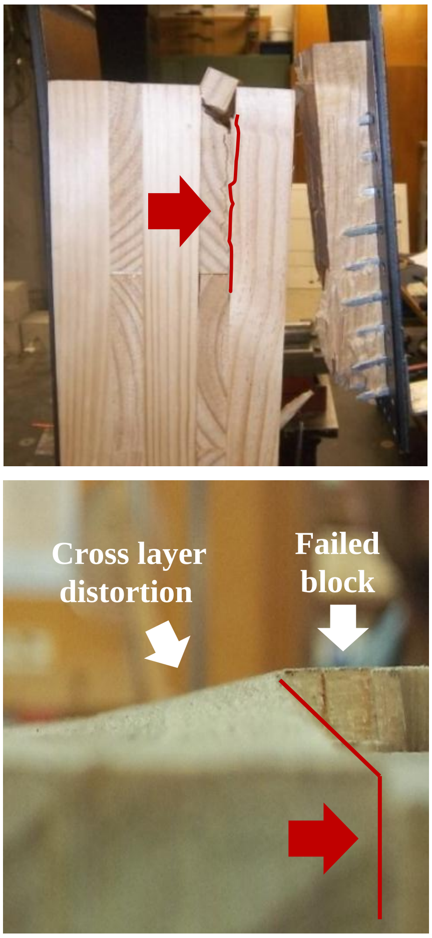

Fig. 10: Samples of failure Mode II, showing rolling shear failure of the interface between the cross layer and the parallel planks adjacent to the loaded planks

Fig. 11: Samples of failure Mode IV

4.2 Effect of connection configuration

Different configurations were designed for the CLT test groups in order to investigate the effect of connection configurations on the wood resistance under parallel to the outer layer loading. As shown in Fig. 12a to 12c, increasing the connection length (e.g., G2 and G3), increasing the connection width (e.g., G3 and G4), and increasing the end distance (G2 and G5), all resulted in sight increases in the connection wood capacity as expected.

Comparisons of the test series G1 and G8 were used to identify the effect of rivet penetration depth. As shown in Fig. 12d, it appears that the connection wood strength increases as the rivet length increases even after penetrating deep into the cross layer. This can be explained by the fact that the longer rivets have the advantage of mobilizing both the block tear-out capacity of the whole thickness of the first outer layer as well as the rolling and longitudinal shear resistance of the cross layer.

In the case of increasing the cross layer thickness (Fig. 12e), the results for the test series G1 and G2 appear to show a reduction of the connection wood strength. As the thickness of the cross layer increases, the related stiffness which could be determined from the rolling shear deformation of the separated blocks, would decrease. Therefore, this results in the cross layer channelling less of the connection load to the inner parallel layer and thus relying more on the outer layer. Also, the test results appear to demonstrate that an increase of the member width which is corresponding to an increase on the length of the cross layers, affects the connection wood resistance positively (Fig. 12f). Such additional resistance can be associated with the higher contribution from the cross layer due to an increase on its stiffness as a result of a larger rolling shear area. Therefore, the longer cross layers could distribute more portion of the applied load to the inner parallel boards in a distance wider than the connection width.

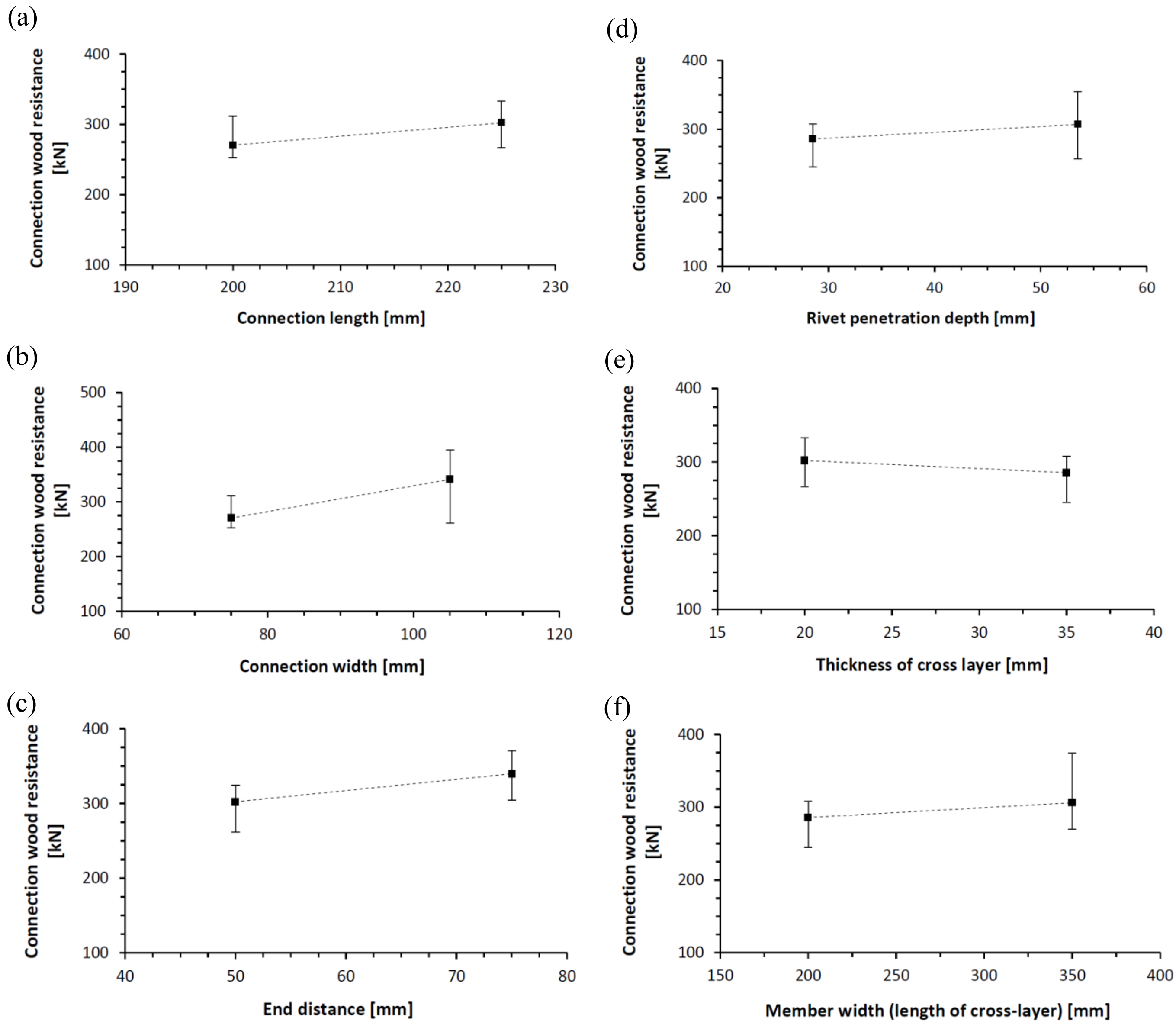

Fig. 12: Connection geometry effect on the wood load-carrying capacity: (a) connection length, (b) connection width, (c) end distance, (d) rivet penetration depth, (e) cross layer thickness, (f) member width (length of cross layer)

4.3 Verification of the proposed model

A comparison between the test failure loads and the predictions of the wood resistance using the stiffness-based approach developed for uniformly layered timbers such as LVL and glulam (Zarnani and Quenneville 2013, 2014) is shown in Fig. 13. The predictions are made assuming that all material is parallel to the grain. The assumed material properties are E = 8000 MPa, G = 533 MPa, G_r = 53 MPa, f_t = 11 MPa, f_s = 5 MPa, and $f_{s,r}$ = 1.7 MPa. One can observe that the predictions using these assumptions are only half of the results. This demonstrates that the stress distribution within the different outside and interior layer boards is more complex and different from the stress distribution assumed in uniform section with all layers running in one direction. As shown in Fig. 14, the proposed stiffness-based model for CLT lead to better predictions as it takes advantage of the increase in resistance for the failure modes due to the reinforcing effect of transverse layers. It should be noted that in the current tests, the lateral planes were not located at the planks interface. Therefore, the predictions could be even closer to the test results and less conservative if the contribution from the lateral shear planes were included in the model. As already described, any contribution from the lateral shear planes is disregarded in the model since there is no control on the positioning of the lateral planes of the joint cluster relative to the unbounded interface of the parallel planks.

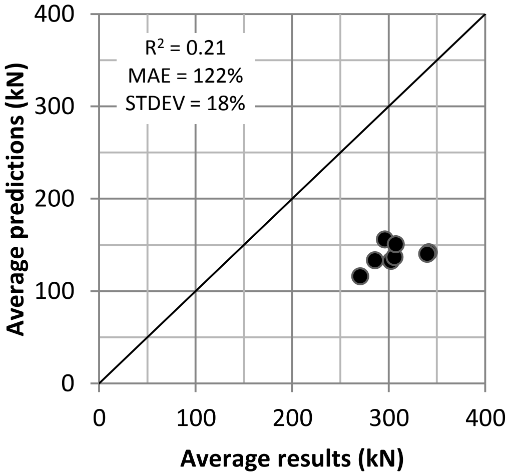

Fig. 13: Comparison of experimental results vs predictions using the previous model developed for uniformly layered timber (e.g. LVL, glulam)

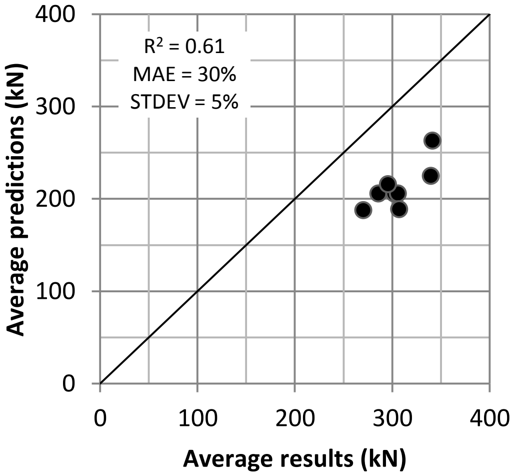

Fig. 14: Comparison of experimental results vs predictions using the proposed model for CLT

5 Conclusions

Through the emergence of advanced engineered timber products such as CLT, many international building standards are revising their codes to accept high-rise timber buildings. In these structures where the joints need to transfer huge loads, the brittle group failure of the joint is more susceptible and more critical. A stiffness-based design approach which has already been developed by the authors and verified in LVL, glulam and lumber has been adapted to determine the block-tear out resistance of connections in CLT by considering the effect of perpendicular layers. The comparison between the test results on riveted connections and the predictions using the new model and the one developed for uniformly layered timber products show that the proposed model provides higher predictive accuracy and can be used as a design provision to control the brittle failure of wood in CLT connections.

Acknowledgements

The authors wish to thank Olivier Perret who conducted the experimental tests as part of his internship at the University of Auckland and also the technical assistance of Mark Byrami.

References

CSA O86 (2009). “Engineering Design in Wood”. CSA Standards, Mississauga, ON, 2009.

FPInnovations. (2011). “CLT Handbook: Cross-laminated timber”. Gagnon, S., and Pirvu, C. (Eds). *Canadian Ed., Special Publication SP-528E,* Quebec, QC.

International Organization for Standardization (ISO). (1983). ISO 6891 Timber structures - Joints made with mechanical fasteners - General principles and determination of strength and deformation characteristics.

Mohammad, M., Salenikovich, A., Munoz, W., Zarnani, P., and Quenneville, P. (2014). "Brittle failure modes in CLT connections." *13th World Conference on Timber Eng.*, Quebec, Canada.

Uibel, T., and H. J. Blass (2006). Load carrying capacity of joints with dowel type fasteners in solid wood panels. Proceedings of the 39th CIB-W18 meeting, Florence, Italy.

Uibel, T., and H. J. Blass (2007). Edge joints with dowel type fasteners in cross-laminated timber. Proceedings of the 40th CIB-W18 meeting, Bled, Slovenia.

Zarnani, P., and Quenneville, P. (2012). Wood effective thickness in brittle and mixed failure modes of timber rivet connections. Proc., 12th World Conference on Timber Eng., Auckland, New Zealand.

Zarnani, P., and Quenneville, P. (2013). Wood block tear-out resistance and failure modes of timber rivet connections – A Stiffness-based approach. Journal of Structural Engineering, ASCE, 140(2): 04013055.

Zarnani, P., and Quenneville, P. (2014). Strength of timber connections under potential failure modes - An improved design procedure. Construction and Building Materials, Elsevier, 60: 81-90.

INTER

International Network on Timber Engineering Research

STUDY ON NAIL CONNECTIONS IN DEFORMED STATE

S Svensson

Technical University of Denmark

J Munch-Andersen

Danish Timber Information

DENMARK

Presented by S Svensson

H Blass commented that the present rope effect in EC5 is based on a theory that does not take into consideration actual fasteners. The angle φ needed in the study depends on splitting tendency. In this present EC5 this is not considered because the value of the angle is unsure. He asked how do you provide assurance of the value of the angle φ. S Svensson responded that in the elastic part the angle φ is approximately 1, 1.5, 2 degrees. In full plasticity for mild steel the angle φ is approximately 4 to 5 degrees. H Blass asked how to guarantee this angle before localized splitting of the timber. S Svensson agreed that this is a topic of future research. J Munch Andersen added that this paper aims to gain more understanding and insight with physically correct approach. H Blass asked can you quantify the contribution of the rope effect which has two parts one of which is already in the EC5. There was discussion that if the contribution is not that much, is it worthwhile to consider this because the angle φ may be different.

JW van de Kuilen referred to an old paper from TU Delft from J Kuipers and T van der Put on the same topic. He asked as annular ringed nails were used what type of yield moment was calculated for this type of fasteners. S Svensson responded that the values came from the manufacturer. JW van de Kuilen stated nails with cutoff round head will also behave differently.

I Smith commented about Johansson's work in 1941.

Study on Nail Connections in Deformed State

STAFFAN SVENSSON

Technical Univeristy of Denmark

JØRGEN MUNCH-ANDERSEN

Danish Timber Information, Denmark

Keywords: Deformed state equilibrium, Double lap shear, Friction, Material yielding.

1 Introduction

In Johansen (1949) a theory for the lateral load-carrying capacity of timber connections is presented. Substantial amount of research efforts have continued the work of K. W. Johansen. Investigations of material parameters required by the model both concerning wood and fasteners are for example presented in Whale & Smith (1986), Whale & Smith (1987), Ehlbeck & Werner (1992), Blass & al. (2000), and Jorissen & Leijten (2005). Other research found that for the case with slender, yielding fasteners (Larsen, 1977) the Johansen's model underestimates the load carrying capacity of the connections. This is especially significant for screws and modern ringed nails, c.f. Görlacher (1995), Bejtka & Blass (2002) and Hansen (2002).

The so-called European yield model (EYM) originates from Johansen's model but also includes correction terms for the rope-effect in order to improve the model precision (Blass & al., 1995). The EYM is in turn the base for the current European design rules for connections in timber structures (EN 1995-1-1, 2004).

The work presented here is another look into the theory of connections as an attempt to show the underlying mechanical behavior of a fastener in order to improve the EYM. The model herein presented is derived from the deformed state equilibrium of a fastener.

2 Theory

When a timber connection is laterally loaded until failure the fasteners rotate and deform together with the adjacent wood materials. For the case where the timber components of the connection do not split during loading, the attained rotations and deformations are large enough to influence the mechanical equilibrium. In the following two elementary equilibrium cases for a single fastener in deformed state are derived. The derived equations will of course coincide with non-deformed state theory (Johansen 1949) when the angle of connector rotation, φ, is close to zero so the contribution from the axial force can be neglected.

The load carrying capacity of a connection is found as the ultimate magnitude of total lateral forces, $(\Sigma F_v)_{ult}$. The force F_v is a function of the dowel force F_{vd} and the rope force F_{vr}. The dowel force and the rope force contributes directly to F_v being its components and indirectly being the normal action on adjacent wood surfaces sliding against each other hence causing in friction. The lateral force becomes:

$$F_v = F_{vd} \cdot cos\varphi + F_{vr} \cdot sin\varphi + \mu_{ww} \cdot (F_{vr} \cdot cos\varphi - F_{vd} \cdot sin\varphi) \qquad (1)$$

where μ_{ww} is the friction coefficient for wood sliding on wood. The forces and angle in (1) are illustrated in figure 1.

2.1 Equilibrium of rigid fastener in deformed state

A rigid fastener does not develop a plastic hinge during the loading of the connection. In figure 1 a rigid fastener isolated from the rest of the connection is shown. The cut over the fastener, to the left in figure 1, is at the connection's over-lap and assumed to be a mechanically condition of anti-symmetry. The outer forces acting on the fastener at the cut, F_{vd} and F_{vr}, as well as the embedment and withdrawal capacities, q and q_v, are illustrated in figure 1.

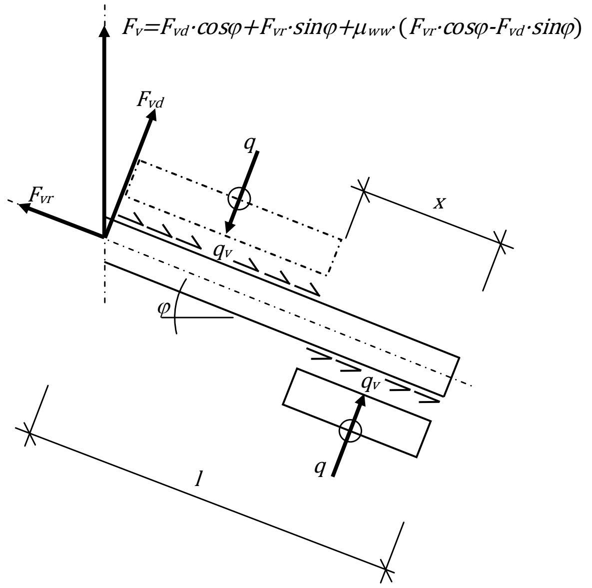

Figure 1. *Sketch of the right part of a rigid fastener in deformed state with anti-symmetry condition at left boundary (cut).*

The mechanical equilibrium of the rotated fastener in deformed state is mathematically described by equations (2), (3) and (4).

$$(\nwarrow) \quad F_{vr} - q_v \cdot l = 0 \qquad (2)$$

$$(\nearrow) \quad F_{vd} - q \cdot (l - 2 \cdot x) = 0 \qquad (3)$$

$$(\curvearrowright) \quad F_{vd} \cdot l - q \cdot \left(\frac{l^2}{2} - x^2\right) = 0 \qquad (4)$$

From (3) and (4) x is determined as:

$$x = l \cdot (1 - \tfrac{\sqrt{2}}{2})$$

and then the dowel and rope forces can be determined:

$$F_{vd} = q \cdot l \cdot \left(\sqrt{2} - 1\right) \qquad (5)$$

$$F_{vr} = q_v \cdot l = q \cdot \mu_{sw} \cdot l \qquad (6)$$

where μ_{sw} is the coefficient of friction between the fastener surface and the wood. The lateral force of the fasteners is found when (5) and (6) is inserted in (1) as:

$$F_v = q \cdot l \cdot \left(\left(\sqrt{2} - 1\right) \cdot (cos\varphi - \mu_{ww} \cdot sin\varphi) + \mu_{sw} \cdot (sin\varphi + \mu_{ww} \cdot cos\varphi)\right) \quad (1a)$$

The assumption that the fastener is rigid requires that the fastener remains in the elastic range. This condition can be formulated as:

$$M_{max} = q \cdot x^2 = q \cdot l^2 \cdot \left(\frac{3-\sqrt{8}}{2}\right) < f_y \cdot W_E \quad (7)$$

where f_y is the yield strength and W_E the elastic section modulus of the fastener.

2.2 Equilibrium of slender fastener in deformed state

A slender fastener develops a plastic hinge during the loading of the connection. In figure 2 a slender fastener isolated from the rest of the connection is shown. The cut over the fastener, to the left in figure 2, is at the connection's over-lap and assumed to be a mechanically condition of anti-symmetry. The outer forces acting on the deformed fastener at the cut, F_{vd} and F_{vr}, as well as the capacities, M_y, q, q_{ax}, q_m and q_v, are illustrated in figure 2. By considering the deformed fastener in mechanical equilibrium, see equations (8), (9) and (10), the distance z is readily determined when using $q_v = q \cdot \mu_{sw}$.

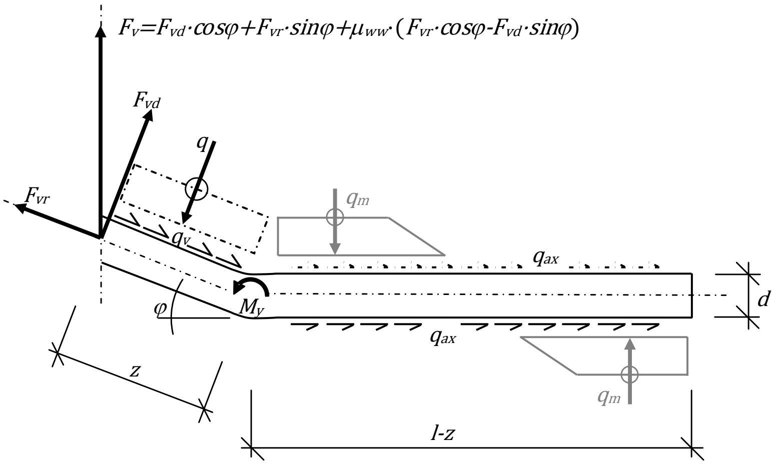

***Figure 2**. Sketch of the right part of a slender fastener with anti-symmetry condition at left boundary (cut).*

$$(\leftarrow) \quad F_{vr} \cdot cos\varphi + q \cdot z \cdot sin\varphi - q_v \cdot z \cdot cos\varphi - q_{ax} \cdot (l - z) - F_{vd} \cdot sin\varphi = 0 \quad (8)$$

$$(\uparrow) \quad F_{vd} \cdot cos\varphi - q \cdot z \cdot cos\varphi - q_v \cdot z \cdot sin\varphi + F_{vr} \cdot sin\varphi = 0 \quad (9)$$

$$(\curvearrowleft) \quad M_y - F_{vd} \cdot z + q \cdot \frac{z^2}{2} = 0 \quad (10)$$

The length, z, is solved from the systems of equations (8, 9 and 10) as:

$$z = \frac{q_{ax} \cdot l \cdot sin\varphi}{q + 2 \cdot q_{ax} \cdot sin\varphi} + \sqrt{\left(\frac{q_{ax} \cdot l \cdot sin\varphi}{q + 2 \cdot q_{ax} \cdot sin\varphi}\right)^2 + \frac{2 \cdot M_y}{q + 2 \cdot q_{ax} \cdot sin\varphi}} \quad (11)$$

and the dowel force and rope force are simplified from (8) and (9) to:

$$F_{vd} = q \cdot z - q_{ax} \cdot (l - z) \cdot sin\varphi \quad (12)$$

$$F_{vr} = q_v \cdot z + q_{ax} \cdot (l - z) \cdot cos\varphi \quad (13)$$

The lateral force of the fasteners is found when (12) and (13) is inserted in (1) as

$$F_v = q \cdot z \cdot \left(cos\varphi \cdot (1 + \mu_{sw} \cdot \mu_{ww}) + sin\varphi \cdot (\mu_{sw} - \mu_{ww}) \right) + q_{ax} \cdot (l - z) \cdot \mu_{ww} \quad (1b)$$

The assumption that the fastener is slender requires that the fastener develops a plastic hinge. It is the rigidity of the embedment to the right of the hinge in figure 2 that will determine if a hinge will develop or not. Since no shear force transfers through the yield point - because the moment has its maximum value there - the forces perpendicular the fastener in figure 2 to the right of the hinge must be self-balancing. A condition for fully developed hinge may therefore be formulated from the moment equilibrium of this part of the nail, assuming that q_m has reached full embedment capacity q and is evenly distributed.

$$M_{hinge} = q \cdot \frac{(l-z)^2}{4} > f_y \cdot W_P = M_y \quad (14)$$

where W_P is the plastic section modulus of the fastener. Out of practical convenience the criterion in (14) is usually written as a minimum penetration length:

$$l > z + 2 \cdot \sqrt{\frac{M_y}{q}} \quad (15)$$

3 Test set-up and results

All tests in this study were conducted on double lap shear specimens, where both center member and the fish plates (side members) were made of laminated veneer lumber (LVL). The material direction was always aligned so that the main wood fiber direction and the load carrying direction of the specimens coincided. Figure 3 shows a sketch of the specimen.

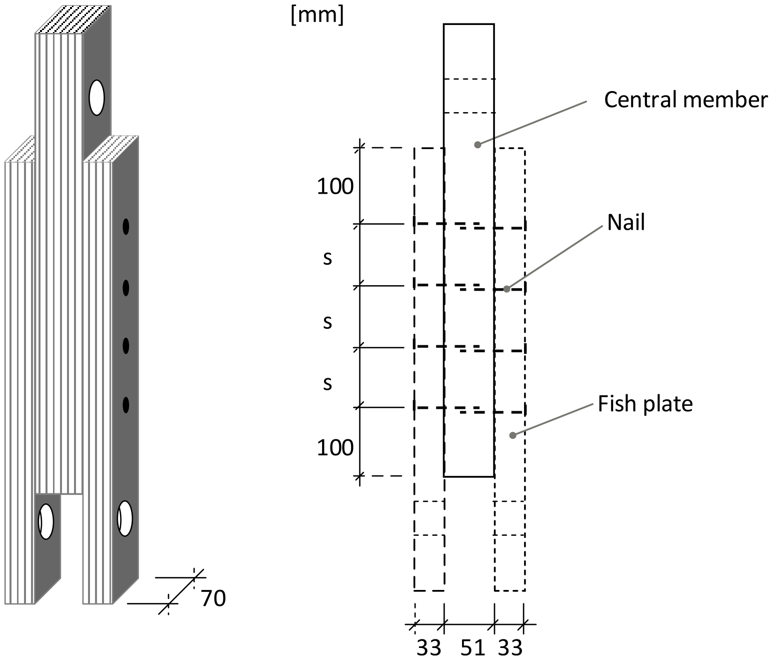

Figure 3. *Drawing of the double lap shear specimen used.*

All specimens were tested following the requirements of the test method given in EN 14592 (2012), with the exception that the LVL was conditioned at 23° C and 65 % RH both before and after the nailing.

In all tests the specimen width was 70 mm and the thickness of the center member and the fish plates were 51 mm and 33 mm, respectively. The nails had diameter d = 3.4 mm and length 64 mm including the point length (1.5*d*). They were placed along the center line, inserted from both sides with a pneumatic nail gun. The number of nails, *n*, per specimen was in total eight or 14, four or seven from each side. Two different nail spacing distances, *s*, where used, 40 mm and 80 mm. The loaded end distance was 100 mm (30*d*) and non-loaded edge distance was 35 mm.

The nails were ringed and of mild or hardened steel. The yield moments for the nails were determined, in accordance with EN 409 (2009) by the manufacturer as 4.5 Nm for the mild steel nail and 7.7 Nm for the hardened, but otherwise the nails were identical. The friction between the timber members was varied by coating the abutting wood surfaces with Teflon on selected specimens. The friction coefficient of the Teflon used is according to the manufacturer in the range 0.05 to 0.1. The Teflon was applied to the wood surfaces as long tape stripes parallel the main grain direction. This was done in order to minimize the reinforcing effect of the Teflon in the weak direction perpendicular to the grain. In table 1 data is provided for each specimen.

Table 1. *Test specimen data. n is number of nails, s is nail spacing, φ_{pu} is the average bending angle after failure in central member, and F_{obs} is the measured failure load. Further the calculated capacity according to Eq. (1b) is given, along with the components according to Eq. 12 and 13. In the specimem-ID M stands for mild steel, H for hardened steel and T for Teflon.*

ID	n [-]	s [mm]	φ_{pu} [°]	F_{obs} [kN]	$n{\cdot}F_v$**(1b)** [kN]	$n{\cdot}F_{vd}$**(12)** [kN]	$n{\cdot}F_{vr}$**(13)** [kN]
M1	4x2	80	13.3	17.65	16.55	9.92	14.50
H1	4x2	80	2.4	18.55	16.70	11.74	15.00
MT1	4x2	80	20.5	15.28	16.10	10.82	14.99
HT1	4x2	80	1.7	16.38	13.16	11.69	14.95
M2	7x2	40	15.1	29.04	29.81	10.13	25.59
H2	7x2	40	2.5	30.06	29.29	11.75	26.26
MT2	7x2	40	7.8	20.86	21.16	9.38	24.68
HT2	7x2	40	1.0	24.50	22.65	11.65	26.07
M3	4x2	40	9.6	16.28	15.51	9.54	14.23
H3	4x2	40	1.7	17.85	16.51	11.69	14.95
MT3	4x2	40	9.9	13.91	12.75	9.57	14.26
HT3	4x2	40	1.7	14.70	13.14	11.69	14.94

The selected twelve specimens failed in the central member without wood splitting in any timber component. After testing the specimens were opened and all nails were photographed, se figure 4. The bending angles after failure, φ_{pu}, were measured in the photos. In all cases the nail is pulled out of the center piece, rather than the head being pulled in.

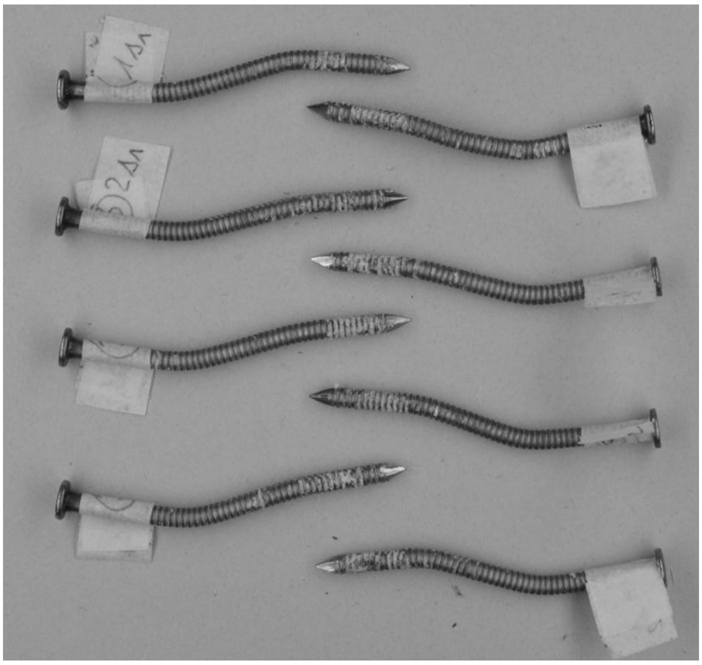

Figure 4. *Nails after testing, specimen MT1. (Photo: Paul Bavière).*

In the following, the results are shown graphically as calculated load carrying capacity of the connections vs. measured failure load of the same connection. In table 1 the failure loads for the ten connections are presented. In table 2 the model parameters are given. It is assumed that the point length ($1.5 \cdot d$) of the nails does not contribute to the load carrying capacity of the connection. The effective embedment length is therefore taken as 26 mm.

Table 2*. Model parameters; where nail geometry, yield moment and teflon friction value were attained from manufactures and the other parameter values were estimations based on values found in literature (Mckenzie & Karpovich, 1968, Möhler & Maier, 1969 and Smith, 1983).*

M_y [Nm], "mild" nail	4.4	$q = f_h \cdot d$ [N/mm]	$40 \cdot 3.4$
M_y [Nm], "hard" nail	7.7	$q_{ax} = f_{ax} \cdot d$ [N/mm]	$13 \cdot 3.4$
d [mm]	3.4	l [mm], (pen. length)	26
Length [mm]	64	μ_{ww} (wood-wood)	0.3
$\mu_{ws} = q_v/q$ (nail-wood)	0.8	μ_{tt} (teflon-teflon)	0.07

Figure 5 shows the outfall of modelled capacity of the connections in relation to the measured values. The diamond markers represent results according to the presented theory using equation (1b) with the average bending angle from table 1. The cross markers are the results estimated with the EYM (including rope-effect as described in Eurocode 5) using the appropriate model parameters of table 2.

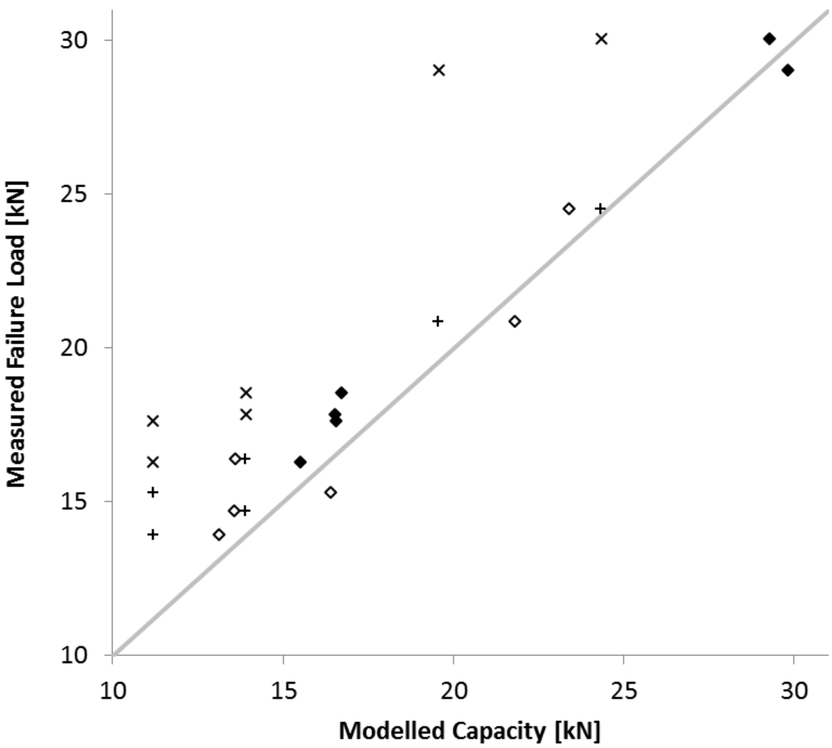

Figure 5. *Measured failure load versus estimated capacity. Diamond markers represent modelled capacities based on presented theory calculated on the values given in table 2, whereof the open markers represent the specimens with Teflon coated abutting surfaces. Cross markers represent modelled capacities using EYM with parameters given in table 2, where + indicates Teflon coated surfaces.*

4 Discussion and conclusions

The model given in equation (1b) is seen to represent the measured load-carrying capacities quite well. The coefficient of variation is only 7 %. The model deviates especially from the EYM by including the bending angle that enables a direct rope force as well as friction between abutting members of the connection. The model also works very satisfying when comparing ringed and smooth nails, see Svensson and Munch-Andersen (2014).

It is seen that the bending angle is small for the hardened nails, but ignoring the nail yielding and consider the nails rigid as in equation (1a) will lead to serious overestimation of the load-carrying capacity. This is believed to be due to the friction force between nail and timber $q_v = q \cdot \mu_{sw}$ being significantly larger than the withdrawal strength q_{ax}.

The small bending angle of the hardened nails has activated the axial force and the axial force is mainly a result of the withdrawal resistance. This coincides with the EYM, which uses the withdrawal strength to estimate the rope effect, being on the safe side even when Teflon is used, as seen in figure 1.

For the model to be practical a method to estimate the bending angles must be developed. Further, the measured angles indicate that the bending decreases as the nail spacing decreases. This ought to be investigated further. If it is confirmed, row effects might be taken into account by reducing the bending angle.

Acknowledgements

All tests on connections presented were conducted by Mr. Daniel Ramerez Opisso as a part of his thesis work for MSc in Civil Engineering. The nails and the LVL were kindly donated by ITW Construction Products, Denmark and Metsä Wood Denmark respectively. Their contributions are very much appreciated.

References:

Bejtka, I., H. J. Blass, 2002: Joints with inclined screws. Proceedings from the CIB-W18, meeting 35, Kyoto, Japan.

Blass, H. J., P. Aune, B. S. Choo, R. Görlacher, D. R. Griffiths, B. O. Hilson, P. Racher, G. Steck (Editors), 1995: Timber Engineering STEP1, Basis of design, material properties, structural components and joints. Centrum Hout, The Netherlands.

Blass, H. J., A Bienhaus, V Krämer, 2000: Effective bending capacity of dowel-type fasteners. Proceedings from the CIB-W18, meeting 33, Delft, The Netherlands.

Ehlbeck, J., H Werner, 1992: Softwood and hardwood embedding strength for dowel-type fasteners, Background of the formulae in Eurocode 5. Proceedings from the CIB-W18, meeting 25, Åhus, Sweden.

EN 1995-1-1, 2004: Eurocode 5, Design of timber structures: Part 1-1, General – Common rules and rules for buildings. CEN, Bussels, Belgium.

EN 409, 2009: Timber structures - Test methods - Determination of the yield moment of dowel type fasteners

EN 14592 + A1, 2012: Timber structures - Dowel-type fasteners – Requirements. CEN, Bussels, Belgium.

Görlacher, R., 1995: Load-carrying capacity of steel-to-timber joints with annular ringed shank nails. Proceedings from the CIB-W18, meeting 28, Copenhagen, Denmark.

Hansen, K. F., 2002: Mechanical properties of self-tapping screws and nails in wood. Can. J. of Civ. Eng. Vol 29, 5.

Hill, R., 1950: The Mathematical Theory of Plasticity, Oxford University Press.

Johansen, K. W., 1949: Theory of timber connections. IABSE publications vol. 7.

Jorissen, A., A. Leijten, 2005: The yield capacity of dowel-type fasteners. Proceedings from the CIB-W18, meeting 38, Karlsruhe, Germany.

Larsen, H. J., 1977: K. W. Johansen's nail tests. Bygningsstatiske meddelelser Vol 48, 1.

Mckenzie, W. M. and H. Karpovich, 1968: The frictional behavior of wood. Wood Science and Technology, Vol 2, 2.

Möhler, K and G. Maier, 1969: The coefficient of friction of spruce timber in view of the efficiency of timber-connections using frictional resistance (In German). Holz als Roh- und Werkstoff, Vol 27, 8.

Smith, I., 1983 Coefficient of friction values applicable to contact surfaces between mild steel connectors such as bolts and dry European whitewood. J. of the Institute of Wood Science, Vol 9, 5.

Svensson, S., J. Munch-Andersen, 2014: Theory of timber connections with yielding mechanical fasteners. Submitted to Engineering structures.

Whale, L. R. J., I. Smith, 1986: The derivation of design clauses for nailed and bolted joints in Eurocode 5. Proceedings from the CIB-W18, meeting 19, Florence, Italy.

Whale, L. R. J., I. Smith, H. J. Larsen, 1987: Design of nailed and bolted joints. Proposals for the revision of existing formulae in draft Eurocode 5 and the CIB Code. Proceedings from the CIB-W18, meeting 20, Dublin, Ireland.

INTER

International Network on Timber Engineering Research

DESIGN MODEL FOR INCLINED SCREWS
UNDER VARYING LOAD TO GRAIN ANGLES

R Jockwer
Empa, Swiss Federal Laboratories for Materials Science and Technology, Structural Engineering Research Laboratory, Dübendorf
ETH Zurich, Institute of Structural Engineering IBK, Zurich

R Steiger
Empa, Swiss Federal Laboratories for Materials Science and Technology, Structural Engineering Research Laboratory, Dübendorf

A Frangi
ETH Zurich, Institute of Structural Engineering IBK, Zurich,

SWITZERLAND

Presented by R Jockwer
H Blass asked why this type of connections was considered when you would have openings. R Jockwer responded that for the reinforcement case such as notched beams this has relevance. H Blass asked would you not incline the screws to avoid opening effect even in the reinforcement cases. In the notch case there is an opening component. Also for example CLT wall connected at the corner there would be an opening case. H Blass received confirmation that in such cases where the opening reduced the embedment, the withdrawal length was also reduced.
H Blass stated that back calculation of the embedment strength can be affected by the existence of friction forces even though Teflon was used. Friction can still be transferred where the calculated embedment in the paper is significantly higher than the values in literature. R Jockwer agreed.
J Munch Andersen commented about the contribution of the head of the screw potentially increasing the fastener capacity due to rope effect.
M Frese commented that pulling test of the inclined screws at 45 degree, relative movement of both pieces was observed. In the case of the notched beam, the beam is bonded which will restrict horizontal movement. He asked if the tests reflect reality. R Jockwer responded that in the test only at larger deformation such lateral movement was observed so the test should be valid.
S Svensson asked did you monitor the bending angles of all of the screws. R Jockwer stated only a few cases were observed and they did not keep the failed screws. S Svensson asked why the compression mode was not tried. R Jockwer responded that similar tests were done in the literature; their results offered comparisons for this study.

1st INTER Meeting, 01 to 04 September, Bath, United Kingdom

Design model for inclined screws under varying load to grain angles

Robert Jockwer[1,2], René Steiger[1], Andrea Frangi[2]
[1] Empa, Swiss Federal Laboratories for Materials Science and Technology, Structural Engineering Research Laboratory, Dübendorf, Switzerland
[2] ETH Zurich, Institute of Structural Engineering IBK, Zurich, Switzerland

Keywords: Timber, dowel-type fastener, joint, reinforcement, stiffness, strength, perpendicular to grain loading, test

1 Introduction

Fully threaded screws are used in various applications for the purpose of connecting or reinforcing structural timber elements. The screws are easy to apply and exhibit high performance. Like other dowel type fasteners, fully threaded screws show highest strength and stiffness properties when being loaded in axial direction. Hence, the optimal inclination (shank versus grain direction) of the screws has to be chosen with respect to the acting forces in the joint.

Different situations where screws are applied as reinforcing elements are shown in Fig. 1 (a-d). In the cases of pure compression or pure tension perpendicular to the grain, the screws should be set perpendicular to the grain. For reinforcement purposes in zones subjected to high shear stresses the screws, however, should be applied with an angle of $\gamma = 45°$ between shank and grain direction.

Examples with screws used as connecting elements are shown in Fig. 1 (e-g). In lateral connections screws are installed with an angle $\gamma = 45°$ to the grain. Compression stresses between the members increase the load-carrying capacity of the joint. In joints where shear

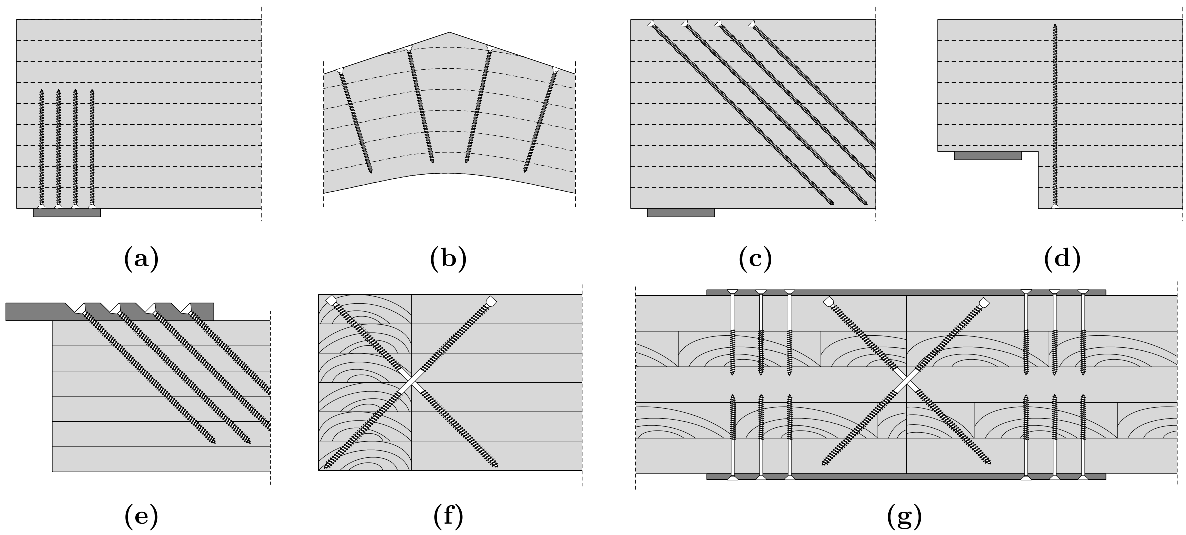

Fig. 1: Applications of self-tapping screws as reinforcing elements in zones subjected to compression (a) and tension (b) perpendicular to the grain, shear stresses (c) and combined shear and tension stresses perpendicular to the grain (d) and applications of self-tapping screws in a lateral connection (e), shear connection (f) and moment and normal force connection (g).

forces have to be transferred between two elements the screws are often installed with angles $\gamma = \pm 45°$. This allows for an optimal transfer of shear forces in both directions. In applications where both shear and tensile forces have to be transferred between elements, it is most commonly assumed that the screws carry the loads mainly in tension.

Examples of situations where combined loads in directions parallel and perpendicular to the grain occur are reinforcement of e.g. notches or connections of CLT plates. For the design of such connections or reinforcement, information regarding the load-carrying capacity and stiffness of fully threaded screws for different shank to grain angles are required.

Approaches and models published so far only account for the individual loading in direction parallel or perpendicular to the grain. Interaction formulas as they exist e.g. for threaded nails in EC5 (2008b) are not accurate and are not suitable to describe the stiffness of screws in such situations. Hence, for a more comprehensive understanding of the structural behaviour of self-tapping screws and for a more precise design, there is a need for a specific approach for the calculation of the load-carrying capacity and the stiffness of inclined screws under varying parallel and perpendicular to the grain loading.

2 State of the art

2.1 Geometrical properties of screws

The most important geometrical parameters of screws are specified in Fig. 2. In general it is distinguished between lag screws (Fig. 2 (a)) and self-tapping screws (Fig. 2 (b-d)). Lag screws used in the traditional timber design have part of the shank without thread which divides the length l of the screw in a threaded part of length l_g and a shank part. Lag screws require predrilled holes. In contrast, self-tapping screws do not require predrilled holes. However, it can be beneficial to insert self-tapping screws into predrilled holes, especially when screws of larger diameter are installed near to the endgrain. Self-tapping screws can exhibit a shank, which enables pre-tensioning of the screw (Fig. 2 (b)). In timber to timber shear connections self-tapping screws with a central shank part and two different thread pitches are used (Fig. 2 (c)). For reinforcing purposes fully threaded screws should be used in order to allow for a continuous load transfer along the whole length of the screw.

In EN 14592 (2008a) the key parameters of screws are specified. The geometrical parameters are outer thread diameter d, inner thread diameter d_1 (or core diameter d_core). These parameters are chosen by the manufacturer and should be in the range of $0.6d \leq d_1 \leq 0.9d$ and 2.4 mm $\leq d \leq 24$ mm for applications specified in EN 14592 (2008a). In case the plastic hinges developing in the threaded part of the screw the effective diameter $d_\mathrm{ef} = 1.1d_1$ is used in the EC5 (2008b) design equations. The yield moment M_y can be determined according to

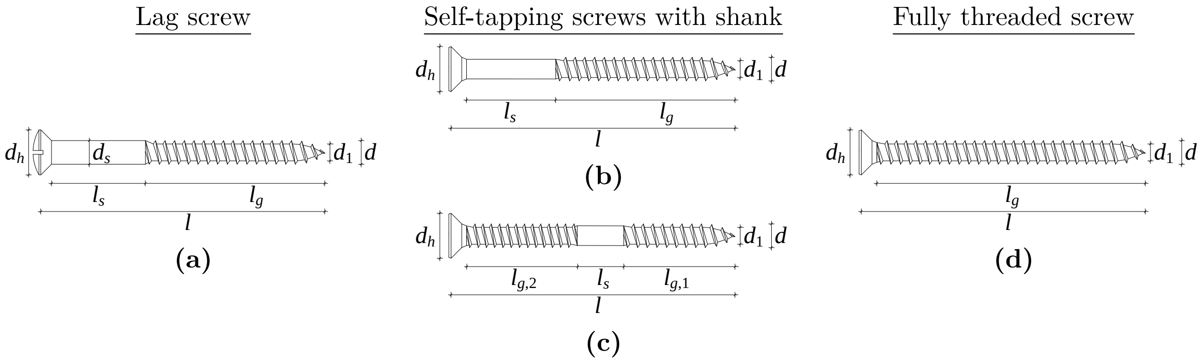

Fig. 2: Geometrical parameters of screws: l = length, l_g = threaded length, d = outer thread diameter, d_1 = inner core diameter, d_h = diameter of the screw head.

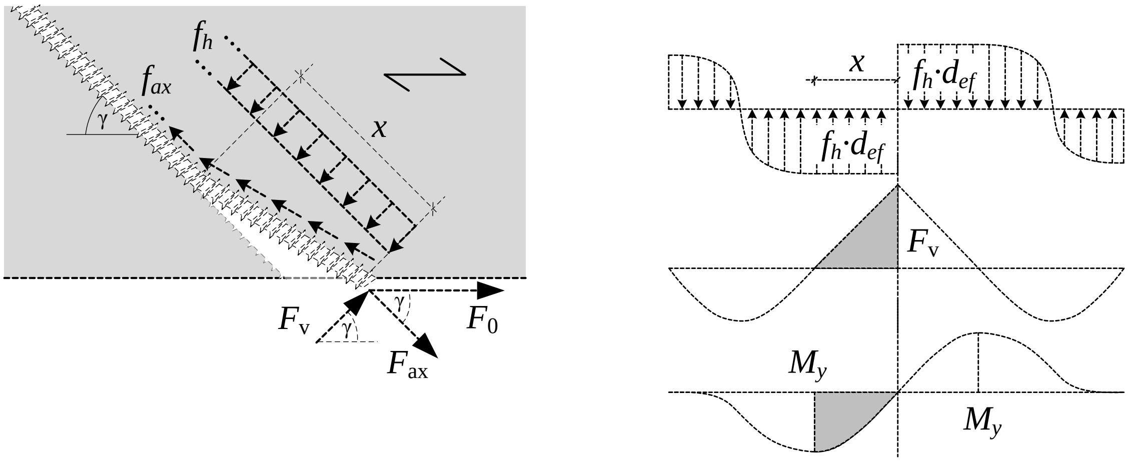

(a) (b)

Fig. 3: Stresses acting in a screwed joint when loaded in shear (a) and respective lateral forces (F_v) and bending moments (M) acting in the screw (b).

EN 409 (2009b) and depends mainly on the yield strength of the screw material. The embedment strength of the timber f_h (determined according to EN 383 (2007)) and the withdrawal strength f_ax of the thread (determined according to EN 1382 (1999)) depend mainly on the density of the timber and the load to grain direction.

2.2 Lateral load-carrying capacity

The load-carrying capacity of screws in lateral direction is calculated as it is done for other dowel-type fasteners i.e. by applying the European Yield Model (EYM) (Johansen 1949). For the ductile failure mode of the screw the load-carrying capacity R_v of a timber to timber connection can be calculated from the equilibrium of forces in the plastic hinge according to Fig. 3(b) using the yield moment M_y, the embedment strength of the timber f_h and the effective diameter of the screw d_ef.

$$R_\mathrm{v} = \sqrt{2 M_\mathrm{y} f_\mathrm{h} d_\mathrm{ef}} \tag{1}$$

Bejtka (2005) determined the embedment strength f_h of self-tapping screws in dependency of the density ρ of the timber and the load to grain angle γ (Eq. 2). Additional parameters like e.g. the geometry of the screw were not considered in the determination of f_h.

$$f_\mathrm{h,mean} = \frac{0.022 \rho^{1.24} d^{-0.3}}{2.5 \cos^2\gamma + \sin^2\gamma} \tag{2}$$

In connections with screws loaded in lateral direction a friction force is acting between the members. This effect arises from the relative contraction of the screw during loading and is called rope effect. EC5 (2008b) proposes to use a friction coefficient $\mu = 0.25$ for timber-timber connections.

2.3 Pull-out capacity

Due to their high slenderness fully threaded screws exhibit low strength and stiffness only when being loaded in lateral direction. Much better performance can be observed for axially loaded screws. The pull-out capacity of fully threaded screws has been studied in detail e.g. by Bejtka (2005), Pirnbacher et al. (2009). The withdrawal parameter f_ax is used to calculate the pull-out capacity of the screw in dependency of the cross-section of the threaded part screw embeded in the timber $d \cdot l_{\text{ef}}$. Bejtka (2005) determined the withdrawal capacity of self-tapping screws with the withdrawal parameter $f_{\text{ax,mean}} = 0.6d^{-0.5}l_{\text{ef}}^{-0.1}\rho_{\text{mean}}^{0.8}$ as follows.

$$R_{\text{ax,mean}} = \frac{\sqrt{d}l_{\text{ef}}f_{\text{ax,mean}}}{1.2\cos^2\gamma + \sin^2\gamma} \tag{3}$$

2.4 Inclined screws

The load-carrying capacity of connections with inclined screws loaded in axial and lateral direction is described in Bejtka and Blaß (2002). The resistance of the connection when being loaded in direction parallel to the grain R_0 can be calculated from the resistances in axial (R_{ax}) and lateral (R_{v}) direction of the screw (Fig. 3a). In addition the friction is accounted for by using the friction coefficient μ (EC5 (2008b)).

$$R_0 = R_{\text{ax}}\left(\mu\sin\gamma + \cos\gamma\right) + R_{\text{v}}\left(\sin\gamma - \mu\cos\gamma\right) \tag{4}$$

2.5 Load-carrying capacity of screws loaded to combined axial and lateral loads

The load-carrying capacity of screws subjected to combined lateral $F_{\text{v,Ed}}$ and axial loads $F_{\text{ax,Ed}}$ can be estimated using the interaction formula (Eq. 5) valid for threaded nails (EC5 (2008b)). In EC5 the lateral and axial load-carrying capacity are denoted $F_{\text{v,Rd}}$ and $F_{\text{ax,Rd}}$, respectively.

$$\left(\frac{F_{\text{ax,Ed}}}{F_{\text{ax,Rd}}}\right)^2 + \left(\frac{F_{\text{v,Ed}}}{F_{\text{v,Rd}}}\right)^2 \leq 1.0 \tag{5}$$

2.6 Stiffness of inclined screws

The stiffness of connections loaded in direction parallel to the grain with inclined screws was studied by Tomasi et al. (2010). The resulting stiffness K_0 can be calculated from the stiffness of the screw in lateral (K_{v}) and axial direction (K_{ax}).

$$K_0 = K_{\text{v}}\sin\gamma\left(\sin\gamma - \mu\cos\gamma\right) + K_{\text{ax}}\cos\gamma\left(\cos\gamma + \mu\sin\gamma\right) \tag{6}$$

For screws the stiffness in lateral direction is specified similar to other dowel type fasteners, i.e. $K_{\text{v}} = \rho^{1.5}d/20$ N/mm (EC5 (2008b)). Bejtka (2005) determined the axial stiffness of screws in experiments and published the following formula: $K_{\text{ax}} = 234(\rho d)^{0.2}l_{\text{ef}}^{0.4}$ N/mm. The stiffness according to the technical approval (DIBt 2011) is $K_{\text{ax}} = 25dl_{\text{ef}}$ N/mm .

A design model for the calculation of the load-carrying capacity and the stiffness of connections with inclined screws loaded in tension perpendicular to grain is proposed in Jockwer et al. (2014). This model will be explained in detail in Section 4.

3 Experimental investigations

A test series has been carried out by the authors in order to determine the strength and the stiffness of connections with screws set in the timber with varying shank to grain angles γ and subjected to forces with different force to grain angles (Jockwer et al. 2014, Jockwer 2014). The parameters shank to grain angle, load to grain angle and density have been varied. For each configuration, 3-8 similar specimens were tested (Tab. 1).

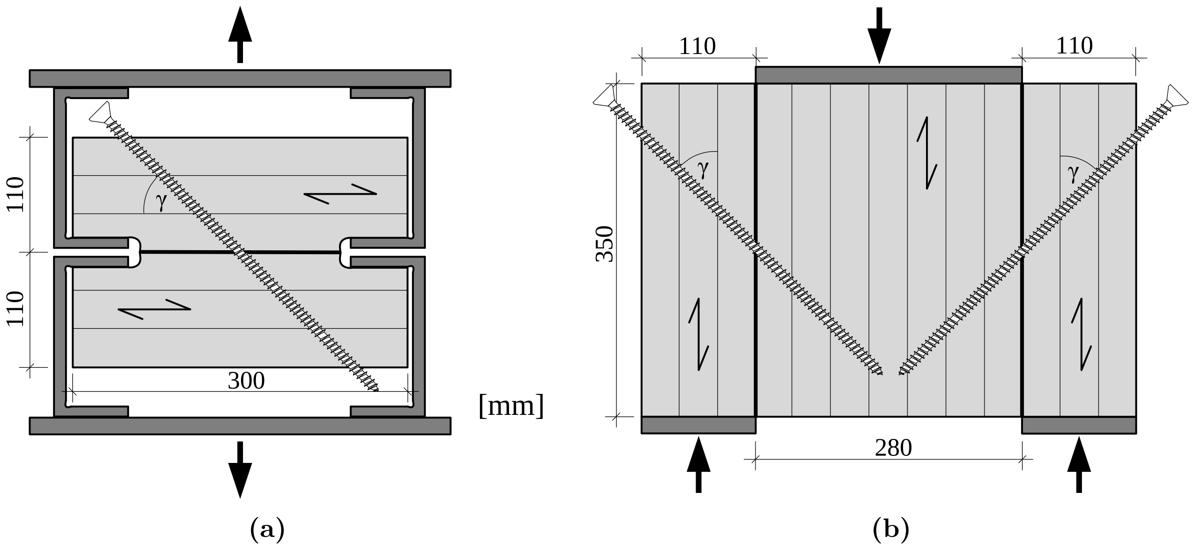

Fig. 4: Test-setups for pulling (a) and shearing (b) tests of joints with inclined screws.

3.1 Methods

The load-carrying capacity and stiffness of connections loaded parallel and perpendicular to the grain was assessed as illustrated in Fig. 4. The setup for the pulling test consisted of two glulam members, whereas the test setup for the shearing tests consisted of three elements i.e. was similar to a block shear setup. In the shearing tests the glulam pieces were separated by means of a Teflon foil of 1.5 mm thickness in order to avoid friction. The inclination of the screws was varied between three different shank to grain angles ($\gamma = 90°,\ 60°$ and $45°$). Tests with $\gamma = 90°$ served as a reference to analyse the withdrawal and embedment strength of screws. The deformations were measured in the timber at the positions of the screw by means of LVDT and by additionally applying the optical system NDI .

3.2 Material

The specimens consisted of two different glulam grades. A higher density glulam sample was produced using boards with $\rho_{\text{mean,high}} = 464$ kg/m^3 ($CoV = 2.5\%$). The second sample with a low density was produced from boards with $\rho_{\text{mean,low}} = 360$ kg/m^3 ($CoV = 1.8\%$). The density distribution of the two samples of boards together with the density of all boards of the graded bulk is shown in Fig. 5. The density of this bulk of boards corresponds well to the one of solid timber of strength class C24 (EN 338 (2009a)). The moisture content of the glulam specimens was approximately $MC = 10\%$.

Self-tapping fully threaded screws of type SFS® WR-T-13xL400 as specified in the technical approval (DIBt 2011) have been used in the tests. The key geometrical properties of measure were: $d = 13$ mm, $d_{1(core)} = 8.5$ mm and $l = 400$ mm (Fig. 2). The screws were predrilled with a diameter of 8 mm. The effective length of the threaded part of the screws in the side members in both block shear tests and pulling tests was $l_{ef} = 110$ mm, 127 mm and 155 mm ($8.5d, 10d$ and $12d$) for screw axis to grain angles of $\alpha = 90°,\ 60°$ and $45°$, respectively. Two parallel screws were used per connection.

In order to determine the yield moment of the screws three-point bending tests have been carried out with a free span of the screw of 76 mm and 100 mm. Based on two tests the yield moment was found to be $M_{\text{y,mean}} \approx 120$ Nm, which is considerably higher than the value of $M_{\text{y,k}} = 80$ Nm given in the technical approval (DIBt 2011).

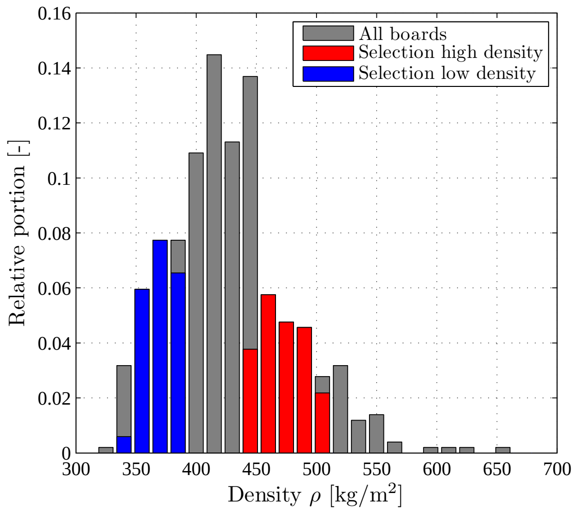

Fig. 5: Density distribution of the bulk of boards and of the two samples of boards with high and low density.

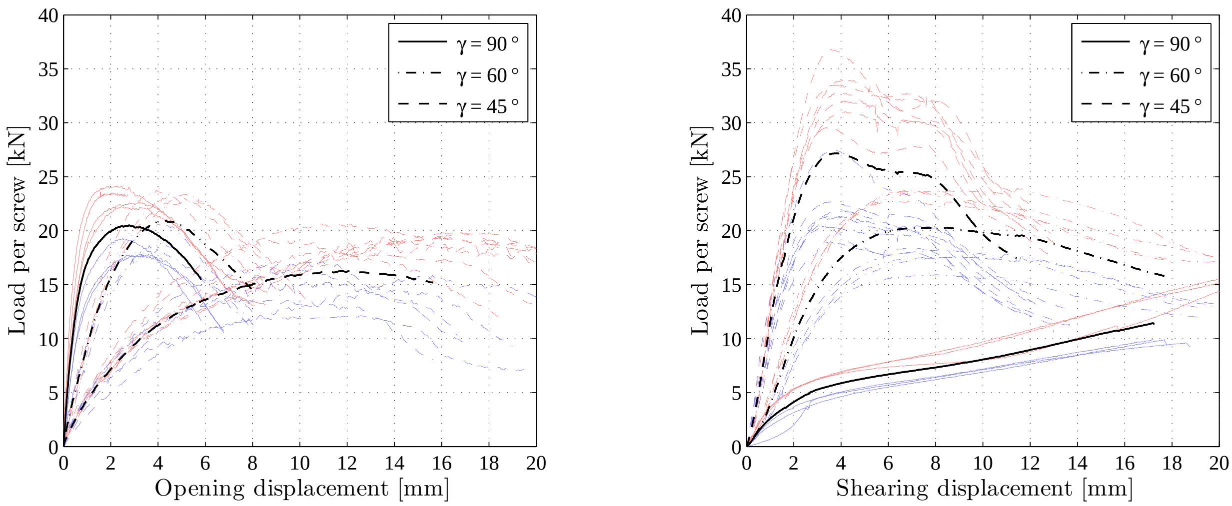

(a) **(b)**

Fig. 6: Joint behaviour in (a) pulling and (b) shearing tests. Individual results in grey, normalised values for $\rho \approx 410$ kg/m^3 in black with solid line for $\gamma = 90°$, dashed-dotted line for $\gamma = 60°$ and dashed line for $\gamma = 45°$.

Tab. 1: Test results normalized to a reference density $\rho = 420$ kg/m^3 and parameter k describing the impact of density on strength and stiffness

			Load-carrying capacity		Stiffness	
	α [°]	n [-]	F_{ult} [kN] (CoV)	k [-]	K_{ser} [kN/mm] (CoV)	k [-]
Pulling	90	7	21.2 (3%)	0.96	28.3 (25%)	2.12
	60	7	21.6 (4%)	0.85	8.9 (15%)	0.63
	45	14	17.7 (8%)	0.89	3.0 (17%)	-0.15
Shearing	90	6	10.5 (5%)	0.94	1.9 (22%)	1.46
	60	8	20.5 (4%)	1.32	5.9 (8%)	1.50
	45	15	27.4 (10%)	1.50	13.6 (16%)	1.21

3.3 Results

The load displacement curves of the six test series are shown in Fig. 6 in red and blue for specimens with high and low density, respectively. In black the mean curves for a density of $\rho = {}^1\!/\!_2\,(464 + 360) \approx 410$ kg/m^3 are given. The density of the timber and the inclination γ of the screw turned out the parameters with the highest impact on the load-carrying capacity and the stiffness of the screws in both the shearing and pulling tests. The effective stiffness K_{ser} was determined in the range of 0.1 F_{ult} and 0.4 F_{ult} by linear regression following EN 12512 (2001). The ultimate load F_{ult} was taken as the maximum load at up to 15 mm deformation. This value, that is lower compared to the 30 mm according to EN 12512, was chosen due to the intended application of the screws as reinforcement, where only small deformations are wanted. The impact of density was determined according to Eq. 7 and strength and stiffness values were normalized to a reference density of $\rho = 420$ kg/m^3. The impact of density on the strength and stiffness is shown in Tab. 1.

$$F_\rho = F_{\rho=420}\left(\frac{\rho}{420\text{kg/m}^3}\right)^k \tag{7}$$

The embedment strength of the timber can be calculated by means of Eq. 1 with R_{v} from the shearing tests with $\gamma = 90°$ and with mean value of the yield moment $M_{\text{y,mean}}$. Values of $f_{\text{h,mean}} = 29.2$ N/mm^2 and $f_{\text{h,mean}} = 48.8$ N/mm^2 are resulting for a shear deformation of 10 mm and 15 mm, respectively. The different values of embedment strength are result of the friction force acting between the timber members despite the fact that a teflon foil was used. This friction force leads to an increased load for shearing displacements > 9 mm for $\gamma = 90°$ in Fig. 6 (b).

In the tests the mean value of withdrawal strength was determined $f_{ax,mean} = 14.8$ N/mm^2, whereas in the technical approval (DIBt 2011) a withdrawal parameter $f_{ax,k} = 80 \cdot 10^{-6} \cdot \rho_k^2$ is given, resulting in a value of $f_{ax} = 14.1$ N/mm^2 for $\rho = 420$ kg/m^3. Bejtka (2005) suggested a mean withdrawal parameter for a variety of self-tapping screws of $f_{ax,mean} = 13.1$ N/mm^2.

The mean value of connector stiffness in shank direction can be expressed by $K_{\text{ax}} = 40\, d\, l_{ef}$ compared to $K_{\text{ax}} = 25 d l_{\text{ef}}$ N/mm as suggested in the technical approval (DIBt 2011).

4 Analytical model for inclined screws

Inclined screws loaded perpendicular to the grain show low load-carrying capacities and low stiffness (Fig. 6). Large deformations of the screws are combined with failure of a timber layer at the surface of the specimens. The structural behaviour of the connection can be described by adequately modifying the EYM. Forces in the screw are separated into components acting in axial and lateral directions as shown in Fig. 7 (a).

In lateral direction the screw is supported by a layer of timber in which the reaction force is oriented against the surface of the timber member. At the very surface, the layer resisting the embedment loads has zero thickness. As a result, no embedment stresses can be carried by this layer. In tests compression and splitting failure were observed in this zone. The full embedment strength f_{h} acts at a distance x_1 from the surface, where the timber layer perpendicular to the screw axis is thick enough to resist the loading from embedment stresses along two shear planes at both sides of the screw. The dominating strength parameter in the shear planes is the rolling shear strength $f_{\text{v,roll}}$. The resulting length x_1 along which only reduced embedment stresses can be transferred is given in Eq. 8 and illustrated in Fig. 7 (a).

$$x_1 = \frac{f_h\ d_{ef}}{2\ \tan\gamma\ f_{v,roll}} \tag{8}$$

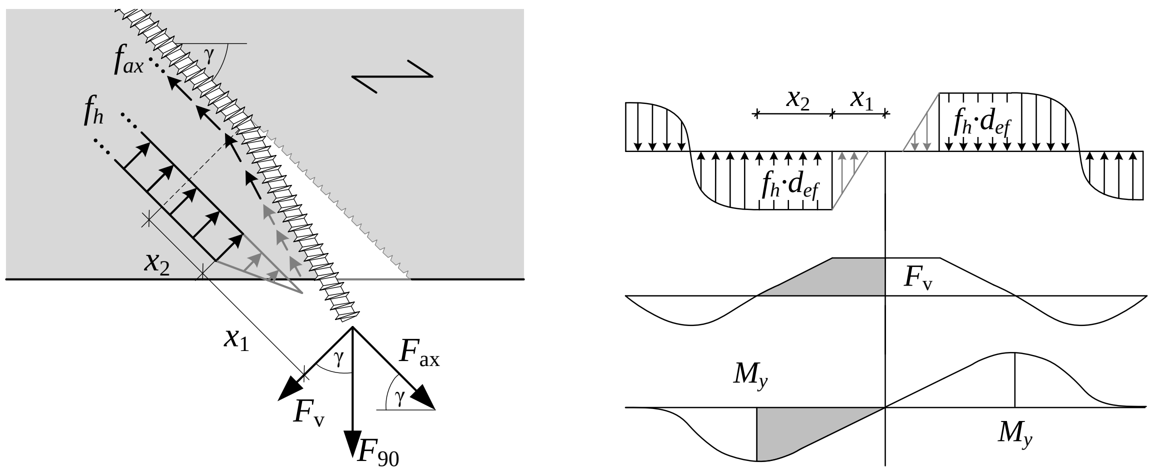

(a) (b)

Fig. 7: Stresses acting in a screwed joint when loaded perpendicular to the grain (a) and respective lateral forces F_v and bending moments M acting in the screw (b).

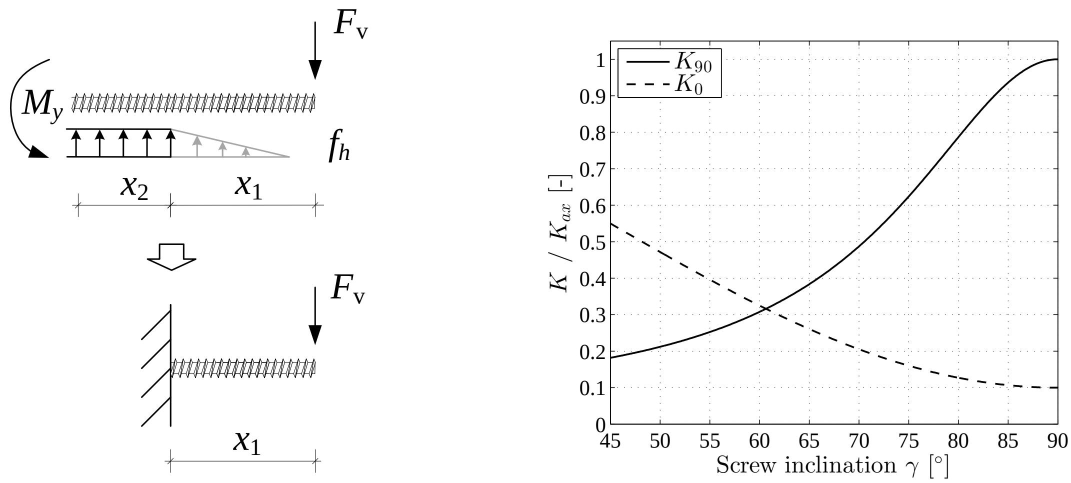

(a) (b)

Fig. 8: Detailed and simplified stiffness model with reduced embedment (a) and impact of screw axis to grain angle γ on the relative stiffness K/K_ax (b).

In the EYM the length of reduced embedment can be accounted for by inserting a zone with a decreased embedment stress as illustrated in Fig. 8 (b). For simplification zero embedment strength is assumed along the length x_1 leading to a linear transition of the bending moment in the screw. The load-carrying capacity can be calculated as follows:

$$R_\mathrm{v,pulling} = -f_\mathrm{h}\ x_1\ d_\mathrm{ef} + \sqrt{(2M_\mathrm{y} + f_\mathrm{h}\ x_1^2\ d_\mathrm{ef})\ f_\mathrm{h}\ d_\mathrm{ef}} \tag{9}$$

In axial direction of the screw, the effective length l_ef is reduced by the length of reduced embedment x_1, since to load transfer is reduced in that zone. The resulting load-carrying capacity of the connection with an inclined screw loaded perpendicular to the grain R_{90} can be determined by means of Eq. 10 in equivalence to the interaction equation (Eq. 4) assuming zero friction ($\mu = 0$) between the elements due to opening of the gap.

$$R_{90} = R_\mathrm{ax}\,(\sin\gamma) + R_\mathrm{v,pulling}\,(\cos\gamma) \tag{10}$$

In the zone of reduced embedment the stiffness of the connection depends on the screw only. The according structural system is a cantilever beam with elastic clamping, whose stiffness can be approached assuming fixed clamping as a simplification according to Eq. 11 (Fig. 8 (a)).

$$K_{\text{v,pulling}} = \frac{3\ E_{\text{steel}}\ \pi\ d_1^4}{64\ x_1^3} \tag{11}$$

The stiffness of a shear connection is the sum of the portions in lateral and in axial direction according to Eq. 6 as suggested by (Tomasi et al. 2010). This model is similar to two springs acting parallel. In contrast to that, in connections loaded perpendicular to the grain the two portions of stiffness are acting in series. Hence, the effective stiffness K_{ser} is equal to the sum of the inverse values of the stiffnesses in lateral (K_{v}) and axial (K_{ax}) direction.

$$\frac{1}{K_{90}} = \frac{1}{K_{\text{v,pulling}}} + \frac{1}{K_{\text{ax}}} \tag{12}$$

The progression of the stiffnesses in direction perpendicular (K_{90}) and parallel (K_0) to the grain according to Eq. 12 and Eq. 6 is shown in Fig. 8 in dependency of the inclination γ of the screw.

5 Discussion

The comparison of test results and predicted strength and stiffness values according to Eq. 9 and 11 and according to EC5 (2008b), Bejtka (2005) and Tomasi et al. (2010) is shown in Tab. 2 and in Fig. 9. The required material parameters for the predicted values are taken from the reference tests with $\gamma = 90°$ and from (Bejtka 2005) and (DIBt 2011). The mean value of rolling shear strength $f_{\text{v,roll}} = 1.8\ \text{N/mm}^2$ was calculated from the characteristic value given in EN 14080 (2013) by assuming a ratio $f_{\text{mean}}/f_{\text{char}} = 1.5$. The maximum length

Tab. 2: Test results compared to the proposed design model and to values from literature

	γ [°]	Load-carrying capacity: Tests F_{ult} [kN] (CoV)	EC5 (2008b) R_{k} [kN]	Bejtka (2005) $R_{0,\text{mean}}$ [kN]	Eq. 10 $R_{90,\text{mean}}$ [kN]
Pulling	90	21.2 (3%)	16.2	18.7	21.2
	60	21.6 (4%)	12.3		19.2
	45	17.7 (8%)	11.8		18.4
Shearing	90	10.5 (5%)	6.8	6.2	
	60	20.5 (4%)	8.6	15.0	
	45	27.4 (10%)	11.8	20.3	

	γ [°]	Stiffness: Tests K_{ser} [kN/mm] (CoV)	Tomasi et al. (2010) $K_{0,\text{mean}}$ [kN/mm]	Eq. 12 $K_{90,\text{mean}}$ [kN/mm]
Pulling	90	28.3 (25%)		28.6
	60	8.9 (15%)		7.5
	45	3.0 (17%)		3.6
Shearing	90	1.9 (22%)	2.5	
	60	5.9 (8%)	6.3	
	45	13.6 (16%)	10.2	

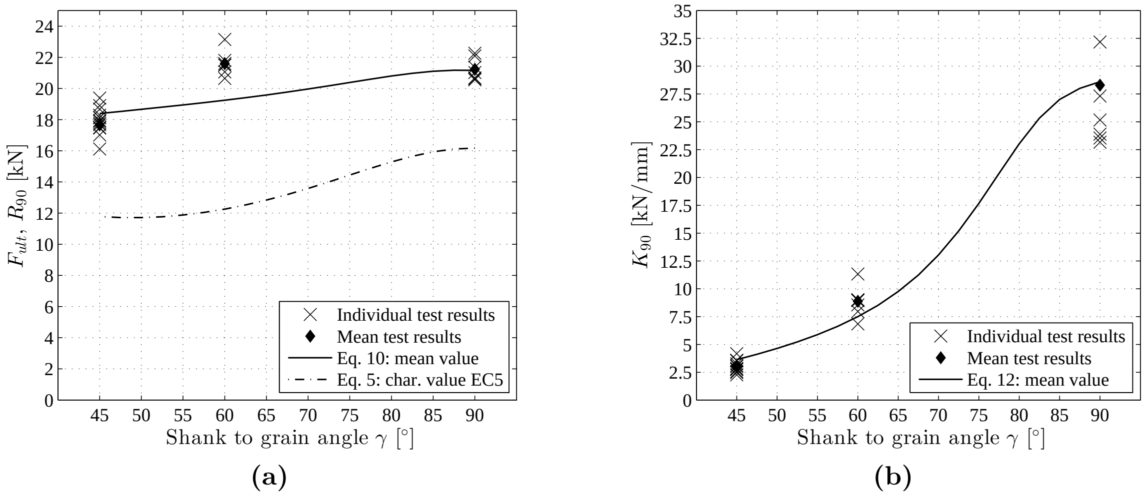

Fig. 9: Comparison of the load-carrying capacity perpendicular to the grain according to Eq. 10, Eq. 5 and test results and comparison of the stiffness K_{90} according to Eq. 12 and test results.

of reduced embedment of approximately $x_1 = 30$ mm in the $\gamma = 45°$ pulling tests corresponds well with the observations made in the tests. The differences between the test results and the predicted load-carrying capacities and stiffnesses can be attributed to the differences between the individual properties of the screw and the generalised specifications in EC5 (2008b) and other literature (Bejtka 2005).

Fig. 9 shows that the influence of the screw to grain angle γ on the stiffness of the connection can be modelled in appropriate way using Eq. 12 and accounting for the reduced embedment length. Since the model for the perpendicular to grain strength and stiffness requires free horizontal movement when reaching ultimate load, it can only be applied to connections offering this movement and to other connections and reinforcement in the range of small deformations, respectively.

6 Conclusions

Fully threaded self-tapping screws can be used in various applications for reinforcement purposes or as connecting elements. They show highest strength and stiffness in axial direction. It is important to choose the optimal angle between screw shank and grain direction. Current design approaches do not cover the whole range of possible applications of fully threaded self-tapping screws. Based on the analysis of the structural behaviour of connections with inclined screws loaded parallel and perpendicular to the grain a model accounting for the reduced embedment length of the screws was proposed. The model shows good agreement with the test results and describes the impact of the screw inclination in appropriate way. For a reliable estimation of the structural behaviour of self-tapping fully threaded screws more specific property values than currently given in EC5 (2008b) and related codes are needed.

References

Bejtka I. (2005): Verstärkung von Bauteilen aus Holz mit Vollgewindeschrauben. PhD Thesis, Fakultät für Bauingenieur-, Geo- und Umweltwissenschaften, Universtität Karlsruhe, Karlsruhe, Germany

Bejtka I., Blaß H.J. (2002): Joints with inclined screws. In: Proc. of the CIB-W18 Meeting 35, Kyoto, Japan, Paper No. CIB-W18/35-7-4

CEN (1999): EN 1382: Timber structures - Test methods - Withdrawel capacity of timber fasteners. European Committee for Standardization CEN, Bruxelles, Belgium

CEN (2001): EN 12512: Timber structures - Test methods - Cyclic testing of joints made with mechanical fasteners + A1 (2005). European Committee for Standardization CEN, Bruxelles, Belgium

CEN (2007): EN 383: Timber structures - Test methods - Determination of embedment strength and foundation values for dowel type fasteners. European Committee for Standardization CEN, Bruxelles, Belgium

CEN (2008a): EN 14592: Timber structures - Dowel-type fasteners - Requirements. European Committee for Standardization CEN, Bruxelles, Belgium

CEN (2008b): EN 1995-1-1/A1: Eurocode 5: Design of timber structures - Part 1-1: General - Common rules and rules for buildings. European Committee for Standardization CEN, Bruxelles, Belgium

CEN (2009a): EN 338: Structural timber - Strength classes. European Committee for Standardization CEN, Bruxelles, Belgium

CEN (2009b): EN 409: Timber structures - Test methods - Determination of the yield moment of dowel type fasteners. European Committee for Standardization CEN, Bruxelles, Belgium

CEN (2013): EN 14080: Timber structures - Glued laminated timber and glued solid timber - Requirement. European Committee for Standardization CEN, Bruxelles, Belgium

DIBt (2011): Allgemeine bauaufsichtliche Zulassung Z-9.1-472, SFS Befestiger WT-S-6,5; WT-T-6,5; WT-T-8,2; WR-T-9.0 und WR-T-13 als Holzverbindungsmittel. Deutsches Institut für Bautechnik, Berlin, Germany

Jockwer R. (2014): Structural behaviour of glued laminated timber beams with unreinforced and reinforced notches. PhD thesis, Institute of Structural Engineering, ETH Zurich, Switzerland

Jockwer R., Steiger R., Frangi A. (2014): Fully threaded self-tapping screws subjected to combined axial and lateral loading with different load to grain angles. In: Aicher S., Reinhardt H.W., Garrecht H. (eds) Materials and Joints in Timber Structures, RILEM Bookseries, vol 9, Springer Netherlands, pp 265–272

Johansen K.W. (1949): Theory of timber connections. IABSE publications 9:249–262

Pirnbacher G., Brandner R., Schickhofer G. (2009): Base parameters of self-tapping screws. In: Proc. of the CIB-W18 Meeting 42, Dübendorf, Switzerland, Paper No. CIB-W18/42-7-1

Tomasi R., Crosatti A., Piazza M. (2010): Theoretical and experimental analysis of timber-to-timber joints connected with inclined screws. Construction and Building Materials 24:1560–1571

INTER

International Network on Timber Engineering Research

CALCULATION OF CYLINDRICAL SHELLS FROM WOOD OR WOOD BASED PRODUCTS AND CONSIDERATION OF THE STRESS RELAXATION

P Aondio
S Winter
H Kreuzinger
J-W van de Kuilen

Lehrstuhl für Holzbau und Baukonstruktion
Technische Universität München

GERMANY

Presented by P Aondio
H Blass asked about extrapolation from the 90 days tests and would one be able to use the LVL. P Aondio responded that there was no extrapolation and the LVL cannot be used because something is needed to distribute the stresses in the ring direction.
R Harris asked about plotting the relaxation versus time in terms of log of time. P Aondio stated that this has not been considered. R Harris stated that bonding wood is commonly done with for example glue laminated beams. P Aondio explained utilization factor and that the curve glue-laminated beams calculations from Eurocode are different. Also lower capacity of curved glulam beams would come from Eurocode.
S Svensson asked if there is an effect on how many plies. P Aondio responded that the study only dealt with 3 plies because thicker laminates would be too stiff. S Svensson commented that in slide 7 the curved glulam was painted and there should be no moisture gradient in the wood and that in actual service climate the condition can be more variable than stated in service class one.
M Fragiacomo received confirmation that 3% strain on top and bottom of the member and that the stress relaxation model was linear. M Fragiacomo recommended checking the stress level with respect to validity of linearity of the model.

Calculation of cylindrical shells from wood or wood based products and consideration of the stress relaxation

P. Aondio[1], J.-W. van de Kuilen[2,3], S. Winter[1] and H. Kreuzinger[1]

[1]Lehrstuhl für Holzbau und Baukonstruktion

Technische Universität München

[2]Holzforschung München, Technische Universität München

[3]Faculty of Civil Engineering and Geosciences, TU Delft the Netherlands

Keywords: wood, wood based products, cylindrical shells, curved members, internal stresses, stress relaxation

Abstract

The present paper deals with the load-bearing capacity of cylindrical shells and curved members made of wood or wood based products. The possibility to create curved members by bending plane produced panels is examined. The bending process induces high internal stresses in ring direction of shells. This should be taken into account in static calculations. Hereby, the associated stress relaxation in ring direction should be considered and its influence on the load bearing capacity of the member needs to be addressed.

1 Introduction and Background

Shells are highly efficient, curved structures featuring a minimal consumption of material. Until now most shells are built as grid shells due to the limited dimensions of wood. Here, many small pieces have to be connected by fasteners to create arches, rhombuses or grids. All these connections are time-consuming during erection and can be the basis of damages.

Recent developments in the timber-product-industry have resulted in many new wood based products, which can be utilized to create simple curved shells. Currently, the industry is able to produce wood based panels with maximum dimensions up to 4,50 x 60,00 meters [1]. These panels are usually produced as plane elements, a production of curved elements is very expensive, but allows for reduced material use.

2 Cylindrical shells made of wood based products

2.1 General

The basic idea of the concept presented in this paper, is to use conventionally produced, large, plane panels to create simple curved shells. The most important parameters are the available dimensions of the panels and the possible radius of curvature. The possible radius of curvature depends on the modulus of elasticity of the boards, the thickness of the panels and the lay-up. Depending on the curvature, stresses are induced in ring-direction of the shell, and a high geometric stiffness in longitudinal direction is activated. Lifting off of the panels can be prevented by fastening the panels to a framework (see Fig. 1).

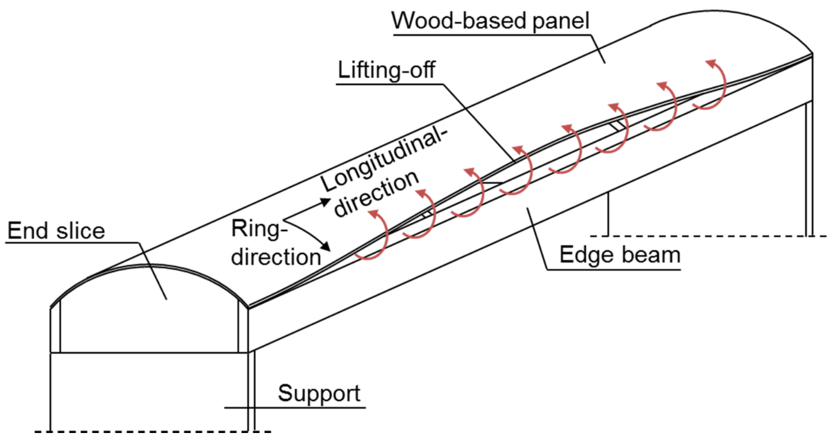

Fig. 1: Example of a simple curved shell

2.2 Determination of the internal stresses

An important aspect in the calculation of cylindrical shells or curved members in general is the accurate consideration of the internal stresses. Two possibilities exist which are described in the following. One possibility is to describe the occurring internal stresses by adding two bending moments at the edge of the curved panel. The value of the bending moments depends on the panel-stiffness and the chosen radius of curvature. An important prerequisite in this method is that the radius of curvature is constant (see Fig. 2). This method is recommended if there are no edge beams, otherwise the bending moments have no influence on the panel.

Alternatively, the occurring internal stresses can be incorporated by a virtual temperature load. The virtual temperature load depends on the thickness of the panel, the expansion coefficient and the chosen radius. Varying radiuses of curvature over the radial cross-section are possible (see Fig. 3).

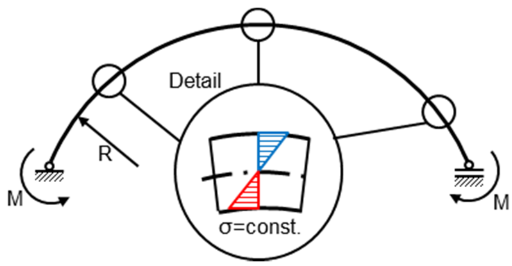

Fig. 2: Edge moments

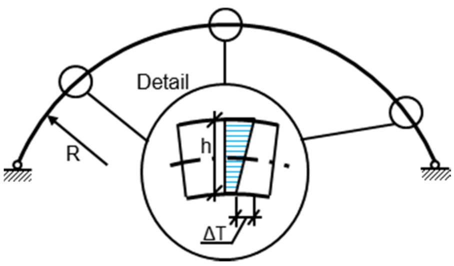

Fig. 3: Virtual temperature load

$$M = \frac{1}{R} \cdot EI \qquad (1)$$

$$\Delta T = \frac{1}{R} \cdot \frac{h}{\alpha_T} \qquad (2)$$

Several studies have shown that the virtual temperature load is more suitable to simulate internal stresses. It is possible to calculate different shell structures with the shear analogy [2], [3] and commercial static programs. To get an idea of possible radiuses of curvature, different standards of production of cross laminated timber (CLT) and glued laminated timber (GLT) have been examined.

When applying boards in a curved situation with the main stresses parallel to the grain, the following observations can be made. In curved members, the elements are generally bended flatwise, whereas strength class assignment is generally based on edgewise bending. The edgewise strength value is normalized at a reference depth of 150 mm with a span/depth ratio of 18. It is expected that the flatwise bending strength is in the order of magnitude of 15 to 20% higher than the edgewise bending strength, here 1,15 is assumed. To be on the safe side, no depth effect is taken into account here, as parts of the depth effect may be covered by the assumed ratio between flatwise and edgewise bending strength and the existence of a depth effect is still very much discussed [4].

The stresses in the curved boards are calculated on the basis of the mean value for the modulus of elasticity, coinciding with a mean bending strength that is about 60 to 70% higher than the characteristic value, based on an assumed coefficient of variation between 20 and 25%. Such a coefficient of variation is normal even for machine graded timber. It means that for a C24 graded board, the mean bending strength is at least about 24 * 1,6 * 1,15 = 44 MPa This is considered on the safe side compared to the results given in [4] where a mean bending strength has been determined of 41 MPa in edgewise bending for all depths of 50 mm or more.

If boards are curved to a maximum curvature corresponding with a bending stress of 24 MN/m², the load level can be estimated at 24/44 ≈ 55% of the mean short term strength. After this bending, a stress relaxation process starts that is influenced by two effects. Firstly, there is the ´standard´ mechanical stress relaxation in wood. Here a number of literature references indicate a decrease in stress between 40 and 50% of the original value. Secondly, in the outer layers of the curved boards, a mechano-sorptive stress relaxation process occurs, as water is diffusing from the glue into the wood, increasing the stress relaxation. This increase is estimated on the basis of literature to be an additional 20-30%. [5]

3 Stress relaxation

3.1 Stress relaxation in GLT

3.1.1 Material and test specimen

To gain insight on the extent of stress relaxation, a 25 year old glued laminated timber beam was investigated. It had been constantly stored in an environment with room temperature throughout the year of ~20°C and a relative humidity of 30÷50%, consistent with Service Class 1 according to Eurocode 5. The lamellas of the laminated timber beam were made of spruce, featuring a thickness of 10 mm and a width of 90 mm (see Fig. 4 and Fig. 5).

Fig. 4: Investigated GLT-beam

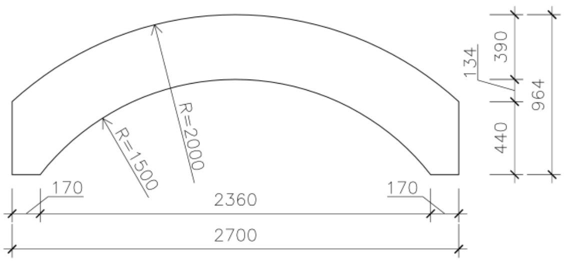

Fig. 5: Dimensions [mm]

3.1.2 Method

Two lamellas were extracted. The change in curvature of the lamellas indicated the amount of stress relaxation.

3.1.3 Results

The curvature of the lamellas was determined before and after the extraction by the corresponding geometric functions and their derivatives. From the change of curvature it was possible to calculate the internal stress after 25 years. An assumption for the stress calculation was that there was neither a change in the modulus of elasticity nor in the geometry of the lamella. Comparing the stresses after 25 years $\sigma_{t=25a}$ with the stresses at the moment of the production $\sigma_{t=0}$, a percentage value of remaining stresses could be calculated (see equation 3).

Fig. 6: Extraction of lamella

$$\vartheta = \frac{\sigma_{t=25\,a}}{\sigma_{t=0}} \cdot 100\% \quad = \quad \frac{|\Delta\kappa| \cdot E \cdot \frac{d}{2}}{|\kappa_1| \cdot E \cdot \frac{d}{2}} \cdot 100\% \quad = \quad \frac{|\kappa_1 - \kappa_2|}{|\kappa_1|} \cdot 100\% \qquad (3)$$

κ_1 … curvature before extraction

κ_2 … curvature after extraction

This value can be used to estimate the stress relaxation:

$$\chi = 100\,\% - \vartheta = \left(1 - \frac{|\kappa_1 - \kappa_2|}{|\kappa_1|}\right) \cdot 100\,\% \qquad (4)$$

For both lamellas, equation (4) was evaluated along the arch length. An example for the solution of the upper lamella is given in figure 7. Calculation results showed that the internal stresses were reduced by about 57% (mean value).

The lamellas were kept in the same climatic conditions for the following year, with boundary conditions that enabled a free deformation. Observing the lamellas over the following year showed an ongoing hygroscopic behavior. Taking into account this behavior, estimated stress relaxation values ranged from 57±5% which corresponds with results given in [6].

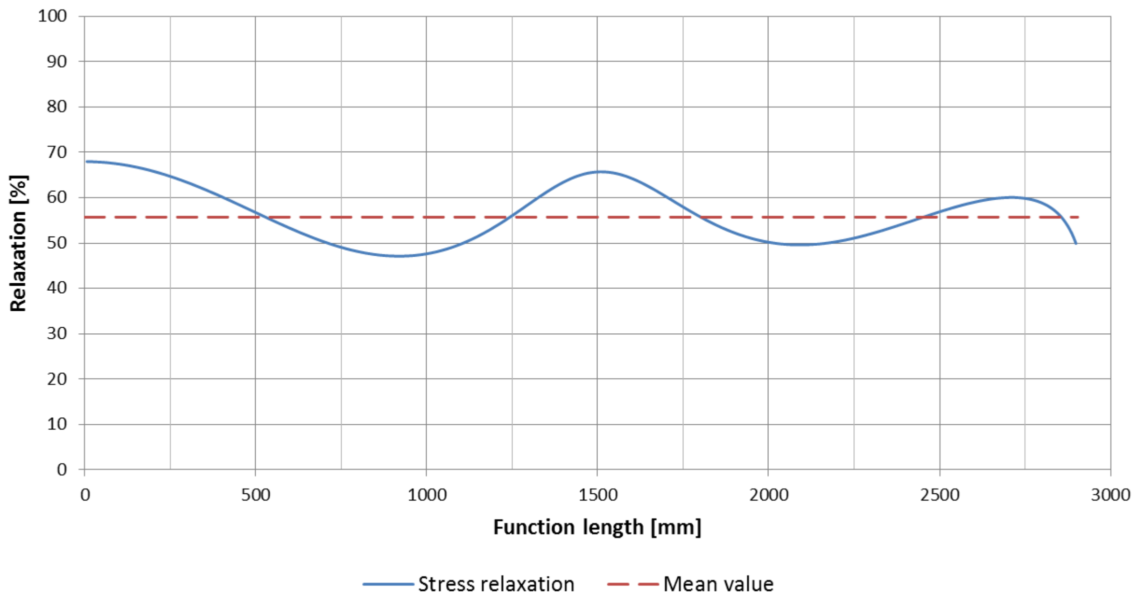

Fig. 7: Stress relaxation in one lamella

3.1 Stress relaxation in solid wood panels

3.1.1 Material and test specimen

Assuming that three layered solid wood panels are eligible for the production of cylindrical shells, the following test setup was arranged.

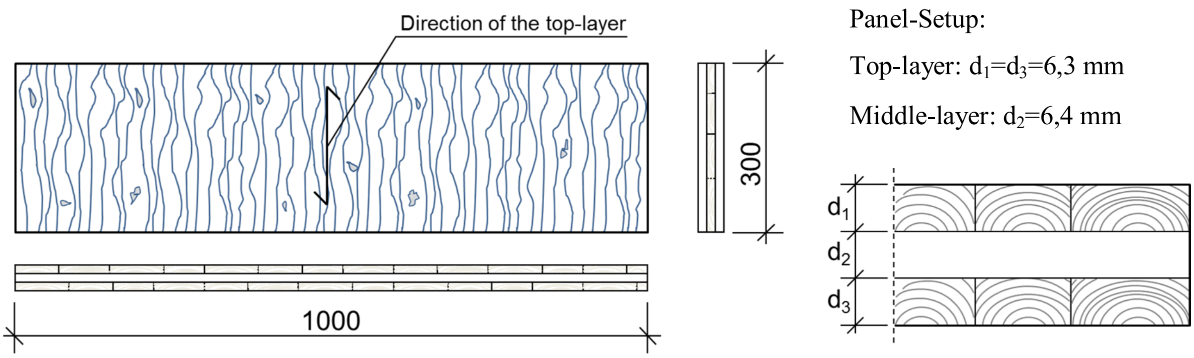

Fig. 8: Examined test specimen in ground view, side view and cross section (dimensions in [mm])

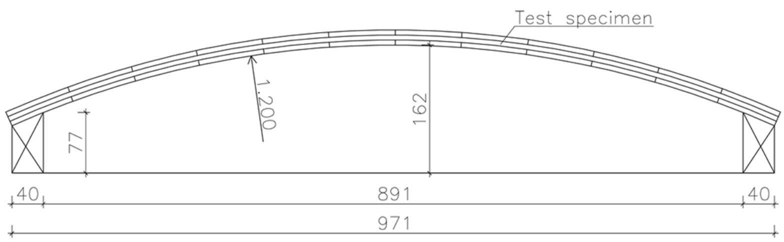

Fig. 9: Test specimen and framework (dimensions in [mm])

The layers consisted of spruce assigned to strength class C24. The edges of the layers were not glued together. To create a constant radius of curvature (R=1.200 mm) the test specimens were fixed to a framework (see Fig. 9).

3.2.2 Method

As described in literature ([7], [8], [9], [10], [11], [12]), the stress relaxation is dependent on the wood moisture content, the relative humidity and the stress level. Here, three different experimental setups were examined. The stress level influence has not been studied at this stage. Each setup consisted of 5 panels which were curved by a constant radius R=1.200 mm. In the first setup the curved panels were stored in constant climate (20°C; 65% RH) for 3 months. In the second experimental setup the panels were stored in the same climatic conditions, but the tension-zone was cyclically moistened with water. The cyclic moistening simulated a post-treatment with the goal to increase stress relaxation. For these two setups, the relaxation was measured after 90 days. To simulate a pre-treatment of the panels a third setup was realized, featuring panels which were saturated with water before bending, and subsequently stored in constant climate (20°C; 65% RH) for three months. For the latter setup, the stress relaxation was measured after 10, 30 and 90 days.

3.2.3 Results

The first experimental setup resulted in a stress relaxation between 33% and 42% in relation to the initial (estimated) stresses. For the second setup a relaxation of 50% to 57% was observed after 90 days. Setup three revealed a stress relaxation between 68% and 71%. A closer examination of the values measured for setup three showed that a large part of stress relaxation occurred during the first ten days (see Fig. 10).

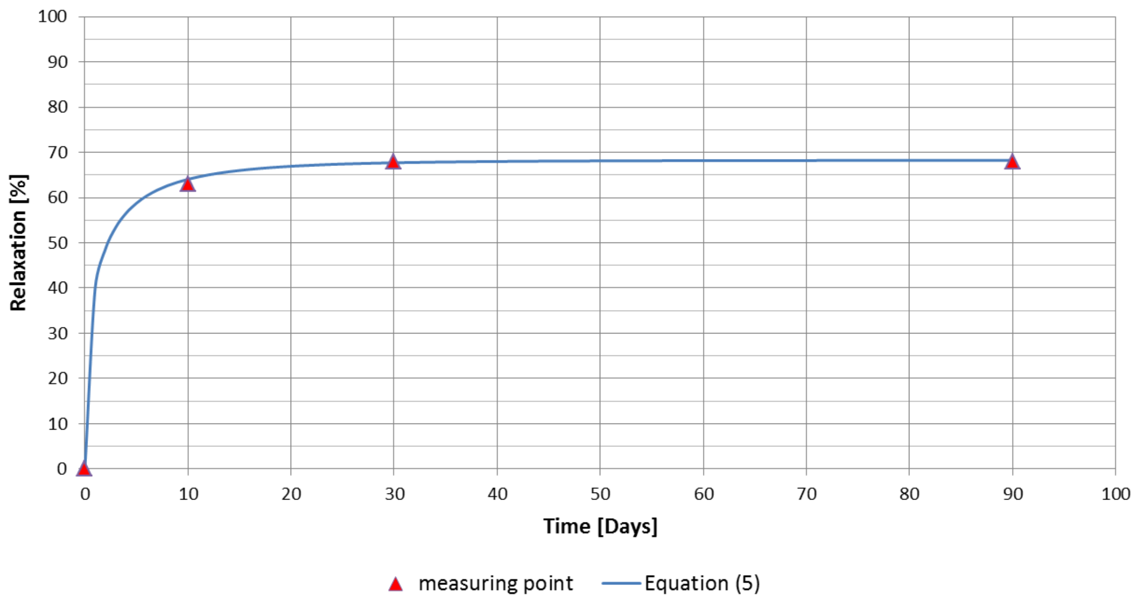

Fig. 10: Measured values of stress relaxation and function

The development during these 90 days can be described by the function of a rheological model, based on a non-linear damper and two linear springs. This model assumes a finite creep deformation and has been determined by the creep behaviour of concrete [10]. The appropriate function can be written as:

$$\chi = \left[1 - \frac{1}{1+\varphi_\infty} \cdot \left(1 + \varphi_\infty \cdot e^{-\frac{E_0+E_1}{\eta}\cdot\sqrt{t}}\right)\right] \cdot 100\% \tag{5}$$

As most of the stress relaxation has taken place during the 90 days measurement period, it is assumed that $t_{90} \approx t_{\infty}$. As a result, a final value of the stress relaxation $t \rightarrow \infty$ can be calculated by the following equation:

$$\chi = \left(1 - \frac{1}{1+\varphi_{\infty}}\right) \cdot 100\% \tag{6}$$

And a final value of the stress as:

$$\sigma_{\infty} = \sigma_0 \cdot \frac{1}{1+\varphi_{\infty}} \tag{7}$$

The right part of equation (7) is equal to the expressions in EN 1995-1-1:2004, 2.3.2.2, giving information on time and moisture dependent deformation. Corresponding values could be derived from the results of the three experimental setups. Substituting the creep parameter φ_{∞} in expression (7) by the values for k_{def} given in EN 1995-1-1:2004, showed that they correspond very well with the experimental results.

Table 1: Comparison of test results and calculated values

Experimental setup	Stress Relaxation χ after 90 days [%]	Treatment corresponding to Service Class	k_{def} from EN 1995-1-1:2004, Table 3.2	Stress relaxation calculated with equation (6) and k_{def}
1	37-42	1	0,8	44
2	46-58	2	1,0	50
3	68-71	3	2,5	71

4 Implementation of test results into a static calculation

4.1 Loads

The internal stresses $\sigma_{m,K}$ in ring direction of the shell, induced by the curvature of the panels, are dependent on a number of parameters. The radius R is one of the most important to calculate the stresses in ring direction. This parameter is dependent on the industrial production accuracy ΔR. The design value can be calculated by:

$$R_d = R_k \mp \Delta R \tag{8}$$

The influence of the stress relaxation can be considered by an adjustment of the modulus of elasticity, consequently calculating an imaginary modulus of elasticity E_{ima} with equation (9).

$$E_{ima} = E_{mean} \cdot \left(\frac{1}{1+k_{def}}\right) \tag{9}$$

Considering the thickness d of the element, stresses can be calculated:

$$\sigma_{m.K,k} = \frac{d}{2 \cdot (R_{nom} \mp \Delta R)} \cdot E_{mean} \cdot \left(\frac{1}{1+k_{def}}\right) \tag{10}$$

EN 1995-1-1 provides no reference on how to consider restraint stresses. On the basis of EN 1992-1-1 it is recommended to use γ=1,0 when determining the design value.

4.2 Resistance

The design resistance of wood is calculated by factors k_{mod} and γ_M. The parameter k_{mod} considers a possible creep fracture. If this kind of failure can be prevented by e.g. appropriate choice of boundary conditions, it is recommended to set k_{mod} =1,0 in case of structures in Service Class 1. The design bending resistance can then be calculated as:

$$f_{m,d} = \frac{f_{m,k} \cdot k_{\text{mod}}}{\gamma_M} \xrightarrow{k_{\text{mod}}=1,0} f_{m,d} = \frac{f_{m,k}}{\gamma_M} \tag{11}$$

For structures featuring higher expected equilibrium moisture contents, the dependency of strength and stiffness parameters on the moisture content should be taken into account. With these approaches it is possible to calculate and realize cylindrical shells with plane, large-sized wood based panels. Amongst others, these approaches can also be applied to determine the internal stresses in highly curved beams made from glued laminated timber.

5. Sample Calculation

The following cylindrical shell, consisting of three layered solid wood panels and two edge beams, was calculated with the shear analogy method [2], [3].

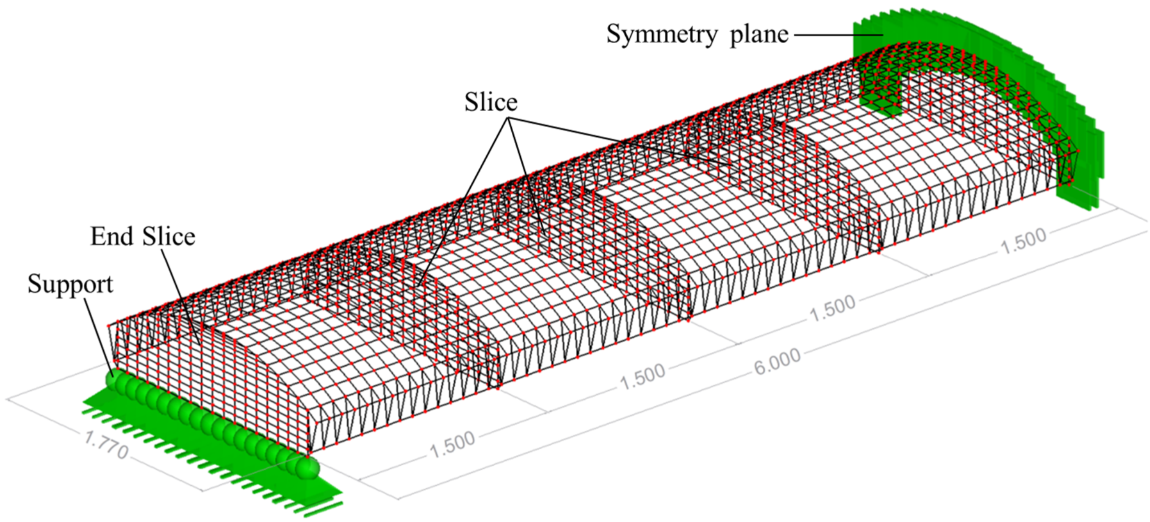

Fig. 11: Grid-Model of the investigated cylindrical shell (dimensions in [mm])

Table 2: Boundary conditions

Geometrical data:	Panel setup:	Edge beam:	Load in vertical direction
L=12.000 mm	d_1=6,7 mm	Material: GL24h	g_k=1,00 kN/m²
B=1.770 mm	d_2=6,6 mm	Dimension: b/h=100/400mm	q_k=1,50 kN/m²
R=1.600 mm	d_1=6,7 mm		

In addition to the given loads, the stresses in ring direction induced by the bending of the panels can be determined with equations (2) and (10).

$$\Delta T_{ideell} = \frac{d}{\alpha_T} \cdot \frac{1}{\left(R_{nom} \mp \Delta R\right)} \cdot \left(\frac{1}{1+k_{def}}\right) \qquad \text{Assumption: } \Delta R=0 \qquad (12)$$

Solutions of the static calculations on design level showed that verification of the load-bearing capacity in ring direction is possible. The parameter k_{def} must be chosen according to the method of bending, respecting a post- or pre-treatment of the panels. If the panels are curved without any post- or pre-treatment (k_{def} =0,8) the verification of the load-bearing capacity results in a unity check value of 1,05. With a post-treatment of the panels (k_{def} =1,0), the verification of the load-bearing capacity can be fulfilled (η=0,77). However with k_{def} =2,5 (pre-treatment with water; corresponding to Service Class 3) the verification of the load bearing capacity was possible. In this case the unity check value was 0,67. In longitudinal direction, the verification of the load-bearing capacity according to EN 1995-1-1 was possible. The unity check value in the plate in longitudinal direction was determined at 0,60.

6. Discussion and conclusion

The research presented has shown that the production of cylindrical shells, using plane, large size, wood-based panels is possible. In static calculations, the stresses induced during the bending process have to be accounted for. The investigation of a curved glued laminated timber beam which was stored for 25 years in Service Class 1 has shown a remaining curvature of about 57%. Further experimental investigations on solid wood panels have revealed that pre- or post-treatment with water significantly influences the stress relaxation. The influence of stress relaxation can be considered by an imaginary modulus of elasticity E_{ima}. This can be implemented in this special case using the creep-factor k_{def} given in EN 1995-1-1:2004. If a creep failure can be prevented by e.g. appropriate choice of boundary conditions, it is recommended to use k_{mod} =1,0 for the stress verification.

Cylindrical shells as structural elements for buildings yield a potential for material savings of around 30% compared to alternative, common construction types [13]. This significant advantage of resource efficiency might be a strong motivation to realize more timber shells in future.

7. References

[1] www.dieffenbacher.de, Download 08.05.2013

[2] Kreuzinger, H.: Platten, Scheiben, Schalen; Ein Berechnungsmodell für gängige Statikprogramme. In: Bauen mit Holz, S. 34-39. Bruderverlag, Karlsruhe. 1999

[3] DIN EN 1995-1-1/NA:2013-08: Nationaler Anhang - National festgelegte Parameter - Eurocode 5: Bemessung und Konstruktion von Holzbauten - Teil 1-1: Allgemeines - Allgemeine Regeln und Regeln für den Hochbau

[4] Stapel P, Rais A, van de Kuilen J-W (2010): Influence of origin and grading principles on the engineering properties of European timber. CIB W18 paper 43-5-2. Nelson, New Zealand.

[5] Echenique-Manrique, R.: Stress Relaxation of Wood at Several Levels of Strain. Wood Science and Technology, Vol. 3, S. 49-73. 1969

[6] Čižek, L.: Dauerfestigkeit und rheologische Eigenschaften von Holz und Holzwerkstoffen. In: Holz als Roh- und Werkstoff, 19. Jahrgang, Heft 3, pp. 83-85. Springer-Verlag. 1961

[7] Kollmann, F.: Technologie des Holzes und der Holzwerkstoffe, Band 1. Springer Verlag, Berlin Göttingen Heidelberg. 1951

[8] Fessel, F.: Probleme beim Holzbiegen. In: Holz als Roh- und Werkstoff, 2. Jahrgang, pp. 56-62. Springer-Verlag. 1951

[9] Gressel, P.: Untersuchungen über das Zeitstandbiegeverhalten von Holzwerkstoffen in Abhängigkeit von Klima und Belastung. Dissertation im Fachbereich Biologie der Universität Hamburg. 1971

[10] Reinhardt, H.-W.: Zur Beschreibung des rheologischen Verhaltens von Holz. In: Holz als Roh- und Werkstoff 31, pp. 352-355. Springer-Verlag. 1973

[11] Hartnack, R.: Langzeitverhalten von druckbeanspruchten Bauteilen aus Holz. Dissertation an der Fakultät für Bauingenieurwesen der Bauhaus-Universität Weimar. 2004

[12] Gressel, P.: Erfassung, systematische Auswertung und Ergänzung bisheriger Untersuchungen über das rheologische Verhalten von Holz und Holzwerkstoffen – Ein Beitrag zur Verbesserung des Formänderungsnachweises nach DIN 1052 „Holzbauwerke“. Abschlussbericht zu den Forschungsvorhaben AIF Nr. 4289/5348 Band 1+2. Versuchsanstalt für Stahl, Holz und Steine, Abteilung Ingenieurholzbau, Universität Fridericiana, Karlsruhe. 1983

[13] v. Halász, R., Cziesielski, E.: Konstruktion und Berechnung hölzerner Zylinderschalen aus Furnierholz. Berichte aus der Bauforschung, Heft 90. Ernst & Sohn Verlag, Berlin. 1973

[14] Kubat, D. G.; Samuelsson, S.; Klason, C.: Stress relaxation in wood (Scots pine veneer). In: Journal of materials science 24, pp. 3541-3548. Chapman and Hall Ltd. 1989

[15] Ranta-Maunus, A.: Creep and effects of moisture in timber. In: Informationsdienst Holz, Holzbauwerke, STEP 3, Grundlagen Entwicklungen Ergänzungen, pp. 4/1-4/21. Fachverlag Holz, Düsseldorf, 1995

INTER

International Network on Timber Engineering Research

HYBRID GLULAM BEAMS MADE OF BEECH LVL AND SPRUCE LAMINATIONS

M Frese

Karlsruher Institut für Technologie

Holzbau und Baukonstruktionen

GERMANY

Presented by M Frese

S Franke commented about the finger joint tests where 4 out of 49 had gluing deficiency. He asked whether they were ignored during the calculations. M Frese responded yes because the deficiencies were due to prototype manufacturing problems.

P Dietsch commented that in the spruce laminate the stresses exceeded the strength on the model and that tests should be done to confirm the simulations. M Frese responded that in reality spruce laminate can fail first and the material can carry additional load resulting from stress redistribution.

E Serrano commented about the failure mode of the Karlsruhe model and wondered how many elements would have failed prior to complete collapse. M Frese said that the information is available from the analysis.

S Svensson discussed shear failure between the LVL and solid wood laminate. M Frese responded that the shear stresses between the interface of the LVL and solid wood was checked. Since only two beech LVL laminate were present, the shear stresses at the interface were not as big as the shear stresses in the center line.

R Brandner asked about the assumption of normality for MOE and whether one could get negative MOE values from the simulations. M Frese responded that the simulation procedure did not seem to show negative MOE values. R Brander also commented on the distance between finger joint in the LVL that there is no need to joint with such high frequencies which would yield even higher results. M Frese responded that this is a manufacturing issue. It might be difficult to bring long length LVL broads into existing glulam plants.

BJ Yeh asked about shear failure model and commented that LVL hybrid glulam is a commercial product in N. America for many years. M Frese agreed that shear failure might occur when large number of LVL laminates is used because the LVL has relatively low shear strength.

J Munch-Andersen commented that one should use distribution of the upper tail MOE rather than the lower tail.

F Lam received confirmation that there is no restriction of finger joint position between adjacent LVL or solid sawn laminations in Europe.

J W van de Kuilen commented that the manufacturers may have different machine settings for MOE which can change its distribution.

S Franke received confirmation that the calculation method is based on glulam values not laminate values.

Hybrid glulam beams made of beech LVL and spruce laminations

Matthias Frese
Karlsruher Institut für Technologie, Holzbau und Baukonstruktionen

Keywords: reinforcement, laminated veneer lumber, Karlsruhe Rechenmodell

1 Introduction

It is most likely that the availability and the use of beech LVL will increase not least because of its high tensile strength. This is the reason to take up again the attempt to examine glulam reinforcements with LVL in the extreme tension zone. Compared to spruce LVL used in former studies [1, 2] beech LVL with parallel-orientated veneers now offers the possibility to increase glulam strength significantly. This may compensate for the additional effort to handle two different materials during manufacture. A positive side effect is that the high and relatively constant strength of beech LVL laminations in the extreme tension zone may crucially reduce the meaning of strength grading regarding the spruce laminations.
The paper aims at showing the achievable mechanical properties of hybrid glulam beams made of beech LVL and spruce laminations (Fig. 1). The properties presented here were determined based on simulations with the Karlsruhe Rechenmodell, a stochastic finite element based computer model, which was specially adopted to the given problem. With regard to the glulam standardisation and probable provisions, it is shown that a calculation method based on a modified theory of composite beams is in principal applicable to determine the effective characteristic bending strength of hybrid glulam, cf. [3-5]. At present, the calculation method shows good agreement with the simulation results. However, it is necessary to verify this calculation method with results of experimental tests on hybrid glulam.

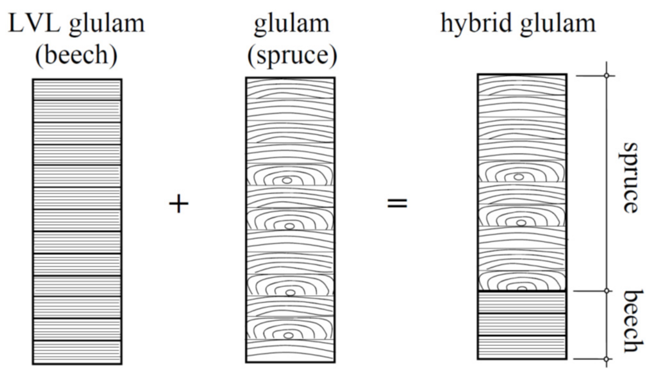

Fig. 1 Composition of hybrid glulam with LVL reinforcement in the tension zone

2 Material and methods

2.1 Computer model and experimental preliminary work

Regarding the technical aspects concerning the simulation of mechanical properties of hybrid glulam beams, the present work is very closely related to a former study on asymmetrically combined glulam, composed of two different strength classes. In this former study, the numerically examined beams were combinations of the strength classes GL20, GL24, GL28 and GL32

(the higher one allocated for the tension zone). The main features of the computer model, relevant for the simulating of the MOE and the bending strength of these strength classes, and the further literature are reported in the corresponding paper [6].
The aspects related to the computer model and given here concern its goal-directed amendment and purposeful application. The amendment affects the simulation of the mechanical properties for the beech LVL laminations. Consequently, new input data are the tensile strength and the MOE of single LVL boards as well as its finger joint tensile strength. The tensile strength of the LVL boards is conservatively represented by a constant value, which reflects the minimum tensile strength of 70 N/mm². This minimum was determined in tension tests [7], which partly form the basis of the current technical approval for beech LVL [8]. The MOE for single LVL boards was determined based on longitudinal vibrations and is empirically represented by a normal distribution with μ = 16600 N/mm² and σ^2 = 805². The resulting distribution shows agreement with the values given in [7]. The tensile strength of finger joints in beech LVL was determined based on tension tests and is also assumed to be normally distributed. The corresponding parameters are μ = 65.4 N/mm² and σ^2 = 6.14². The probability plots in Fig. 2 prove the agreement between the empirical and the assumed theoretical distributions of the MOE and the finger joint strength. In Fig. 2, N denotes the number of the valid specimens in both samples. During the simulation process, both normal distributions were suitably truncated to avoid unrealistic mechanical properties. The report [9] contains a comprehensive description of the corresponding tests. The length of the LVL boards, until now unknown for the reinforcement purpose, is modelled analogously to the spruce material. Hence, the mean length is 4.5 m. The simulated bending strength and MOE values discussed hereafter are in agreement with the provisions of EN 408 [10]. In doing so, the strength is valid for a reference beam depth of 600 mm. The computer model does not involve possible shear failure of the modelled beams.

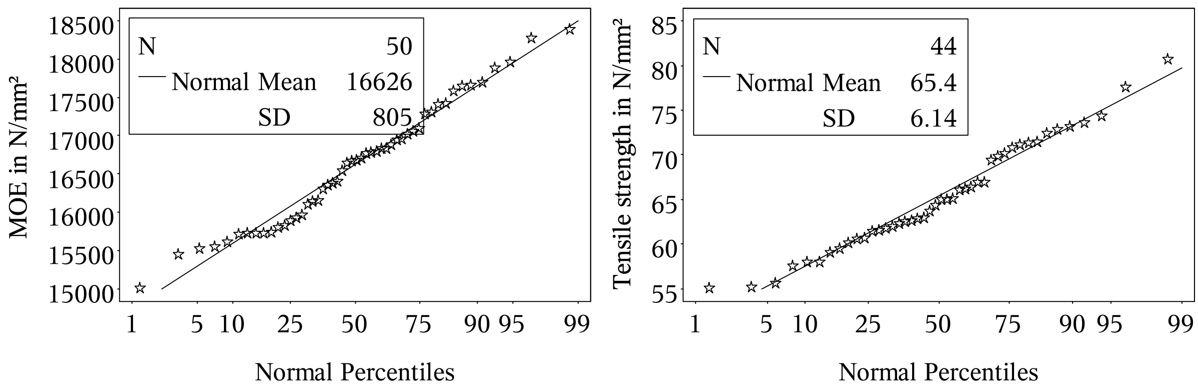

Fig. 2 Test data and fitted normal distributions: MOE in longitudinal direction of beech LVL boards (left) and beech LVL finger joint tensile strength (right)

2.2 Numerical analysis

2.2.1 Pure beech LVL glulam beams

Hybrid glulam is considered as a composition of two different “glulam materials” (Fig. 1) with different characteristic bending strengths. Hence, it is firstly necessary to determine the MOE and the strength distribution of pure beech LVL glulam containing finger joints. For this purpose, one thousand bending tests on such LVL beams were simulated and evaluated. Fig. 3 shows the probability plots of its MOE and bending strength (f_m). According to the given statistics, the mean MOE and characteristic bending strength are

$$E_{\text{mean,LVL}} = 16600\,\text{N/mm}^2 \qquad \text{and} \qquad f_{\text{m,g,k,LVL}} = 60\,\text{N/mm}^2.$$

The mean beam MOE reflects the mean of the source boards. As expected, the standard deviation of the beam MOE is significantly smaller (one fourth) compared to the one of the source boards. The beam strength begins more or less with the minimum finger joint tensile strength of 55 N/mm² (cf. Fig. 2, right) and the maximum slightly exceeds the minimum LVL tensile strength of 70 N/mm². The reason for the casually higher bending strengths compared to the minimum tensile strength of the source boards is the variation in the MOE of the single LVL boards. This causes in more than 25 % of the modelled beams favourable stress distributions, which finally lead to higher bending strengths.

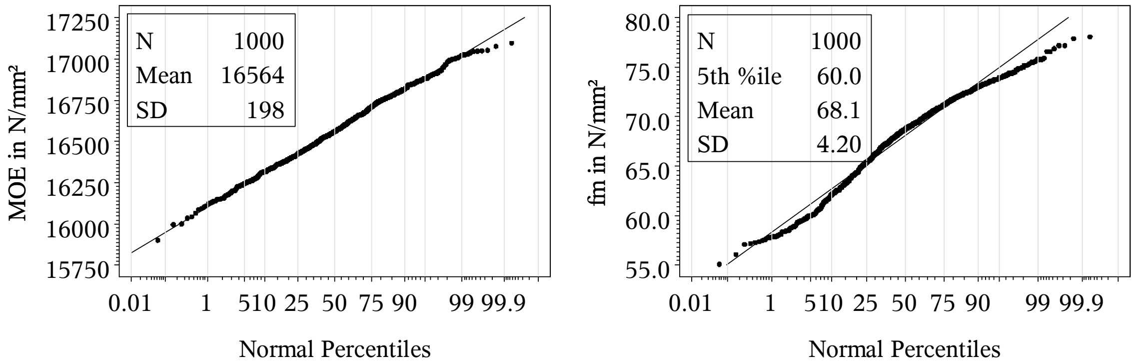

Fig. 3 Simulated mechanical properties of pure LVL glulam containing finger joints

2.2.2 Hybrid glulam beams

Fig. 4 shows the programme for the numerical determination of the MOE and the bending strength of the hybrid beams. The given table contains four variations denoted as type I-hy to IV-hy. The types differ in the glulam strength class in zone 2. Each type was examined for three reinforcement grades, expressed by n. In doing so, up to three beech LVL laminations were modelled in place of spruce laminations. Furthermore, each type and reinforcement grade was examined for the moisture contents u = 12, 16 and 20 %. Each beam consists of 20 laminations.

Type	Zone 1	Zone 2
I-hy	Beech LVL	GL20h
II-hy	Beech LVL	GL24h
III-hy	Beech LVL	GL28h
IV-hy	Beech LVL	GL32h

n Number of beech LVL laminations: 1, 2, 3
Δu Moisture content variation: 12, 16, 20 %
* 20 laminations

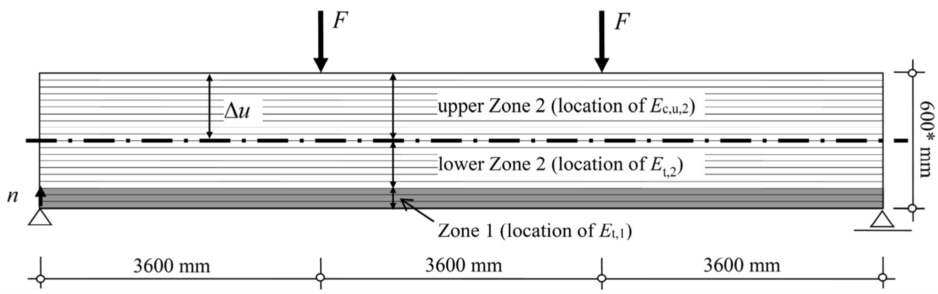

Fig. 4 Test configuration, numerically examined beam types and further details

For the development of the calculation method based on the theory of composite beams Table 1 contains the local MOEs dependent on its zone in which they are present (Fig. 4). The given values for the spruce zones ($E_{t,2}$ and $E_{c,u,2}$) were found by separate simulations of partly unpublished internal studies, which involve bending, tension and compression tests on modelled glulam. In doing so, the phenomenon in elasticity that wood features different MOEs under tension and compression is considered. Consequently, the $E_{t,2}$ values are slightly higher than the $E_{c,12,2}$ values. The given MOEs for compression ($E_{c,16,2}$ and $E_{c,20,2}$) decrease according to the modelled moisture content of 16 and 20 %, respectively.

Table 1 Local tensile and compressive MOEs of the modelled hybrid glulam beams

Type	u %	$E_{t,1}$ N/mm²	$E_{t,2}$ N/mm²	$E_{c,u,2}$ N/mm²	$\alpha = E_{t,1}/E_{t,2}$
I-hy	12 16 20	16600[a]	12500[b]	12200[c] 11200[d] 10300[e]	1.33
II-hy	12 16 20	16600[a]	13000[b]	12600[c] 11600[d] 10600[e]	1.28
III-hy	12 16 20	16600[a]	14100[b]	13800[c] 12700[d] 11600[e]	1.18
IV-hy	12 16 20	16600[a]	16300[b]	15500[c] 14200[d] 13000[e]	1.02

[a] see Fig. 3; [b] mean values from simulations of tension tests; [c] approx. 97 % of $E_{t,2}$, percentage based on simulations of bending and tension tests; [d] 92 % and [e] 84 % of the reference value for 12 % moisture content, see [11]

3 Simulated mechanical properties of hybrid glulam beams

Fig. 5 shows the relation between the bending MOE and the reinforced layup. The first diagram is for 12 % and the last one for 20 % moisture content. Considering 12 % moisture content, the MOE rises from 12.4 GPa (n = 0) to 13.6 (n = 3) for type I-hy and hardly for type IV-hy. The initial MOE values (for n = 0) in each diagram comply with the corresponding mean calculated with $E_{t,2}$ and $E_{c,u,2}$ in Table 1. Casual differences may result from rounding. This agreement, a plausibility check, proves that the simulations correctly reflect the spruce MOEs in Table 1.

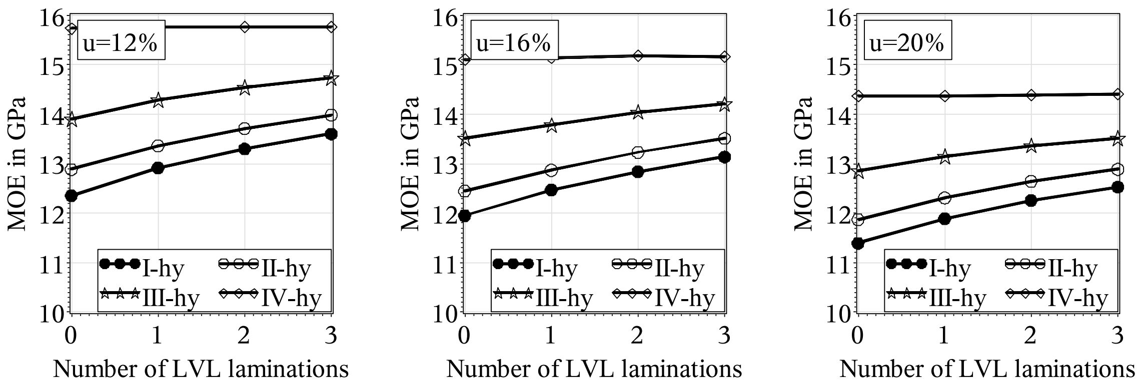

Fig. 5 Simulated effective MOE and gradually converted tension zone

Fig. 6 shows the achievable effective characteristic bending strengths ($f_{m,g,k,eff}$) for the reinforced cross sections (n = 1 to 3) compared to the unreinforced ones (n = 0). According to the prerequisites, each characteristic strength matches the corresponding strength class in case of n = 0. Due to the high minimum strength of beech LVL and of its finger joints, already one to three LVL laminations significantly enhance the bending strength. As the increase in strength is degressive, small reinforcement grades seem to be more efficient than big ones. Furthermore, Fig. 6 shows the influence of the moisture content on the strength. For the unreinforced cross sections, the influence is hardly visible. This is due to the higher compressive strength compared to the strength present in the tension zone. In this case, a change in moisture content has only an effect on the stiffness relations (cf. Table 1) in the cross section and does not affect the beginning of nonlinear material behaviour under compression. However, in the reinforced cross sections the strength in the tension zone far exceeds the compressive strength. Consequently, the compressive stress reaches the strength and modelled plasticity becomes effective in the simulated bending test. For this reason, the neutral axis moves towards the tension zone and the effective bending strength decreases.

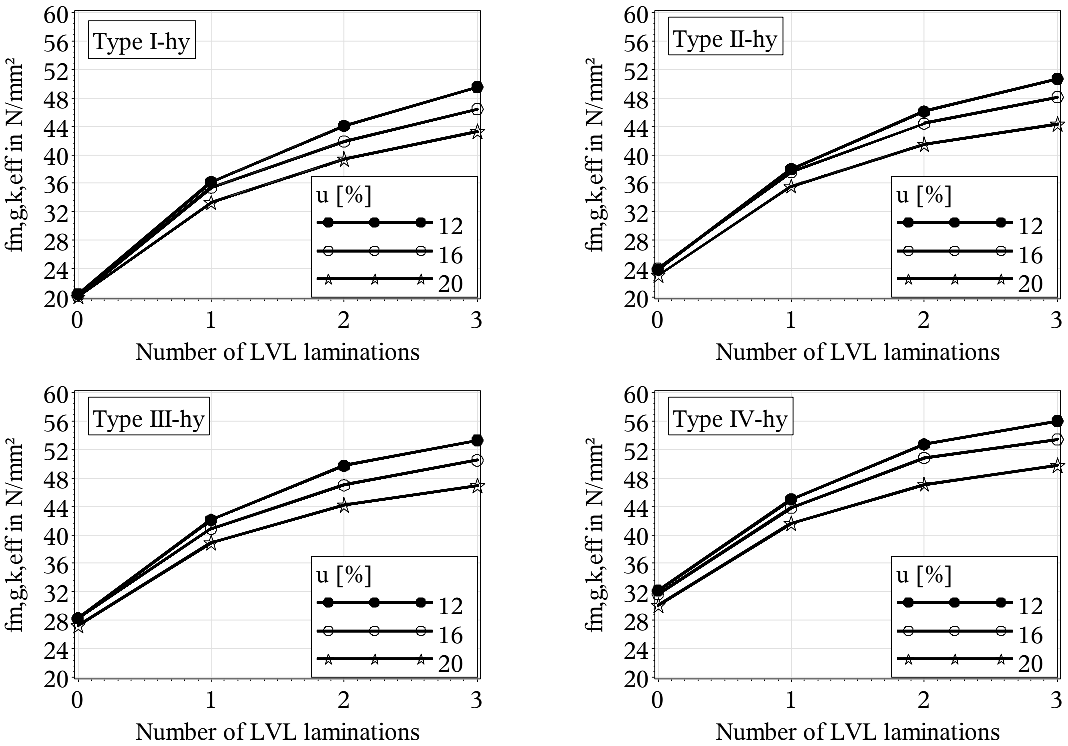

Fig. 6 Simulated effective bending strength and gradually converted tension zone

4 Calculation method based on the theory of composite beams

Simulation processes, shown here, are not a general tool for the glulam user to describe any hybrid configuration, which is of probable relevance for his structure, since the performance of such processes is restricted to scientific computing centres. The following objective concerns, therefore, the development of a verified "hand calculation method" which could be used for the computation of the bending strength of any hybrid beam configuration. In order to be verified, such a method shall adequately reproduce the simulation results. As the theory of composite beams is included in the provisions of EN 14080 [12] – among others in case of asymmetrically glulam – it is purposeful to take this theory as basis for the sought after method. Apart from that, the theory of composite beams suitably reflects the mechanical behaviour in reinforced cross sections [4, 5].

4.1 Theory of composite beams with ideal elastic-plastic behaviour

Fig. 7, left side, exemplifies the calculation of the effective bending strength for type I-hy using the theory of composite beams. A crucial feature of this calculation is the ideal elastic-plastic behaviour of the spruce glulam in the extreme compression zone. Hence, the theory of composite beams is denoted in this preliminary step as nonlinear (NTCB I). The pictorial calculation involves the three reinforcement grades and the moisture content u = 12 %. The diagrams may also be representative for the remaining types, its reinforcement grades and moisture contents. The upper diagram shows the case with n = 1. Based on a linear strain distribution starting with the constant ultimate strain for pure beech LVL glulam beams ($\varepsilon_{\text{bottom}}$ = 0.00361) at the extreme tension fibre, see equation (1), the strain at the extreme compression fibre (ε_{top} = -0.00389) was numerically estimated so that the nonlinear stress distribution (*stepped* or *dashed line*) represents pure bending and horizontal equilibrium is fulfilled, respectively. The given characteristic strength of 36.4 N/mm² applied to the compression zone is the result of separate compression simulations [11].

$$\varepsilon_{\text{bottom}} = \frac{f_{\text{m,g,k,LVL}}}{E_{\text{mean,LVL}}} = \frac{60}{16600} = 0.00361 \tag{1}$$

The equivalent linear stress distribution (*continuous line*) has an effective value of $f_{\text{m,g,k,eff}}$ = 46.3 N/mm². However, this strength is much greater than the simulated one of 36.2 N/mm² (Fig. 6, top left). In this special case, it is not possible to reproduce the simulated strength adequately by means of this nonlinear theory of composite beams. The reasons for the difference between calculated and simulated strength are unrealistically high tensile stresses in the spruce laminations reaching twice the characteristic strength in the extreme tension fibre ($\sigma = 40.5 >> 20$). The issue for $n = 2$ is similar: the effective strength exceeds the simulated one (48.2 > 44), since the tensile stress in the spruce laminations lies still beyond the material strength to a certain extent ($\sigma = 35.7 >> 20$). For $n = 3$, the simulation verifies the calculation (49.7 ≈ 49.5). In this particular configuration, it seems to be possible to permit a stress of $\sigma = 30.7$ N/mm² in the extreme fibre of the spruce laminations (all the same about 150 % of the characteristic strength). This raises the question, whether a particular exceedance of the characteristic strength in the decisive spruce laminations could in principle be permitted. Equation (2) is a suggestion for a format to calculate the degree of such a permissible exceedance. With it, a correspondingly modified characteristic bending strength ($f_{\text{m,g,k,mod}}$) for the spruce laminations in hybrid glulam beams is estimated by a k_{strength} factor. The following sections describe an attempt how the proposed k_{strength} factor could be determined based on the given simulation results.

$$k_{\text{strength}} = \frac{f_{\text{m,g,k,mod}}}{f_{\text{m,g,k}}} \tag{2}$$

4.2 Theory of composite beams with ideal elastic-plastic behaviour and non-consideration of spruce laminations

Fig. 7, right side, exemplifies the application of a modified NTCB. Comparable with possible local (element) failure in the simulation process, the modified NTCB additionally includes non-consideration of such laminations which must not contribute to the equilibrium in order to create agreement between the calculated and the simulated strength. For the configuration $n = 1$, two spruce laminations must not be considered to suit the calculation to the simulation. According to the new equilibrium found for one remaining beech LVL lamination ($\varepsilon_{\text{top}} = -0.00389 \rightarrow -0.00319$) the effective bending strength becomes 34.9 N/mm² and is slightly lower than the simulated value of 36.2 N/mm². The allowable stress in the extreme fibre of the remaining "active" spruce laminations becomes 32.4 N/mm² (= σ). The scheme below exemplifies the configuration $n = 2$. In it, an agreement between calculation and simulation is found after the non-consideration of one spruce lamination. In the case $n = 3$, there is no need for such a "correction". Table 2 summarises the results of the modified nonlinear theory of composite beams (NTCB II) which takes into account the non-consideration of selected laminations: the ratios between calculation and simulation are lower than or equal to one. Hence, they support the assumption that stresses could be effective which significantly exceed the original characteristic strength of the spruce glulam proportion. For the cases discussed here in detail, the increase factors k_{strength} have a range of about 1.5 to 1.6 (Table 2, last column).

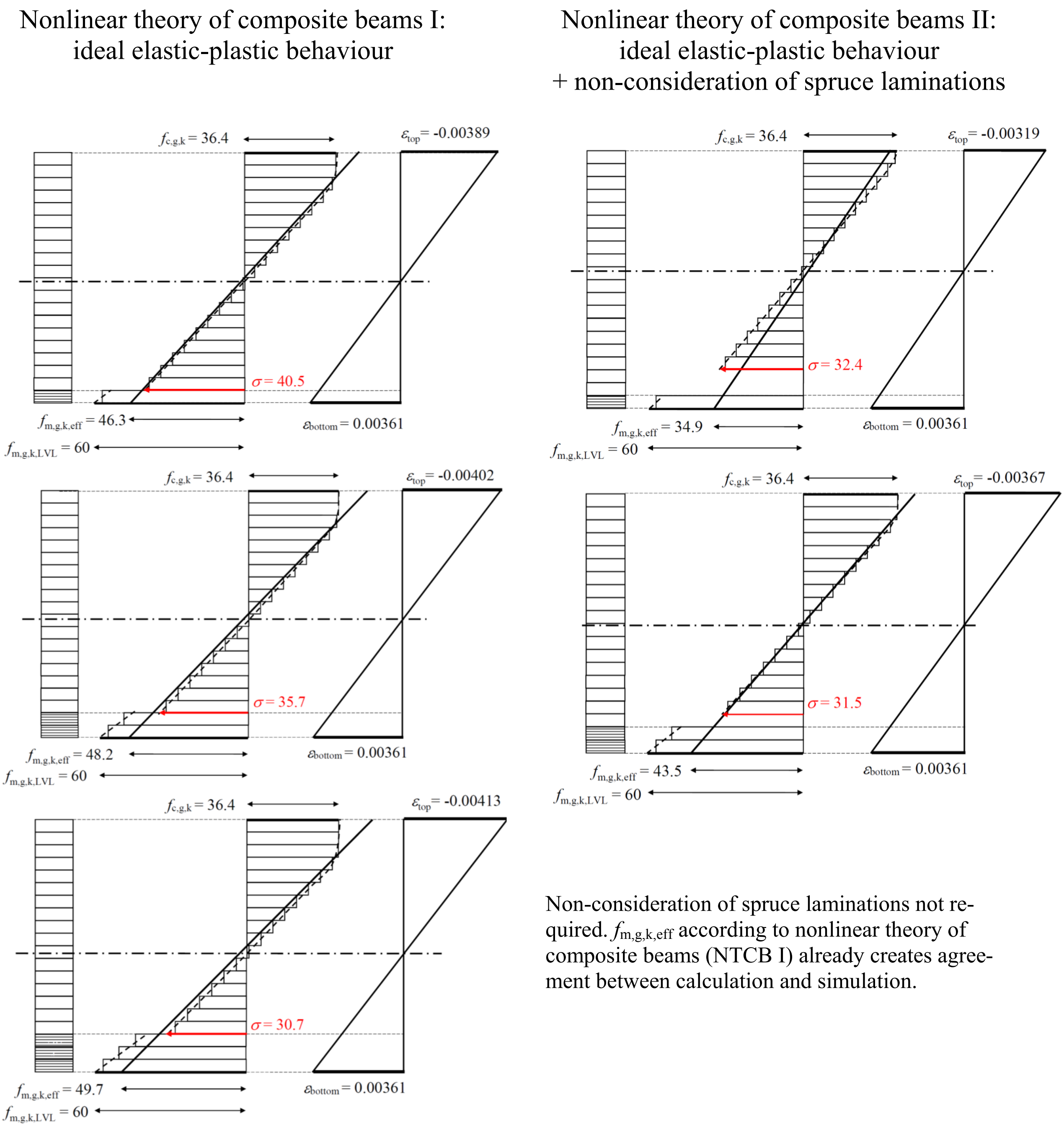

Fig. 7 Stress and strain distribution in the cross section of type I-hy (u = 12 %) and ideal tensile stress (σ) given in red in the extreme fibre of the spruce glulam proportion; reinforcement grade n = 1 (top), n = 2 (middle) and n = 3 (bottom)

Table 2 Exemplary application of the modified nonlinear theory of composite beams; type I-hy used; strength and stress in N/mm²

n	$f_{m,g,k,eff}$ Simulation	$f_{m,g,k,eff}$ NTCB I	$f_{m,g,k,eff}$ NTCB II	$\frac{\text{NTCB II}}{\text{Simulation}}$	σ_{spruce} NTCB II	$k_{strength} = \sigma_{spruce}/20$
1	36.2	46.3	34.9	0.96	32.4	1.62
2	44.1	48.2	43.5	0.99	31.5	1.58
3	49.5	49.7	49.7	1.00	30.7	1.54

The procedure described in Fig. 7 right was completely applied to all types, reinforcement grades and moisture contents. Fig. 9 contains the results. The polygonal courses show comparisons between simulation results and calculations according to the NTCB I and II. It becomes obvious that the NTCB I is an unsuitable method to describe configurations with up to 2 reinforcing LVL laminations. In this case, one to two spruce laminations must not be considered in order to find agreement between calculation and simulation. Except for one single case (IV-hy, n = 3, 12 %), the configurations with n = 3 can be adequately treated with NTCB I.

4.3 Modified strength for the spruce proportion in hybrid glulam beams

According to the assumption of an existing specific modified characteristic bending strength ($f_{m,g,k,mod}$) present in the spruce laminations directly above the reinforcing LVL laminations, all the configurations (4 types x 3 grades x 3 moisture contents) were evaluated in this regard. This led to nominally 36 $k_{strength}$ values, which state the result of a conservative agreement between calculation and simulation. In order to describe these $k_{strength}$ values with a separate function given in equation (3) explanatory variables were identified. These variables and their definitions are given in term (4). The basis of the selection of these variables are mechanical and logical considerations.

$$k_{\text{strength}} = f(x_1, x_2, ...) \tag{3}$$

$$\begin{aligned}
x_1 &= \eta = \frac{f_{\text{m,g,k}}}{f_{\text{m,g,k,LVL}}} = \frac{\text{spruce glulam bending strength}}{\text{bending strength of beech LVL glulam}} \\
x_2 &= \alpha = \frac{E_{\text{t,1}}}{E_{\text{t,2}}} = \frac{\text{MOE of beech LVL glulam}}{\text{MOE of spruce glulam}} \\
x_3 &= \beta = \frac{n_{\text{LVL}}}{n_{\text{total}}} = \frac{\text{number of LVL laminations}}{\text{total number of laminations}} \\
x_4 &= \gamma = \frac{u}{u_{\text{ref}}} \qquad \text{with } u_{\text{ref}} = 12\%
\end{aligned} \tag{4}$$

34 out of 36 $k_{strength}$ values were suitable to be evaluated for a specified form of equation (3). The corresponding result is given in equation (5). With it, the strength increase and the modified characteristic bending strength, respectively, can be estimated. In addition, Fig. 8 exemplifies the relation between the iteratively derived $k_{strength}$ values (as shown in Fig. 7, right and stated in Table 2) and those estimated by equation (5). It is obvious that the selection of explanatory variables and, finally, the equation itself create an adequate means to calculate the modified characteristic bending strength. With it, an estimation of the effective characteristic bending strength of reinforced glulam is theoretically possible.

$$k_{\text{strength}} = \frac{0.608}{\eta \cdot \alpha \cdot \beta^{0.06} \cdot \gamma^{0.08}} \tag{5}$$

5 Conclusions

Simulations on hybrid glulam beams prove that reinforcing spruce glulam with finger jointed beech LVL laminations is an effective method to raise the cross sectional bending strength significantly. It is efficient to reinforce glulam with lower strength classes. Due to the degressive increase in strength dependent on a growing LVL proportion, the LVL laminations should not exceed 15 % of the cross sectional depth. The simulation results support the assumption that a higher bending strength than the characteristic value could be permitted in the spruce laminations arranged directly above the reinforcement. This effect can be used for an arithmetical strength modification in the spruce laminations if the effective cross sectional strength is calculated with the theory of composite beams taking tension failure and non-consideration, respectively, of spruce laminations into account. The strength increase due to the modification is supposed to be 20 % to 60 % of the original characteristic strength of the spruce glulam proportion. The effective factor depends particularly on the difference in strength between the glulam to be reinforced and the beech LVL, the stiffness relations in the hybrid beam and the proportion of the LVL laminations. Further research concern bending tests on reinforced glulam in order to verify the assumption of an arithmetical strength increase. Anyway, such tests may generally prove the benefit of reinforcing glulam with beech LVL laminations. It may be of further use to examine the mechanical properties of finger jointed LVL in detail. More precise input data for the computer model would lead to more reliable simulation results.

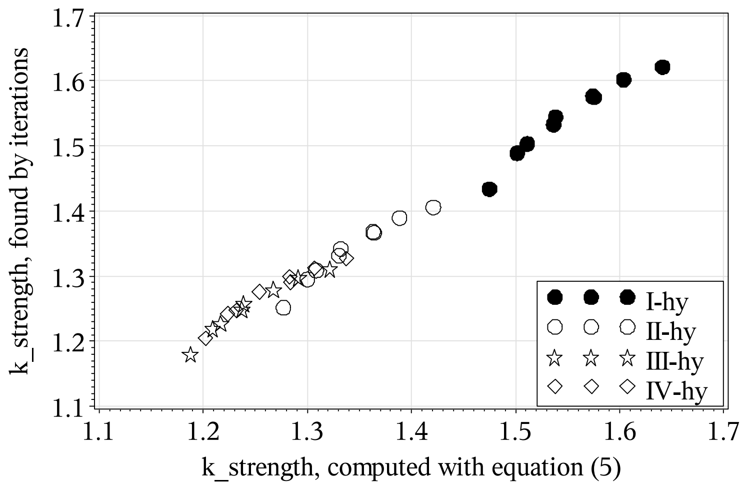

Fig. 8 Comparison between $k_{strength}$ factors

Literature

[1] E. Gehri: Verbindungstechniken mit hoher Leistungsfähigkeit. Holz Roh- und Werkstoff 43 (1985), 83-88

[2] B. Radović: Träger aus Brettschichtholz mit Furnierschichtholz im Zugbereich. Vorhaben I.4-35105, Forschungs- und Materialprüfungsanstalt Baden-Württemberg, Stuttgart 1988

[3] G.P. Krueger: Ultimate-Strength Design of Reinforced Timber. Wood Science 6 (1973), 175-187

[4] T. Schatz: Beitrag zur vereinfachten Biegebemessung von FVK-bewehrten Holzträgern. Bautechnik 81 (2004), 153-162

[5] R.F. Lindyberg, H.J. Dagher: ReLAM: Nonlinear Probabilistic Model for the Analysis of Reinforced Glulam Beams in Bending. Journal of Structural Engineering 138 (2012), 777-788

[6] M. Frese, H.J. Blaß: Asymmetrically combined glulam – simplified verification of the bending strength. CIB-W18/45-12-1, Växjö, Sweden 2012

[7] Holzforschung München: Prüfbericht 10511. Technische Universität München 2012

[8] Deutsches Institut für Bautechnik: Allgemeine bauaufsichtliche Zulassung Z-9.1-838. Berlin 2013

[9] Versuchsanstalt für Stahl, Holz und Steine: Prüfbericht 136147. Karlsruher Institut für Technologie 2013

[10] EN 408:2010+A1:2012 Timber structures –Structural timber and glued laminated timber – Determination of some physical and mechanical properties

[11] M. Frese, M. Enders-Comberg, H.J. Blaß, P. Glos: Strength of spruce glulam subjected to longitudinal compression. CIB-W18/44-12-2, Alghero, Italy 2011

[12] EN 14080:2013 Timber structures – Glued laminated timber and glued solid timber – Requirements

Appendix

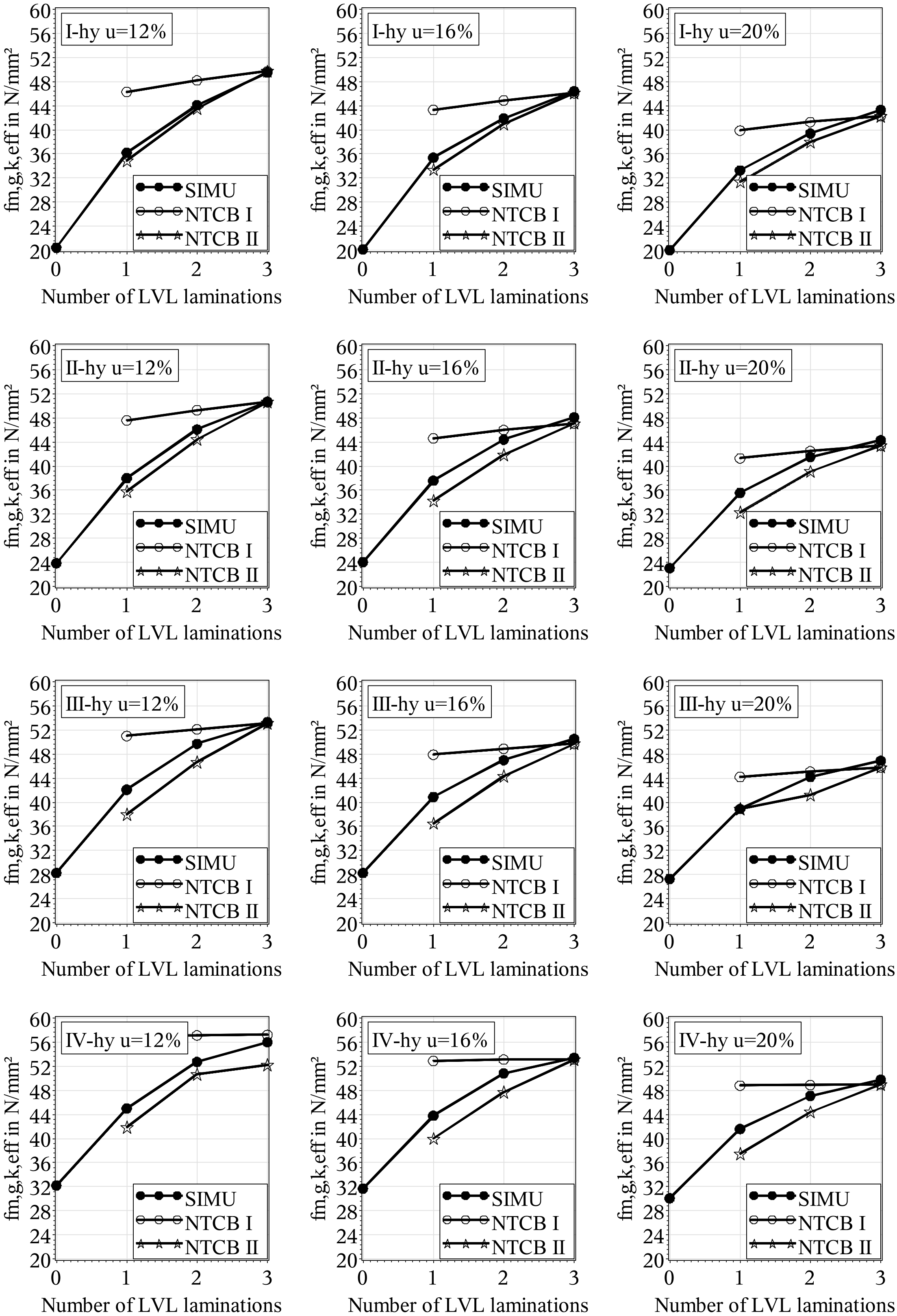

Fig. 9 Effective characteristic bending strength: comparison between simulation results (SIMU), theory of composite beams (NTCB I) and a modified version (NTCB II)

INTER

International Network on Timber Engineering Research

DESIGN FOR THE SPREADING UNDER A COMPRESSIVE STRESS IN GLUED LAMINATED TIMBER

D Lathuilliere
L Bleron
J-F Bocquet
University of Lorraine, ENSTIB/LERMAB

F Varacca
SFS intec

F Dubois
University of Limoges, FST/GEMH

FRANCE

Presented by D Lathuilliere
S Svensson asked was the friction between the loading head and wood considered. D Lathuillier responded no.
F Lam asked about the size effect adjustment Ksb and received confirmation that the coefficient was established from regression.
I Smith stated that more simplification is better and asked about the consideration of B Madsen test results. He received discussions that B Madsen's results were considered via the Eurocode confirmation.
S Franke commented about the use of 1% offset for proportional limit. He stated that one should try different method as the results depend on the specimen depth such that if different specimen depths were considered the 1% offset method would result in difficulties for comparing the results.

Design for the spreading under a compressive stress in glued laminated timber

Damien LATHUILLIERE, Laurent BLERON, Jean-François BOCQUET
University of Lorraine, ENSTIB/LERMAB, France

François VARACCA
SFS intec, France

Frédéric DUBOIS
University of Limoges, FST/GEMH, France

Keywords: Spreading, Compression, Timber, Eurocode 5

1. Introduction

1.1. Background

Since its creation, the use of wood material rises with large-spanned structures building. Glued laminated timber became the material inescapable for these structures. However, the construction of such structures causes localized stress concentrations of compression perpendicular to the grain. This concentration severely penalizes the structure because of weak compressive strength of timber perpendicular to the grain. Today, according to the new standard EN 14080 [1] published in August 2013, the characteristic value of compressive strength perpendicular to the grain $f_{c,90,k}$, determined from the standard EN408 [2], is constant and equal to 2.5 MPa, whatever the resistance class.

However, the spreading effect of the stress allows reducing this mechanic weakness. Today, a current design code, EN 1995-1-1 A1 [3], allows to predict the support bearing capacity solicited in compression perpendicular to the grain taking into account the spreading phenomenon. The design model of the spreading phenomenon is calculated from an effective length ℓ_{ef}. The common case for the calculation of the effective length is the addition of 30 mm on either side of the support, if the sample is long enough. The current calculation criterion, proposed by Pr. Blass [4], is written in such a way that the resistance part has to be lower than the active part. It takes the following form:

$$f_{c,90,d} \cdot k_{c,90} \geq \frac{F_{c,90,d}}{b \cdot \ell_{ef}} = \sigma_{c,90,d} \qquad (1)$$

Due to a ductile behaviour, the standard allows an increase of the design compressive strength perpendicular to the grain via the material factor $k_{c,90}$ taking into account the load configuration. This factor is determined by the change of the SLS design to the ULS design [4]. For glued laminated timber on discrete support whose length is less than 400mm, it is equal to 1.75. In other cases, it is equal to 1.

In agreement with the proposition of the spreading effect of Riberholt [5], the spreading effect of the present standard can be written according to the equation (2) integrating the geometric and material factors.

$$f_{c,90,d} \cdot k_{dif,EC5} \geq \frac{F_{c,90,d}}{b \cdot \ell} = \sigma_{c,90,d} \quad with \quad k_{dif,EC5} = k_{c,90} \frac{\ell_{ef}}{\ell} \tag{2}$$

A problem persists on the use of code for discrete supports upper to 400mm. It imposes an increase of supports length causing an enormous economic problem for their designs. Many studies have been conducted on the understanding of spreading effect [4], [6]–[11]. Thus, many design codes have been proposed by Madsen [12], Van Der Put [13] and Bleron [11] on the prediction of the support bearing capacity. The different models proposed show an evolution taking into account the geometric data of the sample.

According to EN 1995-1-1 A1, the design of the current structure imposes a length four times greater than that calculated by CB71 [14], which is the French design code of wood structures. Building inspections calculated at the CB71 were performed. Analyses show a building exploitation still in progress without apparent degradation of the supports.

However, today's architecture evolves. For this reason, the structures become increasingly complex and varied [15]. By means of these structures, the compressive stress at an angle to the grain under concentrated load has to be understood, as well as the associated spreading phenomenon. Today, it exists two standards, the one of German DIN 1052 [16] and the other European EN1995-1-1 [17], allowing to predict the support bearing capacity solicited in compression at an angle to the grain. The difference noted between these two standards is the integration of the shear strength in the German standard. A study [18] shows that the two standards are similar for the glued laminated timber of GL24H class. Moreover, the German standard is better in terms of prediction of brittle behaviour. Furthermore, today, none of the standards authorize the spreading effect in compression parallel to the grain.

1.2. Objectives

The major objective of this study is to bring a proposition of design code taking into account the diffusion effect of the support solicited in compression at a given angle to the grain. It also integrates the different possible interactions between supports.

In order to answer this objective, the phenomenon of compression perpendicular to the grain is studied by means of the different experimental tests allowing a development of the analytic model. In the second part, compression tests with interaction are performed and compared to this model. Finally, the last part deals with the compression at an angle to the grain.

2. Compression test perpendicular to the grain

2.1. Materials

In order to analyze the spreading effect, the first type of test is performed according to EN408 standard. It consists in carrying out a compression test on the given volume, loaded on his entire surface (*Fig. 1* Case A). This test is called the uniform compression test. The wood used is the glued laminated timber of GL24H class, composed of 45 mm thick lamellas. All specimens were conditioned at 12% moisture content without cracking on the specimen. The displacement of load point is controlled at a constant speed in order to respect the duration of the test of 300s ± 120s.

The second type of test consists in carrying out a compression test with discrete supports. It is compared to the results of uniform compression test associated allowing to quantify the spreading effect of EN 1995-1-1 A1. The experimental conditions and the material are similar to the one in the previous tests. Five configurations (*Fig. 1*) are tested in order to identify the different support conditions. For some configurations, several transverse sections and support lengths are tested in order to study the different geometric effects. The geometric data and the results are summarised in the *Table 1*.

To highlight the spreading effect in the vicinity of support areas, the Digital Image Correlation (DIC) method is introduced. The image capture is performed at a rate of 0.5 frames per second and synchronized with the press displacement. The DIC uses integrated processing algorithms in the software correlation developed by the team at the Prime Photomechanical Institute affiliated with the University of Poitiers (France). The software operating principle calls for the integration of a discrete gray level function distributed by pixels forming a regular grid of the digital image. The displacement of various points on the original image can be estimated by correlating information from two successive images. To acquire precise sub-pixels, the gray levels are interpolated by a bilinear function or cubic spline, which allows obtaining a continuous gray level function over the entire image.

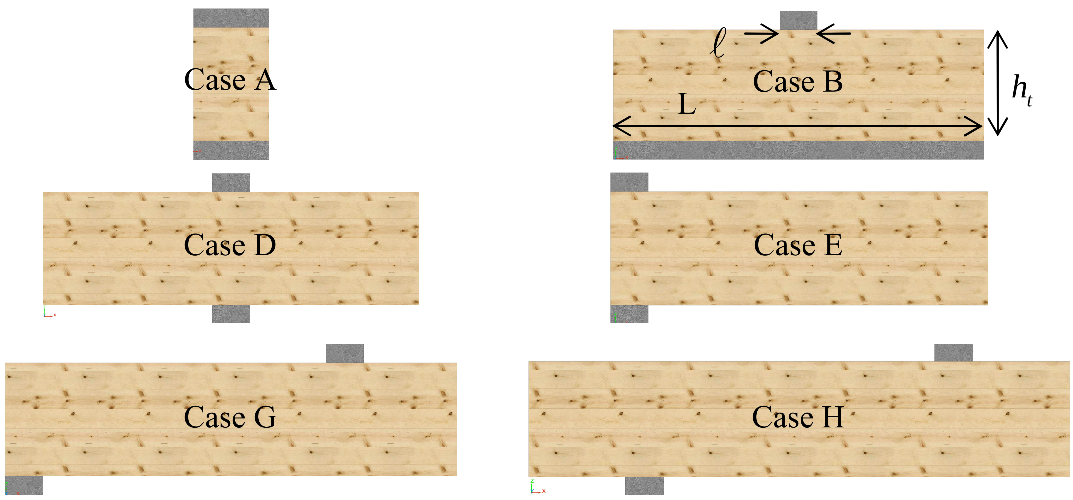

Fig. 1: Configuration of compression test

2.2. Results

In order to have a similar rupture criterion for all configurations, the criterion of EN408 standard is used. It recommends to determine the compression strength for a plastic deformation of 1% (*Fig. 2*). For the strain, the ratio between the displacement and the reference height is performed. For all compression tests, the reference height is the total height of the specimen. The spreading factor of the equation (2) is deducted. All results are synthesized in the *Table 1*.

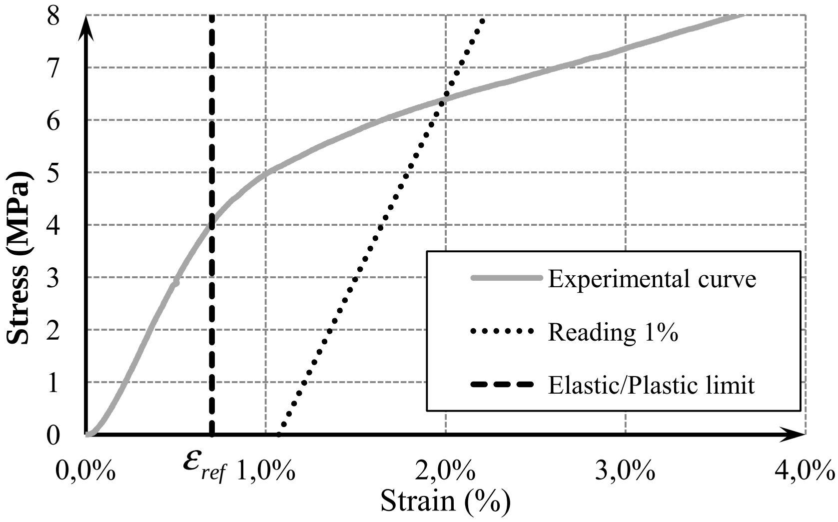

Fig. 2: Determination of the deformation stress. (ε_{ref} is defined as elastic threshold deformation)

Table 1: Compression tests perpendicular to the grain

Series	Width b (mm)	Height h_t (mm)	Specimen length L (mm)	Support length ℓ (mm)	Nb	$\sigma^{1\%}_{c,90,mean}$ (MPa)	COV (%)	$\frac{\sigma^{1\%}_{c,90,mean}}{f_{c,90(CaseA)}}$
A-90-1	78	300	100	10	10	3.01	12	1
A-90-2	90	200	278	278	18	3.29	15	1
A-90-3	160	200	160	160	17	3.49	15	1
B-90-1	78	300	800	100	9	8.08	7	2.45
B-90-2	160	100	600	50	8	6.22	11	1.88
B-90-3	120	300	800	300	3	4.50	13	1.36
D-90-1	78	300	800	100	10	6.34	10	1.92
D-90-2	78	150	800	100	10	6.14	6	1.86
D-90-3	78	300	160	100	10	5.05	7	1.53
D-90-4	90	200	600	50	4	7.48	17	2.27
D-90-6	160	200	600	50	6	6.53	7	1.98
D-90-7	185	200	600	50	2	6.68	2	2.02
D-90-8	210	200	600	50	2	6.56	4	1.99
D-90-9	160	800	1600	600	5	4.25	10	1.29
E-90-1	78	300	800	100	10	5.13	8	1.55
G-90-1	90	315	/	50	3	7.35	18	2.23
G-90-2	120	560	/	119	3	5.41	12	1.64
H-90-1	90	315	/	50	3	8.63	15	2.62
H-90-2	90	315	/	56	6	7.82	18	2.37
H-90-3	120	560	/	119	3	5.89	11	1.78
H-90-4	120	560	/	173	3	5.64	10	1.71
H-90-6	120	560	/	240	3	5.03	15	1.52
H-90-7	160	810	/	119	6	8.16	14	2.47
H-90-8	160	810	/	173	3	6.62	4	2.01
H-90-9	160	810	/	240	3	6.29	7	1.91

2.3. Analysis of the spreading effect in compression perpendicular to the grain

The first result analyzed is the evolution of the support reaction at 1% plastic strain according to the support length. This analysis is performed with series results H-90-3 to H-90-6. These results show a linear relationship between these two parameters. The equation (3) is deducted with $F_{c,90}^{1\%}$, the support reaction at 1% plastic strain and ℓ, the support length.

$$F_{c,90}^{1\%} = A_1 \cdot \ell + B_1 = F_{c,90}(\ell) + F_v \tag{3}$$

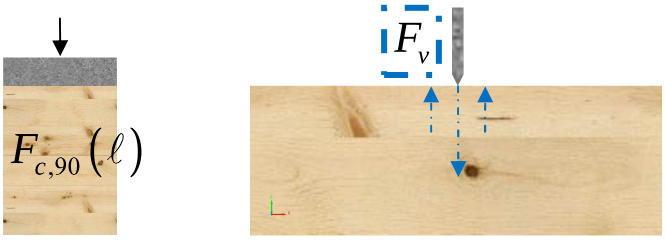

(a) (b)

Fig. 3 : (a) Compression effect (b) Shear effect

This equation is divided by the support surface ($\ell \cdot b$) considered in order to obtain this same equation for stress.

$$\sigma_{c,90}^{1\%} = \frac{A_1}{b} + \frac{B_1}{b \cdot \ell} \tag{4}$$

This expression is composed of two terms. The limit of this equation is calculated when the support length is close to the infinity. In this case, the second term becomes negligible compared to the first. This stress state represents the uniform compression test *Fig. 3*a. Consequently, the first term of the equation may be substituted by the mean compressive strength perpendicular to the grain $f_{c,90,mean}$. On the contrary, when the support length is close to zero, the stress state represents a shear test *Fig. 3*b.

In this case, the term b1 of the equation (4) represents the shear stress, hence the equation (5) determined from the shear strength.

$$B_1 = f_{v,mean} \cdot \frac{2}{3} \cdot b \cdot h \tag{5}$$

The equation (4) may be written with integrating the two analyses (*Fig. 4*):

$$\sigma_{c,90}^{1\%} = f_{c,90,mean} + f_{v,mean} \cdot \frac{h}{\ell} \cdot \frac{2}{3} \tag{6}$$

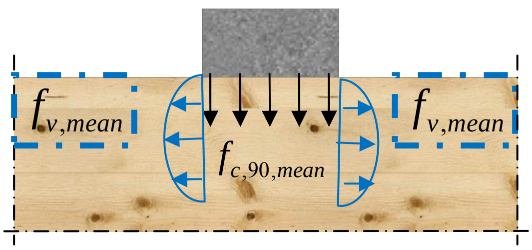

Fig. 4 : Association of the shear and compression effects

The different tests (see *Table 1*) show that a volume effect exists. The results of D-90-4 to D-90-8 show the width influence on the compression strength perpendicular to the grain. It can be deducted that the compression strength perpendicular to the grain becomes constant when the width becomes important.

The measuring device of displacement field allows determining the elastic and plastic domain for each test realized. From this, the strain fields corresponding to the support reaction at 1% plastic strain is kept. It is limited by the reference strain ε_{ref} (see *Fig. 2*). It can be deducted the two strain fields in *Fig.* 5a and 5b, bending and compression respectively.

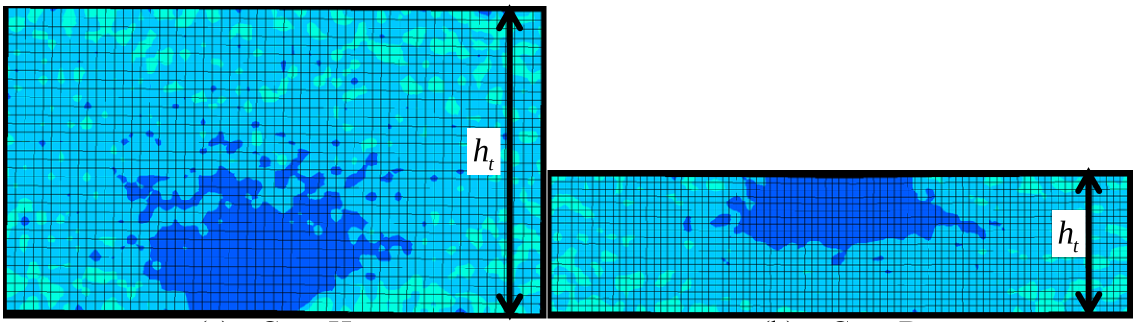

(a) - Case H (b) – Case B

Fig. 5: Strain fields

These two strain fields are represented by two separate areas. The areas dark and light represent the plastic and elastic domain respectively. It can be deducted the plastic height of the different compression and bending tests. This plastic height is represented by a coefficient k_{sh} which is equal to:

$$k_{sh} = \begin{cases} 1/2 \ \textit{case in bending} \\ 1/3 \ \textit{the others cases} \end{cases} \tag{7}$$

Apart from the beam dimensions and by looking the series B-90-1 and D-90-1, we can see that the support type in the lower part of the specimen affects the compression strength perpendicular to the grain. In the presence of continuous support in the lower part, the compression strength perpendicular to the grain is more important of 60% with the geometric sections identical.

Finally, a last effect impacting the spreading effect is the number of side. For this, the couples G-90-1/H-90-1, G-90-2/H-90-3 and D-90-1/E-90-1 are compared. They demonstrate a correlation between the side number and the compression value. Consequently, the side factor n_d is written as follow:

$$n_d = \begin{cases} 1 \ \textit{for end support} \\ 2 \ \textit{for intermediate support} \end{cases} \tag{8}$$

k_{sb} is a first factor which integrates the effect of support width. The second k_{sc} is a support condition. The two last factors are determined in order to minimize the difference between the experimental values and the analytic model. They are written as follow:

$$k_{sb} = b^{-0.325} \tag{9}$$

$$k_{sc} = \begin{cases} 1.51\, configurations\,(B, D, E, F) \\ 1.85\, configuration\,(C) \end{cases} \tag{10}$$

To conclude, the spreading effect is sensitive to the geometric data and the support condition. Consequently, four parameters are integrated to the equation (6).

In this way, the equation (6) combined with the equations (7), (8), (9) and (10) is written as follows:

$$\sigma_{c,90}^{1\%} = f_{c,90,mean} + f_{v,mean} \cdot \frac{k_{sh} \cdot h_t}{\ell} \cdot \frac{2}{3} \cdot k_{sb} \cdot k_{sc} \cdot n_d \tag{11}$$

The equation (11) can be written also by reasoning with the spreading factor of Riberholt [5]:

$$k_{dif} = 1 + \frac{f_{v,mean}}{f_{c,90,mean}} \cdot \frac{k_{sh} \cdot h_t}{\ell} \cdot \frac{2}{3} \cdot k_{sb} \cdot k_{sc} \cdot n_d \tag{12}$$

$$f_{c,90,mean} \cdot k_{dif} \geq \frac{F_{c,90,mean}}{b \cdot \ell} \tag{13}$$

A difference of 9% is observed between the analytic model and the experimental stresses by applying the equation to the different experimental and bibliographic [4] [6]–[11] compression tests perpendicular to the grain of glued laminated timber.

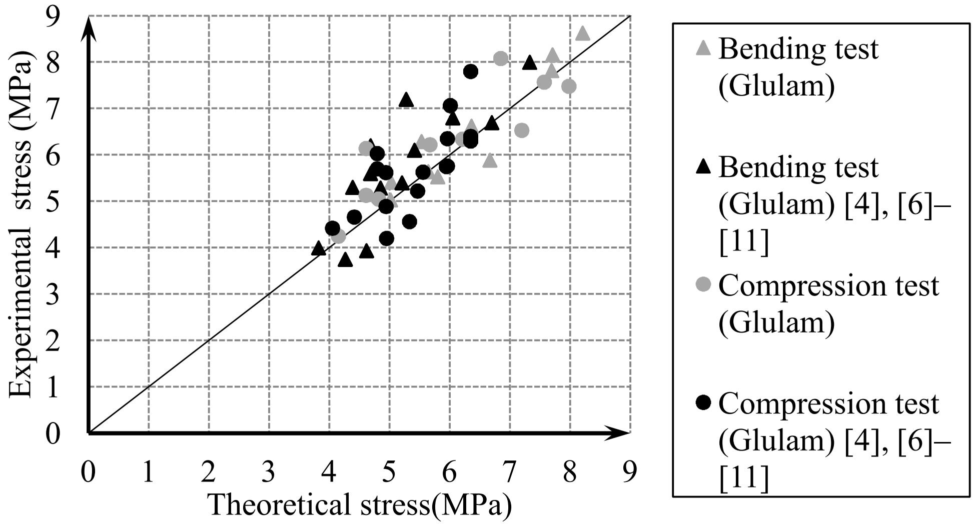

Fig. 6: A review of all mean model predictions vs. mean tests results

2.4.Proposition of analytic model

However, this factor may be expressed in another way that the equation (12). It may be calculated by an effective length and also integrated the different interaction length, as proposed in the EN 1995-1-1 A1 standard. Consequently, the calculation of effective length may be performed according to the equation (14) and integrated in the equation (15):

$$\ell_{ef} = \ell + \min\begin{cases}\ell_{dif} \\ \ell_{le} \\ \ell_{li}/2\end{cases} + \min\begin{cases}\ell_{dif} \\ \ell_{re} \\ \ell_{ri}/2\end{cases} \quad \textit{with} \quad l_{dif} = \frac{f_{v,mean}}{f_{c,90,mean}} \cdot k_{sh} \cdot h_t \cdot \frac{2}{3} \cdot k_{sb} \cdot k_{sc} \tag{14}$$

$$\frac{F_{c,90,mean}}{b \cdot \ell_{ef}} \leq f_{c,90,mean} \tag{15}$$

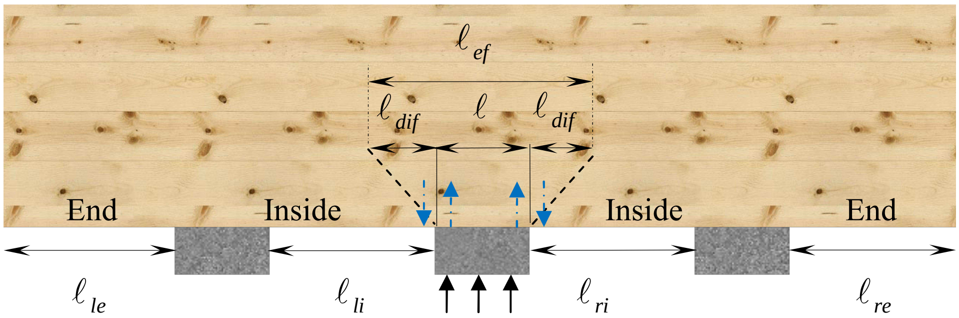

Fig. 7: Determination of effective length

3. Compression tests with interaction

3.1. Materials

In order to valid the interactions of near supports and to confirm the equation (15), three series with spaced supports are performed. The first configuration is composed to two supports of 93.5mm spaced out by 113mm. This configuration is such as the effective length is similar to the effective length of the configuration B-90-3. The second series is similar to the first one, except the space between the two supports, where 50mm are withdrawn. The last series is similar to the first, except the number of support. There are three supports with the spacing between each support of 113mm. For the three series, the height is 300mm and the width is 120mm.

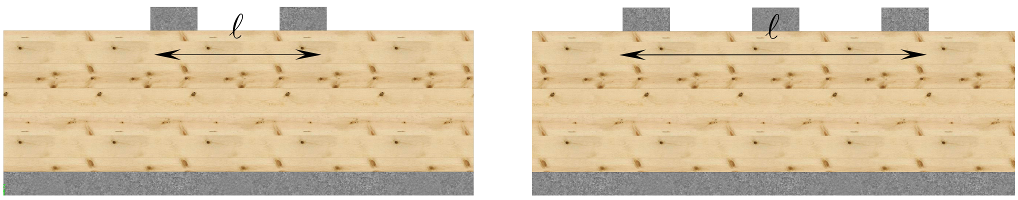

(a) (b)

Fig. 8: Compression tests with interaction: (a) Two supports (b) Three supports

3.2. Results

The determination process of compression strength perpendicular to the grain is still performed for the plastic strain at 1%. The stress is calculated taking into account the total support length ℓ (see Fig. 8). The results are synthesized in the *Table 2*.

Table 2: Compression test with interaction

Series	Nb	$\sigma^{1\%}_{c,90,mean}$ (MPa)	COV (%)	$\frac{\sigma^{1\%}_{c,90,mean}}{\sigma^{1\%}_{c,90,design(15)}}$
B-90-4	3	4.61	9	1.02
B-90-5	3	5.15	14	0.96
B-90-6	3	3.93	9	1.06

3.3.Analysis

The series results of B-90-3 and B-90-4 show a difference of 2% between these two configurations. Moreover, a difference of 2% exists between the analytic model and the experience. The two series are similar for the strength at 1% plastic deformation. A support of 300mm for this configuration may be replaced by two supports of 93.5mm, spaced out by 113mm. In the same perspective, the series B-90-6 is tested with the third support. A difference of 6% exists between the analytic model and the experimental test. However, none of the series authorises the interaction between the supports. The series B-90-5 is performed with an interaction of 50mm between the two supports. The result shows a difference of 4% between the analytic model and the experimental test.

4. Spreading effect in compression parallel to the grain

4.1.Materials and methods

In order to compare the experimental tests with the standards, the experimental tests in compression parallel to the grain are performed according to the configuration A and B, noted A-0 and B-0 respectively. It allows to quantify the spreading effect in the same way as the compression tests perpendicular to the grain. The study conditions are similar to those applied in the compression tests perpendicular to the grain.

4.2.Results

Due to the behaviour parallel to the grain of timber, the criterion used is a fragile criterion. It consists in taking the maximal reaction because it takes place before the reading of reaction at 1% plastic deformation. The geometric data of the sample and the results are synthesized in Table 3.

Table 3: Compression tests parallel to the grain

Series	b (mm)	h_t (mm)	L (mm)	ℓ (mm)	Nb	$\sigma^{1\%}_{c,90,mean}$ (MPa)	COV (%)	$\frac{\sigma^{1\%}_{c,90,mean}}{f_{c,90(CaseA)}}$
A-0-1	100	174	50	50	8	36.79	10	/
B-0-1	100	174	245	50	5	46.95	6	1.28

The results show an increase of 28% between the uniform compression test and the compression test with discrete support. Because of this, a spreading effect exists for compression parallel to the grain, non-quantified in the current standards.

4.3.Analysis

The analytic model proposed previously is confronted with the compression results parallel to the grain with discrete support. By means of the measuring device of displacement field, the plastic height for these tests is deducted. It represents the total height, as you see in Fig. 9. The height factor k_{sh} takes the value of 1 for the compression parallel to the grain.

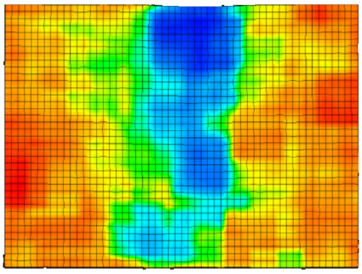

Fig. 9: Displacement fields

Integrating the modification of height factor of equation (12) and replacing the compression strength perpendicular to the grain $f_{c,90,mean}$ by the compressive strength parallel to the grain $f_{c,0,mean}$, the equation (16) may be written. A difference of 2% exists between the design code and the experimental test without cracking.

$$\frac{F_{c,0,mean}}{b \cdot \ell_{ef}} \leq f_{c,0,mean} \; with \; \ell_{ef} = \ell + \min\begin{cases} \ell_{dif} \\ \ell_{le} \\ \ell_{li}/2 \end{cases} + \min\begin{cases} \ell_{dif} \\ \ell_{re} \\ \ell_{ri}/2 \end{cases} \quad with \quad l_{dif} = \frac{f_{v,mean}}{f_{c,0,mean}} \cdot k_{sh} \cdot h_t \cdot \frac{2}{3} \cdot k_{sb} \cdot k_{sc} \tag{16}$$

5. Conclusion

An analytic model of predicting the support bearing capacity solicited in compression perpendicular to the grain is proposed. It integrates the effective length calculation by associating the compression effect and the shear effect. This latter is affected by geometric factors and support conditions. Furthermore, it integrates the interaction possibility between the supports. By means of the compression tests parallel to the grain, a spreading effect is observed. It is quantified by the modification of analytic model proposed for the compression perpendicular to the grain. A complementary campaign of compression tests at given angle to the grain has to be performed in order to estimate the spreading effect for different angles.

Concerning the first problematic of the large support lengths, the model proposed improves lightly the understanding of large support lengths. In order to overcome this weakness of wood, the support reinforcement appears to be the most appropriate solution to ameliorate the supports. Today, two solutions are investigated for the support reinforcement. They consist in shear reinforcing and compression reinforcing.

Finally, a finite element model is developed in order to better understand the spreading phenomenon.

Acknowledgement

Our gratefulness goes to the attention of technician of ENSTIB of University of Lorraine (France) for their collaboration in the realization of tests. We also thank the CODIFAB for funding tests and meeting.

References

[1] EN 14080, : Timber structures - Glued laminated timber and glued solid timber - Requirements. 2013.

[2] EN 408, : Structural timber and glued laminated timber - Determination of some physical and mechanical properties. 2012.

[3] EN 1995-1-1-A1, : EC5 - Eurocode - Design of timber structures - Part 1-1: General - Common rules and rules for buildings. 2008.

[4] H. J. Blass and R. Görlacher, “Compression perpendicular to the grain,” in WCTE, Helsinki, Finland, 2004, pp. 14–17.

[5] Riberholt, “Compression perpendicular to the grain of wood,” COWI-report 42239-1, 2000.

[6] M. Mähr, “Querdruckarmierung mit selbstbohrenden Schrauben,” Fachhochschule Liechtenstein, Vaduz, 2002.

[7] M. Augustin, A. Ruli, R. Brandner, and G. Schickhofer, “Behavior of glulam in compression perpendicular to grain in different strength grades and load configurations,” in CIB-W18, Florence, Italy, 2006, pp. Paper 39–12–6.

[8] K. Nilsson, “Skruvarmering som förstärkning i trä vid belastning vinkelrätt fiberriktningen,” Lunds Tekniska Högskola, Lund, Rapport TVBK- 5112, 2002.

[9] M. Reichegger, “Compressione ortogonale alle fibre negli elementi strutturali lignei secondo le nuove proposte di normative,” Universitá degli Studi di Trento, Trento Italy, 2004.

[10] D. Ed and F. Hasselqvist, “Timber compression strength perpendicular to the grain,” Lund Institute of Technology, 2011.

[11] L. Bléron, L. Cabaton, and E. Sauvignet, “Compression perpendiculaire aux fibres Essais mécaniques - Modélisation,” in CFM, Bordeaux, France, 2009.

[12] B. Madsen, Structural behavior of timber. 1992.

[13] T. A. C. M. Van der Put, “Derivation of the bearing strength perpendicular to the grain of locally loaded timber blocks,” Delft Wood Sci. Found., vol. 66, no. 6, pp. 409–417, 2008.

[14] Règles CB71, : Règle de calcul et de conception des charpentes en bois. 1975.

[15] R. Lefadag, V. Calvi, and C. Eglin, “Allianz Riviera ou l’alliance du bois et du métal pour undéfi géométrique et strucutrel,” presented at the 3ème Forum International Bois Construction, Beaune, 2013.

[16] DIN 1052, Entwurf, Berechnung und Bemessung von Holzbauwerken – Allgemeine Bemessungsregeln und Bemessungsregeln für den Hochbau. 2008.

[17] EN 1995-1-1, : EC5 - Eurocode - Design of timber structures - Part 1-1: General - Common rules and rules for buildings. 2005.

[18] D. Lathuilliere, J. B. Bocquet, L. Bléron, and F. Dubois, “Study of spreading under a compressive stress in glued laminated timber,” in COST Action FP1004, Prague, Czech Republic, 2014, pp. 160–167.

INTER

International Network on Timber Engineering Research

DESIGN OF CLT BEAMS WITH RECTANGULAR HOLES OR NOTCHES

M Flaig

Karlsruher Institut für Technologie

Holzbau und Baukonstruktionen

GERMANY

Presented by M Flaig

I Smith asked how different would the results be compared to stress analysis based on isotropic material. M Flaig responded that the stress concentration factor depends on the ratio of the stiffness so isotropic solution would have errors.

A Buchanan stated that the work of M Fragiacomo on LVL with cross band should be referenced. He asked suppose the beams were made with plywood, would results apply to CLT made with thinner layers. M Flaig responded that no because the shear stress distribution would be different.

BJ Yeh received clarification of the definition of the cross area, size of the hole and side of the CLT. BJ Yeh and M Flaig discussed that the glue space between the board size depends on the width of the laminate.

R Jockwer stated that in slide 17 initial cracking of the notched beam cannot be avoided. M Flaig responded that there is an unglued gap so the vertical bending failure was secondary failure.

E Serrano asked about the local effect in terms of relationship between the corner and the gap in relation to the use of the model and design. M Flaig responded that the model can only take into consideration of the full laminate. There were some tested beams and model of beams with different corners and gaps.

P Quenneville asked how reliable is the model if the torsional contribution is ignored since one cannot control the gap locations. M Flaig responded that this difference is less important with deeper beam relative to notch size. P Quenneville asked what the contribution of the torsional component is. M Flaig responded 100% because the beam would not work without torsional resistance. P Quenneville asked where the size of the crossing area is used. M Flaig responded only 150 mm assuming smaller width.

S. Svensson asked if rolling shear stress was available. M Flaig responded yes near the surface of the beam. There was discussion that the k factor does not depend on the shape of the corner. I Smith added that dry shrinkage will lead to cracks therefore rounded corner should be ignored.

M Fragiacomo asked about edge glue situation. H Blass responded that edge gluing should be ignored and one may assume 150 mm laminar width.

Design of CLT Beams with Rectangular Holes or Notches

M. Flaig
Holzbau und Baukonstruktionen
Karlsruhe Institute of Technology, Germany

Keywords: cross laminated timber, beams, holes, notches, shear design, stress concentrations

1 Objectives and Scope

Beams with holes or notches are commonly used in modern timber structures. The areas around corners of holes and notches are subject to high shear stresses and tensile stresses perpendicular to the grain which severly decrease the load carrying capacity. In glulam beams the areas near holes and notches therefore usually need to be strengthened by means of screws or wood based panels. CLT beams with holes and notches, in contrast, do not need extra reinforcements since tensile forces perpendicular to the beam axis can be transferred by transversal layers that are included in the material. The work presented in this paper is intended to develop design rules for CLT members with holes and notches which at present do not exist in standards and approvals.

In CLT beams loaded in plane direction the crossing areas between longitudinal and transversal layers are subjected to torsional shear stresses and to shear stresses in direction of the beam axis which both result from transverse forces within the beam. In crossing areas near holes and notches both stress components are increased and tensile forces perpendicular to the beam axis cause additional shear stresses in transversal direction.

The design of CLT beams with holes and notches therefore requires *i)* suitable methods to determine the shear stress components in the crossing areas near the corners of holes and notches and *ii)* a failure criterion that takes into account the interaction of simoultaneously occurring shear stress components.

In the first part of the presented work shear stresses in a large variety of CLT beams with holes and notches were determined by means of FE-calculations and the calculated values were used to derive stress concentration factors for a simplified design. The second part part of the work comprises tests with single crossing areas and bending tests with CLT beams with holes and notches. The test series with single crossing areas were designed to verify the failure criterions given in Eq. 1 that were derived from bending tests with prismatic CLT beams by Flaig and Blaß (2013) and take into account the linear interaction of parallel shear stress components at the edges of a crossing area.

$$\frac{\tau_{\text{tor}}}{f_{\text{v,tor}}}+\frac{\tau_{\text{yx}}}{f_{\text{R}}}\leq 1 \qquad \text{and} \qquad \frac{\tau_{\text{tor}}}{f_{\text{v,tor}}}+\frac{\tau_{\text{yz}}}{f_{\text{R}}}\leq 1 \qquad \text{Eq. 1}$$

The main objectives of the bending tests were to determine the load carrying capacity of CLT beams with holes and notches and to investigate the structural behaviour and the failure modes. But the tests were also designed to check the approaches used for the calculation of internal stresses, especially the stress concentration factors obtained from FE calculations.

2 Calculation of stresses in CLT beams with holes and notches

2.1 Finite Element Model

In the FE-model used in this work longitudinal and transversal lamellae of CLT beams are represented by Timoshenko beam elements that are connected to each other via spring elements. The bending and the shear stiffness of the lamellae are represented by the beam elements while the stiffness of the glued connections between crosswise oriented lamellae is assigned to the spring elements. The modulus of elasticity and the shear modulus were assumed with 11,000 N/mm² and 690 N/mm², respectively, and the spring constants were calculated from the expressions given in Eq. 2 with a slip modulus $K = 7.5$ N/mm³ that was derived from the tests described in section 3.1.

$$K_{\mathrm{x}} = K_{\mathrm{y}} = K \cdot A_{\mathrm{CA}} \quad \text{and} \quad K_{\varphi} = K \cdot I_{\mathrm{p,CA}} \qquad \text{Eq. 2}$$

In contrast to the actual situation in CLT where longitudinal and transversal lamellae are continuously connected to each other the beam elements in the FE-model only have punctiform connections. The resulting free length between the nodes allows for additional bending and shear deformation in the beam elements which does not exist in reality. Consequently, some stiffness properties of transversal beam elements had to be modified to be more consistent with the real conditions:

i.) a very high bending stiffness was assigned to beam elements representing transversal lamellae

ii.) beam elements representing longitudinal and transversal lamellae were assigned the shear stiffness that was calculated with the gross thickness of the simulated CLT beams

Figure 1 shows the basic structure of the model and examples of the two beam types.

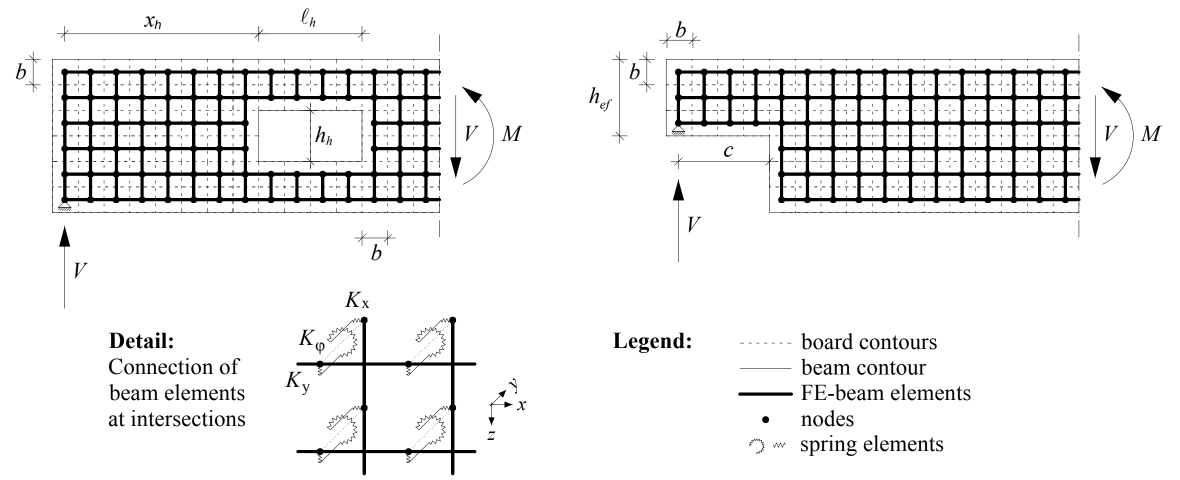

Figure 1: FE-model for the calculation of stresses in CLT beams with holes and notches

2.2 Stress Concentration Factors for CLT Beams with Holes

To determine stress concentration factors for CLT beams with holes the shear stresses in the crossing areas in the hole corners were calculated for beams and holes with various dimensions by means of the FE-model described in the previous section. In all simulated CLT beams the width of longitudinal and transversal lamellae was set to 150 mm and ratios of $t_{\mathrm{net,cross}}/t_{\mathrm{gross}} = 0.20$ and $t_{\mathrm{gross}}/n_{\mathrm{CA}} = 50$ mm were consistantly used. The height of the simulated beams varied between 600 and 1800 mm in steps of 150 mm corresponding to a number m of longitudinal lamellae in direction of the beam height between 4 and 12. Due to the discretisation in the model, the length and the width of the holes were also chosen as integer multiples of the board width b so that in all the simulated CLT beams the edges of holes coincided with the edges of lamellae (cf. Figure 1). The dimensions of the holes varied within the ranges of $b \leq \ell_h \leq h$ (length of the hole), $b \leq h_h \leq 0.5 \cdot h$ (height of the hole) and $1 \leq \ell_h / h_h \leq 4$. For all simulated beams the ratios $k_{h,1}$ and $k_{h,2}$ between the maximum shear stress components at the hole and the shear stress components in an undisturbed beam of equal dimensions were calculated. To determine the functional relationship between the peak stresses and the beam geometry regression analyses were performed from which Eq. 3 and Eq. 4 were derived.

$$k_{h1} = \frac{\tau_{tor,h}}{\tau_{tor}} = 1.81 \cdot \left(\frac{\ell_h}{h} \cdot \frac{h_h}{h - h_h} \right) + 1.14 \qquad \text{Eq. 3}$$

$$k_{h2} = \frac{\tau_{yx,h}}{\tau_{yx}} = 0.103 \cdot \left(\frac{h_h \cdot \ell_h}{h^2} \cdot m^2 \right) + 1.27 \qquad \text{Eq. 4}$$

The regression equations describe the peak stresses with adequate precision as can be seen in the diagrams on the left side of Figure 2 where the stress concentration factors $k_{h,1}$ and $k_{h,2}$ obtained from FE calculations are plotted against the predicted values according Eq. 3 and Eq. 4. The diagrams on the right side show the stress concentrations factors calculated according the regression equations, Eq. 3 and Eq. 4, in dependence of the dimensions of the hole.

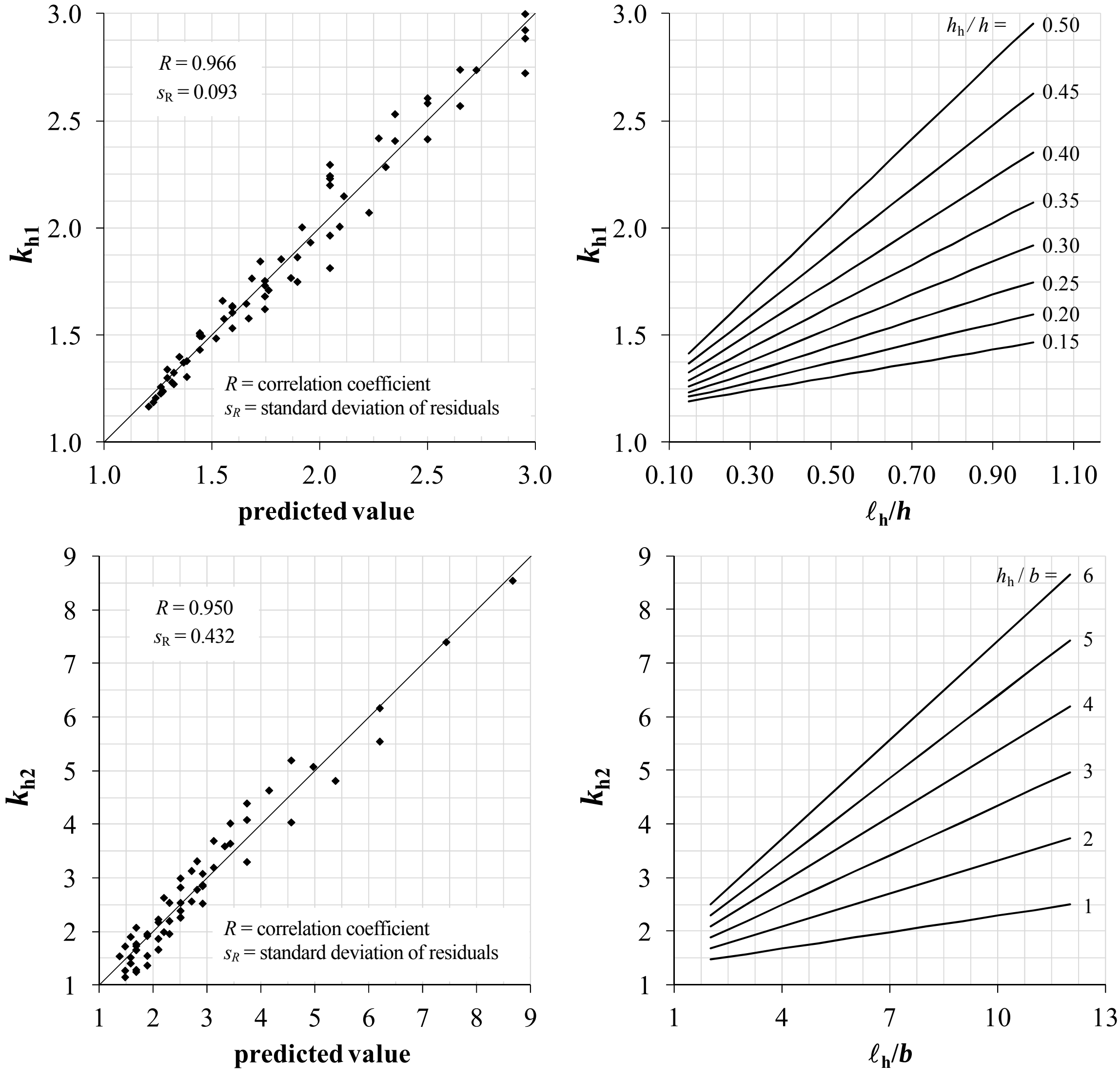

Figure 2: stress concentration factors for CLT beams with holes

The stress concentration factors depend on the ratio between the stiffness of the crossing areas and the stiffness of the lamellae which both are functions of different powers of the board width *b*. The above equations for the calculation of stress concentration factors are therefore only valid for CLT beams consisting of lamellae with a width of 150 mm and should be adapted for board widths b differing from 150 mm. If the board width is within the range between 100 and 200 mm the multiplication with the factor k_b given in Eq. 5 provides good approximations for both factors k_{h1} and k_{h2}.

$$k_b = \left(\frac{b}{150}\right)^{1/3} \qquad \text{Eq. 5}$$

2.3 Stress Concentration Factors for Notched CLT Beams

For notched CLT beams also stress concentration factors were determined by means of the FE-model described in section 2.1 using the same assumptions as for CLT beams with holes, i.e. the width of lamellae was set to 150 mm and ratios of $t_{net,cross}/t_{gross}$ = 0.20 and t_{gross}/n_{CA} = 50 mm were used, consistantly. The height of the simulated beams with notches was varied between 300 and 1200 mm. The height of the notch and the distance between the support and the corner of the notch varied between the width b of one lamella and half the beam height ($b \leq (h\text{-}h_{ef}) \leq 0.5{\cdot}h;\ b \leq c \leq 0.5{\cdot}h$). The ratio between the distance c and the reduced beam height h_{ef} was limited to values equal to or less than one ($c/h_{ef} \leq 1$). As for the holes the dimensions of the notches were chosen as integer multiples of the board width b so that the outlines of the notches coincided with the edges of lamellae (cf. Figure 1). In all simulated beams the shear stress component parallel to the beam axis in the crossing areas at the corner of the notch was smaller than the maximum shear stress component perpendicular to the beam axis. The determination of stress concentration factors for the shear stress component parallel to the beam axis was therefore omitted. To determine stress concentration factors k_n for the torsional shear stress component the ratio between the maximum stress in the corner of the notch and the corresponding value in a beam without notch was calculated for each simulated beam and a functional relationship between the peak stresses and the beam geometry was determined by means of a regression analysis.

$$k_n = 0.877 \cdot \left(\frac{h_{ef}}{h}\right)^{k_c} \quad \text{with } k_c = -1.81 \cdot \left(\frac{c}{h}\right)^{0.479} \qquad \text{Eq. 6}$$

In Figure 3 on the left side the stress concentration factors k_n obtained from the FE calculations are plotted against the values predicted by the regression equation. In the diagram on the right side the values calculated according Eq. 6 are given in dependence of the dimensions of the notch.

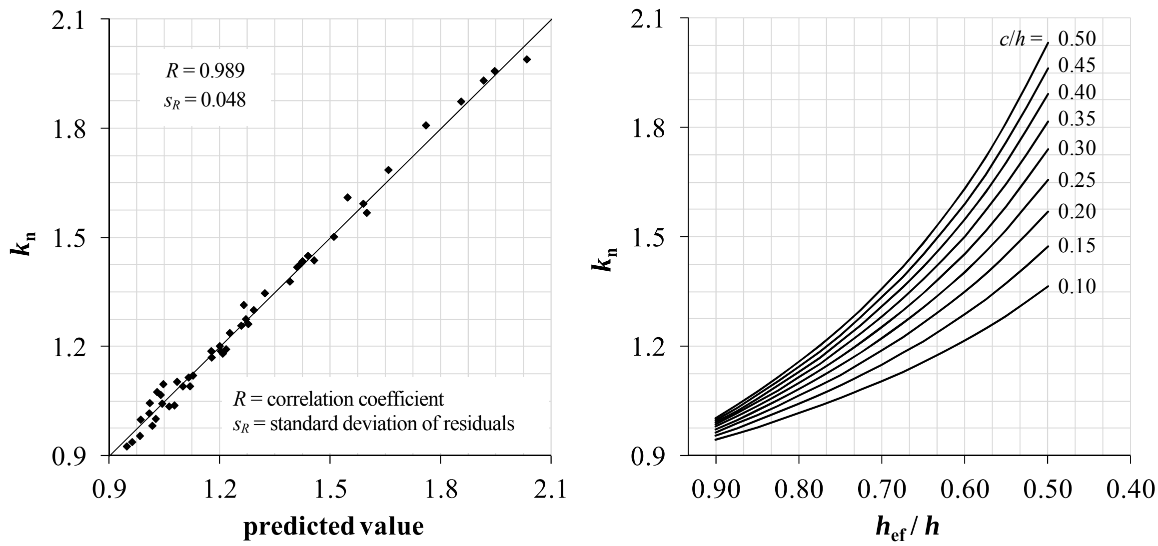

Figure 3: stress concentration factor for notched CLT beams

Due to the assumptions made in the FE model Eq. 6 for the calculation of the stress concentration factor k_n provides accurate results only for beams consisting of lamellae with a width of 150 mm. For beams with smaller or wider lamellae the factor k_n should be adjusted by multiplication with the factor k_b given in Eq. 5.

3 Experimental work

3.1 Single Crossing Areas under combined torsional and unidirectional shear stresses

3.1.1 Materials and Methods

Shear tests with single crossing areas were performed to verify the failure criterion given in Eq. 1. In four different test series the crossing areas of cross shaped specimens were subjected either to a shear force or to a torsional moment or to a combination of both loads. To make sure that the specimens of the different test series had equivalent material properties four sections were cut from one board at a time and then assembled in such a way that always four specimens, one for each series, consisted of sections of the same two boards. For testing, the specimens were fixed into a steel frame that consisted of two crosswise arranged bars as illustrated in Figure 4. The testing apparatus allowed applying arbitrary combinations of torsional and unidirectional shear stresses to the crossing areas by means of two independently controlled loads. Unidirectional rolling shear stresses were induced by a centrically applied vertical force F_v whereas torsional shear stresses were generated by an eccentric load F_{tor} acting at one end of the horizontal bar.

In the first test series (series V100) only a vertical shear force F_v was applied to determine the rolling shear strength of crossing areas as a reference value for the combined loading. In the second and the third series (series V50 and V35) load levels of about 50% and 35% of the mean value of the ultimate load determined in the first series were applied in combined loading. During the testing at first the shear force F_v was increased up to the defined level and kept constant. Only then the second load generating a torsional moment was applied and increased until failure. In the fourth series (series V0) the shear force F_v was set to zero and only a torsional moment was applied.

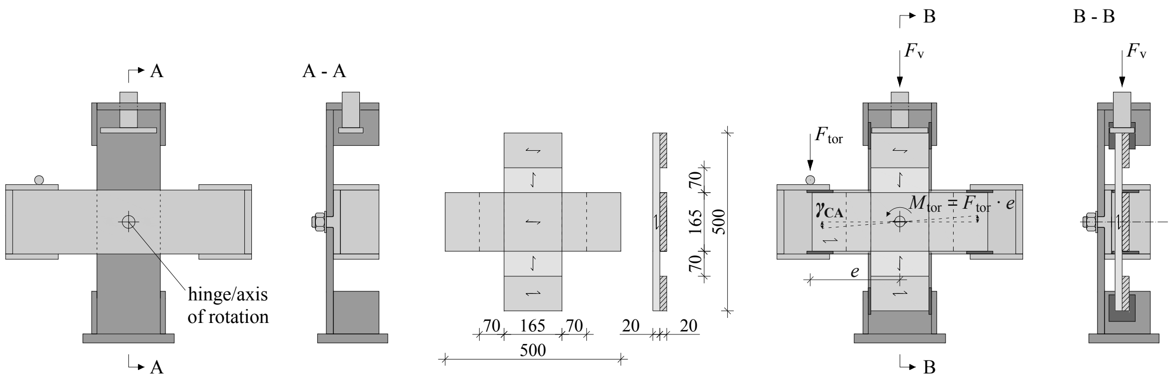

Figure 4: Testing apparatus, test specimens and test setup

3.1.2 Results

From the maximum values of the respective loads the rolling shear stresses and the torsional shear stresses were calculated. The mean values of shear stresses $\tau_{R,mean}$ and $\tau_{tor,mean}$, and the coefficients of variation are given in Table 1. In test series V100 and V0 where only one of the two loads, either shear force or torsional moment, had been applied, the evaluated stresses are the rolling shear strength or the torsional shear strength of the crossing areas, respectively. The mean values of the shear strength evaluated from these two test series were used to calculate the stress levels for all series. The calculated ratios between the actual shear stresses and the mean values evaluated from Series V100 and V0 are plotted in the diagram shown in Figure 5. Due to the linear relationship which is clearly visible the diagram the total utilisation rate η_{tot} for the test series V50 and V35 could be calculated as the sum of the two stress levels.

$$\eta_{\text{tot}} = \frac{\tau_{\text{tor}}}{f_{\text{v,tor,mean}}} + \frac{\tau_{\text{R}}}{f_{\text{R,mean}}} \qquad \text{Eq. 7}$$

In Table 1 the shear strength properties of the two series with combined loading are given that were evaluated by multiplying the total utilisation rate with the mean values of shear strength obtained from series V100 and V0.

$$f_{\text{R,i}} = \eta_{\text{tot}} \cdot f_{\text{R,V100,mean}} \quad \text{and} \quad f_{\text{v,tor,i}} = \eta_{\text{tot}} \cdot f_{\text{v,tor,V0,mean}} \qquad \text{Eq. 8}$$

Table 1: Mean values of shear stresses and shear strengths evaluated from tests with single crossing areas

Series		τ_R *in N/mm²*	f_R *in N/mm²*	τ_{tor} *in N/mm²*	$f_{v,tor}$ *in N/mm²*
V100	*MEAN*		***1.26***	-	
	COV		*0.158*	-	
V50	*MEAN*	*0.66*	*1.29*	*1,51*	*3,07*
	COV	*0.013*	*0.17*	*0,34*	*0,17*
V35	*MEAN*	*0.46*	*1.28*	*1,94*	*3,03*
	COV	*0.002*	*0.14*	*0,22*	*0,14*
V0	*MEAN*	-			***2.97***
	COV	-			*0.09*

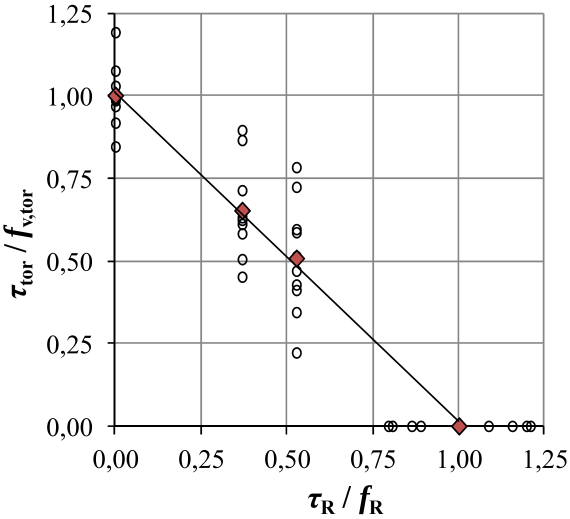

Figure 5: interaction of shear stresses in crossing areas

3.2 Beams with Holes

3.2.1 Materials and Methods

Ten CLT beams with holes were tested destructively to determine the load carrying capacity and to verify the stress concentration factors obtained from FE calculations. All specimens had the same outer dimensions and the same layup that consisted of four longitudinal and two transversal layers. The beams were divided in two series with holes of different height. The smaller holes had a height of 0.4 times the beam height which is the maximum allowable height of holes in glulam beams according to the German National Annex to EC5. The larger height was set to 0.5 times the beam height. In both series the length of the holes was equal to the beam height. In Table 2 the dimensions and the layup of the tested beams are quoted.

Table 2: Dimensions and layup of tested CLT beams with holes

Series	*Number of specimens*	*dimensions in mm* h	t_{gross}	L	h_h	$h_{ra/rb}$	t_{long} / t_{cross}	*layup*
H40	*5*	*600*	*150*	*6300*	*240*	*180*	*30/15*	*l-c-ll-c-l*
H50	*5*	*600*	*150*	*6300*	*300*	*150*	*30/15*	*l-c-ll-c-l*

All specimens were produced from lamellae of strength class T14 according to EN 14080 with a width of 150 mm. The mean density was 459 kg/m^3 in series *H600-0.4* and 456 kg/m^3 in series *H600-0.5* at an average moisture content of 10,4% and 11.0%, respectively. The load carrying capacity of the beams was determined in four point bending tests with a span of 10 times the beam height. The distance between the load application points was reduced to two times the beam height to avoid premature bending failure. The two holes were positioned in the middle between the loads and the supports and in the middle of the beam height. In Figure 6 the test setup and the beam geometry are ilustrated.

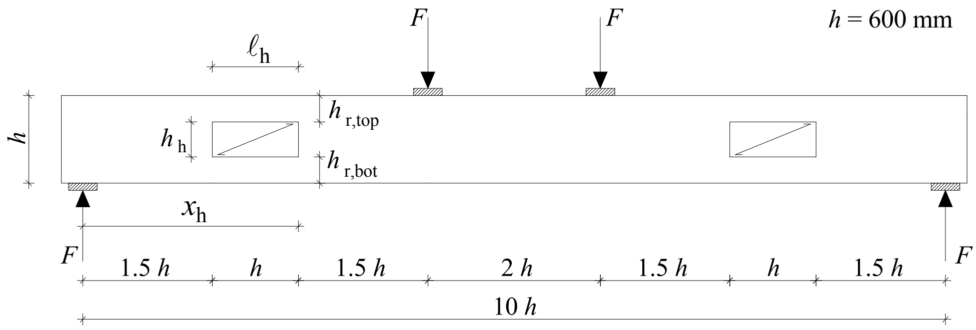

Figure 6: Test setup for beams with holes

3.2.2 Results

Two different types of failure were observed in both test series: Four of five specimens in each series failed due to shear stresses in the crossing areas near the corners of the holes. In the remaining two specimens failure was caused by bending stresses in the reduced cross section at the holes. In Figure 7 examples of the two observed types of failure are shown.

Figure 7: Shear failure in the crossing areas in specimen H50-4 (left), bending failure in the residual cross section below the hole in specimen H40-1 (right)

From the ultimate loads the bending stresses in longitudinal lamellae were evaluated in the middle of the span (Eq. 9) and at the edges of the holes farther from the supports (Eq. 10) where the additional bending moment resulting from the excentricity of shear forces was approximated as $M_V = V/2 \cdot \ell_h / 2$.

$$\sigma_{m,net} = \frac{24 \cdot F_{max}}{t_{net,long} \cdot h} \qquad \text{Eq. 9}$$

$$\sigma_{m,net,h} = \frac{15 \cdot F_{max} \cdot h^2}{t_{net,long} \cdot (h^3 - h_h^3)} + \frac{3 \cdot F_{max} \cdot h}{2 \cdot t_{net,long} \cdot h_r^2} \quad \text{with } h_r = \min\left\{h_{r,top}, h_{r,bot}\right\} \qquad \text{Eq. 10}$$

The tensile forces acting perpendicular to the beam axis at the vertical edges of the holes were calculated according Eq. 11 which is given in the German National Annex to EC5 for glulam beams with holes. A comparison with the results of FE calculations showed that Eq. 11 yields tensile forces that are slightly larger but still in good agreement with the values obtained from the FE model.

$$F_{t,90} = F_V + F_M = F_{max} \cdot \left[\left(\frac{3 \cdot h_h}{4 \cdot h} - \frac{h_h^3}{4 \cdot h^3}\right) + \left(\frac{0{,}008 \cdot x_h}{h_r}\right)\right]; \; x_h \text{ cf. Figure 6} \qquad \text{Eq. 11}$$

Tensile stresses in transversal lamellae at the edges of the holes were calculated using an effective width a_r which was assumed as the smaller value of the actual width of transversal lamellae and the maximum value given in the German National Annex to EC5 for reinforced holes in glulam beams with holes. The nonuniform distribution of tensile stresses within the effective width was taken into account by a factor k_k = 2,0 that was also adopted from the German National Annex to EC5.

$$\sigma_{t,0,cross} = k_k \cdot \frac{F_{t,90}}{a_r \cdot t_{net,cross}}; \text{ with } a_r = \min\{b_{cross}; 0.3 \cdot (h + h_h)\} \qquad \text{Eq. 12}$$

In the evaluation of shear stresses three different failure modes were taken into account, i.e. shear stresses in the gross cross section (FM 1), shear stresses in the net cross section (FM 2) and shear stresses in the crossing areas (FM 3). A detailed description of the different failure modes and the calculation of shear stresses in prismatic CLT beams can be found in Flaig and Blaß (2013). In the tested CLT beams with holes the maximum values of shear stresses in the lamellae and in the crossing areas were calculated according to the equations given by Flaig and Blaß using either the residual cross section (FM 1) or the stress concentration factors k_{h1} and k_{h2} (FM 2 and FM 3) given in section 2.2. The shear stress component $\tau_{yz,h}$ perpendicular to the beam axis was calculated according Eq. 17 assuming a uniform distribution of shear stresses in the crossing areas within the effective length a_r (cf. Eq. 12) and the residual height h_r. In Table 3 the ultimate loads and the evaluated stresses are given.

$$\text{FM 1:} \quad \tau_{xz,gross,h} = \frac{1.5 \cdot F_{max}}{(h - h_h) \cdot t_{gross}} \qquad \text{Eq. 13}$$

$$\text{FM 2:} \quad \tau_{xz,net,h} = k_{h2} \cdot \frac{1.5 \cdot F_{max}}{h \cdot t_{net}} \qquad \text{Eq. 14}$$

$$\text{FM 3:} \quad \tau_{tor,h} = k_{h1} \cdot \frac{3 \cdot F_{max}}{b^2 \cdot n_{CA}} \cdot \left(\frac{1}{m} - \frac{1}{m^3}\right) \text{ and} \qquad \text{Eq. 15}$$

$$\tau_{yx,h} = k_{h2} \cdot \frac{6 \cdot F_{max}}{b^2 \cdot n_{CA}} \cdot \left(\frac{1}{m^2} - \frac{1}{m^3}\right) \text{ and} \qquad \text{Eq. 16}$$

$$\tau_{yz,h} = \frac{F_{t,90}}{n_{CA} \cdot a_r \cdot h_r} \qquad \text{where} \qquad h_r = \min\begin{cases} h_{r,top} \\ h_{r,bot} \end{cases} \qquad \text{Eq. 17}$$

Table 3: Ultimate loads and evaluated stresses for tested CLT beams with holes (failure was caused by <u>underlined stresses</u>)

series	*no.*	F_{max} *in kN*	$\sigma_{m,net}$ *in N/mm²*	$\sigma_{m,net,h}$ *in N/mm²*	$\sigma_{t,0,cross}$ *in N/mm²*	$\tau_{xz,gross,h}$ *in N/mm²*	$\tau_{xz,net,h}$ *in N/mm²*	$\tau_{tor,h}$ *in N/mm²*	$\tau_{yx,h}$ *in N/mm²*	$\tau_{yz,h}$ *in N/mm²*
	1	*93.8*	*31.3*	*<u>42.6</u>*	*14.6*	*2.61*	*15.9*	*1.52*	*0.76*	*0.30*
	2	*111*	*37.1*	*50.5*	*17.3*	*3.09*	*18.9*	*<u>1.81</u>*	*<u>0.91</u>*	*0.36*
H40	*3*	*112*	*37.3*	*50.8*	*17.4*	*3.11*	*19.0*	*<u>1.82</u>*	*<u>0.91</u>*	*0.36*
	4	*117*	*39.0*	*53.1*	*18.2*	*3.25*	*19.8*	*<u>1.90</u>*	*<u>0.95</u>*	*0.38*
	5	*115*	*38.4*	*52.4*	*18.0*	*3.20*	*19.5*	*<u>1.87</u>*	*<u>0.94</u>*	*0.37*
	1	*79.1*	*26.4*	*45.2*	*14.9*	*2.64*	*15.8*	*<u>1.58</u>*	*<u>0.75</u>*	*0.37*
	2	*93.4*	*31.1*	*53.4*	*17.6*	*3.11*	*18.6*	*<u>1.86</u>*	*<u>0.89</u>*	*0.44*
H50	*3*	*83.8*	*27.9*	*47.9*	*15.8*	*2.79*	*16.7*	*<u>1.67</u>*	*<u>0.80</u>*	*0.39*
	4	*95.0*	*31.7*	*54.3*	*17.9*	*3.17*	*18.9*	*<u>1.89</u>*	*<u>0.90</u>*	*0.45*
	5	*76.0*	*25.3*	*<u>43.4</u>*	*14.3*	*2.53*	*15.1*	*1.51*	*0.72*	*0.36*

3.3 Notched CLT Beams

3.3.1 Materials and Methods

To determine the load carrying capacity of CLT beams with notches five specimens with equal were tested. The tested beams had a height of 600 mm and the layup consisted of four longitudinal and two transversal layers with a total thickness of 200 mm. The reduced height h_{ef} at the notched supports was half the beam height and the distance between the centre of the support and the corner of the notch was 300 mm. In Table 4 the dimensions and the layup of the tested beams are given in detail.

Table 4: Dimensions and layup of tested CLT beams with notches

No. of specimens	*h*	t_{gross}	*L*	h_{ef}	*c*	t_{long} / t_{cross}	*layup*
	dimensions in mm						
5	600	200	4800	300	300	40/20	l-c-ll-c-l

Like the tested beams with holes also the notched beams were produced from lamellae of strength class T14 with a width of 150 mm. In longitudinal lamellae the mean density was 425 kg/m^3 at an average moisture content of 12,0%. The beams had notched supports at both ends and were tested in four point bending tests with a span of 7.75 times the beam height. In Figure 8 the test setup used for the notched beams is illustrated.

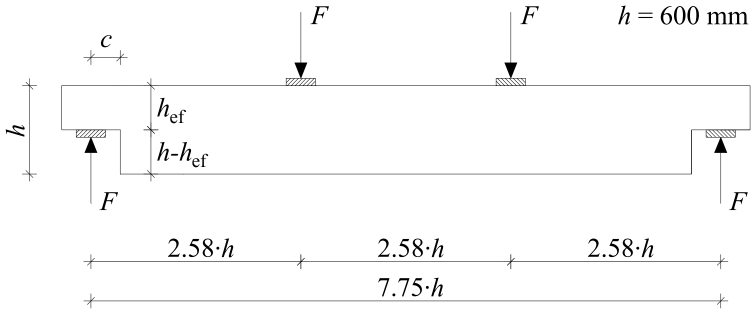

Figure 8: Test setup for notched beams

3.3.2 Results

In spite of the relatively low percentage of transversal layers of only 20% and the resulting high shear stresses in the net cross section of transversal layers (FM 2) failure was caused by shear stresses in the crossing areas in all specimens. Figure 9 shows an example of the failure mode observed.

Figure 9: Shear failure in the crossing areas next to the corner of the notch

From the ultimate loads the bending stresses in the middle of the span and in the reduced cross section at the notched support were calculated according Eq. 18 and Eq. 19. The tensile force perpendicular to the beam axis at the notch was calculated from Eq. 20 that is given in the

German National Annex to Eurocode 5 for notched glulam beams. Like the respective equation for beams with holes Eq. 20 yields tensile forces that are slightly larger than the values obtained from the FE calculations. The maximum tensile stresses in the transversal lamellae next to the notch were calculated according Eq. 21. The factor k_k in Eq. 21 takes into account the nonuniform stress distribution within the effective length ℓ_r. A value of $k_k = 2.0$ and the limitation of the effective length $\ell_r \geq 0.5\cdot(h-h_{ef})$ were adopted from the design rules given in the German National Annex to Eurocode 5 for notched glulam beams. The results of FE calculations showed in addition that in CLT beams the complete tensile force $F_{t,90}$ acts in the transversal lamellae directly next to the notch so that in large CLT beams the effective length should be limited to the width of one transversal lamella.

$$\sigma_{m,net} = \frac{15 \cdot F_{max}}{t_{net,long} \cdot h} \qquad \text{Eq. 18}$$

$$\sigma_{m,net,A} = \frac{6 \cdot c \cdot F_{max}}{t_{net,long} \cdot h_e^2} \qquad \text{Eq. 19}$$

$$F_{t,90} = 1.3 \cdot F_{max} \cdot \left[3 \cdot \left(1 - \frac{h_{ef}}{h}\right)^2 - 2 \cdot \left(1 - \frac{h_{ef}}{h}\right)^3 \right] \qquad \text{Eq. 20}$$

$$\sigma_{t,0,cross} = k_k \cdot \frac{F_{t,90}}{\ell_r \cdot t_{net,cross}}; \quad \text{with} \quad \ell_r = \max\left\{0.5 \cdot (h - h_{ef}); b_{cross}\right\} \qquad \text{Eq. 21}$$

As for beams with holes the shear stresses related to the three failure modes were evaluated from the maximum shear force F_{max}. In FM1, that takes into account shear stresses in the gross cross section (i.e. shear stresses act within the total thickness of a beam), the maximum shear stress occurs in the beam section with reduced height. The actual shear stress in the gross cross section of the test specimen was calculated according Eq. 22. In notched beams the maximum shear stresses in the net cross section (FM 2) arise in the corner of the notch. In the tested CLT beams the shear stresses in the net cross section of transversal layers were calculated from Eq. 23 with the full beam height h and a factor k_n according Eq. 6 taking into account stress concentrations in the corner of the notch. The maximum values of shear stresses in the crossing areas at the notched supports were calculated according Eq. 24 and Eq. 25. In Eq. 24 the increase of the torsional shear stress component in crossing areas next to the notch is again taken into account by the factor k_n according Eq. 6. The shear stress component perpendicular to the beam axis is calculated from the tensile force $F_{t,90}$ given in Eq. 20 assuming a uniform stress distribution within the effective length ℓ_r and the residual height h_r.
The evaluation of shear stresses in the crossing areas acting parallel to the beam axis was omitted since FE calculations and tests showed that this component is not decisive for the design. In Table 5 the ultimate loads reached in the tests and the evaluated bending and shear stresses are summarized.

$$\text{FM1:} \quad \tau_{xz,gross,n} = \frac{1.5 \cdot F_{max}}{h_e \cdot t_{gross}} \qquad \text{Eq. 22}$$

$$\text{FM2:} \quad \tau_{xz,net,n} = k_n \cdot \frac{1.5 \cdot F_{max}}{h \cdot t_{net}} \qquad \text{Eq. 23}$$

$$\text{FM3:} \quad \tau_{tor,n} = k_n \cdot \frac{3 \cdot F_{max}}{b^2 \cdot n_{CA}} \cdot \left(\frac{1}{m} - \frac{1}{m^3}\right) \qquad \text{Eq. 24}$$

$$\tau_{yz,n} = \frac{F_{t,90}}{n_{CA} \cdot \ell_r \cdot h_n}; \quad \text{where} \quad h_n = \min\left\{h_{ef}; h - h_{ef}\right\} \qquad \text{Eq. 25}$$

Table 5: Ultimate loads and evaluated stresses for tested CLT beams with notches (failure was caused by underlined stresses)

series	*no.*	$F_{\max}$ *in kN*	$\sigma_{m,net}$ *in N/mm²*	$\sigma_{m,net,A}$ *in N/mm²*	$\sigma_{t,0,cross}$ *in N/mm²*	$\tau_{xz,gross,n}$ *in N/mm²*	$\tau_{xz,net,n}$ *in N/mm²*	$\tau_{\mathrm{tor,n}}$ *in N/mm²*	$\tau_{\mathrm{yz,n}}$ *in N/mm²*
N600	1	157	25.3	24.5	17.0	3.91	19.9	2.48	0.57
	2	162	26.2	25.4	17.6	4.06	20.6	2.57	0.59
	3	148	23.9	23.2	16.1	3.71	18.8	2.35	0.54
	4	148	23.9	23.2	16.1	3.71	18.8	2.35	0.54
	5	158	25.5	24.6	17.1	3.94	20.0	2.50	0.57

4 Summary and conclusions

In nearly all of the tested CLT beams with holes and notches failure was caused by shear stresses in the crossing areas which shows that an accurate calculation of these stresses as well as a basic understanding of the interaction of different stress components and the knowledge of strength properties of crossing areas are indispensable for a reliable and economic design.
The strength properties that were obtained from the described test series with single crossing areas are relatively low compared to the values determined in earlier studies but the ratio of the two shear strengths lies within the usual range of 2.25 to 2.5.

$$\frac{f_{\mathrm{v,tor,mean}}}{f_{\mathrm{R,mean}}} = \frac{2.97}{1.26} = 2.37 \qquad \text{Eq. 26}$$

The torsional shear strength and the rolling shear strength that were evaluated for the test series with notched beams and beams with holes using the ratio given in Eq. 26 are somewhat larger than those determined for single crossing areas but agree very well with the strength properties of crossing areas found in earlier studies (cf. Table 6).
Together with the failure criterion that was derived from the tests with single crossing areas the equations and the stress concentration factors used for the calculation of shear stresses in the crossing areas of CLT beams with holes and notches provide an adequate design method for CLT beams with holes and notches.
Another finding of the performed test series with CLT beams is that the shear strength in sections through the unglued joints between the lamellae of one direction which is needed for the verification of shear stresses in the net cross section of CLT members is significantly larger than previously assumed.

Table 6: Shear strength properties of crossing areas

Test series		$f_{\mathrm{v,tor,mean}}$ *in N/mm²*	$f_{\mathrm{R,mean}}$ *in N/mm²*
This work	*CLT Beams with Notches*	*3.78*	*1.59*
	CLT Beams with Holes	*3.54*	*1.49*
	Single crossing areas	*3.03*	*1.28*
Earlier work	*Blaß and Görlacher (2002)*	*3.59*	-
	Jöbstl (2004)	*3.46*	-
	Wallner (2004)	-	*1.51*
	Blaß and Flaig (2013)	-	*1.43*

5 Symbols

A_{CA}	crossing area
b	width of lamellae
c	distance between the corner of a notch and the centre of the support
F_{max}	ultimate load
$F_{t,90}$	tensile force acting perpendicular to the beam axis
f_R	rolling shear strength
$f_{v,tor}$	torsional shear strength of crossing areas of orthogonally bonded lamellae
h	beam height
h_n	smaller height above or below the corner of a notch
$h_{r,top/bot}$	residual height above or below a hole
h_h	hole height
h_{ef}	reduced height at notched support
$I_{p,CA}$	polar moment of inertia of a single crossing area
K	slip modulus of crossing areas in N/mm per mm²
k	factor
ℓ_h	length of hole
m	number of longitudinal lamellae within the beam height
n_{CA}	number of crossing areas within the beam thickness
t_{gross}	total thickness of a CLT beam
$t_{net,long}$	net thickness of longitudinal layers
t_{net}	smaller of the net thickness of longitudinal and the net thickness of transversal layers
η	stress level, utilisation rate
$\sigma_{t,0,cross}$	tensile stress in transversal layers
$\sigma_{m,net}$	bending stress in longitudinal layers
$\tau_{xz,gross}$	shear stress in the gross cross section
$\tau_{xz,net}$	shear stress in the net cross section
τ_{tor}	torsional shear stress in crossing areas
τ_{yx}	unidirectional shear stress acting parallel to the beam axis in crossing areas
τ_{yz}	unidirectional shear stress acting perpendicular to the beam axis in crossing areas

Indices

CA	crossing area
h	hole
n	notch
gross	related to the total thickness of a CLT beam
net	related to the net thickness; here: the sum of the thicknesses of transversal layers
long	related to longitudinal layers/lamellae
cross	related to transversal layers/lamellae

6 References

Aicher, S. (2012): “Glulam beams with internally and externally reinforced holes – tests, detailing and design“ In: Proceedings. CIB-W18 Meeting 44, Alghero, Italy, 2011, Paper 44-12-4.

Aicher, S.; Höfflin, L. (2010): “Glulam beams with holes reinforced by steel bars” In: Proceedings. CIB-W18 Meeting 42, Dübendorf, Switzerland, 2009, Paper 42-12-1.

Bejtka, I.: “Cross (CLT) and diagonal (DLT) laminated timber as innovative material for beam elements”. Karlsruher Berichte zum Ingenieurholzbau, Bd. 17, KIT Scientific Publishing, 2011

Bogensperger, T.; Moosbrugger, T.; Silly, G.: “Verification of CLT-plates under loads in plane”. In: Proceedings. 11th World Conference on Timber Engineering, Riva del Garda, Italy, 2010

Bogensperger, T.; Moosbrugger, T.; Schickhofer, G.: “New Test Configuration for CLT-Wall Elements under Shear Load”. In: Proceedings. CIB-W18 Meeting 40, Bled, Slovenia, 2007, Paper 40-12-3

Bosl, R.: “Zum Nachweis des Trag- und Verformungsverhaltens von Wandscheiben aus Brettsperrholz”. Dissertation, Universität der Bundeswehr, München, Germany, 2002

Flaig, M.; Blaß, H.J.: “Shear Strength and Shear Stiffness of CLT beams Loaded in Plane” In: Proceedings. CIB-W18 Meeting 46, Vancouver, Canada, 2013, Paper 46-12-3

Flaig, M.; Blaß, H.J.: “Bending Strength of Cross Laminated Timber Beams Loaded in Plane” In: Proceedings. World Conference on Timber Engineering (WCTE), Quebec, Canada, 2014

Flaig, M: „Biegeträger aus Brettsperrholz bei Beanspruchung in Plattenebene“. Dissertation, Karlsruher Berichte zum Ingenieurholzbau, Bd. 26, KIT Scientific Publishing, 2013

Jockwer, R.: “Structural behaviour of glued laminated timber beams with unreinforced and reinforced notches” Dissertation, ETH Zurich, Swizerland, 2014

Jöbstl, R.A.; Bogensperger, T.; Schickhofer, G.: “In-Plane Shear Strength of Cross Laminated Timber”. In: Proceedings. CIB-W18 Meeting 41, St. Andrews, Canada, 2008, Paper 41-12-3

Jöbstl, R.A.; Bogensperger, T.; Schickhofer, G.: “Mechanical Behaviour of Two Orthogonally Glued Boards”. In: Proceedings. 8th World Conference on Timber Engineering, Lahti, Finland, 2004

Moosbrugger, T.; Guggenberger, W.; Bogensperger, T.: “Cross Laminated Timber Wall Segments under homogeneous Shear — with and without Openings”. In: Proceedings. 9th World Conference on Timber Engineering, Portland, Oregon, USA, 2006

Schickhofer et al.: “BSPhandbuch - Holz-Massivbauweise in Brettsperrholz”. Technische Universität Graz, holz.bau forschungs gmbh, Karlsruher Institut für Technologie, Technische Universität München, Eidgenössische Technische Hochschule Zürich, 2009

Traetta, G., Bogensperger, T., Schickhofer, G.: “Verformungsverhalten von Brettsperrholzplatten unter Schubbeanspruchung in der Ebene”. In: 5. Grazer Holzbau-Fachtagung, September 2006

INTER

International Network on Timber Engineering Research

PROPERTIES OF CROSS LAMINATED TIMBER (CLT) IN COMPRESSION PERPENDICULAR TO GRAIN

R Brandner
Graz University of Technology, Institute of Timber Engineering and Wood Technology
Competence Centre holz.bau forschungs gmbh

G Schickhofer
Graz University of Technology, Institute of Timber Engineering and Wood Technology

AUSTRIA

Presented by R Brandner
Erik Serrano asked for clarification of the uplift. R Brandner responded that under eccentric loading there could be uplift if the unloaded side was not restrained. Erik Serrano asked how to handle the unbonded edge joint. R Brandner responded that the spreading of load from first layer was neglected.
S Svensson stated that there are mechanic based solutions from Green's book for orthotropic material.
W Seim asked should moisture dependency not be covered by kmod. R Brandner responded that this is a topic for discussion but the compression perpendicular to grain case is particularly sensitive to moisture influence.
J Schmidt received confirmation that the 20% increase compared to glulam can be attributed to locking effect. J Schmidt asked if this effect can be expected if the product was made at high moisture content compared to in service conditions. R Brandner responded that the capability to glue at green condition is questionable. In any case locking effect will still be present.
R Tomasi and R Brandner discussed horizontal stresses in the compression component in the 1st layer and horizontal stresses in tension in the 2nd layer in that tension transfer should be restricted.

Properties of Cross Laminated Timber (CLT) in Compression Perpendicular to Grain

R BRANDNER [1) 2)]; G SCHICKHOFER [1)]

Graz University of Technology, Institute of Timber Engineering and Wood Technology [1)]

Competence Centre holz.bau forschungs gmbh [2)]

***Keywords**: Compression Perpendicular to Grain; Cross Laminated Timber; CLT; Discrete Loading; Discrete & Continuous Support; Stress-Distribution Model*

1 Abstract

The high load-bearing potential of CLT and its versatile applicability inspire architects and engineers designing pin- and line-supported structures. Due to its orthogonal layup and possible two-dimensional load transfer, CLT features some specifics, which differentiate it clearly from structural timber and glulam. Motivated by the need for adequate characteristic properties and design procedures for CLT in compression perpendicular to grain we analyse tests of Ciampitti (2013), conducted on point and line loaded, discretely or continuously supported CLT elements. On the basement of the state-of-knowledge correction factors for adapting $f_{c,90}$ and $E_{c,90}$ to the reference moisture content $u = 12$ % are given. The influence of the size of contact area on strength and stiffness, the share of elastic strain as well as current examination of $f_{c,90}$ and $E_{c,90}$ are discussed and new approaches presented. We adapt the stress-dispersion model of van der Put (1988) for two-dimensional load transfer in orthogonal layered CLT elements and verify it with data of several sources.

2 Introduction

Timber in compression perpendicular to grain, shows a unique sigmoid non-linear stress-strain-relationship, featuring a delayed hardening at the beginning followed by a continuous hardening without a stress peak until strains of ≥ 10 %, see Fig. 1. The apparent continuous hardening after exceeding a critical stress at the end of a roughly linear elastic branch follows from a flow mechanism. Hereby internal microscopic fractures, caused by local stability failures (buckling) and crushing of cell walls, occur (Kollmann, 1957, 1959; Madsen et al., 1982). The sigmoid stress-strain relationship impedes the determination of the modulus of elasticity $E_{c,90}$, as arbitrary number only valid for at least one point of the curve itself (Kollmann, 1959). In absence of a meaningful stress peak, for the design of timber structures the compression perpendicular to grain "strength" $f_{c,90}$ is a matter of notation, as stress at a certain strain or as stress at the intersection between a shifted secant-modulus and the stress-strain curve. These notations and the specifications for determination of basic properties for the design differ significantly from code to code (e.g. Leijten and Jorissen, 2010).

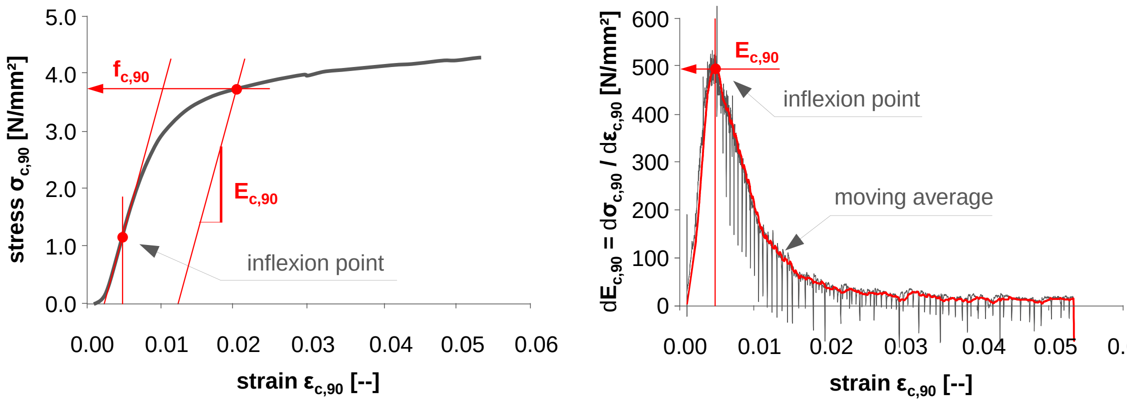

Fig. 1: (left) typical stress-strain relationship of a full-surface loaded prism; (right) change in $E_{c,90}$ per strain-increment vs. strain

The transfer from basic test results, with focus on material properties often determined on full-surface loaded prisms (e.g. EN 408:2012), to versatile configurations apparent in timber structures, with concentrated loads on discrete or continuously supported beams, is challenging. This is in particular the case as the properties of timber in compression perpendicular to grain depend on the geometric conditions (e.g. Madsen et al., 1982). These are i.e. (i) the depth (and width) of the timber member stressed in compression, (ii) the edge distance and the distance in-between stressed zones, (iii) the support conditions (continuous or discrete (point or line) support), and (iv) the size of the load introduction plate or contact area A_c (e.g. Graf, 1921). This is because of the spatial distribution of compression perpendicular to grain stresses to adjacent timber zones, activated to contribute to the load bearing. The load spreading is taken into account by an effective area $A_{\text{eff}} \geq A_c = w_c \cdot l_c$ (with w_c and l_c as width and length of the contact are A_c). This is done by considering a load distribution angle α (e.g. van der Put, 2008, 2012; Salzmann, 2011) or by extending the contact length in grain direction (e.g. Madsen et al., 1982; Blaß and Görlacher, 2004; EN 1995-1-1:2008). This increase in resistance is usually expressed by the factor $k_{c,90} = f_{c,90,\text{member}} / f_{c,90,\text{prism}}$, with $f_{c,90,\text{member}}$ and $f_{c,90,\text{prism}}$ as compression strengths perpendicular to grain of a discrete loaded timber member and of a full-surface loaded prism, respectively. Following Föppl (1904) values for $k_{c,90}$ of up to 2.5 to 3.0 are possible for central loaded timber members.

2.1 Models Considering the Activated Volume for Linear Members

There exists a controversial discussion on the definition of the additional volume contributing to the bearing of locally loaded members. Madsen et al. (1982), in reference to Hall (1980), reports on analysis made on a continuously supported centrically loaded timber member applying the theory of a beam on elastic foundation as well as by performing elastic-plastic finite element analysis (FEA). They report a maximum contributing length on both sides of the compressed area, named as “decay length”, of 1.5-times the member depth. The thickness of the beam on elastic foundation is identified with approximately 17 % of the total depth. Thus the deeper member the more load is spread away. Overall, a non-linear dependency of $k_{c,90}$ from the ratios l_c / d and d / l, respectively, with d and l as depth and length of the timber member is observed.

Blaß and Görlacher (2004) define a model assuming independency between strength and member depth. Based on the design proposal of Madsen et al. (1982) and own tests a constant length of maximum 30 mm per protruding side is found, with

$$A_{\text{ef}} = w \cdot \left[l_c + \sum_{i=1}^{n} \min\left(a_i; l_c; 30\text{ mm}\right) \right], \tag{1}$$

with $i = 1, 2$ and a_i as end- or half in-between distance of two discrete loadings, and $k_{c,90} = 1.00$ and ≤ 1.75 for ultimate (ULS) and serviceability limit state (SLS) design, respectively. This approach is currently anchored in EN 1995-1-1:2008 but extended by values for $k_{c,90} \leq 1.75$ for ULS design, regulated in dependency of the load configuration and the timber product.

Van der Put (1988, 2008, 2012), Leijten and Jorissen (2010) and Leijten et al. (2012) outline the relationship between member depth and strength. Based on an elastic-plastic stress dispersion model of van der Put (1988) the simple power model

$$f_{c,90,\text{member}} = \frac{F_{c,90}}{w \cdot l_c} = f_{c,90,\text{prism}} \cdot \sqrt{\frac{l_{\text{ef}}}{l_c}}, \tag{2}$$

is proposed, with l_{ef} calculated assuming a stress dispersion angle of α = 45° and 33.7° corresponding to a stress at strain of 3 to 4 % and 10 %, respectively, with the last one dedicated to ultimate stress. Preventing other premature failures, the model is limited to $d / w \leq 5$. Meanwhile this model approach has been manifold applied for explaining divergences between test results, test methods and design approaches. Regulations in EN 1995-1-1:2004 are partly akin to the proposed model anchoring a stress dispersion angle of 71.6° and $k_{c,90} \leq 4.0$ at 10 % strain.

Kollmann (1959) give test data gained from centrically loaded and continuously supported small clear wood prisms of beech (*Fagus sylvatica*) with and without v-shaped notches of depth 1, 3 or 5 mm processed on both sides of the contact area. Statistics of strength data indicate no influence by notches.

2.2 The Influence of the Dimension of the Contact Area

Föppl (1904) reports a decreasing resistance in compression perpendicular to grain of full-surface loaded cubic specimen with increasing surface. Graf (1921) investigated experimentally the resistance of centrally loaded and discretely supported timber beams at constant strain limits. At $w_c = w$ he observed a significant increase in strength with decreasing contact area A_c, proportional to the ratio of $A_c / A_{c,\mathrm{ref}}$ with the power of 0.25. In case of equal A_c but $w_c < w$ a lower increase in strength compared to tests with $> A_c$ is observed. This indicates stress dispersion in grain direction higher than transversely. Madsen et al. (1982) confirm the general made observations and mentions an increase in strength with $l_{c,\mathrm{ref}} = 150$ mm, of 13 and 40 %, for $l_c = 75$ mm and 25 mm, respectively. This increase corresponds to a power of 0.19.

2.3 The Influence of Moisture

Föppl (1904) reports a 5 % change in $f_{c,90}$ per percentage change in moisture content (1 % Δu). Data of Kollmann (1959), gained from beech specimen, indicate a reduction in $E_{c,90}$ and $f_{c,90}$ of 1.8 to 2.5 % and approximately 4 %, respectively, per 1 % Δu within $8\,\% \leq u \leq 20\,\%$. This is observed independently from strain limits used for the determination of strength. Forest Products Laboratory (2010) proposes for $E_{c,90}$ a change of 2 % per 1 % Δu. Test results from different timber species (groups) in Madsen et al. (1982) reflect a change of 3.5 to 4.3 % per percent change in moisture content for both, $E_{c,90}$ and $f_{c,90}$. European test (e.g. EN 408:2012) and design standards (e.g. EN 1995-1-1:2008) provide currently no explicit regulations for adapting $E_{c,90}$ and $f_{c,90}$ to $u \neq 12$ % or service classes (SC), beside the different modification factors for SC 1 / 2 and SC 3.

2.4 State-of-Knowledge Regarding Cross Laminated Timber (CLT)

As outlined so far, the majority of publications address linear timber members and products, e.g. structural timber and glued laminated timber (glulam, GLT), e.g. Föppl (1904), Graf (1921), Larsen (1975), Madsen et al. (1982), Korin (1990), Gehri E (1997), Hoffmeyer et al. (2000), Blaß and Görlacher (2004), Ruli (2004), Augustin et al. (2006), van der Put (1988, 2008, 2012), Leijten and Jorissen (2010) and Leijten et al. (2012). Only a few concern two-dimensional timber products like cross laminated timber (CLT), e.g. Halili (2008), Serrano and Enquist (2010), Salzmann (2010) and Bogensperger et al. (2011). In general, the high potential of CLT in load bearing and versatile possibilities for applications inspire architects and engineers designing pin- and line-supported structures. Thus, there is a remarkable interest in the load bearing behaviour of CLT in compression perpendicular to grain. Due to its orthogonal layup and the possibility of a two-dimensional load transfer, CLT features some specifics, which differentiate it clearly from structural timber and glulam.

Halili (2008) compares CLT and GLT by testing uniformly stressed prismatic specimens with a squared surface of 160 mm × 160 mm and a depth of 200 mm made of Norway spruce (*Picea abies*). All specimens are without gaps and produced in the laboratory using board segments of equal width and strength class C24+ according to EN 338:2009. He focuses on the influence of (i) the number of layers, (ii) the ratio between the thicknesses of neighbouring layers, and (iii) of grain orientation. Higher strength and stiffness in CLT in comparison to glulam are found which is dedicated to a "locking effect" caused by alternating reinforcement provided by the orthogonal layering. Consequently, an increase in stiffness and strength with increasing number of layers (decreasing layer thickness) is observed together with a minor reduction in the dispersion. Concerning (ii) by trend higher strength and stiffness occur in specimens composed of layers of equal thickness. This is dedicated to a reduced reinforcement effect in cases of too thin neighbouring layers. CLT specimens composed of side boards, stressed mainly in radial direction, feature a higher E-modulus but a lower resistance. Overall no significant relationship is observed for $E_{c,90}$ and $f_{c,90}$ vs. density ρ_{12} but a minor correlation between $E_{c,90}$ and $f_{c,90}$ ($r \approx 0.55$). In comparison to GLT, CLT features 70 % and 30 % higher stiffness and strength, respectively. Some tests are also made on discrete loaded, continuously and discrete supported CLT-plates. These tests give a first impression of the expectable amount of stress dispersion in a two-dimensional, orthogonal layered element.

Salzmann (2010) gives test results for four different layups of industrially produced five-layer CLT-elements of Norway spruce (*Picea abies*) with average density $\rho_{12} = 440$ to 470 kg/m³ and total thickness $t_{\mathrm{CLT}} = 150$ to 197 mm. He focuses on the influence of different configurations of point-loads (steel plate, $A_c = 160$ mm × 160 mm) on a continuously supported plate. Comparison between tests on full-surface loaded prisms and data of Halili (2008) gives widely congruent results; also similar correlations between $f_{c,90}$, $E_{c,90}$ and ρ_{12} are found. As expected, centrically loaded CLT shows highest resistances (stress dispersion activated on four sides) whereas strength and stiffness is lowest at the corners (stress dispersion activated on two sides). FE-analysis extends the tests by simulating (i) the influence of annual ring orientation, (ii) different layups, and (iii) discrete point-loadings on continuous or line-supports. He successfully verifies strengths and elastic moduli gained from FEA by introducing a load-distribution angle in the range of $\alpha = 20°$ to 30°, smeared over the orthogonal layering.

Serrano and Enquist (2010) report on tests of Hasuni et al. (2009) conducted on industrially produced three-layer CLT-elements of Norway spruce (*Picea abies*) with $t_{\mathrm{CLT}} = 120$ mm subjected to line-loading (50 mm wide steel bars) and varying edge-distances, intended to simulate CLT-slabs clamped by walls. A clear dependency of the resistance from edge-distance and positioning of the line-load in respect to the orientation of the top-layer is observed. Allowing free deformation of the CLT-element during testing they report a more brittle than plastic failure in case of line-loading at the edge and parallel to the grain of the top layers which indicates premature failures by rolling shear as consequence of the shear coupling effects. They outline the complexity of regulations for the resistance of CLT against compression perpendicular to grain.

Bogensperger et al. (2011) provide a comprehensive summary of previous results with focus on CLT. They extend the FEA of Salzmann (2010) simulating $k_{c,90}$-factors for point-loaded and fully supported CLT-elements. This is done by simulating a three-dimensional CLT-element in Abaqus of linear-elastic orthotropic material but elastic-plastic behaviour with linear hardening in radial direction, formulated by means of a flow rule. The effect of member depth on resistance and on $k_{c,90}$-factors is outlined and found to be linear. A comparison of numerical results with test data of Salzmann (2010) in Tab. 1 shows overall good congruence. Furthermore, numerical results reflect increasing resistance with decreasing A_c and with increasing CLT thickness of discrete loaded CLT-elements.

Tab. 1: $k_{c,90}$-factors for different load configurations on discrete loaded, continuously supported CLT-elements

	numerical result [1)]		**test results** [2)]
load configuration	t_{CLT} **= 165 mm**	t_{CLT} **= 200 mm**	t_{CLT} **= 150 to 197 mm**
centrically loading	1.83	1.93	1.91
edge loading parallel to top layer	1.58	1.66	1.58
edge loading transverse to top layer	1.47	1.53	1.57
loading at the corner	1.25	1.30	1.50

1) Bogensperger et al. (2011)

2) Salzmann (2010): values base on $f_{c,90,\mathrm{prism,mean}} = 3.33$ N/mm², calculated by averaging test data from CLT prism, published in Bogensperger et al. (2011)

Motivated by (i) questions regarding the resistance and behaviour of CLT in case of line-loads and line-supports, raised by Serrano and Enquist (2010), (ii) the missing verification of some numerical results in Bogensperger et al. (2011), and (iii) the missing regulations concerning the vulnerability of $f_{c,90}$ and $E_{c,90}$ to moisture content lead to a further research project. Furthermore, input for the ongoing discussion on load-spread models is envisaged.

3 Materials and Methods

We report on results based on Ciampitti (2013). We focus on (a) the dependency of compression perpendicular to grain properties on the dimension of the contact area A_c, (b) the difference between CLT as floor elements clamped between two columns or walls versus a column or wall on a continuously supported floor, and (c) on the influence of moisture, see Fig. 2. Tests are conducted on industrially produced five-layer CLT-elements of Norway spruce (*Picea abies*) with layer thicknesses (from top to bottom layer) of $t_l = 40, 20, 40, 20, 40$ mm, total thickness of $t_{CLT} = 160$ mm, produced without edge-bonding. Regarding (a) tests are made using thick steel plates for load introduction with $A_c = 100 \times 100$ mm², 150×150 mm² and 200×200 mm² for point-loads, representing columns, and 100×400 mm² and 150×400 mm² for line-loads, representing walls. Line-loading is realised by using (I) only the steel plates, (II) two to three steel stripes of cross-section 30×30 mm² beneath the steel plate, for simulating only the longitudinal layers of a CLT-wall element resting on the floor, and (III) like (II) but with additional timber stripes, simulating the cross layers of a CLT-wall element too (Fig. 2 (f)). Deformations, afterwards averaged, are measured globally by means of inductive displacement transducers positioned on all four corners of the steel plate. Investigations for (b) are made using various load configurations (centre (M), corner (E), and edge parallel (L) and perpendicular to the grain of the top layer (Q)) and support conditions (discrete (point- or line-support; D) or continuous support (V)), see Fig. 2 (a-d). Discrete supports are realised in size equal to the steel-plates used for loading and arranged on the opposite direction. To prevent lifting of discrete loaded specimens they are clamped. The influence of moisture (c) is examined by three sub-samples of prisms $150 \times 150 \times 160$ mm³ conditioned to equilibrium average moisture contents of 8.8 %, 12.7 % and 15.3 %. Additional reference tests on full-surface loaded prisms have a cross section equal to A_c of the point-loads; see Fig. 2 (e). Tests are according to EN 408:2012. Some tests run three hysteresis loops at different stress levels. This is done for examining the share of plastic deformation in the non-linear part of the stress-strain curve, see Fig. 1. Test data are evaluated in accordance with EN 408:2012. As the initial part of the stress-strain curve dedicated to delayed hardening exceeds several time the 10 % stress limit for the determination of $E_{c,90}$, in general a linear regression analysis is applied in the apparent linear-elastic part using flexible limits and by conditioning a correlation of $r \geq 0.999$. Sample size of cubic specimens is ten; every load configuration and support condition on CLT-elements comprises five tests. All samples are density matched. Statistics for $f_{c,90}$ and $E_{c,90}$ are calculated by applying A_c. Some values are excluded from further data processing due to deficiencies in determination of $E_{c,90}$ and in cases of local deficiencies influencing strength and stiffness.

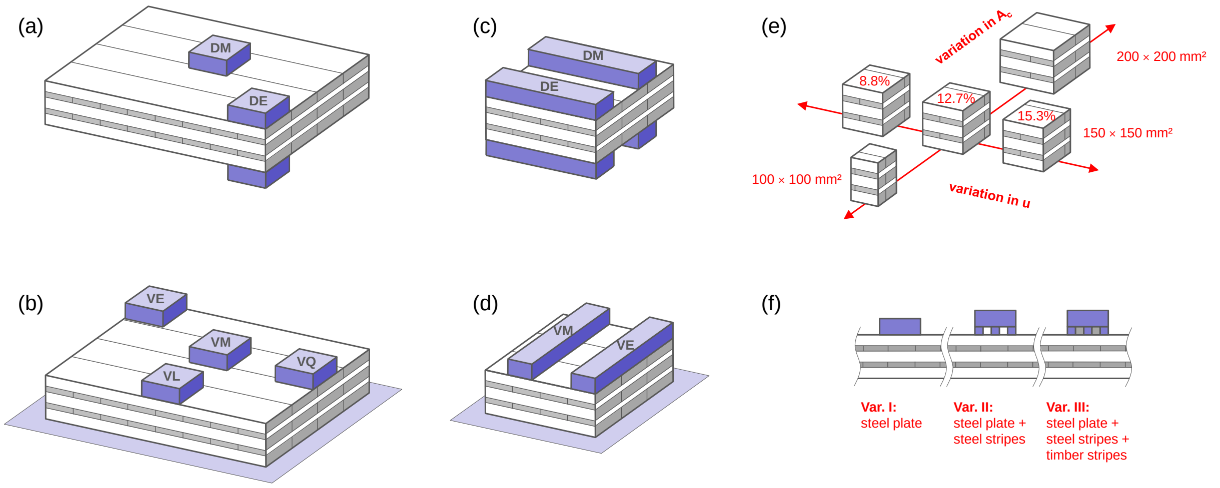

Fig. 2: Test setup: (a) discrete point loads and discrete point supports; (b) discrete point loads and continuous support; (c) discrete line loads and discrete line support; (d) discrete line loads and continuous support; (e) prisms for full-surface testing with variation on surface area and moisture content; (f) variants in testing line loads and line supports

4 Results and Discussions

4.1 Influence of Moisture Content

Tab. 2 gives statistics from three density-matched samples of full-surface loaded prisms. Whereas observing a significant reduction in strength with increasing moisture, the data of $E_{c,90,u}$ reflects an unexpected peak in group $u = 12.7$ %. Seven of ten tests in this group are tested with a steel plate of 150×150 mm², bevelled at the edges. Although no influence is observed for strength an influence on

$E_{c,90,u}$ cannot be excluded. Based on $f_{c,90,u,\text{mean}}$ and $E_{c,90,u,\text{mean}}$ of groups $u = 8.8$ % and 15.3 %, assuming linearly decreasing mechanical properties with increasing moisture content within the investigated bandwidth and with reference to the mean values at $u = 12.7$ % (in case of $E_{c,90,u}$ gained by taking the average of groups $u = 8.8$ % and 15.3 %) correction factors of 3.7 % and 0.5 % per 1 % Δu for adapting $f_{c,90,\text{mean}}$ and $E_{c,90,\text{mean}}$, respectively, are found. Comparable coefficients are given for the 5 %-quantiles. The outcome is well in-line with the literature, see chapter 2.3; an extrapolation to 8 % ≤ u ≤ 20 % is judged as possible. Thus, **for $f_{c,90}$ and $E_{c,90}$ an adaptation of 4 % and 1 % per 1 % Δu, respectively, is proposed** and further applied; the last value also in view of regulations in EN 384:2010.

Tab. 2: Statistics gained from full-surface loaded prisms 150 × 150 mm² at varying moisture contents

statistics	u_{mean} = 8.8 % | CoV[u] = 2.6 %			u_{mean} = 12.7 % | CoV[u] = 2.3 %			u_{mean} = 15.3 % | CoV[u] = 2.2 %		
	ρ_{12} [kg/m³]	$f_{c,90,u\|12}$ [N/mm²]	$E_{c,90,u\|12}$ [N/mm²]	ρ_{12} [kg/m³]	$f_{c,90,u\|12}$ [N/mm²]	$E_{c,90,u\|12}$ [N/mm²]	ρ_{12} [kg/m³]	$f_{c,90,u\|12}$ [N/mm²]	$E_{c,90,u\|12}$ [N/mm²]
quantity	10	10 | 10	10 | 10	10	10 | 10	10 | 10	9	9 | 9	9 | 9
Mean	**457**	**3.87 | 3.38**	**368 | 357**	**458**	**3.54 | 3.64**	**441 | 444**	**450**	**3.03 | 3.43**	**357 | 368**
$X_{50,\text{empD}}$ 1)	**457**	**3.91 | 3.41**	**370 | 357**	**459**	**3.59 | 3.64**	**426 | 430**	**443**	**3.04 | 3.43**	**349 | 361**
CoV [%]	2.1	5.5 | 5.5	7.3 | 7.3	4.0	7.4 | 7.0	9.0 | 8.9	4.2	6.2 | 5.9	10.0 | 9.8
$X_{05,\text{empD}}$ 2)	445	3.54 | 3.08	331 | 321	431	3.17 | 3.28	406 | 408	432	2.76 | 3.14	314 | 325
$X_{05,\text{2pLND}}$ 3)	442	3.53 | 3.08	326 | 316	428	3.13 | 3.23	379 | 382	420	2.73 | 3.11	301 | 312

1) & 2) median & 5 %-quantile, based on rank statistics | 3) 5 %-quantile, based on lognormal distribution

4.2 Variation of Contact Area: Influence on Strength and Stiffness

4.2.1 Full-Surface Loaded Prisms

Tab. 3 contains statistics of full-surface loaded prisms with different surface area. Approximately a linear increase in strength and stiffness with increasing A_c is observed. Reasoning for the made observations are (i) the local variability of timber properties and growth characteristics, (ii) the occurrence of gaps, and (iii) the test configuration itself. Concerning (i) and (ii) an increasing encapsulation of growth and production characteristics with increasing surface area can be expected. Concerning (iii) the aspect of non-parallel support- and loading-planes may also have a more distinct influence on prisms with smaller surface area but equal depth. Focusing on reference mechanical properties for CLT for compression perpendicular to grain **a reference cubic specimen of 150 × 150 × 150 mm³, corresponding to a five-layer CLT element with t_l = 30 mm and a reference board width of 150 mm, is proposed**. A comparison of the statistics for 150 × 150 mm², $f_{c,90,12,\text{mean}}$ from Tab. 3 and $f_{c,90,12,k}$ calculated according to EN 14358:2006, with that in Bogensperger et al. (2011) shows overall good agreement; the values in the present study are a bit higher ($f_{c,90,12,\text{mean}}$: 3.48 vs. 3.33 N/mm²; $f_{c,90,12,k}$: 3.06 vs. 2.85 N/mm²). In contrast, $E_{c,90,12,\text{mean}}$ = 391 N/mm² in Tab. 3 is lower than reported in Bogensperger et al. (2011; $E_{c,90,12,\text{mean}}$ = 450 N/mm²). Comparison of $f_{c,90,12,k}$ and $E_{c,90,12,\text{mean}}$, based on Tab. 3, with the corresponding statistics for GLT in Bogensperger et al. (2011) gives overall 30 % higher resistance and stiffness in CLT. However, a correction of the statistics to the reference moisture content u_{ref} = 12 % is not made in the referenced publication. Thus **$f_{c,90,12,\text{prism},k}$ = 3.0 N/mm²** (CoV[$f_{c,90,12}$] ≈ 8 %) and **$E_{c,90,12,\text{prism},\text{mean}}$ = 400 N/mm²** appear reasonable.

Tab. 3: Statistics gained from full-surface loaded prisms of varying surface area

statistics	100 × 100 mm²			150 × 150 mm² 4)			200 × 200 mm²		
	ρ_{12} [kg/m³]	$f_{c,90,12}$ [N/mm²]	$E_{c,90,12}$ [N/mm²]	ρ_{12} [kg/m³]	$f_{c,90,12}$ [N/mm²]	$E_{c,90,12}$ [N/mm²]	ρ_{12} [kg/m³]	$f_{c,90,12}$ [N/mm²]	$E_{c,90,12}$ [N/mm²]
quantity	10	10	10	29	29	29	10	10	10
Mean	**444**	**3.26**	**380**	**455**	**3.48**	**391**	**455**	**3.87**	**436**
$X_{50,\text{empD}}$ 1)	**441**	**3.33**	**386**	**457**	**3.47**	**379**	**452**	**3.89**	**425**
CoV [%]	4.0	5.4	9.2	3.5	6.8	13.3	3.9	5.8	7.9
$X_{05,\text{empD}}$ 2)	422	2.99	333	432	3.07	322	434	3.56	402
$X_{05,\text{2pLND}}$ 3)	416	2.97	325	430	3.10	311	427	3.51	382

1) & 2) median & 5 %-quantile, based on rank statistics | 3) 5 %-quantile, based on lognormal distribution | 4) averaged from Tab. 2

4.2.2 Discretely Loaded CLT-Elements

Tab. 4 and Tab. 5 contains statistics of point- and line-loaded members, respectively. Due to the small sample sizes of series with line loads caused additionally by testing three different variations of load-introduction (see Fig. 2 (f)), only mean (single) values are presented.

Tab. 4: Statistics of point-loaded, discretely or continuously loaded CLT elements

	"DE" | 100 × 100 mm²			"DM" | 100 × 100 mm²			"VL" | 100 × 100 mm²		
statistics	ρ_{12} [kg/m³]	$f_{c.90.12}$ [N/mm²]	$E_{c.90.12}$ [N/mm²]	ρ_{12} [kg/m³]	$f_{c.90.12}$ [N/mm²]	$E_{c.90.12}$ [N/mm²]	ρ_{12} [kg/m³]	$f_{c.90.12}$ [N/mm²]	$E_{c.90.12}$ [N/mm²]
quantity	5	5	4	5	5	4	5	5	4
Mean	**455**	**5.10**	**609**	**456**	**7.01**	**741**	**451**	**6.96**	**852**
$X_{50,empD}$ 1)	**453**	**5.31**	**605**	**552**	**6.69**	**734**	**452**	**6.66**	**867**
CoV [%]	2.2	9.0	2.5	2.3	11.0	3.8	1.3	14.0	6.7
$X_{05,empD}$ 2)	445	4.61	596	446	6.32	718	445	6.04	785
$X_{05,2pLND}$ 3)	439	4.39	583	439	5.82	695	442	5.49	761
	"VE" | 100 × 100 mm²			"VM" | 100 × 100 mm²			"VQ" | 100 × 100 mm²		
quantity	5	5	5	5	5	4	5	5	5
Mean	**452**	**6.17**	**826**	**452**	**8.62**	**1,241**	**452**	**7.52**	**1,028**
$X_{50,empD}$ 1)	**453**	**6.30**	**848**	**451**	**7.98**	**1,229**	**453**	**6.85**	**1,032**
CoV [%]	1.1	7.5	13.8	1.3	18.2	3.3	1.3	17.8	5.9
$X_{05,empD}$ 2)	445	5.65	682	444	7.00	1,209	444	6.42	974
$X_{05,2pLND}$ 3)	443	5.44	653	442	6.30	1,175	442	5.54	932
	"DE" | 150 × 150 mm²			"DM" | 150 × 150 mm²			"VM" | 150 × 150 mm²		
quantity	5	5	5	5	4	4	5	5	4
Mean	**462**	**5.27**	**484**	**462**	**6.79**	**690**	**453**	**7.22**	**1,051**
$X_{50,empD}$ 1)	**457**	**5.23**	**456**	**457**	**6.83**	**694**	**453**	**7.30**	**1,057**
CoV [%]	4.6	10.6	9.4	4.3	2.3	4.2	4.7	7.6	4.7
$X_{05,empD}$ 2)	446	4.60	447	446	6.60	658	451	6.55	995
$X_{05,2pLND}$ 3)	428	4.41	412	430	6.53	644	450	6.35	972
	"DE" | 200 × 200 mm²			"DM" | 200 × 200 mm²			"VM" | 200 × 200 mm²		
quantity	4	4	4	5	5	5	5	4	4
Mean	**450**	**5.00**	**527**	**449**	**5.79**	**751**	**454**	**7.29**	**999**
$X_{50,empD}$ 1)	**452**	**4.96**	**526**	**451**	**5.94**	**763**	**455**	**7.35**	**997**
CoV [%]	2.1	6.3	3.3	1.9	5.1	8.5	1.5	6.0	10.1
$X_{05,empD}$ 2)	439	4.71	510	439	5.44	686	446	6.80	896
$X_{05,2pLND}$ 3)	435	4.50	499	435	5.32	650	443	6.60	842

1) & 2) median & 5 %-quantile, based on rank statistics | 3) 5 %-quantile, based on lognormal distribution

Tab. 5: Statistics of line-loaded, discretely or continuously loaded CLT elements

	Var. I: A_c = 100 (150) × 400 mm² (2 specimens each)			Var. II: A_c = 60 (90) | 100 (150) × 400 mm²; (2 specimens each)			Var. III: A_c = 100 (150) × 400 mm² (1 specimen each)		
l_c, **config.**	$\rho_{12,mean}$ [kg/m³]	$f_{c,90,12,mean}$ [N/mm²]	$E_{c,90,12,mean}$ [N/mm²]	$\rho_{12,mean}$ [kg/m³]	$f_{c,90,12,mean}$ [N/mm²]	$E_{c,90,12,mean}$ [N/mm²]	$\rho_{12,mean}$ [kg/m³]	$f_{c,90,12,mean}$ [N/mm²]	$E_{c,90,12,mean}$ [N/mm²]
100, DE	449	**3.95**	**329**	450	**4.27 | 2.56**	**374 | 224**	452	**3.82**	**341**
100, DM		**5.00**	**423**		**5.06 | 3.04**	**527 | 316**		**5.48**	**537**
100, VE	449	**5.42**	**538**	450	**7.49 | 4.44**	**781 | 469**	452	**4.93**	**583**
100, VM		**6.96**	**770**		**9.08 | 5.45**	**1,259 | 755**		**7.19**	**868**
150, VE	450	**4.99**	**537**	451	**7.66 | 4.60**	**843 | 506**	455	**5.18**	**566**
150, VM		**6.36**	**751**		**8.59 | 5.15**	**1,114 | 668**		**6.14**	**730**

Data of tests with line loads of Var. I and III are further combined as a significant difference in $f_{c,90,12}$ and $E_{c,90,12}$ between both sub-sets is not observed. Thus tests conducted with stiff steel plates are seen as representative for the practical case of a CLT wall resting on a CLT floor . However, testing two parallel line loads with only a small distance in-between leads to a reduction in strength and stiffness, see Tab. 5. This circumstance is discussed further in chapter 4.3.

Fig. 3 visualises the change in $f_{c,90,12,\text{mean}}$ and $E_{c,90,12,\text{mean}}$ relative to the properties dedicated to the smallest contact area A_c of the common investigated data sets, given as [rel. $f_{c,90,12,\text{mean}}$] and [rel. $E_{c,90,12,\text{mean}}$] versus [rel. A_c]. This graph is motivated by published power relationships between strength and A_c with intrinsic scale invariance. A decrease in the properties with increasing A_c is observed, whereby most of the changes occur in comparing subsets of point- to line-loadings. This is because point-loads applied centrically or at the edge can distribute stresses in four or three directions whereas line-loads, as herein tested, are only able to distribute in two or one direction, respectively (see Fig. 2). Focusing solely on the subset "DE", which involves only data of point-loads, on average roughly no influence of A_c on strength and stiffness is found. However, a certain influence by A_c is expected because the increase in volume activated to load bearing is expected to be disproportional to the increase in contact area. This is discussed further in chapter 4.3. Within sets with point or line loads only a minor decrease is observed for both, $f_{c,90}$ and $E_{c,90}$. There is no distinctive difference between tests made on continuously or discretely supported elements. In comparison to literature, the decrease in strength of the presented tests is overall smaller. Possible reasons are the more homogeneous properties in CLT in general and the orthogonal layering as well. Although the numerical analysis is made for CLT, Bogensperger et al. (2011) report a higher and regressive strength reduction.

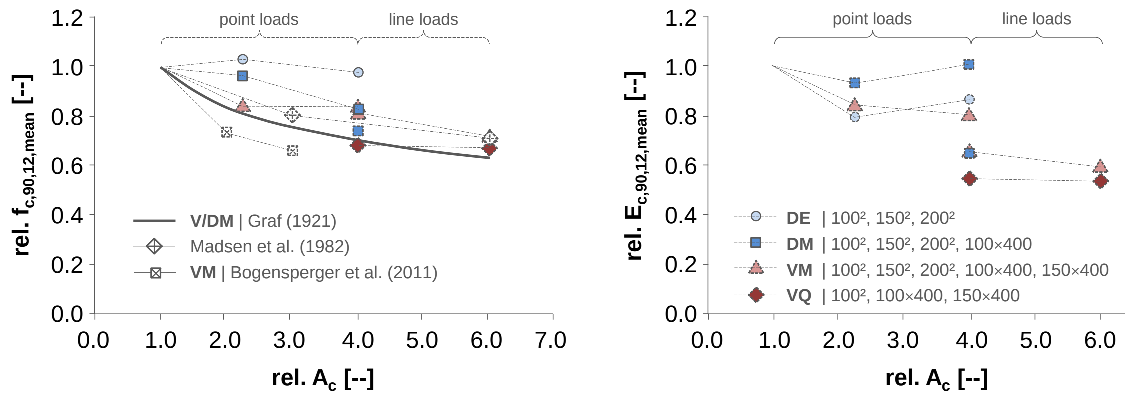

Fig. 3: $f_{c,90,12,\text{mean}}$ and $E_{c,90,12,\text{mean}}$ relative to the properties at min($A_{c,i}$) of the i^{th} subset

4.3 Continuous vs. Discrete Supports and Adaptation of the Stress-Dispersion Model of van der Put

As reflected by statistics in Tab. 3 to Tab. 5, a relationship between CoV[$f_{c,90,12}$] and CoV[$E_{c,90,12}$] on the load configuration is not observed although a decrease in dispersion with increasing volume active in load-bearing is expected. Being on the conservative side and by considering the small sample sizes further investigations concentrate on comparisons between mean values; limitations of this approach later in timber design is not expected. Tab. 6 gives values for $k_{c,90} = X_{\text{member}} / X_{\text{prism}}$, with $X = \{f_{c,90,12,\text{mean}}; E_{c,90,12,\text{mean}}\}$, for all investigated load and support conditions. As reference values for line loads 100 × 400 mm² and 150 × 400 mm² are missing, $f_{c,90,\text{prism},12,\text{mean}}$ and $E_{c,90,\text{prism},12,\text{mean}}$ are estimated by extrapolation from the relationships $X_{12,\text{mean}}$ vs. A_c gained from statistics in Tab. 3.

Tab. 6: $k_{c,90}$ for $f_{c,90,12,\text{mean}}$ and $E_{c,90,12,\text{mean}}$

	100 × 100 mm²		**150 × 150 mm²**		**200 × 200 mm²**		**100 × 400 mm²**		**150 × 400 mm²**	
	$k_{c,90}(f_{c,90})$	$k_{c,90}(E_{c,90})$	$k_{c,90}(f_{c,90})$	$k_{c,90}(E_{c,90})$	$k_{c,90}(f_{c,90})$	$k_{c,90}(E_{c,90})$	$k_{c,90}(f_{c,90})$	$k_{c,90}(E_{c,90})$	$k_{c,90}(f_{c,90})$	$k_{c,90}(E_{c,90})$
"DE"	1.56	1.60	1.51	1.24	1.29	1.21	1.02	0.76	–	–
"DM"	2.15	1.95	1.95	1.76	1.50	1.72	1.30	0.98	–	–
"VL"	2.13	2.24	–	–	–	–	–	–	–	–
"VQ"	2.31	2.71	–	–	–	–	1.40	1.24	1.17	1.14
"VE"	1.89	2.17	–	–	–	–	–	–	–	–
"VM"	2.64	3.27	2.07	2.69	1.88	2.29	1.80	1.78	1.49	1.59

Overall, the coefficients for $k_{c,90}$ of strength in Tab. 6 for continuously supported CLT elements are all higher than published in Bogensperger et al. (2011). Reasoning is seen in differences between applied test configurations. Whereas discretely loaded specimens in Ciampitti (2013) are clamped to prevent lifting, lifting is allowed in numerical calculations and tests of Salzmann (2010), analysed in Bogensperger et al. (2011). However and as expected, discrete loading at the corner of a CLT element leads to lower $k_{c,90}$ than in cases of centrically loading. An increase, comparable to strength, is also observed for $E_{c,90,\mathrm{member},12,\mathrm{mean}}$. Although $k_{c,90}$ basis on mean values the ratios disperse remarkable.

Motivated by the success of the stress-dispersion model of van der Put (1988, 2008, 2012; see Eq. (2)), formulated for linear, unidirectional timber members with $w_c = w$, and the regulations for stress-distribution angles for timber in EN 1995-2:2004, with $\alpha_L = 45°$ and $\alpha_T = 15°$ for longitudinal and transverse direction, respectively, we analyse the applicability of an adapted model for the two-dimensional case of the orthogonal structure of CLT. The stress-dispersion angle $\alpha_L = 45°$ confirms exactly to the recommended angle in van der Put (1988, 2008, 2012) for analysing the compression strength at 3 to 4 % strain as implicitly anchored in EN 408:2012. Applying the two angles α_L and α_T in analysing the stress-dispersion from layer to layer and in dependency of the support conditions (see Fig. 4) allows to explain directly differences between (i) load configurations, (ii) support conditions, (iii) composition and thickness of the CLT elements, and (iv) the edge distances a. This by formulating $A_{\mathrm{ef}} = w_{\mathrm{ef}} \cdot l_{\mathrm{ef}}$. Furthermore, investigating Var. II of line-loaded specimens shows that the zone beneath the steel stripes is multiple compressed by overlapping stress dispersion. This may explain the lower strength and stiffness values for Var. II in comparison to Var. I and III in Tab. 5, calculated at equal A_c.

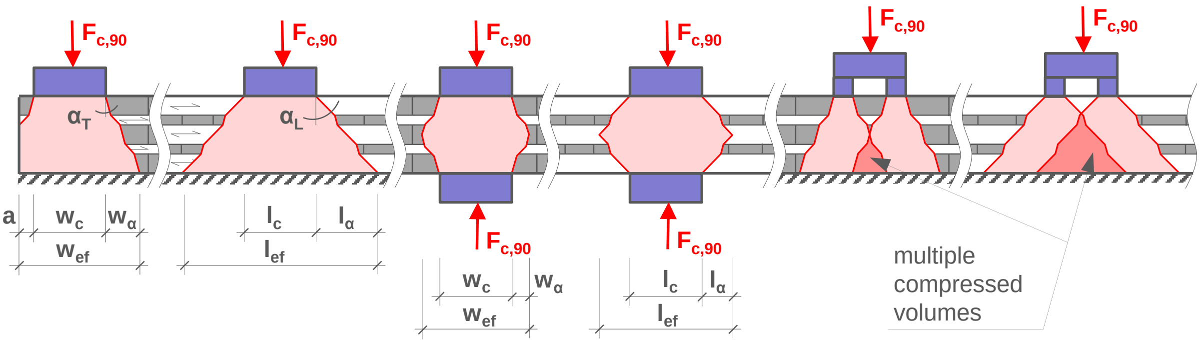

Fig. 4: Distribution model for compression perpendicular to grain stresses in discrete loaded, continuously or discretely supported CLT-elements

Consequently, we formulate an adapted stress dispersion model

$$f_{c,90,\mathrm{member}} = f_{c,90,\mathrm{prism}} \cdot \sqrt{\frac{A_{\mathrm{ef}}}{A_c}} = f_{c,90,\mathrm{prism}} \cdot \sqrt{\frac{l_{\mathrm{ef}} \cdot w_{ef}}{l_c \cdot w_c}} \longrightarrow k_{c,90} = \sqrt{\frac{A_{\mathrm{ef}}}{A_c}}, \tag{3}$$

with $A_{\mathrm{ef}} = w_{\mathrm{ef}} \cdot l_{\mathrm{ef}}$, $w_{\mathrm{ef}} = 2 \cdot (w_c / 2 + \min[a; w_\alpha])$ and $l_{\mathrm{ef}} = 2 \cdot (l_c / 2 + \min[a; l_\alpha])$, $\alpha_L = 45°$ and $\alpha_T = 15°$ and with $a \geq (w_{\mathrm{ef}}; l_{\mathrm{ef}})$. We apply this model for estimating mean values of discretely loaded CLT elements mirroring the investigated load and support configurations in Ciampitti (2013). We further use this model for analysing the data in Salzmann (2010). The ratio $X_{\mathrm{mod}} / X_{\mathrm{test}}$, with $X = \{f_{c,90,12,\mathrm{mean}}; E_{c,90,12,\mathrm{mean}}\}$ is shown in Fig. 5. Beside series "DE | 100 × 400" the model performs well in estimating test results of Ciampitti (2013) within ± 20 % deviation. This is observed for both properties, $f_{c,90,12,\mathrm{member},\mathrm{mean}}$ and $E_{c,90,12,\mathrm{member},\mathrm{mean}}$. As the chosen stress dispersion angles are more dedicated to ULS than to SLS design slightly smaller α_L and α_T are expected for estimating $E_{c,90}$. However, the outcome for Salzmann (2010) is completely different. Overall, the model overestimates the results by roughly 20 %. Two main reasons can be identified: Firstly and as already noted, lifting of discretely loaded specimens opposite to the end tested is allowed in Salzmann (2010) whereas this is prevented in Ciampitti (2013). In view of timber structures clamping by walls and dead load is expected as well although some influence of moments on the resistance in compression perpendicular to grain cannot be excluded completely. Secondly, tests of Salzmann (2010) comprise four different load configurations, all with $A_c = 160 \times 160$ mm², performed on the same CLT element of surface 600 × 600 mm². The orthogonal distance between the loaded zones is only 60 mm on the surface. As all tests exceeded strains of 4 %, micro-cracks and local damage, induced by distinctive non-linear deformation in the volume active in load-bearing, cannot be excluded. A reduction in strength and stiffness of roughly 10 to 20 % is already observed in tests with line loads, Var. II of Ciampitti (2013), see Tab. 5. The second reason is further underlined by smaller deviations between model and test data in case of CLT elements point-loaded at the corner. Furthermore, series “DM-165 | 160²” of Salzmann (2010) and “DM-200 | 160²” of Halili (2008), both representing centrically point-loaded and point-supported CLT elements, not influenced by lifting and pre-damages, agree well with the model predictions, at least for strength.

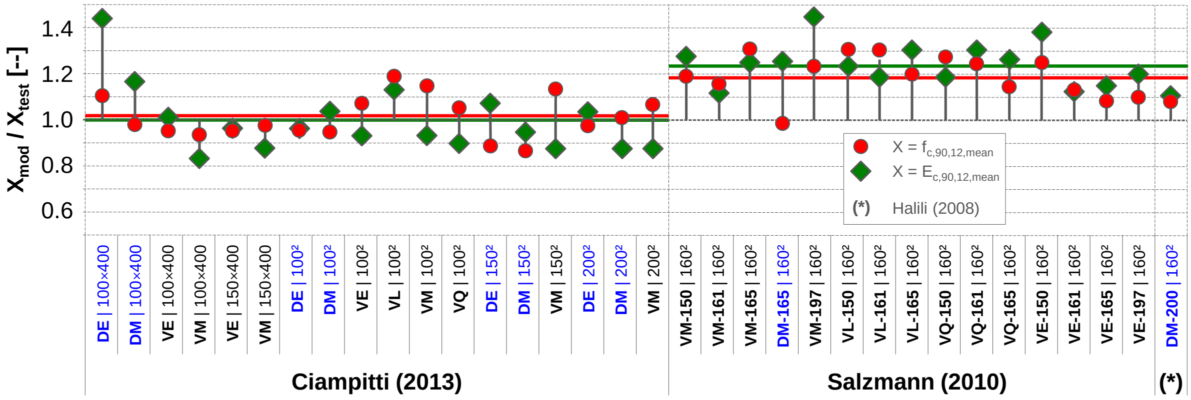

Fig. 5: Comparison between the adapted stress-dispersion model of van der Put (1988) and mean values from testing point- and line-loaded, discretely or continuously supported CLT elements

Overall and in view of the made investigations, **the adapted stress-dispersion model**, based on the works of van der Put (1988, 2008, 2012), presented in Eq. (3) and verified in Fig. 5, **is proposed for estimating the resistance of discretely-loaded and continuously or discretely supported CLT elements against compression perpendicular to grain**.

This model implies, beside a dependency of $k_{c,90}$ on the load and support conditions, also a dependency on the layup of the CLT elements. A brief calculation of $k_{c,90}$ for standard layups of CLT floor elements of one CLT producer, focusing on centrically loaded, point supported members ($A_c = 150 \times 150$ mm²), gives values in the range of $k_{c,90} = 1.42$ to 1.84 and 1.75 to 2.12 for five and seven layers (also comprising double layers), respectively. Thus, **consideration of the layup is mandatory for an economical design of CLT structures in compression perpendicular to grain**.

4.4 Some Comments on the Evaluation of the Mechanical Properties

The procedure for calculating $f_{c,90}$ and $E_{c,90}$ currently anchored in EN 408:2012 requires an iterative optimisation process. This is because of fixed limits of 10 and 40 % of $F_{c,90,\max}$, whereby $F_{c,90,\max}$ is defined by notation as the intersection point of the force-deformation curve with the tangent stiffness evaluated between the mentioned limits and shifted by 1 % of specimens depth. As in our data the 10 % limit is several times exceeded by initial delayed hardening, we applied flexible limits for calculation of $E_{c,90}$, optimised by optical judgement for maximising the approximately linear part of the stress-strain curve and controlled quantitatively by $r \geq 0.999$. Consequently, an iteration procedure is not required. However, the relative change of $E_{c,90}$ from measurement increment to increment, as shown in Fig. 1 (right), outline the sigmoid, non-linear stress-strain relationship inherent in compression tests made on timber. Missing of a linear part in the stress-strain curve, as indicated by the peak in Fig. 1 (right), motivates a new definition for evaluation of $E_{c,90}$, mathematically meaningful as the tangent E-modulus at the inflexion point of the stress-strain curve. Because of noise in the recorded data, in our tests with a measurement rate of 5 Hz, filtering and smoothing is required. Taking this as an outlook further investigations and progress in defining an adequate filtering and smoothing procedure are envisaged.

4.5 Share of Plasticity in the Non-Linear Part of the Stress-Strain Curve

We determined the depth of each specimen of some test series at approximately u = 12 % before testing and after reaching equilibrium moisture content of approximately 12 % in a climate chamber, stored after conducting the oven dry method. Knowing exactly the deformation at the end of each test, we calculate (i) the total strain, (ii) the elastic and (iii) plastic strain. Following test series are involved: DE | 100²; DM | 100², 150²; VE | 100²; VL | 100²; VM | 100²; VQ | 100² and tests on cubic specimens with A_c = 150² (u = 12.7 %) and 200² mm². On average, a total strain of 4.7 % is applied on all tests. The average amount of elastic and plastic strain after relaxation is calculated with 1.0 and 3.7 %, respectively. Thus, the 1 % shift of the tangent E-modulus for determination of the compression strength according to EN 408:2012 delivers on average a strength value at the border between elastic and plastic strain, although determined in the non-linear part of the stress-strain curve. However, Kollmann (1957) conducted cyclic tests and observed a reduction in energy and successive hardening in compression perpendicular to grain, dedicated to the viscoelastic properties and successive collapse of the internal microstructure. Although in tests of Ciampitti (2013) only one loop at about 0.5 % strain and a second loop at about 4 % strain are conducted in prism series of A_c = 150 × 150 mm² and u = 8.8 and 15.3 % the principle stress-strain behaviour, reported in Kollmann (1957) and the non-linear elastic share are confirmed, see Fig. 6.

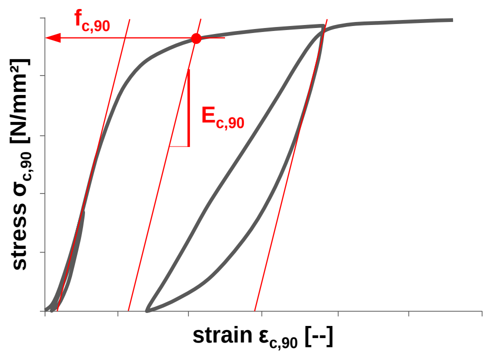

Fig. 6: Stress-strain curve of a prism specimen tested with two hysteresis loops

5 Conclusions

We analysed tests of Ciampitti (2013) conducted on discrete (point and line) loaded, continuously or discretely supported CLT elements and on full-surface loaded prisms. The influence of moisture on the compression perpendicular to grain properties is outlined and correction factors of 4 % and 1 % per 1 % Δu for adaptation of $f_{c,90}$ and $E_{c,90}$ proposed. Reference tests on full-surface loaded prisms reflect increasing strength and stiffness properties with increasing surface area A_c whereas the opposite was found for discrete loaded, discretely or continuously supported CLT elements. Reasoning is given and a reference volume for reference compression perpendicular to grain tests for CLT defined, with 150 × 150 × 150 mm³, corresponding to a five-layer CLT element with t_l = 30 mm and a reference board width w_l = 150 mm. Based on the statistics characteristic properties of $f_{c,90,12,\text{prism},k}$ = 3.0 N/mm² (CoV[$f_{c,90,12}$] ≈ 8 %) and $E_{c,90,12,\text{prism,mean}}$ = 400 N/mm² are found.

We comment the examination procedure for $f_{c,90}$ and $E_{c,90}$ currently anchored in EN 408:2012 and give suggestions for adaptation and an outlook for a new definition of $E_{c,90}$ in general. Furthermore, the share of plastic and elastic strain on total strain is discussed and the current regulation of EN 408:2012 concerning the shift of the tangent E-modulus by 1 % strain for determination of $f_{c,90}$ confirmed.

For modelling the resistance of discrete loaded and discretely or continuously supported CLT elements the stress-dispersion model of van der Put (1988, 2008, 2012), defined for linear, unidirectional timber members, is adapted for two-dimensional load transfer in the orthogonal structure of CLT. The model is successfully verified and further proposed for the design of CLT in compression perpendicular to grain using two different stress dispersion angles α_L = 45° and α_T = 15° for longitudinal and transverse direction, respectively, as already anchored in EN 1995-2:2004. The model allows to explain directly differences between (i) load configurations, (ii) support conditions, (iii) composition and thickness of the CLT elements, and (iv) the edge distance a. The formulation for $k_{c,90}$ makes the consideration of the layup mandatory for an economical design of CLT structures in compression perpendicular to grain.

Overall, the outcome of our study is seen as worthwhile for regulations on test data evaluation (EN 408:2012), for anchoring basic properties of CLT stressed in compression perpendicular to grain (EN 16351:2012) and for the design of point and line loaded and continuously or discretely supported CLT elements (EN 1995-1-1:2008 and EN 1995-2:2004).

6 Acknowledgement

The work and progress made by Alessandro Ciampitti (2013) in frame of his Master thesis as well as the provision of testing equipment and technical support of the Laboratory for Structural Engineering at Graz University at Technology in testing are thankfully acknowledged.

7 References

Hasuni HK, Al-douri K, Hamodi MH (2009) **Compression strength perpendicular to grain in cross-laminated timber (CLT)**. Master thesis, School of Technology and Design, Växjö University, Sweden

Augustin M, Ruli A, Brandner R, Schickhofer G (2006) **Behaviour of glulam in compression perpendicular to grain in different strength grades and load configurations**. International Council for Research and Innovation in Building and Construction, Working Commission W18 – Timber Structures, Meeting 39, CIB-W18/39-12-6, Florence, Italy

Blaß HJ, Görlacher R (2004) **Compression perpendicular to the grain**. World Conference on Timber Engineering (WCTE), Lahti, Finland, pp6

Bogensperger T, Augustin M, Schickhofer G (2011) **Properties of CLT-panels exposed to compression perpendicular to their plane**. International Council for Research and Innovation in Building and Construction, Working Commission W18 – Timber Structures, Meeting 44, CIB-W18/44-12-1, Alghero, Italy, pp15

Ciampitti A (2013) **Untersuchung ausgewählter Einflussparameter auf die Querdruckkenngrößen von Brettsperrholz**. Master Thesis, Institute of Timber Engineering and Wood Technology, Graz University of Technology, pp133 (in German)

EN 338:2009 **Structural timber – Strength classes**. European Committee for Standardization (CEN

EN 384:2010 **Structural timber – Determination of characteristic values of mechanical properties and density**. European Committee for Standardization (CEN)

EN 408:2012 **Timber structures – Structural timber and glued laminated timber – Determination of some physical and mechanical properties**. European Committee for Standardization (CEN)

EN 16351:2012 **Timber structures – Cross laminated timber – Requirements**. European Committee for Standardization (CEN), draft version

EN 1995-1-1:2006 **Eurocode 5: Design of timber structures – Part 1-1: General – Common rules and rules for buildings**. European Committee for Standardization (CEN)

EN 1995-1-1:2008 + A1 **Eurocode 5: Design of timber structures – Part 1-1: General – Common rules and rules for buildings**. European Committee for Standardization (CEN)

EN 1995-2:2004 **Eurocode 5: Design of timber structures – Part 2: Bridges**. European Committee for Standardization (CEN)

EN 14358:2006 **Timber structures – Calculation of characteristic 5-percentile values and acceptance criteria for a sample**. European Committee for Standardization (CEN)

Forest Products Laboratory (2010) **Wood Handbook – Wood as an Engineering Material**. General Technical Report FPL-GTR-190, Madison, WI: U.S. Department of Agriculture, Forest Service, Forest Products Laboratory, 508 p.

Föppl A (1904) **Die Druckfestigkeit des Holzes in der Richtung quer zur Faser**. Mitt. Mechan.-Techn. Lab. D. K. Techn. Hochsch. München, 29–32:7–25 (in German)

Gehri E (1997) **Timber in compression perpendicular to the grain**. International Conference of IUFRO S 5.02 Timber Engineering, Copenhagen, Denmark

Graf O (1921) **Beobachtungen über den Einfluss der Größe der Belastungsfläche auf die Widerstandsfähigkeit von Bauholz gegen Druckbelastung quer zur Faser**. *Der Bauingenieur*, 18:498–501 (in German)

Hall CP (1980) **Behaviour of compression perpendicular to grain loading**. Master thesis, University of British Columbia, Vancouver, B.C.

Halili Y (2008) **Versuchstechnische Ermittlung von Querdruckkenngrößen für Brettsperrholz**. Diploma Thesis, Institute of Timber Engineering and Wood Technology, Graz University of Technology, pp179 (in German)

Hoffmeyer P, Damkilde L, Pedersen TN (2000) **Structural timber and glulam in compression perpendicular to grain**. *Holz als Roh- und Werkstoff*, 58:73–80

Kollmann F (1957) **Über Unterschiede im rheologischen Verhalten von Holz und Holzwerkstoffen bei Querdruckbelastung**. *Forsch. Ing.-Wes.*, 23(1/2):49–54 (in German)

Kollmann F (1959) **Zur Frage der Querdruckfestigkeit von Holz**. *Holzforschung und Holzverwertung*, 11(5):109–121 (in German)

Korin U (1990) **Compression perpendicular to grain**. International Council for Research and Innovation in Building and Construction, Working Commission W18 – Timber Structures, Meeting 23, CIB-W18/23-6-1, Lisbon, Portugal

Larsen HJ (1975) **The design of timber beams**. International Council for Research and Innovation in Building and Construction, Working Commission W18 – Timber Structures, Meeting 5, CIB-W18/5-10-1, Karlsruhe, West Germany

Leijten AJM, Jorissen AJM (2010) **Global test standards and code design rules for compressive strength perpendicular to grain**. World Conference on Timber Engineering (WCTE), Riva del Garda, Italy, pp7

Leijten AJM, Jorissen AJM, de Leijer BJC (2012) **The local bearing capacity perpendicular to grain of structural timber elements**. *Construction and Building Materials*, 27:54–59

Madsen B, Hooley RF, Hall CP (1982) **A design method for bearing stresses in wood**. *Canadian Journal of Civil Engineering*, 9:338–349

Ruli A (2004) **Längs und quer zur Faserrichtung auf Druck beanspruchtes Brettschichtholz**. Diploma Thesis, Institute of Timber Engineering and Wood Technology, Graz University of Technology (in German)

Salzmann C (2010) **Ermittlung von Querdruckkenngrößen für Brettsperrholz (BSP)**. Master Thesis, Institute of Timber Engineering and Wood Technology, Graz University of Technology, pp198 (in German)

Serrano E, Enquist B (2010) **Compression strength perpendicular to grain in cross-laminated timber (CLT)**. World Conference on Timber Engineering (WCTE), Riva del Garda, Italy, pp7

van der Put TACM (1988) **Explanation of the embedding strength of particle board**. Stevin Research Report, 25-88-63/09-HSC6, Faculty of Civil Engineering, TU Delft, Netherlands

van der Put TACM (2008) **Derivation of the bearing strength perpendicular to the grain of locally loaded timber blocks**. *Holz als Roh- und Werkstoff*, 66:409–417, DOI 10.1007/s00107-008-0258-0

van der Put TACM (2012) **Restoration of exact design for partial compression perpendicular to the grain**. *Wood Material Science and Engineering*, DOI 10.1080/17480272.2012.681703

INTER

International Network on Timber Engineering Research

ADVANCED MODELLING OF TIMBER-FRAMED WALL ELEMENTS FOR APPLICATION IN ENGINEERING PRACTICE

T Vogt

W Seim

University of Kassel

Department of Structural Engineering

GERMANY

Presented by T Vogt

P Quenneville asked whether the analysis was liner elastic. T Vogt responded no because the nails are yielding. P Quenneville asked whether different wall configurations will lead to different overstrength factors. T Vogt responded that the paper presented in the last CIB W18 meeting in Vancouver showed different overstrength factors for different connectors. Next step could be to develop overstrength factors for all connection types.

F Lam commented that when a wall undergoes reverse cyclic lateral loading the nails could move at an angle to the long axis of the stud. This movement depends on the wall aspect ratio. He questioned whether the presented approach can fully consider this aspect. T Vogt responded that the overstrength factor was defined as the ratio between the mean values of the response and confirmed that for walls with different aspect ratios the overstrength factors established from this approach is valid.

R Brandner received clarification about the position of the holddown devices and their elastic behaviour.

WY Loo questioned about the force displacements in the timber and commented that the use of Cartesian spring pair may work better.

E Serrano further commented that nonlinear coupled springs rather than single springs are needed to consider the behaviour of the nails.

I Smith stated that overstrength factors should be considered for the entire structure rather than for a wall.

A Buchanan commented that cyclic behaviour is important for seismic and asked whether the procedures can handle reverse cyclic. T. Vogt responded that it is not possible yet.

H Blass commented that the differences from values in EC5 are not that big. T. Vogt agreed. W Seim commented that force based design and time history approach are not appropriate for this model. Performance analysis needs push over analysis as an upper bound. The presented approach can provide this information easily.

M Fragiacomo discussed that this type of approach is still missing in Eurocode and suggested that the approach should aim for upper 95th percentile not the mean strength.

Advanced modelling of timber-framed wall elements for application in engineering practice

Tobias Vogt
Werner Seim
University of Kassel, Department of Structural Engineering,
Kurt-Wolters-Straße 3, 34125 Kassel, Germany.

Keywords: timber-frame, light-frame, push-over, load bearing capacity

1 Introduction

A simple method for the calculation of the load-bearing capacity of timber-framed wall elements is the “pure shear” model, which is standardized in *EC5* [1] as “Method A”. Design provisions in Canada [2] and New Zealand [3] use similar procedures. In contrast to *EC5*, the design provisions in Canada and New Zealand include simplified equations to calculate the stiffness of wall elements. The differences comparing calculated values for load-bearing capacity to experimental test results are striking, which is to be expected because the “pure shear” model is based on the lower bound theorem of the theory of plasticity. In any case, when a reliable prediction of the capacity of shear walls is necessary, advanced calculation methods are needed.

Most engineers decide on the force-based design against earthquake impacts using design spectra to estimate the structural behaviour. Moreover, *EC8* [4] allows for an alternative deformation-based design using the capacity spectrum method. This includes a push-over analysis of full buildings, which has to be carried out using nonlinear behaviour for all structural elements. For this, a simple FE model could be helpful to calculate an elastic-plastic behaviour for wall and slab elements.

Modelling of timber-framed wall elements using the method of finite elements might be an option in engineering practice if numerical tools are available and input parameters are comprehensible. Different material behaviour for the single wall components has to be considered for modelling: While the studs, rails and sheathing normally exhibit linear-elastic behaviour, the fasteners are able to reach high plastic deformations. Elastic-plastic behaviour of the fasteners can be modelled using nonlinear spring elements, which connect the studs and rails to the sheathing. Finite element programmes, as used in engineering practice, provide only spring elements with nonlinear behaviour between two nodes in a predefined direction. The definition of beam elements with bilinear or multilinear deformation characteristics might be suitable to overcome this gap.

This paper presents a comparatively simple FE model for advanced modelling of timber-framed wall elements, which provides more accurate results compared to the “pure shear” model according to *EC5*. The model allows irregular wall geometries and different anchoring situations. This model is not limited to scientific studies and can be applied easily in engineering practice. More detailed information and further applications of this model are given by *Vogt* [5].

2 State-of-the-art

The “pure shear” model, which is used in *EC5*, is a simple method to calculate the load-bearing capacity of timber-framed wall elements under horizontal loading. The main simplification is that the studs and rails are not interconnected, which leads to shear forces only in the axial direction of the studs and rails and to pure shear within the sheathing, as Figure 2.1 illustrates.

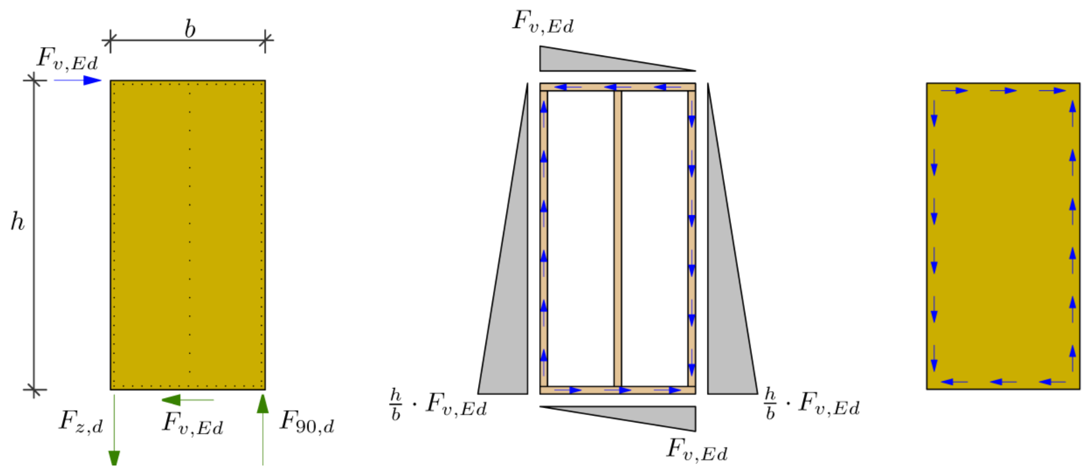

(a) (b) (c)

Figure 2.1: Loading and internal forces of a timber-framed wall element according to the “pure shear” model in EC5; (a) horizontal load and support reactions, (b) and (c) internal forces in studs, rails and sheathing

The capacity of a wall element *i* can be calculated as:

$$F_{v,Rd,i} = \frac{F_{f,Rd} \cdot b_i \cdot c_i}{s} \tag{2.1}$$

with

$F_{f,Rd}$	shear capacity of single fastener
b_i	width of wall element
h	height of wall element
s	spacing of fasteners

$$c_i = \begin{cases} 1 & \text{für } b \geq h/2 \\ \dfrac{b}{h/2} & \text{für } b < h/2 \end{cases}$$

Källsner and Girhammar [6] presented an advanced model also based on the lower bound theorem of the theory of plasticity. This model takes into account different types of anchoring and considers wall elements with openings (see section 5). For this, an effective length of the wall element is calculated. Using the terminology of *EC5*, the equation is:

$$F_{v,Rd} = \frac{F_{f,Rd} \cdot b_{eff}}{s} \tag{2.2}$$

Different procedures for the modelling of timber-framed wall elements have been developed in the last few decades. Some researchers modelled every fastener using two orthogonal so-called non-oriented spring elements (see *Folz and Filiatrault* [7]). This element type has the disadvantage that the non-linear behaviour of the springs is dependent on the angle between force and predefined axes. This leads to an overestimation of capacity and stiffness. *Folz and Filiatrault* solved this problem by the development of the programme “CASHEW”, which increases the distance between the fasteners automatically, according to a calibration on the cyclic testing of fasteners. Other researchers developed oriented spring elements for every fastener, so that the load-displacement behaviour acts along the distance between two defined nodes. *Judd* [8] and *Judd and Fonseca* [9], for example, developed special subroutines which could be implemented in the commercial software *ABAQUS*. Both types of spring elements – oriented and non-oriented – were used predominantly for cyclic behaviour. Therefore, the calibration of parameters is always based on the cyclic testing of connections.

Condensed spring elements for modelling the cyclic behaviour of single wall elements by one or two springs have been developed for the calculation of full building structures (for example, *Folz and Filiatrault* [7] or *Xu and Dolan* [10]). This “single degree of freedom” or diagonal spring elements, which represent the load-displacement behaviour of a full wall element, have to be calibrated by tests on wall elements.

All these methods have an important disadvantage: They can be perfect solutions for research, but are not adoptable in engineering practice. This is because the engineering programmes do not contain the types of spring elements needed and tests on connection units or wall elements are necessary for calibration.

3 Simplified nonlinear FE Model

3.1 Discretization and element types

Figure 3.1 shows the structure of the FE model with all components of a typical wall element. The studs and rails are modelled with two-node beam elements, while the sheathing consists of four-node shell elements. The VM elements represent the fasteners and consist of two-node beam elements with elastic-plastic material behaviour, while studs, rails and sheathing remain elastic.

Mean values for E- and G-modulus according to standards and technical approvals are applied for the linear-elastic behaviour of the timber and sheathing elements. The VM elements are modelled with real parameters for diameter and tensile strength of the steel.

The support conditions are modelled with non-linear orthogonal springs, which consider the load-displacement behaviour of the anchoring elements under tensile and compression stresses. Moreover, vertical loading can be applied on the top rail.

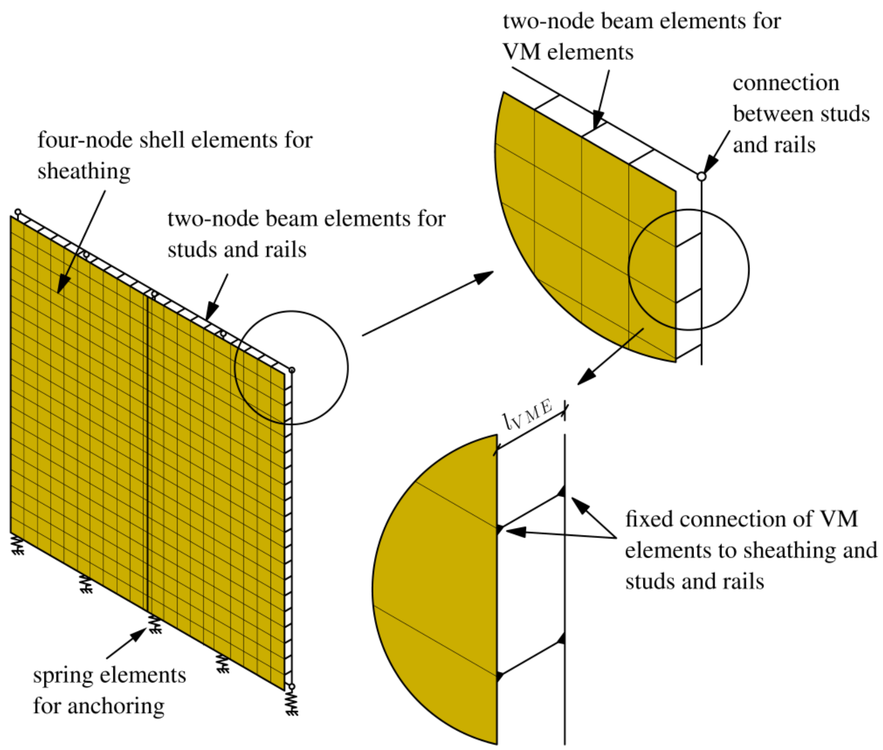

Figure 3.1: Structure of FE model and element types

3.2 Parameter of VM elements

Figure 3.2 shows the static system, the section forces and the deformations of one VM element.

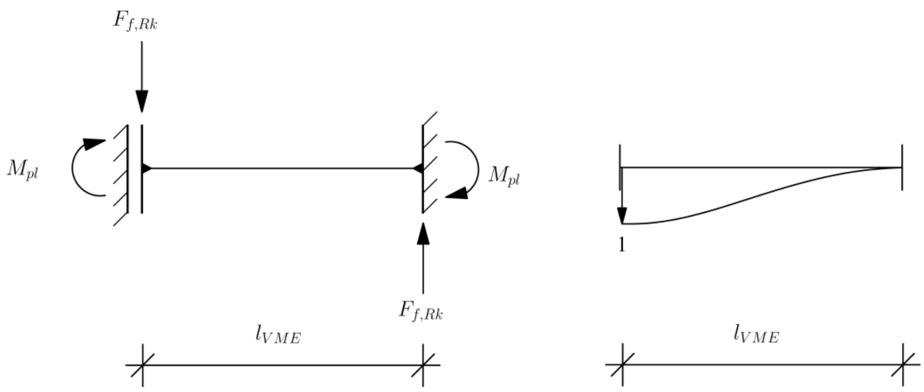

Figure 3.2: Static system, section forces and deformation of VM elements

Plastic hinges on both ends occur when the yielding stress for the steel is reached. The full plastic moment M_{pl} is dependent on the diameter d and the tensile strength f_u:

$$M_{pl} = \frac{1}{6} \cdot f_u \cdot d^3 \tag{3.1}$$

When the shear strength $F_{f,Rk}$ is calculated according to *EC5*, then the length l_{VME} of the fasteners can be determined to:

$$l_{VME} = \frac{2 \cdot M_{pl}}{F_{f,Rk}} \tag{3.2}$$

While the VM element uses the full plastic moment M_{pl} for calculation, it must be pointed out that the shear strength $F_{f,Rk}$ according to *EC5* takes into account the characteristic yield moment $M_{y,Rk}$.

The stiffness of the VM element is highly overestimated if only the E-modulus of steel is taken into account. In addition to the deformations of the fasteners, there are considerable deformations in the timber elements due to embedment. This and a possible slip result in a reduced stiffness. Because of that, the stiffness factor s_l is implemented:

$$s_l = \frac{K \cdot l_{VME}^3}{12 \cdot EI} \tag{3.3}$$

Using K_{ser} according to *EC5* as K is recommended.

According to safety definitions, the mean value of the capacity of connections $F_{f,m}$ is higher than $F_{f,Rk}$ according to *EC5* or other calculation methods (see *Schick et al.* [11]). Over-strength can be calculated directly from test results and applied to the FE model by the over-strength factor r_s, which increases the tensile strength of the VM element:

$$r_s = \frac{3 \cdot F_{f,m} \cdot l_{VME}}{f_u \cdot d^3} \tag{3.4}$$

If a specific number of fasteners are modelled by only one VM element, the diameter d of the VM element can be calculated as:

$$d^* = \sqrt[3]{n \cdot d_1^3} \tag{3.5}$$

Based on this equivalent diameter d^* and the number of fasteners modelled n, the moment of inertia I, the stiffness K and the stiffness factor s_l (see equation 3.3) have to be adjusted. The calculation of the parameters for the VM element will be illustrated in section 4.2.

4 Validation

4.1 Test set-up of wall elements for validation

Table 4.1 shows the configuration of four out of five test series on 20 full-scale wall elements. The dimensions of the walls were 2.50 m × 2.50 m, and the spacing between the studs (140 mm × 60 mm) was 625 mm. Dimensions of the bottom and top rail were 140 mm × 85 mm. The layout of the walls is documented in Figure 4.1. The vertical load was applied at first and kept constant during the test. A horizontal load was transferred to the top rail and the walls were anchored with two hold-downs (HTT22, SIMPSON-StrongTie) on each side of the wall. Horizontal deformations were blocked by two steel plates in front of the two end faces of the bottom rail. More detailed information is presented in *Vogt et al.* [12] and *Seim and Vogt* [13].

Table 4.1: Configurations of wall elements for FE modelling

	A01	**A02**	**A03**	**A04**	**A05**	**A06**
tests	WL-3.3[c1] WL-3.4[c2]	WL-5.3[c1] WL-5.4[c2]	WL-3.1[c1] WL-3.2[c2]	WL-5.1[c1] WL-5.2[c2]	WL-1.1[m] WL-1.2[c1] WL-1.3[c1] WL-1.4[c2]	WL-2.1[m] WL-2.2[c1] WL-2.3[c1] WL-2.4[c2]
sheathing	1 × osb 18 mm	1 × gfb 18 mm	1 × osb 10 mm	1 × gfb 10 mm	2 × osb 18 mm	2 × gfb 18 mm
fasteners Ø - length, spacing [mm]	nails 2.8-65 75 mm	staples 1.53-55 75 mm	nails 2.8-65 75 mm	staples 1.53-55 75 mm	nails 2.8-65 75 mm	staples 1.53-55 75 mm

[m] monotonic; [c1] cyclic according to ISO21581 [14]; [c2] cyclic according to CUREE [15]

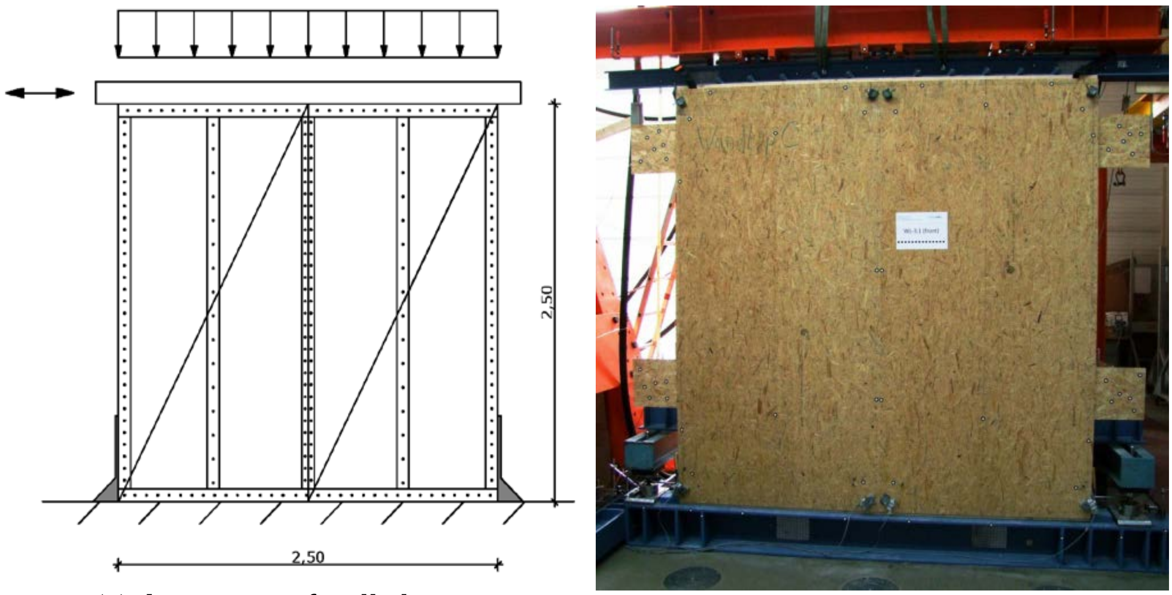

(a) dimensions of wall element *(b) test set-up*

Figure 4.1: Tests on timber-framed wall elements

4.2 Parameters of FE model

Table 4.2 shows the input data for FE modelling and the parameters of the VM elements, which were calculated according to equations 3.1 to 3.4. For wall configurations with staples, all parameters of the VM-elements are specified for only one shank. The mean values of the density ρ_m were calculated by 1.1 × ρ_k for osb-panels and by 1.0 × ρ_k for gfb-panels. The spring elements for support conditions were defined according to test results on anchoring units (see [16]) and used K_t = 11150 N/mm for tensile forces and K_c = 145600 N/mm for compression forces. The resulting load-displacement curves were compared with the envelopes of the hysteresis behaviour (see Fig. 4.2).

Table 4.2: Input data, calculated values and parameters of VM-elements

	remarks	**A01/A05**	**A02/A06**	**A03**	**A04**
d [mm]	fastener	**2.8**	**1.53**	**2.8**	**1.53**
l [mm]	fastener	65	55	65	55
$f_{u,k}$ [N/mm²]		**600**	**900**	**600**	**900**
E [N/mm²]		**200000**	**200000**	**200000**	**200000**
t [mm]	sheathing	**18**	**18**	**10**	**10**
t_{pen} [mm]	l - t	47	37	55	45
$\rho_{m,sh}$ [kg/m³]	sheathing	605	1150	605	1150
$\rho_{k,ti}/\rho_{m,ti}$ [kg/m³]	timber	350/420	350/420	350/420	350/420
M_{pl} [Nmm]	(eq. 3.1)	2195	537	2195	537
$M_{y,k}$ [Nmm]	8.14/8.29 *EC5*	2617	725	2617	725
I [mm^4]		3.017	0.269	3.017	0.269
$f_{h,1,k}$ [N/mm²]	8.22 *EC5/ ETA-03/0050*	42.21	70.07	39.80	41.29
$f_{h,2,k}$ [N/mm²]	8.16 *EC5*	21.07	25.26	21.07	25.26
β [-]	8.8 *EC5*	0.499	0.361	0.529	0.612
$f_{ax,k}$ [N/mm²]	8.25 *EC5*	2.45	2.45	2.45	2.45
$F_{ax,Rk}$ [N]	8.24a *EC5*	322	139	377	169
$F_{f,Rk}$ [N]	8.6 *EC5*	819	365	634	305
K_{ser} [N/mm]	Tab. 7.1 *EC5*	859.5	160.9	859.5	160.9
$F_{f,m}$ [N]	from testing	1110	670	1109	500
l_{VME} [mm]	(eq. 3.2)	**5.36**	**2.94**	**6.92**	**3.52**
s_l [-]	(eq. 3.3)	**0.0183**	**0.0063**	**0.0393**	**0.0109**
r_s [-]	(eq. 3.4)	**1.355**	**1.833**	**1.745**	**1.638**

4.3 Results and conclusions

The following conclusions can be drawn when comparing the load-displacement behaviour of the FE model with test results:

- The FE models using characteristic values reach ca. 15% higher values than calculated according to *EC5*. Additional studies showed that this results from the consideration of the connections between the studs and rails.
- The characteristic values according to *EC5* show about 40% lower values compared to test results, while the FE model using characteristic values results in about 30% lower values.
- If over-strength values are derived directly from sample testing, then the prediction from calculation and results from experimental testing are very close (-8% to +13%). The load-bearing capacity is overestimated about 38% only for gfb-sheathing on both sides.

- While the FE model overestimates the stiffness for osb-sheathed walls with nails using K_{ser} according to *EC5* for the initial stiffness of the fasteners, the stiffness for gfb-sheathed wall elements with staples is underestimated with K_{ser} of staples.

(a) 1x osb-18 mm *(b) 1x gfb-18 mm*

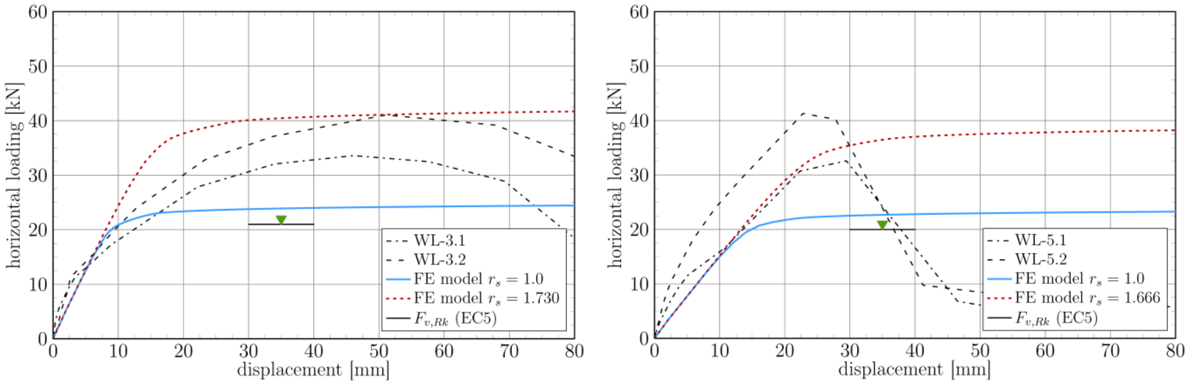

(c) 1x osb-10 mm *(d) 1x gfb-10 mm*

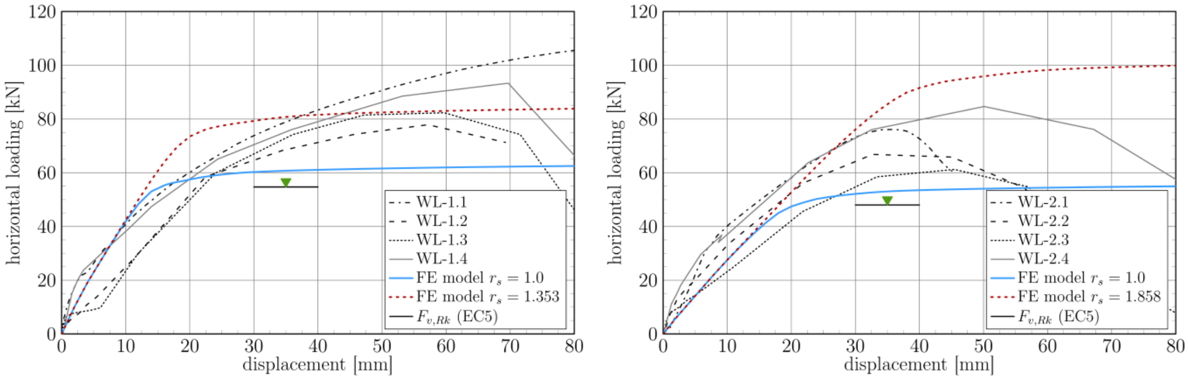

(e) 2x osb-18 mm *(f) 2x gfb-18 mm*

Figure 4.2: Comparison of load-deflection curves – results from modelling and from testing

These results show that the FE model presented is suitable for the calculation of the load-displacement behaviour of timber-framed wall elements under monotonic loadings. Using over-strength factors for the capacity of the fasteners directly from sample testing, the FE model provides values for the load-bearing capacity which are very close to the test results. When characteristic values for the fasteners were taken into account, the load-bearing capacity of the wall element reached more reasonable values than method A from *EC5*. Moreover, the stiffness reached good agreement with the test results, even when K_{ser} for staples seems to underestimate the stiffness of the fasteners.

5 Application

When timber-framed wall elements in *EC5* are calculated using the "pure shear" model, which is based on the lower bound theorem of the theory of plasticity (see section 2), then the most important simplifications and rules are as follows:

- The studs and the rails are considered without contact with each other.
- All wall elements have to be anchored using hold-downs for tensile loading of the studs.
- Wall elements with openings are not taken into account.

Källsner et al. [17], [18], [6] expand this method for application on wall configurations with fully anchored bottom rails instead of stud anchoring with hold-downs. Moreover, wall elements with openings and the influence of the vertical loading were taken into account.

In this section, a wall configuration with opening as presented by *Källsner and Girhammar* [6] was used to compare the results from different calculation methods. In a first step (section 5.1), anchoring using hold-downs was considered without an anchoring of the bottom rail. In a second step (section 5.2), the wall had no hold-downs but a fully anchored bottom rail.

Figure 5.1 shows the wall element, consisting of a part 5 m long with four osb-panels and a smaller part below a window opening. The same material parameters as presented for wall configuration A01 in section 4 were chosen (see Tab. 4.1 and 4.2).

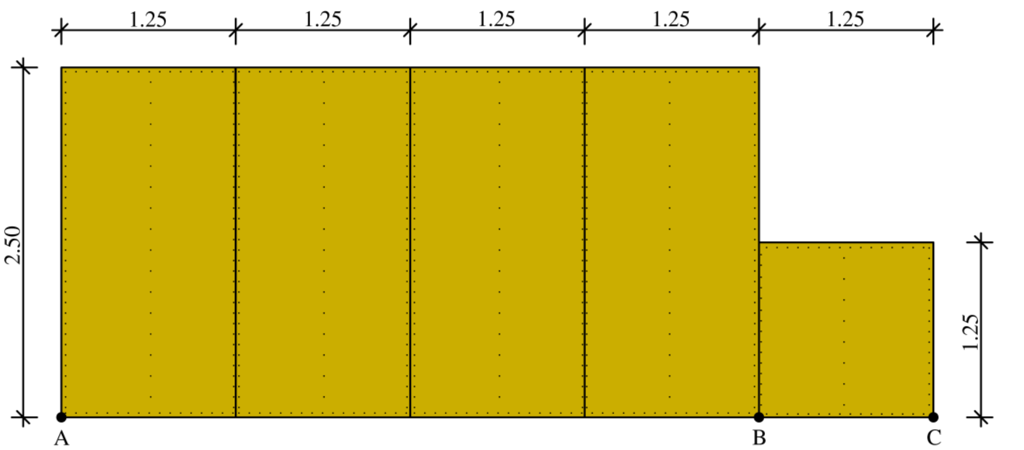

Figure 5.1: Wall element with opening according to Källsner and Girhammar [6]

5.1 Wall element with hold-downs

In order to calculate the load-bearing capacity according to *EC5*, only the wall element without opening is taken into account (b_1 = 5 m):

$$F_{v,Rk,i} = F_{v,Rk,1} = \frac{F_{f,Rk} \cdot b_1 \cdot c_1}{s} \tag{5.1}$$

Figure 5.2 shows the static system and the internal and external loadings of the calculation method according to *Källsner and Girhammar,* where the smaller element is also considered. Here H equals $F_{v,Rk}$ and f_p equals $F_{f,Rk}/s$. Because the stud with tensile loading is anchored with hold-downs, no vertical loads are transferred by the nails between sheathing and bottom rail, so l_1 is zero and l_2 equals 5 m:

$$F_{v,Rk} = \frac{F_{f,Rk}}{s} \cdot \left(\left(\frac{1}{2} \cdot \mu \cdot \alpha_1 + \beta_1 \right) \cdot l_1 + l_2 + \frac{h_l}{h} \cdot l_w \right) \tag{5.2}$$

with

μ = 1.0 (optional factor for loadings perpendicular to the grain)

$\alpha_1 = \frac{l_1}{h} = 0$ ($l_1 = 0$)

$\beta_1 = \sum_{i=0}^{n} \frac{V_i \cdot s}{F_{f,Rk} \cdot h} \cdot \frac{l_1 - s_i}{l_1} = 0$ (no vertical loads are considered)

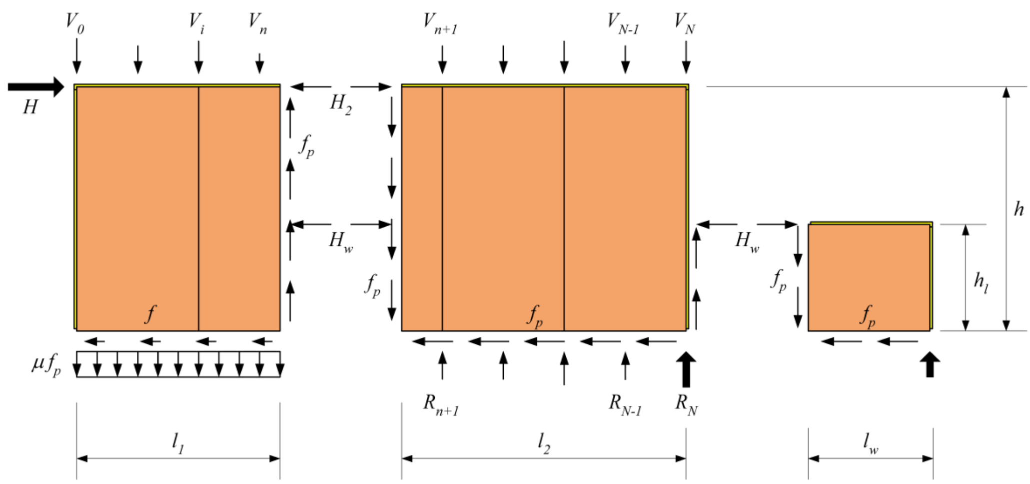

Figure 5.2: Wall element with internal and external loadings according to Källsner and Girhammar (from [6])

The parameters of the VM element in the FE model are given in Table 4.2 (wall configuration A01). Three anchors (A, B and C, see Fig. 5.1) are provided to take tension forces for alternating loading directions.

Figure 5.3 shows a comparison of results according to *EC5*, *Källsner and Girhammar* and the FE model. It can be seen that the consideration of the smaller wall element according to *Källsner and Girhammar* leads to an increase of 13% of the capacity against horizontal loadings. The results of the FE model exhibit 13% higher values compared to *Källsner and Girhammar* and 27% higher values compared to *EC5*. One reason for this is the consideration of the connection between the studs and the rails, as could be seen before in section 4.

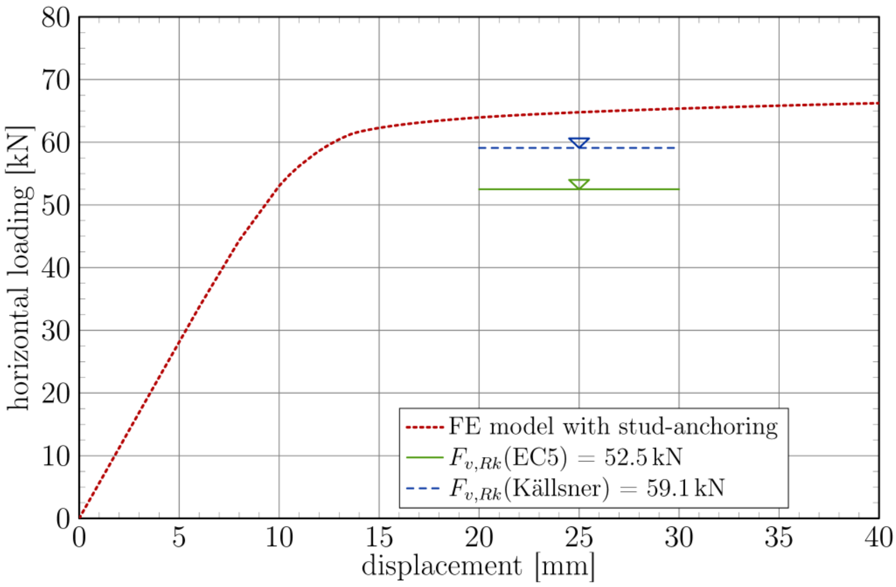

Figure 5.3: Load-bearing capacity with stud-anchoring for different calculation methods

5.2 Wall element with fully anchored bottom rail

In this section, the same wall configuration as presented in section 5.1 was used – only the hold-downs were replaced by a full anchoring of the bottom rail. The same equations as presented in section 5.1 are considered for calculation according to *Källsner and Girhammar*:

$$F_{v,Rk} = \frac{F_{f,Rk}}{s} \cdot \left(\left(\frac{1}{2} \cdot \mu \cdot \alpha_1 + \beta_1 \right) \cdot l_1 + l_2 + \frac{h_l}{h} \cdot l_w \right) \tag{5.3}$$

with

$\mu = 1.0$ (optional factor for loadings perpendicular to the grain)

$$\alpha_1 = \frac{l_1}{h}$$

$$\beta_1 = \sum_{i=0}^{n} \frac{V_i \cdot s}{F_{f,Rk} \cdot h} \cdot \frac{l_1 - s_i}{l_1} = 0 \text{ (no vertical loads are considered)}$$

$$l_1 = \frac{h}{\mu} \cdot (1 - \kappa_1) \text{ with } \kappa_1 = \sum_{i=0}^{n} \frac{V_i \cdot s}{F_{f,Rk} \cdot h} = 0 \text{ (no vertical loads are considered)}$$

It is assumed for the calculation according to *Källsner and Girhammar* that the uplift forces are transferred by the nails between the sheathing and the bottom rail. A vertical connection between the studs with tensile loadings and the bottom rail in the FE model would lead to a similar load flow as an anchoring with hold-downs, so that the uplift forces would be transferred directly from the studs to the bottom rail. Because of that, the vertical connection between the studs with tensile loadings and the bottom rail was removed.

Figure 5.4 shows a comparison of the results according to *Källsner and Girhammar* and to the FE model. It can be seen that the load-bearing capacity is smaller compared to the anchoring with hold-downs for both calculation methods. The maximum load in the FE model is 31% higher compared to the calculated value according to *Källsner and Girhammar*.

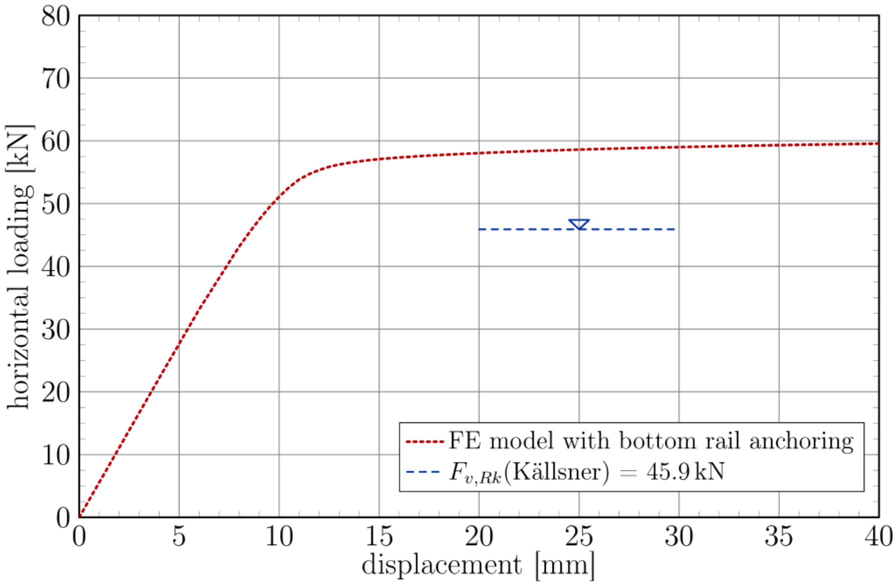

Figure 5.4: Load-bearing capacity with bottom rail anchoring for different calculation methods

6 Summary and outlook

A simple method for an advanced modelling of timber-framed wall elements was presented in this paper. Element types which are used for the studs, rails, nails, and sheathing are provided to be used within commercial FE programmes. The flexibility of the anchoring can be modelled using linear or nonlinear cartesian spring elements.

The model in section 4 was validated based on experimental studies of six different configurations of timber-framed wall elements. The comparison shows a very good accordance when tests on connection units were used to derive over-strength of the connections. The values are about 15% higher compared to the "pure shear" model according to *EC5* [1]. The reason for this is that the FE model, unlike the "pure shear" model, considers the connection between the studs and the rails.

The FE model in section 5 was applied for a wall element with an opening and two different types of anchoring were compared: anchoring of the studs with hold-downs for tensile loadings and a fully anchored bottom rail. The FE model for the configuration with hold-downs resulted in a 27% higher capacity compared to *EC5* and a 13% higher capacity compared to calculation according to *Källsner and Girhammar*. Here, the FE model resulted in 31% higher values compared to *Källsner and Girhammar*.

The results depict that the FE model presented is an efficient tool for calculating the load-bearing capacity and the stiffness of timber-framed wall elements. Because it can be easily applied in engineering practice, it could be a suitable alternative to the calculation methods in *EC5* for timber-framed wall elements.

Further studies should analyse the local stresses and strains in the single components to locate critical points of the wall elements, especially when different types of anchoring and openings are taken into account.

7 References

[1] EN 1995-1-1: *Eurocode 5: Design of timber structures – Part 1-1: General – Common rules and rules for buildings; EN 1995-1-1:2004/AC:2006*. June 2006.

[2] CSA 086-09: *Canadian Standards Association (CSA). Engineering design in wood, Standard 086-09, CSA, Toronto, Canada.* 2010.

[3] NZS 3603: *Timber Structures Standard, Standards New Zealand, Wellington*. 1993.

[4] EN 1998-1: *Eurocode 8: Design of structures for earthquake resistance – Part 1: General rules, seismic actions and rules for buildings*. December 2004.

[5] VOGT, T.: *Entwicklung eines Berechnungsmodells zur Beschreibung des Trag- und Verformungsverhaltens von Holzrahmenwänden unter Berücksichtigung lokaler Effekte*. Dissertation, University of Kassel, In preparation.

[6] KÄLLSNER, B.; GIRHAMMAR, U.A.: *A plastic design method for incompletely anchored wood-framed wall diaphragms*. World Conference on Timber Engineering, 2006.

[7] FOLZ, B.; FILIATRAULT, A.: *Cyclic analysis of wood shear walls*. Journal of Structural Engineering, 127(4):433–441, 2001.

[8] JUDD, J.P.: *Analytical modeling of wood-frame shear walls and diaphragms*. Master's thesis, Brigham Young University, 2005.

[9] JUDD, J.P.; FONSECA, F.S.: *Analytical model for sheathing-to-framing connections in wood shear walls and diaphragms*. Journal of Structural Engineering, 131(2):345–352, 2005.

[10] XU, J.; DOLAN, J.D.: *Development of a wood-frame shear wall model in Abaqus*. Journal of Structural Engineering, 135(8):977–984, 2009.

[11] SCHICK, M.; VOGT, T.; SEIM, W.: *Connections and anchoring for wall and slab elements in seismic design*. CIB-W18 Paper, 46–15–4ff, 2013.

[12] VOGT, T.; HUMMEL, J.; SEIM, W.: *Timber framed wall elements under cyclic loading*. World Conference on Timber Engineering, July 2012.

[13] SEIM, W.; VOGT, T.: *OPTIMBERQUAKE: Deliverable 2B – Timber-framed wall elements – monotonic and cyclic testing*. , Building Rehabilitation and Timber Engineering, University of Kassel, 2012.

[14] ISO 21581: *Timber structures – Static and cyclic lateral load test method for shear walls*, 2010.

[15] KRAWINKLER, H.; PARISI, F.; IBARRA, L.; AYOUB, A.; MEDINA, R.: *Development of a Testing Protocol for Woodframe Structures*. CUREE Publication No. W-02, 2001.

[16] SEIM, W.; HUMMEL, J.; VOGT, T.: *OPTIMBERQUAKE: Deliverable 2C – Anchoring units – monotone and cyclic testing*. , Building Rehabilitation and Timber Engineering, University of Kassel, 2012.

[17] KÄLLSNER, B.; LAM, F.: *Diaphragms and shear walls*. Timber Engineering STEP 3, 15/1–15/16, 1995.

[18] KÄLLSNER, B.; GIRHAMMAR, U.A.; WU, L.: *A simplified plastic model for design of partially anchored wood-framed shear walls*. CIB-W18 Paper, 34–15, 2001.

INTER

International Network on Timber Engineering Research

A BUCKLING DESIGN APPROACH FOR ‘BLOCKHAUS’
TIMBER WALLS UNDER IN-PLANE VERTICAL LOADS

C Bedon
M Fragiacomo
Department of Architecture, Design and Urban Planning, University of Sassari

C Amadio
Department of Engineering and Architecture, University of Trieste

A Battisti
Rubner Haus Spa, Chienes

ITALY

Presented by M Fragiacomo

H Blass asked which shear modulus was considered for G and whether the rolling shear modulus should be considered and would it make a difference. M Fragiacomo agreed that the rolling shear modulus could be used and would make a difference. He also stated that a static friction coefficient μ of 0.2 was used initially but the results were different. There were discussions that the existence of gaps between the layers could decrease the bending stiffness assumed in the model. M Fragiacomo responded that the model is isotropic with smeared results. S Svensson commented that the longitudinal stiffness does not influence the lateral capacity. A Fragiacomo further discussed some of the assumptions in the FE analysis in terms of the interaction between logs and their contacts.

P. Quenneville suggested that half walls to be considered.

G Doudak and M Fragiacomo discussed the issues of modeling elastoplastic buckling, geometric nonlinearity and material nonlinearity. M Fragiacomo stated that the static friction coefficient μ was taken to reflect the mean response. R Tomasi commented that the model for buckling with contribution of torsional and movement out of plane was available in previous paper. M. Fragiacomo added that calibration factors were used in the model.

P Dietsch commented that the geometric eccentricity of L/400 in EC5 applies to one member not a wall with multiple members. Loads will shift in lumber and L/400 may be low for the wall system.

A buckling design approach for 'Blockhaus' timber walls under in-plane vertical loads

Chiara Bedon, Massimo Fragiacomo
Department of Architecture, Design and Urban Planning, University of Sassari, Italy

Claudio Amadio
Department of Engineering and Architecture, University of Trieste, Italy

Annalisa Battisti
Rubner Haus Spa, Chienes, Italy

Keywords: timber log-walls, buckling, analytical models, finite-element numerical modelling, full-scale buckling experiments, buckling design approach.

1 Introduction

Blockhaus systems represent a traditional construction technology where structural resistance is attained by direct contact between multiple timber surfaces obtained via carvings, notches, and ancient corner joints. Although this technology is frequently used in practice for the construction of buildings (Fig.1), due to the complexity of various phenomena (loading perpendicular to the grain, effect of friction, influence of gaps in the joints, creep, etc.), their structural behaviour under specific loading/boundary conditions is not completely known. The interaction between multiple logs, as well as the restraint effectiveness of carpentry timber joints and the anisotropy of timber, can strongly affect the load-carrying capacity of these structural systems [1][2][3][4]. The paper focuses on the assessment of the typical buckling behaviour and resistance of vertically compressed timber-log walls. The effects of various mechanical and geometrical variables such as possible geometrical imperfections, openings (e.g. doors or windows), fully flexible or in-plane rigid inter-storey floors are investigated by means of refined finite-element (FE) numerical models [5] validated on experimental results. Comparisons with analytical solutions are presented and critically discussed, in order to assess the applicability of existing formulations to *Blockhaus* structural systems. Finally, a simplified design approach suitable for implementation in the new Eurocode 5 is proposed for the stability check of timber log-walls under in-plane compressive loads.

2 *Blockhaus* structural systems under in-plane vertical loads

The traditional $H \times L$ *Blockhaus* log-wall is typically obtained by assembling a series of spruce logs with strength class C24 according to EN338 [6] (Fig.1 [7]). These logs have slender $b \times h$ cross-sections ($h/b \approx 1.6\text{-}2.4$) characterized by small notches and protrusions able to provide interlocking between the overlapping logs (Fig.1b). The structural interaction between perpendicular walls is then provided by appropriate corner joints (Figs.1c-1d). Permanent and further imposed gravity loads are transferred onto each main wall by the inter-storey floors (Fig.1e), which typically realize an in-plane rigid diaphragm (e.g. by using OSB panels and timber joists, or glulam panels arranged on their edges) able to prevent the out-of plane deflections of the wall top logs.

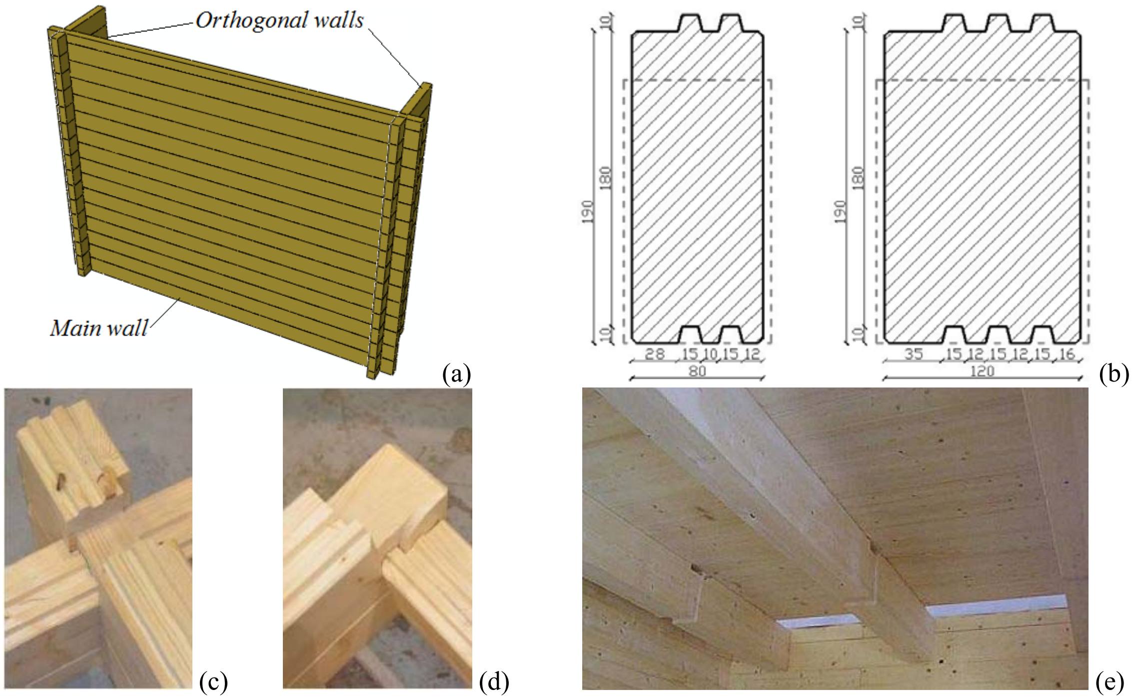

Fig.1. Examples of *Blockhaus* structural components. a) main log-wall; b) 'Tirol' (left) and 'Schweiz' (right) cross-sections of timber logs produced by Rubner Haus AG SpA [7] (dimensions in mm; solid and dashed lines denote currently and previously manufactured cross-sections, respectively);
c) 'Standard' and d) 'Tirolerschloss' corner joints; e) typical inter-storey floor.

The very low modulus of elasticity (MOE) of timber perpendicular to grain makes the typical *Blockhaus* wall susceptible to buckling phenomena - unlike other structural systems such as masonry or concrete walls. Combined to possible load eccentricities, particular geometrical configurations (e.g. large size walls with door and window openings closed to each other and/or to the end of the wall) and geometrical imperfections (e.g. initial curvature of the wall) could have unfavourable effects on the load-carrying capacity of the studied log-walls, hence requiring careful consideration in their design and verification.

2 Existing analytical models

2.1 Fully flexible inter-storey floors (FF)

Few studies have been dedicated to the assessment of the buckling behaviour of timber log-walls under in-plane vertical loads. Buckling experiments on (1:4) and (1:1.4)-scaled specimens made of spruce with various geometrical configurations (no openings; single door opening; door and window openings) are discussed in [8][9]. The specimens were scaled to reproduce the geometry of H= 2.5m tall and L= 3.5m or 4.5m wide log-walls (with a= 0.60m and b/h= 10/17 cm the nominal cross-section of logs, Fig.2). No restraints were introduced at the top of the main log-wall (Fig.2), however, hence suggesting the presence of a fully flexible (FF) inter-storey floor. Based on this experimental investigations (detailed discussion of test results is provided in [8][9]), Heimeshoff and Kneidl proposed an analytical formulation for the buckling design of log-walls, in accordance with the safety rules of DIN1052 standards [10]. Specifically, for $H \times L$ timber log-walls without openings, the critical buckling load could be estimated as:

$$N_{cr,0}^{(E)} = \frac{E_{||} b^3 h^2}{L^3} + 0.8 \frac{G b^3}{L}, \qquad (1)$$

being $b \times h$ the cross-sectional dimensions of logs, with $E_{||}$ and G the MOE in the direction parallel to the grain and the longitudinal shear modulus of timber, respectively.

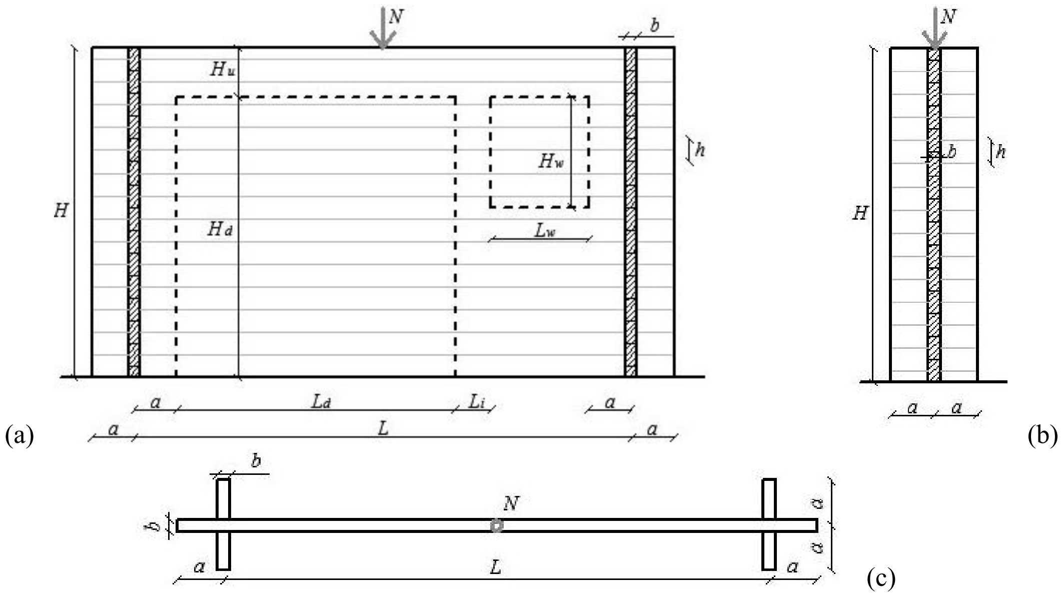

Fig.2. Geometrical properties of (1:4) and (1:1.4)-scaled specimens tested in [8][9].
a) front view; b) lateral view; c) top view.

In the case of log-walls with single openings (e.g. $H_d \times L_d$ door, Fig.2a) or double openings (e.g. $H_d \times L_d$ door and $H_w \times L_w$ window, Fig.2a), the critical buckling load should be respectively calculated as [8, 9]:

$$N_{cr,0}^{(E)} = 0.8 \frac{Gb^3}{L} \left[\frac{H_u}{H} + \frac{H_d}{H} \frac{L - L_d}{L} \right] \tag{2}$$

and

$$N_{cr,0}^{(E)} = 0.8 \frac{Gb^3}{L} \left[\frac{H_u}{H} + \frac{H_d}{H} \frac{L - (L_d + L_i + L_w)}{L} \right] + \pi^2 E_{\perp} \frac{L_i b^3}{48 H^2}, \tag{3}$$

with $E_{\perp}$ signifying the MOE in the direction perpendicular to grain, while the dimensions L_d, L_w and L_i are given in Fig.2a. As highlighted in [8][9], Eqs.(1)-(3) can only roughly estimate the Euler's critical load of a log-wall under in plane vertical load, therefore, based on test results, Heimeshoff and Kneidl introduced a safety factor γ_M resulting in a design buckling resistance:

$$N_{b,Rd} = \frac{N_{cr,0}^{(E)}}{\gamma_M} = \frac{N_{cr,0}^{(E)}}{3.5}. \tag{4}$$

At the same time, Eqs.(1)-(3) do not take into account the strengthening contribution of inter-storey floors typically used in *Blockahus* structural systems, which could significantly improve the global behaviour of the studied log-walls.

2.2 In-plane rigid inter-storey floors (RF)

Due to the presence of in-plane rigid (RF) inter-storey floors in *Blockhaus* structural systems, it is in fact expected that the in-plane compressed log-walls will resist more than in absence of these additional top restraints. At the same time, the assumption of distributed compressive pressures q of total resultant N rather than mid-span concentrate loads N would typically result in a more realistic loading condition, but also in further increase of the actual critical loads for the same log-walls. In this context, simplified formulations derived from classical theory of plate and column buckling could provide rational estimations of the expected critical loads $N_{cr,0}^{(E)}$. For timber log-walls without openings, formulations could be taken from the classical theory of thin plates restrained along the four edges and subjected to in-plane uniformly distributed pressures q [11]. This approach would allow the implementation of the top restraint offered by in-plane rigid floors. Conversely, it would not allow a proper estimation of the interlocking effect between multiple logs, since each timber log-wall would be regarded as '*fully monolithic*', with thickness b, height H, width L and Euler's critical load given by [11]:

$$N_{cr,0}^{(E)} = k_\sigma \frac{\pi^2}{12} \frac{b^3}{L} \frac{E_\perp}{\left(1-\left(\frac{E_\perp}{2G}-1\right)^2\right)}, \tag{5}$$

being $E_\perp$ the average MOE in the direction perpendicular to grain and G the average longitudinal shear modulus. In Eq.(5), k_σ is a buckling coefficient taking into account the effects of various lateral end restraints. Based on the effective clamping restraint provided by orthogonal walls and the adopted corner joints, for practical purposes the coefficient k_σ = f(L/H, *boundaries*) could be rationally set equal to $k_\sigma = 6.97$, like for a panel with fixed unloaded edges and simply supported top-bottom edges [11].

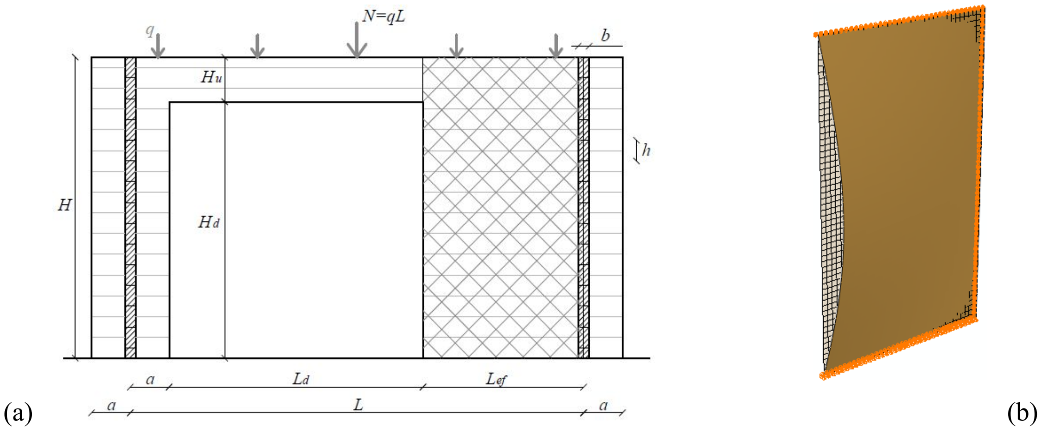

Fig.3. Log-walls with single opening. a) geometry; b) expected buckling shape of the $L_{ef}\times H$ portion.

The same approach, with proper modifications, could be used for an approximate estimation of the critical buckling load of log-walls with single opening. It is in fact expected that their load carrying capacity, with reference to Fig.3, would be strictly related to the buckling resistance of their $L_{ef}\times H$ portion, being L_{ef} the maximum distance between the opening and the lateral restraints of the walls (Fig.3a). Due to the boundary conditions of this portion of wall - namely a free vertical edge and a fixed lateral edge - Eq.(5) could be directly used for a calculation of $N_{cr,0}^{(E)}$, by assuming $L \equiv L_{ef}$ as reference length and $k_\sigma = 1.277$ the corresponding buckling coefficient [11].

In the case of *Blockhaus* walls with double door and window openings, finally, it is expected that their global resistance could depend on the buckling strength of the $b\times L_i\times H_d$ portion comprised between the door and the window (Fig.2a), hence leading to a critical buckling load [11]:

$$N_{cr,0}^{(E)} = \frac{\pi^2 (EJ_{ef})}{\overline{H}^2}, \tag{6}$$

with

$$\overline{H} = 0.7 H_d, \tag{7}$$

the effective buckling length, prudentially estimated as for a clamped-pinned column [11], and

$$EJ_{ef} = E_\perp \frac{b^3 L_i}{12} + 2E_{steel} J_{steel} \tag{8}$$

its flexural stiffness. In Eq.(8), E_{steel} and J_{steel} respectively denote the MOE and second moment of area of steel hollow section profiles usually introduced to reinforce the vertical edges of openings (Fig.4).

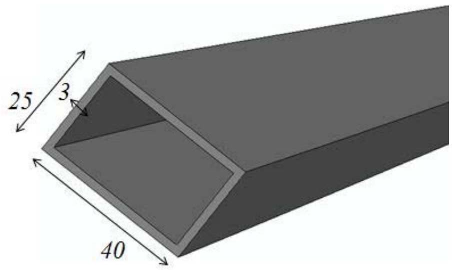

(a)

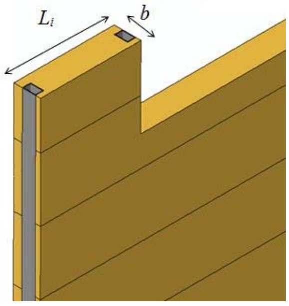

(b)

Fig. 4. Detail of *Blockhaus* walls with double openings. a) steel hollow section profile and b) positioning of the steel profiles along the edges of openings. Dimensions in mm.

It should be noticed, with reference to Eqs.(5)-(6), that the proposed formulations can take into account the strengthening contribution of RF inter-storey floors. In this sense, being not able to describe possible interlocking mechanisms between the overlapping logs, it is expected that Eqs.(5)-(6) will provide an approximate 'upper limit' critical load for *Blockhaus* walls with or without openings. Due to the typical anisotropic behaviour of timber, consequently, as well as the combination of multiple aspects such as possible timber local failure mechanisms in compression, log detachments and initial geometrical imperfections or load eccentricities not explicitly considered in the aforementioned formulation, the effective buckling resistance of the studied walls should be necessarily properly assessed by means of detailed static incremental numerical simulations or full-scale experiments.

3 Extended FE investigation and parametric study

3.1 General numerical approach

In order to perform an extended parametric study on several possible geometrical configurations of technical interest, Finite-Element (FE) models have been implemented in ABAQUS/Standard [5]. The typical Finite-Element (FE) model consists of 8-node, linear brick solid elements with reduced integration (C3D8R), available in the ABAQUS element library. In each simulation, only a single wall has been analyzed (Fig.1a), with appropriate boundary conditions. Restraints have been introduced at the base of each wall (u_x= 0, u_y= 0, u_z= 0) and at the lateral ends of each log. The orthogonal log-walls have been schematized as vertical rollers able to prevent possible out-of-plane and horizontal in-plane displacements of the main walls, hence resulting in linear lateral supports (u_x= 0, u_z= 0). In doing so, the typical geometry of the actual carpentry joints has been taken into account (e.g. contact surfaces between orthogonal logs, Fig.1c), hence the lateral supports effectively resulted in a sort of clamp restraints able to prevent rotations, rather than in simple rollers. Based on earlier works [3], each timber log has been preliminary described with a regular $b \times h$ cross section and the small protrusions along the top and bottom surfaces of logs have been neglected (Fig.1b). Finally, suitable surface-to-surface contact algorithms have been used, to properly describe the mechanical interaction between logs. Possible tangential slidings have been allowed between them (*tangential behaviour*), being μ= 0.5 the static friction coefficient obtained from earlier friction experiments [3]. The possible detachment of logs in the direction perpendicular to the contact surfaces has also been allowed (*normal behaviour*). Concerning the mechanical characterization of timber, C24 spruce has been preliminary described as an isotropic, linear elastic material having density ρ= 420kg/m^3, average MOE $E \equiv E_\perp$= 370MPa and average shear modulus G= 500MPa.

3.2 Assessment of FE-models and modelling assumptions

3.2.1 Inter-storey floors

First of all, the actual restraint provided by inter-storey floors in *Blockhaus* structural systems has been numerically investigated. Linear buckling analyses have been performed in ABAQUS/Standard on a FE-model able to reproduce the effective geometry of a typical floor under uniformly distributed loads (Fig.5a), as well as its connection between the supporting main walls.

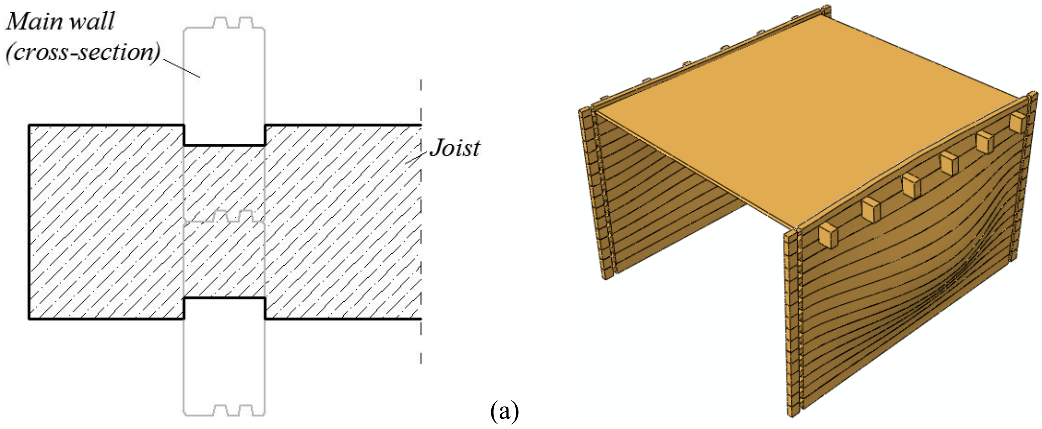

(a) (b)

Fig.5. Example of inter-storey floor in *Blockhaus* structural systems. a) vertical cross-section of joist-to-wall connection; b) buckled modal shape under gravity load (ABAQUS).

Simulations confirmed the diaphragm effect of the adopted floors. The fundamental buckled shape displayed in Fig.5b, for example, refer to a 4m wide × 2.945m high *Blockhaus* wall with 'Tirol' logs and without openings. The obtained modal shape suggests the correctness of the RF restraint assumption, numerically described in the form of continuous simple supports along the top logs of each wall. As a result, further numerical studies have been carried out by taking into account the RF condition only. At the same time, static incremental buckling simulations have been performed, being more accurate than linear buckling analyses and able to provide detailed information for the whole load-deformation behaviour of walls up to failure.

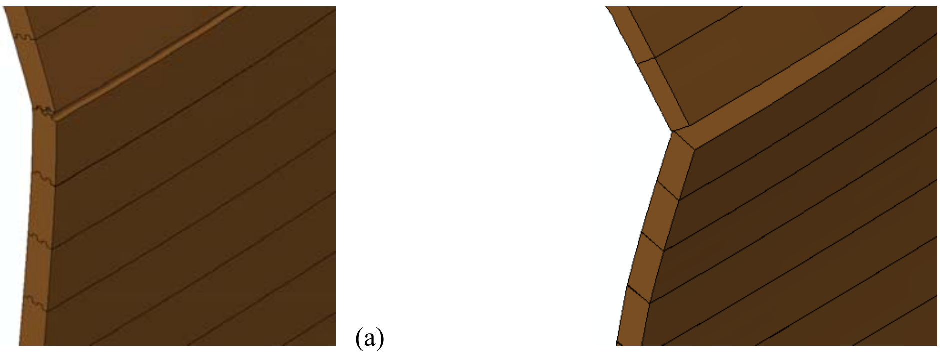

(a) (b)

Fig.6. Effect of geometrical description of $b \times h$ cross section logs, with (a) and without (b) protrusions, on the buckling behaviour of *Blockhaus* walls, deformed shape from ABAQUS.

3.2.2 Geometrical description of logs

Further assessment of FE-models has been carried out for the geometrical description of timber logs. Simulations have been performed on a same *Blockhaus* wall with rectangular $b \times h$ cross section of logs with and without their typical protrusions along the top and bottom surfaces (Fig.1b). A load eccentricity e_{load}= 4cm= $b/2$ was considered in all analyses. Notches and protrusions generally resulted in partial improvement of interlocking between logs (e.g. detail of Fig.6), hence in almost identical stiffness and ultimate buckling resistance for the studied walls (e.g. Fig.7). Consequently, the assumption of geometrically simplified $b \times h$ timber logs was preferred and justified by the markedly improved computational efficiency of these FE-models, compared to the more geometrically refined ones.

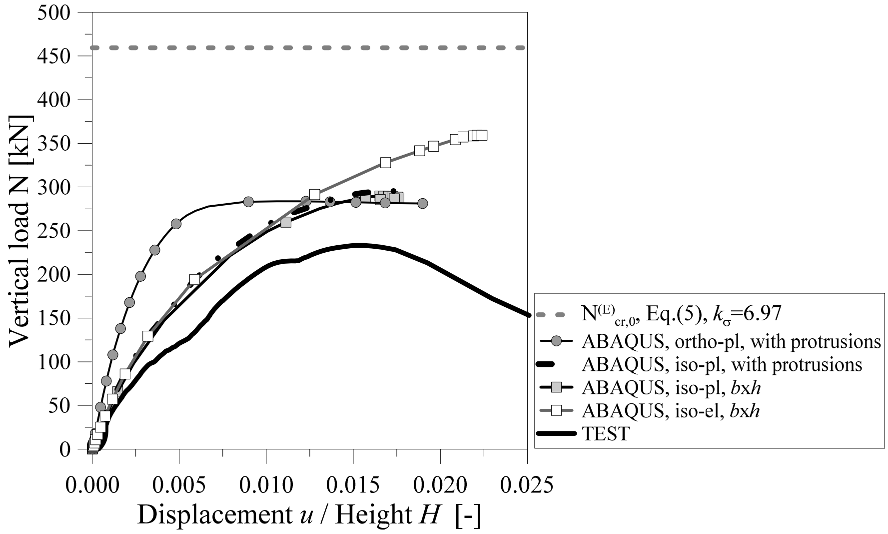

Fig.7. Preliminary analyses. Influence of geometrical description of $b \times h$ cross section logs, timber anisotropy and plasticity in compression. Log-wall: L=4m, H= 2.945m, 'Tirol' logs (load eccentricity e_{load}=4cm=b/2).

3.2.3 Mechanical characterization of timber

The mechanical characterization of timber was successively assessed, in order to investigate the possible effects of its typical anisotropy, as well as of possible local failure mechanisms in compression (e.g. crushing phenomena, etc.), on the buckling behaviour of *Blockhaus* walls. The assumption of an equivalent, isotropic behaviour for C24 spruce (with $E \equiv E_{\perp}$), compared to orthotropic material models (with $E_{||} \approx 30\ E_{\perp}$ the average MOE in the direction parallel to grain [6]), generally resulted in lower initial stiffness for the examined log-walls, but almost in comparable buckling capacity (e.g. ultimate buckling load). This effect is highlighted in Fig.7, where numerical load-lateral displacement plots monitored at the centre of a L= 4m × H= 2.945m ('Tirol' logs) are proposed for various ABAQUS FE-models, and compared to full-scale test results obtained for a *Blockhaus* prototype recently tested at University of Trieste (Italy). As shown, assuming for timber an anisotropic behaviour would lead to an overestimation of the actual bending stiffness *Blockhaus* structural systems, hence resulting in possible non-conservative predictions. Fig.7 also shows that the analytical formulation given in Eq.(5) overestimates the load-carrying capacity of the same log-wall, since the load eccentricity cannot be accounted for, as anticipated in Section 2.2.

Possible local failure mechanisms of logs due to compression perpendicular to grain have been also investigated, and preliminary numerical simulations have been carried-out by replacing the indefinitely linear elastic mechanical behaviour of C24 spruce with an idealized elasto-plastic curve, being $f_{c,90} \approx f_{c,90,k}/0.7$= 3.57MPa the mean compressive strength perpendicular to grain representative of possible crushing phenomena, with $f_{c,90,k}$= 2.5MPa its characteristic value [6]. Numerical investigations highlighted that possible plasticization in compression typically occurs at the centre of log-walls, where the maximum out-of-plane displacements are attained, and these damage phenomena are generally limited to small portions of logs (e.g. few protrusions in compression). Depending on the geometry and possible initial imperfections of walls, however, the assumption of an indefinitely linear elastic material could lead to non-conservative results (e.g. Fig.7). For this reason, based also on assessment of full-scale experiments and further earlier numerical investigations [12], the parametric study has been performed by assuming for timber an isotropic, elasto-plastic mechanical behaviour able to properly reproduce the expected phenomena.

3.3 Extended numerical parametric study

Based on preliminary assessment of FE-models, an extended parametric study has been performed on a wide series of *Blockhaus* log-walls characterized by various geometrical properties (e.g. no openings, single door, double window and door openings) and initial configurations (e.g. possible initial imperfections or load eccentricities). In doing so, FE-models have been calibrated as specified in section 3.2, by assuming for timber the average material properties suggested by standards [6].

3.3.1 Initial imperfections

The buckling resistance of the studied log-walls resulted markedly dependent on the amplitude of possible initial geometrical out-of-plane curvatures u_0. Incremental buckling analyses have been performed on preliminary deformed FE-models, in which the initial geometrical configuration has been obtained as the corresponding fundamental modal shape (RF condition) obtained from linear buckling simulations. The maximum amplitude u_0 of this buckling shape has then been scaled to well-defined ratios, compared to the wall height H. Simulations highlighted that the imperfection u_0 can decrease the expected critical load N_{max} up to 30-40% the ideal value obtained for the same undeformed walls, depending on their geometry. This effect mainly derives, as highlighted by parametric numerical studies, from premature detachment of overlapping logs at the location where maximum displacements are expected (e.g. at the centre of the wall), hence resulting - in conjunction with possible localized damage in compression - in a marked loss of load carrying capacity. As shown in Fig.8, the gradual increase of maximum amplitude u_0 results in a significant decrease of both initial stiffness and maximum sustained load N_{max} for the examined log-wall, as well as in a premature failure due to progressive detachment and overturning of logs. Based on recommendations provided by the Eurocode 5 [13] for stability check purposes (e.g. $u_{0,min}$= 0.002H and $u_{0,min}$= 0.0033H for glulam or solid wood members respectively), the assumption of a minimum initial imperfection of maximum amplitude $u_{0,min}$= 0.0025H should be taken into account in the verification of *Blockhaus* systems.

3.3.2 Load eccentricities

While the typical connection between inter-storey floors and main walls in *Blockhaus* buildings is realized as depicted in Fig.5a, in some circumstances - due to mainly architectural requirements - the floor logs are interrupted within the thickness b of the supporting walls (Fig.9). Simulations performed on log-walls eccentrically loaded typically resulted in further decrease of initial stiffness and corresponding ultimate buckling load N_{max} (Fig.8). Their effect should be consequently properly taken into account. Fig.8 also shows that the analytical solution with k_σ=6.97 corresponding to the boundary conditions of clamped vertical edges and pinned horizontal edges accurately predicts the numerical load-carrying capacity of log walls with little eccentricity (u_0/H=0.0010).

3.3.3 Openings

A wide series of numerical static incremental buckling analyses have then been performed on log-walls characterized by different number and position of openings, overall dimensions and cross-sectional dimensions. Examples of typical buckled modal shapes are proposed in Fig.10 for walls with double or single openings respectively.

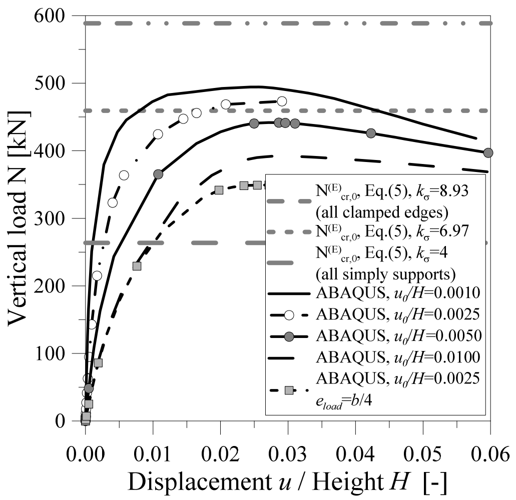

Fig.8. Effect of initial imperfections and load eccentricities.

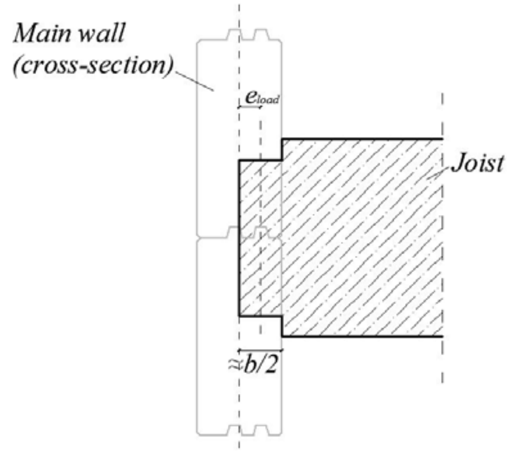

Fig.9. Detail of eccentric joist-to-wall connection for an inter-storey floor.

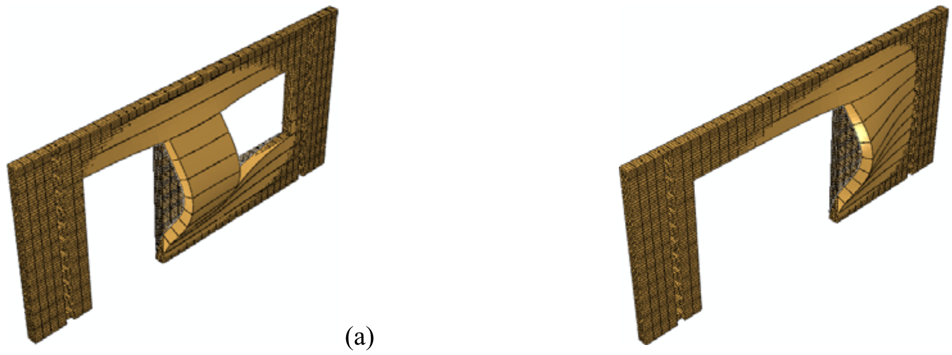

(a) (b)

Fig.10. Buckling failure configuration for *Blockhaus* walls with a) double or b) single openings (ABAQUS).

For walls with double openings, simulations highlighted that the steel hollow section profiles typically provide a stable global behaviour for the central portions of walls, hence resulting in an appreciable increase of their global load-carrying capacity (≈ +25%, depending on the geometry), compared to the same unreinforced walls. In the case of walls with a single door opening, on the contrary, steel profiles resulted only in a moderate increase of the expected critical buckling loads (≈ +10%), compared to unreinforced walls with the same geometry. As confirmed by the analytical predictions, in this latter case, their load-carrying capacity was fully governed by the $L_{ef}\times H$ portion. The use of Eq.(5) with k_σ= 1.277 would capture the effective failure mechanism of the walls, but would neglect the steel reinforcement contribution, hence providing an underestimation for the effective critical load (≈ -30%).

4 Validation to experiments

Full-scale buckling experiments have been recently performed at the University of Trieste (Italy) on various typologies of *Blockhaus* walls under in-plane vertical loads. Specimens having the same L=4m × H=2.945m overall dimensions ('Tirol' logs, Fig.1b), with or without door and window openings differently spaced, have been tested. An appropriate test setup consisting of two metal bracings has been used, to reproduce the desired RF restraint condition - although by means of concentrated rather than continuous supports - for the top logs. During each buckling experiment, out-of-plane displacements and vertical shortening of specimens have been monitored at 9 and 4 control points respectively. Fig.11 refers to a specimen without openings and eccentrically loaded (e_{load}= 4cm, control point at the centre of the wall). The log-wall manifested a typical "plate buckling" behaviour up to failure, which occurred due to the detachment and partial overturning of few top logs (Fig.11a). Compared to analytical calculations (Eq.(5)), the tested log-wall showed the marked sensitivity of experimental predictions to load eccentricities (Fig.11b). Excellent agreement, in this context, was found between test results and numerical predictions obtained by the implemented FE-model, being this latter able to account for the assigned load eccentricity and the actual RF top restraint, hence justifying the modelling assumptions discussed in Sections 2 and 3.

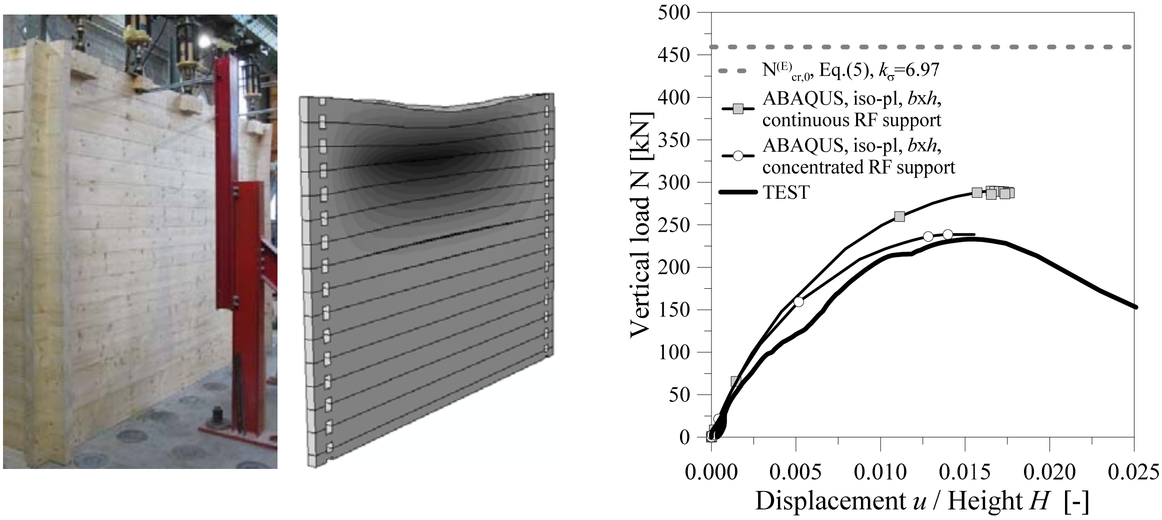

(a) (b)

Fig.11. Full-scale buckling experiment. a) test setup and deformed shape at failure, compared to ABAQUS FE-model; b) comparison of test results to analytical critical load (Eq.(5)) and numerical load N-lateral displacement u to height H ratio plots (ABAQUS; control point at the centre of the wall).

5 Simplified design approach

5.1 General method

Detailed analysis of numerical, analytical and experimental results partly discussed in this paper and earlier contributions [12] for log-walls with or without openings has been finally performed in order to provide a simplified and practical analytical approach for the stability check of *Blockhaus* log-walls under in-plane compressive loads. In doing so, the design MOE $E_{\perp,d}$, the corresponding shear modulus G_d and the design compressive strength perpendicular to grain $f_{c,90,d}$ are considered and used to replace the corresponding mean values, being [13]:

$$E_{\perp,d} = \frac{E_{\perp}}{\gamma_M}, \qquad G_d = \frac{G}{\gamma_M} \quad \text{and} \quad f_{c,90,d} = \frac{k_{\mathrm{mod}} f_{c,90,k}}{\gamma_M} \qquad \text{(9a) (9b) (9c)}$$

with γ_M= 1.3 the partial safety factor of wood and k_{mod} the partial modification factor for moisture and load duration influence, assumed 0.7 for the case of service class 1 and 2, and imposed load of long-term duration.

Under the assigned design loads N_{sd}, it is expected that the examined log-walls should be able to offer a design buckling strength $N_{b,Rd}$ satisfying the condition:

$$N_{b,Rd} = \chi_{imp} \frac{\left(N_{cr,0}^{(E)}\right)_d}{\gamma_1} \geq N_{sd}, \qquad (10)$$

γ_1 being a buckling calibration factor of the simplified formulas on the numerical and experimental behaviour, and χ_{imp} a reduction coefficient taking into account the effects of initial imperfections.

Based on parametric numerical results and comparative calculations, according to safety requirements and recommendations of Eurocode 5 [13], the value $\gamma_1 = 2$ is suggested for log-walls without openings or double door/window openings. For log-walls with single opening, based on analytical models discussed in Section 2.2 and further numerical calibrations, $\gamma_1 = 1$ is proposed. Concerning the buckling coefficient χ_{imp} representative of initial curvatures or load eccentricities, this can be estimated for a generic timber log-wall under in-plane compression as:

$$\chi_{imp} = \left(1 - \frac{e}{b}\right), \tag{11}$$

e being representative of the assigned imperfections or load eccentricities ($e \equiv (u_{0,max} + e_{load})$, with $u_0/H = 0.0025$ the minimum recommended amplitude for initial curvatures [13]), and b signifying the log-wall thickness (e.g. width of the log-walls).

Concerning the design Euler's critical load $\left(N_{cr,0}^{(E)}\right)_d$ in Eq.(10), its value should be properly estimated for log-walls with or without openings. In the latter case, $\left(N_{cr,0}^{(E)}\right)_d$ is given by Eq.(5), with $k_\sigma = 6.97$ and the design moduli provided by Eqs.(9a) and (9b). In presence of double openings (door and window), conversely, $\left(N_{cr,0}^{(E)}\right)_d$ should be calculated by means of Eq.(6). For log-walls with single opening, finally, $\left(N_{cr,0}^{(E)}\right)_d$ could be properly calculated by means of Eq.(5), with $k_\sigma = 1.277$ and $L \equiv L_{ef}$.

In Fig.12, the design buckling resistance $N_{b,\mathrm{Rd}}$ obtained from incremental buckling analyses performed on a wide series of log-walls with or without openings ($u_0/H > 0$ or $e_{load} > 0$, or both, being $E_{\perp,d}$, G_d and $f_{c,90,d}$ estimated for C24 spruce [6]) are compared with the corresponding analytical calculations of $N_{b,Rd}$, Eq.(10). Although it is clear that further validation of the proposed design method is required before final conclusions can be drawn, the simplified approach presented in this work leads to fairly accurate and conservative estimations of the numerical buckling loads.

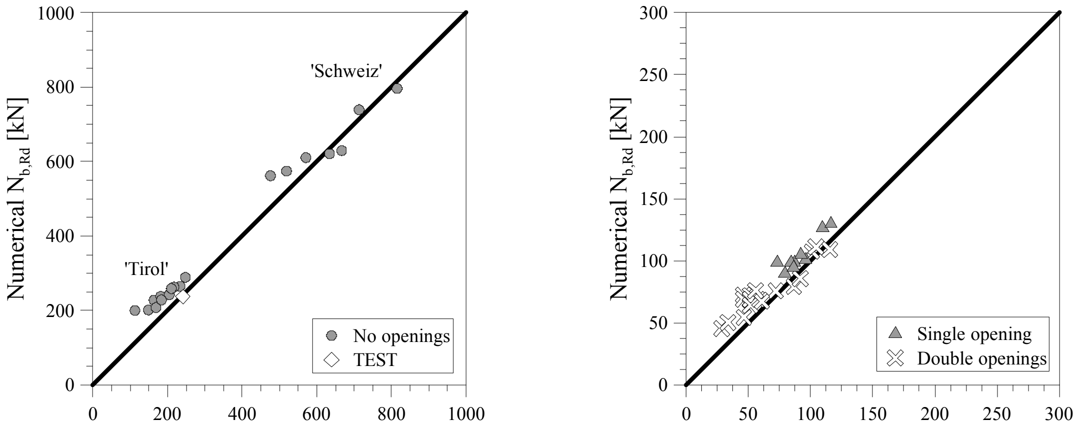

Fig.12. Assessment of analytically estimated design buckling strengths $N_{b,Rd}$ (Eq.(10)), compared to numerical predictions (ABAQUS), for *Blockhaus* walls with initial imperfection ($u_0/H > 0$), load eccentricity ($e_{load} > 0$) or both. Log-walls (a) without openings or (b) with single/double openings ('Tirol').

5.2 Proposal for the new generation of Eurocode 5

While the current version of the Eurocode 5 [13] provides recommendations for the stability check of single members (cap. 6.3 *"Stability of members"*), no design rules are given for log-haus structural systems. Based on the detailed discussion presented in this paper, the same chapter 6.3 could include a new section (e.g. 6.3.2 *"Log-haus walls* *subjected to in-plane vertical loads"*) where the design buckling rules and recommendations for log-walls with generic geometrical properties (e.g. number and cross section of logs; overall dimension of walls; number, position and size of openings; etc.) and eccentricities (due to load and/or initial curvature), as proposed in Section 5.1, are implemented.

6 Conclusions

The buckling behaviour of *Blockhaus* timber log-walls under in-plane compressive loads has been investigated by means of numerical and analytical models, as well as preliminary full-scale experiments. Compared to other structural systems, due to the lack of metal connections as well as to timber logs having typical slender cross-sectional aspect ratios, *Blockhaus* systems could be susceptible to buckling phenomena. As shown through detailed numerical models, inter-storey floors generally provide a full-restraint to the connected walls and a stiffening contribution that should be properly taken into account in calculations. Several mechanical and geometrical variables such as small initial imperfections, load eccentricities as well as the number, size and position of openings (e.g. doors and windows) can markedly reduce the effective load-carrying capacity of this structural system. Based on extended parametric numerical simulations, simple analytical formulations are derived from classical theory of plate buckling or column buckling, and applied to log-walls with generic geometrical properties. Finally, based on the obtained numerical results and on recommendations of Eurocode 5 for the design of timber structures, a simple analytical method is presented and discussed for the buckling design and verification of the studied timber walls under in-plane compressive loads. Although further validation of the presented method should be provided by additional experimental and numerical studies, the simplified design approach proposed in this paper was found to be conservative and suitable for implementation in codes of practice such as the new generation of the Eurocode 5.

Acknowledgements

Rubner Haus AG SpA is gratefully acknowledged for the financial and technical support.

References

[1] Branco, J., Araújo, J.P., 2010. Lateral Resistance of Log Timber Walls subjected to Horizontal Loads. *Proc. WCTE 2010*.
[2] Branco, J., Araújo, J.P., 2012. Structural behaviour of log timber walls under lateral in-plane loads. *Engineering Structures*, 40: 371-382.
[3] Bedon, C., Fragiacomo, M., Amadio, C., Sadoch, C., 2013. Experimental and numerical investigation of "Blockhaus" shear walls under in-plane cyclic loads. *Proc. XV ANIDIS Conference*, 30 June-4 July 2013, Padua, Italy.
[4] Tomasi, R., Sartori, T., Grossi, P., Wenzel, L. (2012). Sistema costruttivo Blockhaus: prove su giunzioni d'angolo. *Internal Report (in Italian)*. University of Trento, Italy
[5] Simulia, 2012. ABAQUS v.6.12 [Computer Software], Dassault Systems, Providence, RI, USA.
[6] EN 338:2009. Structural timber-strength classes.
[7] Rubner Haus AG SpA, www.haus.rubner.com
[8] Heimeshoff B, Kneidl R. Zur Abtragung vertikaler Lasten in Blockwänden – Experimentelle Untersuchungen. *Holz als Roh – und Werkstoff 50(1992): 173-180. Springer-Verlag 1992.*
[9] Heimeshoff B, Kneidl R. Bemessungsverfahren zur Abtragung vertikaler Lasten in Blockwänden. *Holz als Roh – und Werkstoff 50(1992): 441-448. Springer-Verlag 1992.*
[10] DIN1052 Teil 1: Holzbauwerke; Berechnung and Ausführung, 1988.
[11] Timoshenko SP, Gere JM (1961). Theory of Elastic Stability, McGraw-Hill, International Book Company.
[12] Bedon, C., Fragiacomo, M., Amadio, C., Battisti, A. 2014. Buckling of Blockhaus walls under in-plane vertical loads. Proc. WCTE2014, 10-14 August 2014, Quebec City, Canada.
[13] EN 1995-1-1:2009. Eurocode 5 - Design of timber structures - Part 1-1: General-common rules and rules for buildings.

INTER

International Network on Timber Engineering Research

CAPACITY DESIGN APPROACH FOR MULTI-STOREY TIMBER-FRAME BUILDINGS

D Casagrande

T Sartori

R Tomasi

Department of Civil, Environmental and Mechanical Engineering, University of Trento

ITALY

Presented by R Tomasi

A Buchanan commented that the paper is good. In high ductility system where the weak link is to be identified for yielding to take place, other components are to be oversized. In multistory building using this approach of minimum ☐ values, is there possibility of soft storey collapse? If so which storey should be chosen? R Tomasi responded that yielding in each storey should be closely sequenced. This is similar to a braced system. The current model can't calculate so accurately. The designers can decide on the accuracy and which storey is allowed to become a soft storey in small buildings. In medium ductility class same issues exit. Here all the fasteners can yield.

P Quenneville commented that slide 16 shows the rigid and fuse items are not isolated from each other. Incompatibility of deformation between the two systems can occur. He suggested additional provisions be provided. R Tomasi agreed.

I Smith asked how to identify systems prone to disproportional damage. R Tomasi responded that simple cantilever model was considered in this paper. In practice there are secondary elements that can improve the robustness of the building. This should not be a practical problem. He further stated that using q factor of 5 may not be consistent with the behaviour of some of the buildings.

M Fragiacomo questioned plasticization along the entire wall or just assumed the ground floor plasticizing. He stated that distributed plasticization is another method to dissipate energy and wondered which method is better. R Tomasi responded that distributed plasticization was not found in time series analysis and further discussion on the topic is needed. M Popovski stated that in experiments of platform frame, plasticization occurred in one storey not the entire wall.

Capacity design approach for multi-storey timber-frame buildings

Daniele Casagrande, Tiziano Sartori, Roberto Tomasi
Department of Civil, Environmental and Mechanical Engineering, University of Trento, Italy

Keywords: Seismic design, Capacity design, Ductility, Timber frame buildings.

1 Introduction

The traditional seismic design of a structure adopts a force-based method. The capacity of the structure to support the seismic action is usually obtained by dissipating the seismic energy via its structural damaging and hence assuming a nonlinear structural behaviour. Seismic linear analyses are usually carried out, dividing the elastic seismic forces by the behaviour factor q, depending on the global structural ductility. The global behaviour of a structure, and in particular its ductility, strongly depends both on the mechanical properties of structural components and on the global failure mechanism. For this reason, in order to achieve high values of q, local and global brittle failure mechanisms should be prevented.

In timber structures the energy dissipation cannot be achieved in timber elements because, as known, they are characterized by a brittle failure. Hence the capability of the structure to dissipate the seismic energy is obtained from the yielding of the mechanical connection devices, which should be designed so that their local ductility is consistent with the global ductility of the structure assumed in the design phase, and represented by the behaviour factor q.

Regarding timber frame buildings a high upper limit value of the behaviour factor q is usually suggested by Standards (i.e. equal to 5 for European Standards for seismic design [1]), setting this structural type in the high ductility class (DCH). The main reason is that the a great amount of fasteners (to connect the sheathing panels to timber frames) and connection devices (hold-downs, angle brackets) are used, hence a high and well-distributed energy dissipation is expected.

Nevertheless, unlike what for other material structural types (concrete or steel), no well-defined criteria about the global failure mechanism to guarantee a consistent global ductility of the structure are reported in Standard. Moreover, it is not clear which connection type should be chosen (fasteners, hold-down or angle brackets) as the weakest element (where the ductility capacity of the structure is concentrated) and no analytical expression is suggested for the application of the capacity design approach for timber-frame buildings.

In this paper a proposal for the application of the capacity design applied to timber-frame building is reported. Two main approaches are presented: the first one consistent with a medium ductility class, the second one to achieve a higher global energy dissipation.

2. Capacity design approach to timber building

The capacity design (CD) for structures under seismic loads, can be illustrated through the chain model, originally developed in [2]. As the strength of a chain is the strength of its weakest link, one ductile link may be used to achieve ductility for the entire chain. According to the Eurocode 8 provisions [1], in timber structures the ductile link must be only concentrated in joint (e.g. dowel type joint) whereas the timber elements behave elastically (figure 1).

Therefore a reliable strength prediction of the joint and its components is essential for applying the CD and ensuring the required ductility. Potentially brittle mechanisms have in fact to be prevented by checking that their actual strength exceeds the strength demand. To this aim, an over-strength coefficient can be adopted in the design of the timber element:

$$R_{b,Rd} \geq \gamma_{Rd} \cdot R_{d,Rd} \tag{1}$$

where $R_{b,Rd}$ is the design strength of the brittle (timber) element, $R_{d,Rd}$ is the design strength of ductile element (mechanical connection) and γ_{Rd} is a suitable over strength factor (see [3] and [4]).

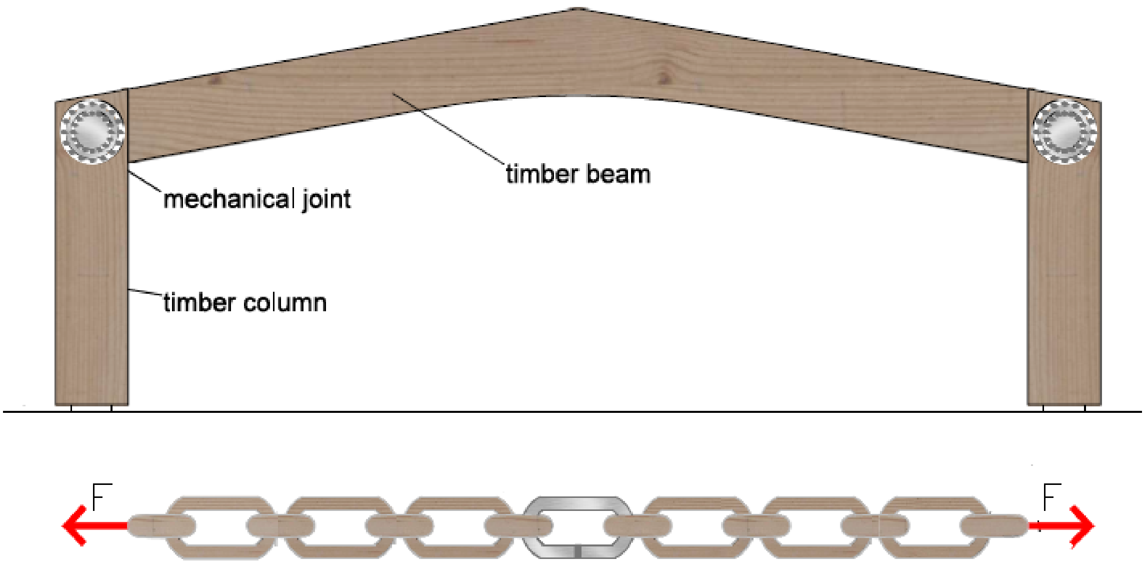

Figure 1. *The chain model applied to hyperstatic timber frames [5]*

The application of this concept is quite simple for most structural types (hyperstatic timber frames, timber hyperstatic beams) as presented in [4] an [5].

Concerning timber frame buildings the global failure mechanism of the structure is not described in Standards and hence it is not evident how to apply the CD concept correctly to this structural type. In the common practice all connection types (sheathing to framing connections, hold-downs, angle brackets) are usually considered as dissipative zones and are designed for the design load from the analysis (taking account of the behaviour factor q). Few prescriptive provisions are reported regarding the geometrical parameters in sheathing to framing connections (minimum thickness of the sheathing material and maximum nail diameter), without explicitly indicating this as the weakest component. On other hand was experimentally demonstrated [6] that the ductility of most commercial hold-downs and angle brackets looks pretty lower than the ductility obtained from sheathing-to-framing fasteners.

3 Linear elastic rheological model of a multi-storey timber framed shear wall

A timber frame shear wall subjected to a distributed vertical load and a horizontal force can be assumed as a statically determinate system, and can be represented by an elastic model represented in figure 2a, presented in [7] and in [8]. An equivalent representation is given by a rheological model composed by four in series spring (figure 3a), each of which is related to a single deformation contribution, namely: sheathing-to-framing connection (SH); sheathing panel shear (P); rigid body translation (A); rigid body rotation (H).

Assuming the hypothesis of an elastic-perfectly plastic behaviour for the mechanical connections, according the chain model, the global ductile failure occurs when the failure mechanism is related to the first one of the following structural components: sheathing-to-framing (SH), angle brackets (A), or hold-down (H). When the component associated of the weak mechanism is individuated, the other elements remain in the elastic range and can be defined as stronger components, according to CD approach (eq. 1). The global ductility of the wall depends only on the ductility of the weakest component. Hence, the provisions about ductility should be applied only to the weakest connection component whereas an elastic design can be used for other devices. It can be easily demonstrated that generally the wall ductility is lower than the weakest component ductility: they are equal only if the stiffness of the stronger components can be assumed infinity [8].

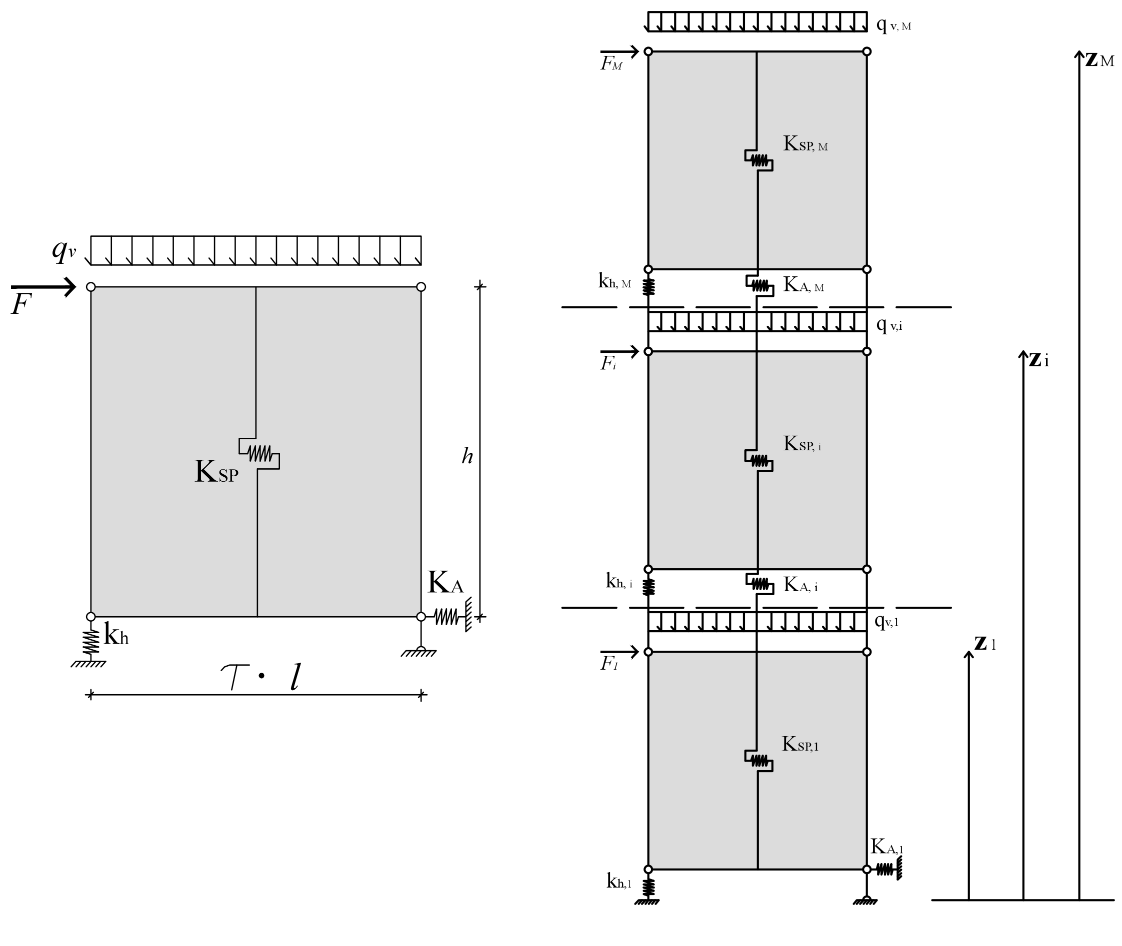

a) *b)*

***Figure 2.** Elastic model for one-storey and multi-storey timber frame wall ([7] and [8])*

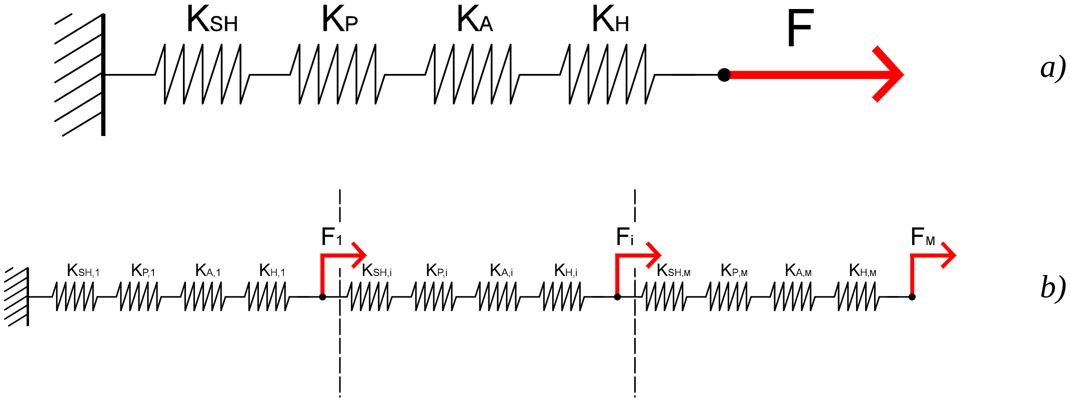

Figure 3. *Rheological model for one-storey and multi-storey timber frame wall ([7] and [8])*

The case of a M-storey timber frame wall can be analysed in a similar way of 1-storey wall. A simple model for a M-story wall can be obtained by means of the superimposition of M one-storey walls (figure 2b). It is not difficult to show that also this model is a statically determinate system. The rheological model used to represent its behaviour under a series of horizontal forces is in fact obtained linking in series M one-storey rheological models and adding all horizontal forces F_j (figure 3b).

As in the previous case, assuming an elastic-perfectly plastic behaviour for the mechanical connections, the structure yielding occurs when at least one component yields. In this case the weakest element of the chain should be determined in relation to the ratio between its strength and the tensile force. Hence, only one spring in the model described in figure 3b should be assumed as dissipative zone (for example the SH component at the i^{th} floor) whereas all other components should be considered as stronger components.

However, the described mechanism failure does not assure the participation of all the stories to the dissipation of the earthquake input energy, and for this reason a “soft-storey” global failure may occur. For this reason, according to the CD philosophy, aimed to obtain a better distributed ductile mechanism along the height of the walls, in section 4 a new design method is proposed.

4 Capacity design approach for a high ductility class

As reported in section 2 Standards assume that timber frame buildings are characterized by a high capacity to dissipate energy because a great amount of small diameter fasteners are used. When fasteners used to connect the sheathing panels to the timber frame are characterized by a local ductility consistent with the high value of the behaviour factor[1], it is reasonable assuming as dissipative zones the sheathing-to framing connections (SH). Since the proposed expressions are rigorously based on the CD concepts and only the sheathing-to framing connection is considered as dissipative zone (usually characterized by high ductility, as experimentally demonstrated in [9]), the method seems suitable for a high ductility class (HDC) of buildings.

[1] According to the Eurocode 8 the dissipative zones shall be able to deform plastically for at least three fully reversed cycles at a static ductility ratio of 6 for ductility class, without more than a 20% reduction of their resistance.

4.1 One-storey shear wall

Assuming the sheathing-to-framing connection (SH) as the weakest ductile component, therefore it has to be designed taking account of the external design analysis force acting on the shear wall F_{Ed} . Once the single fastener design capacity $F_{f,Rd}$ is known, the maximum fastener spacing $s_{f,max}$ between the connectors along the edge of the sheathing panel can be calculated. According to [10] we get:

$$s_{f,max} = \frac{\sum_{j=1}^{N} 1{,}2 \cdot F_{f,Rd} \cdot b_j \cdot c_j \cdot n_{bs}}{F_{Ed}} \tag{2}$$

where N is the number of sheathing panels, b_j is the width of the j^{th} panel, c_j is a reduction factor that takes account of the shape of the panel and n_{bs} is the number of the braced sides of the wall (1 or 2).

Adopting the real fastener spacing $s_f \leq s_{f,max}$ (but lower than 150 mm, according to [10]) it is possible to carry out the shear wall capacity $F_{sw,Rd}^{SH}$ related to the sheathing-to-framing (SH) failure mechanism.

$$F_{sw,Rd}^{SH} = \sum_{j=1}^{N} \frac{1{,}2 \cdot F_{f,Rd} \cdot b_j \cdot c_j \cdot n_{bs}}{s_f} \geq F_{Ed} \tag{3}$$

On the contrary the design of angle brackets (A) and hold-downs (H) should be carried out according to the CD approach. Therefore the design loads are not obtained from the analysis, but they are related to the design capacity of the wall ($F_{sw,Rd}^{SH}$).

Regarding the angle brackets the minimum number $n_{a,min}$ to permit a strong mechanism can be calculated as:

$$n_{a,min} = \frac{F_{sw,Rd}^{SH} \cdot \gamma_{Rd}}{F_{a,Rd}} \tag{4}$$

where $F_{a,Rd}$ is the strength of an angle bracket and $\gamma_{Rd}$is a suitable over-strength factor.

Adopting the real number of angle brackets $n_a \geq n_{a,min}$ is possible to carry out the shear wall capacity related to the angle brackets failure mechanism $F_{sw,Rd}^{A}$ as:

$$F_{sw,Rd}^{A} = n_a \cdot F_{a,Rd} \geq F_{sw,Rd}^{SH} \tag{5}$$

The tensile design force acting on the hold-down can be carried out by means the following equation derived from the rotational equilibrium considerations (see figure 4):

$$F_{h,Ed} = \frac{F_{sw,Rd}^{SH} \cdot \gamma_{Rd} \cdot h}{\tau \cdot l} - \frac{q_v \cdot l}{2 \cdot \gamma_{LOAD}} \leq F_{h,Rd} \tag{6}$$

where l and h are length and height of the wall, τ is the coefficient that takes into account that the internal level arm may be lower than l (from 0.95 to 1), q_v is the uniform vertical load. In the load analysis the 95th percentile for the value q_v of the vertical load is adopted. Since q_v has a positive effect of in reducing the action on the hold-down, it has to be reduced by means of the coefficient $\gamma_{LOAD} = q_v / q_{v,k,0,05}$ to get the 5th percentile value.

The shear wall capacity related to the hold-down failure mechanism $F_{sw,Rd}^{H}$ is therefore:

$$F_{sw,Rd}^{H} = \left(F_{h,Rd} + \frac{q_v \cdot l}{2 \cdot \gamma_{LOAD}}\right) \cdot \frac{\tau \cdot l}{h} \geq F_{sw,Rd}^{SH} \tag{7}$$

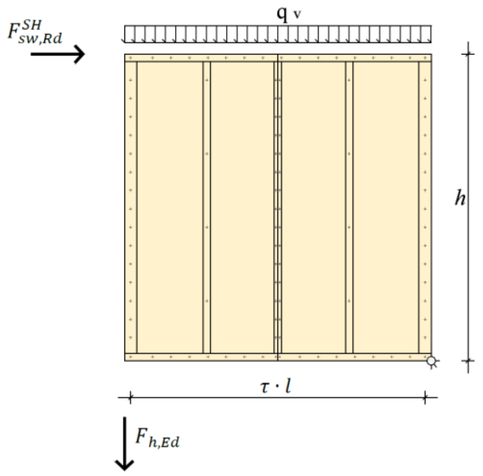

Figure 4. *Tensile force of the hold-down applying capacity design*

The brittle failure mechanism of compression (8) and tension (9) on the timber studs, of compression perpendicular to the grain in the bottom beam (10) and of shear stress on the sheathing panel (11) are represented by the following design equations, according to Eurocode 5 [10]:

$$\sigma_{c,0,d} = \frac{\frac{F^{SH}_{sw,Rd} \cdot \gamma_{Rd} \cdot h}{\tau \cdot l} + \frac{q_v \cdot l}{2}}{A_{stud}} \leq k_{c,y} \cdot f_{c,0,d} \tag{8}$$

$$\sigma_{t,0,d} = \frac{\frac{F^{SH}_{sw,Rd} \cdot \gamma_{Rd} \cdot h}{\tau \cdot l} - \frac{q_v \cdot l}{2 \cdot \gamma_{LOAD}}}{A_{stud}} \leq f_{t,0,d} \tag{9}$$

$$\sigma_{c,90,d} = \frac{\frac{F^{SH}_{sw,Rd} \cdot \gamma_{Rd} \cdot h}{\tau \cdot l} + \frac{q_v \cdot l}{2}}{A_{eff}} \leq k_{c,90} \cdot f_{c,90,d} \tag{10}$$

$$\tau_d = \frac{F^{SH}_{sw,Rd} \cdot \gamma_{Rd}}{l \cdot t} \leq f_{v,d} \tag{11}$$

Where A_{stud} is the area of the external stud of the wall, A_{eff} is effective area under compression in the bottom beam, t is the sheathing panel thickness. The other symbols are in accordance with the Eurocode 5 [10]. The previous equations can be easily obtained by the simple equilibrium considerations substituting the acting force F_{hEd} with the shear wall capacity $F^{SH}_{sw,Rd}$ multiplied by the over-strength factor γ_{Rd} (see figure 4).

4.2 Multi-storey shear wall

Similar expressions can be written in case of multi-storey walls. In according to the model presented in the section 3, the statically determinate multi-storey walls are connected at each level with mechanical devices counteracting translation and rotation of the single storey walls.

Consistently with the method previously introduced for one-storey wall, the energy dissipation can be assumed concentrated in the sheathing-to-framing connections. In order to guarantee a well-distributed energy dissipation along the height of the building, an approach similar to the proposed one for designing steel *X*-braced frames could be adopted according Eurocode 8 [1], where the global mechanism failure is characterized by the yielding of the diagonal elements at each storey level. The diagonals in fact should be designed so that the ratio between their strength and the tensile design force is uniform along the height of the same braced frame. In this way a soft-storey floor failure mechanism is prevented.

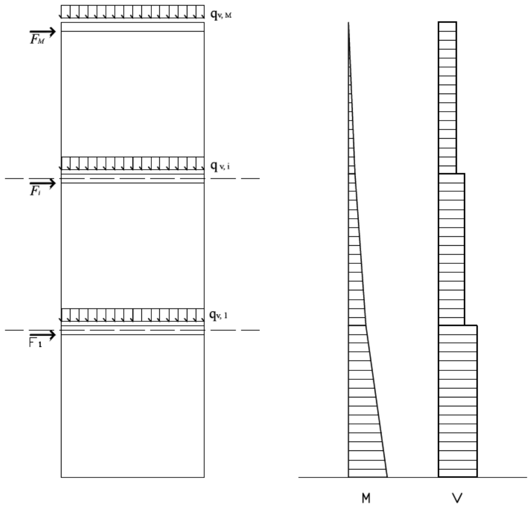

Figure 5. *Multi storey timber frame building: the cantilever model*

For a multi-storey timber frame wall, once the seismic design shear action $V_{Ed,i}$ is known from the seismic analysis (see figure 5), at each level i^{th} ($i = 1 \ldots\ldots M$, where M is the number of storeys) the maximum fastener spacing $s_{f,max,i}$ along the edge of the sheathing panel can be calculated.

$$s_{f,max,i} = \frac{\sum_{j=1}^{N} 1{,}2 \cdot F_{f,Rd} \cdot b_j \cdot c_j \cdot n_{bs}}{V_{Ed,i}} \tag{12}$$

Adopting the real spacing $s_{f,i} \leq s_{f,max,i}$ (but lower than 150 mm) is possible to carry out the shear wall capacity at each floor $F_{sw,Rd\,,i}^{SH}$ related to the sheathing-to-framing failure mechanism (SH$_i$).

$$V_{sw,Rd,i}^{SH} = \frac{\sum_{j=1}^{N} 1{,}2 \cdot F_{f,Rd} \cdot b_j \cdot c_j \cdot n_{bs}}{s_{f,i}} \tag{13}$$

The over strength factor α_i at the i^{th} storey can be calculated as:

$$\alpha_i = \gamma_{Rd} \cdot \frac{V_{sw,Rd,i}^{SH}}{V_{Ed,i}} \tag{14}$$

Assuming the wall as a statically determinate system the global over strength factor for the wall is therefore:

$$\alpha = min(\alpha_i) \tag{15}$$

In order to guarantee a well-distributed energy dissipation along the height of the wall uniform values of α_i should be obtained. This could be guaranteed by the following expression:

$$\alpha_{max} \leq \varphi \cdot \alpha \leq q \tag{16}$$

where φ is a suitable parameter that should be proposed for timber frame walls (e.g. for X-braced steel frames in [1] it is equal to 1.25).

The CD approach for the design of the stronger components (H$_i$ and A$_i$) can be adopted at each level in relation to the shear wall over-strength factor α. Hence, the design shear force on the angle brackets $V_{d,A,i}$ should satisfy the following expression:

$$V_{d,A,i} = \alpha \cdot V_{Ed,i} \leq V_{Rd,A,i} \tag{17}$$

where $V_{Rd,A,i}$ is the shear wall design strength at the i^{th} storey related to angle brackets.

With the same criterion, the tensile force acting on the hold-down at the level i^{th} can be calculated as:

$$F_{h,Ed,i} = \alpha \cdot F_{h,Ed,E,i} - \sum_{j=i}^{M} \frac{q_{v,j} \cdot l}{2 \cdot \gamma_{LOAD}} \leq F_{h,Rd,i} \tag{18}$$

where $F_{h,Ed,E,i}$ is the design tensile force on the hold-down obtained from the seismic analysis at the i^{th} storey and $F_{h,Rd,i}$ is the design hold-down strength at the same storey. Also in this case a load coefficient γ_{LOAD} is introduced to reduce the vertical loads to the 5th percentile.

Similar expression to equations from (8) to (11) can be written for the failure mechanism, related to timber elements at each level:

$$\sigma_{c,0,d} = \frac{\alpha \cdot F_{h,Ed,E,i} + \sum_{j=1}^{N} \frac{q_{v,i} \cdot l}{2}}{A_{stud}} \leq k_{c,y} \cdot f_{c,0,d} \tag{19}$$

$$\sigma_{c,90,d} = \frac{\alpha \cdot F_{h,Ed,E,i} + \sum_{j=1}^{N} \frac{q_{v,i} \cdot l}{2}}{A_{eff}} \leq k_{c,90} \cdot f_{c,90,d} \tag{20}$$

$$\sigma_{t,0,d} = \frac{\alpha \cdot F_{h,Ed,E,i} - \sum_{j=1}^{N} \frac{q_{v,i} \cdot l}{2 \cdot \gamma_{LOAD}}}{A_{stud}} \leq f_{c,0,d} \tag{21}$$

$$\tau_d = \frac{\alpha \cdot V_{Ed,i}}{l \cdot t} \leq f_{v,d} \tag{22}$$

It has to be underlined a proper design need to keep the values of the α over-strength coefficient as uniform as possible according to the limitation reported in eq. 16, with the aim to promote the sheathing to framing connection yielding of more than one storey. However this approach needs that fastener spacing and number of braced side (1 or 2) may vary at each level and at each shear wall. Moreover, since the maximum spacing of the sheathing to framing fastener is limited according to the code provisions, this method could present some difficulties to be applied, especially in the case of low seismic design action. For this reason, a possible strategy for building characterized by at least three storeys, could be not to apply the limitation of eq. 16 for the top storey, considering that its seismic design shear force is usually much lower than the bottom storey ones.

5 Capacity design approach for a medium ductility class

In this section a second approach for the application of the CD method to multi-storey timber frame walls is presented. Differently from the method for HDC reported in section 4, this method is not rigorously based on the CD concepts. Coherently with the common practice all sheathing-to-framing fasteners and connection devices (hold down and angle brackets) are considered as dissipative zones. Their design force is obtained from the seismic analysis and the CD approach is applied only to timber elements (studs, bottom beams and sheathing panels). Since angle brackets and hold-downs are considered in this case dissipative zones, the provisions regarding their local ductility reported in Eurocode 8 [1] should be satisfied (the dissipative zones shall be able to deform plastically for at least three fully reversed cycles at a static ductility ratio of 4 for ductility class, without more than a 20% reduction of their resistance). However, many studies demonstrated that most commercial devices are not characterized by a high local ductility and are usually designed in relation to their strength. For this reason the approach proposed in this section should be applied in case of a medium ductility class (MDC) and hence a reduced behavior factor should be adopted. Further studies are necessary in the future to calibrate this value.

5.1 Multi storey shear wall

Since SH, H and A components are assumed as dissipative zones, the loads from the seismic analysis can be used in the design phase and the CD approach is not applied. Hence the following expression should be satisfied at each level i^{th} ($i = 1 \ldots..M$, where M is the number of storeys):

$$V_{sw,Rd,i}^{SH} = \frac{\sum_{j=1}^{N} 1{,}2 \cdot F_{f,Rd} \cdot b_j \cdot c_j \cdot n_{bs}}{s_{f,i}} \geq V_{sw,Ed,i} \tag{23}$$

$$V_{sw,Rd,i}^{A} = n_a \cdot F_{a,Rd} \geq V_{sw,Ed,i} \tag{24}$$

$$F_{h,Rd,i} \geq F_{h,Ed,i} = F_{h,Ed,E,i} - \sum_{j=1}^{M} \frac{q_{v,i} \cdot l}{2} \tag{25}$$

Since the CD should be applied to timber elements, the over strength factor of the entire wall β should be calculated. This is defined as the minimum of the over strength factor β_i at the i^{th} level:

$$\beta = min(\beta_i) \tag{26}$$

$$\beta_i = min\left(\frac{\gamma_{Ra} \cdot V_{sw,Rd,i}^{SH}}{V_{Ed,i}}; \frac{\gamma_{Rd} \cdot V_{sw,Rd,i}^{A}}{V_{Ed,i}}; \frac{\gamma_{Rd} \cdot F_{h,Rd,i} + \sum_{j=i}^{M} \frac{q_{v,j} \cdot l}{2}}{F_{h,Ed,E,i}}\right) \tag{27}$$

The brittle failure mechanisms for timber elements can be verified at each level applying the CD as in the approach for HDC buildings, using the factor β.

$$\sigma_{c,0,d} = \frac{\beta \cdot F_{h,Ed,E,i} + \sum_{j=1}^{N} \frac{q_{v,i} \cdot l}{2}}{A_{stud}} \leq k_{c,y} \cdot f_{c,0,d} \tag{28}$$

$$\sigma_{c,90,d} = \frac{\beta \cdot F_{h,Ed,E,i} + \sum_{j=1}^{N} \frac{q_i \cdot l}{2}}{A_{eff}} \leq k_{c,90} \cdot f_{c,90,d} \tag{29}$$

$$\sigma_{t,0,d} = \frac{\beta \cdot F_{h,Ed,E,i} - \sum_{j=1}^{N} \frac{q_i \cdot l}{2 \cdot \gamma_{LOAD}}}{A_{stud}} \leq f_{c,0,d} \tag{30}$$

$$\tau_d = \frac{\beta \cdot V_{Ed,i}}{l \cdot t} \leq f_{v,d} \tag{31}$$

6 Conclusion

In this paper two analytical approaches for the application of the capacity design to timber frame buildings are presented. The first one (method HDC) assumes that only the sheathing-to-framing connection components can dissipate energy since, if well-designed, may be characterized by a high ductility. Assuming a timber frame wall as a statically determinate system, other connection devices (angle brackets and hold-downs) should be designed in relation to the strength of the weakest component according to the design capacity approach. The provisions regarding the local ductility should be satisfied only to the sheathing-to-framing connections and it seems correct to adopt a q factor related to a high ductility class of the structures. The second method (approach MDC) is simplified and considers both fasteners and connection devices able to dissipate energy. All of them are designed in relation to the analysis loads and the capacity design approach is applied only to timber elements. There is not a global control on the mechanism failure (the weakest component may be a fastener, an angle bracket or a hold-down) and the provisions about the local ductility are to be applied to all components (SH, A and H). In this case, since the ductility of connection devices is usually lower the fastener one, a reduced value of the behaviour factor q should be adopted.

Some practical rules and expressions are proposed to apply the capacity design approach as requested by Standards. However, further studies should be carried on, in order to select the value of the behaviour factor q for the two approaches (with particular regard to the second one for medium ductility class), and to calibrate the value of the parameter φ, so to have a sufficient distributed energy dissipation.

7 References

[1.] EN 1998-1/A1 Eurocode 8. Design of structures for earthquake resistance - Part 1: General rules, seismic actions and rules for buildings,2013. Brussels, Belgium: CEN, European Committee for Standardization

[2.] Pauley T, Priestley MJN. Seismic design of reinforced concrete and masonry buildings. Wiley Ed.; 1992

[3.] Schick M., Vogt T., Seim W., Connection and anchoring for wall and slab elements in seismic design. In: Proceedings of CIB W18/46-15-4, Vancouver, Canada, 2013

[4.] Jorissen, A., Fragiacomo, M. General notes on ductility in timber structures (2011) Engineering Structures, 33 (11), pp. 2987-2997

[5.] Tomasi, R., Zandonini, R., Piazza, M., Andreolli, M. Ductile end connections for glulam beams (2008) Structural Engineering International: Journal of the International Association for Bridge and Structural Engineering (IABSE), 18 (3), pp. 290-296

[6.] Tomasi, R., Sartori, T. Mechanical behaviour of connections between wood framed shear walls and foundations under monotonic and cyclic load (2013) Construction and Building Materials, 44, pp. 682-690.

[7.] Casagrande, D., Rossi, S., Sartori, T., Tomasi, R. Analytical and numerical analysis of timber framed shear walls (2012) World Conference on Timber Engineering 2012, WCTE 2012, 5, pp. 497-503

[8.] Casagrande, D., Study of timber-frame building seismic behaviour by means of numerical modelling and full-scale shake table testing (2014), PhD Thesis, Department of Civil, Environmental and mechanical Engineering, University of Trento

[9.] Sartori, T., Tomasi, R. Experimental investigation on sheathing-to-framing connections in wood shear walls (2013) Engineering Structures, 56, pp. 2197-2205.

[10.] EN 1995-1-1/A1 Eurocode 5. Design of timber structures Part 1-1: General common rules and rules for building, 2008. Brussels, Belgium: CEN, European Committee for Standardization

INTER

International Network on Timber Engineering Research

DESIGN MODELS FOR CLT SHEARWALLS AND ASSEMBLIES BASED ON CONNECTION PROPERTIES

I Gavric
FPInnovations, Advanced Building Systems
Vancouver, BC

M Popovski
FPInnovations, Advanced Building Systems
Vancouver, BC

CANADA

Presented by M Popovski

A Buchanan stated that the out of plane wall contributions offers big potential for CLT structures but depends on connection between the orthogonal walls. The use of nails or screws devices means that there is no attempt to come up with uncoupled devices between tension and shear. M Popovski agreed and further commented that we do not know the real resistance of the building even though buildings have been built.

W Seim stated that comparing different models is important to establish upper and lower bounds. He stated that model D3A is pure rocking and questioned equilibrium in this model. M Popovski answered that it is assumed that some device such as shear key will take the sliding mode.

I Smith stated that design code should not tell engineers how to do structural analysis. M Popovski agreed.

R Tomasi asked about the rules for the position of the holddown devices. M Popovski stated that it is up to the designers but the position of the holddown devices will make a difference and should be considered. There were discussions whether the presence of lintel beams in the 3-D model affect the structural performance.

M Fragiacomo stated that the 3-D system is conservative because out-of plane wall contributions were not considered in design. M Popovski responded that this is not always the case as it depends on the placement of the connection devices.

Design models for CLT shearwalls and assemblies based on connection properties

Igor Gavric
Visiting Scientist, FPInnovations, Advanced Building Systems
Vancouver, BC, Canada

Marjan Popovski
Principal Scientist, FPInnovations, Advanced Building Systems
Vancouver, BC, Canada

Keywords: Shearwalls, Design models, Lateral loads, Cross-laminated timber, Cyclic tests

1 Introduction

Use of cross-laminated timber (CLT) as a construction material for floor, wall and roof panels has increased exponentially over the last few years. Applications include residential and non-residential low-rise buildings, renovations, building retrofits, and recently, mid-rise and high-rise buildings. Design provisions for CLT as a structural system, however, currently do not exist in any building code or national standard around the world. Consequently, the design approach is left at discretion of the structural engineer.

FPInnovations has undertaken a multi-disciplinary research project on determining the properties of CLT products and help early adopters of CLT in construction [1]. One of the objectives of the project was to quantify the seismic performance of CLT wall assemblies and CLT structures. In 2010, a series of monotonic and cyclic CLT wall tests were conducted with different configurations and connection details [2]. Different types of connectors (hold-downs, brackets) and fasteners (ring nails, spiral nails, self-threaded screws, timber rivets) were used, as well as different wall aspect ratios, types of walls (single walls, coupled walls with step joints) and different levels of vertical loads. With objective to investigate the 3-D system behaviour of CLT structures subjected to lateral loads, a two-storey full-scale model of a CLT house was tested under quasi-static monotonic and cyclic loading [3]. Parameters such as direction of loading, number of hold-downs and number of screws in perpendicular wall-to-wall connections were varied in the tests.

The work presented in this paper is a continuation of the FPInnovations' research project. As currently there are no agreed methods for determining the lateral load resistance of CLT shearwalls based on connection properties, there is a need for development of such method as well as for development of a design procedure for CLT as a lateral load resisting system. The most common approach for determining the resistance of CLT walls under lateral loads currently used in North America and Europe assumes that the lateral resistance of a CLT wall is a simple summary of the shear resistances of all connectors at the bottom of the wall. The uplift forces due to global overturning moments are taken by hold-downs in the corners of the building [4, 5] or by hold-downs in the corners of each wall [6, 7]. Although this approach is simple to use, it does not take into account the fact that kinematic behaviour of CLT walls under lateral loads is a combination of rocking and sliding of the entire panel or each individual wall segment, in case of multi-panel walls. Consequently, all connectors at the bottom of the wall are subjected to a combination of shear and uplift loads. Moreover, the behaviour of multi-panel CLT walls is influenced by the step joints used to connect the panels [8, 9].

The main goal of the study presented in this paper was to develop different models for quantifying the resistance of CLT shearwalls under lateral in-plane loads and compare the models with the available resistance of CLT walls available from experimental data. Experimental results from CLT wall tests performed at FPInnovations, Canada [2] and CNR IVALSA, Italy [9] were used to evaluate the effectiveness and consistency of the newly developed design models, and compare them with the existing design approaches (models) that are currently used in North America and in Europe. In addition, to investigate the behaviour of the models when applied to 3-D structures, the models were used for analytical-experimental comparison of lateral resistance of the two-storey CLT house tested at FPInnovations [3]. Based on the findings, the most suitable model for further development of the design procedure for CLT wall systems is proposed.

2 Kinematic models for CLT walls

CLT wall elements were considered as linear elastic rigid bodies in the analytical models and it was assumed that all wall deformations come from connections in terms of wall slip (horizontal displacement) and wall rotation that causes vertical displacements (uplift). Since models deal with forces that are at or below the factored resistance levels, connection behaviour was assumed to be linear elastic as well. Friction forces in the wall to floor/foundation contact area were not taken into account. It was also assumed that each shear bracket takes equal part of total shear force applied to the wall. On the other hand, it was considered that each uplift connector takes proportional part of total uplift force, depending on its position in the wall with respect to the point of rocking, following a triangular distribution of forces and depending on the proportion of connection stiffness ratios. CLT connection tests demonstrated that for walls designed according to capacity based principles yielding of the screws in the vertical joint between adjacent panels occurs before yielding of the nails in the brackets/hold-downs [10, 11]. Consequently, the connections in the step joints were considered to reach their factored resistances before brackets or hold-downs do. The strength of connections in step joints remains constant after that. Factored resistance of CLT walls under lateral loads was considered to be achieved when first bracket or hold-down at the bottom reaches its factored resistance, while the step-joints have already reached their factored resistance.

In total five different analytical design models were considered and analyzed in this study. Each design model had different assumptions of the behaviour of the connectors such as: resisting tension (uplift) forces only, resisting shear forces only, as well as resisting uplift and shear forces in combination under different interaction formulae (Fig. 1). The first two design models (D1 and D2) are currently used in Europe [4, 5, 6, 7]. These models do not take into account uplift resistance of brackets and because of their similarity to the design approaches for light wood-frame walls they have become the choice of designers in North America as well. Design model D1 (pure sliding) assumes that all brackets resist shear forces while resistance of hold-downs is not taken into account. Overturning resistance of CLT wall systems in this design model shall be verified on the building level. In Design model D2 corner brackets or hold-downs are able to take uplift forces (have uplift resistance), while inner brackets resist shear forces. Newly proposed design models (D3-D5) take into account uplift resistance component of the brackets, as well as different interaction of shear and uplift resistance. Design model D3 takes into account full uplift resistance of hold-downs and full shear and uplift resistance of all brackets. This model was included more as an academic exercise, as full resistance of connections in both directions is not usually possible. In addition, two sub-models D3A and D3B of this model were also considered. If it is assumed that the wall is only rocking, than the wall resistance is determined using uplift contributions of the brackets only (D3A). If the wall is experiencing sliding deformations only with engaging full resistance of connections in shear (sub-model D3B), that sub-model is same as model D1. Design models D4 and D5 consider shear-uplift interaction of load carrying capacity in the brackets due to two directional loading. Two different shear-uplift interaction domains (circular and triangular) were applied (Fig. 1 and Section 3).

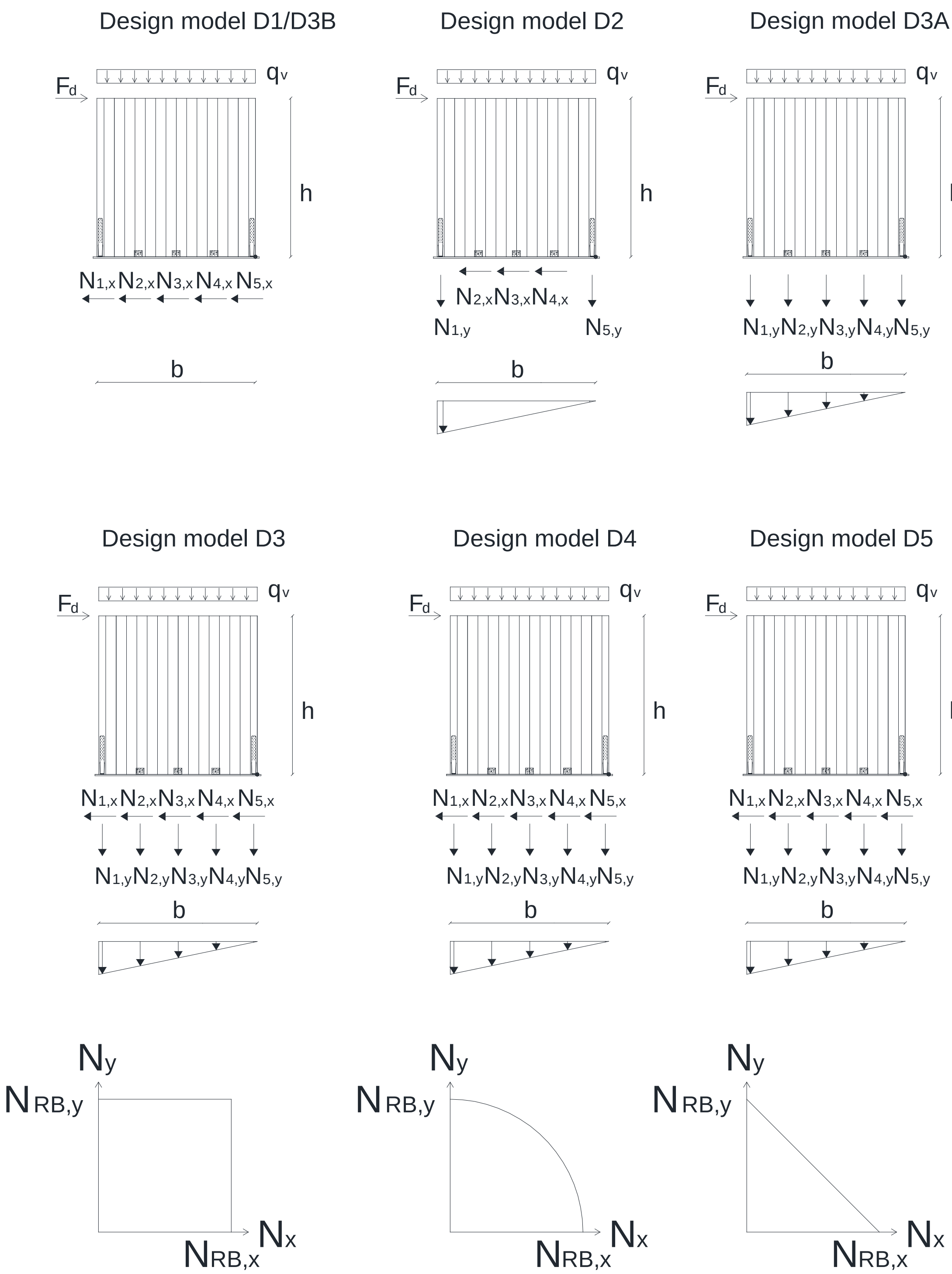

Figure 1 Analytical models used for determining the lateral resistance of CLT shearwalls

3 Calculation procedure

In this section a calculation procedure to determine the factored lateral resistance of a CLT wall is presented. As an example the procedure for design model D4 is presented in detail, while the procedure of other models can be derived from it. All design models can be easily programmed and implemented in calculation software such as Excel, Matlab or Mathcad.

3.1 Factored (design) resistance of CLT connections

An embedment strength formula for dowel-type fasteners (nails, screws) in CLT has been proposed by Uibel and Blaß [12]. The proposed embedment formula was developed using a characteristic wood density (5^{th} percentile) based on 12% moisture content weight and volume for short duration of load. As the lateral resistance of fasteners in Canadian standard CSA O86 [13] is based on 5^{th} percentile density values on a 15% moisture volume and weight basis, with relative density values on mean oven-dry weight and volume basis at standard load duration, a modified equation was used. After the conversion, the following embedment strength expression was obtained:

$$f_{CLT} = 95.6 d_F^{-0.5} G^{1.05} \ (N / mm^2) \tag{1}$$

where f_{CLT} is specified embedment strength based on 15% moisture volume and weight basis, d_f is fastener diameter (in mm) and G is mean relative density based on oven-dry weight and volume. Once the embedment strength properties of fasteners in CLT connections were established, their factored lateral resistance was calculated using Johansen's yield model. In this study, the yield model equations for lateral load resistance given in CSA O86-09 were used. Factored resistance values of connectors (N_{RH} for hold-downs and N_{RB} for brackets) were calculated by multiplying factored lateral resistance of one fastener (nail or screw) with the number of fasteners used in one connector. It should be noted that this assumption can only be used in cases where the resistance of a connection is governed by the total resistance of fasteners in the connection. For that, the number of nails in hold-downs and brackets shall be selected so that the yielding occurs in the nails and not in the connectors (brackets). Based on observations from the CLT wall tests [2, 9] and the results from the CLT connection tests [10], hold-downs do not provide significant resistance in shear direction, thus such resistance was not taken into account in the analytical models. On the other hand, shear is the primary load carrying direction for the brackets. However, experimental tests on CLT metal connectors [10] showed that almost equal amount of load can be transferred in tension (uplift) direction as well. Therefore, equal strength properties of brackets in uplift and shear direction were assumed in the kinematic analytical models ($N_{RB,x} = N_{RB,y} = N_{RB}$). As the brackets resist loads in two directions (shear and uplift), the combined resistance of the bracket is usually lower than its unidirectional resistance. In some of the models, the reduction of strength was assumed using two different interaction domains (Eq. (2) and Eq. (3)), according to ETA-07/0055, Annex B [14]:

$$\left(\frac{N_x}{N_{RB}}\right)^2 + \left(\frac{N_y}{N_{RB}}\right)^2 \leq 1 \ \rightarrow \ N_x^2 + N_y^2 \leq N_{RB}^2 \tag{2}$$

$$\frac{N_x}{N_{RB}} + \frac{N_y}{N_{RB}} \leq 1 \ \rightarrow \ N_x + N_y \leq N_{RB} \tag{3}$$

where N_x is horizontal force in the bracket, N_y is vertical force in the bracket and N_{RB} is factored lateral resistance of bracket in a single direction.

3.2 Factored (design) resistance of CLT walls

Factored (design) resistance of a CLT wall (F_d) under lateral loads is equal to the horizontal force on the top of the wall when first bracket or hold-down at the bottom reaches its factored resistance (N_{RH} for hold-downs and N_{RB} for brackets), while the step-joints (if present) have already reached their factored resistance (N_{RS}). It was assumed that connections reach their yield point at the factored resistance level. Fig. 2 shows the distribution of reaction forces in the connections of a coupled CLT wall with two hold-downs and four brackets with a step-joint according to the design model D4. The geometry of the CLT wall (b, h), vertical load q_v, and the factored resistances of the connections (hold-downs, brackets, step joint) are known.

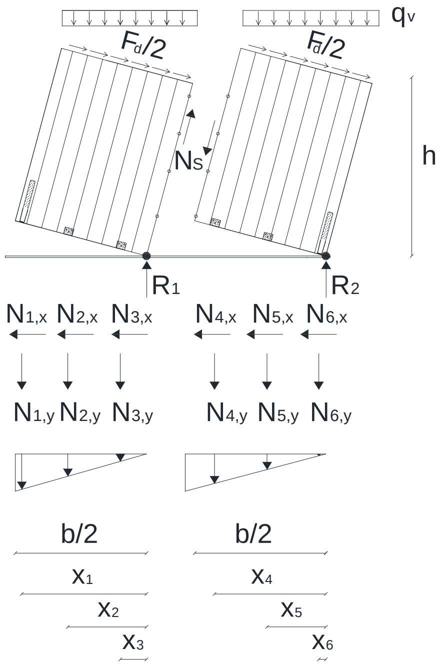

- F_d = factored lateral resistance of the CLT wall
- q_v = vertical load
- h = height of the CLT wall
- $b/2$ = width of one CLT wall segment
- N_i = reaction force in the connection “i”
- N_S = force in the step-joint
- R_i = reaction force of a CLT wall segment
- x_i = distance from the centre of connection ‘i’ to the right edge (rotation point) of each CLT wall segment

Figure 2 Distribution of reaction forces in a coupled CLT wall according to the design model D4

In the first step, the resistances of the CLT wall due to shear forces and due to overturning moments are calculated based on the equilibrium of forces in horizontal direction and moment equilibrium about lower right corner without taking into account the shear-uplift interaction of the brackets due to bidirectional loading. The minimum of these resistances gives so called unreduced factored wall lateral resistance (F_d^*):

$$F_d^* = \min \begin{cases} F_{d,S}^* = 4 \cdot N_{RB,x} \\ F_{d,M}^* = \dfrac{q_v \cdot b^2}{4 \cdot h} + \dfrac{N_{RH} \cdot x_1}{h} + \dfrac{N_{RB}}{h \cdot x_1}\left(x_2^2 + x_3^2 + x_4^2 + x_5^2\right) + N_{RS}\dfrac{b}{2 \cdot h} \end{cases} \tag{4}$$

As presented earlier in the paper, hold-downs are considered to be without shear resistance, thus $N_{1,x} = N_{6,x} = 0$, and the contribution of vertical reaction of the right hold-down can be neglected ($N_{6,y} = 0$). Static equilibrium of forces for the left wall segment in vertical direction give the expression for the reaction R_1:

$$R_1 = N_{RH} + N_{RB}\left(\frac{x_2}{x_1}\right) + N_{RB}\left(\frac{x_3}{x_1}\right) + q_v \, {}^{b}\!/_{2} - N_{RS} \tag{5}$$

where the hold-down has reached its factored resistance, while the vertical reaction forces in the brackets are based on the triangular proportion, and the force in the step joint is equal to its factored resistance. If $R_1 < 0$, the wall segments are not rocking as separate walls, as the factored resistance of the step-joint is greater than the sum of factored resistance of hold-downs and brackets, and the contribution of the vertical load. In such case, the number of screws in the vertical joint shall be reduced to achieve so called coupled wall behaviour. In the second step a reduction of strength for each bracket is taken into account through shear-uplift interaction formula (Eq. (2)). Total factored lateral resistance of CLT wall panel (F_d) can be assessed with an iterative method of reducing the strength of the connections until requirements from the interaction formula are satisfied. This process is shown in Fig. 3.

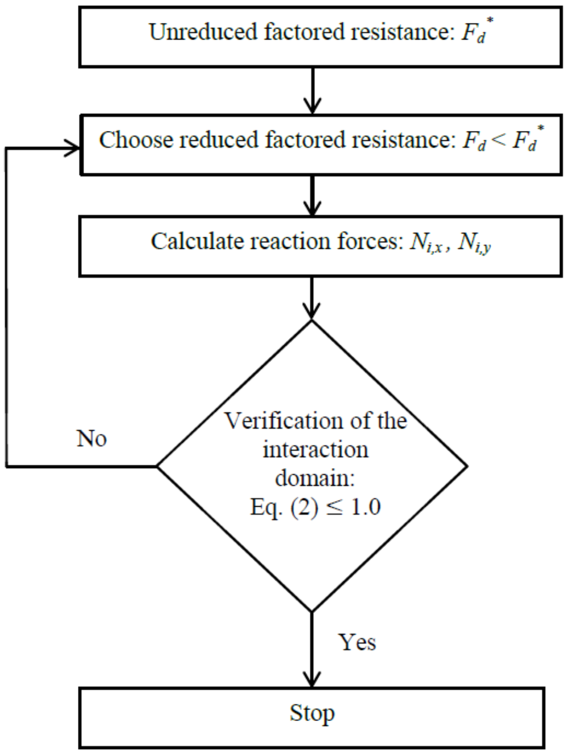

Figure 3 Assessment of CLT wall panel factored resistance F_d with iteration steps

4 Comparison of CLT design values to test results

4.1 2-D CLT wall tests

The models that describe the current design practice as well as new proposed analytical design models were used to obtain the factored lateral load resistances (design resistances) of various CLT wall configurations that were tested cyclically at FPInnovations, Canada [2] and at CNR IVALSA, Italy [9]. The analyzed walls had different aspect ratios and segmentation, different vertical load levels, different connection layouts and different fasteners in the connections. Design model D1 and sub-model D3B have the same theoretical background (Fig. 1) and lead to same results, thus their results are presented in the same column. Model D3 calculates the resistance of the walls due to pure rocking and pure sliding and then choses the lower value as wall resistance. Sub-model D3A considers only rocking of the wall. Since in almost all wall examples analyzed in this study, CLT wall factored resistances obtained using model D3 were due to rocking component (as it was lower than the sliding one), the results for model D3 will also be equal to the results obtained using models D3A (except for Wall I.1, Table 2). The experimental-analytical comparisons are shown in Table 1 for FPInnovations tests and in Table 2 for CNR IVALSA tests. The maximum resistances obtained from the experimental tests ($F_{ult,exp}$) were compared with the design values obtained using the various analytical models (F_d). In the experimental results average values of positive and negative ultimate forces were considered. Although limited number of walls was tested, basic statistical analysis assuming Normal Distribution was performed. Average values and coefficient of variations of experimental vs design ratios were determined, as well as 5th and 95th percentiles of $F_{ult,exp}/F_d$ ratios (Table 1 and Table 2). The ratio between experimental resistance and analytical design value of a CLT wall when using a specific model represents the "safety margin" of that model. The average values of $F_{ult,exp}/F_d$ ratios indicate how conservative the design models are (higher $F_{ult,exp}/F_d$ ratio means more conservative design model). The deviation of $F_{ult,exp}/F_d$ ratios from the average "safety margin" within the model was taken as a measure of consistency of that model. This is represented with COV values and with the 95th perc./5th perc. ratios (Table 1 and Table 2). The lower these values are, the higher the level of consistency the model has. In other words, a design model that has a higher level of consistency has narrower (more uniform) prediction of the design resistance over various wall configurations. Consequently, such model was deemed more suitable for further development of the design procedure of CLT walls under lateral loads. Due to a relatively low number of samples (wall tests) and due to various types of samples (different types of wall configurations) statistical values presented here can only be taken as an approximation. Additional experimental data or results from numerical parametric analyses are needed to cover various wall parameters such as wall geometry, aspect ratio, layout of connectors, type and number of fasteners used in the connectors, vertical load, etc.

Table 1 Comparison of experimental ultimate forces ($F_{ult,exp}$) and factored lateral resistance values (F_d) calculated with different models (FPInnovations CLT wall tests)

Wall name		$F_{ult,exp}$ [kN]	Design Model									
			D1/D3B		D2		D3/D3A		D4		D5	
			F_d [kN]	$\frac{F_{ult,exp}}{F_d}$	F_d [kN]	$\frac{F_{ult,exp}}{F_d}$	F_d [kN]	$\frac{F_{ult,exp}}{F_d}$	F_d [kN]	$\frac{F_{ult,exp}}{F_d}$	F_d [kN]	$\frac{F_{ult,exp}}{F_d}$
1	CA-SN-00	88.9	90.8	**0.98**	21.9	**4.06**	34.8	**2.55**	32.4	**2.74**	25.0	**3.56**
2	CA-SN-02	90.3	90.8	**0.99**	33.4	**2.70**	46.3	**1.95**	42.2	**2.14**	33.3	**2.71**
3	CA-SN-03	98.1	90.8	**1.08**	44.9	**2.18**	57.8	**1.70**	51.5	**1.90**	41.6	**2.36**
4	CA-S1-05	102.7	115.2	**0.89**	50.8	**2.02**	67.2	**1.53**	60.4	**1.70**	48.3	**2.13**
5	CA-S2-06	100.1	94.8	**1.06**	45.9	**2.18**	59.3	**1.69**	53.0	**1.89**	42.7	**2.34**
6	CA-SNH-08	118.2	68.1	**1.74**	45.2	**2.62**	65.3	**1.81**	55.3	**2.14**	43.1	**2.74**
7	CA-SNH-08A	107.1	68.1	**1.57**	39.5	**2.71**	59.6	**1.80**	53.1	**2.02**	41.6	**2.57**
8	CA-SN-11	79.5	81.6	**0.97**	38.1	**2.09**	39.3	**2.02**	37.6	**2.11**	32.8	**2.42**
9	CA-SN-12	92.5	90.8	**1.02**	36.8	**2.51**	38.0	**2.43**	36.5	**2.53**	31.7	**2.92**
10	CA-SN-12A	90.6	90.8	**1.00**	36.8	**2.46**	38.0	**2.38**	36.5	**2.48**	31.7	**2.86**
11	CB-SN-14	190.9	113.4	**1.68**	70.2	**2.72**	111.8	**1.71**	88.7	**2.15**	72.8	**2.62**
12	CB-SN-16	130.2	113.4	**1.15**	46.7	**2.79**	51.9	**2.51**	49.4	**2.64**	43.1	**3.02**
13	CA-SN-20	152.1	158.9	**0.96**	44.9	**3.39**	80.0	**1.90**	73.2	**2.08**	58.6	**2.60**
14	CA-SN-21	54.1	30.4	**1.78**	15.2	**3.56**	30.4	**1.78**	27.7	**1.95**	25.0	**2.16**
15	CA-SN-23	72.2	53.2	**1.36**	30.3	**2.38**	42.1	**1.71**	36.7	**1.97**	30.9	**2.34**
Average				**1.22**		**2.69**		**1.96**		**2.16**		**2.62**
COV [%]				26.3		21.4		17.2		13.9		14.1
5th percentile				0.69		1.75		1.41		1.67		2.01
95th percentile				1.74		3.64		2.52		2.66		3.23
95th perc./ 5th perc.				**2.52**		**2.08**		**1.79**		**1.59**		**1.61**

Table 2 Comparison of experimental ultimate forces ($F_{ult,exp}$) and factored lateral resistance values (F_d) calculated with different models (CNR IVALSA CLT wall tests)

Wall name		$F_{ult,exp}$ [kN]	Design Model									
			D1/D3B		D2		D3/D3A		D4		D5	
			F_d [kN]	$\frac{F_{ult,exp}}{F_d}$	F_d [kN]	$\frac{F_{ult,exp}}{F_d}$	F_d [kN]	$\frac{F_{ult,exp}}{F_d}$	F_d [kN]	$\frac{F_{ult,exp}}{F_d}$	F_d [kN]	$\frac{F_{ult,exp}}{F_d}$
1	I.1	70.7	36.0	**1.96**	46.7	**1.51**	36.0/56.9	**1.96/1.24**	35.2	**2.01**	31.9	**2.22**
2	I.2	104.2	72.0	**1.45**	46.7	**2.23**	70.1	**1.49**	57.5	**1.81**	45.6	**2.29**
3	I.3	100.5	72.0	**1.40**	33.0	**3.05**	56.5	**1.78**	49.9	**2.01**	37.5	**2.68**
4	I.4	106.7	72.0	**1.48**	46.7	**2.28**	70.1	**1.52**	57.5	**1.86**	45.6	**2.34**
5	II.1	97.2	72.0	**1.35**	46.7	**2.08**	70.1	**1.39**	57.5	**1.69**	45.6	**2.13**
6	II.2	92.3	72.0	**1.28**	46.7	**1.98**	70.1	**1.32**	57.5	**1.61**	45.6	**2.02**
7	II.3	84.4	72.0	**1.17**	40.3	**2.09**	46.6	**1.81**	43.2	**1.95**	39.2	**2.15**
8	II.4	93.1	72.0	**1.29**	39.3	**2.37**	49.8	**1.87**	49.6	**1.88**	38.8	**2.40**
9	III.1	102.5	72.0	**1.42**	46.7	**2.19**	70.1	**1.46**	57.5	**1.78**	45.6	**2.25**
10	III.2	91.8	72.0	**1.28**	41.9	**2.19**	48.2	**1.90**	45.6	**2.01**	40.4	**2.27**
11	III.3	102.9	72.0	**1.43**	40.1	**2.57**	50.6	**2.03**	50.3	**2.05**	39.0	**2.64**
12	III.4	82.4	72.0	**1.14**	41.9	**1.97**	48.2	**1.71**	45.6	**1.81**	40.4	**2.04**
13	III.5	86.4	72.0	**1.20**	41.9	**2.06**	48.2	**1.79**	45.6	**1.89**	40.4	**2.14**
14	III.6	63.4	72.0	**0.88**	28.2	**2.25**	34.6	**1.83**	32.8	**1.93**	30.6	**2.07**
Average				**1.34**		**2.20**		**1.70/1.65**		**1.88**		**2.26**
COV [%]				17.9		15.5		13.4/14.9		6.9		8.9
5^{th} percentile				0.94		1.65		1.33/1.25		1.67		1.93
95^{th} percentile				1.73		2.76		2.08/2.06		2.10		2.59
95^{th} perc./ 5^{th} perc.				**1.84**		**1.67**		**1.56/1.65**		**1.26**		**1.34**

Ratios between the maximum experimental and the analytically determined factored resistance values showed different levels of consistency of the models. Tables 1 and 2 show that for the analyzed walls Design model 1 (D1/D3B) and Design model 2 (D2), which are currently used for CLT wall design in Europe and North America, are less consistent than the newly proposed design models D3/D3A, D4 and D5. Use of design model D1 resulted in both overestimation and underestimation of the CLT walls strength. The reason for overestimation of the wall resistances were mostly due to the fact that the analytical models predicted pure sliding failure mechanism, while in experimental tests failures occurred due to predominant rocking motion.

As shown above, design models D3-D5 proved to be more appropriate, as they have shown significantly lower level of difference in the ratios (higher level of consistency) compared to models D1-D2. Namely, the difference between the 5^{th} percentile and the 95^{th} percentile for $F_{ult,exp}/F_d$ ratios are less than 80% (FPInnovations walls, Table 1) and less than 65% (CNR IVALSA walls, Table 2), while this difference is significantly higher for design models D1 and D2 (up to 152% for D1 and 108% for D2). Furthermore, design models D4 and D5 are more consistent compared to the Design model D3, which on the other hand has less complex calculation procedure. Since design models D4 and D5 take into account shear-uplift interaction of brackets the consistency of the $F_{ult,exp}/F_d$ ratios improves further and for these two models 95^{th} perc./5^{th} perc. ratio is around 60% (FPInnovation walls) and less than 35% in case of CNR IVALSA walls. The linear shear-uplift interaction domain used in model D5 was more rigorous in comparison to the circular interaction domain used model D4, thus giving lower design values of lateral wall resistance. As the sub-model D3A assumes only rocking behaviour of the wall it was less suitable for CLT wall design in cases where resistance of CLT walls was mostly governed by sliding resistance (Wall I.1, Table 2).

Both FPInnovations and CNR IVALSA comparisons showed the same trend and outcomes, namely the analytical model with the highest level of consistency of $F_{ult,exp}/F_d$ ratios was the model D4, followed by models D5 and D3, while the models D1 and D2 showed the largest deviation of $F_{ult,exp}/F_d$ ratios from the mean values. Lower percentages of COV values and 95th perc./5th perc. values in the case of CNR IVALSA experimental-analytical comparison were due to the lesser variations of wall configurations compared to the FPInnovation walls. Namely, all hold-downs and brackets were of same type, using same type and number of fasteners, while the vertical load, number and position of connectors, type and strength of the vertical joint between the adjacent coupled wall segments was varied. Therefore, this comparison showed that among the analyzed analytical design models (and for the available test results used in this study), model D4 is the most suitable for future development of the design procedure for CLT walls. Additional parametric numerical analyses with different configurations of wall geometry, segmentation of walls, types of connectors and fasteners are needed to further justify this claim.

The analyzed analytical models also showed different "safety margin" levels. In general, all structural elements are designed with certain consistent level of safety, which is the difference between their factored resistance and the ultimate load (probable resistance). The ratio between the factored resistance and average experimental ultimate load levels from cyclic tests for wood-frame shear walls in CSA O86-09 is approximately 2.5. The desired level of safety for the CLT walls models can be achieved by introducing a multiplication factor, which can be defined as "wall safety adjustment factor" γ_w. The factored resistance values (F_d) obtained from the analyzed CLT walls can then be multiplied with this factor to reach the desired level of wall safety.

4.2 3-D CLT house tests

The analytical design models presented in this paper were also used to evaluate the lateral resistance of a two-storey CLT house that was subjected to lateral cyclic loading at FPInnovations [3]. The house was tested in two directions, one direction at a time. Fig. 4a shows the CLT house ready for loading in N-S direction. In both directions the failure condition of the house was reached due to the exceeded shear resistance in the lower storey.

(a)

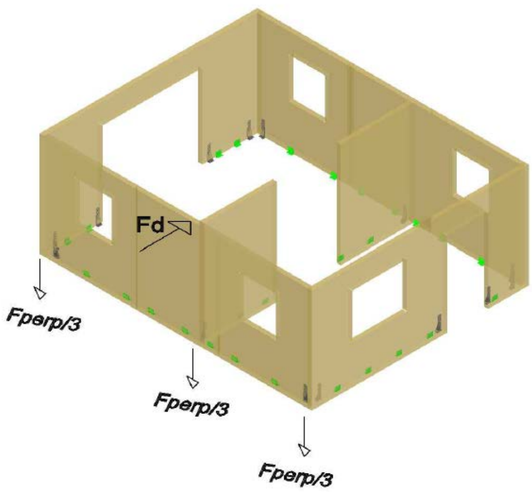

(b)

Figure 4 (a) Two-storey CLT house before loading in N-S direction; (b) Scheme of the first storey for the case when the uplift resistance of perpendicular walls is taken into account in the analytical design models (loading in N-S direction)

Two different cases were analyzed in this analytical study. In the first case only the lateral resistance of the walls in the loading direction was taken into account when determining the house lateral strength (F_d), while in the second case the uplift resistance of the walls perpendicular to the loading direction (so called "perpendicular walls") F_{perp}, was also considered. In both cases 2-D kinematic CLT wall models presented earlier in the paper were used. In the second case the walls were modelled with additional uplift resistance force at the end of the walls being the sum of uplift resistances of the connectors from perpendicular walls (Fig. 4b).

The purpose of this part of the research work was to determine the influence of perpendicular walls on the lateral resistance of the house and to study the differences of presence of perpendicular walls in the analytical design models. Table 3 shows the experimental lateral load resistances for the house in both directions and the values obtained from the analytical models, with and without taking into account the influence of perpendicular walls. Also, ratios between the experimental and design strength values are shown for both cases. Furthermore, the experimental vs design ratios obtained for the house (3-D specimen) are compared to those of the 2-D CLT walls (Section 4.1). In addition, experimental failure modes were compared to the failure modes obtained with the analytical models with (s) being the failure mode due to sliding (exceeded shear resistance), and (r) being the failure mode due to rocking (exceeded overturning moment resistance).

Table 3 Experimental vs design lateral resistances of the CLT house and comparison of average $F_{ult,exp}/F_d$ ratios

Case Name	$F_{ult,exp}$ [kN]	Design Model											
		D1/D3B		D2		D3		D3A		D4		D5	
		F_d [kN]	$\frac{F_{ult,exp}}{F_d}$	F_d [kN]	$\frac{F_{ult,exp}}{F_d}$	F_d [kN]	$\frac{F_{ult,exp}}{F_d}$	F_d [kN]	$\frac{F_{ult,exp}}{F_d}$	F_d [kN]	$\frac{F_{ult,exp}}{F_d}$	F_d [kN]	$\frac{F_{ult,exp}}{F_d}$
E-W (par.)	365.2 (s)	56.2 (r)	6.50	63.8 (r)	5.72	73.8 (r)	4.95	73.8 (r)	4.95	69.0 (r)	5.29	56.6 (r)	6.45
E-W (par. + perp.)		106.4 (s)	3.43	76.0 (s)	4.81	106.4 (s)	3.43	120.4 (r)	3.03	101.2 (s)	3.61	95.4 (s)	3.83
N-S (par.)	356.5 (s)	73.5 (r)	4.85	39.7 (r)	8.98	58.9 (r)	6.05	58.9 (r)	6.05	55.0 (r)	6.48	42.7 (r)	8.35
N-S (par. + perp.)		103.6 (s)	3.44	85.9 (s)	4.15	89.0 (s)	4.01	116.6 (r)	3.05	86.7 (s)	4.11	81.3 (s)	4.38
Average values													
$F_{ult,exp}/F_d$ (par.)		5.68		7.35		5.50		5.50		5.89		7.40	
$F_{ult,exp}/F_d$ (par. + perp.)		3.44		4.48		3.72		3.04		3.86		4.11	
$F_{ult,exp}/F_d$ (CLT walls)		1.22		2.69		1.96		1.96		2.16		2.62	

Experimental-to-analytical strength ratios ($F_{ult,exp}/F_d$) were very high (conservative) in the case when only walls in the direction of loading (denoted as 'par.') were taken into account. The average ratios varied between 5.50 and 7.40. In cases where perpendicular walls were taken into account (denoted as 'par. + perp.'), significant increase in analytical design resistance was obtained. Average $F_{ult,exp}/F_d$ ratios in this case varied between 3.04 and 4.48. In both cases for the 3-D house, however, the ratios were substantially higher than those obtained in case of individual 2-D CLT walls. This means that in 3-D structures there is an additional source that contributes to the lateral resistance of the house such as sliding and rocking resistance of perpendicular walls. All design models predicted rocking as a failure condition when no perpendicular walls were taken into account. To the contrary, when perpendicular walls were taken into account, sliding became the governing design condition because of increased overturning design resistance of the house due to the perpendicular walls. Thus, design models which included perpendicular walls predicted the governing failure condition correctly (sliding), while in case of design models without perpendicular walls, the prediction was wrong (rocking governing condition). The only exception was model D3A which does not include verification of shear forces (Fig. 1.). The analytical models that do not take into account the influence of perpendicular walls can lead to very conservative design values and inadequate predictions of kinematic behaviour of the CLT buildings under lateral loads.

5 Conclusions

Currently there are no standardized methods for determining the resistance of CLT shearwalls under lateral loads. In this paper some new analytical models for predicting of the design (factored) resistance of CLT walls under lateral loads were developed based on connection properties. These new models were evaluated for their consistency along with the models that are currently used in North America and in Europe. Newly developed models that account for sliding-uplift interaction in the brackets (models D3-D5) showed higher level of consistency compared to existing ones (D1 and D2). The analytical model D4 that accounts for sliding-uplift interaction according to a circular domain, proved to be the most suitable candidate for future development of design procedures for determining resistance of CLT walls under lateral loads. The influence of perpendicular walls shall be included in the analytical design models of CLT walls. The next step in the development of design procedure for CLT walls under lateral loads is implementation of capacity based design principles, which will take into account statistical distributions of connection resistances.

6 References

[1] Gagnon S., Pirvu C. CLT Handbook: Cross-Laminated Timber. FPInnovations, Canada, 2011.

[2] Popovski M., Schneider J., Schweinsteiger M. Lateral resistance of cross-laminated wood panels. *Proc. of the 11th World Conference on Timber Engineering*, Riva del Garda, Italy, 2010.

[3] Popovski M., Gavric I., Schneider J. Performance of two-storey CLT house subjected to lateral loads. *Proc. of the 13th World Conference on Timber Engineering*, Quebec City, Canada, 2014.

[4] Ceccotti A. New technologies for construction of medium-rise buildings in seismic regions: The XLAM case. *Journal of the International Association for Bridge and Structural Engineering*, 2-2008, 156-165.

[5] Dujic B., Strus K., Zarnic R., and Ceccotti A. Prediction of dynamic response of a 7-storey massive XLam wooden building tested on a shaking table. *Proc. of the 11th World Conference on Timber Engineering*, Riva del Garda, Italy, 2010.

[6] Follesa M., Christovasilis I.P., Vassallo D., Fragiacomo M., and Ceccotti A. Seismic design of multi-storey CLT buildings according to Eurocode 8. *Ingegneria Sismica/International Journal of Earthquake Engineering, Special Issue on Timber Structures*, October-December 2013, 27-53.

[7] Tomasi R. Seismic behaviour of connections for buildings in CLT. *Proc. of COST Action FP1004 Conference on The State-of-the Art in CLT Research*, Graz, Austria, 2013.

[8] Gavric I., Fragiacomo M., Popovski M., Ceccotti A. Behaviour of cross-laminated timber panels under cyclic loads. *Proc. of RILEM Conference: Materials and Joints in Timber Structures – Recent Advancement of Technology*, Stuttgart, Germany, October 2013.

[9] Gavric I., Fragiacomo M., Ceccotti A. Cyclic behavior of cross-laminated timber (CLT) wall systems: Experimental tests and analytical prediction models. *ASCE Journal of Structural Engineering*, submitted.

[10] Gavric I., Fragiacomo M., and Ceccotti A. Cyclic behaviour of typical metal connectors for cross-laminated (CLT) structures. *Materials and Structures*, published online, 2014, DOI: 10.1617/s11527-014-0278-7.

[11] Gavric I., Fragiacomo M., Ceccotti A. Strength and deformation characteristics of typical CLT connections. *Proc. of the 12th World Conference on Timber Engineering*, Auckland, New Zealand, 2012.

[12] Uibel T., Blaß H. J. Load carrying capacity of joints with dowel type fasteners in solid wood panels. *Proc. of the 43rd CIB-W18 Meeting*, Paper 39-7-5, Florence, Italy, August 2006.

[13] CSA O86-09. Engineering design in wood. Canadian standards association, Mississauga, Ontario, Canada, 2009.

[14] ETA-07/0055. Three-dimensional nailing plate European technical approval. European organisation for technical approvals, Charlottenlund, Denmark, 2007.

INTER

International Network on Timber Engineering Research

EFFECTS OF DESIGN CRITERIA ON AN EXPERIMENTALLY-BASED EVALUATION OF THE BEHAVIOUR FACTOR OF NOVEL MASSIVE WOODEN SHEAR WALLS

L Pozza

R Scotta

D Trutalli

Department of Civil, Environmental and Architectural Engineering, University of Padova

A Polastri

Trees and Timber Institute, Italian Research Council (CNR-IVALSA)

A Ceccotti

University IUAV of Venezia

ITALY

Presented by D Trutalli

BJ Yeh asked that the hysteresis loops of the staple wall did not seem to reach the ultimate capacity. D Trutalli stated that they did not have breakage of the staples.

G Doudak asked how to justify q=4 between rigid and deformable panels. D Trutalli answered that test results are needed to help justify q=4.

F Lam received clarification that the staple system is the Hundegger system.

A Buchanan questioned the use of q as a wall ranking method. He questioned how to account for the poor performance of low stiffness walls with high q.

H Blass stated that the gaps between members and the performance of the base connections will also influence the wall response. D Trutalli responded that the base connectors were chosen with respect to the deformability of the panels.

M Fragiacomo asked what kind of failures was observed. D Trutalli answered that normal failures were observed with glued walls. With the unglued walls staples did not break.

I smith asked about the peak acceleration in the building. D Trutalli said that they do not have the information.

M Yasumura asked whether vertical load was applied. D Trutalli answered that 18.5 kN/m vertical load was applied. He also confirmed that 15 earthquakes were used in simulations to establish the q factor.

Effects of design criteria on an experimentally-based evaluation of the behaviour factor of novel massive wooden shear walls

L. Pozza, R. Scotta, D. Trutalli

Department of Civil, Environmental and Architectural Engineering, University of Padova, Italy

A. Polastri

Trees and Timber Institute, Italian Research Council (CNR-IVALSA), Italy

A. Ceccotti

University IUAV of Venezia, Italy

Keywords: Timber shear walls, Massive timber panels, Seismic design, Behaviour factor

1 Introduction

The growing use of timber structures in seismic regions has led to the development of numerous innovative construction systems using massive timber shear walls (e.g. Cross Laminated Timber - CLT) or timber frames (e.g. Platform Frame). CLT typology has been widely studied through experimental tests and numerical simulations (e.g., Ceccotti et al. 2006, Ceccotti 2008, Sandhaas et al. 2009, Dujic et al. 2010, Popovski et al. 2010, Fragiacomo et al. 2011, Gavric et al. 2011, Yasumura 2012, Ceccotti et al. 2013, Gavric et al. 2013, Pei et al. 2013, Pozza et al. 2013a, Gavric et al. 2014, Popovski et al. 2014, Pozza and Scotta 2014). However, other construction systems using massive timber elements assembled with various techniques have been developed by numerous companies, in order to improve the favourable characteristics of timber structures, e.g., prefabrication, structural efficiency, material economies, rapidity of construction, mechanical properties, environmental compatibility.

These novel structural systems require the assessment of mechanical properties, in order to quantify the safety level against vertical and lateral loads and to develop a suitable design procedure. The most important parameters that describe the behaviour of structures when subjected to earthquake are stiffness, strength, ductility and dissipative capacity (Elanshai and Di Sarno, 2008). Tests are therefore necessary to quantify these parameters that can be fully assessed for timber structures with quasi-static cyclic-loading tests on entire specimens (CEN 2006). Numerical modelling permits then to replicate these tests and perform non-linear analyses to extend results to entire structures and quantify other important parameters, e.g., Peak Ground Acceleration that leads the structure to near-collapse condition and relative Behaviour Factor or Seismic Force Modification Factor (termed “R” in ASCE 7-10 and NBCC and “q” in the Eurocodes) (ASCE 2010, IRC 2010, CEN 2013), which summarizes the post-elastic behaviour and energy dissipation capacity of a structure. The most suitable behaviour factor value - henceforth also called 'q-factor' - for innovative timber construction systems is still required to be defined, since there are no explicit references in available codes and no explicit seismic-design methods for these new structural systems.

One of the most relevant issues in the definition of such factor is the assessment of both the "intrinsic" q-factor, and design over-strength. The intrinsic q-factor takes into account the energy dissipation capacity and all intrinsic over-resistances (e.g. due to post-elastic hardening behaviour); the design over-strength is used to quantify the difference between the required and the actual strength of a material, a component or a structural system (Elnashai and Di Sarno 2008). Codes generally refer to a unique factor that takes into account energy dissipation, intrinsic over-resistances and overdesign, since the design acceleration is typically smaller than yield acceleration (Fajfar 2000). In other words, q-factor is not only an "intrinsic" property of the structure, but it is also strictly related to the adopted seismic design code and the safety level assumed by designers.

In this work, three massive wooden shear-wall systems have been analysed by means of experimental tests and numerical simulations. Test results are presented to characterize these structures in terms of strength, stiffness, ductility, and hysteresis behaviour. Main steps of numerical modelling are described in order to evaluate the dissipative capacity and to estimate the suitable intrinsic q-factor for increasing damage level of walls.

2 Experimental tests

Here the main details of the experimental phase are briefly given. For further details, see (Pozza et al. 2014).

2.1 Description of tested walls

The tests presented here were part of three experimental campaigns performed at the Laboratory of Mechanical Testing, CNR-IVALSA, at San Michele all' Adige (Trento, Italy). The test configurations and connection systems to the foundations were not the same for the various walls, since the tests were partly commissioned by private companies for research and development projects: the companies had used different connection systems in order to optimize the mechanical response.

Four wall configurations corresponding to three massive wooden shear-wall systems were studied (Fig. 1): two Cross-Laminated-Glued (CLT) walls, Cross-Laminated-Stapled panels, and Layered Panels with dovetail inserts. In CLT walls, the panels were composed gluing together alternatively oriented perpendicular layers. In Cross-Laminated-Stapled walls, glue was replaced by metal staples. In Layered walls, the layers of vertically oriented boards were connected with perpendicular dovetail inserts. The connection systems adopted in the different test configurations, i.e. hold-downs and angle brackets, fastened with nails or screws, are summarised in Table 1.

CLT walls were assembled with 5-layer panels, made of C24 timber boards, for an overall thickness of 85 mm. The first wall represents a typical CLT wall anchored to the foundation by the use of hold-downs and angle brackets (Fig. 1a) (un-jointed CLT wall). In the case of the second wall, two panels have been connected using a half-lap joint: the CLT panels were grooved symmetrically to half the depth of the panel at the edge, so that they could be coupled with screws inserted orthogonally to the joints (Fig. 1b) (jointed CLT wall).

The stapled wall specimens (Fig. 1c) were made of 5 crossed layers of C24 spruce boards, nominal thickness 28.5 mm; the layers were stapled to each other. Layered wall with dovetail inserts was made up of 3 layers of vertical sawn spruce boards, nominal thickness

60 mm, coupled with 5 pairs of horizontal spruce elements inserted horizontally creating a so called dovetail joint (Fig. 1d).

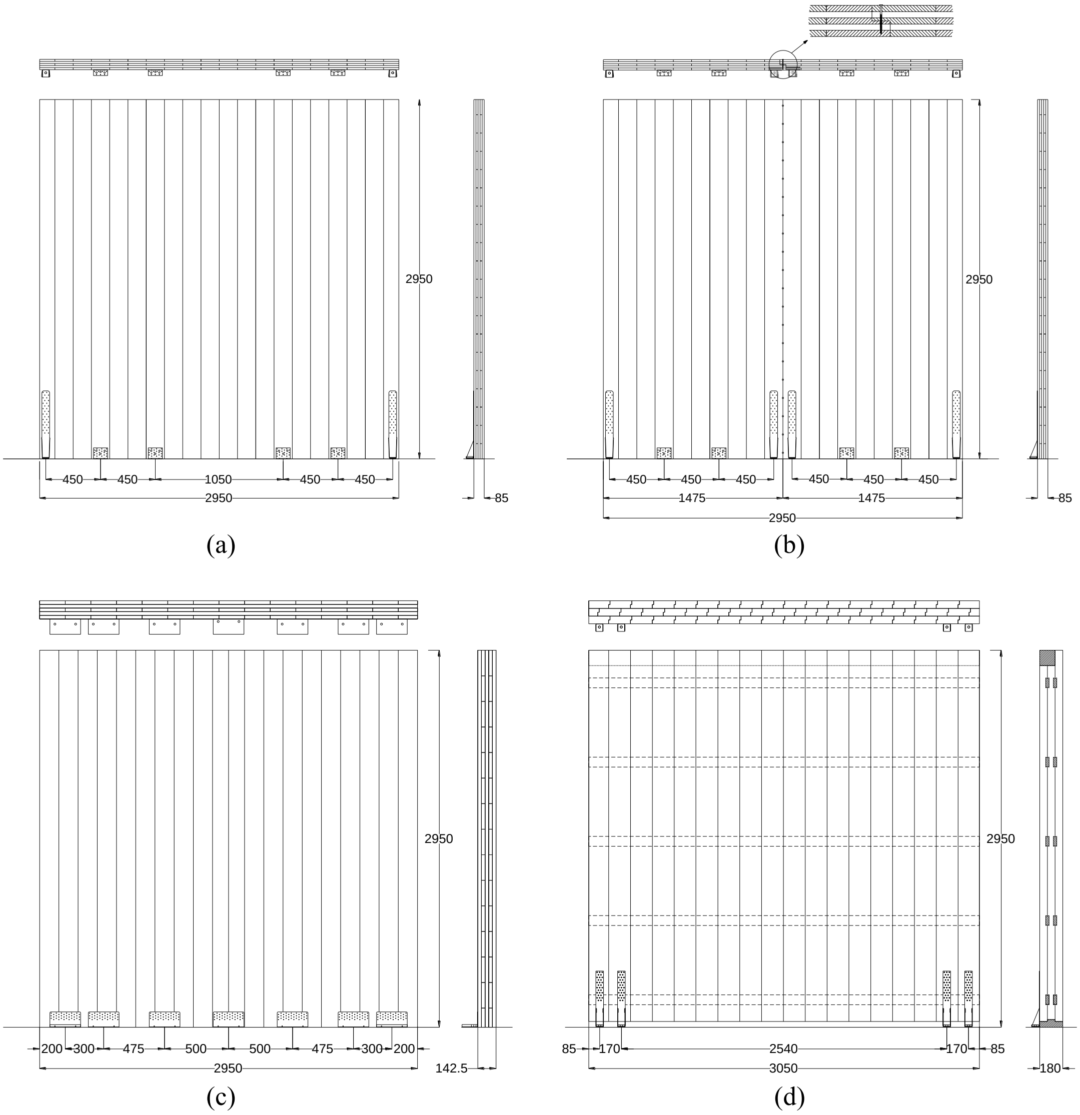

Figure 1 Geometric arrangement and connection systems of tested walls. (a) Un-jointed CLT wall; (b) jointed CLT wall; (c) Stapled wall and (d) Layered wall.

Table 1 Adopted connection system (dimensions in mm).

Specimen	Connectors		Anker type nails or screws	
	Type	No.	Size	No.
Un-jointed CLT	Hold-down - foundation	2	4x60	12
	Angle bracket - foundation	4	4x60	11
Jointed CLT	Hold-down - foundation	4	4x60	12
	Angle bracket - foundation	4	4x60	11
	Screw – vertical joint	10	8x100	
Stapled	Angle bracket- foundation	7	4x100	36
Layered	Hold-down - foundation	4	4x60	30
	Inclined screw - foundation	18 pairs	8x200	-

The specimens were tested with the quasi-static cyclic loading protocol recommended by EN 12512 (CEN 2006). An identical test protocol was adopted for all the studied walls and the chosen reference displacement (yielding point) was equal to 20 mm. The applied vertical load was 18,5 kN/m.

2.2 Experimental results and analytical interpretation

2.2.1 Failure modes

At the end of the test procedures, no evident failures in the massive wall panels have been registered. CLT walls showed evident failure due to large deformation in the connection systems (hold-downs and angle brackets) (Fig. 2a and 2b). Moreover, the jointed wall showed failure of the middle half-lap joint between the two panels (Fig. 2b). This last failure mode revealed rigid rotation of the two panels, which, subjected to large displacements, behaved independently. For the un-jointed CLT wall the main deformations are concentrated in the angle brackets (Fig. 2a).

At the end of testing, although stapled and layered walls did not show an evident failure mode, extensive large shear deformation and consequent sliding between boards occurred: in case of stapled wall it is possible to observe evident deformation between the vertical timber elements due to staple deformation (Fig. 2c), while layered wall evidenced sliding between the vertical boards after plastic deformation of the dovetail inserts subjected to compressive stress perpendicular to the grain (Fig. 2d).

(a)

(b)

(c)

(d)

Figure 2 Tested walls at the end of testing procedure: (a) Un-jointed CLT; (b) Jointed CLT; (c) Stapled wall and (d) Layered wall.

2.2.2 Analysis of results

Performed quasi-static cyclic loading tests allow to define characteristic parameters that are elastic and post-elastic stiffness, yielding point, failure condition, and ductility ratio (CEN 2006, CEN 2013). These parameters are fundamental for design and modelling of novel structural systems and are fully defined using a suitable bi-linearization method of the envelope force-displacement curve. Actually, various methods are proposed to compute this point (CEN 2006, Muñoz et al. 2008). In this work an equivalent-energy method with post-elastic hardening branch was used (Pozza et al. 2012). Fig. 3 shows the evaluation of yielding points. Three limits of ultimate top displacements (i.e., inter-storey drift) were imposed, which correspond to three levels of increasing damage of the structure: 80 mm (2.67% - no data for higher imposed drifts were available therefore this was assumed as ultimate failure drift of specimens 3 of the 4 panels), 60 mm (2.00% - ultimate drift for the un-jointed CLT specimen) and 40 mm (1.33%). For each limit the proper evaluation of the yielding point is given in order to obtain the appropriate data as input for the numerical analyses and q-factor calculation described below.

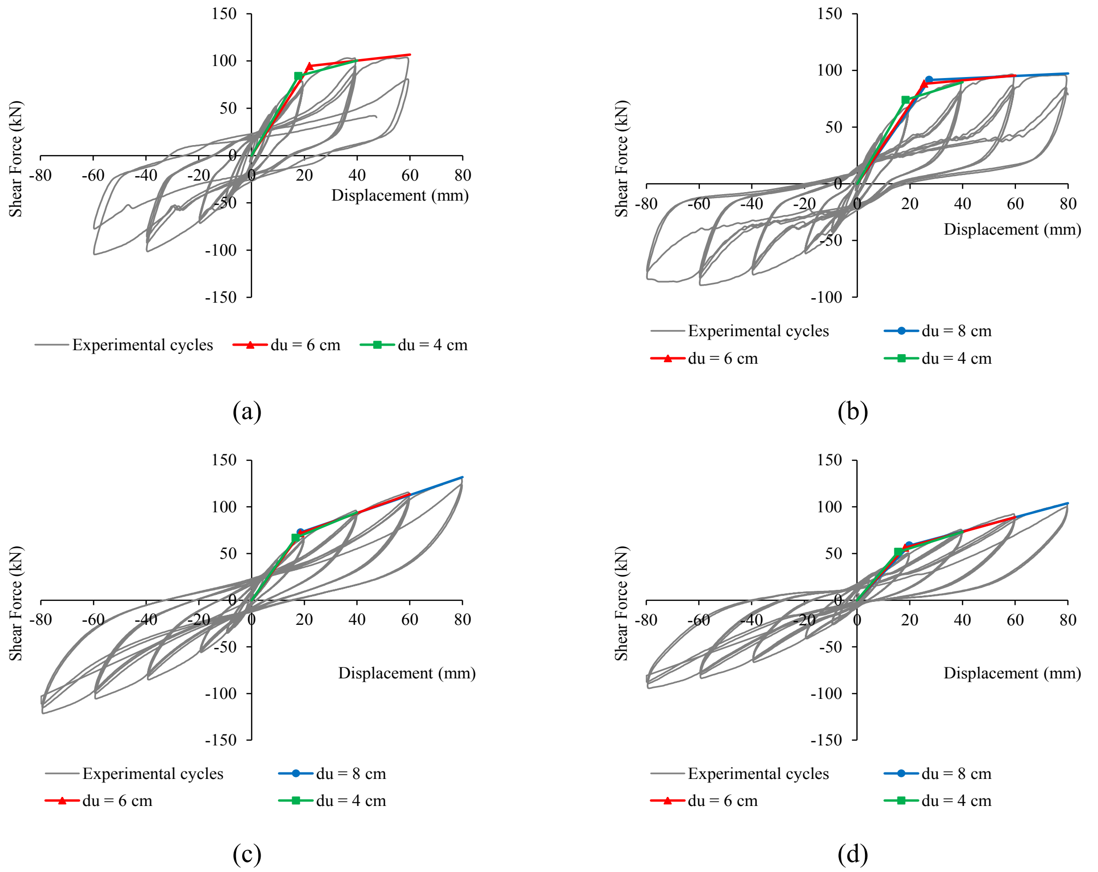

Figure 3 Experimental cycles and definition of yielding point for each imposed ultimate displacements: (a) Un-joined CLT wall; (b) Jointed CLT wall; (c) Stapled wall; (d) Layered wall.

3 Numerical modelling

A simplified numerical model of the tested shear walls was considered. The modelling criteria were essentially those reported in (Ceccotti 2008). In detail, the panels were modelled as lattice modules composed of stiff elastic truss elements at the perimeter and non-linear springs adopting the hysteresis model of Elwood (Elwood and Moehle 2006) as diagonals. According to this model, all the nonlinearities due to the base connections and specific composition of the panel are concentrated in the diagonal elements. The parameters of non-linear diagonal springs were obtained by fitting the experimental cyclic behaviour under lateral loads. The research-oriented numerical code “Open System for Earthquake Engineering Simulation - OPENSEES” (McKenna et al. 2000) was used to implement the numerical model and perform the analyses.

Each numerical model of shear walls was calibrated on experimental results, reproducing the base shear force for each imposed top displacement according to the cyclic-loading protocol given by CEN (2006). Fig. 4 shows the numerical hysteresis cycles compared to the experimental ones.

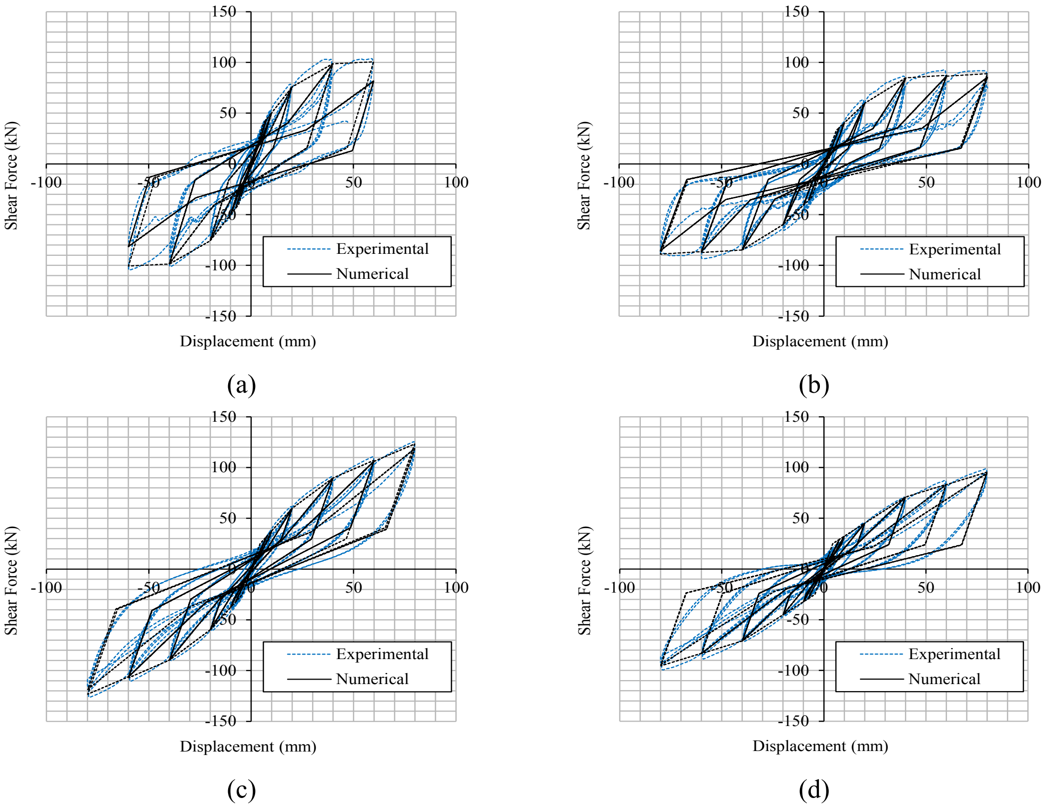

Figure 4 Hysteresis cycles of: (a) Un-jointed CLT wall, (b) Jointed CLT wall, (c) Stapled wall, (d) Layered wall.

4 Assessment of q-factor

Proper definition of the q-factor is essential in the force-based seismic design (Chopra 1995) of timber structures, particularly for innovative timber construction systems, for which there are no explicit references in available codes.

4.1 Methods for the q-factor evaluation

According to Ceccotti and Sandhaas (2010), the method based on experimental tests and numerical simulations results the most efficient for newly developed timber systems. According to this method the definition of q-factor of the sample building refers to the design condition, defined by the design PGA (PGA_d), and the ultimate condition, defined by PGA_u: the former can be analytically or experimentally evaluated, the latter is numerically obtained. Q-factor values are then calculated as ratio between the PGA_u and the corresponding PGA_d. Differences between design and modelling phase introduce then uncertainties in the final values of q-factor that can be influenced mainly by design over-strength. A correct evaluation of the intrinsic q-factor should take into account all intrinsic capacities of the system, i.e., dissipative capacity, ductility, redundancy, post-elastic hardening behaviour, and strength reserve. However, each over-resistance of the walls induced by design criterion, (e.g. safety level assumed by designers or simplified analytical methods for design) should not influence this value and can be computed in addition.

Imposing the design condition coinciding with that of yielding of the structure allows to calculate the intrinsic value of the q-factor. It is clear that such design condition depends only on the bi-linearization method adopted to evaluate the yielding limit from the experimental load-displacement curve. This approach is therefore based on the following issues: it is dependent on need to define a yielding and near-collapse condition, whereas it is independent on the design of the structure (e.g., over-design factors and safety level assumed), and on the available seismic codes (e.g. the factored resistances of materials).

The near-collapse condition of timber wall systems must be defined both in design and modelling phase assuming a criterion based on the maximum displacement or distortion capacity that the structure can reach without collapsing. Various limits of near-collapse can be imposed, e.g., the first collapse of a connection element (Ceccotti 2008) or the achievement of an inter-storey drift beyond which the structure is no longer safe and suffers severe damage (Schädle and Blaß 2010). These limits can be evaluated from full-scale quasi-static tests on entire wall specimens or imposed in the design phase. In this work the inter-storey drift has been used as near-collapse condition (Fig. 3).

It is necessary to note that the applied method allows to define an intrinsic q-factor, which is specific only for the examined sample building. In order to obtain a more general result it is necessary to extend the study varying the sample building (geometry, wall arrangement, number of storeys etc..) and performing additional analyses (Pozza et al. 2013a).

4.2 Case-study configuration and design criteria

A simplified numerical model of a shear-wall of a three-storey building, formed by stacking three levels of the experimentally tested panels, was considered. Design earthquake forces on the case-study shear walls were calculated by means of an equivalent static analysis considering elastic response spectrum for building foundations resting on type A soil (rock soil, corresponding to S=1.0, T_B=0.15s, T_C=0.4s T_D=2.0s), q-factor=1, and building importance factor γ_I=1, according to Eurocode 8 (CEN 2013). In order not to introduce effect of design over-strength in the evaluation of q-factor, the equivalence of the design base shear force to the experimentally evaluated yielding force (i.e., $PGA_d = PGA_y$) had to be imposed. Assuming the first mode period of each wall in the plateau range of the spectral responses and the first mode participating seismic mass equal to 14 t, for all the shear walls, the PGA_y were determined from the experimentally evaluated yielding shear force proper of each wall for each imposed drift, applying the linear static analysis according to (CEN 2013), see Fig. 5. Then the initial hypothesis that all first mode periods were in the plateau range was confirmed, since the fundamental periods of all shear walls resulted to be in the range between 0,36 and 0,40 s, i.e., between T_B=0.15s and T_C=0.4s.

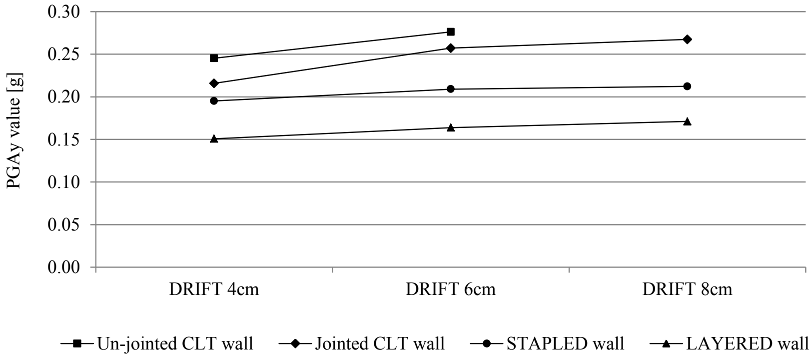

Figure 5 PGA_y values for the investigated systems at the three imposed drifts.

4.3 Q-factor evaluation

A series of non-linear dynamic analyses (NLDA) was carried out in order to extend the experimental results and assess the seismic performance of the examined shear walls.

Performing simulations with increasing intensity of earthquake signals allowed us to compute the effective PGA_u and compare it with PGA_d. Then, according to the adopted method, q-factor was evaluated as the ratio between PGA_u and PGA_d. Such NLDA were carried out considering 15 seismic shocks, artificially generated in order to meet the spectrum compatibility requirement with the design elastic spectra. Two types of software were used to generate the shock signals: SIMQKE_GR (Gelfi 2012) and SeismoArtif (Seismosoft 2013). Dynamic equilibrium equations were integrated with a not-dissipative Newton-Raphson scheme and time-steps of 0.001 s, introducing an equivalent Rayleigh viscous damping of 2%, according to (Ceccotti 2008). Results are reported in Fig. 6 and 7 and in Table 2. It is well known that when performing non-linear time history analyses the structural response is strongly dependent on the frequency content of the adopted seismic signals and the elastic periods of the structures. Therefore q-factor depends not only on the shear strength of the walls, but also on their ductility and dissipative capacities and on the frequency content of the seismic motion. All these factors can be evaluated only by means of non-linear time-history analyses.

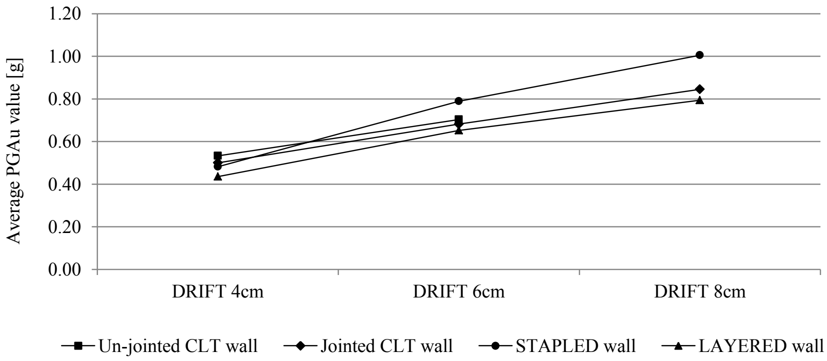

Figure 6 Average PGA_u values for the investigated systems at the three imposed drifts.

PGA_u values provide the first comparison among walls in terms of resistance to seismic actions because the walls have the same mass and geometry. Fig. 6 shows that stapled wall guarantees the highest resistance to lateral loads. Even un-jointed CLT wall shows a good behaviour for low drift thanks to high strength and stiffness of the wall (Fig. 3).

Q-factor values obviously increase with the drift level, even if not proportionally. The significant value of q-factor is that achieved at the real ultimate capacity of the walls and, due to the high number of numerical simulations performed, average results represent a reliable estimation of the intrinsic q-factor of the investigated shear walls (Table 2). The un-jointed CLT panel demonstrates the lowest dissipative and ductility capacity. The other three panels have a greater ultimate drift capacity (2,67%), for which they assure higher q-factors. The high value for stapled and layered panels, if compared with CLT walls, is due not only to higher dissipative capacity, but also to the hardening behaviour of those two panels. This type of post-elastic behaviour involves intrinsic strength reserve after yielding, that increases the PGA_u value, and a lower PGA_y, because of the lower values of yielding strength (Fig. 3, 5 and 6). Both the increase of PGA_u and the decrease of PGA_y imply a rise of q-factor for systems with marked post-elastic hardening behaviour. The comparison between the examined CLT walls shows that the un-jointed panel presents less displacement capacity and less ductility than the jointed one. Therefore the jointed panel ensures a reserve of ductility and energy dissipation until reaching a state of near-collapse condition for a greater drift, for which a greater q-factor can be obtained, despite an ultimate strength less than that of the un-jointed wall. This is because the shear failure mechanism of an un-jointed wall, is replaced by a rocking failure mechanism in which the two CLT panels rock and slide relative to one another at the joint between them. The jointed CLT wall results more performant for use in seismic-prone areas, because of the reaching of higher displacements before failure and consequent increase of q-factor (Pozza et al. 2013a). The above reported remarks are obtained comparing average values of q-factor. The standard deviation is however not the same among walls and for the three drift limits (Fig. 7 and Table 2). It has to be noted that stapled and layered walls present higher dispersion of results for drift higher or equal than 6 cm. The consequence is that difference among walls in terms of more precautionary values than average ones (e.g. 5% characteristic) becomes lower.

Table 2 Obtained q-factor values.

	Un-Jointed CLT			Jointed CLT			Stapled wall			Layered wall		
T_1 (s)	*0.36*			*0.37*			*0.40*			*0.37*		
DRIFT (cm)	*4.00*	*6.00*	*8.00*	*4.00*	*6.00*	*8.00*	*4.00*	*6.00*	*8.00*	*4.00*	*6.00*	*8.00*
MIN	1.79	2.03	-	1.78	2.00	2.51	1.90	2.54	3.53	2.36	2.90	3.47
MAX	2.82	3.43	-	3.31	3.74	4.25	3.08	5.02	6.22	3.52	5.07	5.88
AVERAGE	2.18	**2.55**	-	2.32	2.65	**3.16**	2.47	3.78	**4.74**	2.89	3.98	**4.64**
ST. DEV.	0.34	0.38	-	0.45	0.44	0.46	0.35	0.73	0.81	0.34	0.66	0.70

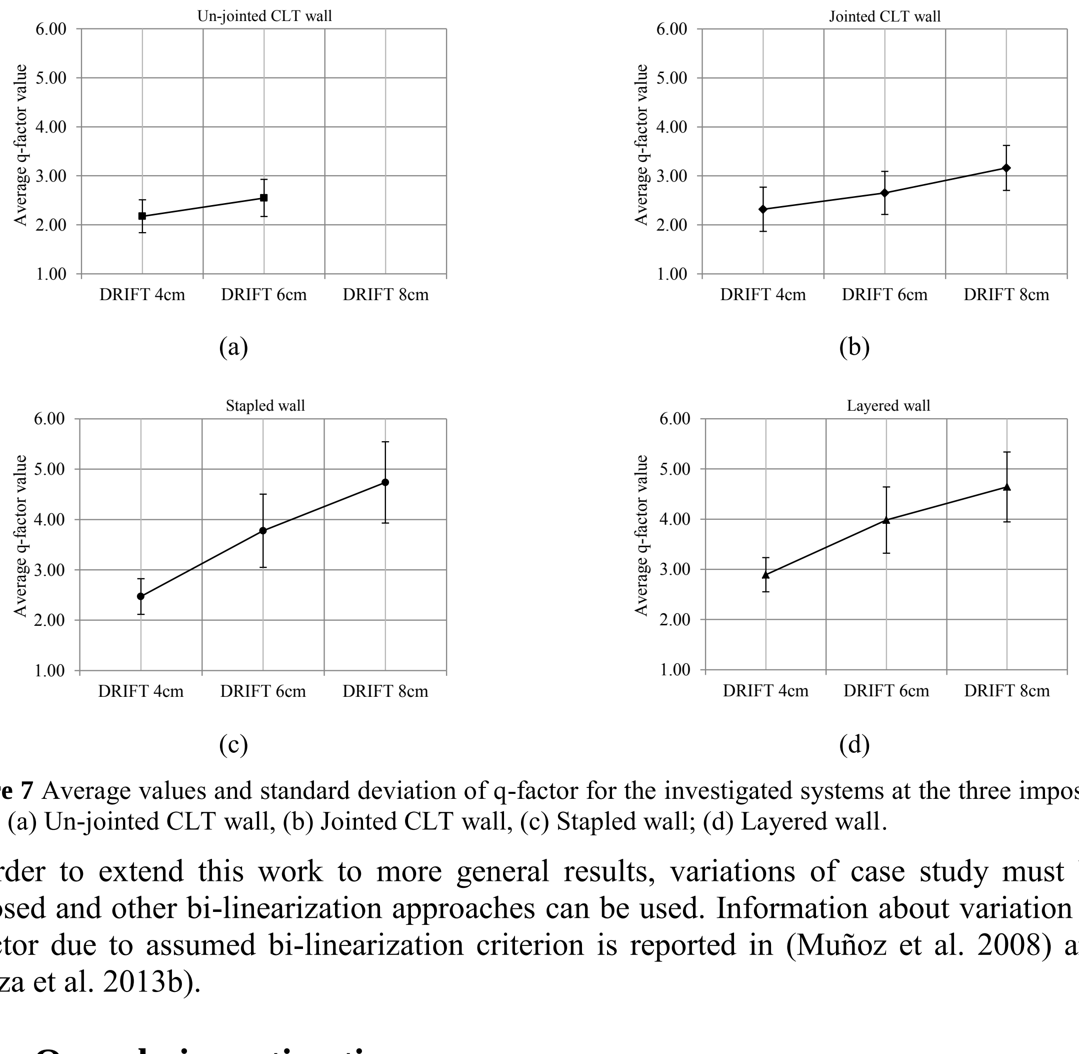

Figure 7 Average values and standard deviation of q-factor for the investigated systems at the three imposed drifts: (a) Un-jointed CLT wall, (b) Jointed CLT wall, (c) Stapled wall; (d) Layered wall.

In order to extend this work to more general results, variations of case study must be imposed and other bi-linearization approaches can be used. Information about variation of q-factor due to assumed bi-linearization criterion is reported in (Muñoz et al. 2008) and (Pozza et al. 2013b).

4.4 Over-design estimation

The effect of the over-design on the q-factor can be obtained defining the PGA_d value. According to (Elnashai and Mwafy 2002), the final estimation of the q-factor can be obtained multiplying the intrinsic q-factor by the design over-strength, defined as the ratio of the yielding to the design lateral strength (i.e., PGA_y/PGA_d). For shear walls the design lateral strength can be analytically evaluated, and is equal to the force that causes the failure of a component (e.g. hold-down, angle brackets, wooden panel), suitably modified to take into account code statements and safety levels. For CLT structures this value can be computed as the minimum of the resistances associated to failure on angle brackets, hold-downs or vertical joints, depending on number and resistance of fasteners. The per-fastener resistances can be calculated according to the so-called Johansen yield theory (Johansen 1949, CEN 2009). For the other two examined systems no code guidelines are available for the calculation of the design lateral strength. For the newly developed building systems the design strength is generally given by the product certification (e.g., ETA etc.).

It is clear that the main issue in the calculation of the over-design is the reliable definition of both design and yielding resistance. The design resistance is strongly dependent from both the design method and resistant mechanisms assumed by designer. Otherwise the yielding resistance is only dependent from the adopted bi-linearization criterion.

In this work different design methods and resistant mechanisms have been considered obtaining over-design ranges from 1.05 to 1.50 for CLT walls, from 1.00 to 1.25 for stapled wall and from 0.70 to 1.00 for layered wall. The proposed ranges are valid only for the method adopted in this work to estimate the yielding limit. If other bi-linearization methods are used, both intrinsic q-factor and over-design factor vary and additional investigations are required. The theme of dependence and variability of the intrinsic q-factor and of the over-design factor from the design and yielding limit is not fully defined in literature and requires additional investigations and researches.

5 Conclusions

Results from experimental tests and numerical simulations demonstrated that the four examined massive wooden shear walls represent a viable technique for construction in seismic-prone area.

A proper choice of the yielding and of the failure limit ensures a reliable estimation of the intrinsic q-factor of the examined system. The criteria used to design the system (i.e. definition of the PGA_d) could affect the results in terms of q-factor values introducing over-design effect. By imposing the experimental yielding limit equal to the design condition (i.e. $PGA_d = PGA_y$), the over-design effects are avoided.

The calculation of the q-factor at different inter-storey drifts, shows the relevance of the choice of the near-collapse condition in the seismic response of the examined shear walls. Results show that wall systems characterized by deformable wooden panel sound more efficient in terms of q-factor than systems with rigid wooden panel.

An intrinsic q-factor up to 3 can be used for the seismic design of shear walls with rigid wooden panel ($q \leq 2.5$ for un-jointed CLT wall and $q \leq 3$ for jointed CLT wall). This range is also consistent with values proposed in literature (Ceccotti 2008, Pozza and Scotta 2014). Otherwise an intrinsic q-factor of 4 is suitable for wall systems with deformable panel ($q \leq 4$ for both stapled and layered walls). Such values should be modified using suitable over-design factor taking into account the design approach, the calculation methods and code guidelines.

Acknowledgements

The authors would like to thank Lignaconstruct, Soligno and TIS Innovation Park, Bolzano (Italy) for their cooperation during testing.

References

ASCE. (2010). “Minimum design loads for buildings and other structures”. *ASCE 7-10*, Washington, DC.

Ceccotti, A., Lauriola, M.P., Pinna, M., and Sandhaas, C. (2006). “SOFIE Project – Cyclic Tests on Cross-Laminated Wooden Panels.” *Proc., World Conference on Timber Engineering WCTE.* Portland, USA.

Ceccotti, A. (2008). “New technologies for construction of medium-rise buildings in seismic regions: the XLAM case.” *Struct. Eng. Int.*, 18(2), 156-165.

Ceccotti, A., and Sandhaas, C. (2010). “A proposal for a standard procedure to establish the seismic behaviour factor q of timber buildings.” *Proc., 11th World Conference on Timber Engineering WCTE,* Riva del Garda, Italy.

Ceccotti, A., Sandhaas, C., Okabe, M., Yasumura, M., Minowa, C., and Kawai, N. (2013). “SOFIE project – 3D shaking table test on a seven-storey full-scale cross-laminated timber building.” *Earthquake Engng Struct. Dyn.*, 42, 2003-2021.

Chopra, AK. (1995). “Dynamics of structures - theory and applications to earthquake engineering.” Upper Saddle River, NJ, Prentice Hall.

Dujic, B., Strus, K., Zarnic, R., and Ceccotti, A. (2010). “Prediction of dynamic response of a 7-storey massive XLam wooden building tested on a shaking table.” *Proc., World Conference on Timber Engineering WCTE.* Riva del Garda, Italy.

Elnashai, A.S., and Mwafy, A.M. (2002). “Overstrength and force reduction factors of multistorey reinforced-concrete buildings.” *Struct. Design Tall Build.*, 11, 329-351.

Elnashai, A.S., and Di Sarno, L. (2008). “Fundamentals of earthquake engineering.” *Wiley, United Kingdom*.

Elwood, K.J., and Moehle, J.P. (2006). “Idealized backbone model for existing reinforced concrete columns and comparisons with FEMA 356 criteria”, *Struct. Design Tall Spec. Build.*, 15(5), 553-569.

European Committee for Standardization (CEN) (2006). “EN 12512 - Timber structures – Test methods – cyclic testing of joints made with mechanical fasteners.” Brussels, Belgium.

European Committee for Standardization (CEN) (2009) “Eurocode 5 - design of timber structures, Part 1-1, General - Common rules and rules for buildings.” Brussels, Belgium.

European Committee for Standardization (CEN) (2013). “Eurocode 8 - design of structures for earthquake resistance, part 1: General rules, seismic actions and rules for buildings.” Brussels, Belgium.

Fajfar, P. (2000). “A nonlinear analysis method for performance based seismic design.” *Earthquake Spectra,* 16(3), 573-592.

Fragiacomo, M., Dujic, B., and Sustersic, I. (2011) “Elastic and ductile design of multi-storey crosslam massive wooden buildings under seismic actions.” *Engineering Structures*, 33, 3043–3053.

Gavric, I., Ceccotti, A., and Fragiacomo, M. (2011). “Experimental cyclic tests on cross-laminated timber panels and typical connections.” *Proc., ANIDIS*. Bari Italy.

Gavric, I., Fragiacomo, M., and Ceccotti, A. (2013). “Capacity seismic design of x-lam wall systems based on connection mechanical properties.” *Proc., meeting 46 of the Working Commission W18-Timber Structures, CIB.* Vancouver, Canada, paper CIB-W18/46-15-2.

Gavric, I., Fragiacomo, M., Popovski, M., and Ceccotti, A. (2014). “Behaviour of Cross-Laminated Timber Panels under Cyclic Loads.” *Materials and Joints in Timber Structures*, 9, 689-702, RILEM Bookseries.

Gelfi, P. (2012). “SIMQKE_GR, version 2.7.” University of Brescia. Available from http://dicata.ing.unibs.it/gelfi, Italy. (Software).

Institute for Research in Construction, (2010). “National Building Code.” National Research Council of Canada, Ottawa, Ontario.

Johansen, K. W. (1949). “Theory of timber connections.” *International Association of Bridge and Structural Engineering*, Bern, Publication n. 9, pp. 249 - 262

McKenna, F., Fenves, G. L., and Scott, M. H. (2000). “Open System for Earthquake Engineering Simulation.” Pacific Earthquake Engineering Research Center. (Software).

Muñoz, W., Mohammad, M., Salenikovich, A., and Quenneville, P. (2008). “Need for a harmonized approach for calculations of ductility of timber assemblies.” *Proc., Meeting 41 of the Working Commission W18-Timber Structures, CIB,* St. Andrews, Canada, paper CIB-W18/41-15-1.

Pei, S., van de Lindt, J., and Popovski, M. (2013). “Approximate R-Factor for Cross-Laminated Timber Walls in Multistory Buildings.” *J. Archit. Eng.*, 19(4), 245–255.

Popovski, M., Schneider, J., and Schweinsteiger, M. (2010). “Lateral load resistance of Cross-Laminated wood panels.” *Proc., World Conference on Timber Engineering WCTE.* Riva del Garda, Italy.

Popovski, M., Pei, S., van de Lindt, J.W., and Karacabeyli, E. (2014). “Force Modification Factors for CLT Structures for NBCC.” *Materials and Joints in Timber Structures*, 9, 543-553, RILEM Bookseries.

Pozza, L., Scotta, R., Polastri, A., and Ceccotti, A. (2012) “Seismic behaviour of wood-concrete frame shear-wall system and comparison with code provisions.” *Proc., Meeting 45 of the Working Commission W18-Timber Structures, CIB*, Växjö, Sweden, paper CIB-W18/45-15-2.

Pozza, L., Scotta, R., Trutalli, D., Ceccotti, A., and Polastri, A. (2013a). “Analytical formulation based on extensive numerical simulations of behavior factor q for CLT buildings.” *Proc., Meeting 46 of the Working Commission W18-Timber Structures, CIB,* Vancouver, Canada, paper CIB-W18/46-15-5.

Pozza, L., Trutalli, D., Polastri, A., and Ceccotti, A. (2013b). “Seismic design of CLT buildings: definition of the suitable q-factor by numerical and experimental procedures.” *Proc., Second International Conference ICSA,* Guimaraes, Portugal, Structures and Architecture 9, 90–97, Print ISBN: 978-0-415-66195-9, DOI: 10.1201/b15267-13.

Pozza, L., Scotta, R., Trutalli, D., Pinna, M., Polastri, A., and Bertoni, P. (2014). “Experimental and numerical analyses of new massive wooden shear-wall systems”. *Buildings*, 4(3), 335-374, DOI: 10.3390/buildings4030355.

Pozza, L., and Scotta, R. (2014). “Influence of wall assembly on q-factor of XLam buildings” *Institution of Civil Engineers - Journal Structures and Buildings* - ISSN: 0965-0911 E-ISSN: 1751-7702 (*in press).*

Sandhaas, C., Boukes, J., van de Kuilen, J.W.G., and Ceccotti, A. (2009). “Analysis of X-lam panel-to-panel connections under monotonic and cyclic loading.” *Proc., meeting 42 of the Working Commission W18-Timber Structures, CIB.* Dübendorf, Switzerland, Paper CIB-W18/42-12-2.

Schädle, P., and Blaß, H. J. (2010). “Earthquake behaviour of modern timber construction systems.” *Proc. 11th World Conference on Timber Engineering WCTE*, Riva del Garda, Italy.

Seismosoft. (2013) “SeismoArtif v2.1.” Available from http://www.seismosoft.com. (Software).

Yasumura, M. (2012). “Determination of failure mechanism of CLT shear walls subjected to seismic action.” *Proc., meeting 45 of the Working Commission W18-Timber Structures, CIB.* Växjö, Sweden, paper CIB-W18/45-15-3.

INTER/47-15-6

INTER

International Network on Timber Engineering Research

AN ELASTOPLASTIC SOLUTION FOR EARTHQUAKE RESISTANT RIGID TIMBER SHEAR WALLS

Wei Yuen Loo
P Quenneville
N Chouw

Department of Civil and Environmental Engineering
The University of Auckland

NEW ZEALAND

Presented by WY Loo

I Smith commented about pounding against the ground and asked about the pounding within the structure itself. WY Loo responded that strong bracketed connections can be used and architecture details can be designed to prevent pounding against other parts of the structure.

W Seim received clarification of the friction device and explanations of the re-centering concept. He questioned how this system would work with wind loads where the loading is in mostly one direction only. WY Loo answered that wind load is not a problem because the system is very rigid.

M Fragiacomo commented that re-centering without restoring force is surprising. WY Loo responded that with this connection which emulates a plastic hinge that has special attributes numerical simulations results show that re-centering is available. With CLT walls which work as load bearing structures self centering is expected.

A Buchanan commented about the relatively large wall with small shear key therefore the sliding plates must provide some resistance to lateral sliding. WY Loo responded that the perpendicular to grain sliding plates can sway and are not expected to provide shear resistance.

M Fragiacomo pointed out that the static test show residual set. WY Loo responded that the numerical result of dynamic analysis shows re-centering was observed.

An elastoplastic solution for earthquake resistant rigid timber shear walls

Wei Yuen Loo, Pierre Quenneville, Nawawi Chouw

Department of Civil and Environmental Engineering, the University of Auckland

Auckland, New Zealand

Keywords: Shear walls, elasto-plastic, slip-friction connectors, energy-dissipation, ductility.

1 Introduction

In terms of seismic performance, timber structures have been observed to perform well, in spite of timber being an inherently non-ductile material. This is due mainly to the ductility of the steel-to-timber connections, and the way in which they interact with the timber material. If these connections are detailed to deform plastically, while keeping the timber members elastic, the overall structure achieves ductility. For nailed sheathing-to-framing shear walls and floor diaphragms, the New Zealand structural timber code, NZS3603:1993 [1] allows ductilities of up to four to be assumed. The issue with such an approach is that in a design level earthquake, the deformations required to achieve ductility often renders the structure irreparable, or at least requiring expensive repairs. Recent developments in engineered lumber products have seen the availability of mass timber panels of tremendous strength and stiffness. These include CLT (cross laminated timber) and LVL (laminated veneer lumber) panels. Under typical loading conditions these panels are essentially rigid, and the experiments of Popovski and Karacabeyli [2] demonstrate that the hysteretic behaviour is largely governed by the plastic deformations in the steel bracket connections attaching the walls to the floor. The hysteretic loops bear some resemblance to those of sheathing to framing shear walls, the main difference being they are more tightly pinched. The seismic performance of such walls is adequate, however, damage is still a consequence after an earthquake.

The authors propose implementing energy dissipating slip-friction device as hold-down connectors in shear walls (see Fig. 1(a)). By adjusting the slip-force of the connectors, the strength of the wall can be tuned to a desired strength, and overturning moment (and hence activated base shear) capped below a certain threshold. Because the force-displacement behaviour of the connectors is highly elasto-plastic (see Fig. 1(b)), it is expected that this characteristic would be reflected in the hysteretic behaviour of the walls in which they serve as hold-downs. Numerical modeling has demonstrated the promise of such a concept [3].

This paper introduces experiments carried out on a 2.4 m × 2.4 m LVL wall with slip-friction connectors. To facilitate controlled rocking, a novel shear key is adopted, that contributes to the damping of the system. The respective contributions to wall strength of the shear key and the slip-friction device can be quantified by a simple analytical relationship, and the predicted results align closely with the experimental results.

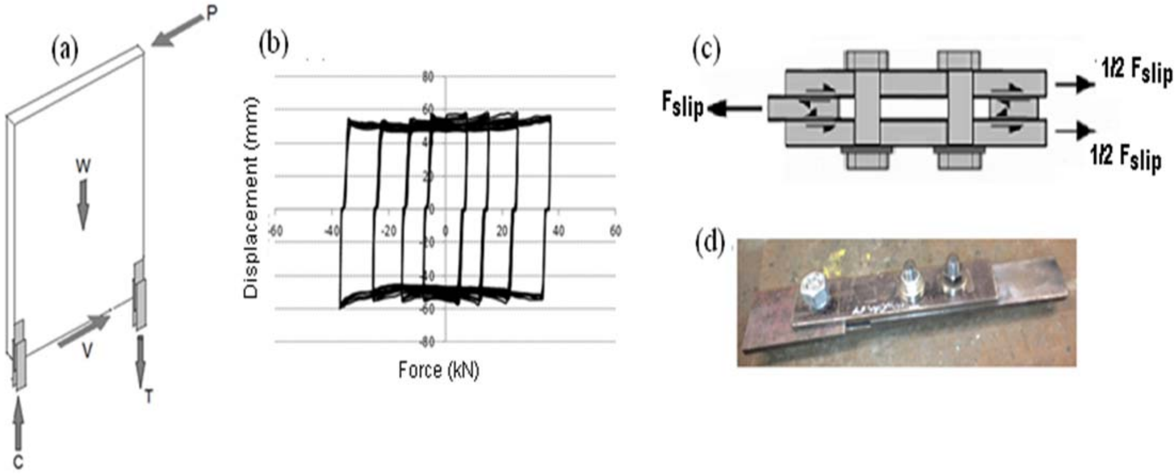

Figure 1 (a) General concept (frictional effects from shear key not shown), (b) hysteretic behaviour of slip-friction connector from component test, (c) forces on connector, and (d) connector specimen.

Implications to the way in which such a system could be designed, and considerations unique to them are discussed. The modelling of the wall and connectors is covered, and earthquake simulations are used to investigate the seismic performance of the wall. The results are presented and discussed.

2 Slip-friction connectors

The type of slip-friction connector (see Figure 1(d)) adopted as wall hold-downs has a symmetric sliding mechanism, in which the two outside plates resist in equal proportion the external load applied to the centre-plate (see Fig. 1(c)). Other researchers have used slip-friction connectors in steel frames [4] - however those typically have an asymmetric mechanism, in which external load is only applied to the centre plate, and one of the outside plates. Butterworth [5] provides a detailed discussion of the sliding mechanism of both symmetric and asymmetric connectors. Symmetric connectors were explored in great detail by Popov and Grigorian [6], and to date, these have typically required the use of brass shims between mild steel surfaces in order to facilitate sliding. Without brass shims, it has been shown that sliding is extremely erratic. However, in the connector design for the shear wall, the authors decided to forgo the use of shims altogether, and instead simply use a centre-plate of abrasion resistant steel (typically Bisalloy 400), in direct sliding against external mild steel plates. All steel surfaces were prepared to the clean mill scale finish prior to use, and extensive tests carried out by Loo et al. [7] show that with some minor preconditioning of the surfaces, while keeping the connectors clamped together, excellent elasto-plastic behaviour can be achieved (see Fig. 1(b)).

3 Experimental wall with slip-friction connectors

A 2.44 m × 2.44 m wall was assembled from two separate 1.22 m × 2.44 m LVL panels of 45 mm in thickness (see Fig. 2(a)). Loo et al. [8] describes the set-up of the experimental wall; the panels were fabricated through the use of screws connecting the panels through end studs, and top and bottom plates. These plates were fabricated from the same material as the main wall. In the design, a maximum racking force of approximately 120 kN was considered (the actual maximum tested force was between 65 and 70 kN).

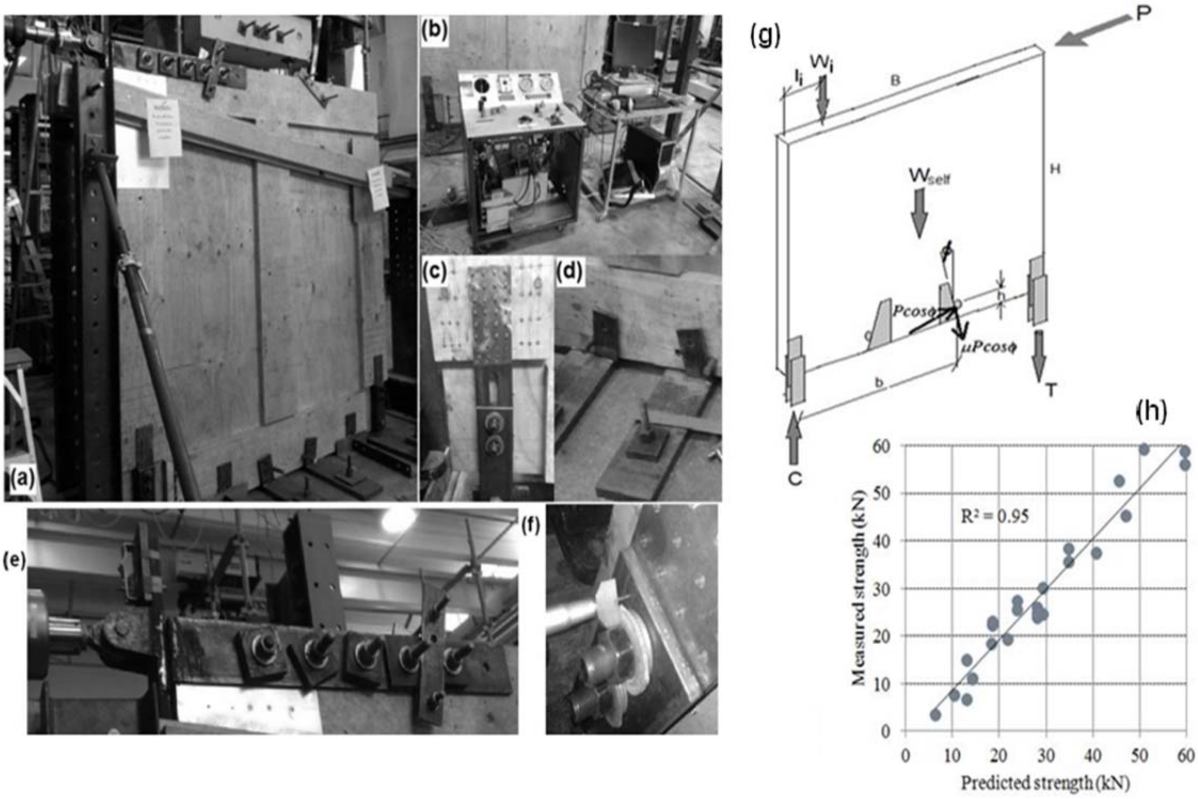

Figure 2 (a) General setup, (b) actuator controller and data acquisition system, (c) slip-friction connector shown extended, (d) shear key, (e) plates to transfer racking force, and (f) use of depth micrometre to measure deflection of Belleville washer stack. (g) Forces on wall about to uplift, with racking force P applied at the top corner. (h) Measured strength vs. predicted strength.

A slip-friction connector riveted to an end chord is shown in Fig. 2(c), and the shear key of two vertical steel plates and solid steel rod inserts is shown in Fig. 2(d). Because the wall in itself is almost rigid and the actual material yield strength would be well beyond the range of the test values, its strength is controlled by the slip-friction connectors. Belleville washers were again employed to provide the desired preload. This preload in the bolts is a function of the way the Belleville washers are stacked in parallel and series, and the deflection applied to the stack. Loo et al. [8] derived expressions to find the Belleville stack height for a desired slip-force. A depth micrometre was used to gauge the deflection of the Belleville washers (see Fig. 2(f)). When the slip-force of the connector is achieved, the wall will uplift and rock. In order for rocking to occur in a relatively unimpeded manner, a shear key is proposed in which solid steel rods passing through the timber panel are made to bear on mild steel shear plates on both sides of the wall. These plates are rigidly fixed to the foundation, and the bearing surface is set at a slight angle from the vertical.

The free body diagram of the wall just about to uplift is shown in Fig. 2(g), and the expression for racking force is:

$$\mathbf{P} = \frac{\mathbf{F_{slip}B} + \frac{\mathbf{W_{self}B}}{\mathbf{2}} + \sum_{\mathbf{i=1}}^{\mathbf{n}} \mathbf{W_i l_i}}{\mathbf{H} - \mathbf{K_{mrp}}} \tag{1}$$

where K_{mrp} encapsulates the effect and contribution of the shear key:

$$K_{mrp} = (h^2 + b^2)^{1/2} \cos\emptyset \left[\mu\cos\left(\emptyset - \tan^{-1}\left(\frac{h}{b}\right)\right) - \sin\left(\emptyset - \tan^{-1}\left(\frac{h}{b}\right)\right)\right] \tag{2}$$

Loo et al. [8] describes 25 tests carried out on the wall, with the experimentally measured strengths corresponding well with the values from Eq. 1 (see Fig. 2(h)). No damage to the wall was observed. The connectors each underwent at least 14 m of cumulative sliding travel, with little evidence of deterioration in strength or stiffness. Fig. 3(a) shows a typical hysteretic result, and Fig. 3(b) shows the uplift displacement time history at the slip-friction connector locations. One end of the wall readily descends, while the other end uplifts. This capability to re-centre under only self-weight (approximately 2.8 kN), demonstrates the accuracy obtained in setting the connector force (the difference in the slip-force between connectors is required to be less than the combined gravity effects [8] for re-centring to take place), and this capability is naturally an important prerequisite for minimising residual drifts following an earthquake.

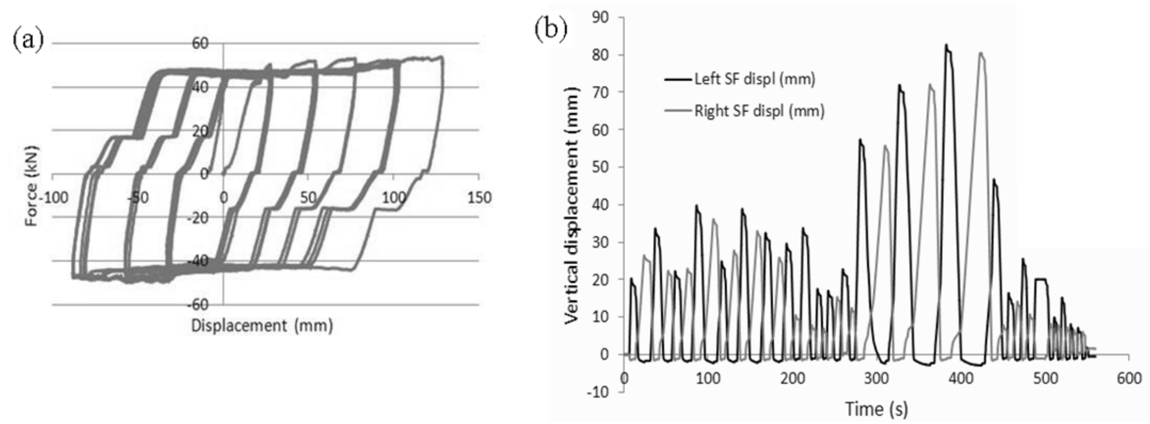

Figure 3 (a) Force-displacement behaviour for wall of approximate 45 kN strength. (b) Vertical displacement time history at slip-friction connector locations.

The reader is referred to Loo et al. [8] for a detailed presentation and analysis of the experimental results.

4 General design imperatives

4.1 Ductility

Slip-friction connectors applied to rigid walls can readily enable elasto-plastic behaviour. The amount of ductility is limited only by the length of travel allowed by the slot within the centre-plate of the connector. Such a slot should provide enough sliding distance to correspond to little or no damage during a design level earthquake, and even perhaps a maximum credible earthquake. In extreme circumstances, this drift could be exceeded, and the priority under such a circumstance is to shift the ductility demand to the other steel connections within the structure, ensuring the structure maintains strength and avoids brittle damage.

For timber structures, definitions of yield strength and ductility have varied [9]. Yield strength can be somewhat difficult to define, because in reality the load-slip relationship of timber connections is not strictly linear at any portion of the load-slip envelope. Nevertheless, 50% of ultimate strength has been commonly used in the past for sheathing to framing shear walls. For CLT walls, strengths are currently defined as 40% that of the ultimate strength [10]. The overall ductility μ is found by dividing the failure displacement,

δ_{max}, (typically the displacement at which the strength falls to 80% of the peak load) by the yield displacement δ_y. These definitions are illustrated in Fig. 4(a). For walls with slip-friction connectors, the same approach can be adopted to define overall ductility, μ. Fig. 4(b) shows that within the overall ductility, such walls enjoy a damage free phase, as well as a quite distinct region involving inelastic damage. The damage free zone is associated with the slip-friction connectors undergoing sliding, and thereby capping forces at or below the yield strength of the wall (i.e 50% of ultimate load for sheathing to framing walls, and 40% of ultimate load for CLT walls). The measure of slip-friction enabled ductility is $\mu_{sf} = \delta_{sf} / \delta_y$. It is intended that during earthquakes the structures remains in the damage free zone with a high level of probability.

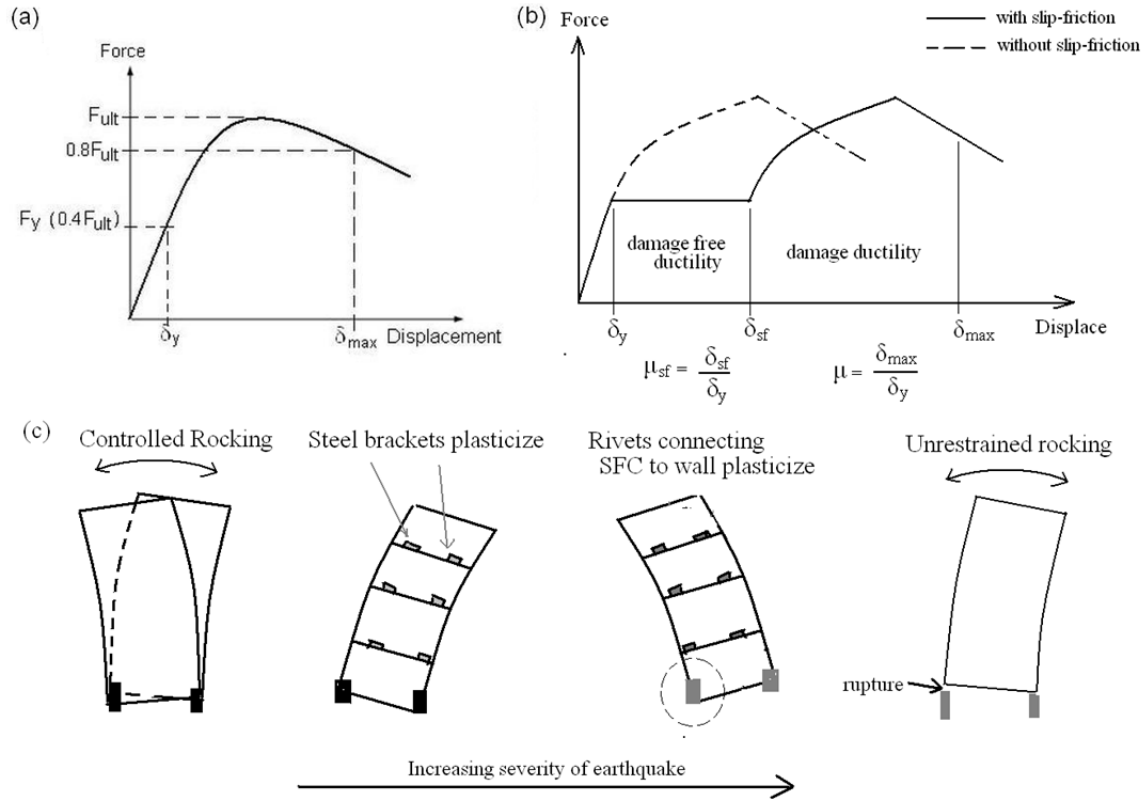

Figure 4 (a) Definitions of wall strength and maximum displacement. (b) Total and slip-friction enabled ductility for wall with slip-friction connectors, and (c) a possible progression of nonlinearity for CLT wall structure.

The designer would decide on an appropriate value for δ_{sf}, corresponding to relevant code recommendations of drift for a ULS or MCE event. It is emphasised that the continued ductile behaviour of the wall beyond δ_{sf} (second phase ductility), depends on sufficient overstrength being provided when designing the other connections of the structure. For sheathing-to-framing walls, this second phase ductility would be supplied by the deformation of the nail connections, while for CLT walls, it would arise from the the ductil plasticization of the steel bracket connections.

Within the structure, sources of ductility are the slip-friction connector, and the steel brackets at each storey connecting the wall to the floor below. The rivets connecting the slip-friction connector to the wall should be designed for a ductile failure mode. A possible order of 'non-linearization' is illustrated in Fig. 4(c).

Naturally the first stage involves sliding of the slip-friction connectors and uplift and rocking of the wall. It is intended that for almost all design level events, and for most maximum credible events, the non-linear behaviour of the wall structure will remain in this range. However an extreme event could cause the wall to attempt to uplift past the range permitted by the connector slot-lengths. A second phase of nonlinear behaviour is then intiated (the post-plateau part of Fig. 4(b)). During this phase, ductility is achieved through the plasticization of the steel brackets, and some rocking of the non-ground floor wall panels – in fact this is the mechanism currently depended upon to provide adequate seismic performance [2]. But whereupon in current practice, the ductile behaviour of the steel brackets constitutes the first stage of ductility, in the proposed concept it will serve as reserve ductility only.

If for some reason ductility in the inter-storey steel bracket connections is not manifested in the manner desired, or the event is so extreme as to cause extremely large displcements, the third stage of non-linearity is provided by the riveted connection between the slip-friction connector and the timber wall (note that the assumption is that it is preferable to have damage first occur in the steel bracket connectors, rather than risk the rupturing away of the slip-friction connector from the wall). The slip-friction connector should be designed for a ductile mode of failure, and this is readily achieved through reference to the work of Zarnani and Quenneville [11, 12]. Upon the complete loss of strength in the riveted connection, the wall will freely rock.

It should be emphasised that the final stage may superficially appear to mean collapse, but this is not necessarily the case. In fact something akin to free rocking is already assumed as providing adequate behaviour in current design practice of CLT walls [10]. Regardless of the intensity of an earthquake event, brittle failure of the timber members should be avoided. Thus it is also necessary to check that the actions associated with the overstrength levels of all the connectors, will not cause any of the timber members to exceed their respective yield strengths.

4.2 Rocking and shear amplification

In the case of MDOF structures designed to rock, numerical studies have shown that higher mode effects can play a part in increasing the shear action above those predicted by the equivalent static method (which is based on the fundamental mode of vibration). Kelly [13] carried out a series of numerical analyses, and from this proposes the following dynamic amplification factor, ω_v, to be used to increase the shear actions.

$$\omega_v = 1 + a_{VN}DF \quad \text{for } N > 1 \tag{3}$$

where DF is the ductility and a_{vn} is a shear amplification factor with values of 0, 0.1, 0.15, 0.40, 0.60, and 0.90 for 1, 2, 3, 4, 5, and 6 story buildings, respectively. A detailed discussion of this factor and its development is provided by Kelly [13]. The authors adopt Eq. 3 in the discussion of earthquake simulation results in Section 6.

5 Numerical model

5.1 Multi-storey wall

In order to demonstrate the benefits of slip-friction connectors, a five storey shear wall is designed, modelled, and placed under earthquake simulations. The software package SAP2000 [14] was used. The model wall is considered to be one of the perimeter walls of a 6 m × 6 m box structure. It is assumed that only the perimeter walls resist earthquake forces. Storey heights are 2.6 m, and the concentrated seismic mass at all levels is 15 tonnes. Walls are of 140 mm thick CLT panels at every storey, and are modelled by a thick shell element. The shell elements have an elastic modulus of 10200 MPa, and shear modulus of 525 MPa. In terms of gravity, only self-weight is considered. The wall was designed for the seismically active area of Napier, New Zealand, and intermediate soil type conditions. The design ductility is 4, and the fundamental period found to be approximately 0.7 s. Based on the spectral acceleration and procedure of NZS 1170.5:2004 [15], the lateral forces F_i at each level are calculated. These are presented in Table 1, together with the shear and bending actions.

Table 1 Distributed forces and actions on shear wall

Floor	h (m)	m (kg)	$m_i h_i$	$m_i h_i$ /sum($m_i h_i$)	F_i (kN)	V (kN)	M (kNm)
5	13	15000	195000	0.33	27.0	27.0	0.0
4	10.4	15000	156000	0.27	17.1	44.2	70.3
3	7.8	15000	117000	0.20	12.9	57.0	185.1
2	5.2	15000	78000	0.13	8.6	65.6	333.4
1	2.6	15000	39000	0.07	4.3	69.9	504.0
0	0		585000			69.9	685.7

5.2 Connections

5.2.1 Steel brackets

Steel bracket connections were adopted in connecting the walls to the floor panels below. For simplicity of modelling, the same bracket type was used, with the required overturning resistance obtained by varying the distribution of the brackets. The assumed mechanism of the rocking wall with plasticizing bracket connections is shown in Fig. 5(a).

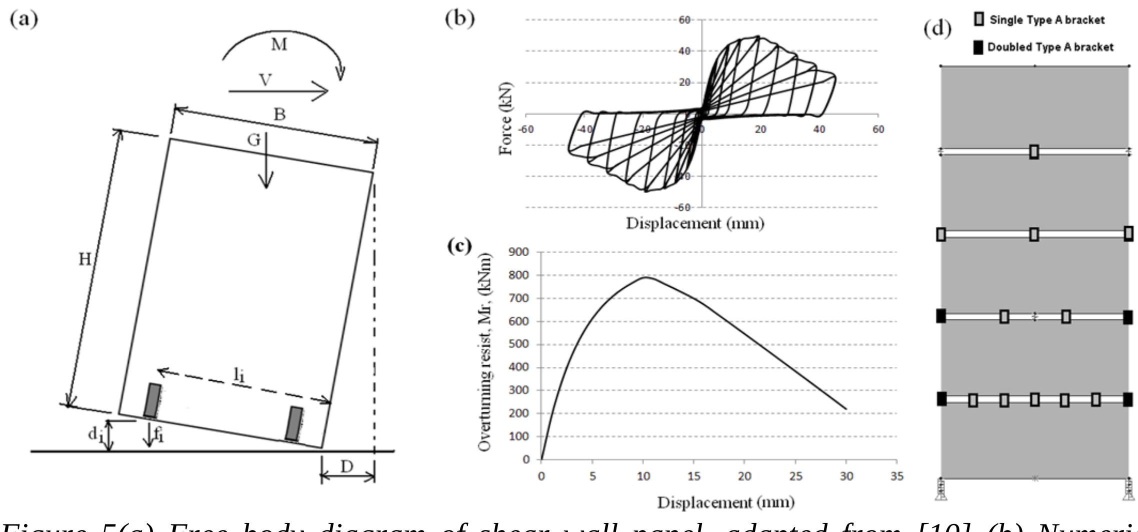

Figure 5(a) Free body diagram of shear wall panel, adapted from [10] (b) Numerical hysteretic behaviour of Type A bracket. (c) Resistance to overturning as a function of displacement, D, for a 2.6 m high by 6 m wide wall with doubled Type A brackets at the ends and singles at l_i = 2 m and 4 m. (d) Distribution of brackets in model wall.

If the wall had *n* brackets, the overturning resistance M_r is

$$M_r(D) = \sum_{i=1}^{n} l_i f_i \langle \frac{l_i}{H} D \rangle + \frac{L}{2} G \quad (4)$$

Note that f_i is a function of (l_i D / h). To resist a design level overturning action (peak value divided by 2.5), brackets must be designed and laid out in such a way so that

$$M_r \geq V\,H + M \tag{5}$$

The bracket adopted for modelling is reported on by Shen et al. [16]. Averaged hysteretic parameters from cylic tests on a SIMPSON strong tie steel 90×48×3×116 mm bracket with eighteen 3.8 × 89 mm spiral nails (conveniently called bracket Type A) are provided by Shen et al., and these are reproduced in Table 2. Adopting these parameters and using a multilinear plastic link, the method of Loo et al. [17] was used to model the force-displacement behaviour of Type A brackets. This method is largely based on the behaviour on the well known Foschi load-slip curve for steel connections in timber structures.

A result from a numerical test on a single Type A bracket is shown in Fig. 5(b). Fig. 5(c) shows the moment-resistance / racking-displacement relationship (from Eq. 4) for a 6 m wide by 2.6 m high wall, with single connectors at l_i = 2 m and 4 m, and doubled connectors at the ends. For the model wall, the connection arrangements for each wall panel are shown in Fig. 5(d) (note that the distributions do not necessarily reflect a practical implementation, but serve to investigate the adopted design principles and how they perform under simulation).

5.2.3 Slip-friction connector

The slip-friction connector is modelled using a gap, hook, and multilinear plastic element. The gap element prevents the downward displacement of the wall at its corner, the hook element defines the slot-length available for sliding (i.e. uplift), and the multilinear plastic link with kinematic hysteris behaviour provides the elasto-plastic characteristics of the connector. Loo et al. [3] describes in detail the modelling of slip-friction connectors. In the research of this article, the slip-friction connector is placed in series with the element representing the rivet connection to the wall (see Fig. 6(a)).

The sliding strength, F_{slip}, of the slip-friction connector is set as:

$$F_{slip} = \frac{M_o}{B} - \frac{G}{2} \tag{6}$$

where M_o is the overturning moment on the wall, and G the total gravity effects including self-weight. M_o for the model wall is 686 kNm (see Table 1) and G (assuming self-weight only, and 450 kg/m^3 for CLT) is 48.2 kN. Thus, F_{slip} is set to 90 kN. The slot length was set for a maximum allowable uplift of 150 mm, i.e corresponding to 2.5% drift.

5.2.4 Rivet connections

Timber rivets provide an excellent solution in timber structures, where both a stiff connection and high force to transfer area ratio, is required. This suits the requirements of the connection between the slip-friction connector and shear wall (see Fig. 2(c)). In general, riveted connections should be designed for a ductile failure mode, and brittle failure modes such as block pull-out and splitting should be avoided. Zarnani and Quenneville [11, 12] investigated rivets in timber and provide design equations enabling their ductile design. Popovski and Karacabeyli [18] tested rivets on braced frames and obtained averaged force-displacement properties for various timber types such as glulam, parallel strand lumber, and laminated veneer lumber (LVL). Zarnani and Quenneville have investigated CLT - however these are yet to be published. Thus the values for laminated veneer lumber are adopted for modelling purposes, and presented in Table 2. For comparison, results for a nail connection are also shown.

Table 2 Averaged Foschi parameters for single rivet, nail, and bracket Type A

Foschi parameter	[1]Rivet (40 mm long)	[2]Nail (3 mm dia)	[3]Bracket Type A (18 spiral nails)
Ultimate strength, F_{ult} (kN)	3.2	1.37	49.1
Displacement at ultimate strength, δ_{ult} (mm)	3.3	9	20
Strength at failure (80% of F_{ult}), F_{fail} (kN)	2.6	1.1	39.2
Displacement at failure, δ_{fail} (mm)	7.7	14.9	29.4
Initial stiffness, K_0 (kN/mm)	3.8	1.2	11.93
Tangent stiffness at peak load, K_1 (kN/mm)	0.41	0.05	0.012
Post peak strength envelope gradient, K_2 (kN/mm)	-0.15	-0.042	-1.05
Unloading stiffness, K_3 (kN/mm)	3.6	1.1	11.3
Pinching strength, F_1 (kN)	0.27	0.19	4
Y-intercept strengthe, F_0 (kN/mm)	1.9	0.92	49.27

[1]adopted (or estimated by authors) from Popovski and Karacabeyli [18]
[2] adopted (or estimated by authors) from Dolan and Madsen [19]
[3] adopted (or estimated by authors) from Shen et al. [16]

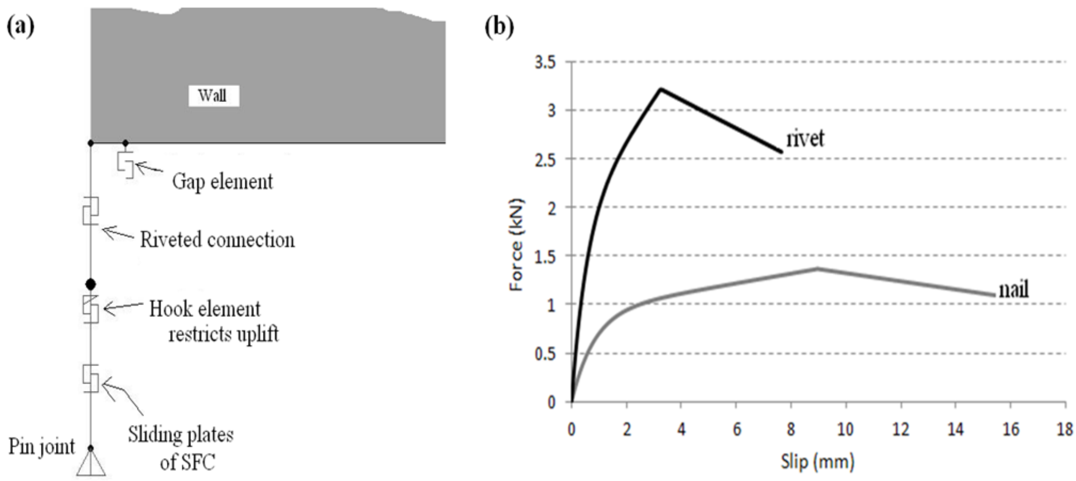

Figure 6 (a) Riveted connection combined with slip-friction elements. (b) Foschi load-slip curves for a timber rivet, compared with a 3 mm diameter nail.

The Foschi envelope curve for the rivet is compared to that of the 3 mm diameter nail in Fig. 6(b), and the differences in strength and stiffness are apparent. While rivets do exhibit high levels of ductility (around 15 for LVL), only a very small displacement post-peak load will cause failure, and this is an important consideration when it comes to providing post-sliding ductility to the structure (see Fig. 4(c)). Rivet connections are modelled using a multilinear plastic element of a pivot hysteresis type. Note that a connection with *n* rivets has *n* times the strength and stiffness values of Table 2 (the assumption being that significant displacements remain the same [17]). Fig. 6(a) shows the element representing the rivet as part of the overall slip-friction connector.

6 Earthquake simulations – results and discussion

The wall was subjected to five earthquake simulations. The acceleration records and their respective scale factors are shown below.

Table 3 Earthquake acceleration records[a]

Event	Station	Bearing	PGA (g)	Scale Factor, k_1[b]	Scaled PGA (g)
El Centro, Imperial Valley, 1940	117 El Centro Array #9	180°	0.313	0.9	0.282
Loma Prieta 1989	47125 Capitola	0°	0.529	0.6	0.317
Northridge 1994	24303 LA – Hollywood Stor	90°	0.231	1.5	0.347
Kobe 1995	0 JMA	0°	0.821	0.3	0.246
Chihuahua 1979	6621 Chihuahua	282°	0.254	0.9	0.229

[a]From PEER [20]

[b]Scaled for building period of 0.7 s. Location Napier, NZ, 500 yr return period, Site C soils.

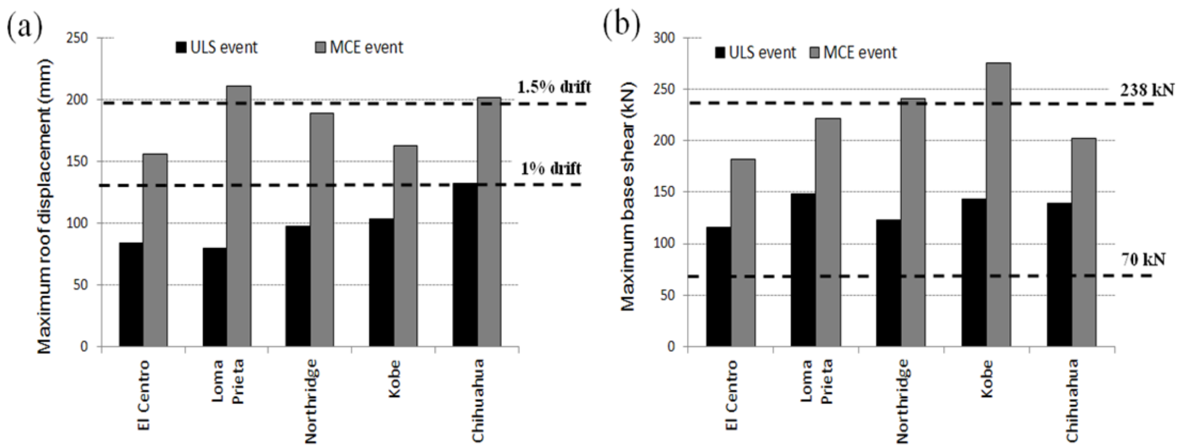

Figure 7 (a) Maximum displacements, and (b) maximum base shears

From Fig. 7(a) it can be seen that the maximum roof displacements are generally below a 1% drift limit, while drifts for two of the MCE event are slightly above 1.5%. From a performance based approach this is promising, as the NZS1170.5 [15] limit for the ULS state allows 2.5%. It should be noted that residual drifts are not shown. This is because in all cases, both the ULS and MCE residual drifts were close to, if not zero, and all well below the 0.2% limit for realistic self-centring structures [21].

Base shears are shown in Fig. 7(b). It is seen that the equivalent static predicted value of 70 kN is significantly exceeded in both the ULS and MCE events. This is due to higher mode effects on the structure that amplifying the base shears initiating uplift. From Eq. 3, the dynamic amplification factor is ω_v = 3.4 for a 5 storey structure, and this gives a value of 238 kN. Fig. 7(b) shows this value as conservative for the ULS case, but appropriate to the MCE case.

In the modelling of the wall, the brackets, slip-friction connectors, and the rivets connecting the slip-friction connector to the wall were designed for the same level of actions, with no overstrength between them. However, in Fig. 4(c), a possible progression of nonlinearity was presented. In order to explore the impact of a 'weak' rivet connection and a 'strong' bracket connection, the model is adjusted, and the slot length reduced to 50 mm (from the original 150 mm), in order to allow the second phase of ductile behaviour shown in Fig. 4(b) to develop. The El Centro MCE simulation was applied, and the hysteretic result from one of the rivet connections is shown in Fig. 8(a). Clearly the rivet connection (attaching the slip-friction connector to the wall) is more or less behaving elastically, and has undergone little damage, in spite of the reduction in slot length.

With the same slot length of 50 mm retained –the strength and stiffness of the Type A brackets within the wall were then increased by 1.5.

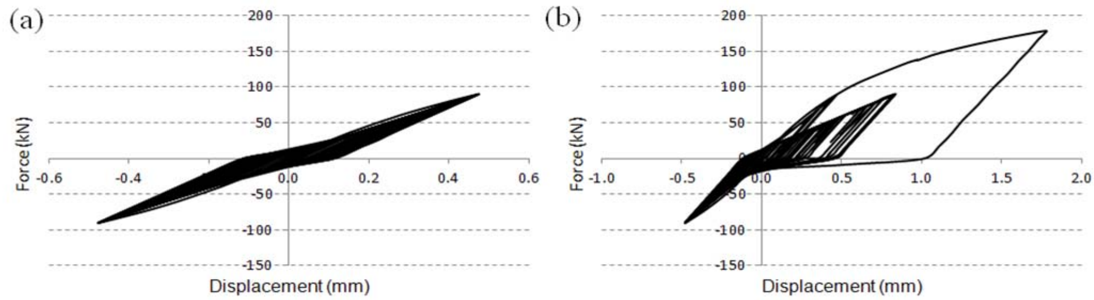

Figure 8 Hysteresis of rivets when (a) wall is not overstrengthened, and (b) when wall is overstrengthened. Note the difference in scale of the horizontal axis.

The impact on the same rivet connection is startling, and Fig 8(b) shows evidence of significant non-linear damage. With further excitations, failure of this connection is highly likely. Clearly, careful consideration should be given, when overstrengthening the nonlinearly responding parts of the structure relative to one another.

7 Conclusions

Experimental work on a rocking wall with slip-friction connectors demonstrate the feasibility of the concept, and the wall manifests excellent elasto-plastic behaviour and readily rocks back into place as long as the connector strengths are within a range no larger than the gravity loads on the wall. That this occurs under just self-weight indicates that the method of directly measuring Belleville washer displacement in order to modulate the slip-force in the connectors can be achieved with reasonable precision.

Slip-friction connectors allow available ductility to be directly determined through the provision of slot lengths corresponding to particular target rotational drift levels. Two measures of ductility can thus be defined. Slip-friction enabled ductility represents a damage free zone of ductile behaviour, while total ductility (failure displacement divided by yield displacement) includes both this damage free range and also a zone where plasticization of the brackets connecting the walls to the floor below occurs.

Slip-friction connectors thus have the potential to enhance the already adequate seismic performance of CLT walls, by allowing the wall to avoid damage for a large range of drift, but with a backup reservoir of ductility provided through the ductile bracket connections connecting each wall panel to the storey directly below it, as is currently the case. However care must be taken to avoid premature failure of the very stiff rivet connection. This can be done by ensuring the riveted connection is designed for actions that are the same, or preferably higher than those of the brackets.

Numerical parametric studies are currently being conducted to determine the ranges of uplift that correspond to design level and maximum credible earthquakes within and their probabilities of non-exceedance.

References

[1] Timber structures standard, NZS3603, Standards New Zealand, Wellington, New Zealand; 1993.

[2] Popovski M, Karacabeyli E. Seismic behaviour of cross-laminated timber structures. Auckland, New Zealand: Proc of World Conference on Timber Engineering; 2012.

[3] Loo WY, Quenneville P, Chouw N. A numerical study of the seismic behaviour of timber shear walls with slip-friction connectors. Eng Struct 2012; 34(22):233-243.

[4] Khoo HH, Clifton GC, Butterworth JW, MacRae G, Ferguson G. Influence of steel shim hardness on the Sliding Hinge Joint performance. J Constr Steel Res 2012; 72(2012):119-129.

[5] Butterworth J. Ductile concentrically braced frames using slotted bolted joints. J Struct Eng Society of New Zealand 2000; 13(1):39–48.

[6] Popov E, Grigorian C, Yang T. Developments in seismic structural analysis and design. Eng Struct 1995; 17(3):187–97.

[7] Loo WY, Quenneville P, Chouw N. A new type of symmetric slip-friction connector. J Constr Steel Res; 94(March 2014): 11-22.

[8] Loo WY, Kun C, Quenneville P., Chouw N. Experimental testing of a rocking timber shear wall with slip-friction connectors. Earthq Eng Struct D 2014; DOI: 10.1002/eqe.2413

[9] Munoz W, Salenikovich A, Mohammad M, Quenneville P. Determination of yield point and ductility of timber assemblies: in search for a harmonised approach. In: Proceedings of Meeting 41 of CIB-W18, St Andrews, Canada; 2008

[10] Gagnon S, Pirvu C. CLT Handbook: Cross-Laminated Timber. FPInnovations, Canada, 2011.

[11] Zarnani P, and Quenneville P. Strength of timber connections under potential failure modes - An improved design procedure. Constr Build Mater, 60(June 2014): 81-90.

[12] Zarnani P, and Quenneville P. Wood block tear-out resistance and failure modes of timber rivet connections – a stiffness-based approach. J Struct Eng 2014; 140(2), 04013055.

[13] Kelly TE. Tentative seismic design guidelines for rocking structures. B NZ Soc for Earthq Eng 2009; 42(4):239-274.

[14] Computers and Structures, Inc. SAP2000 v14: Integrated solution for structural analysis and design. Berkeley, California; 2009.

[15] Structural design actions - Part 5: Earthquake actions, NZS1170.5, Standards New Zealand, Wellington, New Zealand; 2004.

[16] Shen Y-L, Schneider J, Tesfamariam S, Steimer S, Mu Z-G. Hysteresis behavior of bracket connection in cross-laminated-timber shear walls. Eng. Struct; 48(November 2013): 980-991.

17] Loo WY, Quenneville P, Chouw N. A numerical approach for simulating the behaviour of timber shear walls, Struct Eng Mech 2012; 42(3): 383-407.

[18] Popovski M, Karacabeyli E. Seismic performance of riveted connections in heavy timber construction. Vancouver, Canada: 13th World Conference on Earthquake Engineering; 2004.

[19] Dolan JD and Madsen B. Monotonic and cyclic nail connection tests. Can. J. Civil 1992; 19 (1): 97-104.

[20] Pacific Earthquake Engineering Research Center (PEER). PEER strong motion database.<http://peer.berkeley.edu/smcat/>. [accessed 18.10.09].

[21] Henry RS, Sritharan S, Ingham JM. Recentering requirements for the seismic design of self-centering systems. Auckland, New Zealand: Proc of ninth Pacific Conference on Earthquake Engineering; 2011.

INTER

International Network on Timber Engineering Research

IN-PLANE RACKING TESTS OF CONTINUOUS SHEATHED WOOD STRUCTURAL PANEL WALL BRACING

T D Skaggs
E L Keith
Borjen Yeh
APA – The Engineered Wood Association

P Line
American Wood Council

N Waltz
Weyerhaeuser

U.S.A

Presented by T Skaggs
P Quenneville received confirmation that the deflections being sensitive to boundary conditions are sensitive at 40% as well as at the predicted load.
J Marcroft asked whether there was vertical load on the return wall. T Skaggs responded no and the return wall only had anchor bolts.

In-Plane Racking Tests of Continuous Sheathed Wood Structural Panel Wall Bracing

Thomas D. Skaggs, Edward L. Keith, Borjen Yeh
APA – The Engineered Wood Association, U.S.A.
Philip Line, American Wood Council, U.S.A.
Ned Waltz, Weyerhaeuser, U.S.A.

Keywords: Racking Tests, Wood Structural Panels, Bracing

1 Introduction

The "continuous sheathed wood structural panel" (CS-WSP) wall bracing method in the *International Residential Code* (IRC) (ICC, 2009) is favored by designers due to its high strength and stiffness that result in reduced lengths for individual bracing segments and smaller total lengths of required bracing relative to other bracing methods. In addition, the end restraint options available for the CS-WSP bracing option include details that permit 610 mm (24 in.) long return corner walls to be used in lieu of hold-down anchorage for wall segments less than 1220 mm (48 in.).

Due in part to the attractive attributes of the IRC's CS-WSP bracing provisions, ICC-Evaluation Service has developed acceptance criteria for proprietary sheathing products to gain recognition for use in CS-WSP braced wall applications. *AC269.1: Acceptance Criteria for Proprietary Sheathing Attached to Wood Light-Frame Wall Construction Used and Braced Wall Panels Under the IRC (*AC269.1*)* (ICC-ES, 2013) provides criteria intended to provide alternative proprietary sheathing panel manufacturer with a means to evaluate whether their product performs in a manner consistent with CS-WSP bracing. The criteria include a series of in-plane wall racking tests that address a range of different boundary conditions and wall configurations and require the proprietary product to meet or exceed a series of performance targets to gain recognition as a CS-WSP bracing substitute.

The IRC's CS-WSP bracing provisions are not based on tests of the specific CS-WSP bracing configurations described in AC269.1. In the absence of a test basis for the specific perforated wall configurations, performance targets for perforated wall configurations in AC269.1 are based on the perforated shear wall calculation method summarized in the American Wood Council's *Special Design Provisions for Wind and Seismic* (SDPWS, 2008). However, the perforated shear wall calculation method is intended to provide conservative design strengths and has generally been assumed to under-predict actual test-based strengths. As a result, using the calculation method may result in establishment of non-conservatively low strength performance targets for the recognition of alternative sheathing products.

Testing summarized herein was undertaken as part of a collaborative effort between American Wood Council, Weyerhaeuser, and APA-The Engineered Wood Association for the purposes of documenting the in-plane racking performance of WSP sheathed walls in the specific CS-WSP bracing configurations described in AC269.1. In-plane racking tests were conducted on WSP sheathed walls in two separate laboratories. One laboratory conducted the ASTM E72 wall racking tests as described in AC269.1. Both laboratories conducted tests on a full series of the CS-WSP bracing configurations described in AC269.1, including the baseline wall, corner return wall, and perforated walls. Each laboratory tested three baseline walls and either one or two walls for each additional configuration. A total of 21 walls were tested.

2 Test Method

Testing was conducted in general conformance with requirements of AC269.1 for the wall configurations depicted in Table 1. For Wall Types 1-7, racking tests were in accordance with AC269.1's modifications to ASTM E 564 *Standard Practice for Static Load Test for Shear Resistance of Framed Walls for Buildings* (ASTM, 2006). The applied shear loading at both laboratories was in compression and directed from left to right based on orientation of walls depicted in Table 1.

In addition to testing of Wall Types 1 - 7, ASTM E72 wall racking tests were also conducted in accordance with AC269.1's modifications to ASTM *E72 Standard test Methods of Conducting Strength Tests of Panels for Building Construction* (ASTM, 2010).

Table 1. Test wall configurations for an AC269.1 evaluation of CS-WSP bracing.

Wall type	Description	Wall size height x length (m)	Clear opening height, %H	Sheathed segment aspect ratio (H/L_s)	Full-height sheathed length (m)	Hold-down	Wall configuration
-[1]	ASTM E 72	2.4 x 2.4	-	1:0	2.4	Yes	-
1	Baseline	2.4 x 2.4	-	1:0	2.4	Yes	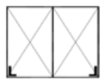
2	Corner return	2.4 x 3.7	-	1:1.5	3.7	No	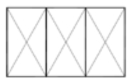
3	Full-height opening	2.4 x 3.7	-	2:1	2.4	Yes	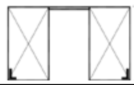
4	Window opening	2.4 x 3.7	-	2:1	2.4	Yes	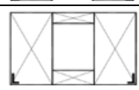
5	Door opening	2.4 x 4.1	-	3:1	1.6	Yes	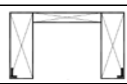
6	Two window openings	2.4 x 4.3	-	4:1	1.8	Yes	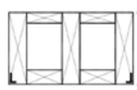
7	Window & door openings	2.4 x 4.6	65% window 85% door	4:1, 3:1	2.2	Yes	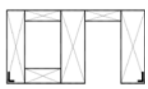

(1 ft. = 0.3048 m)

[1] Wall racking tests conducted in accordance with AC269.1 modifications to ASTM E72 to address the capacity of the sheathing and sheathing-to-framing attachment

3 Specimens

The ASTM E72 walls were fabricated in accordance with AC269.1's modifications. Wall Types 1-7 were fabricated in general conformance with the available requirements and details outlined in AC269.1. To minimize differences in interpretation of wall construction details for specific wall assemblies of AC 269.1, detailed drawings were developed for each wall configuration and used by each laboratory to fabricate test walls. The detailed drawings removed potentially different judgments between laboratories for wall construction details that could influence the measured performance such as minimum anchor capacity, exact anchor bolt placement, corner stud attachment, framing nail type and placement. Figure 1 illustrates a typical test wall in the test frame used by each test laboratory. Other relevant materials and details of construction used in fabrication of the Wall Type 1-7 test specimens were as follows:

- **Framing:** Studs and plates were 38 x 90 mm (2x4 nominal) Douglas-Fir "Standard or Better" grade. Stud spacing was 406 mm (16 in.) o.c. except where wall configurations required smaller stud spacing adjacent to openings. All end studs where hold-downs were used were built-up (2) 38 mm thick members. Headers were single-ply 38 x 290 mm (2x12 nominal) Douglas-Fir No. 2 Grade. Headers were supported at each end by one jack stud. All of the stud and plate framing that received perimeter WSP nailing was pre-screened to ensure that the average oven-dry specific gravity was 0.50 ± 0.03.
- **Sheathing:** All WSP sheathing used by both laboratories was 9.5 mm (3/8 in.) oriented strand board (OSB) obtained from the same single bundle that was purchased on the open market and produced in accordance with Performance Standard for Wood-Based Structural Use Panels (DOC-NIST, PS2-10).
- **Sheathing nails**: Sheathing nails were 6d common (50 x 2.87 mm) (2.0 x 0.113 in.) fasteners spaced at 150 mm (6 in.) at panel edges and 300 mm (12 in.) in the field of the panel. The fasteners were installed to maintain a 9.5 mm (3/8 on.) minimum edge distance at all OSB panel perimeters. The nails used by both laboratories were manufactured by the same nail manufacturer.
- **Framing nails:** Framing nails were installed in accordance with prescribed minimum nailing from the IRC unless otherwise noted. Headers were toe-nailed to full-height studs at each end using (4) 8d box nails (65 x 2.87 mm) (2.5 x 0.113 in.). Top plate to header nailing consisted of 75 x 3.33 mm (3.0 x 0.131 in.) nails at 610 mm (24 in.)o.c. Window sills were end-nailed to studs using (2) 16d box (90 x 3.43 mm) (3.5 x 0.135 in.) at each end. Jack studs were nailed to king-post with 75 x 3.33 mm (3.0 x 0.131 in.) nails spaced at 610 mm (24 in.)o.c.
- **Anchor bolts:** Anchor bolts were 15.9 mm (5/8 in.) diameter with 75 x 75 x 5.82 mm (3 x 3 x 0.229 in.) square plate washers between the bottom plate and the nut. Anchor bolts were spaced at 610 mm (24 in.) o.c. An anchor bolt was located 300 mm (12 in.) from ends of each bottom plate except for walls with openings where anchor bolts were located within 300 to 600 mm (6 to 12 in.) from each end of each bottom plate.
- **Hold-downs:** "HDQ8-SDS3" hold-downs were used for Wall Types 1, 3, 4, 5, 6 and 7. In all cases, eight screws attached each hold-down to double end studs. The number of screws used for overturning anchorage attachment was determined such that the hold-down-to-end stud connection was only slightly greater in strength than the wall's allowable stress wind design overturning force of 9.96 kN (2,240 lbf). The overturning force represents the wind design allowable unit shear value for Wall Type 1 times the wall height of 2.4 m (8 ft) (e.g. 4.1 kN/m x 2.4 m) (e.g. 280 plf x 8 ft). Hold-downs in Wall Types 3, 4 5, 6, and 7 are sized for this same unit shear force to enable the tension side end panels to develop the same unit shears as associated with Wall Type 1. Nailing between the two-ply end studs consisted of (15) 75 x 3.33 mm (3 x 0.131 in.) nails evenly-spaced to match the ASD shear wall overturning force.

Figure 1: Example Wall Type 7 specimen at Laboratory A (left) and Example Wall Type 2 – corner return specimen at Laboratory B (right)

The combination of 9.5 mm (3/8 in.) thick WSP sheathing and 6d common sheathing nails used for all of the test specimens in this study is associated with the minimum requirements for CS-WSP bracing described in the IRC. This same sheathing and attachment are also linked to the 8.2 kN/m (560 plf) minimum shear strength target that AC269.1 requires for the ASTM E72 wall racking test specimens. This capacity target was based upon the 8.2 kN/m (560 plf) shear wall nominal unit shear for wind design that the SDPWS tabulates for the same combination of sheathing and sheathing nailing with framing that has a specific gravity of at least 0.50.

As illustrated in Table 1, all walls utilized a hold-down at ends except for Wall Type 2. Wall Type 2 was framed with 610 mm (24 in.) sheathed corner returns which were used to provide alternative end restraint. Details of construction of the corner return walls used in this study are depicted in Figure 2. A three-stud corner with a 32 mm (1-1/4 in.) gap between adjacent studs was used to represent a typical framed corner in accordance with the IRC.

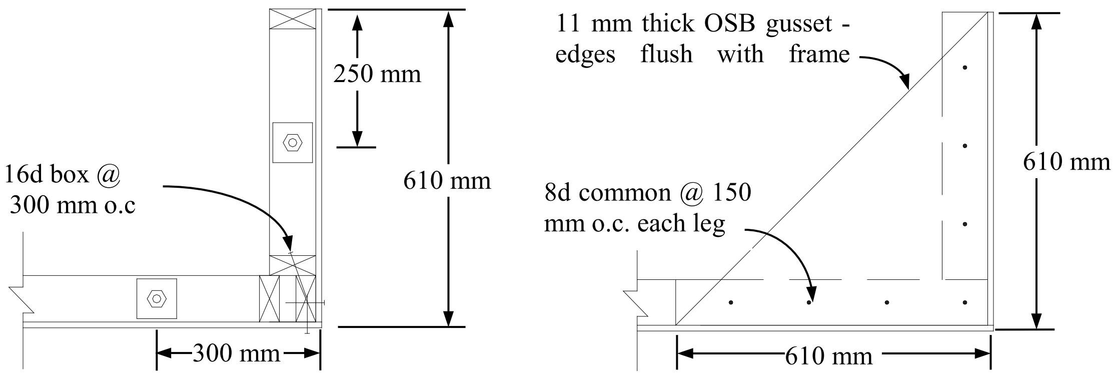

Figure 2. Wall Type 2 corner return: location of bottom plate anchor bolts (left), and attachment of triangular OSB gusset to wall top plates (right). (1 in. = 25.4 mm)

4 Test Results

Detailed test results are provided in Table A.1. Table 2 provides a summary of the strength-based criterion of interest in this study. Load deflection curves for Wall Types 1-7 from Series A data are shown in Figure 3 (left) as an example of typical load deflection behavior. Load deflection curves for the ASTM E72 walls are shown in Figure 3 (right). In each summary table and figure, the data has been divided into "Series," with each Series representing the test data from one of the two laboratories involved in the test program. It should be noted that in Figure 3 (left), the x-axis represents the racking deflection at the top of wall in mm. In figure 3 (right), per ASTM E72, the x-axis represents the "net" racking deflection at the top of the wall with the rigid body rotation and translation components of deflection removed. Table 2 and the y-axes of Figure 3 provide the measured racking strength as a normalized ratio calculated in accordance with Equation 1:

$$Strength\ ratio = \frac{(load\ unit\ shear)}{(Peak\ load\ unit\ shear)_{Baseline}} \qquad \text{Eq. 1}$$

where:

(load unit shear) = load for the wall configuration divided by the total wall length, kN/m (plf)

(Peak load unit shear)$_{Baseline}$ = Average peak load unit shear divided by Wall Type 1 length of 2.4 m (8 ft), kN/m (plf)

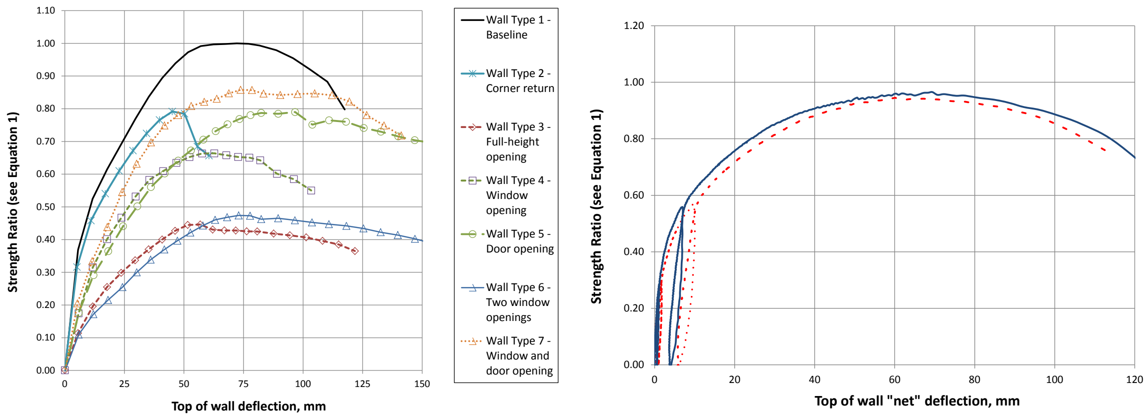

Figure 4. Series A load - deflection curves for Wall Types 1-7 (left), and Series A load - deflection curves for ASTM E72 walls (right). (1 in. = 25.4 mm)

Failure modes included a combination of nail withdrawal from the framing, nail heads pulling through the thickness of the sheathing (commonly referred to as "nail head pull through"), and sheathing edge tear-out. Bearing failures at panel edges were observed at the corners of walls with openings. Panel buckling and panel shear failures were not observed. All studs were judged to be intact and capable of supporting gravity loads at the conclusion of the test.

Table 2. Summary of peak load test results.

Wall type	Wall description	Data series A		Data series B		Combined data	
		Peak load kN/m	Normalized strength ratio	Peak load kN/m	Normalized strength ratio	Strength ratio	
						Average	Lower-Bound
-	ASTM E72	9.72[(1)]	0.96	-	-	-	-
1	Baseline	9.11 11.06 10.33		9.60 10.58 8.61			
	Average: COV:	**10.17** 0.098	**1.00**	**9.60** 0.103	**1.00**	**1.00**	**-**
2	Corner return	8.29	0.82	7.47[(1)]	0.78	0.80	-
3	Full-height opening	4.61	0.45	4.85	0.51	0.48	0.43
4	Window opening	6.89	0.68	7.43	0.77	0.73	0.66
5	Door opening	3.28	0.32	3.11	0.32	0.32	0.29
6	Two window openings	4.89	0.48	4.16	0.43	0.46	0.41
7	Window & door openings	4.25	0.42	4.07	0.42	0.42	0.38

(1 plf = 0.01459 kN/m)

[(1)] Represents average of 2 tests

[(2)] Lower bound is based on average minus 1 standard deviation

5 Evaluation of Measured Strength Parameters

5.1 ASTM E72 Pre-Qualification:

AC 269.1's pre-qualification requirements for CS-WSP bracing recognition require the sheathing and sheathing attachment to achieve a peak shear capacity of at least 8.2 kN/m (560 plf) when tested in general accordance with ASTM E72 using Douglas-fir framing. In addition, the system must demonstrate racking loads of at least 2.9 kN/m (200 plf) and 5.8 kN/m (400 plf) at net deflections of 5.1 and 15.2 mm (0.2 and 0.6 in.), respectively. Review of Table 2 and Table A.1 shows that WSP sheathed walls in this study satisfied these targets. The average peak shear capacity of 9.72 kN/m (666 plf) was 19% greater than the minimum peak unit shear capacity requirement of AC269.1. The 2.9 and 5.8 kN/m (200 and 400 plf) deflections averaged 1.3 and 9.4 mm (0.05 and 0.37 in.), respectively. These findings confirm that the WSP sheathed walls met the pre-qualification requirements.

5.2 Continuous Sheathed Baseline (Wall Type 1):

Once the pre-qualification requirements have been satisfied, additional CS-WSP bracing criteria of AC269.1 are applicable and include testing of Wall Type 1. Wall Type 1 serves as a baseline used for relative evaluation of the other six specific wall types with end returns and openings. Acceptability is based upon how well those walls perform compared to the performance of Wall Type 1.

While the performance of Wall Type 1 becomes critical for the review, AC269.1 does not currently impose minimum strength or stiffness targets. If Wall Type 1 were to be tested with weak anchorage or other detailing, it is possible that a non-conservative review for the remaining configurations may result. For Series A, the minimum peak unit shear is 9.11 kN/m (624 plf). For series B, the minimum peak unit shear is 8.61 kN/m (590 plf). For all Wall Type 1 walls in both series A and B, average top of wall deflection did not exceed 5.1 mm (0.2 in.) at a unit shear of 2.9 kN/m (200 plf) and 15.2 mm (0.6 in.) at a unit shear of

5.8 kN/m (400 plf). To avoid a non-conservative review for alternative proprietary product, it may be appropriate for AC269.1 to impose the ASTM E72 wall strength and stiffness requirements upon Wall Type 1. WSP sheathed walls tested in this study would have supported this suggested minimum performance level.

5.3 Continuous Sheathed Wall Comparisons:

A comparison of test-based peak strength ratios in accordance with Equation 1 and the current minimum "reference" strength ratios required by AC269.1 is provided in Table 3. Column 3 provides minimum required reference strength ratios assigned by AC269.1 to each wall configuration. Column 4 provides average test-based strength ratios at peak load. For comparison purposes, Column 6 provides the ratio between Columns 4 and 5. Values greater than 1.0 indicate that test-based strengths exceed the reference strength targets. From Column 6, it is seen that average test-based strengths in this study exceeded the reference calculation-based strengths for the perforated configurations by varying margins ranging from 1.20 to 1.63. This suggests that the average WSP bracing performance measured in this study for the walls with perforations was 20-63% greater than the current minimum targets in AC269.1. This finding was not unexpected given that the AC269.1 targets were generated using the SPDWS perforated wall calculation method believed to be conservative for design purposes.

Column 5 provides newly proposed lower-bound – average minus one standard deviation – strength ratios for perforated wall configurations that might be considered for incorporation as potential new minimum targets for AC269.1. The standard deviation estimate used for all wall configurations was based upon an assumed 10% coefficient of variation (COV). The COV for the Wall Type 1 configuration obtained by combining the six replicates from Series A and B was 9.5%. Using a reasonable lower bound target has precedent in other ICC-ES acceptance criteria and provides some flexibility to account for the limited number of samples required as part of an AC269.1 evaluation. The average minus one standard deviation approach helps to account for the likelihood that any given small sampling may fall above or below a population average. From Column 7, it is seen that even the proposed lower bound test-based strengths would exceed the existing reference calculation-based strength ratios for walls with openings by varying margins ranging from 1.08 to 1.46.

Table 3. Comparison of reference and test-based strength ratios.

[Col 1]	[Col 2]	[Col 3]	[Col 4]	[Col 5]	[Col 6]	[Col 7]
Wall type	Wall description	Reference strength ratio[1]	Test-based peak strength ratio (average)	Test-based peak strength ratio (lower-bound)[2]	$\frac{\text{Col 4(Test)}}{\text{Col 3(Ref)}}$	$\frac{\text{Col 5(Test)}}{\text{Col 3(Ref)}}$
1	Baseline	1.00	1.00	-	1.00	-
2	Corner return	0.79	0.80	-	1.01	-
3	Full-height opening	0.40	0.48	0.43	1.20	1.08
4	Window opening	0.51	0.73	0.65	1.42	1.27
5	Door opening	0.21	0.32	0.29	1.54	1.38
6	Two window openings	0.28	0.46	0.41	1.63	1.46
7	Window & door openings	0.29	0.42	0.38	1.45	1.31

(1) Reference strength ratios for walls with openings (Wall types 3, 4, 5, 6, and 7) are calculated in accordance with the perforated shear wall strength ratio equation: F=r/(3-2r) where r = sheathing area ratio (see Commentary to AWC, 2008). Reference strength ratio is called the "reduction factor" in AC269.1 and used in both strength and stiffness evaluations of CS-WSP bracing.

(2) Lower bound values based on average minus one standard deviation estimates from test data where COV of baseline wall data was 0.10.

5.4 Corner return wall (Wall type 2):

Unlike the reference strength ratio for the five wall perforated configurations, the required minimum reference strength ratio of 0.79 for the corner return wall used by AC269.1 was not based on the perforated shear wall calculation method. While it is based on prior testing; the specific factor of 0.79 is not directly prescribed in corner return wall test reports (Dolan, 1997 or HUD, 2001). It is also worth noting that AC269.1 does not currently specify the corner return framing configurations and that corner return details specified in the IRC have evolved with time. For corner return walls constructed in accordance with details reported herein, the average strength ratio is 0.80 which is considered to be in support of the continued use of the current reference strength ratio of 0.79 based on prior testing.

5.5 Stiffness/deflection evaluation:

In addition to the minimum required relative strength, the CS-WSP bracing criteria of AC269.1 also contain stiffness targets that are numerically equivalent to the minimum strength ratios. Test-based stiffness ratios are determined in accordance with Equation 2:

$$Stiffness\ ratio = \frac{\left(\frac{Reference\ load}{\Delta\ @\ Reference\ load}\right)}{\left(\frac{Reference\ load}{\Delta\ @\ Reference\ load}\right)_{Baseline}} \qquad \text{Eq. 2}$$

where:

Δ = top of wall deflection, in.

Test-based stiffness ratios determined at 40% of each wall's peak unit shear capacity (kN/m or plf), as required by the current criteria, showed high variability and resulted in both large increases and decreases in stiffness targets relative to current AC269.1 values. Under the current AC269.1 approach, unit shear is calculated as load divided by the overall wall length. Test-based stiffness ratios evaluated at 40% of each wall's peak capacity (kN or lbf) were also highly variable but met or exceeded current stiffness targets when data from series A and B were averaged. It is observed that measured deflections are both small in magnitude and can vary significantly between laboratories on a percentage basis. Also, while 40% of peak load is intended to approximate a region of generally elastic response, varying levels of non-linearity are present such that slight increases in load can lead to relatively large increases in deflection.

An alternative stiffness ratio analysis is provided in Table 4 where deflection is taken at a load more representative of an allowable "reference" design load and calculated as: 4.1 kN/m x wall length x the reference ratio. The alternative stiffness ratio analysis was investigated to evaluate stiffness ratio at load levels associated with a load level approximating an allowable stress design of the shear walls with openings in accordance with the perforated shear wall method. Results of the analysis are shown in Table 4. Such load levels are intended to represent the elastic response region of the load deflection curve, For Wall Types 3-7, the test-based stiffness ratios are observed to vary significantly between laboratories. When data series A and data series B are averaged, test-based ratios are observed to range from 0.88 to 1.29 times the reference ratios with an overall average ratio of 1.04. Based on averaged results for each configuration, the alternative analysis shows that the stiffness ratio from testing is greater than the reference ratio for Wall Types

3, 4 and 5 but less than the reference ratio for Wall Types 6 and 7. Where tested stiffness ratio was less than the reference ratio, the maximum difference was 12% for Wall Type 7. However, in general, the overall average test/reference ratio of 1.04 for the test program suggests reasonable agreement between the tested and predicted perforated wall stiffnesses at the design load level.

Table 4. Comparison of reference and test-based stiffness ratios at the reference design load.

Wall type	Wall description	Reference ratio	Reference design load (kN)	Series A test-based stiffness ratio	Series B test-based stiffness ratio	Combined data from Series A and B	
						Test-based average stiffness ratio	$\frac{\text{Test}}{\text{Reference}}$
1	Baseline	1.00	9.96	1.00	1.00	1.0	1.0
2	Corner return	0.79	11.8	1.11	0.73	0.92	1.16
3	Full-height opening	0.40	5.98	0.33	0.71	0.52	1.29
4	Window opening	0.51	7.56	0.50	0.56	0.53	1.05
5	Door opening	0.21	3.45	0.21	0.21	0.21	1.00
6	Two window openings	0.28	4.85	0.33	0.16	0.25	0.89
7	Window & door openings	0.29	5.54	0.31	0.20	0.26	0.88
						Overall Average	1.04

6 Findings and Recommendations

In addition to documenting results from testing wood structural panel sheathed walls in specific CS-WSP bracing configurations in AC269.1, information reported herein is intended to assist in further refinement of procedures for evaluation of equivalence to CS-WSP bracing. Findings and recommendations from this testing program include the following:

a. This test program confirmed that wood structural panel sheathing satisfies the racking pre-qualification requirements for strength and stiffness based upon an ASTM E72 racking test. The pre-qualification requirement provides for a standard evaluation of the sheathing and sheathing-to-framing attachment.
b. The strength and stiffness of Wall Type 1 is essential for establishing strength and stiffness ratios for CS-WSP bracing configurations in AC269.1. While testing indicates relative low strength variability for the baseline wall tests, additional clarification of requirements for baseline tests is recommended. This includes clarification of fabrication details, such as the minimum overturning anchorage capacity, and compliance of the baseline walls with minimum strength and stiffness requirements similar to that of the ASTM E72 racking test provisions.
c. Results of testing-specific wall configurations in AC269.1 confirm the conservatism of the perforated shear wall calculation method in SDPWS for estimating design strength. This conservatism for design; however, translated into minimum strength performance targets in AC269.1 that are non-conservative relative to the tested performance of wood structural panel sheathed walls.
d. Revised minimum strength performance targets for perforated shear wall configurations in AC269.1 are proposed using an “average minus one standard deviation” basis. These test-based strength performance targets for the perforated configurations ranged from 1.08 to 1.46 times the current strength performance targets. For corner return walls constructed in accordance with details reported herein, the

average strength ratio is 0.80 which supports the continued use of the current reference strength ratio of 0.79 based on prior testing.

e. Additional construction details for fabrication of walls are recommended to improve consistency in results. Details that have the potential to impact the results include: location and installation of anchor bolts, measurement of corner return wall lengths, header framing size and support methods, and framing nailing guidance. Revised guidance for a minimum hold-down size that aligns the hold-down strength with the expected wall racking strength is also recommended.
f. Methods used for calculation of strength and stiffness ratios are currently dependent on footnoted information in AC269.1. Further clarification or re-organization of the calculation method used for evaluation of strength and stiffness is recommended.
g. In recognition of observed stiffness variability in Wall Types 2-7 and that only a single test of each of those configurations is required by AC269.1, it is proposed to remove stiffness performance requirements for Wall Types 2-7 provided that minimum strength and stiffness requirements are met for Wall Type 1. Alternatively, the stiffness targets for specific CS-WSP bracing configurations should be revised to reflect the results of this study based on the construction details in this study. The load levels used for the unit stiffness determinations should also be revised and clarified to account for non-linear deformation behavior and variability.

7 Summary

Testing of wood structural panel sheathed walls in specific CS-WSP bracing configurations described in AC269.1 was undertaken in two separate laboratories. Test-based strength performance of the CS-WSP bracing configurations with perforations are 20% to 63% greater than the existing calculation-based reference minimum strength performance targets used by AC269.1 for evaluating proprietary sheathing materials. While test data confirmed the expected conservatism of the perforated shear wall calculation method used to establish the existing targets, it also shows that AC269.1's strength performance targets based on calculations underestimate actual tested strengths of specific wall configurations. Alternative strength ratio performance targets ranging from 1.08 to 1.46 times current calculation-based levels for perforated wall configurations are suggested. Stiffness ratios based on deflection at 40% of peak load observed in this study did not mirror the strength ratios as assumed by AC269.1. The approach used by AC269.1 for the unit stiffness evaluation of Wall Types 2-7 should be replaced with alternative criteria or revised to reflect the results of this study.

8 References

1. APA. 2011. Voluntary Product Standard – PS2-10, Performance Standard for Wood-Based Structural-Use Panels, Form S350. APA – The Engineered Wood Association, Tacoma, WA.
2. ASTM. 2006. ASTM E564 Standard Practice for Static Load Test for Shear Resistance of Framed Walls for Buildings. American Society for Testing and Materials, West Conshohocken, PA.
3. ASTM. 2010. ASTM E72 Standard test Methods of Conducting Strength Tests of Panels for Building Construction, American Society for Testing and Materials, West Conshohocken, PA.

4. AWC. 2008. Special Design Provisions for Wind and Seismic (SDPWS) with Commentary. American Wood Council, Leesburg, VA.
5. Dolan, J.D. and C. Heine. 1997. Sequential Phased Displacement Tests of Wood-framed Shear Walls with Corners. Report No. TE-1997-003. Brooks Forest Products Research Center, VPI&SU, Blacksburg, VA.
6. HUD. 2003. Wood shear walls with corners. U.S. Department of Housing and Urban Development, Washington, DC. (publication available through **www.huduser.org**)
7. ICC. 2009. International Residential Code, International Code Council, Falls Church, VA.
8. ICC-ES. 2013. ICC ES AC269.1 Acceptance Criteria for Proprietary Sheathing Attached to Wood Light-Frame Wall Construction Used and Braced Wall Panels Under the IRC. International Code Council Evaluation Service, Falls Church, VA.
9. Keith, E., 2014. APA Report T2013P-18 Wood Structural Panel Shear Wall Tests in Accordance with ICC-ES AC269.1, APA-The Engineered Wood Association, Tacoma, WA.
10. Line, P, Waltz, N., Skaggs, T. 2008. "Seismic Equivalence parameter for Engineered Wood-frame Wood Structural Panel Shear Walls," Wood Design Focus (Summer), Forest Product Society. Madison, WI.
11. Waltz, N. 2012. Benchmark Monotonic and Cyclic Tests of Fully-Restrained Wood Structural Panel Braced Walls," Weyerhaeuser Engineering Laboratory Experiment No. 2379A. Weyerhaeuser, Boise, Idaho.
12. Waltz, N. 2013. ICC-ES AC269.1 Continuous Sheathing Review of Oriented Strand Board, Weyerhaeuser Engineering Laboratory Experiment No. 2407. Weyerhaeuser, Boise, Idaho.

Table A.1. Detailed data summary.

Wall type	Ref/Item	Wall Length (m)	OSB (mm)	Sheathing nails	Fastener spacing (edge/field) (mm)	Open-ings	Drift at 2.9 kN/m (mm)	Drift at 5.8 kN/m (mm)	40% Peak load		Peak load		Ultimate load[1]		Gravity load system intact	Failure[2]
									Load (kN)	Drift (mm)	Load (kN)	Drift (mm)	Load (kN)	Drift (mm)		
-[3]	[A]/A21	2.4	9.5	6d com	150/300	No	1.5	10.8	9.4	3.0	23.4	60.1	18.8	113.0	Yes	P, T, W
-[3]	[A]/A22	2.4	9.5	6d com	150/300	No	1.2	7.9	9.6	2.2	23.9	69.4	19.2	116.5	Yes	P
1	[B]/1	2.4	9.5	6d com	150/300	No	6.7	10.3	8.9	8.3	22.2	80.4	17.8	139.9	Yes	W, T, P
1	[B]/2	2.4	9.5	6d com	150/300	No	2.7	12.2	10.8	6.0	27.0	74.5	21.6	124.1	Yes	P, W
1	[B]/3	2.4	9.5	6d com	150/300	No	3.6	14.3	10.1	6.4	25.2	75.5	20.2	117.2	Yes	W, T, P
1	[C]/4	2.4	9.5	6d com	150/300	No	-	9.3	9.4	-	23.4	59.3	18.7	97.2	Yes	P, W
1	[C]/5	2.4	9.5	6d com	150/300	No	1.0	5.7	10.3	2.4	25.8	70.0	20.6	98.9	Yes	P, W
1	[C]/6	2.4	9.5	6d com	150/300	No	1.7	12.7	8.4	2.6	21.0	55.9	16.8	127.7	Yes	P, T
2	[B]/7	3.6	9.5	6d com	150/300	No	-	-	12.1	5.3	30.3	48.0	24.3	62.1	Yes	T at end return bottom
2	[C]/8	3.6	9.5	6d com	150/300	No	-	-	11.0	2.8	27.5	36.2	22.0	49.7	Yes	T
2	[C]/9	3.6	9.5	6d com	150/300	No	-	-	10.8	3.3	27.1	47.8	21.7	65.5	Yes	T
3	[B]/10	3.6	9.5	6d com	150/300	Yes	-	-	6.7	10.3	16.9	59.1	13.5	124.0	Yes	T, P, W
3	[C]/11	3.6	9.5	6d com	150/300	Yes	-	-	7.1	2.4	17.7	39.4	14.2	109.5	Yes	P, W
4	[B]/12	3.6	9.5	6d com	150/300	Yes	-	-	10.1	9.2	25.2	60.6	20.1	106.6	Yes	B, P, T
4	[C]/13	3.6	9.5	6d com	150/300	Yes	-	-	10.9	5.5	27.2	56.4	21.7	80.4	Yes	P, T
5	[B]/14	4.1	9.5	6d com	150/300	Yes	-	-	5.3	14.2	13.3	94.4	10.7	165.5	Yes	P, T, B
5	[C]/15	4.1	9.5	6d com	150/300	Yes	-	-	5.0	6.0	12.6	57.4	10.1	125.9	Yes	B, P, T
6	[B]/16	4.3	9.5	6d com	150/300	Yes	-	-	8.4	14.3	20.9	75.2	16.7	158.0	Yes	B, T, P
6	[C]/17	4.3	9.5	6d com	150/300	Yes	-	-	7.1	10.9	17.7	72.6	14.2	122.8	Yes	T, B, P
7	[B]/18	4.6	9.5	6d com	150/300	Yes	-	-	7.9	12.0	19.9	77.1	15.9	146.0	Yes	B, T, P
7	[C]/19	4.6	9.5	6d com	150/300	Yes	-	-	7.6	7.8	19.0	65.3	15.2	150.6	Yes	B, T, P

Notes

(1 ft = 0.3048 m, 1 in. = 25.4 mm, 1 plf = 0.01459 kN/m, 1 lbf = 0.004448 kN)

[1] Point where the wall capacity is 80% of the peak.

[2] Failure description: W-sheathing nail withdrawal from framing, P – sheathing nail head pull-through the panel, T-sheathing nail edge tear-out of panel, B – bearing failure of sheathing panel at edges.

[3] These walls were tested using matched materials in accordance with the racking test method of ASTM E72. The reported drifts represent the net lateral deflection after rigid body rotation and translation have been analytically removed. The drift reported for the remaining walls represents the total lateral movement from all sources.

Appendix Table References:
[A] Waltz (2012), [B] Waltz (2013), [C] Keith (2014)

INTER/47-15-8

INTER

International Network on Timber Engineering Research

DESIGN OF FLOOR DIAPHRAGMS IN MULTI-STOREY TIMBER BUILDINGS

D Moroder

T Smith

S Pampanin

A Palermo

A H Buchanan

University of Canterbury, Christchurch

NEW ZEALAND

Presented by A Buchanan

WY Loo and A Buchanan discussed about wall flexibility in that it is the relative stiffness of the floor and wall and that the torsional response is important.

R Tomasi commented on the definition of flexibility of diaphragm and suggested that perhaps we need rules based on the type of construction (concrete topping floors for example). A Buchanan stated that we should be consistent rather than specifying such rules.

M Popovski provided information that in Canada diaphragm flexibility is now defined by 50% of the diaphragm deflection is greater than the deflection of the lateral load resistance system. This affects the R factor. I smith stated that in tall buildings you will not do this type of design. All agreed as wind rather than seismic will govern.

Design of Floor Diaphragms in Multi-Storey Timber Buildings

Daniel Moroder, Tobias Smith, Stefano Pampanin, Alessandro Palermo, Andrew H. Buchanan

University of Canterbury, Christchurch, New Zealand

Keywords: diaphragm, over-strength, ductility, multi-storey, seismic resistance, capacity design, displacement incompatibility, earthquakes

Abstract

This paper discusses the design of timber diaphragms with respect to new-engineered timber products, in response to the growing interest in multi-storey commercial timber structures, and the lack of unified regulations regarding the seismic design of timber structures.

Proper performance of floor diaphragms is required to resist all lateral loads, but design for earthquake loads is much more complex than design for wind loads. This paper shows that the seismic design of a diaphragm is intimately linked to the seismic design of the whole building. For this reason, the state-of-the-art in the seismic design of multi-storey timber buildings is reviewed, with special attention to diaphragms.

The paper summarises international code requirements for diaphragm design, and provides suggestions for improvements. It is shown that some current design recommendations for plywood sheathing on light timber framing can be applied to solid wood diaphragms, but proper connection detailing and stress verification in diaphragm panels is still required. It is strongly recommended that diaphragms be designed as elastic elements, by applying dynamic amplification and the over-strength factors derived from the lateral load resisting system. Diaphragm flexibility and displacement incompatibilities between the floor diaphragms and the lateral resisting systems also need to be accounted for.

1 Introduction

The recent construction of a number of engineered multi-storey timber buildings around the world has attracted growing interest from developers, researchers, engineers, and the timber industry. As part of this push for taller timber buildings, several feasibility studies on high-rise timber buildings were published [1-7]. More tall timber buildings are to be built in Canada and Norway [8], some with government subsidies promoting innovation.

This new interest in medium to high-rise multi-storey timber buildings creates the need for a more rigorous approach in design. The presence of some of these structures in seismically active countries highlights knowledge gaps surrounding their performance under earthquake loading, with a special focus on the design of diaphragms.

1.1 Role of diaphragms

Floor diaphragms are critical components of all buildings. Aside from acting as slabs under gravity loads, diaphragms tie all other structural elements together and transfer horizontal wind and seismic loads to the Lateral Load Resisting System (LLRS). A loss of diaphragm action could have catastrophic consequences in severe wind storms or earthquakes.

Several authors have highlighted poor design and detailing of diaphragms, mostly due to a lack of understanding of diaphragm functionality, and inadequate code provisions. It has been shown that flexible diaphragms can change the global dynamic behaviour of buildings [9, 10], that floor accelerations are often underestimated with traditional design methods [11-13] and that displacement incompatibilities between the floor diaphragm and the LLRS can compromise the load path [12, 14, 15].

Although this paper focuses on seismic design, similar principles regarding force distribution and connection detailing apply to the design of diaphragms for wind loads or other lateral loads on buildings. All forces created within the diaphragm or deriving from load applications along the diaphragm edges need to be transferred to the LLRS. Concentrated forces, floor openings or re-entrant corners create stress concentrations, which need to be accounted for to prevent premature failures. All components of floor diaphragms (chord beams, collectors and strut beams, panel elements and the various connections) need to resist the anticipated forces guaranteeing a clearly defined load path through the structure from the points of load application to the foundations. Under seismic forces, dissipation and ductility should be provided by the vertical LLRS, leaving the diaphragms to work as a whole in the elastic range.

1.2 Importance of seismic design philosophy

In recent decades, the majority of research and development in engineered timber structures has been in Europe, with a few exceptions in North America and elsewhere. Because of the relatively low seismic risk in these areas however, little effort was put into the understanding the seismic behaviour of such buildings. Light Timber Frame (LTF) buildings are common in high seismic zones such as North America and New Zealand; however, these buildings are mostly low-rise, residential, and constructed using prescriptive design codes and very little detailed calculation. These two facts have led to a knowledge gap regarding the seismic design of medium to high-rise multi-storey timber buildings. It is also worth noting that the performance limits states for seismic loading can vary significantly from those for wind loading design. In general seismic loading will have higher allowable drift limits and as such increased displacements under design loadings. These increased displacements must also be considered during design of diaphragms.

1.2.1 Capacity design

The capacity design philosophy developed in New Zealand in the Seventies [16, 17] for the seismic design of reinforced concrete structures, has since been included in many international design methods and codes for concrete, steel and masonry structures and lies at the heart of modern seismic design.

The capacity design procedure outlined in Figure 1 requires the selection of a mechanism with designated ductile regions or ductile connections. These ductile components must be designed to withstand large cyclic deformations while dissipating energy in a stable manner, and all other (less ductile or brittle) elements must be designed with proper over-strength. Similar to a chain where the maximum capacity is dictated by the weakest link (Figure 2), when the weakest link is ductile, the overall chain is ductile.

Chose a kinematically admissible mechanism – i.e. define the position of the ductile connections which dissipate energy. ⇨ Design the connections to fail in a ductile manner, with their capacity as close as possible to the demand. ⇨ Design all other elements for strength greater than the over-strength capacity of the ductile connections.

Figure 1: Capacity design procedure

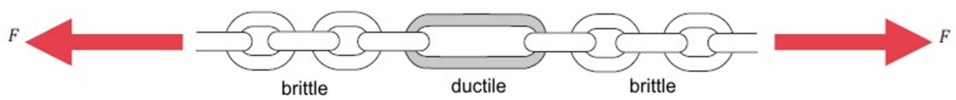

Figure 2: The principle of capacity based design of a chain with a ductile link (modified from [18])

For wind loading, or if dissipation is neither required nor achieved under earthquake loading, structures can be designed to remain elastic. Even then, the overall structure should be designed to behave in a ductile manner under extreme overload conditions.

1.2.2 Over-strength

In order to ensure that the ductile link in the system is indeed the weakest component along any given load path an 'over-strength' factor is defined for the ductile link and all other links are designed accordingly. Paulay and Park [17] state that the over-strength takes into account all factors that may increase the strength of the weakest element or connection. These factors include higher-than-specified material strength, strain hardening at large deformations, sections sizes larger then assumed etc.

2 Review of current code design provisions

2.1 Code provisions for the seismic design of timber structures

While timber design codes in Europe, New Zealand, Canada and the US discuss seismic design, the provisions and information provided is relatively limited. Recent international developments in the seismic design of structural steel and reinforced concrete buildings have not generally been adopted into timber building codes.

Most codes and standards for seismic design of timber buildings are based on LTF construction, with light weight timber studs and joists sheathed in wood-based panel products such as plywood and Oriented Strand Boards (OSB). Ductility, over-strength and dynamic amplification factors are occasionally mentioned, but definitions differ greatly, and missing values are left to engineering judgement.

A review of international codes [19-28] regarding the seismic design of timber structures shows there is inadequate attention to the principles of capacity design for timber structures. Due to this, many timber structures do not have any strength hierarchy, kinematically admissible ductile failure mechanisms are not present and theoretically dissipative connections (the 'weak links') might be overdesigned, leading to possible catastrophic brittle failures instead of ductile behaviour. Furthermore, the implications of choices like structure ductility and over-strength are often unknown to designers.

2.2 Code implementation of capacity design principles for diaphragms

For the design of diaphragms in timber structures minimal reference is made to capacity design principles as can be seen in Table 1. No consensus can be found regarding the requirement of elastic diaphragm design. Over-strength values are implied by most codes, but values and their specific application are often left to the designer's choice.

It is worth noting that the Eurocode 8 [19] and the NTC 2008 [28] are misleading about the design of diaphragms, because although they give over-strength factors for diaphragm design, they do not explicitly prohibit the design of ductile diaphragms. This means that a designer may erroneously attempt to create a ductile diaphragm system that is not the weakest component due to the presence of code defined over-strength factors.

2.2.1 Provisions for over-strength factors in codes and recent literature

The term 'over-strength' is used in many different ways in current seismic codes, some of them inconsistent with the general principles given in 1.2.2. So called over-strength factors are sometimes used to reduce the seismic design spectra [29] or create load combinations for special elements such as collector beams [21], or are used to protect the diaphragm as a whole or its individual parts [19, 23, 24, 27]. Significant research [30-35], gives no consensus on a common approach of how to determine over-strength values and what factors (i.e. statistical scatter, approximation of analytical expressions, over-capacity, hidden reserves from mechanical effects etc.) should be included.

Table 1: Comparison of design codes regarding 'capacity design'

	Europe EN 1995:2008, EN 1998:2010 (ECs 5 and 8) [19, 20]	**Italy** NTC2008 [28]	**Switzerland** SIA 265:2003, SIA 261:2003 [27, 36]	**New Zealand** NZS 3603:1993, NZS 1170.5:2004 [24, 25]	**US** ASCE 7-10, IBC 2012 and SDPWS 2008 [21, 22, 37]	**Canada** O86-09 and NBCC 2010 [23, 26]
Elastic versus yielding diaphragm design	No explicit provisions are given.			Elastic (localized yielding at boundaries allowed[1)])	Elastic	Provisions for elastic and yielding diaphragms.
Design of diaphragms	Provides over-strength factors for diaphragms.	Diaphragms loads need to be increased by 30%.	For all non-ductile timber members and connections an over-strength factor of 1.2 needs to be applied.	For LTF walls and diaphragms all non-ductile elements and connections need to be designed with an over-strength of 2.	Equations for diaphragm forces provided. Collectors need to be designed for a load combination with over-strength [2)]. Special provisions for diaphragm anchorage are provided.	Overcapacity factors for the design of elastic and yielding diaphragms need to be calculated based on the actual strength of the LLRS.
Capacity design of timber members	For timber members over-strength factors need to be applied (but no values provided).					

[1)] Even though NZS3603:1993 requires an over-strength factor for diaphragm chords, assuming that the connection between the panels might yield, NZS 1170.5:2004 states that diaphragms should be designed as elastic.

[2)] Structures with LTF shear walls are exempt from this rule, i.e. collector beams are designed with the standard load combination.

2.3 Code provisions for diaphragm design

A review of six timber design codes showed that only limited guidance is available on the design of diaphragms. Furthermore, all codes were based on the design of traditional LTF diaphragms consisting of wooden sheathing panels connected by metallic fasteners to timber framing. Table 2 summarises admissible aspect ratios, requirement of blocking, load application, required design verifications, evaluation of diaphragm deformation, and design for openings. Whereas North American codes provide tabulated capacity values derived from testing, all other codes are based on mechanics-based principles.

Table 2: Comparison of codes regarding the design of timber diaphragms

	Europe EN 1995-1-1:2008 [20]	**Germany** DIN EN 1995-1-1/NA:2010-12 [38]	**Switzerland** SIA 265:2003 [27]	**New Zealand** NZ3603:1993 [24]	**USA** ANSI/AF&PA SDPWS-2008 [22]	**Canada** O86-09 [23]
Diaphragm construction	Timber framing and sheathing panels					
Aspect ratio (L/W)	2-6	≤ 6	N.R.	N.R.	≤ 3 (unblocked), ≤ 4 (blocked)	N.R.
Blocked/ unblocked	Blocked	Not required if additional requirements are satisfied	Blocked	Blocked	Tabulated shear capacity values for both	
Load	Uniformly Distributed Load (UDL) along the edge	UDL along the edge or smeared over the diaphragm	UDL along the edge	N.R.	Wind and seismic, UDL along the edge	N.R.
Statical system	Simply supported beam	Continuous beams treated as simply supported beams	Continuous beam on supports.	N.R.	N.R.	N.R.
Verifications	Chords, shear in panels, fasteners	Chords, shear and buckling of panels, fasteners	Chords and fasteners	Chords, panels, fastener.	Tabulated capacity values for shear in nails and panels; Chord strength needs to be verified	
Deformation	N.R.	Can be omitted if certain conditions are satisfied (Equation in [39])	Needs to be considered under SLS (Equation in [18])	Equation provided for blocked simply supported diaphragms		
Openings	N.R.	Can be ignored if of very limited size	Need to be considered	Need to be considered, refers to Shear Transfer Method [40]	N.R.	N.R.

N.R. = no requirements

To determine the force demand in sheathed timber diaphragm components, the New Zealand approach is based on the girder/deep beam analogy [41, 42], the German and Swiss approach is based on the further enhanced 'shear field analogy' [39, 43]. In North America, the deep beam analogy is used in combination with transfer diaphragms for force concentrations deriving from openings, re-entrant corners or other irregularities [44].

2.3.1 Flexible vs rigid diaphragms

The definition of flexible versus rigid floor diaphragm behaviour has always been a point of discussion, especially for LTF timber construction. The flexibility of the floor diaphragm may change the dynamic response of the whole building and will impact on the distribution of lateral forces into the LLRS. The standard assumption is that a rigid diaphragm will distribute lateral loads to the LLRS in proportion to the stiffness of the LLRS, whereas a flexible diaphragm will distribute loads in proportion to tributary areas.

Definitions of "flexible" diaphragms vary widely (for example see Figure 3), and the provisions of some codes on this matter are quite difficult to understand. Some timber design codes provide different prescriptive detailing rules for rigid diaphragms, but their application is questionable for more recent floor materials and panel layouts.

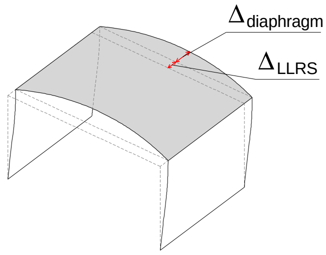

A diaphragm is flexible if:

ASCE 7-10, NZS 1170.5:2004:
$\Delta_{diaphragm} \geq 2\ \Delta_{LLRS}$

Eurocode 8, NTC 2008:
$\Delta_{diaphragm} \geq 1.1\ \Delta_{LLRS}$

Figure 3: Flexible diaphragm definitions according to New Zealand/US codes and European codes

3 Diaphragm design

3.1 Loads on timber diaphragms

All components of floor diaphragms must be designed to resist anticipated loads, including wind loads, seismic inertial loads and any transfer forces. A significant difference between wind and seismic loads is that while wind pressure on the building façade is normally represented as a Uniformly Distributed Load (UDL) on the edge of the diaphragm, seismic loads are inertial and generated within the diaphragm itself. Seismic loads therefore should be represented as horizontal pressures on the diaphragm. Although this does not significantly alter the stress distributions in the diaphragms, for wind loads where forces from the façade are normally introduced over the chord beams, the connections between the panels and the chord beams must account for forces perpendicular to the panel edges. For LTF diaphragms only the German National Appendix to Eurocode 5 [38] differentiates between different load sources.

Transfer forces can be generated by changes in the LLRS up the height of the building, or by interaction between different types of LLRS (i.e. combinations of wall, frame and tube systems), amplified by the large displacements mentioned in Section 1.2, especially if a high level of building ductility is required. Additional diaphragm loads can also be created by the three dimensional nature of earthquake attack. While common practice is to separately design orthogonal LLRs (in case of regular building configuration), the lateral movement of the structure in a principal direction will also create out-of-plane movement of any orthogonal LLRS, which must be allowed for in the design.

3.2 New developments in timber diaphragm systems

Traditionally, timber diaphragms have been structural elements built from wooden sheathing on light timber framing. Recent innovations have opened the possibility of using larger solid timber panels made of LVL, CLT or glulam, as well as pre-assembled Structural Insulated Panels (SIPs) and timber-concrete composite floors. Almost no code provisions are available for diaphragms made of these new materials.

For large solid timber panels, available research on CLT structures focuses mainly on residential construction, where a single panel could span over the whole diaphragm. Structural analysis for such buildings generally adopts a rigid diaphragm assumption, since the connections between the panels are normally designed with sufficient over-strength [45-47].

The use of solid timber diaphragms in multi-residential and commercial buildings however might require multiple rows of panels to cover the diaphragm depth and the span of the whole diaphragm may become significant. Such a layout tends to increase the diaphragm flexibility.

3.3 Timber diaphragm design

Whereas design approaches with the deep beam analogy [42, 49-51] with its improvements found in the 'shear field analogy' [39, 43] and transfer diaphragms [44] have led to satisfactory designs for LTF diaphragms, little is known about the behaviour of diaphragms made of solid timber panels.

Wallner-Novak et al. [48] discuss the design of floor diaphragms made from CLT panels and refer also to the deep beam analogy as shown in Figure 4. The panels and panel connections which resist the shear and tension/compression forces along the edges are taken by chord beams or need to be transferred by appropriate connectors. For earthquake attack perpendicular to the panel length (Figure 4c), the diaphragm can be assumed to work as a series of beams in parallel. A finite element analysis in Canada [52] confirmed the shear force distribution in Figure 4a, but the tension and compression forces in Figure 4b could not be evaluated because the panels were connected with rigid links perpendicular to the panel edges.

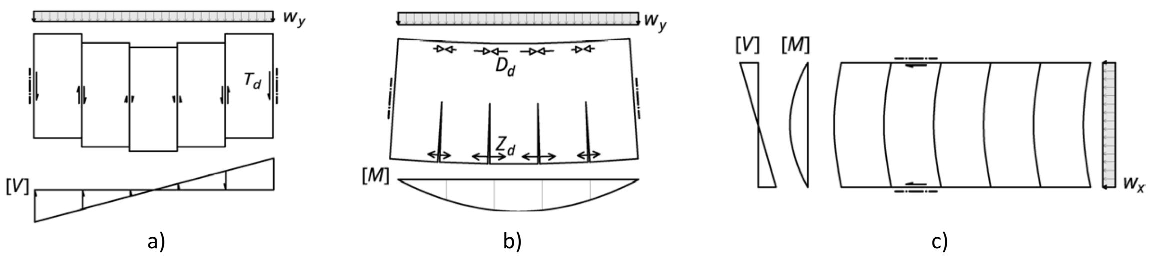

Figure 4: Failure mechanism of floor diaphragms: a) shear along panel connection, b) chord forces, c) diaphragms as series of beams [48]

To verify the deep beam analogy for solid timber diaphragms, the authors carried out a simple FEM analysis in SAP2000 [53]. CLT diaphragm panels of 1.2 x 4.8 m were modelled as orthotropic membrane elements (E_1 = 8 GPa, E_3 = 4 GPa, E_3 = 0.5 GPa, G_{12} = 600 MPa, G_{13} = 500 MPa, G_{23} = 100 MPa, υ_{12} = 0.07, $\upsilon_{13} = \upsilon_{23}$ = 0.35) [52] and the panel connections, 30° inclined Ø8 mm fully threaded screws at 150 mm on a lap joint, were modelled with linear elastic link elements (K_{ser} = 6600 N/mm and K_{ser} = 3000 N/mm parallel and perpendicular to the panel edge, respectively). Figure 5 shows the stress distributions for a simply supported diaphragm (4.8 x 10.8 m) with and without chord beams. The contours show normal stresses (tension/compression stresses parallel to the span) and shear stresses in the panels.

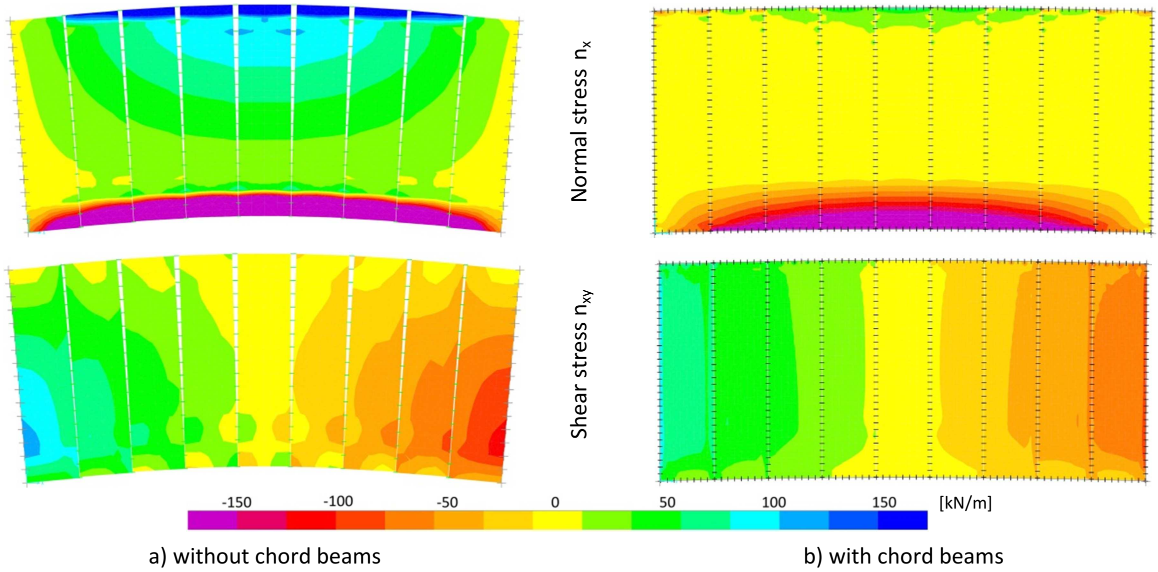

Figure 5: Simply supported diaphragms a) without and b) with chord beams

For both setups the stress distributions were as assumed in the deep beam analogy. For diaphragms with chord beams the majority of the tension/compression forces were resisted by the chords, otherwise tensile forces need to be transferred by the panel connections. The absence of chord beams as shown in Figure 5 a) created high tensile stresses. In panels without cross-layers (glulam, LVL) these high tensile forces may lead to brittle failure. Figure 5 also shows that the deflection is much bigger for the diaphragm without chord beams.

These studies confirm that the deep beam analogy can be adopted for both traditional and solid timber diaphragms with simple geometries and no major openings. For more complex floor layouts the adoption of the shear field analogy or the approach with transfer diaphragms, or a strut-and-tie model could be considered, however further research on the applicability is required. Due to the increased use of computer software in design offices, truss methods [43, 54] and Finite Element Modelling (FEM) are increasing in popularity.

With modern computer software it is not difficult to construct a simple FEM model of a floor diaphragm made from solid wood panels, to assess the fastener forces and diaphragm displacements. However, if designers wish to use a FEM model for analysis of the whole building, it may be inappropriate (very likely un-conservative and thus unsafe) to use only one rigid shell element for the whole floor diaphragm, so orthotropic elements with a simple mesh and linear springs for the connections should be adopted to capture the stress flow, stress concentrations and fastener forces.

3.3.1 Forces around openings, re-entrant corners and other irregularities

All floors have openings for access and vertical services, which can create local stress concentrations in the floor diaphragm. Similarly, non-rectangular or other unusual floor plates cause additional related problems. Different approaches to calculating these stresses are available for traditional diaphragms, whose applicability to solid timber panels still needs to be verified.

The diaphragm simulation in Figure 6 shows that high stresses need to be transferred between the panels close to floor irregularities. These forces need to be evaluated and if no additional reinforcement (strut beams, steel plates etc.) is placed around these disturbed zones, local panel connections need to be reinforced.

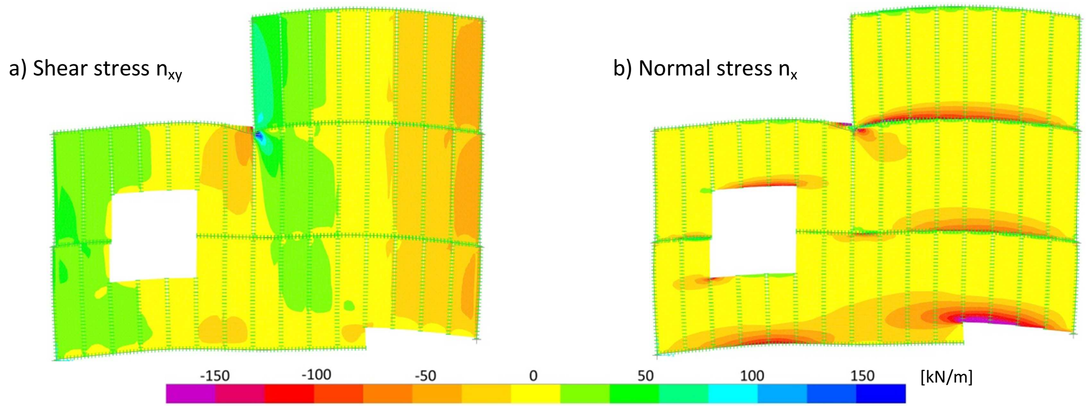

Figure 6: Stress distributions of an irregular diaphragm with chord and collector beams with a re-entrant corner and an opening; a) n_{xy} shear stresses and b) n_x normal stresses

3.4 Rigid versus flexible diaphragm design

Equations for deformations of LTF shear walls and diaphragms are available in most codes (or commentaries) so that the definition of flexible diaphragm as stated in Section 2.3.1 can be checked. For solid timber diaphragms little guidance on deformations or in-plane stiffness is given. Most publications regarding CLT structures assume that the diaphragms are rigid [1, 45-47]. Other researchers have however shown that the rigid-floor assumption is not always guaranteed since it depends on the stiffness of the connection between the single panels [55] and on the relative stiffness of the diaphragm and the LLRS [52]. In general the diaphragm in-plane stiffness can be evaluated as a combination in series of the stiffness contribution from the floor "plate" consisting of panel units and their connections and the contribution of the connectors between the floor plate and the LLRS [56].

Although finite element modelling of diaphragm with solid panels is feasible, hand based evaluation of the diaphragm deflections are still missing. Canadian guidelines [1, 57] suggest an envelope be established by applying both the flexible and rigid diaphragm assumptions to determine both upper and lower bound force distributions into the vertical LLRS. This approach makes theoretically sure that wall-to-slab connections are designed for the highest possible force, but it is potentially dangerous because walls could be overdesigned, hence not yield and therefore attract higher seismic forces. Unforeseen mechanisms with premature failure of one or more shear walls might activate torsional effects in the floor diaphragms or change their support conditions.

3.5 Elastic versus plastic diaphragm design

Even for ductile building designs, the authors recommend that the floor diaphragms be designed to remain elastic, by designing the vertical LLRS as the ductile link. An over-strength factor related to the LLRS should be applied to the diaphragm demand. The recommendation for elastic diaphragms is due to their essential role in carrying gravity and horizontal forces. Limited yielding might be allowed in confined areas of the diaphragm with stress concentrations, provided that the connections have some guaranteed ductility.

In spite all this, in order to adhere to the basic requirement of collapse prevention under higher-than-expected seismic loading, the diaphragm as a whole should have sufficient ductility and ultimate deformation capacity, either through the non-linear behaviour of the connections to the LLRS or between panels. Similarly, when special buildings of high importance level are designed for a 'maximum considered earthquake' (MCE, 2500 years return period), given the level of design forces involved, some diaphragm yielding can be allowed, with designated ductile connections and prevention of brittle failures.

3.6 Determination of diaphragm forces and higher mode effects

With the exception of ASCE 7-10 [21] (see Table 1), no codes explicitly address the calculation of seismic diaphragm forces. Several researchers [9-13] have shown that floor accelerations can be significantly higher than those obtained from simplified methods like equivalent static or modal analysis. Simplified methods are normally able to predict the seismic forces acting on the LLRS, but neglect the fact that acceleration peaks can lead to much higher forces on a diaphragm and its connections. Flexible diaphragms may further enhance this increase in floor accelerations [9, 10]. Higher mode effects and the over-strength of the vertical LLRS need to be considered in order to guarantee the elastic behaviour of diaphragms. The applicability to post-tensioned Pres-Lam frames and walls [58, 59] of design methods suggested by Bull [12] or Priestley et al. [60] is currently being researched. Whatever method is chosen, over-strength values for timber LLRS are still missing in design codes as pointed out by Follesa et al. [47].

3.7 Connections between diaphragm panels

The flexibility of solid timber diaphragms is mainly influenced by the stiffness of the connection between the single panels. Depending on the type and location of fasteners, the stiffness of these connections might vary along and perpendicular to the panel edges.

The deep beam action of diaphragms not only requires the establishment and transfer of shear forces, but also of tension and compression forces along the edges perpendicular to the load direction. Chord beams are therefore essential for LTF diaphragms. Many CLT structures studied under seismic action are designed without chords [1, 45-47, 52, 55], so high tensile forces need to be transferred by the panel connections, leading to a different force distribution along the diaphragm panels as shown in Figures 5 and 7 b). Even in the presence of chord beams, connections will have to carry nominal tensile forces as shown in Figure 7 b), requiring careful design. For example the diaphragm simulation shown in Figures 5 provided a tensile force in the top connector of the central panels of 2 kN and 36 kN with and without chord beams respectively.

Figure 7: Force distribution in diaphragm panel connections with solid panel elements

3.8 Displacement incompatibilities

Careful design and detailing is essential to avoid damage from displacement incompatibilities within diaphragms or between diaphragms and the LLRS. This problem, which applies to all structures [12, 14, 61-63], has been investigated at the University of Canterbury for the low damage post-tensioned Pres-Lam system with post-tensioned frame, wall [64, 65] and core structures [66]. The rocking behaviour in Pres-Lam systems is not unique, as it also occurs at the base of CLT walls [67] or other timber walls with supplemental damping such as friction dampers [68]. Displacements can occur at beam-column connections in any ductile moment resisting timber frame structures [69].

Beam elongation in frame structures and uplift and rotation of walls as shown in Figure 8 can cause horizontal or vertical displacement incompatibilities in the diaphragms or their connections. Experience from concrete structures shows that frame elongation can result in the failure or 'tearing' of the connection between the floor diaphragm and the LLRS thus impairing the development of the fundamental load path for seismic resistance [12]. Rocking of walls tends to bend the floor slabs out-of-plane leading to floor damage and higher axial loads in the wall itself [61].

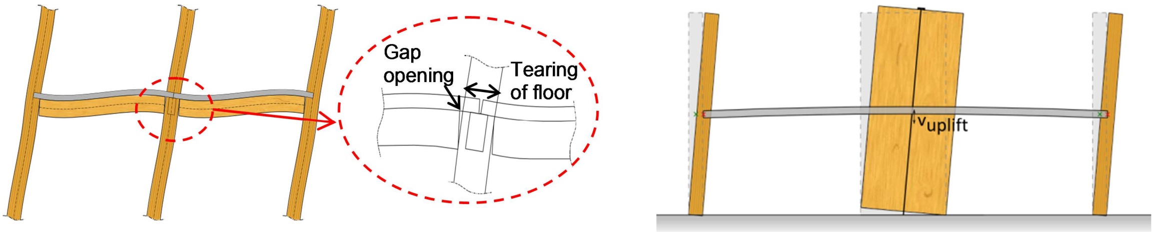

Figure 8: Floor displacement incompatibilities due to frame elongation (left) and wall uplift and rotation (right)

These displacement incompatibility issues need to be considered when detailing floor diaphragms and their connections, to guarantee the predicted behaviour of the structure under seismic actions. Experimental testing has shown that the flexibilities of timber members and steel fasteners can, in many cases, accommodate the required displacements without compromising the diaphragm behaviour [64].

4 Conclusions

The following conclusions can be drawn from the review of literature, code design provisions and research carried out by the authors:

General principles

- Diaphragms have an essential role in the lateral load resistance of buildings and special care should be taken in their design.
- Buildings which require ductility to reduce seismic loads must be designed using a hierarchy of strength (capacity design) to ensure that the ductility occurs only in the intended locations in the Lateral Load Resisting System (LLRS).
- All diaphragms should be designed to remain elastic under seismic loading, by applying an over-strength factor (related to the LLRS) to the diaphragm demand as a whole. All designs should provide ductile behaviour for higher-than-expected forces or displacements under extreme loading conditions.
- Diaphragm flexibility (including connections to the LLRS) can change the load distribution to the LLRS and the dynamic behaviour of the whole building.

Design of timber diaphragms

- Timber floor diaphragms must be designed to resist all anticipated forces, including inertial forces and any transfer forces from other parts of the structure, with special attention to forces around openings and at re-entrant corners.
- The general design principles for traditional plywood sheathed diaphragms can be applied to solid wood floor diaphragms, for regular floor geometries.
- The design and detailing of connections between the diaphragm and the LLRS must take into account any possible displacement incompatibilities.
- Dynamic amplification from higher mode effects needs to be considered for diaphragms.

Timber Design Codes

- Different international codes have widely differing provisions for the design of timber diaphragms, so more international collaboration is strongly recommended.

- The same applies to all aspects of seismic design for timber structures.
- All codes should have a clear statement of their seismic design philosophy for timber buildings, incorporating capacity design of the LLRS and over-strength factors to ensure that the diaphragms and their connections remain elastic under seismic loading, with some ductility available for extreme loading conditions.
- All codes should have requirements for clearly defined load paths in diaphragms and their connections to the LLRS, and provision for assessing and preventing damage from any displacement incompatibilities during extreme loading events.

Future Research needs

- Derivation of dynamic amplification factors for tall timber structures with and without flexible diaphragms.
- Strength and stiffness evaluation for diaphragms built with solid timber panels.
- Determination of over-strength factors for timber building systems and fasteners.
- Evaluation of alternative post-yielding mechanisms and solutions to achieve ductile behaviour and low-damage design.

References

[1] FPInnovations (2013). *Technical Guide for the Design and Construction of Tall Wood Buildings in Canada. 90% DRAFT.* E. Karacabeyli. Vancouver.

[2] O. M. Skidmore, LLP (2013). *Timber Tower Research Project*.

[3] Berg | C.F. Møller Architects (2013). *Wooden Skyscraper*. Retrieved 30th May, 2014, from http://www.cfmoller.com/r/Wooden-Skyscraper-i13265.html.

[4] mgb ARCHITECTURE + DESIGN, Equilibrium Consulting, LMDG Ltd and BTY Group (2012). *THE CASE FOR Tall Wood BUILDINGS - How Mass Timber Offers a Safe, Economical, and Environmentally Friendly Alternative for Tall Building Structures*.

[5] J. W. G. Van De Kuilen, A. Ceccotti, Z. Xia and M. He (2011). *Very tall wooden buildings with Cross Laminated Timber*. Procedia Engineering 14: 1621-1628.

[6] A. Waugh, M. Wells and M. Lindegar (2010). *Tall Timber Buildings: Application of Solid Timber Constructions in Multi-Storey Buildings*. International Convention of Society of Wood Science and Technology and United Nations Economic Commission for Europe - Timber Committee. Geneva, Switzerland.

[7] CEIArchitecture (2011). *40-Storey Wood Office Tower*. Retrieved 30th May, 2014, from http://www.ceiarchitecture.com/project/naiop-design-competition-2012.

[8] The Norwegian Barents Secretariat (2009). *Barents House*. Retrieved 30th May, 2014, from http://www.barents.no/barents-house.4607296-139566.html.

[9] R. B. Fleischman, K. T. Farrow and K. Eastman (2002). *Seismic Performance of Perimeter Lateral-System Structures with Highly Flexible Diaphragms*. Earthquake Spectra 18(2): 251-286.

[10] H. J. Lee, M. A. Aschheim and D. Kuchma (2007). *Interstory drift estimates for low-rise flexible diaphragm structures*. Engineering Structures 29(7): 1375-1397.

[11] S. D. Nakaki (2000). *Design guidelines for precast and cast-in-place concrete diaphragms*, Earthquake Engineering Research Institute.

[12] D. K. Bull (2004). *Understanding the complexities of designing diaphragms in buildings for earthquakes*. Bulletin of the New Zealand Society for Earthquake Engineering 37(2): 70-88.

[13] M. E. Rodriguez, J. I. Restrepo and A. J. Carr (2002). *Earthquake-induced floor horizontal accelerations in buildings*. Earthquake Engineering & Structural Dynamics 31(3): 693-718.

[14] fib (2003). *Seismic design of precast concrete building structures: state-of-art report*. Lausanne, Switzerland, Fédération internationale du béton, Bulletin n. 23 (Chairmen R. Park, F. Watanabe).

[15] R. Fenwick, D. K. Bull and D. Gardiner (2010). *Assessment of hollow-core floors for seismic performance*. Research Report, Civil and Natural Resources Engineering. University of Canterbury.

[16] J. Hollings (1968). *Reinforced concrete seismic design.* Bulletin of the New Zealand Nation Society for Earthquake Engineering 2(3): 217-250.

[17] T. Paulay and R. Park (1975). *Reinforced concrete structures: R. Park and T. Paulay*. New York, Wiley.

[18] R. Brunner, P. Jung, et al. (2010). *Erdbebengerechtes Entwerfen und Konstruieren von mehrgeschossigen Holzbauten ("Seismic design of multistorey timber buildings")*. Zürich, Switzerland, Lignum, Holzwirtschaft Schweiz.

[19] European Committee for Standardization (2004). *EN 1998-1:2004/AC:2009 Eurocode 8: Design of structures for earthquake resistance.* Part 1: General rules, seismic actions and rules for buildings.

[20] European Committee for Standardization (2008). *EN 1995-1-1:2004/A1:2008 Eurocode 5: Design of timber structures*. Part 1-1: General - Common rules and rules for buildings.

[21] American Society of Civil Engineers (2010). *Minimum design loads for buildings and other structures*. Reston, Va, American Society of Civil Engineers.

[22] AF&PA American Wood Council (2008). *ASD&LRFD. Wind & Seismic. Special Design Provisions for wind and seismic*. ANSI/AF&PA SDPWS-2008. Washington DC, USA.

[23] Standards Council of Canada (2009). *Engineering design in wood*. O86-09. Ottawa, Canada.

[24] Standards New Zealand (1993). *Timber Structures*. NZS 3603:1993. New Zealand.

[25] Standards New Zealand (2004a). *NZS 1170.5 - Structural Design Actions Part 5: Earthquake Actions - New Zealand*. Wellington, New Zealand.

[26] Canadian Commission of Building and Fire Codes (2010). *User's guide - NBC 2010 - Structural Commentaries (Part 4 of Division B)*. National Research Council of Canada. Ottawa, Canada.

[27] SIA Swiss Society of Engineers and Architects (2003). *SIA 265:2003 Timber Structures*. Zurich, Switzerland.

[28] Consiglio Superiore dei Lavori Pubblici (2008). *Norme tecniche per le costruzioni ("Design code for structures")*. DM 14 gennaio 2008. Rome, Italy.

[29] Canadian Commission of Building and Fire Codes (2010). *National Building Code of Canada*. National Research Council of Canada. Ottawa, Canada.

[30] BRANZ (1999). *Evaluation and Test Method EM1: Structural Joints - Strength and Stiffness Evaluation*. Porirua City, New Zealand.

[31] M. Popovski and E. Karacabeyli (2005). *Framework for lateral load design provisions for engineered wood structures in Canada*. CIB W18. Karlsruhe, Germany.

[32] A. Jorissen and M. Fragiacomo (2011). *General notes on ductility in timber structures*. Engineering Structures 33(11): 2987-2997.

[33] I. Sustersic and B. Dujic (2011). *Influence of connection properties on the ductility and seismic resistance of multi-storey cross-lam buildings*. CIB W18. Alghero, Italy.

[34] F. Brühl, J. Schänzlin and U. Kuhlmann (2014). *Ductility in Timber Structures: Investigations on Over-Strength Factors*. Materials and Joints in Timber Structures. S. Aicher, H. W. Reinhardt and H. Garrecht, Springer Netherlands. 9: 181-190.

[35] M. Schick, T. Vogt and W. Seim (2013). *Connections and anchoring for wall and slab elements in seismic design*. CIB W18. Vancouver, Canada.

[36] SIA Swiss Society of Engineers and Architects (2003). *SIA 261:2003 Actions on Structures*. Zurich, Switzerland.

[37] International Code Council (2011). *2012 International Building Code*, International Code Council.

[38] DIN Deutsches Institut für Normung (2010). *DIN EN 1995-1-1:NA:2010 National Annex - Nationally determined parameters - Eurocode 5: Design of timber structures*. Part 1-1: General - Common rules and rules for buildings. Berlin.

[39] M. H. Kessel (2004). *Erläuterungen zur DIN 1052:2004-08. Entwurf, Berechnung und Bemessung von Holzbauwerken ("Commentary to the DIN 1052:2004-08. Design of Timber Structures")*, DGfH Innovations- und Service GmbH.

[40] J. A. Dean, P. J. Moss and W. Stewart (1984). *A design procedure for rectangular openings in shearwalls and diaphragms*, Pacific Timber Engineering Conference.

[41] J. A. Dean (1982). *Sheated Construction*. Timber Engineering Seminar. University of Canterbury.

[42] P. C. Smith, D. J. Dowrick and J. A. Dean (1986). *Horizontal timber diaphragms for wind and earthquake resistance*. Bulletin of the New Zealand Society for Earthquake Engineering 19(2): 135-142.

[43] M. H. Kessel and T. Schönhoff (2001). *Entwicklung eines Nachweisverfahrens für Scheiben auf der Grundlage von Eurocode 5 und DIN 1052 neu ("Development of a design methodology for diaphragms on the base of Eurocode 5 and DIN1052:2008")*. Fraunhofer IRB Verlag, Technical University Braunschweig.

[44] R. T. Malone and R. W. Rice (2012). *The Analysis of Irregular Shaped Structures - Diaphragms and Shear Walls*, McGraw Hill.

[45] A. Ceccotti (2008). *New technologies for construction of medium-rise buildings in seismic regions: The XLAM case*. Structural Engineering International: Journal of the International Association for Bridge and Structural Engineering (IABSE) 18(2): 156-165.

[46] B. Dujic, K. Strus, R. Zarnic and A. Ceccotti (2010). *Prediction of dynamic response af a 7-storey massive XLam wooden building tested on a shaking table*. World Conference on Timber Engineering. Riva del Garda, Italy.

[47] M. Follesa, I. P. Christovasilis, et al. (2013). *Seismic design of multi-storey cross laminated timber buildings according to Eurocode 8*. Ingegneria Sismica (4).

[48] M. Wallner-Novak, J. Koppelhuber and K. Pock (2013). *Brettsperrholz Bemessung - Grundlagen für Statik und Konstruktion nach Eurocode ("Cross Laminated Timber Design - Construction and Design according to Eurocode")*. Vienna, Austria, proHolz Austria.

[49] H. G. L. Prion (2003). *Shear Walls and Diaphragms*. Timber engineering. S. Thelandersson and H. J. Larsen. New York, J. Wiley: 383-408.

[50] D. Countryman (1952). *Lateral tests on plywood sheathed diaphragms. Laboratory Report No. 63*. Douglas Fir Plywood Association. Tacoma, WA.

[51] ATC (1981). *Guidelines for the design of horizontal wood diaphragms*. Berkeley, California, Applied Technology Council.

[52] S. Ashtari (2009). *In-plane Stiffness of Cross-laminated Timber Floors*. Civil Engineering. Vancouver), The University of British Columbia.

[53] CSI Computers and Structures Inc. (2004). *SAP2000: Static and Dynamic Finite Analysis of Structures*. Berkeley, CA, USA.

[54] A. P. Hrennikoff (1941). *Solution of Problems of Elasticity by the Framework Method*. Journal of Applied Mechanics 8: A169-175.

[55] M. Fragiacomo, B. Dujic and I. Sustersic (2011). *Elastic and ductile design of multi-storey crosslam massive wooden buildings under seismic actions*. Engineering Structures 33(11): 3043-3053.

[56] A. Brignola (2010). *Evaluation and Control of the In-Plane Stiffness of Timber Floors for the Performance-Based Retrofit of URM Buildings*. Bulletin of the New Zealand Society for Earthquake Engineering 42(3): 204.

[57] S. Gagnon, C. Pirvu and FPinnovations (2011). *CLT handbook: cross-laminated timber*. Québec, FPInnovations.

[58] A. Palermo, S. Pampanin, A. Buchanan and M. Newcombe (2005). *Seismic Design of Multi-Storey Buildings using Laminated Veneer Lumber (LVL)*. New Zealand Society for Earthquake Engineering Conference. Wairakei, New Zealand.

[59] Structural Timber Innovation Company (STIC) (2013). *Design Guide Australia and New Zealand - Post-Tensioned Timber Buildings*. Christchurch, New Zealand.

[60] M. J. N. Priestley, G. M. Calvi and M. J. Kowalsky (2007). *Displacement-Based Seismic Design of Structures*, IUSS Press.

[61] R. S. Henry, J. M. Ingham and S. Sritharan (2012). *Wall-to-floor interaction in concrete buildings with rocking wall systems*. New Zealand Society of Earthquake Engineering Conference. Christchurch.

[62] D. A. Latham, A. M. Reay and S. Pampanin (2013). *Kilmore Street Medical Centre: Application of a post-tensioned steel rocking system*. Steel Innovations Conference. Christchurch, New Zealand.

[63] M. R. Eatherton (2010). *Large-scale cyclic and hybrid simulation testing and development of a controlled-rocking steel building system with replaceable fuses*. Urbana, Illinois, University of Illinois at Urbana-Champaign.

[64] D. Moroder, F. Sarti, et al. (2014). *Seismic design of floor diaphragms in post-tensioned timber buildings*. WCTE. Quebec, Canada.

[65] D. Moroder, T. Smith, et al. (2014). *Experimental behaviour of diaphragms in post-tensioned timber frame buildings*. Second European Conference on Earthquake Engineering and Seismology. Istanbul, Turkey.

[66] A. Dunbar, D. Moroder, S. Pampanin and A. H. Buchanan (2014). *Timber Core-Walls for Lateral Load Resistance of Multi-Storey Timber Buildings*. WCTE. Quebec, Canada.

[67] I. Sustersic, B. Dujic and M. Fragiacomo (2014). *Influence of the Connection Modelling on the Seismic Behaviour of Crosslam Timber Buildings*. Materials and Joints in Timber Structures. S. Aicher, H. W. Reinhardt and H. Garrecht, Springer Netherlands. 9: 677-687.

[68] W. Y. Loo, C. Kun, P. Quenneville and N. Chouw (2014). *Experimental testing of a rocking timber shear wall with slip-friction connectors*. Earthquake Engineering & Structural Dynamics.

[69] D. Wrzesniak, C. Amadio, G. Rinaldin and M. Fragiacomo (2013). *Non-linear cyclic modelling of moment-resisting timber frames*. ANIDIS. Padua, Italy.

INTER

International Network on Timber Engineering Research

FIRE DESIGN OF GLUED-LAMINATED TIMBER BEAMS WITH REGARD TO THE ADHESIVE PERFORMANCE USING THE REDUCED CROSS-SECTION METHOD

M Klippel
ETH Zürich, Institute of Structural Engineering IBK, Zürich
SWITZERLAND

J Schmid
SP Wood Technology, Stockholm
SWEDEN

A Frangi
G Fink
ETH Zürich, Institute of Structural Engineering IBK, Zürich

SWITZERLAND

Presented by J Schmid

BJ Yeh asked how to define adhesive quality system. J Schmid answered that there is no adhesive classification system that focuses on fire performance. This paper showed non-structural adhesives go below 0.3. Adhesive industry would like to see a certification process but this is not available. BJ Yeh commented that a heat durability standard has been available in N. America for 7 years requiring adhesives to be qualified for heat durability to eliminate low performance adhesives. This is also in the ISO standard.

W Seim asked how to define the strength at 100 C. J Schmid responded that KΘ can't be established from fire tests. This can be established only from backward calculations of fire test data of joints – lap shear tests.

K Ranasinghe asked about the glue line. J Schmid responded that since the glue line deals with shear strength, it is a different issue.

A Buchanan discussed the reduced cross section method and commented that in this paper the zero strength layer varied from 3 mm to 22 mm is a concern. He received confirmation from J Schmid that the zero strength layer depended on sectional size and the number sides exposed. A Buchanan stated that there was overlapping response between good and bad adhesives; therefore, the lack of influence of adhesive is not expected. J Schmid responded that the work was compared to fire test results using mean values and agreed that more details are needed.

S Svensson asked about the conductivity of wood and adhesive. J Schmid stated that the same conductivity was considered for wood and adhesive. S Svensson stated that glue can lead to heat transfer which can affect the results.

F Lam asked whether vertical or horizontal finger joints were used and whether there would be an influence in terms of heat transfer of the glue. J Schmid stated horizontal finger joints were used and that he is not sure whether there is a finger joint orientation effect.

Fire design of glued-laminated timber beams with regard to the adhesive performance using the Reduced Cross-Section Method

Michael Klippel*

Joachim Schmid**

Andrea Frangi*

Gerhard Fink*

* ETH Zürich, Institute of Structural Engineering IBK, Zürich, Switzerland

** SP Wood Technology, Stockholm, Sweden

Keywords: Fire design model, Reduced Cross-Section Method, Adhesive, Finger joint, Glued-laminated timber beams, Numerical analysis, Probabilistic investigation

Abstract

For timber structures with requirements in fire resistance, design models usually take into account the loss in cross-section due to charring and the temperature-dependent reduction in strength and stiffness of the residual cross-section. In EN 1995-1-2, for bonded timber elements like glued-laminated timber beams it is assumed that structural adhesives used do not influence the fire resistance of structural timber members. However, further specifications of adequate adhesive requirements is missing.

To investigate the influence of different adhesives a comprehensive research project ("Fire safety of bonded structural timber elements") was recently performed at the ETH Zurich: Within the first steps of this project, fire resistance tests on finger-jointed wooden lamellas were conducted under tensile loading and ISO-fire exposure. The results of the fire tests were used to determine temperature-dependent strength relationships for finger-jointed connections, similar to those for timber given in EN 1995-1-2. In the next step, a finite element (FE) model was developed to investigate the influence of different adhesives on the fire resistance of glued-laminated timber beams. The model considers both the variable strength and stiffness of timber boards and finger joint connections. In the last step, the results from the extensive FE simulations were used and evaluated in terms of the *Reduced Cross-Section Method* given in EN 1995-1-2.

As a result of this investigation, a modification of the zero-strength layer thickness of 7 mm currently used in EN 1995-1-2 should be considered for glued-laminated timber loaded in bending in a future release of EN 1995-1-2. However, an increase of the zero-strength layer considering the finger joint strength depending on the approved structural adhesive is not needed.

1 Introduction

Fire reduces the cross-section as well as the stiffness and strength of the heated timber beyond the char layer. The *Reduced Cross-Section Method*, being a popular fire design method for structural timber products, according to EN 1995-1-2 [1] considers the strength and stiffness reduction of the residual cross-section by adding an additional depth d_0 (called zero-strength layer) to the charred layer $d_{char,n}$ (see Figure 1). The effective cross-section can be calculated by reducing the residual cross-section at a specific time of fire exposure by the zero-strength layer, which is assumed to have no strength nor stiffness. EN 1995-1-2 [1] gives a constant value of 7 mm for the zero-strength layer, independent on the application. However, it has previously been shown on the basis of advanced calculation methods [2] as well as based on the analysis of numerous fire tests [3] that the use of a constant value of 7 mm might lead in some application to a non-conservative design.

For bonded timber elements, like glued-laminated timber beams (glulam), EN 1995-1-2 assumes that the adhesive does not influence the fire resistance and thus, the *Reduced Cross-Section Method* does not include any consideration of the adhesive. However, a possible influence of the adhesive on the load-bearing behaviour of glulam beams in fire was recently shown [4]. To assess the fire performance of finger-jointed lamellas glued with various adhesives, an extensive testing series of 49 tensile tests under standard ISO-fire exposure was recently performed [5, 6]. In this campaign, 12 different structural adhesives, which are approved according to current European standards [7, 8, 9] for the use in structural timber engineering (1C PUR, PRF, MUF, EPI) and non-structural adhesives of common types (1C PUR, MUF, UF, PVAc) were tested in fire tests on finger-jointed connections loaded in tension (see section 2). The tests on finger-jointed timber lamellas were used to determine the "effective" temperature-dependent tensile strength reduction of finger-jointed lamellas depending on the adhesive, as already given for timber in EN 1995-1-2, as simplified bi-linear functions with a breakpoint at 100°C (see section 3.1). The temperature-dependent strength reduction does not reflect the "real" material properties at elevated temperatures but can directly be used as material input properties for a finite element thermal-mechanical analysis of structural finger-jointed timber members. Section 3.2 of this paper presents a 3D finite element model of glulam beams implemented in Abaqus considering the natural variability of the timber strength and stiffness on the bases of [10]. The model allows for performing probabilistic investigations on the fire resistance of glulam beams with different strength classes (GL24h and GL36h), a further extension to other grades is possible. With this model, the influence of different temperature-dependent strength approaches of finger joints on the fire resistance of glulam beams was investigated. Concluding, the zero-strength layer was determined depending on the adhesive strength in the finger joint (see section 3.3) for glulam beams in bending.

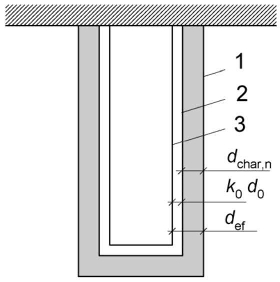

Key:
1 Initial surface of member
2 Border of residual cross-section
3 Border of effective cross-section

Figure 1. Definition of residual cross-section and effective cross-section.

2 Fire tests

Fire tests were performed on the model-scale horizontal furnace with dimensions of 1.0 × 0.8 m using fire exposure according to ISO 834 [11] at the Swiss Federal Laboratories for Materials Science and Technology (Empa) in Dubendorf/ Switzerland. The fire behaviour of finger-jointed timber boards was studied in a first series investigating three types of adhesives [5]. This investigation was recently extended by further tests on the same specimen dimensions [6]. The results of totally 49 fire tests using 12 different adhesives in the finger joints constitute an adequate background to evaluate the influence of adhesives on the fire resistance of finger-jointed timber boards. Further, the specimens designed in this investigation should describe the real behaviour of finger joints in a fire situation relevant for glulam beams. Figure 2 shows the fire resistance of the specimens constantly loaded with 30% of the mean tensile strength obtained in normal temperature tests. Additionally, the four typical types of failure are given and illustrated. The specimens which showed a failure along the fingers show most likely an influence of the adhesive on the fire resistance. In the case of the other three failure types, the fire resistance was mainly limited by the tensile strength of timber and the adhesive still sustained enough strength.

A detailed description and the results of the fire tests as well as tests at normal temperature are presented in the testing report [6]. The fire tests form the basis for the numerical model to investigate the behaviour of finger-jointed timber lamellas and glulam beams exposed to fire, which is described in the following.

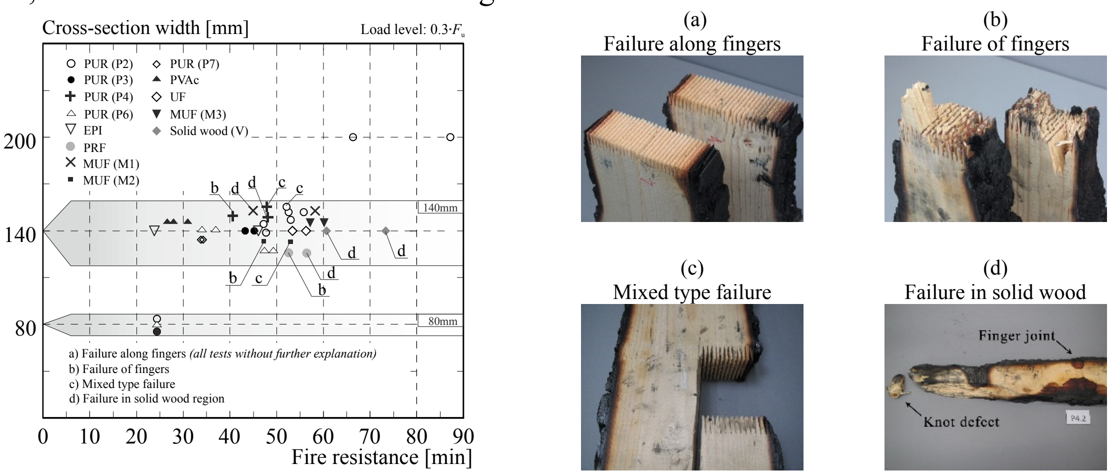

Figure 2. Fire resistance as a function of the cross-section width (80, 140 and 200 mm) depending on the adhesive in the finger joint. Additionally, the types of failure observed in the fire tests are given.

3 Numerical simulations

3.1 Numerical simulations on single finger-jointed lamellas

Non-linear three-dimensional Finite Element (FE) simulations were performed with Abaqus to study the load-bearing behaviour of finger-jointed timber lamellas exposed to standard ISO fire. The thermal-mechanical analyses use the test data obtained in the fire tests introduced above. The reduction of strength with increasing temperature of finger-jointed specimens were derived, in accordance to the temperature-dependent reduction of the timber strength given in [1], also as a simplified bi-linear approach with a breakpoint at 100°C. Figure 3 shows the assembly of the finite element model as well as the description of the material model used. The “Concrete Damaged Plasticity” (CDP)-model provided by the Abaqus material library was used to describe the linear elastic brittle behaviour under tensile loading. The same constitutive material property was later used for the FE simulations of glulam beams. The CDP-model is able to model both the linear elastic brittle behaviour of timber in tension and the linear elastic-plastic behaviour under compression taking into account the reduction of temperature-dependent strength, see Figure 3 (right). The reduction of stiffness was defined according to [1] for timber in tension, since the CDP-model allows for using only one stiffness property and failure of the beam is assumed in the tension zone. The input parameters for the thermal analysis to simulate the temperature development inside the ISO-fire exposed timber cross-section were taken from [1].

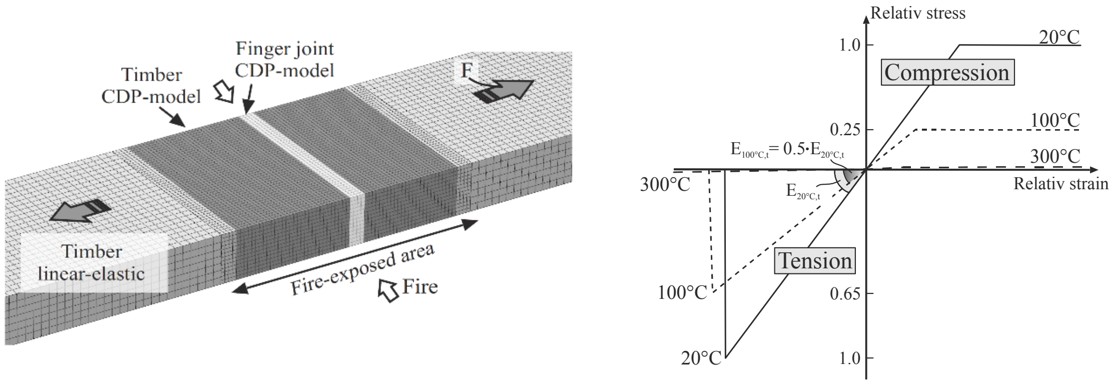

Figure 3. Model to determine the temperature-dependent strength reduction of finger-jointed specimens (40 × 140 mm^2). The middle part of the model was exposed to ISO-fire from the sides. As in the fire tests, a constant tensile load (10 N/mm^2) parallel to the grain is applied, until the fire resistance is reached (left); Modelling the mechanical properties of timber at elevated temperatures (right).

About 170 tensile tests on finger-jointed timber boards of structural size were performed at normal temperature [6, 12]. For all these reference tests, a mean tensile strength of $f_{t,j}$ = 35.5 N/mm^2 (COV = 0.20) was calculated. The load-bearing capacity at normal temperature was limited by the timber tensile strength. The tensile strength of finger-jointed specimens reached about 85% of the tensile strength of unjointed solid wood specimens (f_t = 42.9 N/mm^2). For the FE study on finger-jointed specimens, the mean tensile strength $f_{t,j}$ = 35.5 N/mm^2 at normal temperature was used. The reduction of strength with increasing temperature was modelled with a simplified bi-linear approach using the reduction factor $k_{\Theta=100°C}$ to characterize the behaviour. A low relative strength at 100°C (e.g. $k_{\Theta=100°C}$ = 0.1) represents an adhesive more sensitive to the influence of temperature and vice versa.

The reduction factor $k_{\Theta=100°C}$ for finger-jointed specimens was determined, assuming the previously described bi-linear temperature-dependent strength approach. Therefore, the mean fire resistance of the tests with the same adhesive in the finger joint was used. Fire tests, in which an early failure occurred because of defects, were neglected. Further, the fire tests in which failure occurred in the finger joint due to exceeding the timber tensile strength (failure of the fibres, e.g. failure of the finger-joint root) were neglected in this evaluation, since the adhesive had still sufficient strength. In such a case, a value of $k_{\Theta=100°C}$ = 0.2 was calculated (see Figure 4, curve "for early timber failure"). Such low strength of the finger joint could occur independent on the adhesive in the finger joint. Thus, the failure reason occurring in the finger joint is classified into two groups:

1. Failure along the fingers, which shows most likely an influence of the adhesive and

2. Failure of the fingers due to exceeding the timber tensile strength.

The latter one usually leads to an earlier failure and the adhesives' fire resistance is higher than the reached value. The temperature-dependent strength approach for finger-jointed members loaded in tension is an "effective" approach similar to the work by König and Walleij [13], who determined the temperature-dependent relationships for timber given in EN 1995-1-2, and does not reflect the "real" material

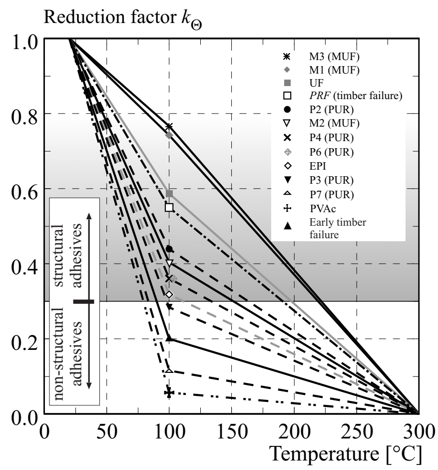

Figure 4. Bi-linear approach describing the residual tensile strength for finger-jointed lamellas depending on the adhesive.

properties. An advantage of this procedure is that complex effects, e.g. due to mass transport (e.g. vapour), are considered by the effective material properties. Thus, the values can directly be used as material input properties for a FE thermal-mechanical analysis of structural members. With respect to the effective material properties of adhesives it should be noticed that the PRF adhesive did not govern the fire resistance, because in both tests failure occurred due to exceedance of the timber's tensile strength. The approach in Figure 4 (right), represents, therefore, only a lower boundary of the strength reduction for PRF. The actual temperature-dependent strength approach lies above the given curve. For structural adhesives, which are approved according to current European standards, at least a value of $k_{\Theta=100°C} = 0.3$ was derived.

3.2 Numerical simulations on glued-laminated timber beams

After studying the load-bearing resistance of single finger-jointed timber boards, a FE-model of a full-scale beam was developed in Abaqus. This FE-model is capable of taking into account timber's variable material properties (see Figure 7, left) and finger joint properties depending on the adhesive. Glulam beams were modelled using the probabilistic material model developed by Fink [10], see example of a beam in Figure 56. The modelled glulam beams consisted of several boards and finger-jointed lamellas.

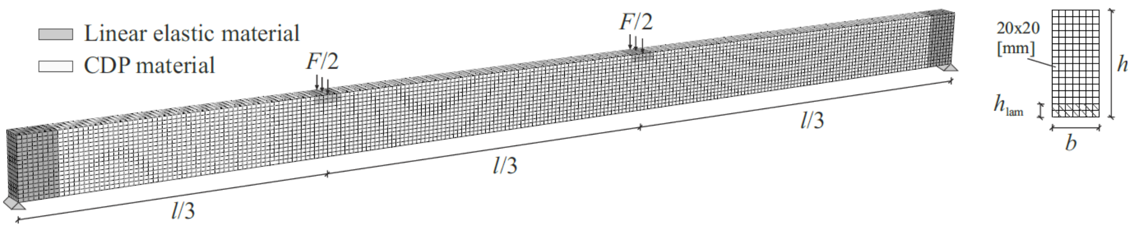

Figure 5. Finite element model set-up.

Each lamella was described with two elements in the height. This size was fine enough to provide accurate results with respect to both the determination of the bending strength at normal temperature and the determination of the fire resistance. Glulam beams with a height h = 320 mm and a span l = 5760 mm were modelled following the span to height relationship according to EN 408 [14] of $l = 18 \cdot h$. The beams width was b = 140 mm. At normal temperature, it is assumed that the bending strength of the beam is either limited by the tensile strength parallel to the grain of the lamellas in tension or of the finger joint connection. Failure occurs when the tensile strength is reached and the load cannot further be increased. The maximum applied load is then used to determine the bending strength of the beam. The FE model was first verified using tests performed by Fink et al. [15,20]. The bending strength and stiffness in the simulations had a good agreement with the experiments.

For the presented investigation, glulam beams with well-known material properties were simulated based on the probabilistic approach developed by Fink [10] (see also [21,22] for a detailed description). Figure 6 illustrates an example of a simulated glulam beam. The beam simulation was implemented in a Matlab script to generate the input files for the subsequent Abaqus simulations. In the final step, the output data from the FE simulations were automatically evaluated. Thereby, the stress in lengthwise direction of the beam for each element located in the tension zone was compared with the ultimate strength allocated to this element. When the ultimate strength of one element was reached, the location of this element was detected. At this stage, the load could not be increased, the ultimate bending strength was reached.

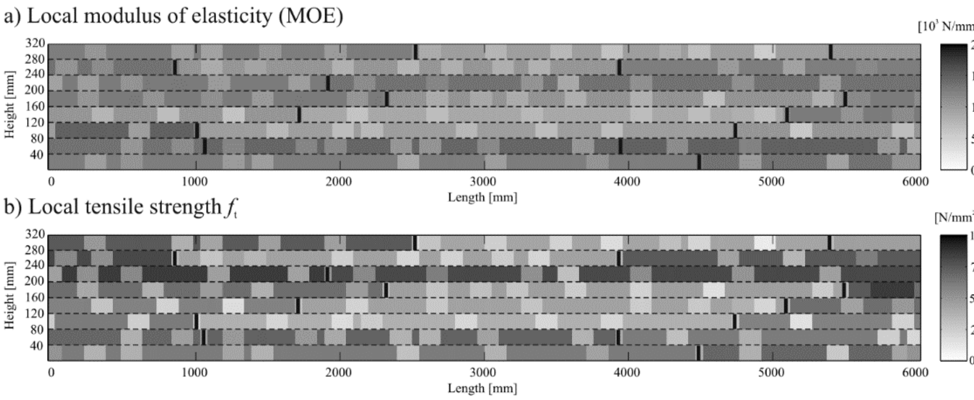

Figure 6. Example of local material properties (stiffness and strength) allocated to the elements of the FE model; the vertical black lines indicate the position of finger joints.

The influence on the fire resistance of glulam beams was studied for the following parameters:

- Timber strength class (GL24h and GL36h)
- Distance [m] between the finger joints: short(ened) boards: L~N(2.15, 0.50) and long boards L~N(4.30, 0.71) according to [16, 17]
- Temperature-dependent strength of finger joints, representing different adhesives in the finger joint: $k_{\Theta=100°C}$ = [0.1, 0.3, 0.6, 0.8]

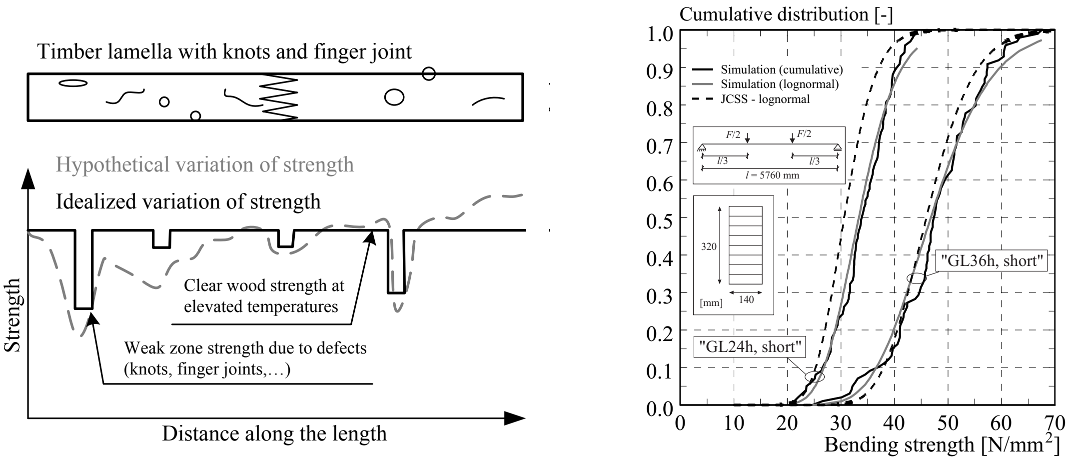

Figure 7. Description of variation of strength along the length of a timber lamella (left), Simulated cumulative distribution (n=100) of bending strength for strength grades classes GL24h and GL36h using short boards (right).

The tensile strength of a finger joint at normal temperature was assumed to be equivalent to the tensile strength of a knot cluster section with a tKAR-value of 0.2 [10]. For each type of glulam beam, one hundred simulations were performed with different material properties. Figure 7 (right) shows that the cumulative distribution of the bending strength of 100 simulations follows approximately the lognormal distribution proposed by the Joint Committee on Structural Safety (JCSS) [18]. This diagram shows the cumulative bending strength distribution of beam type “GL24h, short” and “GL36h, short”; whereas the name of the beam type is composed of the strength grade and the distance between the finger joint, which is equivalent to the board length (long and short(ened) boards).

About 1600 simulations were performed to investigate the influence of the adhesive used in a finger joint of a glulam beam on the fire resistance. The evaluation of the simulations contains the fire resistance and failure location of each beam as well as the type of failure [finger joint, clear wood, weak section (defined here as tKAR > 0.1)]. Among others, some important conclusions from the numerical simulations can be summarized as follows:

- In general, the fire resistance of glulam beams decreases with increasing sensitivity to elevated temperature of the finger joints, i.e. a lower value of $k_{\Theta=100°C}$, as illustrated in Figure 8 (left).
- The fire resistance of higher strength glulam beams is more sensitive to the temperature-dependent strength performance of finger joints than lower graded timber.
- For the finger joints glued with structural adhesives, the effective temperature-dependent strength at 100°C ($k_{\Theta=100°C}$) was determined to be in the range of 30% up to 60% of the initial strength at normal temperature, see Figure 4. In cases where the adhesive limits the fire resistance of the finger joint the following statement can be given: The fire resistance for those adhesives varied between 73% and 96% (for GL36h) in relation to the reference finger joint strength approach, which was defined to exhibit 80% ($k_{\Theta=100°C}$ = 0.8) of the initial strength at normal temperature. For GL24h beams, the relative fire resistance was between 86% and 98%. This is in line to fire tests performed in the past [4].

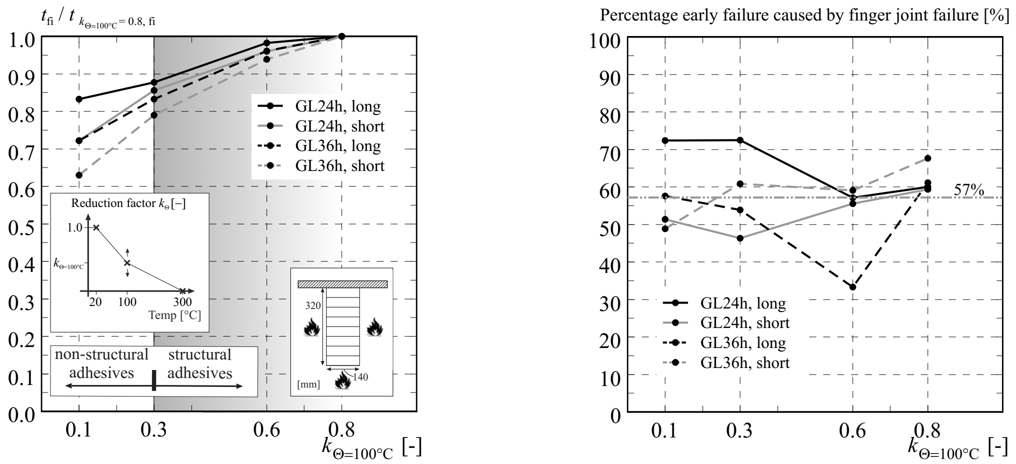

Figure 8. Relative fire resistance for glulam beams depending on the finger joint strength reduction (left); Percentage of finger joint failure (related to the observed number of finger joint failure) for the beams that reached a fire resistance below the mean fire resistance for each beam type (right).

Figure 8 (right) shows that a finger joint failure leads in about 57% of the cases to an early failure of the beam. Early failure occurs when the simulated beam reached a fire resistance below the mean fire resistance of each beam type. As a consequence, there is no clear tendency for all analysed beams that a failure in a finger joint leads to early failure of the glulam beam. Moreover, such early failure of glulam beams exposed to fire is attributed to failure of both finger joints and weak section failure and is independent of the finger joint strength and the strength grade. It can be concluded that taking into account the different failure types no significant difference of the fire resistance depending on the structural adhesive used can be found. Although differences between the finger joints made from different adhesives can be observed in many cases the fire resistance was governed by other properties.

3.3 Further evaluation of numerical simulations on glued-laminated timber beams with regard to the Reduced Cross-Section Method

The zero-strength layer d_0 was derived for the simulated glulam beams loaded in bending and fire exposed on three sides with the help of equation 1 [19]. The beams were loaded with 30% of the mean bending resistance of the 100 simulated beams of each beam type at normal temperature. The calculation is based on the notional charring rate β_n, which was determined for each individual beam at the time of failure.

Equation 1 explains the determination of the zero-strength layer thickness. The bending strength at normal temperature for each beam equals the ratio of load resistance at fire exposure $M_{R,fi}$ to the section modulus of the effective residual cross-section $W_{fi,ef}$. In other words, the thickness of the zero-strength layer was determined by comparing the depth of the unburned residual cross-section in fire (temperatures in the cross-section below 300°C) with the required depth of the effective residual cross-section to obtain the same load resistance.

$$f_m = \frac{M_{R,fi}}{W_{fi,ef}} = \frac{6 \cdot M_{R,fi}}{b_{fi} \cdot h_{fi}^{\ 2}} = \frac{6 \cdot M_{R,fi}}{\left(b - 2 \cdot (\beta_n \cdot t + d_0)\right) \cdot \left(h - (\beta_n \cdot t + d_0)\right)^2} \tag{1}$$

where

f_m	is the bending strength under normal temperature conditions
$M_{R,fi}$	is the load resistance at fire exposure
$W_{fi,ef}$	is the section modulus of the effective cross-section
b	is the original width of the cross-section
h	is the original height of the cross-section
t	is the fire resistance
β_n	is the notional charring rate

The thickness of the zero-strength layer was determined for each of the 1600 simulated beams. The mean value of the zero-strength layer is plotted in Figure 9, in which each point reflects the mean of 100 simulations. Based on these results, some important conclusions regarding the thickness of the zero-strength layer from the numerical simulations can be summarised as follows:

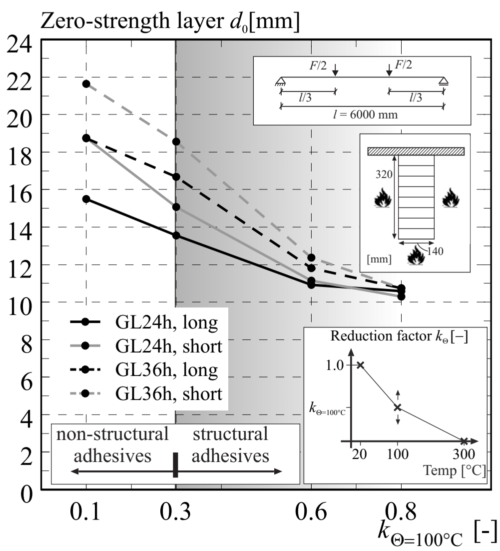

Figure 9. Zero-strength layer for glulam beams depending on the finger joint strength reduction.

- Based on this numerical evaluation and the results from the fire tests [6], a modification of the zero-strength layer thickness given in EN 1995-1-2 should be discussed for glulam loaded in bending in a future release of EN 1995-1-2. The lowest thickness of the zero-strength layer was determined independently of the strength grade to be about 10 mm. A greater value than 7 mm, as given in EN 1995-1-2, for timber members in bending is in accordance with earlier studies on similar cross-section dimensions as the present one [3].
- The zero-strength layer thickness of glulam beams loaded in bending was determined for two different strength class (GL24h and GL36h). In general, slightly higher mean d_0-values (about 2.5 mm) were determined for the higher strength class GL36h.

- The influence on the zero-strength layer of different temperature-dependent strength approaches for the finger joints was determined. The smallest mean value of the zero-strength layer was determined to $d_0 \approx 10.0$ mm (for $k_{\Theta=100°C} = 0.8$).
- The effect of finger joints glued with structural adhesives ($k_{\Theta=100°C} > 0.3$) in a fire exposed glulam beam is about the same as of knots and other defects (see Figure 4). Thus, an additional zero-strength layer to consider the effect of fire exposure on finger joints beside the effect on strength and stiffness of wood is not needed.

4 Conclusions

On the basis of model-scale fire tests with full-scale specimens the “effective” temperature-dependent reduction of strength for finger joints glued with different adhesives was determined with the help of finite element simulations. Further, probabilistic finite element simulations were performed on glulam beams, which were loaded in bending and exposed to standard ISO-fire. The *Reduced Cross-Section Method* was used to evaluate the results obtained from the numerical simulations. Particular interest was paid to the evaluation of the zero-strength layer thickness. The following main remarks can be concluded:

- The zero-strength layer thickness of glulam beams loaded in bending was determined for two different strength classes (GL24h and GL36h). In general, slightly higher mean d_0- values were determined for the higher strength classes.

- The influence on the zero-strength layer of different temperature-dependent strength approaches for the finger joints was determined. The smallest mean value of the zero-strength layer was determined to $d_0 \approx 10.0$ mm. As a consequence of this evaluation, an increase of the zero-strength layer thickness given in EN 1995-1-2 should be discussed for timber members loaded in bending in a future release of EN 1995-1-2. An increase taking into account the adhesive is not feasible and should be disregarded (Figure 4).

5 References

[1] EN 1995-1-2:2004, Eurocode 5: Design of timber structures – Part 1-2: General – Structural fire design. European Standard. European Committee for Standardization. Brussels. 2004.

[2] Klippel, M., Schmid, J., Frangi, A.: "The Reduced Cross-section Method for timber members subjected to compression, tension and bending in fire "; International Council for Research and Innovation in Building and Construction, Working Commission W18 – Timber Structures, Meeting 45; CIB-W18 Meeting 2012; Växjö, Sweden; CIB-W18/45-16-1; 2012.

[3] Schmid, J., Klippel, M., Just, A., Frangi, A.: "Review and analysis of fire resistance tests of timber members in bending, tension and compression with respect to the Reduced Cross-Section Method"; *Fire safety journal*; 68 (0); 81-99; 2014.

[4] König, J., Norén, J., Sterley, M.: "Effect of adhesives on finger joint performance in fire"; *Proceedings of 41th CIB-W18 Meeting*; St. Andrews, Canada; 2008.

[5] Klippel, M., Frangi, A., Hugi, E.: "Experimental Analysis on the Fire Behavior of Finger-Jointed Timber Members"; *ASCE Journal of Structural Engineering*; 140 (3); 2014.

[6] Klippel, M., Frangi, A.: "Fire tests on finger-jointed timber boards"; Institute of Structural Engineering (IBK), ETH Zürich; No 354; 2014.

[7] EN 301: "Adhesives - Phenolic and aminoplastic - For load-bearing timber structures - Classification and performance requirements"; 2013.

[8] EN 15425: "Adhesives - One component polyurethane for load bearing timber structures - Classification and performance requirements"; EN 301 CEN/TC 193; 2008.

[9] EN 16254: "Adhesives - Emulsion polymerized isocyanate (EPI) for load-bearing timber structures - Classification and performance requirements"; EN 16254; CEN/TC 193; 2013.
[10] Fink, G.: Influence of varying material properties on the load-bearing capacity of glued laminated timber; PhD thesis, ETH No. 21746; ETH Zurich, Switzerland, 2014.
[11] ISO 834: Fire-Resistance Tests - Elements of Building Construction - Part 1: General Requirements International Organisation for Standardisation. 1999.
[12] Frangi, A., Bertocchi, M., Clauss, S., Niemz, P.: "Mechanical behaviour of finger joints at elevated temperatures"; *Wood Science and Technology*; 46 (5); 793-812; 2012.
[13] König, J., Walleij, L.: "One-Dimensional Charring of Timber Exposed to Standard and Parametric Fires in Initially Unprotected and Postprotection Situations"; Trätek, Report I 9908029; SP Technical Research Institute of Sweden, Wood Technology; Stockholm, Sweden; 1999.
[14] EN 408: "Timber structures – Structural timber and glued laminated timber – Determination of some physical and mechanical properties"; Brussels, Belgium 2010.
[15] Fink, G., Köhler, J., Frangi, A.: "Bending tests on glued laminated timber beams with well-known material properties: Test report"; IBK Bericht Nr. 350; vdf Hochschul-Verlag an der ETH Zürich; Zürich; 156; 2013.
[16] Larsen, H.J.: "Strength of Finger Joints"; Otaniemi; Proceedings of 13th CIB-W18 Meeting; 1980.
[17] Ehlbeck, J., Heimeshoff, B.: Biegefestigkeit von Brettschichtholz in Abhängigkeit von Rohdichte, Elastizitätsmodul, Ästigkeit und Keilzinkung der Lamellen, der Lage der Keilzinkung sowie von der Trägerhöhe: Teil A: Karlsruher Untersuchungen, Teil B: Münchner Untersuchungen; Fraunhofer IRB Verlag, 1987.
[18] JCSS: "Probabilistic Model Code"; Joint Committee on Structural Safety; www.jcss.byg.dtu.dk; 2007.
[19] Schmid, J., Just, A., Klippel, M., Fragiacomo, M.: "The Reduced Cross-Section Method for evaluation of the fire resistance of timber members - Discussion and determination of the zero-strength layer"; *Fire Technology*; 2014.
[20] Fink, G., Frangi, A. & Kohler: "Bending tests on GLT beams having well-known local material properties", accepted for publication in Materials and Structures, 2014
[21] Fink, G. & Kohler, J. (submitted 2014). Probabilistic modelling of the tensile related material properties of timber boards and finger joint connections, Submitted to European Journal of Wood and Wood Products.
[22] Fink, G. & Kohler, J. (2014). Model for the prediction of the tensile strength and tensile stiffness of knot clusters within structural timber, European Journal of Wood and Wood Products, 72 (3), pp 331-341.

6 INTER Notes, Bath, United Kingdom 2014

Critical Discussion on Properties of Beech LVL **- C Sandhaas, M Frese**

Withdrawal Strength Dependency on Timber Conditioning **- J Munch-Andersen**

Execution of Timber Structures **- K Nore, T Toratti, J Munch-Andersen, J Schmid, A Just**

Cross laminated Timber Made of Regional Wood from Shizuoka Area -
Part 1: Project Outlines and Mechanical Properties of CLT **- K Kobayashi, M Yasumura**

Cross Laminated Timber Made of Regional Wood from Shizuoka Area -
Part 2: Seismic Performance of CLT Structures **- M Yasumura, K Kobayashi, M Okabe**

Modelling the Bending Strength of Glued Laminated Timber using Machine-Grading Indicators **- G Fink, A Frangi, J Köhler**

Critical discussion on properties of beech LVL

Carmen Sandhaas, Matthias Frese
Karlsruhe Institute of Technology (KIT), Germany

Keywords: **engineered wood products, laminated veneer lumber, mechanical properties, stability**

1 Introduction

Since September 2013, a technical approval for laminated veneer lumber (LVL) made of beech is available where two different products are regulated, LVL with all veneers oriented in one direction (LVL-L) and LVL with some veneers oriented transversely to the main direction (LVL-C) [1]. Characteristic material properties and design rules for e.g. joints are given which allow structural engineers to use these two products LVL-L and LVL-C in timber structures. In December 2013, a further technical approval for glulam made of beech LVL-L without finger joints was issued [2].

Independently from flatwise or edgewise bending of the material[i], beech LVL has exceptionally high tension strength values parallel-to-grain in comparison to other wood products. However, the MoE and the compression strength parallel-to-grain are not increased accordingly. Consequently, in bending members, the deflections can get comparatively high and the compression zone will be stressed beyond the elastic limit before the bending capacity of the member is reached.

During bending tests on LVL-L beams with a cross section of 95x600 mm^2 and a length of 12 m, stability problems occurred that could not be resolved without a continuous lateral support of the compression zone with hollow steel sections. These problems gave the impetus for this note which discusses chances, but also issues related to the exceptional mechanical properties of novel wood products such as beech LVL. Such materials open new application fields for engineered timber structures. However, they may also lead to difficulties so far unknown to timber engineers as they do not occur with commonly used wood products. By discussing the stability issue as an example, possible design difficulties are reflected. This should lead to a conscious use of novel products and a clear communication to timber design engineers.

2 Current state of the art

Since the release of the technical approvals, beech LVL is more and more subject of research. Apart from the necessary tests to derive the mechanical properties, tests with beech LVL joints were carried out together with investigations on promising application fields. In Table 1, an overview is given about recently published research results where beech LVL was used (older literature is given in [3]).

Table 1. Literature overview with information on investigated topic

Material properties	
Knorz and van de Kuilen [3]	Determination of strength and stiffness of beech LVL-L and LVL-C
Dill-Langer and Aicher [4]	Glulam made of beech LVL-L, focus on compression parallel-to-grain
Joint properties	
Kobel, Frangi and Steiger [5, 6]	Embedment behaviour and joints with dowel-type fasteners
Innovative applications fields	
Enders-Comberg and Blaß [7]	Use of beech LVL for multiple step joints
Boccadoro and Frangi [8]	Timber-concrete slabs using beech LVL-C
Frese [9] (this meeting)	Spruce glulam with beech LVL laminations in the tension zone

3 Material properties

In Table 2, chosen material parameters for beech LVL and different wood products are given. Three aspects are highlighted:

- Beech LVL-L has by far the highest tension to compression strength ratio parallel-to-grain and the tension strength is equal to the bending strength.
- If comparing beech LVL-L to D70 (solid timber with the same characteristic bending strength), the MoE is low.
- The mean shear modulus is rather low, e.g. if compared to the highest strength class for beech glulam, GL48c.

Table 2. Some characteristic strength and mean stiffness values of wood products (only values for edgewise bending are given), strength and stiffness in MPa, density in kg/m^3. The factor k_h given for beech LVL-L and spruce LVL-L needs to be applied to reduce the characteristic bending strength of beams with a depth > 300 mm.

	Beech LVL-L [1]	Glulam of beech LVL-L [2]	Spruce LVL-L [10]	Beech glulam GL48c [11]	Spruce glulam GL24h [12]	D70 [13]
$f_{m,k}$	70	70	48	48	24	70
k_h	$(300/h)^{0.12}$		$(300/h)^{0.12}$			
$f_{t,0,k}$	70	55	38	21	19.2 (16.5)*	42
$f_{t,90,k}$	1.5	1.2	0.8	0.5	0.5 (0.4)	0.6
$f_{c,0,k}$	41.6	49.5	38	25	24	34
$f_{c,90,k}$	14	8.3	6	8.4	2.5 (2.7)	13.5
$f_{v,k}$	9	4.0	4.4	3.4	3.5 (2.7)	5.0
$E_{0,mean}$	16800	16700	13800	15100	11500 (11600)	20000
$E_{0.05}$	14900	15300	11600	14700	9600 (9400)	16800
$E_{90,mean}$	470	470	300	690	300 (390)	1330
G_{mean}	760	850	500	1000	650 (720)	1250
ρ_k	680	680	480	650	385 (380)	900

* values in parenthesis are from EN 1194 [14].

4 Four-point bending tests

In Karlsruhe, four-point edgewise bending tests were carried out according to EN 408 [15] as part of the test protocol to derive the characteristic edgewise bending strength for beech LVL-L (all other tests were carried out at Holzforschung München). For the initial test (denoted as A), five lateral supports were used with a resulting ℓ_{ef} of approximately 1.80 m. During the test however, buckling occurred, see Figure 1 left, and continuous lateral supports of the compression zone had to be used to force a failure in the tension zone.

The five properly tested beams (T1[ii] to T5) with a cross section of 95x600 mm^2 featured the following mean values: density: 750 kg/m^3, moisture content (MC): 8.5%, local MoE parallel-to-grain: 14200 MPa and bending strength (when failing in the tension zone): 74 MPa (COV 7%). The initial test without continuous lateral support was interrupted at a bending stress of 65 MPa where the beam already buckled as shown in Figure 1 left. The deflection at failure amounted to about 250 mm, see Figure 1 right.

The moisture content of (freshly produced) beech LVL-L is low; the mean MC of all edgewise bending specimens at Holzforschung München was 7.2% [16]. As the MC is important above all for the compression strength, also data from the compression tests parallel-to-grain are mentioned here [16]: For instance, the reported minimum compression strength was $f_{c,min,8.5} = 54.8$ MPa at a mean MC of 8.5%. If service class 1 with a mean MC of 12% is considered, the corrected minimum compression strength value[iii] would be $f_{c,min} = 49$ MPa.

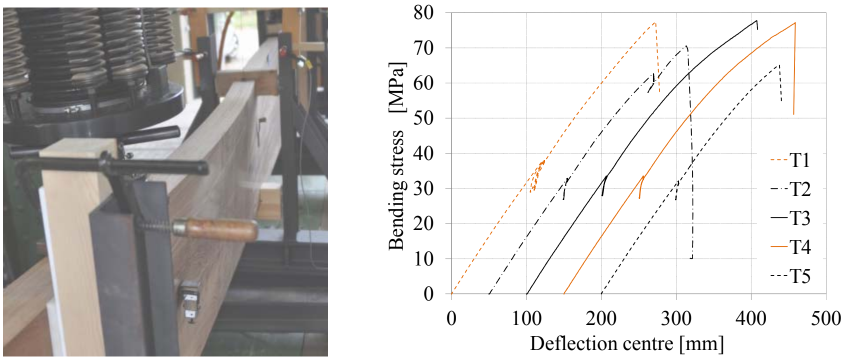

Figure 1. Left: Lateral torsional buckling of compression zone. Right: bending stress - deflection curves of five tested beams T1 to T5 with continuous lateral support. Loops indicate where additional wedges were inserted between beam and jack to increase the deflection until failure in the tension zone.

5 Discussion

σ_{crit}

For a 95x600 mm^2 beam with $\ell_{ef} = 1.80$ m, the value for the critical bending stress σ_{crit} was calculated according to equation 6.31 of Eurocode 5 [17]. Considering a MoE of 16800 MPa from Table 2 and taking G_{mean} to 1000 MPa which is the value for GL48c, the resulting critical bending stress is $\sigma_{crit} = 102$ MPa. This value for an ideal, linear elastic bending member is only 38% higher than the experimentally established bending strength of 74 MPa for a real system which gives a different safety margin than that of commonly used products such as D70, GL48c or GL24h.

Theoretical stress distributions

Figure 2 schematically shows a theoretical, linear elastic bending stress distribution over the cross section on the left for a MC of 12% and a nonlinear distribution on the right for 20% MC.

For 12%, the design bending strength of $0.9 \cdot 70/1.3 = 48.5$ MPa associated with M_d/W is still smaller than the minimum compression strength $f_{c,min}$. However, for 20% MC the design bending strength would exceed the corresponding compression strength, reflected by 41.6 MPa[iv] which means that the extreme compression zone will be beyond the elastic limit.

Therefore, the question arises if the current stability design rules are still valid for these types of strongly nonlinear stress distributions as the current k_{crit}-factors are derived considering linear elastic material behaviour (without scatter) of an ideal system. This is not expected to be a problem for service loads as then the consideration of partial safety factors for the loading lead to a reduced design bending stress of about $48.5/1.4 = 35$ MPa which is lower than $f_{c,0,k}$. However, for any exceptional loading case in service class 2 (MC < 20%) and/or combination of assumption errors, the current design rules are not valid any more.

Furthermore, the influence of moisture content on the compression strength and stiffness values has to be addressed together with a thorough discussion of the influence of the MoE in compression that is different from the MoE in bending.

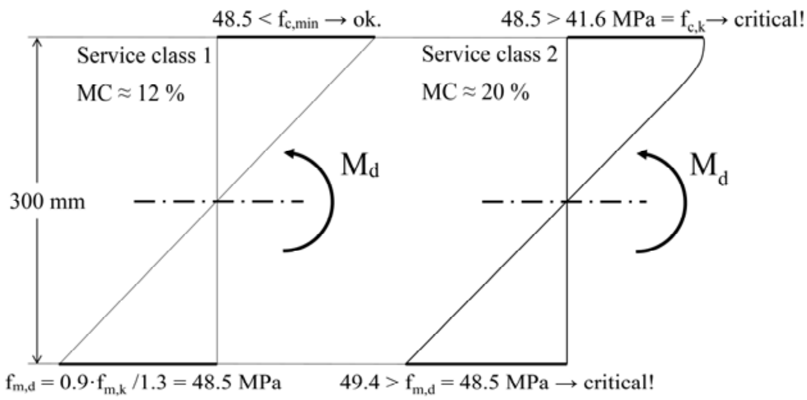

Figure 2. Linear and nonlinear stress distributions. Both cross sections are subjected to the same design moments M_d leading to a bending stress of 49.4 MPa in the extreme tension zone for the nonlinear case. $f_{c,min} = 49$ MPa at 12% MC (see section 4).

References

[1] Z-9.1-838 (2013) Laminated veneer timber made of beech for the construction of bar-shaped and flat load-bearing structures. "Beech LVL with longitudinal layers". "Beech LVL with crosswise layers". *German technical approval*. Deutsches Institut für Bautechnik, Berlin, Germany.

[2] Z-9.1-837 (2013) Glued laminated timber made from beech laminated veneer lumber. *German technical approval*. Deutsches Institut für Bautechnik, Berlin, Germany.

[3] Knorz M and Van de Kuilen JWG (2012) *Development of a high-capacity engineered wood product - LVL made of European beech (Fagus sylvatica L.)*. 12th World Conference of Timber Engineering WCTE. Auckland, New Zealand.

[4] Dill-Langer G and Aicher S (2014) Glulam composed of glued laminated veneer lumber made of beech wood: superior performance in compression loading. In: *RILEM bookseries. Materials and joints in timber structures. Recent developments in technology*. pp. 603-613. Stuttgart, Germany.

[5] Kobel P, Steiger R and Frangi A (2014) Experimental analysis on the structural behaviour of connections with LVL made of beech wood. In: *RILEM bookseries. Materials and joints in timber structures. Recent developments in technology*. pp. 211-220. Stuttgart, Germany.

[6] Kobel P, Frangi A and Steiger R (2014) *Dowel-type connections in LVL made of beech wood*. INTER first meeting, Paper 47-7-2. Bath, UK.

[7] Enders-Comberg M and Blaß HJ (2014) Treppenversatz - Leistungsfähiger Kontaktanschluss für Druckstäbe. *Bauingenieur*, **4**:162-171.

[8] Boccadoro L and Frangi A (2014) *Timber-concrete composite slabs made of beech*. Doktorandenkolloquium. Stuttgart, Germany.

[9] Frese M (2014) *Hybrid glulam beams made of beech LVL and spruce laminations*. INTER first meeting, Paper 47-12-2. Bath, UK.

[10] Z-9.1-100 (2011) Furnierschichtholz "Kerto S" und "Kerto Q". *German technical approval*. Deutsches Institut für Bautechnik, Berlin, Germany.

[11] Z-9.1-679 (2009) BS-Holz aus Buche und BS-Holz Buche-Hybridträger. *German technical approval*. Deutsches Institut für Bautechnik, Berlin, Germany.

[12] *EN 14080* (2013) Timber structures - Glued laminated timber and glued solid timber. Requirements. Comité Européen de Normalisation (CEN), Brussels, Belgium.

[13] *EN 338* (2009) Structural timber - Strength classes. Comité Européen de Normalisation (CEN), Brussels, Belgium.

[14] *EN 1194* (1999) Timber structures - Glued laminated timber - Strength classes and determination of characteristic values. Comité Européen de Normalisation (CEN), Brussels, Belgium.

[15] *EN 408* (2012) Timber structures - Structural timber and glued laminated timber - Determination of some physical and mechanical properties. Comité Européen de Normalisation (CEN), Brussels, Belgium.

[16] Knorz M and Van de Kuilen JWG (2012) Ergebnisse der Zulassungsversuche für eine 'allgemeine bauaufsichtliche Zulassung' (abZ) von Furnierschichtholz aus Buche. *Prüfbericht Nr. 10511*. Holzforschung München, Technische Universität München, Germany.

[17] *EN 1995 1-1* (2010) Eurocode 5. Design of timber structures - Part 1-1: General -Common rules and rules for buildings. Comité Européen de Normalisation (CEN), Brussels, Belgium.

---

i Flatwise: LVL is loaded perpendicular to the veneers. Edgewise: LVL is loaded parallel to the veneers

ii Initial beam A was re-used as beam T1.

iii The compression strength is reduced by 3% per 1% less MC.
Therefore (from 8.5% MC to 12% MC): $f_{c,min} = 54.8 - (0.12-0.085)\cdot 3\cdot 54.8 = 49$ MPa

iv The characteristic value as derived by Holzforschung München accounted to 53.7 MPa at a mean MC of 8.5% [16]. Therefore, it is assumed that the used characteristic value of 41.6 MPa (see Table 2) was adjusted to a MC of 20% for service class 2. The MoE in compression was not measured.

Withdrawal strength dependency on timber conditioning

Jørgen Munch-Andersen

Danish Timber Information, jma@traeinfo.dk

Keywords: Withdrawal, conditioning, staples, nails

Introduction

According to prEN 1382 Withdrawal capacity of timber fasteners (CEN, 2014), smooth fasteners shall be installed in timber conditioned at 85 % RH and then stored for at least a week at 65 % RH before being tested. Other fasteners can be installed in timber conditioned at 65 % RH, since the effect of the moisture content for screws and ringed nails are negligible, so there is no need for the complicated procedure with two moisture levels. However, it is not known if staples with resin-coated legs should be regarded smooth or non-smooth.

This paper investigates the influence of bringing test specimens in equilibrium with 85 % RH before inserting the fasteners, compared to inserting them in timber conditioned at 65 % RH. Tests are carried out with three types of fasteners: ringed nails, smooth nails and coated staples.

Kevarimäki (2005) investigated the influence of the conditioning for nails, but to the authors knowledge it has never been investigated for staples.

Tests and results

Three makes of each of three types of fasteners was selected, see Table 1. Six different boards of spruce was used, see Table 2. The boards were halved and one half were conditioned at 65 % and the other at 85 % RH. Each half board could contain six fasteners and the three makes of two types of fasteners were used in both halves, so the fasteners were tested in pairs with different moisture conditions. Six pairs of each of the nine different makes of fasteners were tested, so a total of 72 tests were carried out. The fastener types were mixed, so two boards had smooth and ringed nails, two had smooth nails and staples and two had ringed nails and staples. (It would have been preferable to use boards long enough to contain all nine fasteners, but that was not possible).

Table 1. Characteristics of the fasteners. d is diameter, l is total length, l_{point} is the length of the point and t_{pen} is the penetration depth during the test, excluding the point length for the nails.

Fastener no	1	2	3	5	6	7	9	10	11
d, mm	3,23	3,06	2,96	3,05	2,73	2,44	1,80	2,00	1,53
l, mm	90	75	62	90	63	64	60	65	50
l_{point}, mm	4,4	4,1	3,8	5	4,7	4	-	-	-
t_{pen}, mm	75,6	60,9	48,2	75	48,3	50	2 x 52	2 x 57	2 x 42

Note: Fastener no 1 is the reference nail mentioned in Munch-Andersen and Svensson, (2013)

Table 2. Densities of the 6 boards used. The value is determined when conditioned at 65 % RH.

Board no	1	2	3	4	5	6	Mean	CoV
Density, kg/m^3	444	415	408	455	421	412	426	4,4 %

The observed pairs (F_{max65}; F_{max85}) are shown in Figure 1, where index 85 refers to conditioning at 85 % and storage at 65 % RH. One pair for a smooth nail is regarded as an outlier, having the 85%-observation much larger than the 65%-observation, see × on Figure 1.

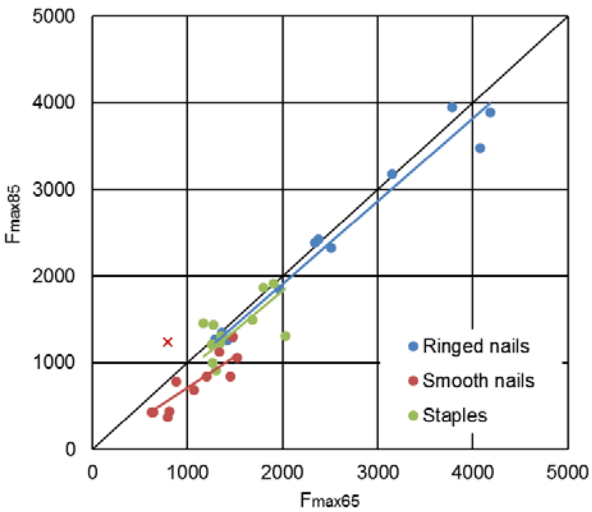

Figure 1. Observed pairs of withdrawal force when conditioned at 85 % RH respectively 65 % RH. A disregarded outlier for a smooth nail is marked with ×.

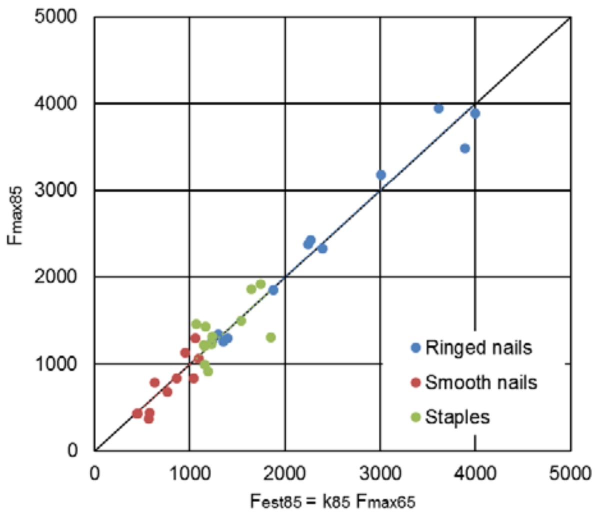

Figure 2. The factor k_{85} for each fastener type is determined such that the slope of F_{max85} versus $F_{est85} = k_{85}\, F_{max65}$ becomes unity for each type of fastener.

Estimation

Since the tests were done in pairs, the influence of the conditioning procedure can be revealed by determining three factors k_{85}, one for each of the three fastener types such that the error of the model

$$F_{est85} = k_{85}\, F_{65} \tag{1}$$

is minimized. The factors k_{85} are determined using Figure 2 such that F_{max85} versus F_{est85} for each type lies as close as possible to a line with slope 1. The factors are seen in Table 3 together with the mean and standard deviation of the error

$$\Delta_d = \ln(F_{85}/F_{est85}) \tag{2}$$

for each type of fastener. Due to the logarithm, the standard deviation of Δ_d is equal to the coefficient of variation of the factor k_{85}. The estimation method is in line with Annex D in Eurocode 0 (CEN, 2004).

Table 3. The correction factors k_{85}, the mean error and the standard deviation of each k_{85}.

	k_{85}	mean(Δ_d)	sd.(Δ_d)
Ringed nails	0,955	0,000	0,065
Smooth nails	0,715	-0,054	0,202
Staples	0,915	0,009	0,189

It was expected that the k_{85}-value would be close to unity for ringed nails and significantly smaller for smooth nails. This is confirmed. It is seen that the effect of the conditioning method also is small for staples, but larger than for ringed nails.

The coefficient of variation of k_{85} is much smaller for ringed nails than for smooth nails and staples. The mean value of Δ_1 will be zero if the ratio F_{max85}/F_{max65} is Log-normally distributed. For smooth nails, this is not quite the case, since the mean value is -0,054. This is just a statistical coincidence related to limited number of tests and the high coefficient of variation.

A further statistical analysis, not reported here, showed that the coefficient of variation for the nails were very similar for conditioning at 65 % and 85 % RH, whereas it for staples were almost three times higher when conditioned at 85 % than when conditioned at 65 % RH (0,16 versus 0,06).

Previous results

Kevarimäki (2005) tried conditioning and storing at 65 % RH as a reference, conditioning at 85 % RH and storing at 40 % RH (about 7 weeks, until equilibrium) and conditioning at 65 % RH and storing at 85 % RH. This was done with three makes of nails, a smooth nail with longitudinal groves, a normal ringed nail and a nail with a coarser profile than a normal ringed nail. The average withdrawal strengths when conditioned at 65 % RH were found to be 7,2 MPa, 5,6 MPa and 9,4 MPa, respectively. The average density at 65% RH was close to 360 kg/m^3.

Storing at 85 % RH after inserting the nails did not change the withdrawal strength at all, but the fairly harsh drying to 40 % RH reduced the strength to 67 % for the ringed nails and to 38 % for the smooth nail.

Conclusions

Conditioning the timber at 85 % RH before assembling the specimens, as required in prEN 1382 (CEN, 2014) for smooth fasteners, reduces the average withdrawal capacity of ringed nails with about 5%, and 10 % for staples compared to conditioning at 65 % RH. For smooth nails the capacity on average was reduced by about 30 %, so for smooth nails the complicated procedure seems appropriate, whereas it is unnecessary for ringed nails.

For staples the influence of the conditioning might not be negligible, but the coefficient of variation almost triples when the timber is first conditioned at 85 % RH in-stead of 65 % RH. This indicates that it is preferable to carry out tests with the simple method and then reduce the withdrawal strength by a prescribed factor. However, the high coefficient of variation for staples when conditioned at 85 % ought to be confirmed before doing that.

The previous test carried out by Kevarimäki (2005) show similar tendencies, but since the conditionings used are different from those used for the present study, the estimated sensitivities cannot be confirmed.

It should be considered if design rules should take the effect of drying on the withdrawal strength into account, as also pointed out by Kevarimäki.

Acknowledgement

The test were carefully carried out by Jette Byberg and Signe Tolberg Andersen, Wood Fasteners R & D Center, ITW, Denmark.

References

CEN (2004): Eurocode 0, Basis of structural design. EN 1990:2004.

Kevarimäki, A. (2005): Nails in spruce – Splitting sensitivity, end grain joints and withdrawal strength. CIB-W18, Meeting 38. Karlsruhe, Germany. August 2005.

Munch-Andersen, J and Svensson, S. (2013): Fasteners and connections in the next Eurocode 5. CIB-W18, Meeting 46. Vancouver, Canada. August 2013.

CEN (2014): Timber Structures - Test methods -Withdrawal capacity of timber fasteners. prEN 1382:2014.

Execution of Timber Structures

Kristine Nore, Tomi Toratti, Jørgen Munch-Andersen, Joachim Schmid and Alar Just
Norwegian Institute of Wood Technology, Norway; RTT, Confederation of Finish construction product industries, Finland; Danish Timber Information, Denmark; SP Wood Technology, Sweden and Tallin University of Technology, TUT, Estonia

Keywords: **execution, timber structure, industry, moisture control, fire safety, stability during construction**

1 Introduction

To a large degree, building failures are caused by poor execution [1]. The guidelines for execution, given in Eurocode 5 [2] are quite limited. Therefore, the procedures and entrepreneurs plan and perform proper execution according to their experience and anticipation of site conditions. NEXT-Timber, a Novel EXecution Tool for Timer structures, is a project that aim to coordinate available execution tools to provide a common open execution standard for the Nordic countries. This paper summarises the fields of interest and anticipated results as a basis for future execution standards.

NEXT-Timber includes study of performance requirements and respective solutions for some critical performances: vibrations, acoustics, fire and moisture load. This will be a platform for future developments. In order to ensure the use of the same terminology and concepts by all stake holders a review will be carried out. This will focus on the description on element joints to enable the use of elements from different sources and materials.

The assembly of prefabricated elements is a very central part of the execution of a building. Usually an assembly plan is required. This plan defines the responsibilities of the parties involved and solutions for:

- Structural stability during each phase of the erection,
- Fire safety during the site work,
- Control of moisture during the site work, protection methods, element storage and related inspections.

2 Current code for execution standard

Currently Eurocode 5 has some pages related to detailing and execution of timber structures. These are given in chapter 10 and this consists of only 3 pages. In TC250/SC5 there is a plan to produce a full execution standard for timber structures, which will be (most probably) a separate standard from the Eurocode (as with other building materials).

In several European countries, national standards are developed for the execution of timber structures simultaneously. In Finland the national execution standard has recently been published [3]. In NEXT-Timber, Nordic views on this document will be discussed and this discussion will also be brought up in the respective CEN groups.

Attention towards execution guidelines are also found in recent publications from Australia on fire during construction [4] and moisture controls [5] and on tall timber buildings in general in Canada [6]. Such initiatives will increase the professionalism of the timer construction industry.

3 Performance requirement principles

Performance requirements for timber buildings may regard fire, acoustics, vibrations and structural stability. Solutions for planning and design can be according to performance requirements. A way to express essential performance requirements, both in building regulations and for clients who require higher performance, is one aim of NEXT. We seek to provide guidance on how to fulfil these requirements at different levels.

Interface principles will be provided, which facilitate the use of new developments with respects to vibrations, acoustics and fire. This may be used as a platform for future innovative developments.

An overview of the present performance requirements and how they are expressed in regulations and guidelines will be published. Generalization of experience will ease judgment of performance level during design.

4 Tolerances

Tolerances are clearly different according to material. Joints include several materials and the serviceability of each material must be understood in order to ensure durability. Tolerances are seldom measured or argued. However, with the increased degree of prefabrication, defined tolerances are necessary in the construction process. Well-defined and agreed tolerances will simplify the communication between de different parties.

Tolerances are needed for:

- Material sections
- Joint placing
- Prefabricated elements
- Assembly placing

Although the allowable material tolerances are usually given in material product standards, there might be a need to specify further tolerances and/or to tighten the general tolerances in order to ensure the performance of joints, especially between different materials. Tolerance classes have to be defined and these should be dependent on the execution class/consequence class.

Examples of the above are given in the Finnish execution standard [3]. These have been drafted together with the national professionals and designers. No international discussion on this has yet followed.

5 Moisture

Moisture is one main cause of building failures [1]. Moisture control during assembly is of vital importance. A new standard on measuring wood moisture primarily in the building phase is soon to be released in Norway [7]. A moisture control plan, as found in [3, 7], can ensure sound construction with minimal undesirable moisture influence. At first, a level of weather protection in the building process must be defined. Further, all states must be followed from fabrication, transport, delivery and storage and assembly and use.

Wooden buildings will always shrink and swell according to the ambient moisture content. In Växjö the 8-storey timber project Limnologen is carefully logged on vertical displacements [8]. In total the shrinking was 23 mm. Constructed with the platform principle such settlement should not be noticeable or severe in any case. Daily fluctuations of the entire building is around 1-1.5 mm. However, new construction principles may arise in order to attain improved stability or cost efficiency.

Expected moisture shrinkage must be estimated and followed in the construction process and buildings service life to avoid building damage.

6 Fire

The process of execution has high importance for the overall fire safety of the completed building. While fire safety of members can be estimated by means of calculation models or fire tests the possibilities for a verification of assembled structures are limited, e.g. there are few methods available to evaluate the performance of joints. Cavities may have a considerable influence on the system performance in the fire situation while they might be concerning other aspects.

Execution with respect to the fire performance comprises the phases of planning when details are developed as well as the erection phase of the building. In this last phase the documentation and controlling of sensitive details is essential to achieve the requested level of fire safety. Due the importance and the sensitivity of this last phase check lists and documentation tools were developed recently. Further, sufficient fire safety during any building phase has to be achieved as other requirements, e.g. stability. The lack of planned active and passive protection may require special planning for different phases.

7 Practical use

The procedures described in the Finnish standard [3], have received a varying feedback from the building professionals in Finland. In general, structural designers are most positive on these guidelines, as these help on their everyday design work on problems encountered. A common question has been on ensuring sufficient human resources for the designer tasks. Some professionals regard the requirements of the standard as too complicated, although they concern actions and decisions that should be considered in any case. The use of templates in such standards would be easier to apply in practice when information technologies are more widely applied for the construction process.

Systems to handle documentation and communication during a building process are widely available. A review to provide an overview of existing web tools for execution of timber buildings is part of NEXT-Timber. The applications available are not yet structured to handle all aspects, like from structural design to order to material handling to building maintenance.

8 Conclusion

The project NEXT will provide a common basis on the timber building execution standard for the Nordic countries. It is a target that this standard will ensure a high quality level for the building and errors encountered in past experience may be avoided.

This standard will meet the needs of a more professional urban tall timber building culture.

References

[1] Lisø, K.R., T. Kvande, og J.V. Thue. «Learning from experience – an analysis of process induced building defects in Norway». Proceedings of the 3rd International Building Physics Conference, August 27-31, 2006: 425–432 *Research in Building Physics and Building Engineering*. Design sheet 700.110 Building failures. SINTEF Building and Infrastructure, Oslo, Norway.

[2] EN 1995 1-1:2010 Eurocode 5. Design of timber structures - Part 1-1: General -Common rules and rules for buildings. Comité Européen de Normalisation (CEN), Brussels, Belgium.

[3] SFS 5978:2014 Execution of timber structures. Rules for load-bearing structures of buildings (In Finnish, an unofficial English translation is available).

[4] MacKenzie C. 2012 Impact and Assessment of Moisture-affected Timber-framed Construction Technical Design Guide. Forest and Wood Products, Australia.

[5] England P. 2014 Fire Precautions During Construction of Large Buildings. Timber-framed Construction Technical Design Guide. Forest and Wood Products, Australia.

[6] Karacabeyli E and Lum C. 2014. Technical Guide for the Design and Construction of Tall Wood Buildings in Canada. Special Publications SP-55E. FPInnovations, Canada.

[7] prNS 3512:2014 Measurement of wood moisture content, Standard Norway, Oslo.

[8] Serrano E. Enquist B. and Vessby J. 2014 Long term in-situ measurements of displacement, temperature and relative humidity in a multistory residential clt-building. World Conference on Timber Engineering, Quebec City, Canada.

Cross Laminated Timber made of regional wood from Shizuoka area Part 1: Project outlines and mechanical properties of CLT

Kenji Kobayashi and Motoi Yasumura
Shizuoka University, Japan

Keywords: CLT, Regional wood, Bending property, Shear property

1. About Shizuoka CLT project

The utilization of CLT is increasing more and more around the world. In Japan, Japanese Agricultural Standard (JAS) about CLT materials was established on December 2013. Although average and 5th percentile values of representative CLT layups are prescribed in JAS standard, they are determined based on limited test results and calculations.

Shizuoka CLT project was started in Shizuoka University to investigate the performance and clarify the feasibility of the utilization of CLT made of regional wood from Shizuoka area. This project includes various types of tests from material tests of lamina to full scale test of CLT structures. All tests can be compared with common axis – made of same lamina from Shizuoka area. Test series of this project are listed as follows:

a) Mechanical grading of lumber and strength distribution of lamina

   Logs from Shizuoka area were sawn and dried and the lumbers were classified by mechanical grading based on MOE values. Besides, bending tests of lamina were conducted to determine MOE and MOR of each lamina.

b) Bending and out-of-plane shearing tests of CLT

   Two types of material tests were conducted according to Japanese Agricultural Standard for CLT materials (CLT-JAS) in Japan. It was confirmed whether produced CLT would satisfy the requirements in JAS standard.

c) Shearing tests of screw joints

   Three types of screw joints were tested to determine characteristic values. Joint details were determined so as to estimate the performances of CLT shear walls or diaphragms.

d) Static and pseudo-dynamic tests of CLT Wall

   Reversed cyclic loading tests and pseudo-dynamic tests of CLT shear walls were conducted to clarify the effects of joints on the seismic behavior of CLT shear walls.

e) Lateral loading tests of CLT walls with opening and full scale vertical diaphragms

Ten CLT shear walls with openings and two full scale CLT structures were tested to clarify the effects of the size and configuration of wall panels on the lateral resistance and deformability of CLT structures.

In this paper, we report about material properties of lamina itself and manufactured CLT.

2. Material properties of lamina from Shizuoka area

2.1. Outline of experiment

Details of lamina used for CLT is shown in Table 1. Japanese Sugi (*Cryptmeria japonica*) and Hinoki (*Chamaecyparis obtusa*) produced at east area of Shizuoka region were used. MOE of each board was measured by grading machine and classified in several groups.

Bending test of lamina was conducted according to CLT-JAS – three point bending test for MOE values, and four point bending test for MOR values. Test specimens have cross section of 123x30mm and length of 720mm. Both specimens with and without finger joint were prepared for the test.

Table 1 Details of lamina used for CLT

Name	Species	Grade	Range of MOE [a] (GPa)	Average MOE at Grading (GPa)
S-M60	Sugi	M60	4.5-9.0	7.84
S-M90	Sugi	M90	7.5-12.0	10.29
H-M90	Hinoki	M90	7.5-12.0	10.33
H-M120	Hinoki	M120	10.5-15.0	12.77

a) Range of MOE is described in JAS standard

2.2. Test results

The relationship between MOE and MOR on each series is shown in Figure 1. Bold lines in the figure show 5% values of MOR which is prescribed in CLT-JAS. MOR values derived from test results showed higher than 5% values in each grade. S-M60 and S-M90 specimens with finger joint showed almost the same MOR values in spite of the difference of MOE value.

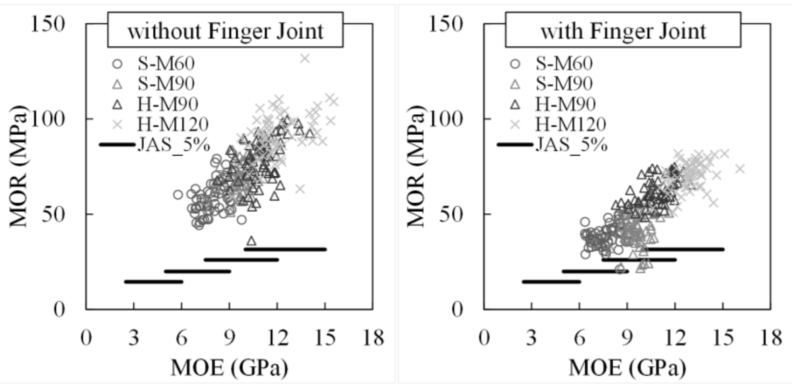

Figure 1 Relationship between MOE and MOR on each series

3. Bending and out-of-plane shearing tests of CLT

3.1. Outline of experiment

Bending and shearing test specimens are shown in Table 2. S60, S90 types consist of same grade lamina – M60 and M90 grades with the same species respectively. Mx120 types have H-M120 lamina (Hinoki) for outer layer and S-M60 lamina (Sugi) for inner layer. All layers have thickness of 30mm. Water based polymer isocyanate adhesive was used for layer lamination and finger jointing and no glue was applied to the edge joint of lamina.

Bending tests and out-of-plane shearing tests were conducted according to CLT-JAS – four point bending test and short span three point bending test. Supporting spans were 21*h* for bending test and 5*h* for shearing test (*h*: height of the specimen).

3.2. Test results

Apparent MOE and MOR values derived from four point bending tests were shown in Figure 2 and 3. These values decreased with the increasing of the height of the specimen (number of layers). Rolling shear failures often observed in SH-Mx120 specimens.

Apparent shear strength f_s derived from short span three point bending test were shown in Figure 4. Similar tendency to MOE values was observed against number of layers. They did not depend on MOE of lamina but species. The lowest value was observed in the specimens with 210mm height.

Mechanical properties of CLT made of regional wood were enough higher than CLT-JAS values.

Table 2 Bending and shearing test specimens

Specimen	Outer layer	Inner layer	number of layer	width (mm)	height (mm)
S-S60-3	S-M60	S-M60	3	300	90
S-S60-5	S-M60	S-M60	5	300	150
S-S60-7	S-M60	S-M60	7	300	210
S-S90-3	S-M90	S-M90	3	300	90
S-S90-5	S-M90	S-M90	5	300	150
S-S90-7	S-M90	S-M90	7	300	210
H-S90-3	H-M90	H-M90	3	300	90
SH-Mx120-3	H-M120	S-M60	3	300	90
SH-Mx120-5	H-M120	S-M60	5	300	150
SH-Mx120-7	H-M120	S-M60	7	300	210

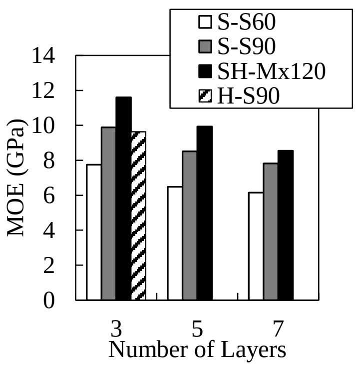

Figure 2 Comparison of MOE values

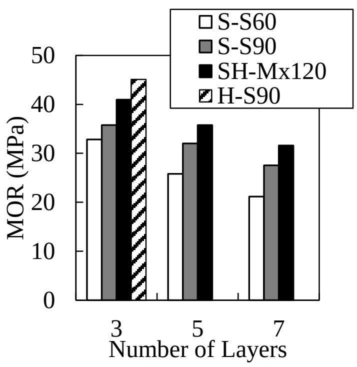

Figure 3 Comparison of MOR values

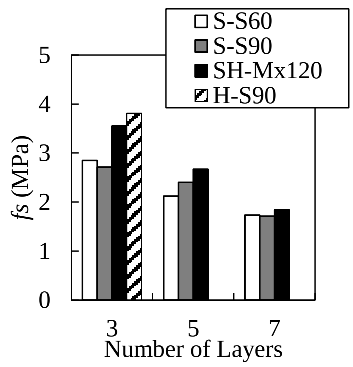

Figure 4 Comparison of f_s values

Cross Laminated Timber made of regional wood from Shizuoka area Part 2: Seismic performance of CLT structures

Motoi Yasumura, Kenji Kobayashi and Minoru Okabe

Shizuoka University, Japan

Keywords: CLT, shear walls, reversed cyclic, pseudo dynamic, opening, full-scale test

1 Introduction

The seismic performance of CLT structures depend much on the size and configulation of wall panel elemens and the boundary conditions of each panel element. In general large wall panels including openings are used for CLT structues, however there will be also possibility to use smaller wall panels. In the first place, the reversecd cyclic lateral loading tests and pseudo dynamic tests were conducted on CLT shear walls to clarify the effects of joints on the seismic behaivior of CLT shear walls, and then two full scale CLT structures with large wall panels and small wall panels were conducted to clarify the effects of the size and configulation of wall panels on the laterall resistance and deformability of CLT structures. As the cracks appeared at the corner of openings in the structure with large CLT panels with openings, reversed cyclic lateral loading tests on CLT wall panel with an opening were also conducted to study the effects of size and configulation of opening on the load carrying capacity of CLT shear walls with opening.

2 Lateral loading tests on CLT shear walls

2.1 Outline of experiment

Reversed cyclic lateral loading tests and pseudo dynamic tests were conducted on CLT shear walls consisting of two 1m-by 3m Sugi (*Cryptomeria japonica*) and Hinoki (*Chamaecyparis obtusa*) CLT panels of 3ply 90mm thickness. Two CLT panels were connected by 65mm screws of 5.5mm diameters and steel plats and they were connected to the steel base with steel restrains and 65mm screws of 5.5mm diameters. Asumming the design maximum load bearing capacity of 50kN, number of screws were determined by applying reliability based analysis[1].Two failure modes were assumed. One is the failure mode where the failure of the vertical restrain at the end of wall panel preceds the yielding of the joints connecting two CLT panels, and the other is that the failure mode where the failure of the joints connecting two CLT panels preceds the failure of the vertical restrain. The number of screws determined for the vertical restrain and shear joints are shown in Table 1.

Reversed cyclic horizontal loads based on ISO 21581 was applied togather with the vertical constant loads of 15kN/panel (total 30kN). Pseudo dynamic tests were also conducted using 1995 JMA KOBE NS (PGA 818gal) and artificial waves of BCJ LEVEL2 (PGA356gal).

Table 1 Determined number of screws for design maximum load bearing capacity of 50kN

Specimen	Spieces	Criteria	Number of screws		Vertical load
			Vertical restrain	Panel-panel	(kN/panel)
H-T12-S8	*Hinoki*	Panel-panel	12	8	15
H-T8-S34	*Hinoki*	Vertical restrain	8	34	15
S-T20-S10	*Sugi*	Panel-panel	20	10	15
S-T12-S44	*Sugi*	Vertical restrain	12	44	15

2.2 Experimental results

The maximum displacement responses of the specimens with the precedence of the failure of vertical restrain were 25.7mm and 15.8mm for *Sugi* and *Hinoki* specimen, respectively. They were 30 to 36% of those with the precedence of the failure of the joints between CLT panels that were 70.4mm and 52.1mm for *Sugi* and *Hinoki* specimen, respectively.

Most specimens designed for the failure of the joints between CLT panels attained ultimate state with the excitation of 1995 JMA KOBE NS 100%, but almost no apparent failures were observvwd in the specimens with the failure criteria of vertical restrains.

3 Lateral loading test of full scale CLT structures

3.1 Outline of experiment

Two story CLT structures of 6m in length, 4m in width and 5.82m in height were subjected to reversed cyclic lateral loads. Two specimens were prepared as shown in Fig.1. One specimen had large CLT panels of 6m in length and 2.7m in height, and another consisted of small panels of 1m-by 3m. Assuming the building of 3 story, weights of 72kN and 126kN were fixed on 2nd floor level and roof level, respectively. So, total weight of the specimen was 251kN, and the design maximum horizontal capacity of 251kN was assumed considering the base shear coefficient of 1.0. The number of screws in vertical restrains and shear plates were determined from the linear analysis by Finite Element Method of the structure. The number of screws obtained by FEM is shown in Table 2. Reversed cyclic lateral loads were applied at the top of the 2nd story by actuators.

Fig.1(a) Specimen with large CLT panels

Fig.1(b) Specimen with small CLT panels

Table 2 Determined number of screws in vertical restrains of full scale specimen by FEM

Joint position		1	2	3	4	5	6
Large	2nd str	8					8
Panels	1st str	14			6	4	10
Small	2nd str	8	6	6	6	6	8
Panels	1st str	14	12	12	12	12	14

3.1 Experimental results

Both specimens with large and small CLT panels showed high load bearing capacity of more than 400kN, while the design maximum capacity was 251kN. Cracks appeared at the corner of opening with the specimen with large panels after the design load, but vigolous decrease of horizontal load was not observed, and the load continued to increase as the development of the cracks. The initial stiffness of the structure with large panel was approximative twice as high as that with small panels, and the maximum displace of the former was about a half of the later.

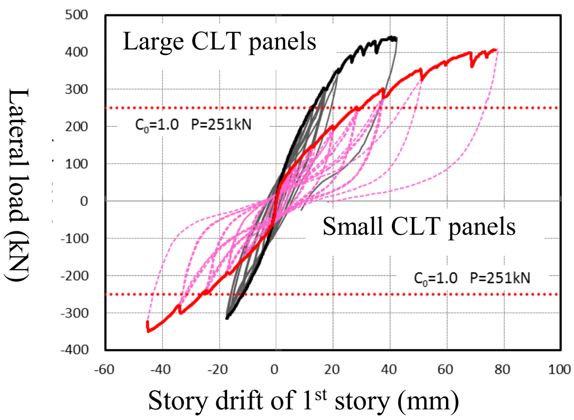

Fig.2 Load-story drift relation of 1st story

4 Lateral laoding test of CLT shear walls with an opening

4.1 Outline of experiment

Reversed cyclic lateral loading test was conducted on CLT wall panels with an opening of various size and configuration. Specimens had 3.5m length and 2.7m height and opening of 1000x1500mm, 1400x1500mm, 2000x1500mm and 1400x2300mm. Both bottom ends of wall was connected tightly to steel base and the horizontal loads were applied at the end of timber beam of 90x 240mm which was connected tightly to the top of the wall.

4.2 Test results

Figure 3 shows relation between capacity for 1/300rad. displacement (○), maximum load bearing capacity (◇) and opening area ratio. It shows that both 1/300rad. capacity and the maximum load bearing capacity were proportional to the opening area ratio. It indicates the necessity to check the stress at the corner of opening in large CLT panels if the shear stress is comparatively high and the opening area is comparatively large.

[1] Motoi Yasumura, Determination of failure mechanism of CLT shear walls subjected to seismic action, Proc. CIB-W18, pp. 1-9, paper 45-15-3, 2012

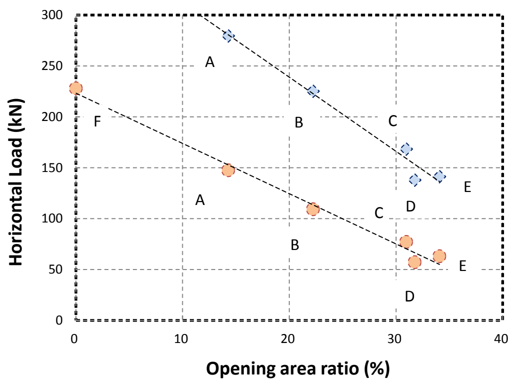

Fig.3 1/300 capacity (○), maximum load bearing capacity (◇) v.s. opening area ratio

Modelling the Bending Strength of Glued Laminated Timber – using Machine-Grading Indicators

Gerhard Fink[1)], Andrea Frangi[1)], Jochen Kohler[2)]
[1)] ETH Zurich, Institute of Structural Engineering, Zurich, Switzerland
[2)] NTNU, Department of Structural Engineering, Trondheim, Norway

1 Introduction

The most common way to model the mechanical performance of GLT beams are by using simulation models. Thereby, at first GLT beams are simulated using probabilistic models. Afterwards, their load-bearing capacities are estimated using e.g. numerical models. Well-known examples for such probabilistic models are the *Model of Foschi and Barrett* [1], the *Karlsruher Rechenmodel* [2, 3, 4], or more recent the model presented at the 46$^{\mathrm{th}}$ CIB-W18 meeting [5], see also [6] for a detailed description.

To describe the characteristics of the timber boards, all the above mentioned models are using strength and stiffness related indicators measured in the laboratory. In general two indicators are used: One global indicator that describes the mean material properties of the timber boards, and one knot-indicator to describe the local strength and stiffness reduction due to knots. For the identification of the latter one, the size and position of all 'relevant' knots have to be measured. It is obvious that such a knot-measurement is very time consuming and thus the resulting knot-indicators are not efficient for practical application. However, nowadays, timber boards are often graded with measurement devices where both indicators (global indicator and knot-indicator) are automatically measured (refereed as to machine-grading indicators). Following, it would be more efficient to develop probabilistic approaches based on machine-grading indicators.

The *GLT model* presented at the 46$^{\mathrm{th}}$ CIB-W18 meeting [5] is based on two strength and stiffness related indicators measured in the laboratory: $E_{\mathrm{dyn,F}}$ and tKAR. However, all the timber boards used for the development of this model were previously graded by the GoldenEye-706 grading device [7]. This is a grading device that measures the dynamic modulus of elasticity based on eigenfrequency (denoted E_{m}) and performs an X-ray measurement to detect knots in size and position. In Fig. 2 (left) an example of one resulting knot profile is given; the knot-indicator measured by the GoldenEye-706 grading device is denoted K_{m}. A comparison between the indicators measured in the laboratory ($E_{\mathrm{dyn,F}}$ and tKAR) and those measured by the grading device (E_{m} and K_{m}) indicate a strong correlation between the two moduli of elasticity and between the knot indicators (Fig. 1): $\rho(E_{\mathrm{m}}, E_{\mathrm{dyn,F}}) = 0.98$ and $\rho(K_{\mathrm{m}}, \mathrm{tKAR}) = 0.77$. As a result of the strong correlation the *GLT model* [5] was extended for machine-grading indicators; i.e. the indicators measured in the laboratory were exchanged by machine-grading indicators.

In this technical note a short summary about this new approach developed within the framework of the PhD thesis *Influence of varying material properties on the load-bearing capacity of glued laminated timber* [6] is presented. Furthermore, the potential of machine-grading indicators in respect to the development of more reliable GLT beams is discussed.

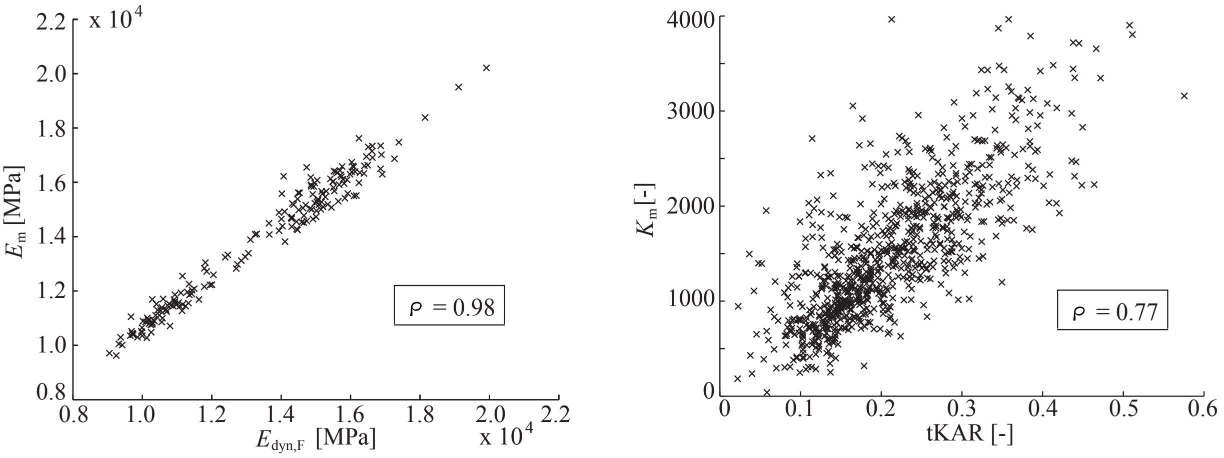

Fig. 1: Correlation between the indicators measured in the laboratory and the machine-grading indicators: (left) global indicator $E_{\mathrm{dyn,F}}$ and E_{m} of 200 timber boards; (right) knot-indicator tKAR and K_{m} of 864 knot clusters.

2 GLT model for machine-grading indicators

The *GLT model* [5] contains four independent sub-models: (1) a probabilistic model to simulate timber boards, (2) a model to reproduce the fabrication process of GLT beams, (3) a material model to allocation of material properties, and (4) a FEM for the estimation of the load-bearing capacity. For the extension to machine-grading indicators a new probabilistic model and a new material model have to be developed. Furthermore, the application of the numerical model has to be validated.

The probabilistic model is developed following the same principle as for indicators measured in the laboratory [8]; i.e. the distance between weak sections (WS) is described using a shifted Gamma distribution and both strength and stiffness related indicators are modelled using hierarchical models. The position and the characteristics of knot clusters were identified based on the knot profile (Fig. 2, left). Knot clusters with $K_{\mathrm{m}} \geq 700$ are defined as WS, knot clusters $K_{\mathrm{m}} < 700$ are neglected.

The material model is developed as described in [9], using (a) the measured tensile stiffness of 864 knot clusters, and (b) the the tensile capacity and the knot profile of 450 timber boards (including 2'987 WS). A comparison with the test results shows a wide agreement. Thus the material model can be applied to estimate the tensile strength and stiffness properties of knot clusters (and clear wood) based on machine-grading indicators.

The application of the numerical model is validated on 24 GLT beams having well-known local material properties; i.e. GLT beams where the exact position of each timber board, each FJ, and each WS as well as the machine-grading indicators E_{m} and K_{m} of each lamella section are precisely-known. The material properties of the lamella sections are estimated using the material model described above. In this example the material properties of FJ are calculated according to Eq. (1). The wide agreement between the estimated and the measured material properties (see e.g. Fig. 2, right) indicate that the numerical model can be used for the estimation of GLT beams with a precisely-known beam setup.

$$E_{\mathrm{t,j}} = \frac{1}{2}\sum_{i=1}^{2} E_{\mathrm{t,CWS},i} \qquad f_{\mathrm{t,j}} = \min_{i=1,2}\{f_{\mathrm{t,WS},i} | K_{\mathrm{m}} = 1200\} \tag{1}$$

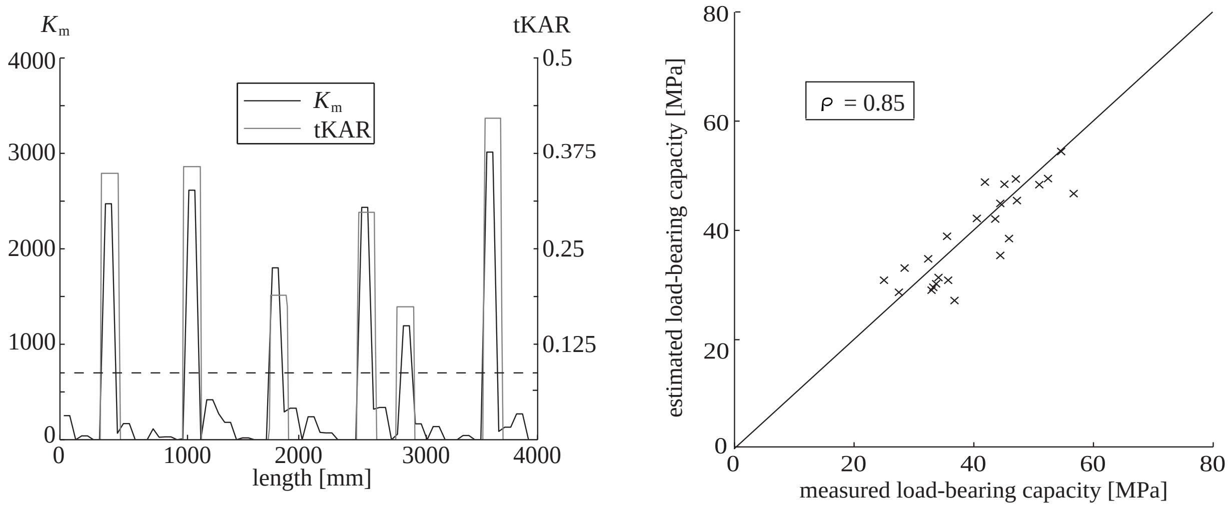

Fig. 2: (left) Knot-indicator profile, (right) Correlation between the measured and the estimated load-bearing capacity.

In [6] the probabilistic approach using machine-grading indicators is applied on selected examples. Summarized it can be stated that realistic values for the bending stiffness and the bending strength were achieved; i.e. the characteristic values as well as the variability of both material properties correspond to values proposed in the literature. In addition also the number of FJ-failure seems to be realistic.

3 Potential of machine-grading indicators

The major advantage of the new approach is that machine-grading indicators are measured automatically during the grading process; i.e. machine-grading indicators (e.g. E_m and K_m) are measured for every timber board graded by grading devices (e.g. GoldenEye-706). As a result, machine-grading indicators can be collected automatically and thus new probabilistic models can be developed with only marginal effort. Such new probabilistic models are essential to describe the characteristics of timber boards of different strength grades, different growing regions, different cross-sections, and so on. A further advantage of machine-grading indicators is that they are reproducible and objective.

However, the presented approach also offers new opportunities to fabricate more reliable GLT beams. Due to a combination of the grading process and the GLT fabrication, GLT beams with a precisely-known beam setup could be fabricated; i.e. GLT beams were the machine-grading indicators of each lamella cross section are known. Using material models such as presented in [6] the tensile strength and stiffness properties of the lamellas can be calculated. Afterwards, the bending stiffness and the load-bearing capacity of the GLT beam can be estimated using numerical models. To fabricate more reliable GLT beams, those with e.g. very low estimated load-bearing capacities could be sorted out.

Another, more complex, example of application could be the fabrication of GLT beams with an optimised beam setup. Knowing the material properties of the timber boards, their arrangement within the GLT beam could be optimized; e.g. timber boards with low estimated material properties could be located in low loaded areas of the GLT beams.

References

[1] R. O. Foschi and J. D. Barrett. Glued-laminated beam strength: a model. *Journal of the Structural Division, American Society of Civil Engineers*, 106(ST8):1735–1754, 1980.

[2] J. Ehlbeck, F. Colling, and R. Görlacher. Einfluß keilgezinkter Lamellen auf die Biegefestigkeit von Brettschichtholzträgern. *European Journal of Wood and Wood Products*, 43(8):333–337, 369–373, 493–442, 1985.

[3] F. Colling. *Tragfähigkeit von Biegeträgern aus Brettschichtholz in Abhängigkeit von den festigkeitsrelevanten Einflussgrößen.* Versuchsanstalt für Stahl, Holz und Steine, Karlsruhe, Germany, 1990.

[4] H.J. Blaß, M. Frese, P. Glos, J.K. Denzler, P. Linenmann, and A. Ranta-Maunus. *Zuverlässigkeit von Fichten-Brettschichtholz mit modifiziertem Aufbau*, volume 11. KIT Scientific Publishing, 2008.

[5] G. Fink, A. Frangi, and J. Kohler. Modelling the bending strength of glued laminated timber - considering the natural growth characteristics. In *Proceedings of the 46th Meeting, International Council for Research and Innovation in Building and Construction, Working Commission W18 - Timber Structures, CIB-W18, Vancouver, Canada*, 2013.

[6] G. Fink. *Influence of varying material properties on the load-bearing capacity of glued laminated timber – Diss. ETH NO. 21746.* PhD thesis, ETH Zurich, Zurich, Switzerland, 2014.

[7] F. Giudiceandrea. Stress grading lumber by a combination of vibration stress waves and x-ray scanning. In *Proceedings of the 11th International Conference on Scanning Technology and Process optimization in the wood Industry (ScanTech 2005)*, Las Veagas, 2005.

[8] G. Fink and J. Kohler. Probabilistic modelling of the tensile related material properties of timber boards and finger joint connections. *submitted to European Journal of Wood and Wood Products*, 2014.

[9] G. Fink and J. Kohler. Model for the prediction of the tensile strength and tensile stiffness of knot clusters within structural timber. *European Journal of Wood and Wood Products*, 72(3):331–341, 2014.